ACCURATE MODELLING OF GLACIER FLOW

by

EDWIN DONALD WADDINGTON

B.Sc., University of Toronto, 1971

M.Sc., University of Alberta, 1973

A THESIS SUBMITTED IN PARTIAL FULFILLMENT OF

THE REQUIREMENTS FOR THE DEGREE OF

DOCTOR OF PHILOSOPHY

in

THE FACULTY OF GRADUATE STUDIES

(Department of Geophysics and Astronomy)

We accept this thesis as conforming

to the required standard

THE UNIVERSITY OF BRITISH COLUMBIA

November, 1981

In presenting this thesis in partial fulfilment of the requirements for an advanced degree at the University of British Columbia, I agree that the Library shall make it freely available for reference and study. I further agree that permission for extensive copying of this thesis for scholarly purposes may be granted by the head of my department or by his or her representatives. It is understood that copying or publication of this thesis for financial gain shall not be allowed without my written permission.

Department of Geophysics and Astronomy

The University of British Columbia
2075 Wesbrook Place
Vancouver, Canada
V6T 1W5

Date February 20, 1982.

ABSTRACT

Recent interest in climatic change and ice sheet variations points out the need for accurate and numerically stable models of time-dependent ice masses. Little attention has been paid to this topic by the glaciological community, and there is good reason to believe that much of the published literature on numerical modelling of the flow of glaciers and ice sheets is quantitatively incorrect. In particular, the importance of the nonlinear instability has not been widely recognized. The purposes of this thesis are to develop and to verify a new numerical model for glacier flow, compare the model to another widely accepted model, and to demonstrate the model in several glaciologically interesting applications.

As in earlier work, the computer model solves the continuity equation together with a flow law for ice. Thickness profiles along flow lines are obtained as a function of time for a temperate ice mass with arbitrary bed topography and mass balance. A set of necessary tests to be satisfied by any numerical model of glacier flow is presented. The numerical solutions are compared with analytical solutions; these include a simple thickness-velocity relation to check terminus mobility, and Burgers' equation to check continuity and dynamic behaviour with full nonlinearity.

An attempt has been made to verify the accuracy of the computer model of Budd and McInnes (1974), Budd (1975) and McInnes (unpublished). These authors have reported problems with numerical instability. If the existing documentation is

accurate, the Budd-McInnes model appears to suffer from mass conservation violations both locally and globally.

The new numerical model developed in this thesis can be used to reconstruct the velocity field within the glacier at each time step; this velocity field satisfies continuity and Glen's flow law for ice. Integration of this velocity field yields the trajectories of individual ice elements flowing through the time-varying ice mass. The trajectories and velocity field are checked by comparison with an analytical solution for a steady state ice sheet (Nagata, 1977). The model in this thesis is not restricted to steady state, and it avoids the violations of mass conservation, and the approximations about the velocity field found in some published trajectory models.

The feasibility of using stable isotopes to investigate prehistoric surging of valley glaciers has been studied with a model simulating the Steele Glacier, Yukon Territory. A sliding velocity and surge duration were specified, based on the observations of the 1966-67 surge. A surge period of roughly 100 years gave the most realistic ice thickness throughout the surge cycle. By calculating ice trajectories and using two plausible relationships between $\delta(O^{18}/O^{16})$ and position or height, longitudinal sections and surface profiles of δ were constructed for times before, during, and after a surge. Discontinuities of up to $0.8^{o}/_{oo}$ were found across several surfaces dipping upstream into the glacier. Each of these surfaces is the present location of the ice which formed the ice-air interface at the time a previous surge began. It may be difficult to observe these surfaces on the Steele Glacier due to

the large and poorly-understood background variability of δ.

The generation of wave ogives has been examined following the theory of Nye (1958[b]), wherein waves are caused by a combination of seasonal variation in mass balance and plastic deformation in an icefall. The wave train generated on a glacier is shown in this thesis to be a convolution of the velocity gradient with an integral of the mass balance function. This integral is the impulse response of the glacier surface to a step in the velocity function. Spatial variations in the glacier width and mass balance also contribute to the wave train. This formulation is used to explain why many icefalls do not generate wave ogives in spite of large seasonal balance variations and large plastic deformations.

TABLE OF CONTENTS

LIST OF TABLES

LIST OF FIGURES

ACKNOWLEDGEMENTS

In the early stages of this work, encouragement and support from my advisor G. K. C. Clarke helped me keep my research going, especially during the periods when the computer programs were uncooperative. His enthusiasm is contagious, and it is delightful to work with him. My appreciation of him grows along with my knowledge of glaciology. Discussions with W. S. B. Paterson, B. B. Narod, W. H. Mathews, D. W. Oldenburg, C. F. Raymond, R. D. Russell, M. C. Quick, R. A. Bindschadler, and W. D. Hibler III have shed light on aspects of glacier dynamics and numerical methods. During the late stages of this project, P. K. Fullagar, completing his Ph.D. thesis in the adjacent office, has been a frequent companion on "the night shift" exchanging ideas and mutual encouragement. B. B. Narod put in long hours proofreading the manuscript and offering helpful suggestions, and he, together with a group of colleagues and friends, helped me through that last hectic night when the manuscript was produced.

Julia Forbes, through her encouragement, interest, and support, has helped me to formulate and to work toward my personal goals. I have made good friends at U.B.C. In particular, Barry Narod, J.G. Napoleoni, Bo Chandra, and Peter Fullagar have shared many happy non-academic experiences with me.

I was supported in part by a National Research Council of Canada postgraduate scholarship, and by an H. R. MacMillan Family Fellowship from the University of British Columbia.

The computations have been carried out at the Computing Centre at U.B.C.

Austin Post, of the U. S. Geological Survey, provided the frontispiece photograph of the Trimble Glacier.

FRONTISPIECE: Wave ogives on the North Branch, Trimble Glacier, Alaska Range, 61°40'N, 152°18'W. Photo by Austin Post, U. S. Geological Survey, 1965.

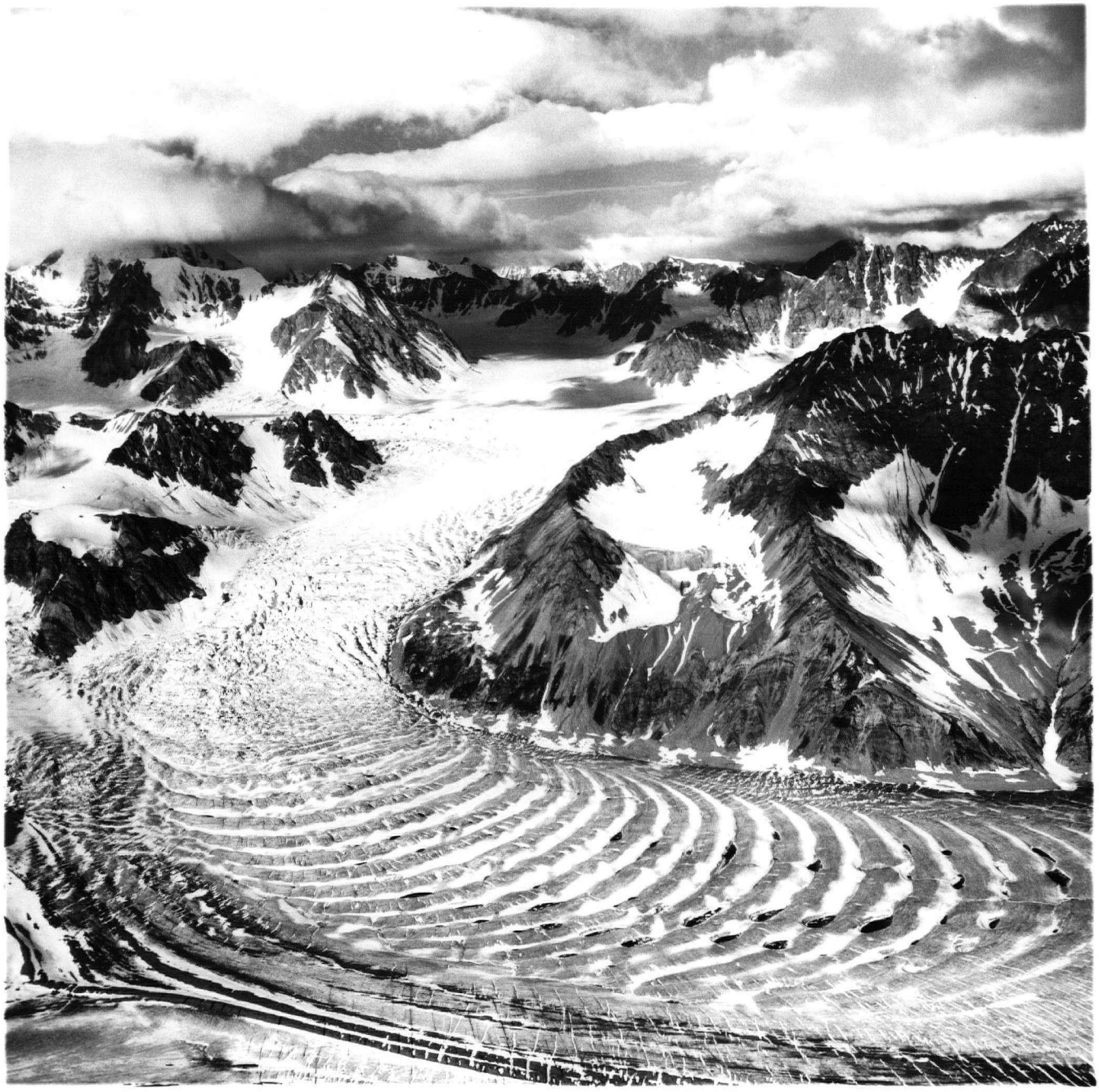

CHAPTER 1: BEGINNINGS

'"Its the job that's never started as takes longest to finish" as my old gaffer used to say.'[1]

1.1 INTRODUCTION

1.1.1 ENDS AND MEANS

Although glaciers and ice sheets often appear to be far-removed from most day-to-day matters, there are a number of compelling reasons to study their behaviour. Advances of some glaciers would threaten roads, dams and mines. Berendon Glacier, British Columbia was studied by Untersteiner and Nye (1968) and by Fisher and Jones (1971) for this reason.

Ice avalanches from glaciers have caused a long history of destruction. For example, a series of four ice avalanches from the Randa Glacier, Switzerland (Agassiz, 1840, p. 158) between 1636 and 1819 destroyed many buildings and fields and killed dozens of citizens. Ice avalanches into moraine-dammed lakes in Peru caused damaging floods (Lliboutry and others, 1977). Advancing glaciers can dam streams or rivers; the resulting lakes often drain catastrophically (Clarke and Mathews 1981; Clarke, in press) when the ice dam fails. Cunningham (1854 (reprinted 1970), p. 100) reported damaging floods on the Indus River in the nineteennth century, and Forbes (1845, p. 262) described the 1818 disaster when the Getroz glacier dammed the

[1] Sam Gamgee, in The Fellowship of the Ring. J. R. R. Tolkien.

Dranse in the Val de Bagnes in Switzerland. Several glacier-dammed lakes threaten a proposed pipeline route in the Yukon Territory (Canada, unpublished).

There is still no universally accepted theory on the cause of ice ages and continental glaciation; an understanding of ice sheet dynamics helps to select and test hypotheses. To correctly interpret the geomorphological record of Pleistocene ice sheets, we must understand the processes of glacial erosion and deposition. This requires a knowledge of glacier mechanics (e.g. Boulton, 1979; Hallet, 1979). The volume, distribution, and rate of growth and decay of the Pleistocene ice sheets (e.g. Paterson, 1972) are important data for the determination of the viscosity of the upper mantle, vertical crustal movements, and sea level changes (e.g. Andrews, 1974).

The isotopic composition of polar ice sheets has been used to reconstruct temperature changes and climate over the past 10^5 years (Dansgaard and others, 1969). To correctly date deep cores, it is necessary to determine the flow pattern within the ice sheet (Dansgaard and Johnsen, 1969[a]; Philberth and Federer, 1971; Hammer and others, 1978).

A current question of some concern is the possibility of global atmospheric warming due to combustion of fossil fuels and clearing of temperate forests (e.g. SMIC, 1971). A multidisciplinary study (NOAA, unpublished) is underway in Boulder, Colorado to investigate the effect increased atmospheric CO_2 would have on the Antarctic ice sheets. Disintegration of the East Antarctic Ice Sheet could raise sea level by 75 m and substantially reduce the albedo of the earth

(Wilson, 1969). Of more immediate concern is the possibility of a surge and disintegration of the West Antarctic ice sheet; this could raise sea level by seven metres in less than 100 years (Thomas and others, 1979). A group at NASA (NASA, unpublished) is using satellite radiometry, altimetry and radar imaging to monitor and to help model variations of the Greenland ice sheet.

Nye (1951, 1952[a], 1953, 1957) made the first quantitative studies of the steady flow of glaciers and ice sheets using analytical models, and Weertman (1958), Lliboutry (1958[b]), and Nye (1960, 1961, 1963[a], 1963[b], 1963[c], 1965[a], 1965[b]) developed the theory of glacier variations, kinematic waves, and response to climate, by using perturbation methods. Many interesting glaciological problems have large temporal variations or complicated boundary conditions; the analytical solutions cannot be used. Answers to some of these more complicated problems can be found by numerical methods using finite differences on digital computers. However, numerical solutions have their own special pitfalls. A numerical solution of a differential equation may differ from the correct solution for many reasons (e.g. Richtmyer and Morton, 1967; Gary, 1975). It is extremely difficult to prove that a numerical model has correctly solved a particular differential equation with complicated boundaries if no analytical check is available; yet this is precisely the type of problem for which numerical models are necessary.

It is essential to first check numerical models against analytical solutions for a variety of simpler problems. The glaciological literature contains very little discussion of

model verification in spite of its obvious importance. There is some indication that much of the published literature on numerical modelling may be quantitatively incorrect.

The major thrust of my work has been aimed at understanding the problems of numerical models, finding ways to avoid the problems, and devising tests to verify the accuracy of the model results. With this in mind, I have developed a new computer model of glacier flow (Appendix 1, and Chapter 2, Section 2.2). Like several previous models (Budd and Jenssen, 1975; Bindschadler, unpublished), this model uses finite differences to solve the mass conservation equation together with a flow law for ice, to give the time-dependent glacier surface for a temperate ice mass in a channel of arbitrary width and bed topography, with an arbitrary mass balance, assuming the flow is driven by gravitational stresses.

I have analyzed the numerical stability and accuracy of this model as thoroughly as is possible for nonlinear equations (Appendix 1). In Chapter 2 I present a set of tests comparing the numerical solutions to analytical solutions to check terminus mobility and both local and global mass conservation, including a case with a nonlinear flow law.

If, in a computer model, the glacier terminus moves incorrectly, it can seriously affect the ice thickness and the velocity throughout the glacier (Section A1.3.4). The physics of the deformation of a glacier snout is complicated (Nye, 1967) for any realistic ice rheology. In the standard numerical approximation (e.g. Budd and Jenssen, 1975; Bindschadler, unpublished, p. 105), the terminus is simply a wedge-shaped

volume with slope and apex chosen so as to conserve mass (see Section A1.3.4). The error in using this kinematic approximation cannot be determined; the correct general solution for the motion of a glacier terminus on an arbitrary slope with Glen's flow in tensor form is still an unsolved problem. However, I have tested the numerical implementation of the wedge terminus by comparing the computed solution to a time-dependent analytical solution with a simpler "rheology" (Section 2.3.2).

Many standard numerical schemes for linear equations break down when applied to nonlinear equations. It is important to test a numerical model with a nonlinear problem. Burgers' equation (Section 2.3.3) is a nonlinear hyperbolic equation with an analytical solution; it is also related to the mass conservation equation. I have compared numerical results with the analytical solution to Burgers' equation to show that my model correctly solves nonlinear problems.

For some glacier flow problems, such as dating ice cores (Dansgaard and Johnsen, 1969[a]) and finding the temperature distribution of cold ice masses (e.g. Jenssen, 1977), it is necessary to know the trajectories of ice particles. My computer model can calculate the velocity field on a vertical longitudinal mesh for a time-dependent glacier, by using Glen's flow law to find the horizontal velocity, and using the continuity equation to then derive the vertical velocity. Particle trajectories are found by a numerical integration of the time-dependent velocity. I tested this part of the computer model against an analytical solution by Nagata (1977) for particle paths in a steady ice sheet.

This numerical model is probably the most thoroughly and accurately tested of its type. The set of tests which I have assembled, or others similar to them, should be used to verify any numerical model of glacier flow. Only then can the models be used with confidence to solve more complicated problems.

I have used this new computer model in two studies. Previous efforts have concentrated on using variations in isotopic ratios in ice cores to investigate climate change, assuming steady state flow. In Chapter 3 I have evaluated the feasibility of using stable isotope measurements to study the surge history of valley glaciers, assuming a constant climate and unsteady flow. The example I considered was the Steele Glacier, Yukon Territory. I found that surging leaves a characteristic pattern in the isotope distribution, but preliminary measurements of $\delta(O^{18}/O^{16})$ suggest that this pattern may be masked by other effects.

Finally, in Chapter 4 I have derived a linear convolution relating the amplitude of wave ogives to the velocity, channel width and mass balance in icefalls. This work is an extension of studies by Nye (1958[b]). I used the computer model to verify the convolution formulation and to determine which features of the icefall on Austerdalsbreen, Norway are most critical to the formulation of its large wave ogives.

1.1.2 CONVENTIONS USED

There are many diverse views on the most appropriate style for a Ph.D. thesis. My aim has been to produce a document which fully describes my work, and which can be understood on its own by those with a basic knowledge of physics or physical glaciology. I have documented all my numerical methods in detail, and summarized the relevant work of others; references substantiate the text rather than substitute for it. This results in a lengthy manuscript. To keep the main text as short as possible, I have placed the numerical methods and the background material in appendices. The work of others should be clearly identifiable. I hope that this level of detail will be appreciated by some readers, since brevity will be required in the version of this work in preparation for publication.

Unless stated otherwise, I have used a righthanded locally orthonormal coordinate system such that the x axis lies along the glacier bed down the centreline of the channel. The y axis is transverse and horizontal, and the z axis is normal to the bed and positive upward in the vertical plane containing the centreline.

The velocity components are (u,w,v) along the (x,y,z) axes. This notation differs from the standard convention (i.e. (u,v,w)) due to historical developments in the thesis.

Underscores are used to indicate tensors. The number of underscores indicates the rank of the tensor, e.g. $\underline{v}$ is the velocity vector, and $\underline{\underline{A}}$ is a coefficient matrix.

The dot symbol $\cdot$, when located above a variable, indicates

a time derivative. When located between two vectors, it represents the standard scalar inner product or dot product, e.g. Malvern (1969, p. 17).

A bar above a variable indicates an average value, usually over a depth range (z direction), or over time (e.g. annual averages).

A list of symbols, together with their meanings and the section in which each is introduced, can be found following Chapter 4.

Equation numbers, and textual references to equation numbers, are enclosed in round parentheses, e.g. (2.2.5), or (A5.6), or (A1.1.3). The characters preceding the first decimal point are the chapter or appendix number. The middle number (if present) identifies the chapter subsection where the equation is given, and the final number is the consecutive equation number in that subsection. References to chapter sections are always identified as such, and the numbers are not enclosed in parentheses.

The LITERATURE CITED is in the style of The Journal of Glaciology. I was not able to obtain the use of some of the very early literature, and some of the literature in languages other than English. In those cases, where I could not verify the citations of others, I have included the citing author in square brackets.

1.2 PREVIOUS WORK

1.2.1 FOUR CENTURIES OF GLACIER FLOW THEORY

The framework within which we currently understand and investigate glacier flow has been assembled in the past three decades. Deep coring techniques (Hansen and Langway, 1966) and radio-echo sounders (Evans, 1963), coming shortly after important experiments on the deformation of ice (Glen, 1952, 1955) and mathematical treatment of the flow of ice sheets and glaciers (Nye, 1951, 1952[a], 1957) started the rapid growth of glaciological research. However, investigation of the flow of glaciers goes back hundreds of years. In Appendix 17, I review the development of ideas on glacier flow in that early period. Some early works were based on fertile imagination and limited observations; others were concise and lucid statements on topics which are subjects of research today. Some misconceptions about glacier flow were raised, debated, and resolved more than once during the period. The main thrust of research during the second half of the nineteenth century was directed by physicists; in the early part of this century, geologists dominated the field (with a few notable exceptions), and research priorities and theories reflected this difference. Contemporary reviews of glacier flow theory were given by Croll (1875, Chapter XXX, p. 495), by Geikie (1894, Chapter 3, p. 25), by Russell (1897, Chapter 9, p. 160), by Hawkes (1930), by Matthes (1942), by Perutz (1947), and by Orowan (1949).

Since 1950, research on glacier flow has progressed

rapidly. The flow law for ice was established for many practical purposes by Glen (1952, 1955) and Nye (1953). Weertman (1957), Lliboutry (1968[a], 1968[b]), Kamb (1970), Nye (1969[b], 1970) and Morland (1976[a], 1976[b]) contributed to the theory of glacier sliding; some aspects of this question are still unresolved. Papers by Nye (1951, 1952[a], 1952[b], 1952[c], 1957, 1959[c]) established realistic analytical solutions for steady glacier and ice sheet profiles, velocities, and stress fields, while identifying many useful approximations. Vialov (1957) used Glen's flow law to derive a steady ice sheet profile which matched the flow line through Mirny, Antarctica. Weertman (1961[b]) examined the effects of longitudinal strain rates on steady ice sheet profiles, and included isostatic depression of the bed. Weertman (1963) considered the effects of fringing mountain ranges on steady ice sheets, and (1966) the effect of a basal water layer.

Although temporal variations of ice masses are difficult to study fully, some useful analytical results have been derived. Kinematic waves on glaciers were observed by Vallot (1900) and were studied by Lliboutry (1958[b]), Nye (1958[a]), and by Weertman (1958) using perturbation methods. Nye, in a series of papers, (1960, 1961, 1963[a], 1963[b], 1963[c], 1965[a], 1965[b]) extended the method to analyze the response of glaciers to climatic change, and to estimate past climate from the record of advance and retreat of glaciers. Bodvarsson (1955) derived equations for a thin ice sheet and analyzed its stability to climatic change. This model is not widely used due to its assumed relation between basal stress and ice flux. Weertman

(1961[a]) performed a similar stability analysis assuming Weertman (1957) sliding. He also derived (1964[a]) the time scales for the growth or decay of a perfectly plastic ice sheet. Jenssen and Radok (1963) obtained a numerical solution for the temperature field in the central region of an ice sheet undergoing thinning.

The study of fully time dependent ice masses with arbitrary boundaries and source terms is a recent development made possible by high speed computers. Numerical solutions of the equations governing ice masses have been obtained for a range of problems by, e.g. Shumskiy (1963), Budd and Jenssen (1975), Mahaffy (1976), Jenssen (1977), Bindschadler (unpublished) and Clarke (1976). The complete solution of the equations of motion, the constitutive equations and the equations of state for a time varying ice mass with arbitrary sources and boundaries is an outstanding problem.

1.2.2 PREVIOUS ICE PROFILE MODELS

Computer models which find the surface height of time-varying glaciers and ice sheets are a relatively new research tool.

Campbell and Rasmussen (1969, 1970) and Rasmussen and Campbell (1973) developed a model which found ice depth at points on a horizontal mesh. They assumed that the ice was a viscous material with a basal friction coefficient determined by mass flux. By arbitrarily lowering the basal friction coefficient they simulated glacier surges.

Budd and others (1971) and Budd and Jenssen (1975) developed a finite difference model to solve the continuity equation for the glacier thickness profile along a flowline. While the equations are similar to those I have used, our numerical methods differ in some respects (see Appendix 16). These authors have included additional important physical properties of ice flow (e.g. the effect of longitudinal stress deviators) and I have devoted more effort toward obtaining an accurate and stable numerical scheme; the additional physical properties will be included later. This model was later developed by Budd (1975) and Budd and McInnes (1974, 1978, 1979) to generate periodic surges. Working from the assumption that basal meltwater can cause sliding, they used the strain energy dissipation to redistribute the basal shear stress, causing large longitudinal strain rates and rapid flow. The sliding behaviour of the model, viewed as a qualitative phenomenon, may be its most important contribution to our ideas on surges.

Bindschadler (unpublished) developed another finite difference profile model similar to the one I describe in this thesis. Bindschadler also did a careful analysis of numerical stability and used a numerical scheme similar to the one I discuss in Appendix 1. He used this model to investigate the changes in the surge-type Variegated Glacier, Alaska, during its quiescent phase.

Mahaffy (Mahaffy, unpublished; Mahaffy 1976; Mahaffy and Andrews 1976; Andrews and Mahaffy, 1976) used a two-dimensional finite difference model to study the ice thickness and lateral extent of the Laurentide ice sheet and the Barnes ice cap.

Jenssen (1977) published the only fully three dimensional model of ice sheets. This model calculated flowlines and temperature as well as ice surface height. Its accuracy was limited by severe computer size limits (Jenssen used a mesh of 12 x 12 x 10 points to represent the whole Greenland Ice Sheet). However, this model is an ambitious development, and probably will be followed by other models of this kind.

1.2.3 PREVIOUS ICE TRAJECTORY MODELS

Quantitative attempts to calculate streamlines date back to the late nineteenth century. Nansen (cited by Shumskiy, 1978, p. 133) calculated flow lines near the ice divide in central Greenland by assuming (1) steady state, (2) constant ice thickness, density and mass balance, and (3) horizontal velocity independent of depth. Haefeli (1963[b]) independently derived the same solution. Reid (1894) and Finsterwalder (1897) independently developed a method of calculating streamlines in steady glaciers using the concept of flow tubes and properties of smooth vector fields. All these methods were only qualitative; none made any use of the constitutive properties of ice.

Haefeli (1961) derived the velocity field in the central portion of a steady isothermal ice sheet, assuming (1) no sliding, and (2) deformation by shear parallel to the bed, using Glen's flow law for ice (Glen, 1955).

Nagata (1977) developed an analytic steady state ice sheet model assuming no horizontal shear deformation; the flow was all

basal sliding following a Weertman-type relation (see A8.3.1). By assuming that the vertical velocity was constant along the ice sheet surface, Nagata also derived the streamlines, and used the results to model the concentration of meteorites by glacier flow in Antarctica (Nagata, 1978). I use this model as a test for my numerical streamline calculations in Section 2.5.2.

Nielson and Stockton (1956) derived the flow field in valley glaciers of constant valley cross-section assuming steady plastic flow, and Shumskiy (1967) found a solution for stress and velocity in a steady glacier with nonlinear viscosity.

Several trajectory models have been derived for regions near ice divides on steady ice sheets in order to date ice cores (Dansgaard and Johnsen, 1969[a]; Philberth and Federer, 1971; Hammer and others, 1978), and to model temperature with depth (Weertman, 1968). All these models make some assumptions about vertical strain rates or temperature gradients.

Budd and others (1971) calculated trajectories along steady state Antarctic flow lines assuming that the vertical strain rate was constant in any vertical column, (p. 51) or weighted by the horizontal velocity variation with depth (p. 55). This process does not appear to satisfy continuity locally. The ice surface elevation was calculated by the numerical model described in Section 1.2.2.

Jenssen (1977) calculated trajectories in a finite difference three dimensional time-dependent ice sheet model, in order to solve for the temperature field.

Jenssen (1978) also found the trajectories of ice particles for a surging model of a flowline through Mirny, Antarctica by

Budd and McInnes (1978). He did not describe the method used to obtain the flowlines. This is the only previous model, of which I am aware, to calculate the trajectories in a time-varying ice mass.

1.3 THE CONTINUITY EQUATION FOR AN ICE MASS

1.3.1 THE GENERAL GLACIER FLOW PROBLEM

The equation of continuity expresses the manner in which the ice mass changes its shape over time, in response to mass input (accumulation or ablation), subject to the physics of deformation and sliding of ice (Sections 1.4 and 1.5), and with the assumptions about the flow field imposed below. I have derived the continuity equation for an ice mass from first principles in Appendix 5, using standard methods of continuum mechanics (e.g. Truesdell and Toupin, 1960; Malvern, 1969; Prager, 1973). In this Section, I will give the resulting equation, the assumptions involved in its derivation, and the physical interpretation of its terms.

The coordinate system I have used in this study is described in Section 1.1.2. The position vector $\underline{x}$ is the triplet [x,y,z], and the velocity vector $\underline{v}(\underline{x})$ is the triplet $[u(\underline{x}),w(\underline{x}),v(\underline{x})]$.

Three basic assumptions of the glacier model are:

1. matter is conserved.
2. momentum is conserved, i.e. acceleration negligible.
3. ice is incompressible (see Appendix 4).

To solve the general set of conservation equations, constitutive equations, and equations of state for the temperature distribution, internal energy content, and all the components of the stress tensor and the velocity field, with boundary conditions on a possibly arbitrary boundary, is a problem to instill a sense of humility in even the most enthusiastic and optimistic glaciologist or numerical analyst. All attempts, of which I am aware, to find solutions to ice flow problems start by making some additional assumptions about the channel geometry (boundaries and symmetry), or about the temperature distribution (e.g. isothermal), and/or about the flow field itself (e.g. plane strain, simple shear, uniform strain rates, etc.). The model I describe in this study is no exception.

1.3.2 RECTANGULAR CROSS-SECTION FLOW MODEL

The glacier flow volume being modelled (see Figure 1.1) is assumed to have a rectangular cross-section, and a width W(x). The two dimensional model includes variations in the third dimension in an approximate way by the assumptions that the velocity components u and v are independent of y, and that the lateral component w varies linearly with y (lateral strain rate independent of y), such that the net velocity $\underline{v}(\underline{x})$ at the margins is parallel to the margins, i.e.

$$\frac{\partial u}{\partial y} = 0 \qquad (1.3.1)$$

$$\frac{\partial v}{\partial y} = 0 \tag{1.3.2}$$

$$\frac{\partial w}{\partial y} = \frac{u(x,z,t)}{W(x)} \frac{dW}{dx} \tag{1.3.3}$$

The glacier thickness h(x,t) is also independent of y.

$$\frac{\partial h}{\partial y}(x,t) = 0 \tag{1.3.4}$$

Nye (1959[c], equation (33)) suggested this method of including lateral variations, and Budd and Jenssen (1975, equation 3.34) incorporated it into their model. Figure 1.1 illustrates the form of this model.

For an ice sheet, W(x) can be the distance between two possibly nonparallel flowlines; the 'walls' of the channel are a mathematical fiction, and the assumptions (1.3.1) through (1.3.4) are reasonable.

For a valley glacier, drag from the valley walls is important, and the ice thickness and glacier bed vary with y. If I attempt to identify W(x) with the valley width, the assumptions (1.3.1) to (1.3.4) may be grossly violated. If, however, I let W(x) be the distance between two flowlines near the glacier centreline, e.g. W(x) may be a few percent of the valley width at the level of the ice surface, then all the assumptions are reasonable, and I obtain a central flowline solution, but with the lateral variation in valley width included to a good approximation.

The effect of the valley sidewall drag can be included in an approximate way by using shape factors (Nye, 1965[c]) to modify the shear stress (see equation (1.4.25) below).

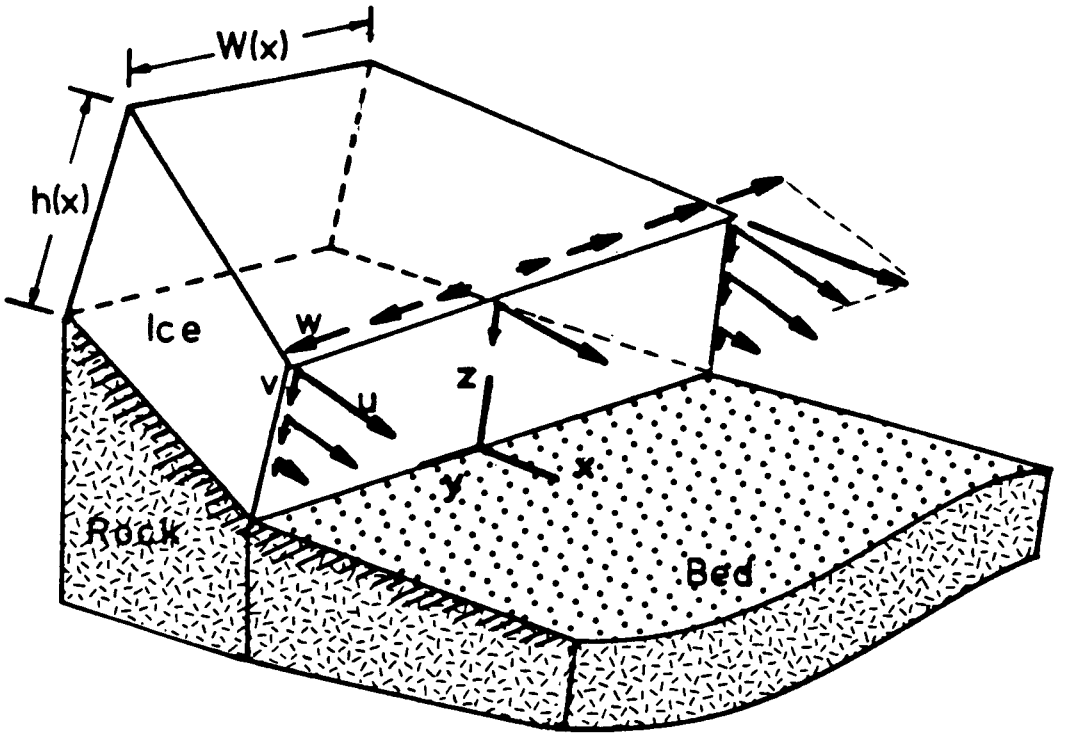

FIGURE 1.1. Rectangular Cross-section Flow.
The triad x-y-z shows the coordinate axes, and the bold arrows u, v, and w are the vector components of the velocity $\underline{v}$. The example shows the velocity in the accumulation zone (v is negative).

1.3.3 THE CONTINUITY EQUATION

With these assumptions, the well-known continuity equation (the derivation of which I show in Appendix 5) is

$$\frac{\partial h}{\partial t}(x,t) + \frac{1}{W(x)} \frac{\partial Q}{\partial x}(x,t) = A(x,t) \qquad (1.3.5)$$

where h(x,t) is the ice thickness normal to the bed, Q(x,t) is the ice flux through a cross-section from bed to surface, and the source term A(x,t) is the net mass balance normal to the bed, i.e. the net accumulation or ablation rate in ice equivalent thickness units per unit time, including snowfall, surface melting, and basal melting and refreezing. The last two

contributions are usually negligibly small (e.g. Rothlisberger, 1972).

The ice flux Q(x,t) is defined by

$$Q(x,t) = W(x)\int_0^{h(x,t)} u(x,z,t)\, dz \qquad (1.3.6)$$

where u(x,z,t) is the velocity component parallel to the bed. It will be derived in the next section. Q(x,t) can also be written

$$Q(x,t) = V(x,t)\, h(x,t)\, W(x) \qquad (1.3.7)$$

where V(x,t) is u(x,t), i.e. the downslope velocity u(x,z,t) averaged between the bed and the surface.

$$V(x,t) = \frac{Q(x,t)}{W(x)\, h(x,t)} = \frac{1}{h(x,t)}\int_0^{h(x,t)} u(x,z,t)\, dz \qquad (1.3.8)$$

Assuming that the upstream end of the glacier section under consideration is at x=0, the boundary condition is

$$Q(0,t) = Q_o(t) \qquad (1.3.9)$$

If x=0 actually represents the physical upper extent of the ice mass, $Q_o(t)$ is identically zero. For the case of an ice divide, this is achieved by setting

$$V(0,t) = 0 \qquad (1.3.10)$$

by a vanishing ice surface slope angle (see (1.4.38)), and letting ice thickness h(0,t) vary. For the case of a valley glacier originating on a slope, the boundary condition (1.3.9) is achieved by setting

$$h(0,t) = 0 \qquad (1.3.11)$$

If the lower end x=L(t) is the glacier terminus, then L(t) is defined implicitly by

$$h(L(t),t) = 0 \qquad (1.3.12)$$

(This is not a mathematical boundary condition, but a physical condition defining the limits of the ice mass.)

An initial condition of the form

$$h(x,0) = H_0(x) \qquad (1.3.13)$$

is also required. For example, one simple initial condition is $H_0(x)=0$, i.e. unglacierized ground.

1.3.4 PHYSICAL INTERPRETATION

Equation (1.3.5) may be interpreted in the following manner. Consider a vertical prism of ice as shown in Figure 1.2, extending from the bed to the surface h(x,t), with width W(x) in the y direction, and thickness δx in the x direction. Let ρ be the constant density of glacier ice. When (1.3.5) is multiplied by the constant $\rho W(x)\delta x\delta t$, the first term is the net change in mass in the prism in a time δt (the prism is then taller or shorter). The second term on the left is the difference in mass between that which flowed out of the prism through the downslope face, and that which flowed into the prism through the upstream face, in the time δt. This is the net loss of mass from the prism into the downstream flow. The term on the right side is just the total mass added to the prism in time δt by snowfall or melting. Thus, (1.3.5) states that the total layer of mass added to the top of the prism at any position x is the sum of the snowfall onto the prism and the net mass left inside the prism by spatial flow variations.

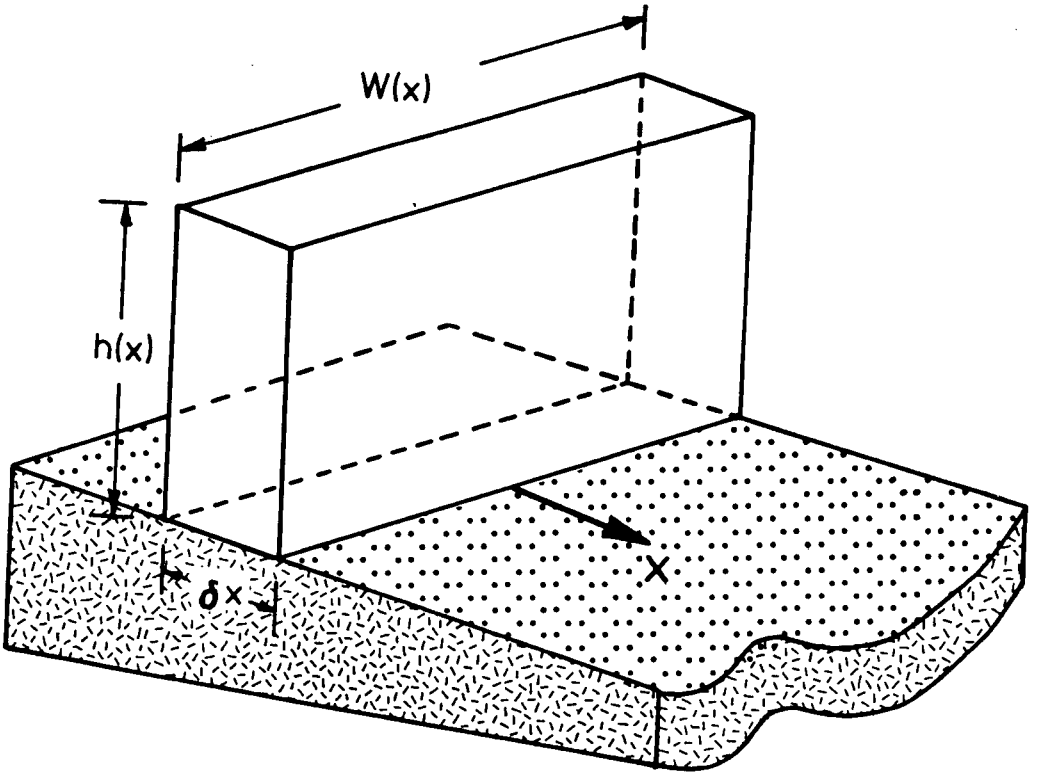

FIGURE 1.2. Vertical Prism For Continuity Interpretation.

1.4 PHYSICS OF ICE DEFORMATION

1.4.1 INTRODUCTION

In this Section, I will outline the derivation of a second equation relating glacier thickness and ice flux so that the continuity equation (1.3.5) can be solved. There are three steps in this derivation. This is a standard procedure in modelling glacier flow (e.g. Paterson, 1980; Raymond, 1980).

Newton's second law establishes relationships between the surface and body forces and the accelerations in any continuum. The stress equilibrium equations are outlined in Section 1.4.2. Second, observations and theory of the deformation of glacier ice establish constitutive relationships between the stresses applied to ice, and the resulting deformation. Glen's flow law

for ice (Glen, 1955, 1958) is presented in Section 1.4.3. Finally, in Section 1.4.4, after making simplifying assumptions, substituting the stress equations of Section 1.4.2 into Glen's flow law to get the strain rate, and integrating over appropriate coordinates, I express the downslope component of the ice velocity in terms of the ice thickness. Since ice flux, thickness, and velocity are related through (1.3.7), this will complete the derivation of a second equation needed to solve the continuity equation (1.3.5) for ice thickness and flux.

1.4.2 STRESS EQUILIBRIUM EQUATIONS

Since glacier ice deforms slowly, the acceleration term in Newton's second law can be neglected, leaving the result that, for any volume V of a slowly deforming continuous medium,

$$\underline{B} + \underline{T} = 0 \qquad (1.4.1)$$

where $\underline{B}$ is the total body force found by integrating the specific body forces (force per unit mass) $\underline{f}(\underline{r})$ at position $\underline{r}$ over all $\underline{r}$ throughout the volume V. Its components are

$$B_i = \iiint_V \rho(\underline{r})\, f_i(\underline{r})\, d^3r \qquad (1.4.2)$$

and $\underline{T}$ is the total surface traction on the surface S enclosing the volume V with surface normal vector $\underline{n}$. The components of $\underline{T}$ are

$$T_k = \iint_S n_j(\underline{r})\, \sigma_{jk}(\underline{r})\, dS \qquad (1.4.3)$$

σ_{jk} is the stress tensor, i.e. the force per unit area on a surface normal to the x_j axis acting in the x_k direction. The

Einstein convention, whereby repeated indices are summed, is used in this section. Orthogonal axes are assumed.

Applying Gauss' Theorem (e.g. Prager, 1973, p. 29) to (1.4.3) and substituting (1.4.2) and (1.4.3) into (1.4.1) by components gives

$$\iiint_V \left[\rho(\underline{r})\, f_i(\underline{r}) + \frac{\partial \sigma_{li}}{\partial x_l}(\underline{r}) \right] d^3r = 0 \qquad (1.4.4)$$

Since the volume V is arbitrary, the global equation (1.4.4) has a local counterpart

$$\rho(\underline{r})\, f_i(\underline{r}) + \frac{\partial \sigma_{ki}}{\partial x_k}(\underline{r}) = 0 \qquad (1.4.5)$$

Assuming that the net angular acceleration is zero, and setting to zero the sum of moments acting on the volume V, gives the result

$$\sigma_{ij} = \sigma_{ji} \qquad (1.4.6)$$

i.e. the stress tensor is symmetric. The development is very similar to (1.4.1) through (1.4.5), and is given in Prager (1973, p. 47).

For a glacier, the only body force is gravity, so

$$\underline{f}(\underline{r}) = \underline{g} \qquad (1.4.7)$$

When the x_1 axis (to be called x) is taken along the glacier bed which is at an angle $\beta(x)$ to the horizontal, the x_3 axis (z) is normal to it and upward, and the x_2 axis (y) is horizontal, then the stress equations (1.4.5) are

$$\frac{\partial \sigma_{xx}}{\partial x} + \frac{\partial \sigma_{xy}}{\partial y} + \frac{\partial \sigma_{xz}}{\partial z} + \rho g \sin(\beta) = 0 \qquad (1.4.8)$$

$$\frac{\partial \sigma_{xz}}{\partial x} + \frac{\partial \sigma_{yz}}{\partial y} + \frac{\partial \sigma_{zz}}{\partial z} - \rho g \cos(\beta) = 0 \qquad (1.4.9)$$

$$\frac{\partial \sigma_{xy}}{\partial x} + \frac{\partial \sigma_{yy}}{\partial y} + \frac{\partial \sigma_{yz}}{\partial z} = 0 \qquad (1.4.10)$$

1.4.3 CONSTITUTIVE RELATION FOR ICE DEFORMATION

The constitutive equations for deformation relate the stresses applied to ice to the resulting deformation rate. The components of the strain rate tensor are

$$\dot{\epsilon}_{ij} = \frac{1}{2}\left[\frac{\partial u_i}{\partial x_j} + \frac{\partial u_j}{\partial x_i}\right] \qquad (1.4.11)$$

where u_i is the ith component of the ice velocity.

Glen (1958) showed that the most general relation between the stress tensor and the strain rate tensor for a nonlinear, originally isotropic material had the form

$$\dot{\epsilon}_{ij} = A(T_1, T_2, T_3)\delta_{ij} + B(T_1, T_2, T_3)\sigma_{ij} + C(T_1, T_2, T_3)\sigma_{ik}\sigma_{kj} \qquad (1.4.12)$$

where δ_{ij} is the Kroenecker delta

$$\delta_{ij} = 0 \quad i \neq j$$

$$= 1 \quad i = j \tag{1.4.13}$$

and T_1, T_2, and T_3 are the first, second, and third scalar invariants of the stress tensor (e.g. Prager, 1973, p. 22)

$$T_1 = \sigma_{ii} \tag{1.4.14}$$

$$T_2 = \frac{1}{2}(\sigma_{ij}\sigma_{ji} - \sigma_{ii}\sigma_{jj}) \tag{1.4.15}$$

$$T_3 = \frac{1}{6}(2\sigma_{ij}\sigma_{jk}\sigma_{ki} - 3\sigma_{ij}\sigma_{ji}\sigma_{kk} + \sigma_{ii}\sigma_{jj}\sigma_{kk}) \tag{1.4.16}$$

Terms in higher powers of σ_{ij} can be eliminated by the Hamilton-Cayley equation (e.g. Prager, 1973, p. 25). The stress-dependent coefficients must be functions of, at most, the scalar invariants, because the relation (1.4.12) is independent of the choice of axes.

The coefficients A, B, and C may be dependent on temperature.

Rigsby (1958) showed that, to a good approximation, the deformation rate of ice crystals was independent of the hydrostatic pressure p, where

$$p = \frac{1}{3}\sigma_{ii} \tag{1.4.17}$$

when the ice temperature was measured relative to the pressure-melting point. This result means that the constitutive relation can be written more simply in terms of the deviatoric stress σ'_{ij}.

$$\sigma'_{ij} = \sigma_{ij} - \frac{1}{3}\delta_{ij}\sigma_{kk} \qquad (1.4.18)$$

By definition, the first scalar invariant T'_1 of σ'_{ij} is zero. By further assumptions, first that the density of glacier ice is constant (see Appendix 4), second, that, for a given stress, the components of strain rate are proportional to the components of the stress deviator tensor, and third, that the second invariant of the strain rate tensor is a function of T'_2 only (see Glen, 1958) the flow law presented by Nye (1953) reduced the general relation (1.4.12) to

$$\dot{\epsilon}_{ij} = B(T'_2)\,\sigma'_{ij} \qquad (1.4.19)$$

When $\dot{\epsilon}$ and τ are the square roots of the second scalar invariants of $\dot{\epsilon}_{ij}$ and σ'_{ij} ($\tau = \sqrt{T'_2}$), Nye (1953) showed that a plausible relationship was

$$\dot{\epsilon} = A\,\tau^{n} \qquad (1.4.20)$$

Using the case of a simple slab deforming by shear parallel to the x axis, combining (1.4.20) with (1.4.19) implies that

$$B(T'_2) = A\,\tau^{n-1} \qquad (1.4.21)$$

and

$$\dot{\epsilon}_{ij} = A\,\tau^{n-1}\,\sigma'_{ij} \qquad (1.4.22)$$

The exponent n in (1.4.20) is independent of temperature. Values in the literature vary from 1.5 (Gerrard and others, 1952) to 4.2 (Glen, 1955), and the value usually used for glacier modelling is n=3 (e.g. Paterson, 1980). The factor A

follows the exponential Arrhenius temperature dependence

$$A = A_0 \exp(-Q/RT) \qquad (1.4.23)$$

where A_0 is a constant, R is the gas constant (8.314 J $K^{-1}mol^{-1}$), Q is the activation energy for creep, and T is the temperature (°K). Values of Q for secondary creep of polycrystalline ice are 60 kJ mol^{-1} for $T < -10°C$, and approximately 139 kJ mol^{-1} for $T > -10°C$ (Paterson, 1981, p. 34). The presence of small amounts of water causes grain boundary sliding (Barnes and others, 1971; Jones and Brunet, 1978) above -10°C. The deformation below -8°C is dominated by basal glide (Barnes and others, 1971).

In this study, the ice is assumed to be isothermal at 0°C, and the flow law parameters used are (Paterson, 1981, Table 3.3, p. 39)

$$n=3 \qquad A = 5.3\ 10^{-15}\ s^{-1}\ kPa^{-3} \qquad (1.4.24)$$

These values apply only for secondary creep, after the initial transient response to loading has died away.

Other constitutive relations have been proposed for glacier ice, such as a hyperbolic sine relation (Barnes and others, 1971), or a polynomial with odd order stress terms (Meier, 1958, 1960; Lliboutry, 1969[a]; Colbeck and Evans, 1973). However, laboratory experiments (e.g. Glen, 1952, 1955; Steinemann, 1958) and field measurements of closure of boreholes and tunnels and deformation of boreholes (e.g. Gerrard and others, 1952; Nye, 1953; Mathews, 1959; Meier, 1960; Paterson and Savage, 1963[a], 1963[b]; Haefeli, 1963[a]; Shreve and Sharp, 1970; Raymond, 1971; Paterson, 1977) and the flow of ice shelves (Thomas, 1973)

indicate that (1.4.22), known as Glen's flow law, is a useful and satisfactory constitutive relation for glacier ice.

1.4.4 SHEAR STRESS AND ICE FLUX

In this section, I will outline the derivation of the shear stress parallel to the bed, and how it can be integrated to give the downslope velocity component and the ice flux. The errors and assumptions are explicitly shown. The details are given in Appendix 7.

The stress equilibrium equation (1.4.8) can be integrated from the surface to a height z above the glacier bed to give the shear stress

$$\sigma_{xz}(x,z) = s\rho g(h-z)\sin\alpha \left[1 + O\left[\frac{2h\,\overline{\partial\sigma'_{xx}}/\partial x + h\,\overline{\partial\sigma'_{yy}}/\partial x}{\rho g h \alpha}\right]\right] \qquad (1.4.25)$$

which is derived from (A7.3.21) in Appendix 7. The leading factor is the standard formula for shear stress in a parallel-sided slab deforming by simple shear parallel to the bed (e.g. Paterson, 1969, p. 91) when the shape factor s is unity (see Appendix 7, Section A7.4). The surface slope α is an effective slope averaged over a distance of at least the order of 4h (Budd, 1968; 1970[a]). The average stress deviators in the second term are defined by

$$\overline{\frac{\partial \sigma'_{xx}}{\partial x}} = \frac{1}{(\overline{h-z})} \int_{z}^{h(x)} \frac{\partial \sigma'_{xx}}{\partial x} \, dz' \qquad z<h$$

$$= 0 \qquad z=h \qquad (1.4.26)$$

with a corresponding definition for the yy component. If I consider the x- and y-directed forces on an ice column from the ice surface to the bed, the correction terms in (1.4.25) are, very roughly speaking, ratios of the normal forces to the basal shear force. These ratios are usually very small for glaciers and ice sheets. Lliboutry (1958[b]), Shumskiy (1961), and Robin (1967) used a correction term similar to this to account for longitudinal strain, and Collins (1968) published a mathematical justification of it. Nye (1969[a]) simplified the analytical formulation by an appropriate choice of axes. My formulation differs in some details, partly because I use the axes of the numerical model (see Section 1.3).

Budd (1968; 1970[a]; 1970[b]; 1971) gave a detailed discussion of stress variations in glaciers, including correction terms and the wavelength ranges for which they may be important. Hutter (in press) gives the most recent and rigorous treatment of stress in glaciers.

The shape factor is an approximate correction between zero and unity for the reduction in the shear stress σ_{xz} along the channel centreline when some of the weight of the glacier is supported by the valley sidewalls. It was first used quantitatively in work on rectilinear flow in rectangular, parabolic, and elliptical channels by Nye (1965[c]). I describe shape factors in more detail in Appendix 7, Section A7.4.

In arriving at (1.4.24) in Appendix 7, I assumed that the slope angles α of the ice surface, and β of the glacier bed were small, i.e.

$$|\alpha(x)| << 1 \tag{1.4.27}$$

$$|\beta(x)| << 1 \tag{1.4.28}$$

I also assumed that α was never negligibly small compared to β. This may not be true near an ice divide.

Although (1.4.8) contains $\sin\beta$, the final result (1.4.25) for the shear stress depends only on $\sin\alpha$. Nye (1952[b]) first pointed out this result. When the small angle assumptions (1.4.27) and (1.4.28) hold, the longitudinal stress gradient term $\partial\sigma_{xx}/\partial x$ in (1.4.8) introduces a term in $(\alpha-\beta)$ which cancels the bed slope dependence, leaving only the surface slope dependence of (1.4.25).

With the assumption that the major shear deformation occurs parallel to the bed, i.e.

$$\left|\frac{\partial v}{\partial x}\Big/\frac{\partial u}{\partial z}\right| << 1 \tag{1.4.29}$$

the shear strain rate

$$\dot{\epsilon}_{xz} = \frac{1}{2}\left[\frac{\partial u}{\partial z} + \frac{\partial v}{\partial x}\right] \tag{1.4.30}$$

is approximately

$$\dot{\epsilon}_{xz} = \frac{1}{2}\frac{\partial u}{\partial z} \tag{1.4.31}$$

which can be integrated directly, from the bed to height z, to give

$$u(x,z) = u_s(x) + \int_0^z \dot{\epsilon}_{xz}\, dz' \qquad (1.4.32)$$

where $u_s(x)$ is the basal sliding velocity discussed in Section 1.5.

If I further assume that τ, the square root of the second invariant of the stress deviator tensor (1.4.19) is approximately equal to the shear stress σ_{xz}, i.e. shear stress parallel to the bed is by far the largest stress deviator component, or

$$\left| \frac{\delta\tau}{\sigma_{xz}} \right| = \left| \frac{\tau - \sigma_{xz}}{\sigma_{xz}} \right| << 1 \qquad (1.4.33)$$

then I can substitute Glen's flow law (1.4.22) for the strain rate $\dot{\epsilon}_{xz}$ in (1.4.32), using σ_{xz} from (1.4.25) for both τ and σ_{xz}, to get the velocity component u(x,z) parallel to the bed.

$$u(x,z) - u_s(x) =$$

$$2A\left[s(x)\rho g \sin(\alpha(x))\right]^n \frac{\left[h^{n+1} - (h-z)^{n+1}\right]}{(n+1)} \left[1 + e(x)\right] \qquad (1.4.34)$$

where the error e(x), i.e. the terms not included in the computer model, has the form

$$e(x) = O\left[n\left[\frac{2h\,\overline{\frac{\partial\sigma'_{xx}}{\partial x}} + h\,\overline{\frac{\partial\sigma'_{yy}}{\partial x}}}{\rho g h \alpha} \right] + (n-1)\frac{\delta\tau}{\sigma_{xz}} - \frac{\partial v}{\partial x} \Big/ \frac{\partial u}{\partial z} \right] \qquad (1.4.35)$$

where the symbol O[x] means "is of the order of x", i.e. the function goes to zero at the same rate as x. I have assumed that

the glacier is isothermal, i.e. temperate, so that the coefficient A of Glen's flow law(1.4.22) can be treated as a constant. If the ice temperature varies with z, the integral can be evaluated numerically.

The downslope ice flux for use in the continuity equation (1.3.5) is

$$Q(x,t) = \int_0^{h(x,t)} u(x,z,t)\, dz$$

$$= u_s(x,t)\, h(x,t) + 2A\left[\frac{s\rho g \sin\alpha}{(n+2)}\right]^n [h(x,t)]^{n+2} [1+ e(x)] \qquad (1.4.36)$$

With the assumptions discussed above, the error term involving e(x) is small; it is neglected in the computer model in its present form.

The average velocity V(x,t) used in Section 1.3 and Appendix 1 is defined as

$$V(x,t) = Q(x,t)/h(x,t) \qquad (1.4.37)$$

which is

$$V(x,t) = u_s(x,t) + 2A\left[\frac{s\rho g \sin\alpha}{(n+2)}\right]^n [h(x,t)]^{n+1} [1+ e(x)] \qquad (1.4.38)$$

The term on the right due to the internal deformation is just (n+1)/(n+2) times the downslope velocity component at the ice surface u(x,h(x),t) from (1.4.34).

1.5 BASAL SLIDING

1.5.1 INTRODUCTION

The one quantity still required to complete the derivation of the downslope velocity u(x,z) and the flux Q(x) is the basal sliding velocity $u_s(x)$ which appeared as an integration constant in (1.4.32). Raymond (1980), in a recent review, gave a summary of sliding behaviour, measurements, and the physical processes possibly involved, and pointed out some difficulties of quantitative modelling of sliding.

In Appendix 8, I summarize current ideas on the physics of sliding, and review the use of sliding in computer models. In this section, I discuss the importance of sliding, the way I treat sliding in Chapter 3, and the reason for my choice.

1.5.2 BASAL ICE TEMPERATURE AND SLIDING

Ice masses which are cold at the base, i.e. have temperatures below the pressure melting point, do not appear to slide. The basal ice is effectively frozen to the glacier bed, and

$$u_s(x) = 0 \qquad (1.5.1)$$

Ice masses which have temperatures at the pressure melting point at the ice-rock interface exhibit sliding velocities which range from zero to values much greater than the velocities due to internal deformation. The model I describe in this study assumes an isothermal ice mass. Due to the existence of the

geothermal heat flux, and the resulting geothermal temperature gradient, the only possible essentially isothermal ice mass is one at the pressure melting point throughout its volume (neglecting a possibly cold surface layer caused by diffusive penetration of the winter cold wave), because only then can the geothermal flux be absorbed at the base by being transformed into energy of fusion. This means that sliding velocities can be an important component of motion for my modelling situations.

1.5.3 PHILOSOPHY OF SLIDING IN THIS STUDY

Correctly modelling the physical processes of glacier sliding is, at the present, very difficult, due to inadequate observations, and the large number of uncontrolled physical variables possibly involved in sliding processes. In Appendix 8, I have outlined the problems of measurements, the physical complications of sliding processes, the present state of sliding theory and its quantitative application in computer models.

In the models presented in this study, I do not attempt to investigate or to simulate the physics of glacier sliding. My aim, in Chapter 3, is to investigate the consequences of surging (defined by a periodic sliding history) on structures within a glacier, given that periodic surging occurs in the defined manner. I do not attempt to induce surges in the model by any particular physical mechanism. This approach to investigating effects of surging was also used by Campbell and Rasmussen (1969) and by Clarke (1976).

I could easily incorporate the theories of Weertman (1957),

Nye (1969[b]; 1970), Kamb (1970), Morland (1976[a]; 1976[b]), or Budd (1975) to calculate the sliding velocities, but the results would be numerically suspect, due to the problems discussed in Appendix 8, and would add nothing to my investigation of the consequences of surging.

My approach is, instead, to use a predetermined sliding function $u_s(x,t)$ (based as closely as possible on the reasonably well inferred sliding history of a surging glacier such as the Steele) as a driving function for periodic surges in the computer model. I calculate the response of the glacier model to this driving function by using continuity and Glen's flow law to find the internal deformation. For my purpose of finding the effects of surging on the internal structure, this approach is no worse than using a numerically inadequate sliding theory, and it has the distinct advantage that I can control the sliding at will while I relate sliding patterns to resulting changes within the ice mass.

CHAPTER 2: MODELS AND TESTS

"Things are seldom what they seem;
Skim milk masquerades as cream."[1]

2.1 INTRODUCTION

2.1.1 OUTLINE

In this chapter, I outline the operation of the computer models and I describe tests used to verify their correct operation. In this introductory section, I explain why I think tests are important. In Section 2.2, I describe the continuity equation glacier profile model, and in Section 2.3, how I have tested it. In section 2.4 I describe the particle trajectory calculations, and in Section 2.5, how they were tested.

2.1.2 IMPORTANCE OF MODEL TESTING

Analytical solutions of initial value problems are most desirable, because the correctness of the solution can be verified for all space and time simply by substituting the solution into the differential equation. Unfortunately, analytical solutions to ice flow problems are restricted to a few cases with simple boundary conditions, uncomplicated rheologies, and, often, steady states.

A finite difference numerical model uses a set of algebraic

---

[1] H.M.S. Pinafore. Gilbert and Sullivan.

equations whose solution closely approximates a digitized version of the true solution of the differential equation, to within a truncation error (see Appendix 1, Section A1.5.3). Numerical solutions can extend the domain of solvable problems to include those with quite general boundary conditions, ice rheology, and temporal variations. The price which is paid for this increased generality, however, is a new inherent uncertainty in the validity of the solution obtained. Substitution of a numerical solution into the finite difference equations, or into the differential equation, can give, at most, the residual errors in the most recent time step. The long term integrated error is unknown. The danger is that a numerical solution will behave in a qualitatively reasonable manner, yet quantitatively may be, over some time scales, grossly wrong. For instance, ice velocities and thicknesses may be in error by tens of percent, and the phase of cyclic phenomena such as surging may become totally unrelated to the phase of the true solution. These possibilities should make us quite cautious about any predictive claims made for numerical models. We could obtain a result no more accurate, at best, than an educated guess, yet be lulled into believing that it was an quantitative prediction of glacier behaviour.

There are two possible sources of error in numerical solutions. First, the computer program may not correctly solve the set of algebraic equations. Programming errors, such as incorrect constants or missing minus signs, sometimes go undetected. Spurious numerical "solutions" of this kind have on occasion found their way into the scientific literature. By

careful program design and the use of consistency checks, these errors can be eliminated, although not all programmers have taken the time to do so.

Assuming then, that the computer program works correctly, there is still another source of error. The numerical scheme used in the computer model may not adequately represent the differential equation at all time scales. One example of this is the linear computational instability (Appendix 1, Section A1.4.2). The solution of the finite difference equations may include an exponentially growing high wavenumber oscillation completely unrelated to the differential equation. Fortunately, this error is usually easy to recognize!

The other cause for concern is the possibility that the numerical solution may drift away from the true solution, yet still look "physically reasonable". This could be caused by any of several factors. For example, inappropriate mesh intervals (Appendix 1, Section A1.5.2) may cause incorrect dispersion and spectral attenuation, distorting the solution to an unacceptable degree. Introducing smoothing schemes in attempts to suppress numerical instabilities can cause similar distortions (and may still fail to totally remove the instabilities). For example, the widely reported ice sheet model of the Melbourne group (Budd and Jenssen, 1975; Budd and Radok, 1971) was used by McInnes (unpublished), who appears to have encountered all of the above difficulties. In an attempt to model surging glaciers in the presence of growing numerical instability, McInnes (p. 64) reported:

> " Different time steps give slightly different surge times and periods and therefore at the same growth time, profiles are not directly comparable. Also due to the different number of steps, and the smoothing scheme not being perfect, the lower the time step the more iterations, which leads to more smoothing which tends to lower either the depth or the base velocity, and therefore affects the surging times."

and further, discussing a criterion to introduce automatic smoothing at the appearance of instability problems (p. 64):

> "Using this test before automatic smoothing, lessens the number of times smoothing is used, and therefore decreases the effect smoothing has on the exact profiles."

There is obviously little cause for optimism in the belief that this numerical model, for instance, was providing a solution that closely matched the true solution at all times. The results of the McInnes study were published by Budd (1975) and by Budd and McInnes (1974; 1978; 1979). I mention this example, not to criticize any particular individuals, but to illustrate the lack of attention paid to this serious question by most members of the glaciological modelling community. Even a major glacier modelling program has apparently had serious difficulties with accuracy, consistency, and mass conservation (see Appendix 16), yet model verification has not been given priority discussion in the published literature.

Because numerical model results cannot be verified for the complicated problems the numerical models are created to solve, it is <u>imperative</u> that numerical schemes be verified by comparing their numerical solutions with analytical solutions for simpler problems <u>before</u> the numerical models are used for new problems. There is always a temptation with a new model to rush into the solution of complicated glaciological problems. This urge to

break new ground in a hurry must be controlled until the numerical model has been demonstrated to work accurately on known ground. Only in this way can there be any confidence in the results.

2.2 CONTINUITY EQUATION PROFILE MODEL

2.2.1 INTRODUCTION

I have written a FORTRAN IV computer program which numerically solves the continuity equation (1.3.5), when provided with a subroutine to calculate the velocity V(x,t) averaged through the ice thickness. The flow equation (1.4.38) based on Glen's flow law (1.4.22) is used for glacier simulations (Chapter 3). I describe the computational scheme in detail in Appendix 1. I summarize the computational aspects in this Section, including the numerical scheme (Section 2.2.2), the boundary conditions (Section 2.2.3), numerical stability (Section 2.2.4), and accuracy (Section 2.2.5).

Inputs to the model are bedrock elevation b(x), mass balance A(x,t), the initial ice thickness $H_0(x)$, the ice flux $Q_0(t)$ through the upslope boundary, and parameters to specify the sliding and flow properties of the deforming medium. Output from the model is the time-varying ice thickness profile.

2.2.2 THE NUMERICAL SCHEME

Complete details of the numerical scheme are given in Appendix 1, Sections A1.1 and A1.2.

I solve the continuity equation (1.3.5) by a finite difference method (e.g. Richtmyer and Morton, 1967). The partial differential equation (1.3.5) is approximated by a set of algebraic equations for the ice thickness $\{h_j \mid j=1,J\}$ at a set of mesh points at equal horizontal intervals of Δx. Starting from an initial condition $\{h_j^0 \mid j=1,J\}$, the solution is obtained by time marching, using a possibly variable time step Δt. The finite difference equations are

$$\frac{h_j^{n+1} - h_j^n}{\Delta t} + \frac{\theta}{W_j}\frac{(Q_{j+1/2}^{n+1} - Q_{j-1/2}^{n+1})}{\Delta x_j} + \frac{(1-\theta)}{W_j}\frac{(Q_{j+1/2}^{n} - Q_{j-1/2}^{n})}{\Delta x_j}$$

$$= \theta A_j^{n+1} + (1-\theta) A_j^n \qquad (2.2.1)$$

$$1 \le j \le J \quad 1 \le n \le N$$

where superscripts indicate the time step, and subscripts indicate the spatial mesh point. Mass balance A_j and ice thickness h_j are measured normal to the bed, and the mesh increments Δx_j are measured along the bed. The weight factor θ is a constant between zero and unity, used to stabilize the scheme. I discuss θ further in Section 2.2.4.

The ice flux $Q_{j+1/2}$ between the meshpoints is related to the ice thickness h_j at the meshpoints, the channel width $W_{j+1/2}$ and the vertically averaged downslope velocity $V_{j+1/2}$ between the meshpoints by

$$Q_{j\pm1/2} = V_{j\pm1/2}\, W_{j\pm1/2}\, \frac{(h_{j\pm1} + h_j)}{2} \qquad (2.2.2)$$

Most of the variables in (2.2.2) are shown in Figure 2.1. The flux is calculated midway between mesh points because of numerical stability considerations.

The set of equations (2.2.1) can be written in matrix form as

$$\underline{\underline{M}}\ \underline{H} = \underline{D} \qquad (2.2.3)$$

where the components of the vector $\underline{H}$ are the unknown ice thicknesses at the mesh points at the future time step $\{h_j^{n+1} | j=1,J\}$, the right side vector $\underline{D}$ contains quantities from the previous time step, and the matrix $\underline{\underline{M}}$ contains coefficients involving velocity at the future time step. Since the velocity is related to the ice thickness (Sections 1.3 and 1.4), this makes (2.2.3) nonlinear, and the system must be solved iteratively. For the first iteration, the velocity profile at the previous time step $\{V_j^n | j=3/2, 5/2, \ldots J+1/2\}$ is used as an estimate of $\{{}_0V_j^{n+1} | j=3/2, 5/2, \ldots J+1/2\}$, to calculate the first estimate of the ice thickness $\{{}_0h_j^{n+1} | j=1,J\}$. Prescripts indicate iteration number. These ice thickness estimates are then used to calculate an estimate $\{{}_1V_j^{n+1} | j=3/2, 5/2, \ldots J+1/2\}$ of the longitudinal velocity profile at the future step. The residuals (2.2.4)

$$r_j^{n+1} = 2p_j\,\theta[Q_{j+1/2}^{n+1} - Q_{j-1/2}^{n+1}] + 2p_j\,(1-\theta)[Q_{j+1/2}^{n} - Q_{j-1/2}^{n}]$$

$$+ h_j^{n+1} - h_j^{n} - \theta A_j^{n+1}\,\Delta t - (1-\theta)A_j^{n}\,\Delta t$$

$$1 \le j \le J \qquad 1 \le n \le N \tag{2.2.4}$$

where

$$p_j = \Delta t/(2\Delta x W_j) \tag{2.2.5}$$

then measure the degree to which the current estimates of ice thickness and velocity fail to satisfy the continuity equation (1.3.5).

By using a linearized equation (2.2.6) to relate residuals to ice thickness corrections δh_j required to make the residuals go to zero,

$$r_j^{n+1} = \sum_{k=1}^{J} \frac{\partial r_j^{n+1}}{\partial h_k^{n+1}}\,\delta h_k \tag{2.2.6}$$

$$\text{or} \qquad \underline{A}\,\underline{\delta h} = \underline{r} \tag{2.2.7}$$

I obtain essentially a multi-dimensional formulation of the Newton-Raphson method (e.g. Carnahan and others, 1969, p. 319) to solve (2.2.4). The iterations terminate when the largest residual in absolute value is smaller than a preset test criterion. I discuss the choice of a criterion in Appendix 11.

2.2.3 BOUNDARY CONDITIONS

The set of equations (2.2.1) with (2.2.2) consists of J equations in J+2 unknowns $\{ h_j^{n+1} | j=0,J+1 \}$. Since equation (1.3.5) is a first order differential equation, it requires one boundary condition selected from (1.3.10) through (1.3.12). This gives one of the required two extra equations.

At an ice divide, zero input flux is modelled by including an image point h_0 at a distance Δx outside the boundary j=1, with

$$h_0 = h_2$$

$$V_{1/2} = -V_{3/2} \qquad (2.2.8)$$

This forces the surface slope to be zero at the boundary, but the ice thickness can vary with time. This situation is illustrated in Figure 2.1.

For a valley glacier originating on a bedrock slope,

$$h_1 = 0 \qquad (2.2.9)$$

and the ice surface slope can adjust to any appropriate value.

To model only a portion of an ice mass such that the upstream end of the model is some distance downslope from the bergschrund or divide (e.g. Chapter 4, where an icefall is modelled), the ice flux must be specified at 1/2 mesh increment above the boundary, i.e.

$$Q_{1/2}^{n} = Q_0(n\Delta t) \qquad (2.2.10)$$

The second extra equation required to balance the number of

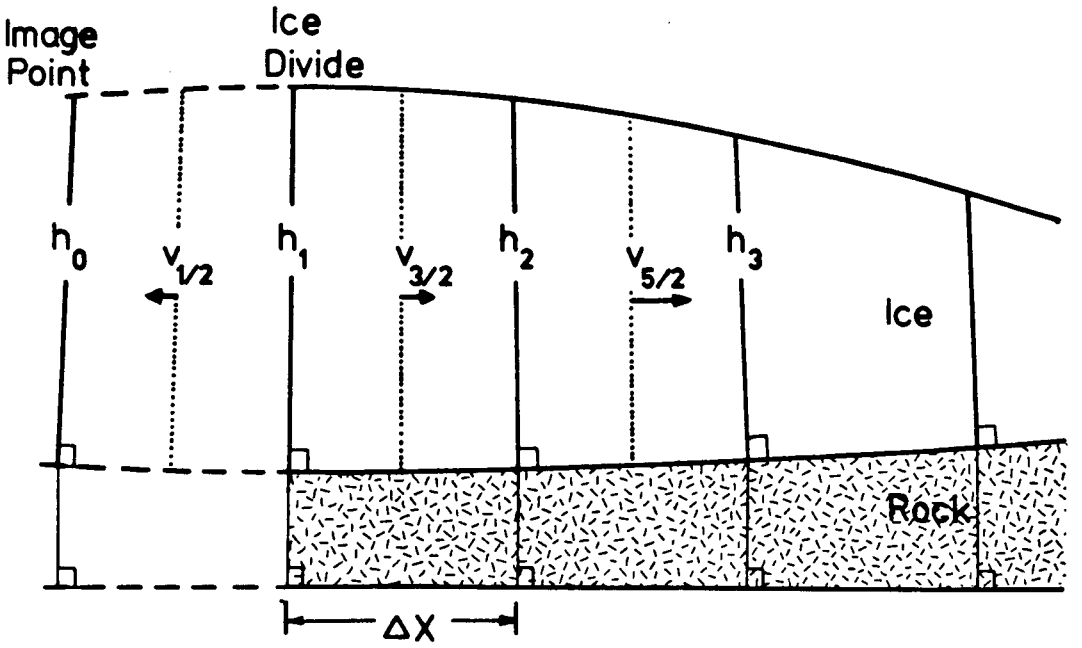

FIGURE 2.1. Numerical Scheme At Ice Divide.

equations and unknowns comes from the treatment of the downslope boundary. If I treat the boundary as fixed in space, and simply allow ice to flow through it and out of the model, I can get the equation by writing h_{J+1} as an appropriate extrapolation of the ice thickness at the meshpoints. I use the second order Newton's divided differences polynomial (e.g. Carnahan and others, 1969, p. 12).

If I choose to follow the actual motion of the glacier snout, defined by x=L(t), I must keep track of L(t) when it falls between the meshpoints, and be able to add or subtract points to or from the mesh as the terminus moves. I assume that the terminus is wedge shaped from the last mesh point J to the snout at L(t), as shown in Figure 2.2. Then, I apply the principle of conservation of mass to the shaded section of the wedge, obtaining the required final equation by balancing the

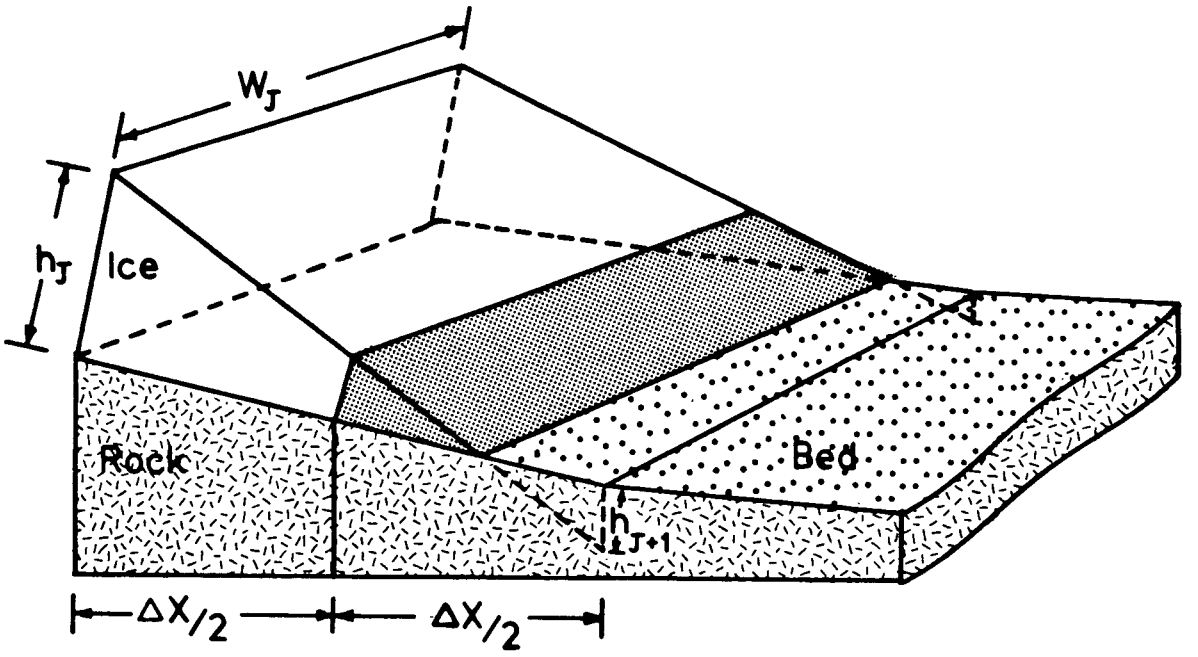

FIGURE 2.2. The Wedge Terminus.

volume change of the wedge against ice flux into the wedge from upslope plus net mass balance on the upper surface, during each time step. The details may be found in Appendix 1, Section A1.3.4. As the terminus moves, the ice thickness h_J at the upstream end, the snout position L(t), and the slope of the ice surface are all free to adjust to changes in the flow. This terminus model is similar in many respects to that used by Bindschadler (unpublished).

2.2.4 NUMERICAL STABILITY

If the finite difference numerical scheme and the mesh increments are chosen unwisely, the finite difference equations may admit a solution quite different from the solution of the differential equation. This usually involves a spurious exponential growth of some wavenumber component which quickly

dominates the desired bounded, physically reasonable solution.

Rigorous stability analysis of nonlinear equations is usually not feasible, but stability criteria for linearized analogues generally give useful guidelines and insights into stability of the nonlinear forms.

The first type of stability problem, the linear computational instability, involves the choice of the mesh increments Δt and Δx. For many systems of finite difference equations, instability can occur when the time step Δt is too large relative to the space step Δx. If $\Delta x/\Delta t$ is much greater than the material velocity V, material travels many mesh intervals per time step, and the system tends to 'forget' the physical solution. The von Neumann method (e.g. Richtmyer and Morton, 1967, p. 70), is one standard stability analysis for linear or linearized equations. The method involves finding the transfer function T(m) in the wavenumber domain which multiplies the Fourier transform of the solution at the previous time step n, to give the Fourier transform of the solution at the future time step n+1. If

$$T(m) \leq 1 \qquad (2.2.11)$$

at all wavenumbers m, no wavenumber can grow, so no instability can exist. After linearizing (1.3.5) by setting the velocity V to a constant in (1.3.7), I find that by choosing

$$\theta \geq 1/2 \qquad (2.2.12)$$

I obtain unconditional linear computational stability for any choice of Δx and Δt.

The second type of numerical instability is called 'the nonlinear instability' (e.g. Phillips, 1959; Mesinger and

Arakawa, 1976, p. 35). This is a problem which arises in any numerical solution of a differential equation using a discrete mesh, and having terms which are nonlinear in some combination of the dependent and the independent variables. In (1.3.5), $\partial Q/\partial x$ has this form.

The nonlinearity pumps energy (squared amplitude of the wavenumber spectrum) from the low wavenumber end to the high wavenumber part of the wavenumber spectrum of the dependent variable, and the aliasing (Appendix 3) due to discrete sampling folds this energy back to the lower wavenumbers, where it distorts the solution. Since the nonlinear instability has an importance which is not widely recognized in the glacier modelling community, I discuss it in detail in Appendix 1, Section A1.4.3.

If a function is known only at discrete intervals Δx, a wellknown result from sampling theory (see Appendix 3) is the fact that its Fourier spectrum can be found only up to a wavenumber m_N, called the Nyquist wavenumber,

$$m_N = \frac{\pi}{\Delta x} \qquad (2.2.13)$$

This is a sampling rate of two samples per cycle. Wavenumbers above this limit are misinterpreted as lower wavenumbers (see Figure A3.2), by being 'folded' back into the spectrum symmetrically about m_N (see Figure A1.3).

It is easy to show (see (A1.4.7) through (A1.4.9)) that multiplying two band-limited Fourier series together gives a product bandlimited to the sum of the bandwidths of the two signals. This happens with the ice flux Q=hV. If both h and V

are always bandlimited to $2/3m_N$, their product is bandlimited to $4/3m_N$, which is aliased back onto the interval from $2/3m_N$ to m_N, but the lower 2/3 of the spectrum remains correct (see Figure A1.3).

It is evident, then, that to avoid the nonlinear instability, the aliased signal at high wavenumbers, i.e. above $2/3m_N$, must be heavily attenuated. At the same time, the attenuation must not distort the low wavenumbers which contain information about the glacier.

Budd and Jenssen (1975) encountered an instability which they attributed to machine roundoff error. I think it was actually the nonlinear instability. Budd and Jenssen attempted to cope with the instability by smoothing the velocity profile whenever it began to oscillate spatially. McInnes (unpublished, p. 58; p. 102) used the same computer programs to simulate surging at Bruarjokull, Iceland. The broken curves in Figure 2.3 (redrawn from McInnes, (unpublished), p. 58) show the instability which arose as he attempted to build up the glacier to a steady state with no sliding, and no smoothing of the profiles. In Appendix 1 Section A1.4.4, I discuss the velocity smoothing method used by Budd and Jenssen (1975), and also, the addition of a purely numerical dissipation term to (1.3.5) to preferentially damp high wavenumbers. I conclude that the use of either of these methods is hard to justify. The two methods I use in this numerical model are superior on physical grounds.

First, if the flow equation for the continuum (e.g. (1.4.34)) depends on the local ice surface slope $\alpha(x)$, then large amplitude bumps in the solution profile should tend to

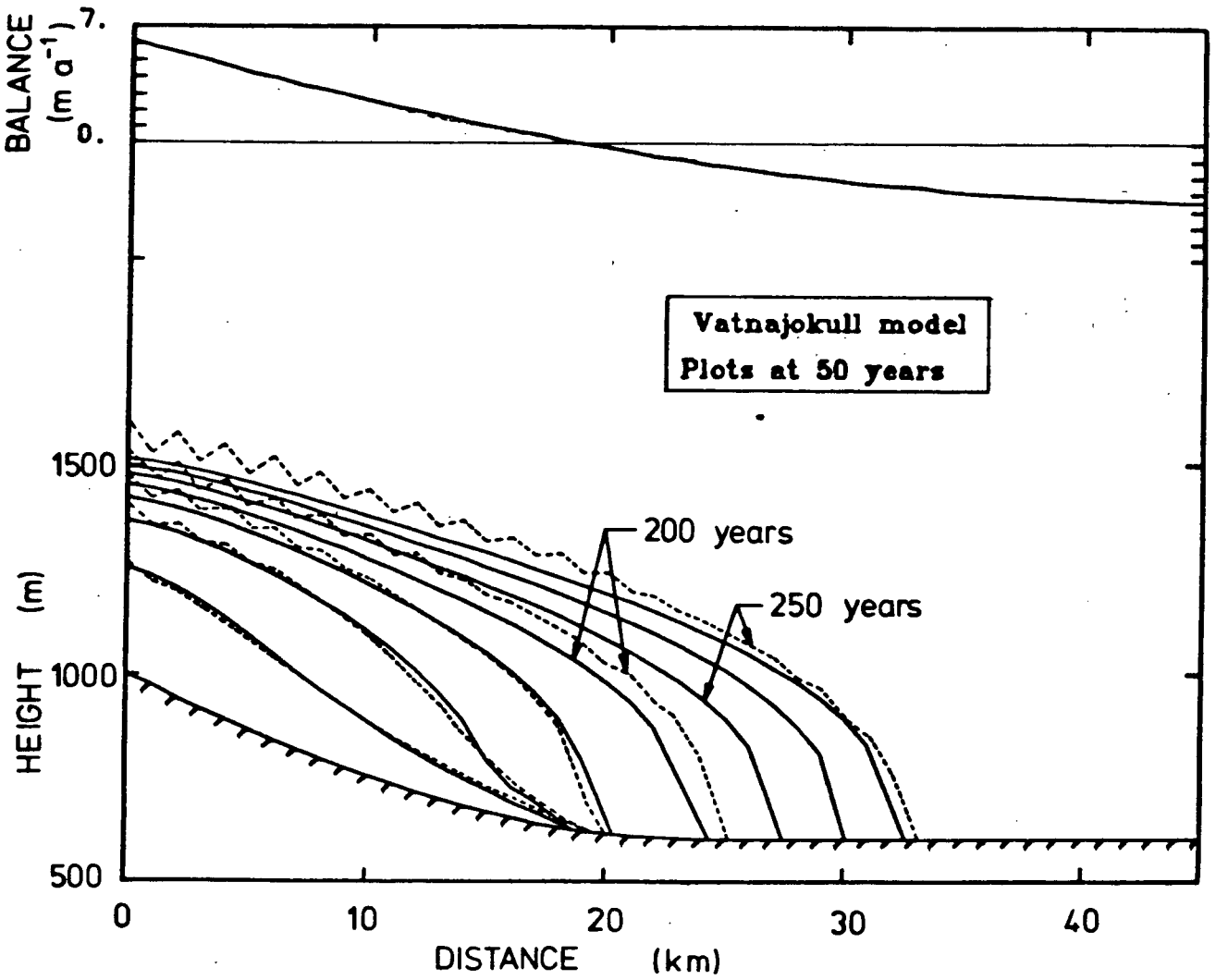

FIGURE 2.3. Example Of The Nonlinear Instability.
The dashed curves redrawn from McInnes (unpublished, p. 58) show the onset of the nonlinear instability on ice surface profiles at 50 year intervals for a flowline on Vatnajokull (Iceland). The Budd-McInnes model did not calculate flux at the midpoints of the mesh intervals for h(x), and therefore was vulnerable to the nonlinear instability. The solid curves are the 50 year profiles from my computer model using parameters in Table 2.1. The Budd-McInnes model also appears to create mass (see Appendix 16).

diffuse out rapidly, due to the physical properties of the medium (See Appendix 6, which relates perturbations of (1.3.5) to a diffusion equation following Nye (1960)). This same process should also efficiently smooth out high wavenumber instabilities. In Appendix 13, I have shown that, when the ice

flux is calculated at the midpoints of the mesh intervals, i.e. at j±1/2, as shown in Figure 2.2, this physical diffusion process is incorporated into the numerical model and controls the nonlinear instability at all wavenumbers.

For example, the broken curves in Figure 2.3 show the onset of the nonlinear instability in the Budd-McInnes (1974) computer model (Budd, 1975; McInnes, unpublished). The original caption on Figure 4.3 of McInnes, from which these profiles are redrawn, was

> "Profiles from the Vatnajökull model at fifty year intervals, showing the increase in the magnitude of the oscillations with time, due to the two point finite difference approximation. In this case, no smoothing was used."

These authors did not calculate the ice flux at the midpoints of their mesh intervals. As a result, the diffusive mechanism of Glen's flow law was unable to prevent serious aliasing at the Nyquist wavelength (in this case, 2 km). The trigger for the instability could have been a large truncation error (Appendix 1, Section A1.5.3) resulting from the use of a forward difference at the boundary (Budd and Jenssen, 1975). The solid

n	A $bar^{-n}\ a^{-1}$	s	g ms^{-2}	ρ $kg\ m^{-3}$	Δx m	Δt a
2	.225	1.0	9.8	910.	1000.	1.0

TABLE 2.1. Parameters for Vatnajökull (Figure 2.3)

curves are the 50 year profiles using my computer model with the parameters in Table 2.1. As far as I can tell, McInnes also used

these values. The nonlinear instability is removed at all wavelengths due to the choice of numerical scheme. As well as the high wavenumber oscillation, the Budd-McInnes model appears to suffer from a mass conservation error. I discuss this further in Appendix 16.

A second method must be used when the ice flux is not a function of the local ice slope. For example, the gravitational stress may be calculated using an intermediate or large scale slope (e.g. Bindschadler, unpublished, p. 92). In this case, I remove the nonlinear instability without distorting the low wavenumber signal at all, by, at the completion of each time step, taking the Fourier transform of both the velocity profile and the ice thickness profile, and multiplying by the lowpass filter in Figure 2.4; this filter has a cutoff at $2/3m_N$. I then perform the inverse Fourier transform to obtain the profiles which are bandlimited at $2/3\ m_N$, and unaffected by aliasing. The nonlinear instability cannot grow, and cannot affect the solution below $2/3m_N$. By a suitably small choice of the mesh increment Δx, m_N can be made large enough so that all physically interesting wavenumbers in the glacier profile are well below the cutoff wavenumber.

Phillips (1959), who originally identified the nonlinear instability, suppressed it in this manner. However, the procedure was quite costly to implement, because his work predated the Fast Fourier Transform algorithm (Cooley and Tukey, 1965). In my work, using the filter of Figure 2.4 with the Fast Fourier Transform method did not dramatically increase the computer execution time for the tests I performed.

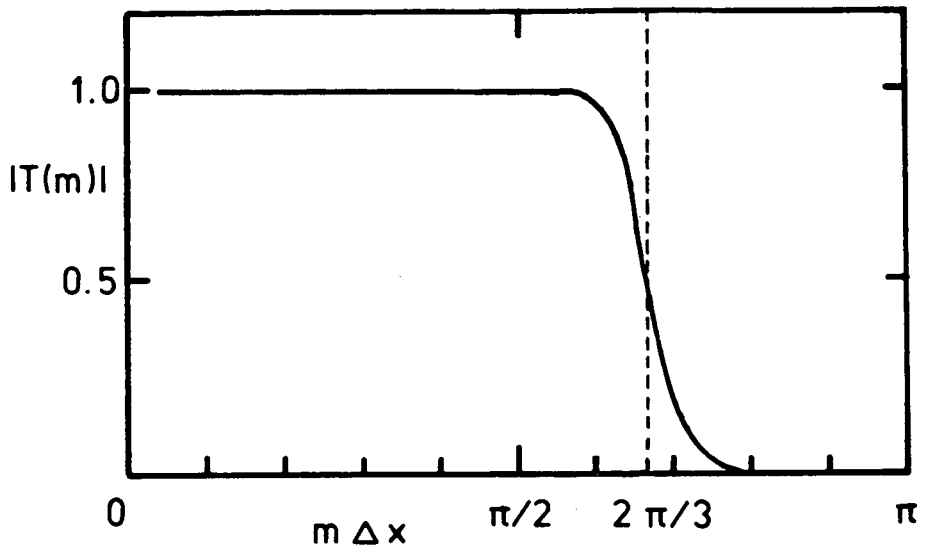

FIGURE 2.4. Filter To Suppress The Nonlinear Instability. The Nyquist wavenumber is at $m\Delta x=\pi$.

2.2.5 ACCURACY

Having achieved a stable scheme, I must now ask how accurately it solves the partial differential equation. In Section A1.5, I examine the accuracy of the numerical scheme by two somewhat complementary methods.

The first method follows from the von Neumann stability analysis in Section 2.2.4. At all wavenumbers m, I compare both amplitude and phase of the transfer function T(m) of the the numerical scheme with those of the partial differential eqation. Errors in amplitude represent incorrect attenuation, and errors in phase represent incorrect propagation speeds and dispersion. For the linear equation, the conclusion is to use

$$\theta = 1/2 \qquad (2.2.14)$$

for the most accurate amplitudes (see Figure A1.7), and to take Δx as small as feasibly possible to get accurate phase (see

Figure A1.8). I use these conclusions as a guide when selecting parameters for the nonlinear model.

The second method is an estimation of the 'truncation error'. This is the difference between an exact solution h(x,t) of the differential equation, and an exact solution $\{h_j^n | j=1,J\}$ of the finite difference equations. It is a spatial domain error estimate, i.e. it estimates the total error at each x position, rather than estimating the error in each sine wave component. After assuming that ice thickness h(x,t) and ice flux Q(x,t) are infinitely differentiable, the finite difference solution can be expressed as truncated Taylor expansions about the solution h(x,t) and Q(x,t) of the differential equation. The error is expressed in terms of the first neglected derivatives. The result is that the truncation error ϵ_j^n has the form

$$\epsilon_j^n = \Delta t \left[\frac{(1-2\Theta)}{2} \frac{\partial^2 h}{\partial t^2}\bigg|_j^n \right] + \Delta t^2 \left[\frac{1}{6} \frac{\partial^3 h}{\partial t^3}\bigg|_j^n \right] + \Delta x^2 \left[\frac{1}{24} \frac{\partial^3 Q}{\partial x^3}\bigg|_j^n \right] \tag{2.2.15}$$

The leading term vanishes with the choice

$$\Theta = 1/2 \tag{2.2.16}$$

This is the same result obtained from the wavenumber analysis (2.2.14). The truncation error is also minimized by keeping the mesh increments as small as possible. The coefficients can be estimated from the third derivatives of h and Q in the numerical model to get a quantitative estimate of the error.

2.3 TESTING THE CONTINUITY MODEL

2.3.1 INTRODUCTION

Two tests are described in this subchapter. The first verifies that the model satisfies continuity with nonconstant width, balance, bed, velocity, and ice thickness, and that the terminus moves correctly. The second test verifies that the programs accurately solve a realistic nonlinear problem in which the flow velocity depends on both h(x,t) and its gradient in x.

Although other tests of numerical models are available (e.g. Waddington, 1979), the tests presented here are a simple, reasonably comprehensive, and stringent trial of any numerical flowline model based on the continuity equation (1.3.5). I think that it is a reasonable proposal that these tests be used as a minimum standard for verification and comparison of all numerical models of glacier flow prior to attempts to use them to model complicated ice masses.

2.3.2 CONTINUITY TEST WITH TERMINUS MOTION

The ability of the glacier model terminus to move correctly, i.e. at a rate consistent with the flow law being used, is critical to accurate simulation of glacier flow (e.g. Nye(1963[a], 1963[b]); Nye in discussion of a paper by Mahaffy and Andrews (1976)). If the model terminus advances too slowly, it will act as a dam, resulting in a glacier solution which is too thick, slow, and short, even though continuity is satisfied everywhere. If the terminus of the model advances more rapidly

h_o	s_o	$\dot{s}$	W_o	W'	c	Δx	Δt
0.1	-1.0	0.01	1.0	1.0	-0.02	0.01	0.5
0.1	-0.1	-0.01	1.0	1.0	-0.02	0.01	0.5

TABLE 2.2. Parameters for continuity test with moving terminus. The first line gives the advancing model, and the second line gives a retreating model. See Figure 2.5 and Figure 2.6.

than the correct rate, the glacier solution will be too thin, fast flowing, and extended.

No simple approximations are available to simplify the stress equations (1.4.8) through (1.4.10) near the glacier terminus. Nye (1967) published a solution for the shape of a glacier terminus. Since this solution assumed steady state, a horizontal bed, and perfectly plastic ice, it is not suitable for inclusion in my numerical model. The terminus model being tested is described in Section 2.2.3 and A1.3.

To check that the numerical model satisfies continuity everywhere and advances or retreats correctly when it is allowed to choose its own terminus position, I use a channel, mass balance, and a flow law giving an analytical solution to the continuity equation (A1.1.1) and show that the model reproduces this solution accurately. My choice is to some extent arbitrary. Other solutions could easily be found. However, the one used below is a good one because it is evident at a glance whether the model results are correct, and it tests the model with a number of nonconstant and nontrivial input functions. Let h_o, s_o, $\dot{s}$, W_o, W', and c be constants, let the channel width W(x) be

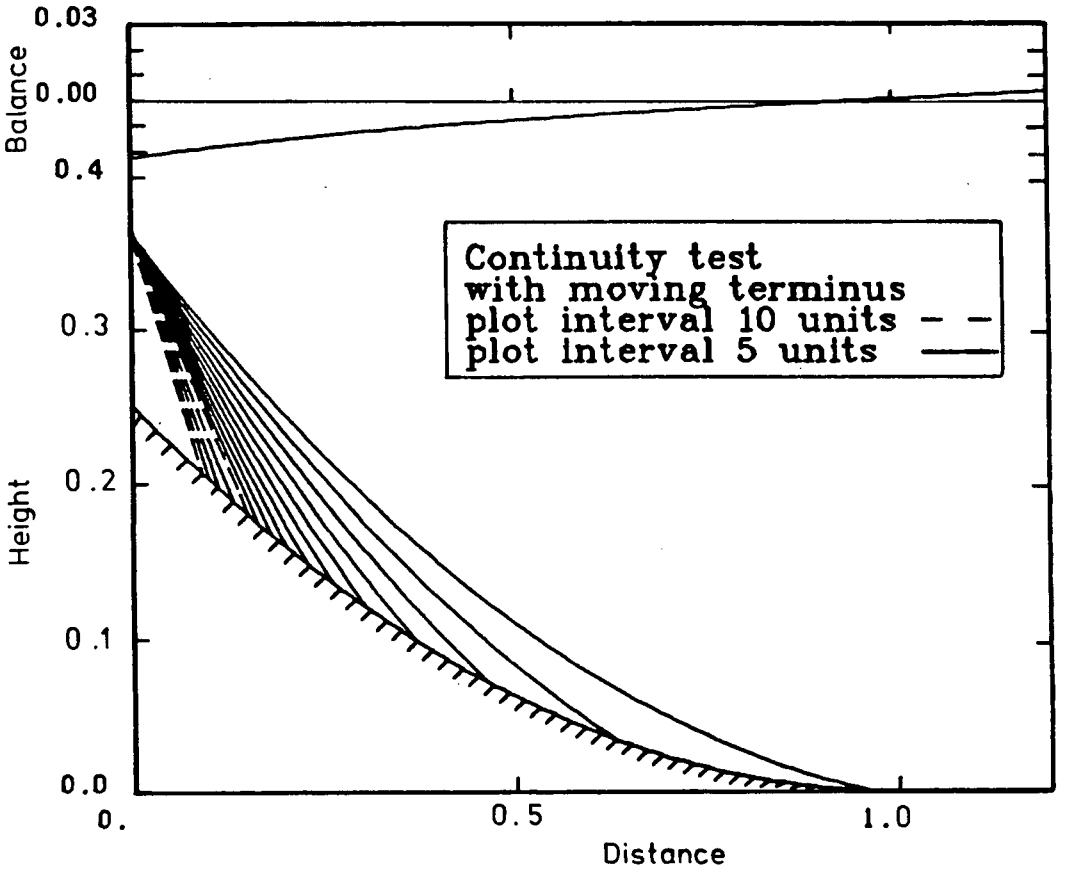

FIGURE 2.5. Continuity Test with Moving Terminus.
Flow is to the right. The solution profiles are shown at intervals of 10 time units up to 40 units, then at 5 units. The model is described by equations (2.3.1) through (2.3.5) with the constants in Table 2.2.

$$W(x) = W_o + W'x \qquad (2.3.1)$$

and the mass balance A(x) be

$$A(x) = \dot{s}x + c/W(x) \qquad (2.3.2)$$

I use a velocity (averaged over depth) given by (2.3.3). This has no physical significance; it is merely a numerical test.

$$V(x,t) = cx/[W(x)(h(x,t)-h_o)] \qquad x \neq 0$$

$$= c/[s(t)W(x)] \qquad x=0 \qquad (2.3.3)$$

where the surface slope s is given by

$$s(t) = s_o + \dot{s}\,t \qquad (2.3.4)$$

(During the numerical solution procedure, care should be taken to avoid the singularity in (2.3.3) when h(x,t) approaches h_o; this can be done by approximating (2.3.3) by a suitably smooth analytical function in the region of h(x,t) near h_o and $h(x,t)>h_o$.) Substitution of (2.3.1) through (2.3.5) into (A1.1.1) verifies that the thickness solution h(x,t) is

$$h(x,t) = h_o + s(t)\,x \qquad (2.3.5)$$

Distance x is measured along the glacier bed. Any bed profile may be used in the numerical model. The thickness h_o at x=0 is constant for all time, and h(x,t) varies linearly with x at all times, resulting in a wedge-shaped "glacier" with slope s(t). This slope s(t) changes linearly with time at the constant rate $\dot{s}$. By solving (2.3.5) for the value of L such that h(L(t),t)=0, the correct glacier terminus position is found to be at

$$L(t) = -h_o/s(t) \qquad (2.3.6)$$

Figure 2.5 shows the numerical results for the advancing model using the constants in the first line of Table 2.2, and the curvilinear bed shown in Figure 2.5. The wedge solution advances to the right and is shown at equal time intervals of 10 nondimensionalized units for the first 40 units, and at 5 units

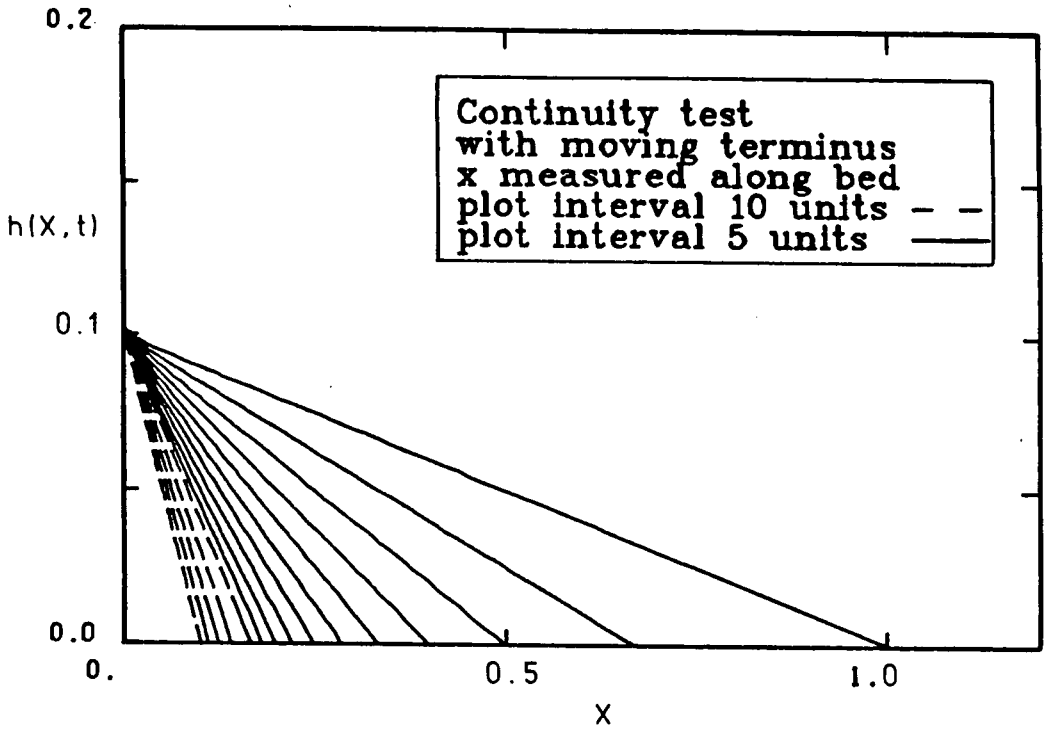

FIGURE 2.6. Continuity Test With Moving Terminus.
Results in Figure 2.5 with bed elevation removed and distance measured along the bed.

thereafter. Figure 2.6 shows the same results with the bed elevation subtracted, and distance x measured along the model bed rather than horizontally, i.e. it should be the solution h(x,t) in (2.3.5). In fact, it reproduces (2.3.5) to within one part in 10^3. The same degree of accuracy is obtained with the retreating model (Table 2.2) which duplicates the curves of Figure 2.6, but in the reverse order. This verifies that the numerical model satisfies continuity everywhere and moves the terminus correctly under quite general conditions; the width

varies with x, the mass balance varies with x, and the velocity varies with h, x, and t.

2.3.3 CONTINUITY TEST WITH BURGERS' EQUATION

The test in Section 2.3.2 verifies that the model works correctly with general geometrical input and a moving terminus. In this section I show that the iterative procedure in the numerical model works accurately by correctly solving a fully nonlinear equation with a realistic form of velocity depending on both ice thickness and slope. The problem solved also includes kinematic waves.

The theory of propagation of shock waves in a gas with diffusion has been investigated by many authors. Contributors to the literature of gas dynamics have included Stokes (1848), Rankine (1870) and Taylor (1910). Methods discussed in the text on nonlinear waves by Whitham (1974) are closely followed here. One standard approach to find the gas density as a function space and time in a shock front is to solve a continuity equation analogous to (1.3.5) (but with no source term on the right hand side) together with an equation analogous to a flow law relating gas flux Q to gas density H. One of the simplest flux relations is

$$Q = Q_1(H) - \nu \frac{\partial H}{\partial x} \qquad (2.3.7)$$

The first term gives the tendency of flux to increase with thickness, and the second term is diffusive damping with diffusion coefficient $\nu>0$. When the variable change

$$c(H) = \frac{dQ}{dH}^{-1}(H) \tag{2.3.8}$$

is introduced to the continuity equation (1.3.5) with mass balance A(x,t) set to zero and width W(x) set to unity, the result is a nonlinear diffusion equation

$$\frac{\partial c}{\partial t}(x,t) + c(x,t)\,\frac{\partial c}{\partial x}(x,t) = \nu\,\frac{\partial^2 c}{\partial x^2}(x,t) \tag{2.3.9}$$

known as Burgers' equation (Burgers, 1948). When the flux law (2.3.7) has the form

$$Q(H) = \alpha H^2 + \beta H + \gamma - \nu\frac{\partial H}{\partial x} \tag{2.3.10}$$

the nonlinear Cole-Hopf transformation (Cole, 1951; Hopf, 1950), reduces (2.3.9) to a linear diffusion equation, to which the analytical solution is well-known. Applying the inverse transformation to the solution gives the analytical solution to Burgers' equation, and thus to (1.3.5) with the flux relation (2.3.10). The details of the solution are given in Appendix 9. Since it is rare to find nontrivial analytical solutions to nonlinear partial differential equations, this result is remarkable. It provides an excellent opportunity for an exact test of the model with a nonlinear flow law.

Burgers' equation has appeared previously in the glaciological literature in papers on kinematic waves of finite amplitude (Johnson, 1968; Lick, 1970; Hutter, 1980).

When the initial condition is

$$c(x,0) = A\,\delta(x) \tag{2.3.11}$$

and the boundary conditions are

$$c(\infty,t) = c(-\infty,t) = 0 \tag{2.3.12}$$

the solution is (see Appendix 9)

$$c(x,t) = \frac{\sqrt{\frac{\nu}{t}}\; e^{x^2/(4\nu t)}\; (e^R - 1)}{\sqrt{\pi} + (e^R - 1)\displaystyle\int_{x/\sqrt{4\nu t}}^{\infty} e^{-z^2}\, dz} \tag{2.3.13}$$

The parameter R is equal to $A/2\nu$. This solution (2.3.13) is a single asymmetric decaying hump which propagates in the positive x direction. A shock (vertical front) tends to form on the leading edge, but is prevented from doing so by diffusion. When $\alpha=1/2$ and $\beta=\gamma=0$, we obtain from (2.3.8)

$$c(x,t) = H(x,t) \tag{2.3.14}$$

so that the solution (2.3.13) is also the solution for $H(x,t)$.

It is worth noting that equation (2.3.9), as well as being a nonlinear test, is also a test of kinematic wave behaviour (Lighthill and Whitham, 1955). For application to waves on glaciers, see Nye (1960). It is readily apparent from (2.3.9) that the diffusive property of $c(x,t)$

$$\frac{dc}{dt}(x,t) = \nu\frac{\partial^2 c}{\partial x^2}(x,t) \tag{2.3.15}$$

is carried as a kinematic wave at velocity

$$\frac{dx}{dt} = c(x,t) \tag{2.3.16}$$

which is thus the kinematic wave velocity. (The left side of (2.3.15) is a total derivative.) this kinematic wave behaviour is included in the complete solution (2.3.13).

To test the numerical solution of (1.4.1) against the analytical solution (2.3.13) and (2.3.14), I set the material

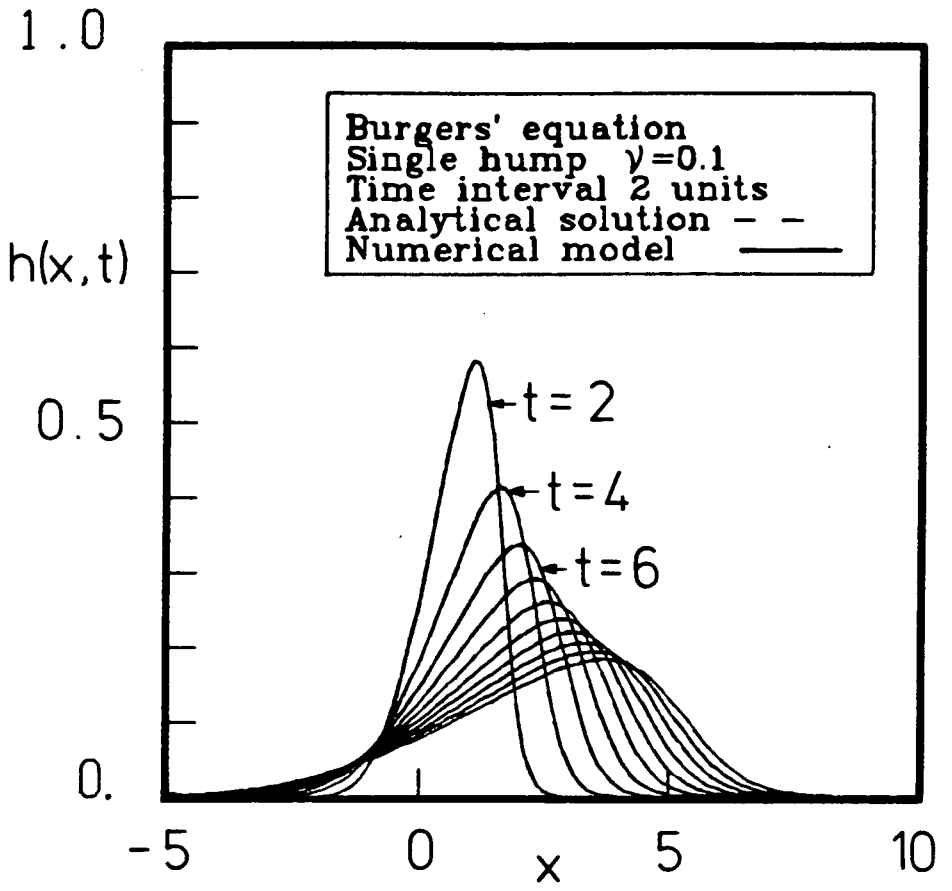

FIGURE 2.7. Nonlinear Test With Burgers' Equation.
Dashed lines indicating the analytical solution (2.3.13) have been superimposed on the numerical model solution for a single hump. Because of the close agreement (one part in 10^3), the curves are indistinguishable in this Figure. Plots are at intervals of 2 time units. The parameters of the model are given in Table 2.3.

velocity V(x,t) to be, using (2.3.10),

$$V(x,t) = \frac{Q(x,t)}{H(x,t)} \qquad H \neq 0$$

$$= 0 \qquad H=0 \qquad (2.3.17)$$

I solve the finite difference equations on the interval [-L,L], choosing L sufficiently large that H(-L,t)=0 adequately approximates (2.3.12). The condition at $+\infty$ is not needed since

A	ν	L	t_o	α	β	γ	Δx	Δt
1.0	0.1	7.5	2.0	1/2	0.0	0.0	0.125	0.05

TABLE 2.3. Parameters for Burgers' equation test.

(1.4.1) is first order.

Since finite difference equations cannot represent the impulse initial condition (2.3.11), I start instead with an initial condition (2.3.13) $c(x,t_o)$ at some small $t_o>0$.

In Figure 2.7, the analytical solution (2.3.13) is superimposed as dashed lines on the numerical model results. The parameters are given in Table 2.3. The agreement is so close (generally to better than three figures) that the dashed lines cannot be distinguished. This test shows that the numerical model conserves mass with fully nonlinear equations. The iterative scheme for nonlinearities works correctly. Since the numerical solution finds the correct time response for the hump, the behaviour of kinematic waves in the numerical solution is also correct.

2.4 THE ICE TRAJECTORY COMPUTER MODEL

2.4.1 INTRODUCTION

I have written a FORTRAN IV computer program which locates the trajectories of specified particles of ice, as they flow through a time-varying glacier. I have described the model in detail in Appendix 2.

The inputs to the model are the bedrock topography, the constants for Glen's flow law (1.4.22), and the number N, and the initial positions, of the ice particles to be tracked. The trajectory model uses the same mesh increments Δx and Δt as the continuity model (Section 2.2), and the same assumptions about the channel geometry. At each time step, the ice thickness profile $\{h_j \mid j=1,J\}$ and the basal sliding profile $\{ u_{s_j} \mid j=1,J\}$ used by the continuity model are also used as input to this model.

2.4.2 THE VELOCITY AND DISPLACEMENT FIELDS

The trajectory of an ice particle is given by $\underline{P}(t)$, its displacement vector as a function of time. For a particle at position $\underline{P}_0$ at time t_0,

$$\underline{P}(t) - \underline{P}_0 = \int_{t_0}^{t} \underline{v}(\underline{P}(t'),t')\, dt' \qquad (2.4.1)$$

where $\underline{v}(\underline{x},t)$ is the ice velocity field (u,w,v). To solve (2.4.1), I start at each time step by finding the velocity field

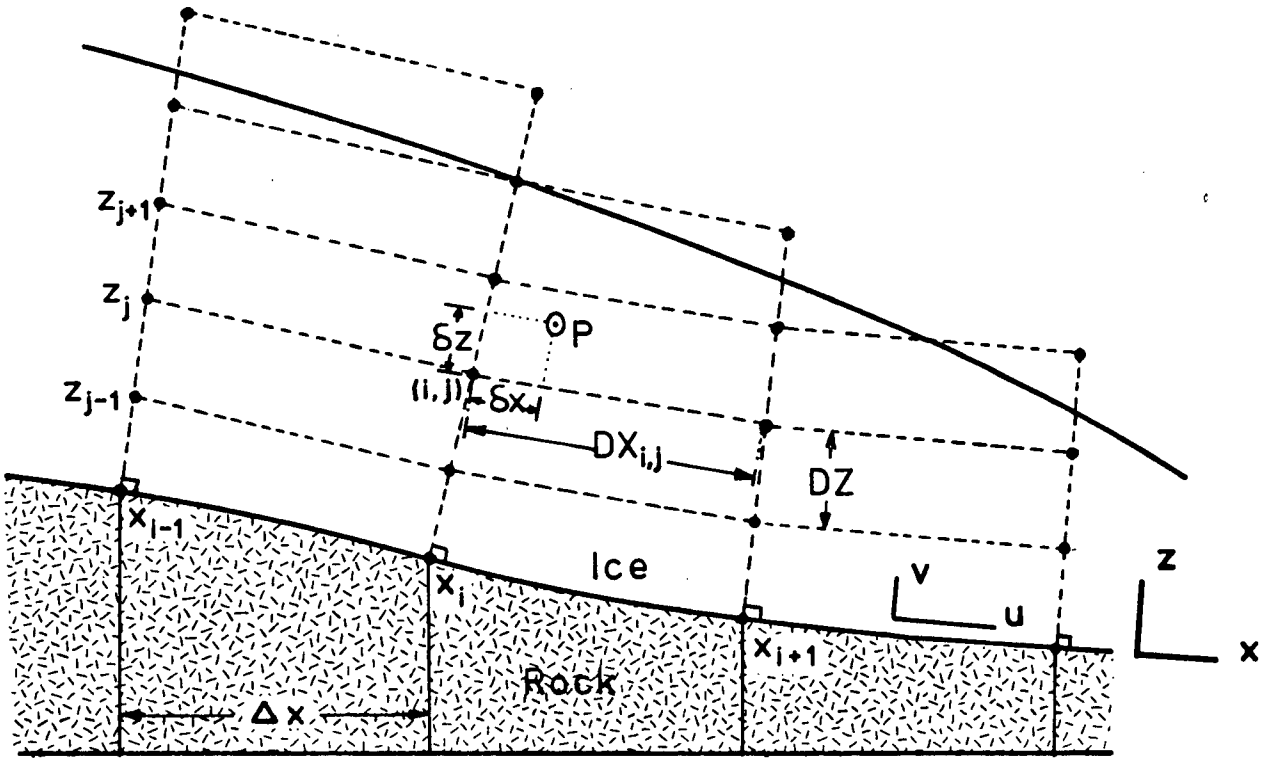

FIGURE 2.8. Meshpoints For Ice Velocity Calculations.

$\underline{v}(\underline{x},t)$ throughout the vertical plane in the glacier centreline, on the x-z mesh shown in Figure 2.8, and described in Appendix 2, Section A2.1. First, the downslope velocity component u(x,z) is found at each meshpoint using the integrated form (1.4.34) of Glen's flow law, with h(x), $\alpha(x)$, and $u_s(x)$ given by the continuity model solution. The longitudinal strain rate $\partial u/\partial x$ is estimated by a finite difference

$$\frac{\partial u}{\partial x}(i,j) = \frac{u(i+1,j) - u(i-1,j)}{DX_{i-1,j} + DX_{i,j}} \qquad (2.4.2)$$

of the downslope velocity from (1.4.34), and the lateral strain rate $\partial w/\partial y$ is given in terms of u(x,z) and the channel width W(x) by (1.3.3).

The incompressibility condition with mass conservation

gives

$$\frac{\partial v}{\partial z} = -\frac{\partial u}{\partial x} - \frac{\partial w}{\partial y} \qquad (2.4.3)$$

Using the approximation (usually very good, e.g. Rothlisberger, 1972) that basal melting is negligible as far as mass balance is concerned, i.e.

$$v(x,0,t) = 0 \qquad (2.4.4)$$

(2.4.3) is integrated numerically by Simpson's rule (e.g. Carnahan and others, 1969, p. 73) from the bed to level z to give v(x,z,t).

The lateral velocity component w(x,y,z) is exactly zero on the flowline down the centre of the channel, and is very small in a narrow flow volume (Figure 1.1) centred on this flowline. The average value of w is zero in this volume. The computer model uses w=0.

When the velocity field has been completely determined at the meshpoints in Figure 2.8, the displacement field of the ice leaving each meshpoint $\underline{P}_o$ and going to a point $\underline{P}$ in a time interval Δt is found by estimating the integral (2.4.1) by

$$\underline{P}(t+\Delta t) - \underline{P}_o(t) = \frac{1}{2}\left[\underline{v}(\underline{P}_o,t) + \underline{v}(\underline{P},t+\Delta t)\right] \Delta t \qquad (2.4.5)$$

i.e., the average of the velocities at the beginning and end of the time interval Δt. The velocity $\underline{v}(\underline{P},t+\Delta t)$ is estimated from the values of $\underline{v}$ at the four surrounding meshpoints at time $t+\Delta t$ using an interpolation scheme described in Appendix 2, Section A2.3.1.

2.4.3 THE ICE PARTICLE TRAJECTORIES

At each time step, and for each of the N particles being tracked, the coordinates ($\delta x, \delta z$) relative to a meshpoint (i,j) are recorded. The displacements of the particles in the time Δt are interpolated from the displacements of ice at the four surrounding meshpoints, and the new coordinates of the particles are then saved.

The program checks whether the new positions are still within the glacier mass, and saves the interpolated times and positions at which ice particles reach the ice surface.

By using $\Delta t<0$, the program is easily adapted to track particles backward in time and upslope (e.g. from a borehole), to find where and when they entered the ice mass as precipitation.

2.4.4 ACCURACY OF THE TRAJECTORY MODEL

The velocity field in this model is obtained by assuming that shearing parallel to the glacier bed is the dominant component of deformation. The downslope velocity u(x,z) is then found using the stress equations and the mechanical properties of ice. This is the only place where the force equations are used. The other velocity components are determined purely kinematically, using continuity and geometric assumptions about the lateral variation of the flow field.

When the assumption of predominantly shear deformation holds, this approach works very well. The fractional error in longitudinal strain rate, and in the vertical velocity, is quite

small. The leading term is approximately the ratio of the unbalanced longitudinal forces on a vertical column, to the basal shear force. The details are given in Appendix 7, equation (A7.5.9), which is repeated here as (2.4.6).

$$e(x) = O\left[\left[n\left[\frac{2h\frac{\partial\overline{\sigma'_{xx}}}{\partial x} + h\frac{\partial\overline{\sigma'_{yy}}}{\partial x}}{\rho g h \alpha}\right] + (n-1)\left[\frac{\delta\tau}{\sigma}_{xz}\right] - \frac{\partial v}{\partial x}\Big/\frac{\partial u}{\partial z}\right]_{max}\right] \qquad (2.4.6)$$

When the assumption of predominantly shear deformation is not accurate, the downslope velocity component u(x,z) is relatively inaccurate. The final term in the error estimate (2.4.6) may be of order unity, or larger, when $\partial u/\partial z$ is small.

The second term in the same equation may also be of order unity, or larger, when stress deviators other than the shear σ_{xz} contribute to the effective stress. Furthermore, the presence of any additional stress components other than σ_{xz} always softens the ice, so there is no possibility of compensating approximations in this term.

This situation may arise at an ice divide, where the predominant motions may be vertical sinking, and longitudinal extension as the ice flows downslope in both directions. Fortunately, the ice velocity is very small at an ice divide, so that the total error in the trajectories is not large. To be safe, the trajectories near an ice divide should be interpreted only qualitatively. Longitudinal stresses are also important in icefalls.

The use of Glen's flow law, and the inclusion of

longitudinal strain rates (to the approximation of (2.4.6)) is an improvement over the trajectory models of Nagata (1977), who assumed that $\partial u/\partial z$ was zero, and Dansgaard and Johnsen (1969[a]) who set $\partial u/\partial z$ to a constant at each x in the lowest 400 metres, and zero above that level, and assumed that $\partial u/\partial x$ was constant for a given z, in a model for the Camp Century, Greenland borehole.

The fact that my model is time dependent is also an improvement over these models.

One advantage of this model is that the mass conservation law is still obeyed globally and locally at all times. This has not been the case with some other trajectory models. For instance, the Weertman (1968) analytical model for ice velocity and temperature at Camp Century, Greenland, assumed a constant vertical strain rate, but used a horizontal velocity given independently by integrating Glen's flow law (1.4.22) to get a result like (1.4.34). Dansgaard and Johnsen (1969[b]) showed that this violation of continuity was the likely cause of a discrepancy of $2^{o}C$ between predicted and measured temperature at the bed at Camp Century, Greenland. The flow model used by Dansgaard and Johnsen (1969[a]) satisfied continuity everywhere, but assumed the form of the horizontal velocity component, instead of using Glen's flow law.

While the model I described in Section 2.2 does not yet include temperature variations, that is a simple development that will not violate mass conservation.

Budd and others, (1971, p. 42) assumed a constant vertical strain rate $\partial v/\partial z$ independent of depth, at each position x,

regardless of the values of the other terms in (2.4.3). They also described another model (p. 43) in which the vertical strain rate was weighted by the downslope velocity u(x,z) at each point. While this makes the vertical strain rate curves more closely resemble the expected shape in a real ice mass, it still does not satisfy continuity locally through (2.4.3). An incompressible continuum flowing with such a velocity field would have to locally create or destroy mass.

Constant vertical strain rate (or a strain rate specified a priori) may be a reasonable approximation when deriving analytical solutions to some flow problems to illustrate the physics involved (e.g. Robin, 1955; for the effect of advection on temperature profiles), and it arises naturally in some simple kinds of flow, i.e. horizontal shearing restricted to the basal layer (e.g. Hill, 1950, p. 233; Nye, 1951; or Nye, 1957). However, given the sophistication of current computer models accepting otherwise quite general inputs, this assumption now appears to be a needless limitation. While the errors involved may turn out, in some situations, to be small, it is preferable to avoid them at no additional complication.

The only model of which I am aware which attempts to use the continuity equation in a manner similar to the way I described in Section 2.4.2 to find the vertical velocity component, and also makes no a priori assumptions about the flow field other than those described in Section 2.4.2, is the preliminary three-dimensional model of Jenssen (1977) for the Greenland ice cap. This model also solves for the temperature distribution, for use in the temperature dependent flow law. The

Jenssen model is still under development to improve the boundary treatment and and to reduce inaccuracy resulting from the coarse grid imposed by computer limitations (Greenland was modelled by a 12x12 map grid, 10 points deep); however, the Jenssen approach is the logical next step that must be taken towards the numerical solution of the complete set of equations for ice sheets.

2.5 TESTING THE TRAJECTORY MODEL

2.5.1 INTRODUCTION

In Section 2.5, I describe two tests of the trajectory model.

In Section 2.5.2, I compare the steady state trajectories and velocity field calculated by my computer model to an analytical solution for a steady state ice sheet (Nagata,1977).

In Section 2.5.3, I use the balance condition (A5.8) at the ice surface to show that continuity is satisfied by the velocity field.

2.5.2 NAGATA ICE SHEET TEST

Nagata (1977) derived an analytical solution for the surface profile, velocity field, and streamlines of a steady two-dimensional ice sheet resting on a flat bed. For the steady state case, streamlines and ice trajectories coincide. I describe the Nagata model in detail in Appendix 15, Section A15.3. Nagata (1978) used this ice sheet model to

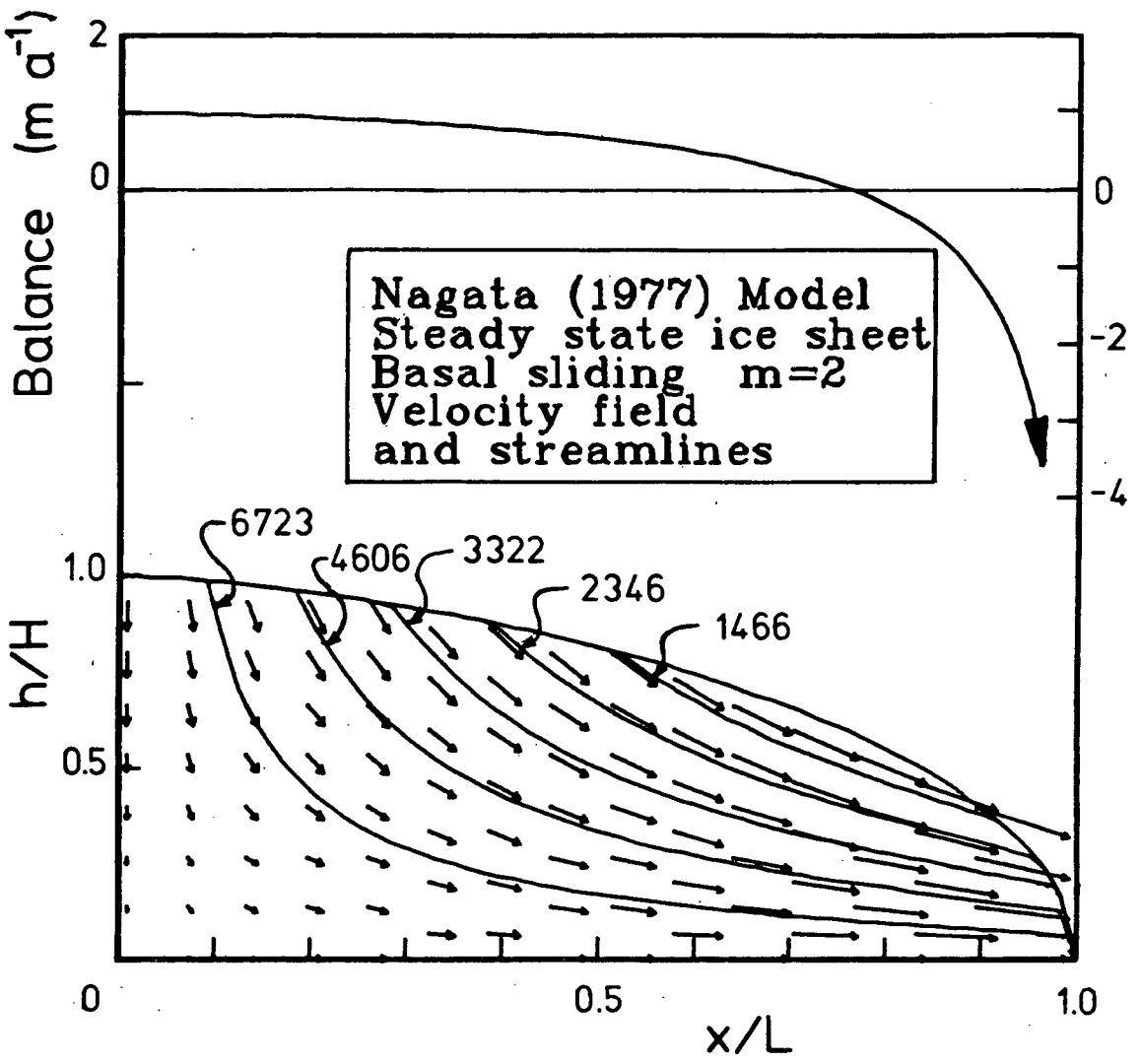

FIGURE 2.9. Nagata Steady Ice Sheet.
The analytical solution for the ice thickness, mass balance, particle paths, and velocity field using the parameters in equation (2.5.2). The velocities have been multiplied by 250 years. The numbers are the time in years for ice to flow the length of each particle path.

explain the concentration of meteorites at the Meteorite Ice Field in Antarctica. The Nagata model assumes that the forward ice velocity u(x) is constant throughout a vertical column and depends on the basal shear stress (1.4.25) through a Weertman-type relation (see Appendix 8, Section A8.3.1) of the

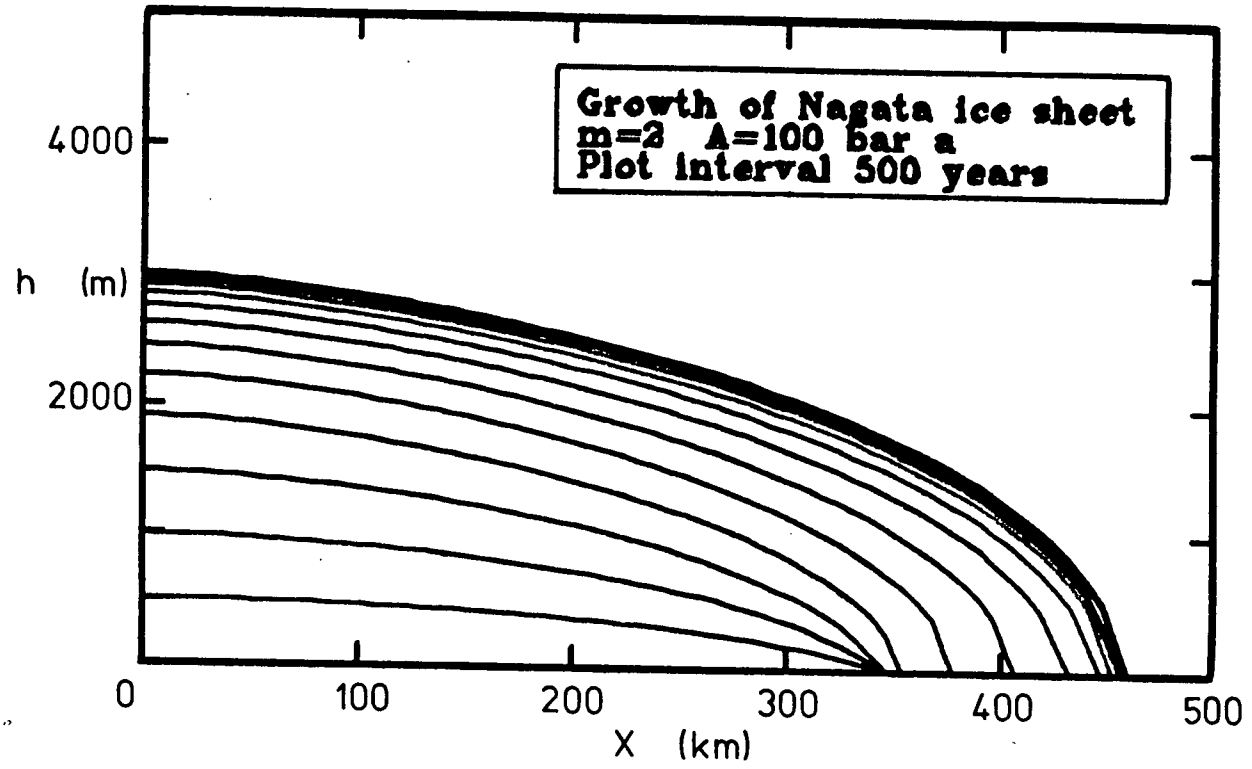

FIGURE 2.10. Growth Of Nagata Ice Sheet.
The ice surface elevation is shown at intervals of 500 years, starting from ice-free conditions. The flow parameters are given in Table 2.4 and the mass balance in Figure 2.9. The steady state ice thickness agrees with the analytical solution by Nagata (1977) to one part in 10^3.

form

$$u(x) = A\,\tau^{m} \qquad (2.5.1)$$

Although it is not clear in the original paper, the Nagata model also assumes that the vertical velocity component v(x,z) is equal to a constant b along the upper surface of the ice sheet. The scale of the ice sheet model is set by H, the thickness at the ice divide.

While the form of the mass balance and the velocity field are not a close representation of real ice sheets, the Nagata model is well suited to testing the accuracy of my numerical

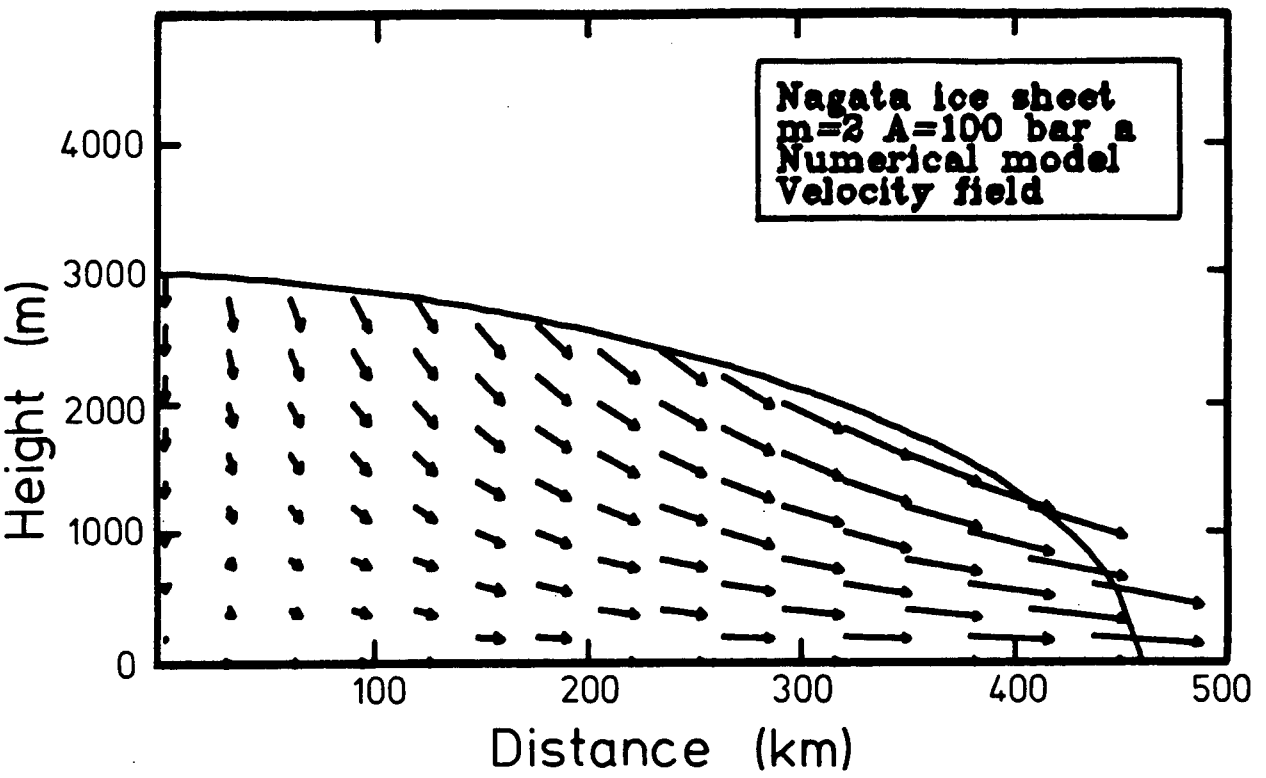

FIGURE 2.11. Velocity Field For Nagata Model.
The velocity vectors calculated by the Waddington trajectory model for the steady state profile in Figure 2.10 and using flow parameters in Table 2.4. The velocities have been multiplied by 250 years (The units of the vectors are displacement).

trajectory program. I compare my numerical results to the Nagata model shown in Figure 2.9 for the constants in Table 2.4.

Figure 2.10 shows the growth of the Nagata ice sheet to steady state using the profile model described in Section 2.2). The steady state profile agrees with the analytical model in Figure 2.9 to within one part in 10^3.

The solid vectors in Figure 2.11 show the steady state velocity field calculated by my numerical model. The velocities have been multiplied by a factor of 250 years. The velocity

m	A $bar^{-2}a^{-1}$	b $m\ a^{-1}$	H m	L km	ρ $kg\ m^{-3}$	g $m\ s^{-2}$
2	100.	1.0	3000	454.6	910.	9.8

Δx km	Δt a
7.215	10.0

TABLE 2.4. Parameters for Nagata ice sheet.

field agrees with the analytical solution (Figure 2.9) to within a few parts in 10^3 (except near the terminus where the agreement is only to two parts in 10^2, because the mass balance in the numerical model remains finite while the analytical mass balance goes to $-\infty$).

Figure 2.12 shows the trajectories for ice entering the ice sheet at time t=0.; these are the same five points shown for the streamlines in Figure 2.9. The arrowheads indicate 250 year intervals. The total residence times along each of the five streamlines are compared to the analytical values in Table 2.5.

The good agreement between the numerical results and the analytical solution indicates that the velocity field is reconstructed accurately and the integration of the velocity field to get flowlines is correct and accurate.

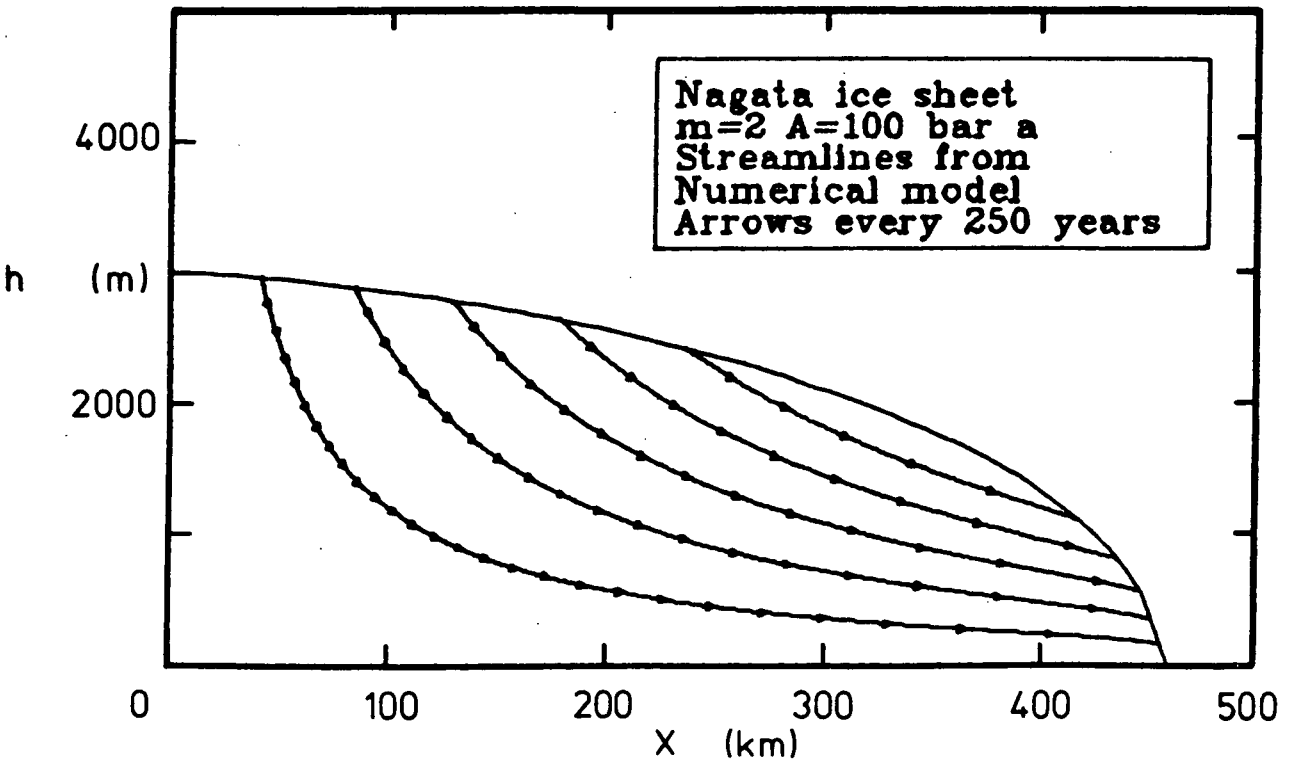

FIGURE 2.12. Trajectories In Nagata Model.
The solid curves are the particle paths calculated by the Waddington trajectory model by integrating the velocity field in Figure 2.11. The arrowheads indicate 250 year intervals. In Table 2.5 the total residence times in the ice sheet are compared to values for the analytical solution.

2.5.3 SURFACE MASS CONSERVATION TEST

Conservation of mass at the glacier surface with normal vector $\underline{n}$ implies that the normal velocity of the ice-air interface is equal to the sum of the normal ice velocity plus the surface accumulation rate, i.e.

$$\frac{\partial \underline{h}}{\partial t} \cdot \underline{n} = \underline{v} \cdot \underline{n} + \underline{a} \cdot \underline{n} \qquad (2.5.2)$$

This equation is derived in Appendix 5, Section A5.2. When ice

Streamline Number	Numerical model years	Analytical model years
1	6746.	6723.
2	4625.	4606.
3	3335.	3322.
4	2350.	2346.
5	1477.	1466.

TABLE 2.5. Residence times in Nagata ice sheet.

thickness change rate $\partial h/\partial t$ and mass balance vector $\underline{a}$ are measured normal to the bed, and the velocity components (u,v) are parallel to and normal to the bed, (2.5.2) becomes

$$\frac{\partial h}{\partial t} = v(x,h) - u(x,h)\frac{\partial h}{\partial x} + A(x) \qquad (2.5.3)$$

where A(x) is now a scalar giving the mass balance. My derivation (Section 2.4.2 and Appendix 2, Section A2.2) of the velocity field uses only incompressibility (2.4.3) and the basal boundary condition (2.4.4); (2.5.3) can be used as an independent check of the degree to which the velocity field conserves mass. Models which use (2.5.3) to derive the vertical velocity (e.g. Weertman, 1968; Budd and others, 1971, p. 42) do not have this consistency check.

Figure 2.13 (a) shows the mass balance A(x) and the surface rise $\partial h/\partial t$ for a typical time step, with parameters described by Table 2.6, during the growth of the Nagata ice sheet model. I apply the test at a time (2500 years) when the ice sheet is growing vigorously because conditions at that time impose the most stringent conditions on accuracy. Figure 2.13 (b) shows the residual of (2.5.3), i.e. the difference between the left and right sides of the equation on substituting the values of h, A,

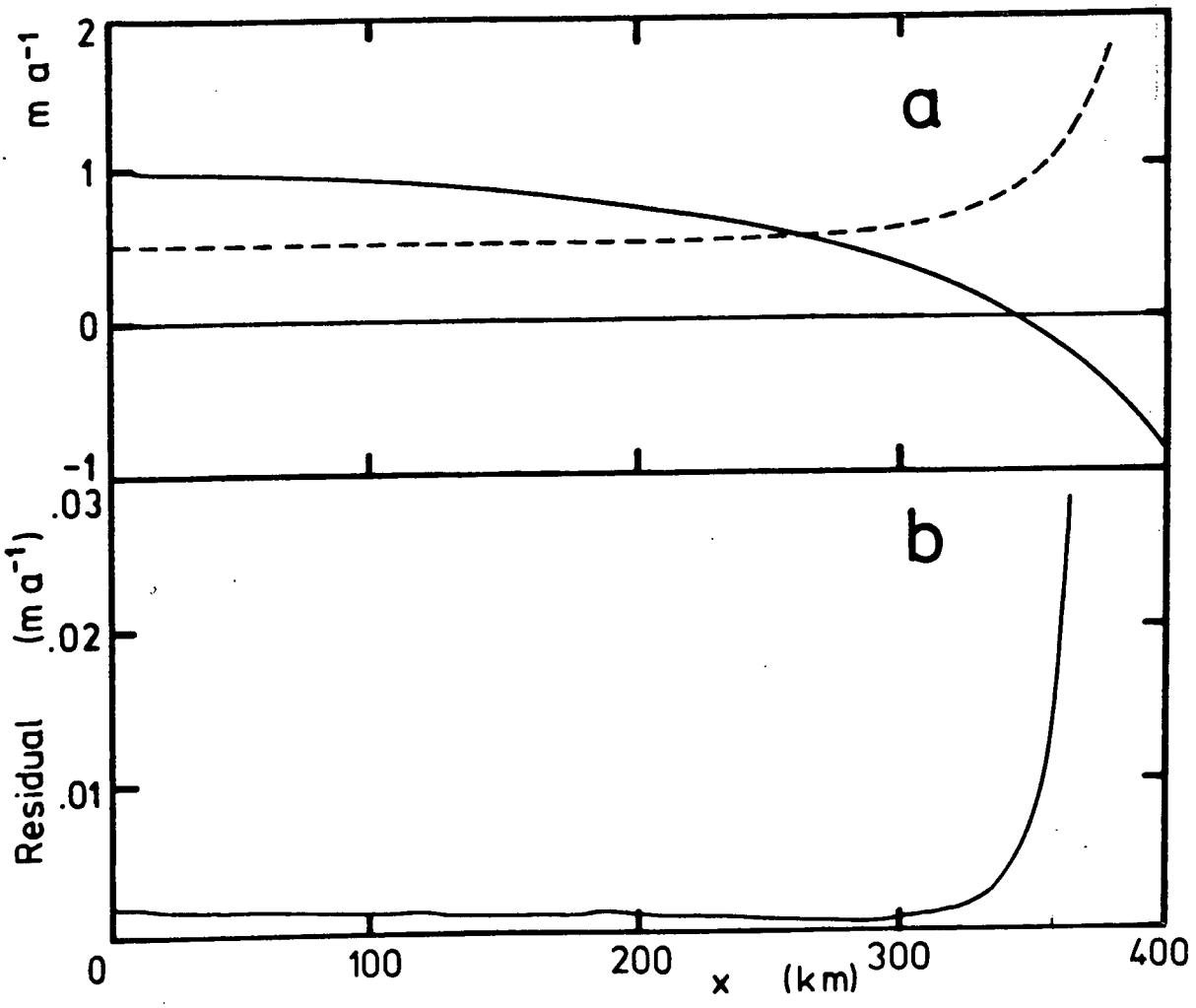

FIGURE 2.13. Surface Mass Conservation Test.
Time=2500 years during the growth of the Nagata ice sheet model to a steady state. (a) shows the mass balance (solid curve) and the rate of surface rise dh/dt (broken curve). (b) shows the residual of (2.5.3). It is very small (note scale change of 10^{-2}, indicating that the velocity field satisfies incompressibility. The terminus is at x=37.8 km. The residual increases near the terminus because there are few meshpoints in each vertical column; vertical integration is inaccurate.

u, and v from the numerical solution. The residual error is three orders of magnitude less than the average magnitude of the mass balance, except near the terminus where there are insufficient mesh points in any vertical column to guarantee accurate vertical integration of (2.4.3). This region has no

Time a	Δx km	DZ m	Δt a
2500.	7.215	150.	10.

TABLE 2.6. Nagata ice sheet surface boundary test.

effect on the trajectories investigated in this work. Similar tests (not shown) on the Steele Glacier Model 1 (Figure 3.3) routinely give residuals of the order of one part in 10^2 of the average mass balance, even though the mass balance is discontinuous (tributaries), the width is variable, and the flow law includes a height-dependent longitudinal strain rate. Results of these tests indicate that the velocity field satisfies the continuity equation (2.3.3) to a very good approximation. This test verifies the accuracy of the trajectory model under time-varying conditions.

CHAPTER 3: CAN STABLE ISOTOPES REVEAL A HISTORY OF SURGING?

3.1 INTRODUCTION

The stable heavy isotopes O^{18} of oxygen and D (deuterium) of hydrogen in glacier ice have been widely used as indicators of climatic change (e.g. Dansgaard and others, 1969; 1971). This procedure requires assumptions about the pattern of glacier flow. In this chapter, I investigate a related problem; assuming that the past climate is known, can the stable isotope distribution be used to reveal the flow history of time-varying glaciers? The example I consider in this chapter is the Steele Glacier, Yukon Territory. This glacier was observed to surge in 1966-1967 (Stanley, 1969). I used the computer models described in Chapter 2 to find the ice surface and the velocity field throughout the surge cycle, and to calculate the ice trajectories. Knowing the trajectories and the isotopic composition (from climate) at the time and place the material was precipitated as snow on the glacier surface, has allowed me to construct longitudinal cross-sections and surface profiles showing the isotopic distribution at a series of times during the surge cycle; this pattern would facilitate the selection of optimum borehole and surface sampling locations for an isotopic study of past flow patterns.

In Section 3.2, I describe the Steele Glacier and its surge history. In Sections 3.3 and 3.4 I describe the computer models I used to simulate the Steele Glacier. Model 1 in Section 3.3 is

a detailed model based on all the available data. Because of limited sliding data and an approximation in the mass balance, it is not at present the best model for particle trajectory calculations. With more complete data and some computer model refinements, it may become so. Model 2 in Section 3.4 is a simplified version better matched to the resolution of the sliding observations. Model 2 is used for the trajectory and isotopic calculations in Sections 3.6 and 3.7. In Section 3.5, I describe the use of stable isotopes in glaciology, and present two possible isotopic relations for precipitation at Steele Glacier. The ice surface profile calculations in Section 3.6 indicate that a surge period of approximately 100 years is appropriate for the Steele Glacier if the present mass balance and the velocity of the 1966-67 surge are representative of the average long-term climate and of the glacier flow pattern. In Section 3.7, I present computed longitudinal cross-sections and surface profiles of the isotopic distribution $\delta(O^{18}/O^{16})$ for a model with a surge periodicity of 97 years. Isotopic discontinuities occur in the ice along surfaces which were at the ice-air interface in the accumulation region when a surge began. Even for the isotopic-precipitation model most favourable to the formation of discontinuities, the discontinuities do not exceed one DEL unit on the Steele Glacier; this amount may be hidden by noise in the Steele Glacier environment.

3.2 STEELE GLACIER

3.2.1 GENERAL DESCRIPTION

Steele Glacier (61°10'N, 140°15'W) is a surging valley glacier on the northeast slopes of the Icefield Ranges (see Figure 3.1) of the St. Elias Mountains, Yukon Territory, Canada. Prior to 1963 it was called the Wolf Glacier. (Sharp (1951) and Bostock (1948, p. 99) state that this is more proper than the often-used notation Wolf Creek Glacier.). The glacier length varies from 34 to 44 km, and the width of the main channel is one to two km. The main channel flows down from 3000 m elevation on the north side of Mt. Steele (Figure 3.2) to 1200 m elevation in Steele Creek, where the ice is stagnant and moraine-covered between surges.

The continental slope of the Icefield Ranges is semi-arid. Annual precipitation drops from 300 cm a^{-1} at Yakutat on the Gulf of Alaska (see Figure 3.1), to about 35 cm at Kluane Lake (Wood, 1972). The firn line on the Steele Glacier is presently very high (2400 m or more). A major source of accumulation is avalanches from the north face (labelled (0) in Figure 3.2) of Mt. Steele (5070 m). In its upper reaches, the Steele is an extensive system of accumulation basins and converging tributaries. These tributary ice streams (see (1) through (5), Figure 3.2) also contribute a substantial fraction of the Steele Glacier mass balance. In its lower reaches, the Steele Glacier makes a 90° bend to the east, and enters a straight and narrow valley formed by the Wolf Creek monocline (Sharp, 1943).

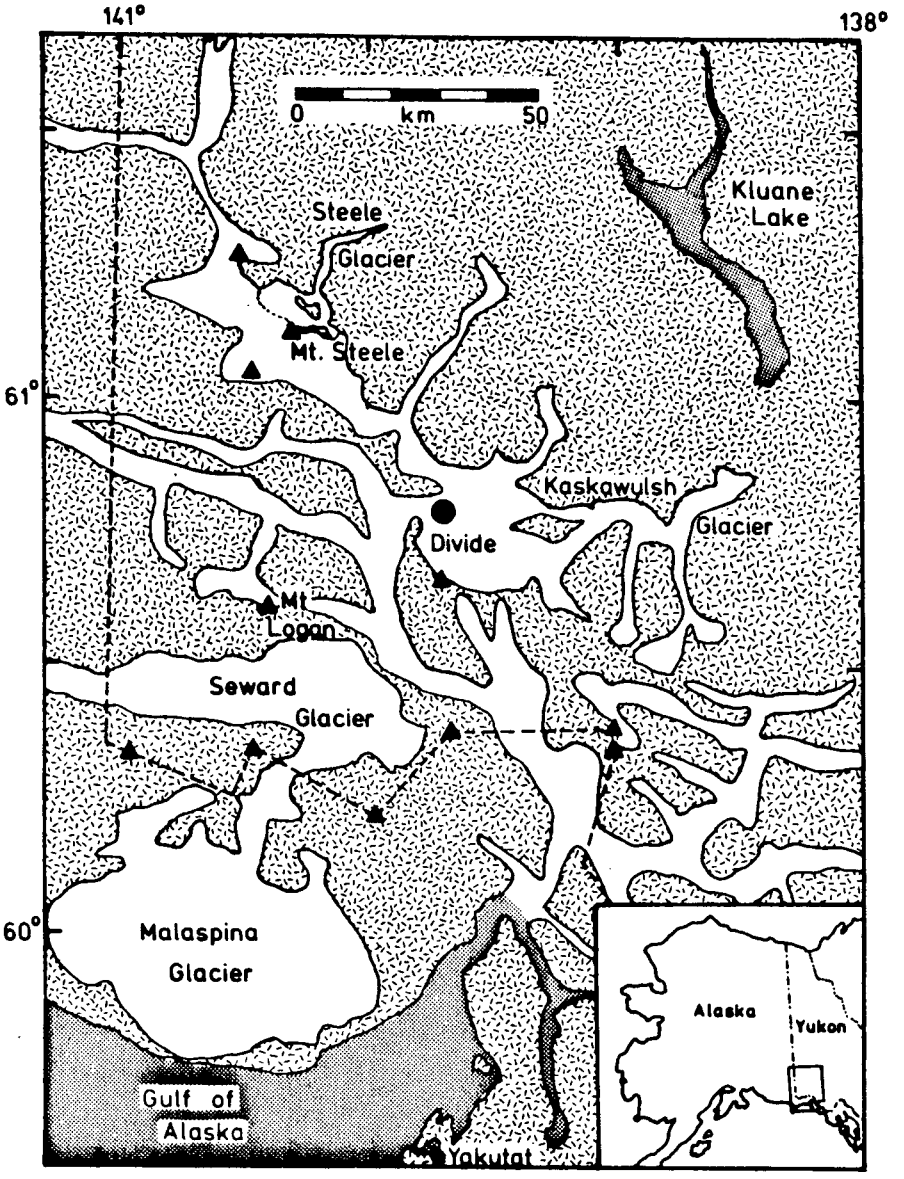

FIGURE 3.1. Icefield Ranges Location Map.
Nonstippled areas are major glaciers and icefields. The triangles indicate major summits of the Icefield Ranges (St. Elias Mountains). The Steele Glacier is on the north-east (continental) slope (top centre).

3.2.2 GLACIER SURGES

A glacier surge (e.g. Meier and Post, 1969) is a short period of very rapid flow, during which ice is transferred from an ice reservoir area to an ice receiving area downstream. A surge is followed by a longer period of stagnation and ablation

in the receiving area, with renewed ice buildup in the ice reservoir; these areas do not necessarily correspond to the accumulation and ablation zones defined by mass balance. For a large valley glacier like the Steele, the maximum velocity during a surge may be 500 m a^{-1} to 10 km a^{-1}, with downstream ice displacement of one to 10 km. Surging appears to be a periodic phenomenon. For glaciers like the Steele, the surge duration is typically one to two years, with a quiescent phase lasting from 20 to 150 years.

Glaciers of all sizes have been observed to surge. Examples are the Trapridge Glacier (in the Steele Creek watershed) which is only three km long, and the Muldrow Glacier on Mt. McKinley, Alaska which is over 50 km long. There has been speculation that the Antarctic ice sheet may surge (Hollin, 1969; Wilson, 1969). Surging glaciers are found in many parts of the world, e.g. Alaska (Tarr and Martin, 1914, p. 168), British Columbia and the Yukon Territory. (Post, 1969), the Arctic Islands (Hattersley-Smith, 1964; Løken, 1969), Iceland (Thorarinsson, 1969), the Karakoram (Hewitt, 1969), the Pamirs, Tien Shan, Caucasus, and Kamchatka (Dolgoushin and Osipova, 1975). Surges occur in both temperate and cold or subpolar glaciers. Surging does not appear to be triggered by climate variations.

The high velocity during surging is generally attributed to rapid basal sliding. Various hypotheses on the mechanism of surging have been put forward. The more plausible ones include thermal regulation (Robin, 1955; Clarke, 1976; Lliboutry, 1969[b]), stress instabilities (e.g. Post, 1960; Robin, 1969) and basal water film instabilities (Weertman, 1962, 1969; Robin

and Weertman, 1973; Budd, 1975). A concensus on the cause of glacier surging has yet to be reached. In this chapter, I investigate the effect of periodic surging on the stable isotope distribution in the Steele Glacier. The amount of basal sliding is important to this question; the mechanism which causes it is not. For this reason, I specify a basal sliding velocity $u_s(x,t)$ consistent with the observations of the Steele Glacier surge of 1966-1967, and I use this as a boundary condition for the computer model.

3.2.3 OBSERVATIONS OF THE STEELE GLACIER

The flow pattern before and during a surge is better known for the Steele Glacier than for most other surging glaciers. Scientific expeditions sponsored by the American Geographical Society and led by W. A. Wood explored the Steele Creek watershed in 1935, 1936, 1939, and 1941. Work included the experimental use of oblique aerial photography for mapping areas of high relief. These air photos and the panoramas from ground control points give information on the ice surface elevation and state of flow during the quiescent phase.

Sharp (1943) described the geology of Steele Creek, observed the glaciers of the Steele Creek basin (Sharp, 1947), and interpreted the glacial history (Sharp, 1951).

The Surveys and Mapping Branch of the Department of Energy, Mines and Resources, Government of Canada, obtained vertical aerial photography of the Icefield Ranges from 10 700 m in the summer of 1951. Flight lines A13232/33 covered the Steele

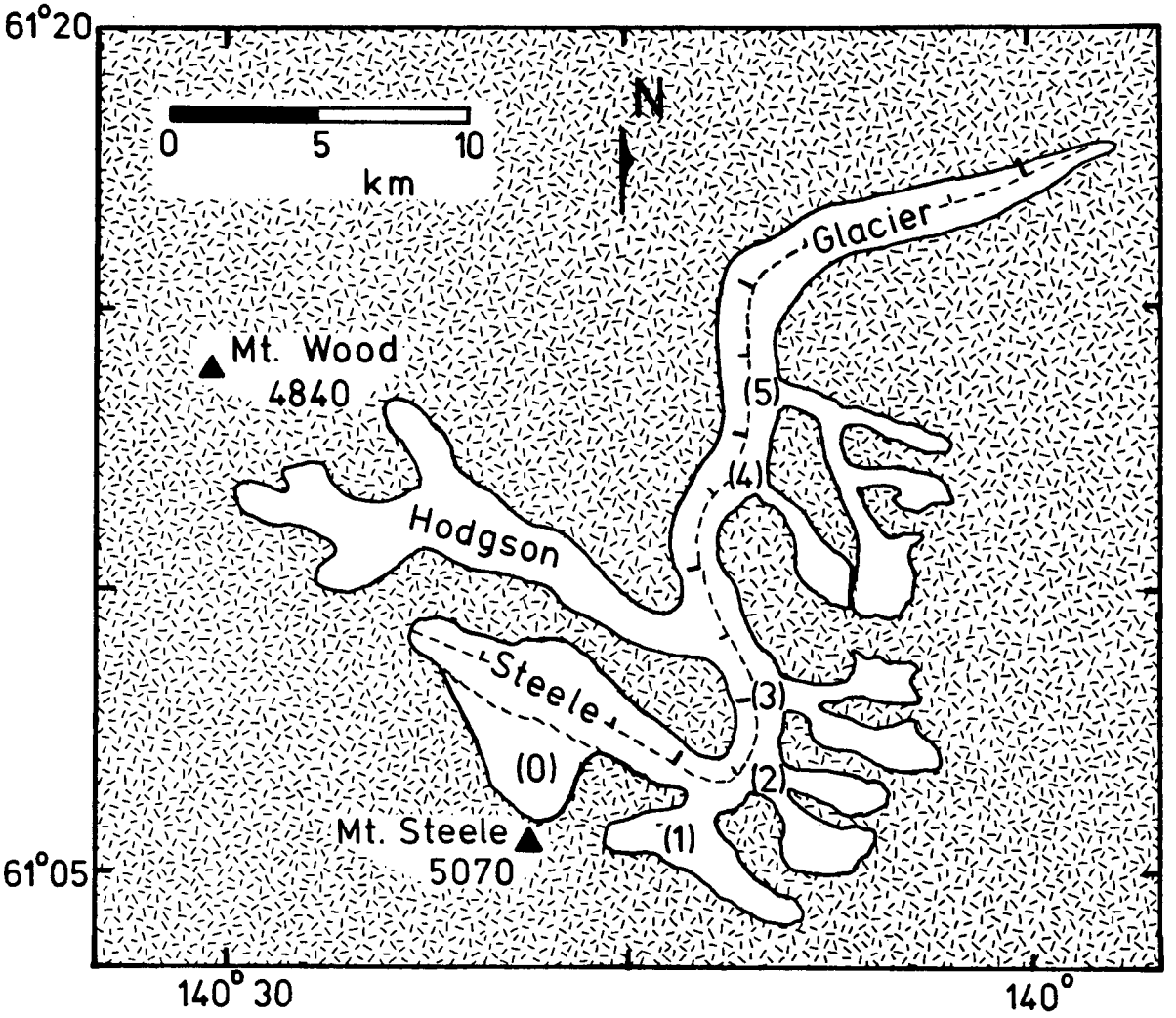

FIGURE 3.2. Steele Glacier And Tributaries.
The central flowline used in the computer model is marked at 2.5 km intervals. The Hodgson Glacier is included in the channel width function (Figure 3.3 (b)) for the main ice stream. For Model 1, the mass contributions from the minor tributaries (0) through (5) are included in the mass balance function (Figure 3.3 (a)).

Glacier. This photography was used to prepare the government map 115F at the scale 1:250,000; it was also used to prepare a map of the Steele Glacier at the scale 1:25,000 (Topographical Survey, 1967). Oblique aerial photography of the Steele Glacier was obtained periodically between 1960 and 1965 by W. A. Wood (American Geographical Society) and by A. Post (U.S. Geological Survey). In 1960, Post predicted an imminent surge for the

Steele Glacier (Wood, 1972), and in 1965, noted the first signs of increased flow on the upper Steele (Wood, 1972).

During the 1966-1967 surge, high oblique aerial photos were obtained by Wood, pre-1941 survey stations were re-occupied, and the Surveys and Mapping Branch obtained vertical air photo coverage on August 13 and September 15, 1966. Wood (1972) and Stanley (1969) measured displacements of identifiable surface markings. Features originally between the Hodgson confluence and the 90° bend (Figure 3.2) all advanced at roughly the same velocity of 5 km a^{-1} during 1966, with a total displacement of roughly 8 km when the surge ended late in 1967. There was no significant lateral variation of velocity beyond 200 m from the glacier margins. Bayrock (1967) observed the details of the terminus advance, and the reactivation of stagnant ice. A bulge of active ice 30 m high moved forward at about 10 m d^{-1} (3650 m a^{-1}). This bulge sometimes has been called the terminus in the literature on the 1966-1967 surge. Alford from the Whitehorse office of the Water Survey of Canada obtained monthly air photographs of the advancing bulge during the winter of 1966-1967. He observed an advance of 6000 feet (1830 m) between September 10, 1966 and January 15, 1967 (Roots, 1967). By August 1967, the active bulge had slowed to 2 m d^{-1} (730 m a^{-1}) (Thomson, 1972).

Stanley (1969) identified three zones based on surface elevation changes during the surge. An upper zone, entirely in the accumulation area, apparently was not involved in the 1966-1967 surge. In a middle zone (the ice reservoir zone) from a point above the firn line (based on Stanley's description, I

locate this point at about x=7 km) to a point about 3 km above the 90° bend (at x=27 km in my model), there was a net lowering of the ice surface, with a maximum value of 130 m above the Hodgson-Steele confluence. In the lower remaining zone (ice receiving area) the surface rose by up to 100 m.

During the winter of 1966-1967, the Hodgson Glacier began a year-long surge during which it pushed the still-surging Steele ice stream to one third of its normal width at the ice surface. The effect of the Hodgson surge on deep ice is unknown. The Hodgson ice formed a large lobe extending three km down the main Steele channel. This tributary surge may have been triggered by a reduced confining stress resulting from the rapid lowering of the Steele Glacier at their confluence.

3.2.4 PERIOD OF STEELE SURGES

Sharp (1951) showed that, based on 1941 observations, the Steele Glacier below the bend had been stagnant since 1916 or earlier. Based on biological recolonization rates inside the most recent trim line, he estimated that the last advance ended in the period 1840-1890, i.e. 115 to 75 years before the 1966-1967 surge.

Wood (1972) pointed out evidence for ice displacements of over two km between 1935 and 1941 near the Steele-Hodgson confluence. The previously smooth ice in that region was heavily crevassed in 1941, and the crevasses looked several years old. The evidence suggests that the Steele Glacier had a minor surge

or a failed attempt at a surge in 1938 or 1939. Sharp's (1951) estimate of the time of the previous terminus advance would then imply a buildup time of 50 to 90 years.

Sharp (1951) pointed out moraines 100 m to 150 m above the 1941 ice surface below the bend. An ablation estimate of 2 m a^{-1} implies the maximum ice elevation occurred 50 to 75 years prior to 1941.

There are no direct observations on the Steele Glacier of regular looped moraines, or of disrupted ogive patterns which could reveal pre-historical surge episodes. The assumption of periodicity is based on observation of surging glaciers elsewhere (e.g. Variegated Glacier, Alaska, (Bindschadler and others, 1977)). The assumption of exact periodicity for the computer model is, at best, an approximation; significant climate variability on the time scale of glacier surges has been widely documented (e.g. Bryson and Goodman, 1980; Gribbon, 1979). If the Steele Glacier surges periodically, the period is in the range 50 to 150 years.

3.3 NUMERICAL MODEL 1

3.3.1 FLOW LAW CONSTANTS AND SHAPE FACTOR

The computer model in its present form assumes that the ice is isothermal. Temperatures in the upper 100 metres of the Steele Glacier (Jarvis and Clarke, 1974; Clarke and Jarvis, 1976) following the 1966-1967 surge were in the range $-1^{\circ}C$ to $-7^{\circ}C$. It is likely that the basal ice, within which most of the shear deformation takes place, is at or near the pressure melting point. The assumption of temperate ice is not unreasonable.

I use the constants (Paterson, 1981, p. 39)

$$A = 5.3\ 10^{-15}\ s^{-1}\ kPa^{-3} \qquad n=3 \qquad (3.3.1)$$

in Glen's flow law (1.4.22) for the Steele Glacier simulation. Since most of the motion in a surge is due to sliding, changes in the flow law constants have little effect on the ice movement.

The shape of the valley cross-section is unknown. I use a shape factor (see Section A7.4) of

$$s = 0.8$$

independent of position x. Since the shape factor is raised to the nth power (see equation (1.4.34)), uncertainty in s introduces substantial uncertainty into the deformation velocity. However, as pointed out above, the internal deformation of the Steele Glacier is a small component of the total motion.

3.3.2 BED TOPOGRAPHY

There are no published ice depth data for the Steele Glacier. Jarvis and Clarke (1974) and Clarke and Jarvis (1976) reached depths exceeding 100 metres with a hot-point drill without any indication of bottom; the glacier is likely much thicker than this. Typical depths of large valley glaciers can exceed 600 metres (e.g. Lowell Glacier, St. Elias Mountains, based on monopulse radio-echo sounding, 1977; G. K. C. Clarke, personal communication). A rough estimate of the depth e.g. above the confluence of the Steele and the Hodgson can be obtained by assuming a basal shear stress σ_{xz} of one bar and measuring the ice surface slope to be α=0.03 from the 1951 map (Topographical Survey, 1969). Assuming a shape factor of s=0.8, the stress relation (1.4.25) gives the depth as (approximately)

$$h = \frac{\sigma_{xz}}{s\rho g\alpha} = 472 \text{ metres} \qquad (3.3.2)$$

Alternatively, assuming flow by simple shear with no sliding, and using the 1951 velocity of 25 m a^{-1} measured at this point by Wood (1972) (1.4.38) with the flow law constants (3.3.1) gives the depth estimate

$$h = \left[\frac{(n+2)V}{2A(s\rho g\alpha)^n}\right]^{1/(n+1)} = 445 \text{ metres} \qquad (3.3.3)$$

Since the motion of the Steele Glacier is obviously not an example of steady nonslip flow in a cylindrical channel, these are merely rough estimates. The presence of basal stress of less than one bar, or of nonzero basal sliding would result in an

overestimate of the true thickness. Neglecting the stress perturbations and lateral asymmetry caused by bends in the channel, I assume the central flowline (x axis) follows the broken curve shown in Figure 3.2. For the Steele Glacier bed topography in Figure 3.3 (c), I use an exponential function having the form

$$h(x) = ae^{-bx} + c \qquad (3.3.4)$$

where a, b, and c are constants determined by fitting the three points:

(1) 2900 metres elevation at the bergschrund of the main ice stream (x=0).

(2) 1200 metres at the 1978 terminus position (x=42 km).

(3) 1650 metres at the confluence of the Hodgson and Steele Glaciers (x=18 km); this value would give an ice depth of about 400 metres at this point in 1951 (Topographical Survey, 1969). The 1951 longitudinal surface profile is shown in Figure 3.3 (c).

The actual topography beneath the Steele Glacier is undoubtedly more complicated. This approximation means that the computer model cannot be expected to quantitatively reproduce the observed ice surface elevations.

3.3.3 CHANNEL WIDTH

The width of the main ice stream of Steele Glacier can be estimated by measuring the separation of the lateral moraine ridges on the topographic map at the scale 1:25,000 (Topographical Survey, 1969). The published government mapsheet 115G and 115F(E1/2), at the scale 1:250,000, (from which Figure 3.2 is drawn), is not a reliable indication of the channel width. Ideally, tributaries should be included in the numerical model as separate ice streams with their own bed and mass balance functions, and coupled to the main ice stream by thickness and flux conditions at the junctions; this option is not available in the computer model in its present form. Instead, I can include the effects of tributaries in approximate ways through the width or mass balance functions. Since the discharge and depth of the Hodgson Glacier are probably comparable to those of the Steele at their confluence, I use the sum of their widths above this point. This is a simple approximation. In fact, their surface gradients are not equal everywhere in this region, their mass balance functions probably differ, and the two glaciers do not surge together (the Hodgson last surged in 1967-68, one year after the Steele). Because of their much shallower depths, to include the minor tributaries (1) through (5) (Figure 3.2) in this way would tend to grossly reduce the thickness and velocity of the main channel. The mass contribution of these tributaries is included in Model 1 by an addition to the mass balance function (Figure 3.3 (a)) at the regions of confluence.

3.3.4 MASS BALANCE

No comprehensive mass balance measurements have been made on the Steele Glacier. Between an average date of July 19, 1974, and an average date of July 2, 1975, Collins (unpublished) measured ablation at eight survey targets near the right angle bend (x=30 km). The measurements ranged from 1.57 m to 2.77 m of ice, with a mean of 2.15 m. All other evidence is indirect. On the lower Steele Glacier, Stanley (1969) estimated the ablation to be 1.5 m a^{-1} based on downwasting of ice shown to be stagnant by Sharp (1951).

Since snowfall can depend strongly on local conditions, extrapolating mass balance information even from adjacent valleys is at best a risky procedure. However, the qualitative patterns of mass balance, and its order of magnitude throughout the Icefield Ranges give some control on reasonable estimates for the Steele Glacier. Marcus and Ragle (1970) reported winter accumulation measurements on a traverse across the Icefield Ranges from the lower Seward Glacier to the Kaskawulsh Glacier. The values for the Kaskawulsh are instructive because both Kaskawulsh and Steele Glaciers occupy similar positions on the east side of the Icefield Ranges (Figure 3.1). The precipitation on the Kaskawulsh increases with elevation. The 1964-65 winter accumulation was 1.7 metres of ice equivalent at 2640 metres elevation, decreasing to 0.35 metres of ice equivalent at 1615 metres elevation. These authors also reported negligible summer melting on the ice plateau at Divide Station 30 km west of the Kaskawulsh Glacier. Divide Station at 2620 metres

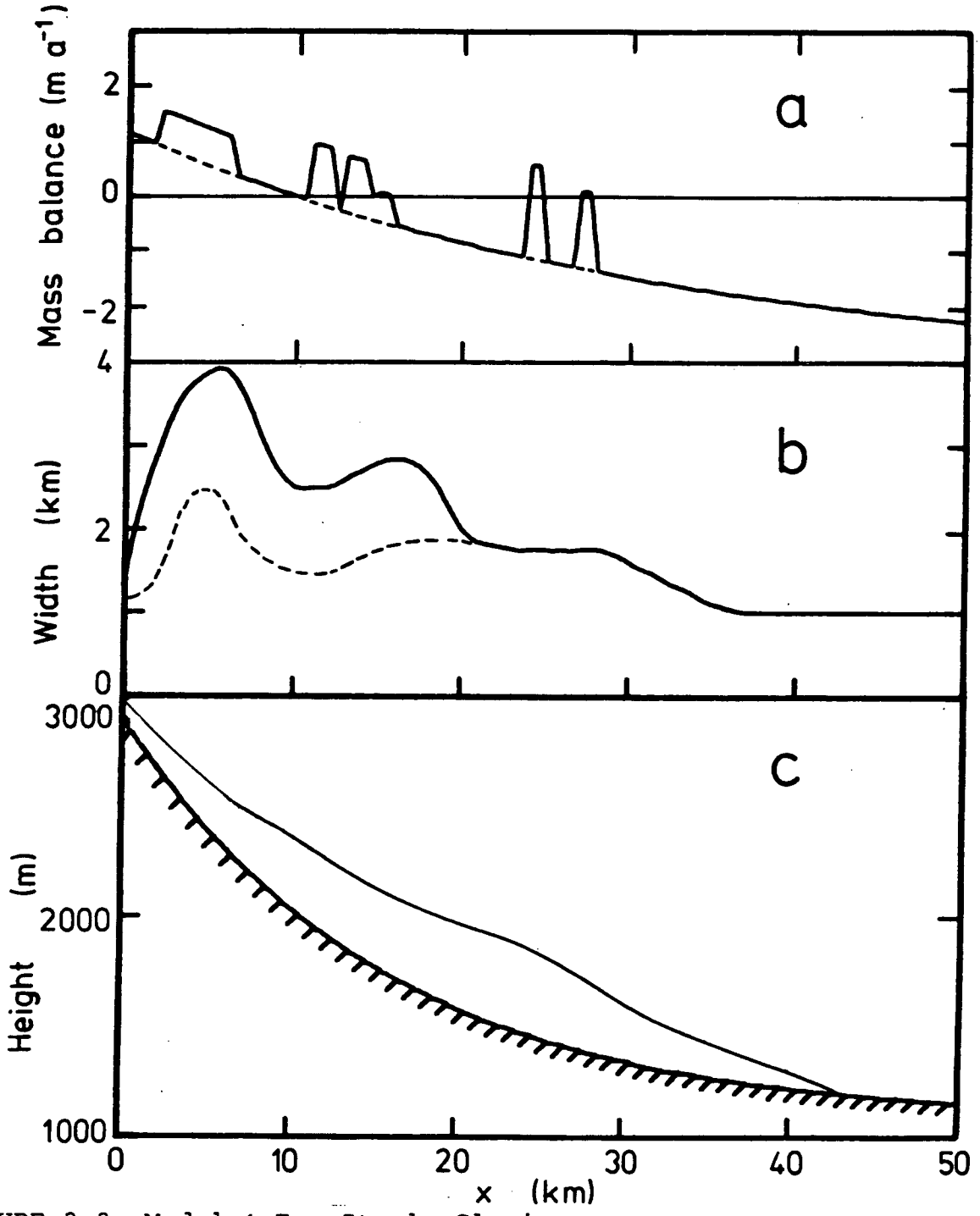

FIGURE 3.3. Model 1 For Steele Glacier.
(a) Mass balance. The dashed curve is balance for the main ice stream. The solid curve includes mass contributions from the tributaries (0) through (5) identified in Figure 3.2.
(b) Glacier width. The broken curve is the width of the main ice stream only. The solid curve includes the width of the Hodgson Glacier.
(c) Bed topography. The ice surface profile in 1951 is also shown.

elevation receives about 2.2 metres (ice equivalent) net accumulation each year; the record there indicates that 1965-66 was a low snowfall year by about 40% in the Kaskawulsh region (Marcus and Ragle, (1970, Figure 7)).

Keeler (1969) reported that, on Mount Logan, 60 km south of the Steele Glacier, elevation has little effect on precipitation above 2500 metres elevation. The net accumulation is about 0.8 metres of ice annually.

Stanley (1969, Figure 1) located the firn line at about 2400 metres on the Steele Glacier based on the 1951 aerial photography. Wood (1972) put the firn line in the higher elevation range of 2750 to 2900 metres. This would leave almost no accumulation area. Sharp (1947) gave the estimate of 8000 to 9100 feet (2440 to 2775 metres).

The broken line in Figure 3.3 (a) shows an estimated mass balance function for the main ice stream of the Steele Glacier consistent with Collins (unpublished) and with the indirect observations. The ice flux from the ith small tributary glacier is included through a perturbation δb_i to the mass balance function. In Appendix 19 I describe two methods of estimating the ice flux from each tributary and how I use this to estimate the δb_i. The solid curve in Figure 3.3 (a) shows the mass balance with the tributary terms δb_i included.

While Figure 3.3 (a) represents the best available estimate of the Steele Glacier mass balance, it should be kept in mind that mass balance may change significantly with longterm climatic change. The decades 1930-1950, upon which much of the data for the Steele Glacier is based, appear to have been an

exceptionally warm period (e.g. Hansen and others, 1981; Schneider and Mesirow, 1976, Chapter 3).

3.3.5 CYCLIC SURGE PATTERN FOR THE MODEL

Because I am investigating consequences of surging, rather than surge mechanisms, I specify a priori the sliding velocity $u_s(x,t)$. This aspect of surge modelling is discussed in Section 1.5.3. I have chosen to use a sliding velocity having the form

$$u_s(x,t) = X(x,t)\ T(t) \qquad (3.3.5)$$

because it can represent the observed sliding of the Steele Glacier reasonably well. Other functional forms of $u_s(x,t)$ could equally well fit the observations of Stanley (1969) and Wood (1972). The time dependent term T(t) is a nondimensional weighting factor between zero and unity. Figure 3.4 (b) shows the form of T(t) for a surge cycle of length t_4. During the quiescent stage, T has some small constant value f (e.g. f=0 gives no sliding). The surge starts at time t_0 and the velocity rises to the peak value by time t_1, remains at the maximum until t_2, then falls back to the nonsurge level by time t_3. The term X(x,t) shown in Figure 3.4 (a) gives the normalized spatial distribution of the sliding velocity at a time $(t-t_0)$. Observations on the Steele Glacier (Stanley, 1969) and on other surging glaciers, and some theoretical work on surging (e.g. Robin, 1969; Robin and Weertman, 1973) suggest that rapid sliding starts in a small region, and the boundaries of this

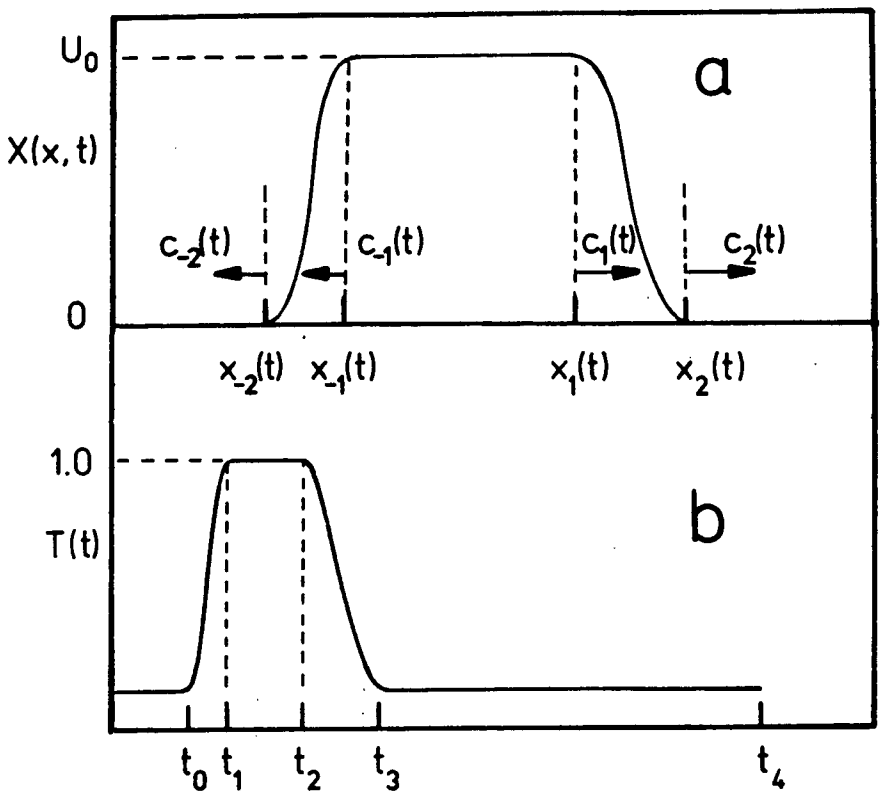

FIGURE 3.4. Sliding Model For Steele Glacier.
(a) X(x,t) gives the normalized spatial dependence of the sliding velocity at time t.
(b) T(t) is the temporal weighting function for the sliding velocity in (a).

zone of rapid sliding then propagate down (and possibly up) the glacier. U_0 is the maximum sliding velocity during the surge. In this model, each transition from a zone of rapid sliding to a zone of no sliding is given by one half cycle of a cosine. The distribution of sliding can change during the surge as the four points $x_{-2}(t)$, $x_{-1}(t)$, $x_1(t)$, and $x_2(t)$ move at velocities $c_{-2}(t)$, $c_{-1}(t)$, $c_1(t)$, and $c_2(t)$ respectively. The data from the surge of the Steele Glacier are not sufficiently complete to allow detailed estimation of the $c_j(t)$. I use constant values for these four velocities, so that the velocity transition points move according to

$$x_2(t) = x_2(t_0) + (t-t_0)\, c_2 \qquad (3.3.6)$$

with similar equations for the other three points. The constants $x_{-2}(t_0)$, $x_{-1}(t_0)$, $x_1(t_0)$, and $x_2(t_0)$ define the extent of the trigger zone.

Observations by Raymond and others (unpublished, Figure 9) on the Variegated Glacier, Alaska, indicate a regular increase of sliding velocity, from 0.05 m d^{-1} (18 m a^{-1}) in 1973, to 0.3 m d^{-1} (110 m a^{-1}) in 1979 in the upper reaches of the glacier. The Variegated Glacier appears to have a surge period of about 20 years, and is expected to surge sometime in the mid-1980's. The simulations which I have carried out for this chapter do not include a pre-surge increase in basal sliding, although it probably could be modelled satisfactorily by the Weertman (1957) sliding mechanism; this option is available in the computer program. However, for the Steele Glacier, the observed pre-surge velocities (Wood, 1972) are low, and are not sufficiently detailed to warrant this additional complication.

The leading edge of the zone of rapid sliding (i.e. $x_1(t)$ to $x_2(t)$) is a region of compressive flow. The instability of regions of compressive flow is widely recognized (e.g. Paterson, 1969, p. 207). For nonsurging glaciers, the surface rise resulting from compressive flow in the ablation area is largely balanced by surface melting. A surge lasting only one or two years occurs too quickly for melting to have any appreciable control on surface elevation; to avoid a growing bulge or shock wave moving with the leading edge of the zone of rapid sliding, the velocities c_1 and c_2 of the velocity disturbance must be

sufficiently greater than the material velocity U_0 that the velocity change can move ahead of any bulge forming in the ice. For the elementary case of ice with sliding velocity U_0 and thickness h_0 advancing into thinner stagnant ice of thickness h_1 in a channel of constant width, a simple continuity argument in Appendix 18 shows that when $c_1=c_2$, the velocity disturbance must move at least at the speed

$$c_1 \geq U_0 \left[\frac{h_0}{h_0 - h_1} \right] \qquad (3.3.7)$$

to prevent the development of a shock front in the advancing velocity transition. Equation (3.3.7) can be used to estimate the ice thickness h_0 and h_1; for the Steele Glacier, I have used it only to choose reasonable values of c_1 and c_2.

3.4 STEELE GLACIER MODEL 2

3.4.1 PROBLEMS WITH STEELE MODEL 1

I ran the Steele Glacier model 1 (Figure 3.3) using the flow law parameters (3.3.1) with no sliding. The numerical parameters are given in Table 3.1. The surface profiles at 50 year intervals starting from ice-free conditions are shown in Figure 3.5. The individual tributaries coalesced by 250 years. The maximum velocity (averaged over depth) in steady state is 33 m a^{-1} at x=12.5 km. The corresponding velocity at the ice surface is (see Section 1.4.4) (n+2)/(n+1) times this, i.e. 41 m a^{-1}. The final steady state length is 35.5 km, and the

n	A $kPa^{-n}\ s^{-1}$	s	g ms^{-2}	ρ $kg\ m^{-3}$	Δx m	Δt a
3	$5.3\ 10^{-15}$	0.8	9.8	900.	500.	1.0

TABLE 3.1. Parameters for Steele steady state.

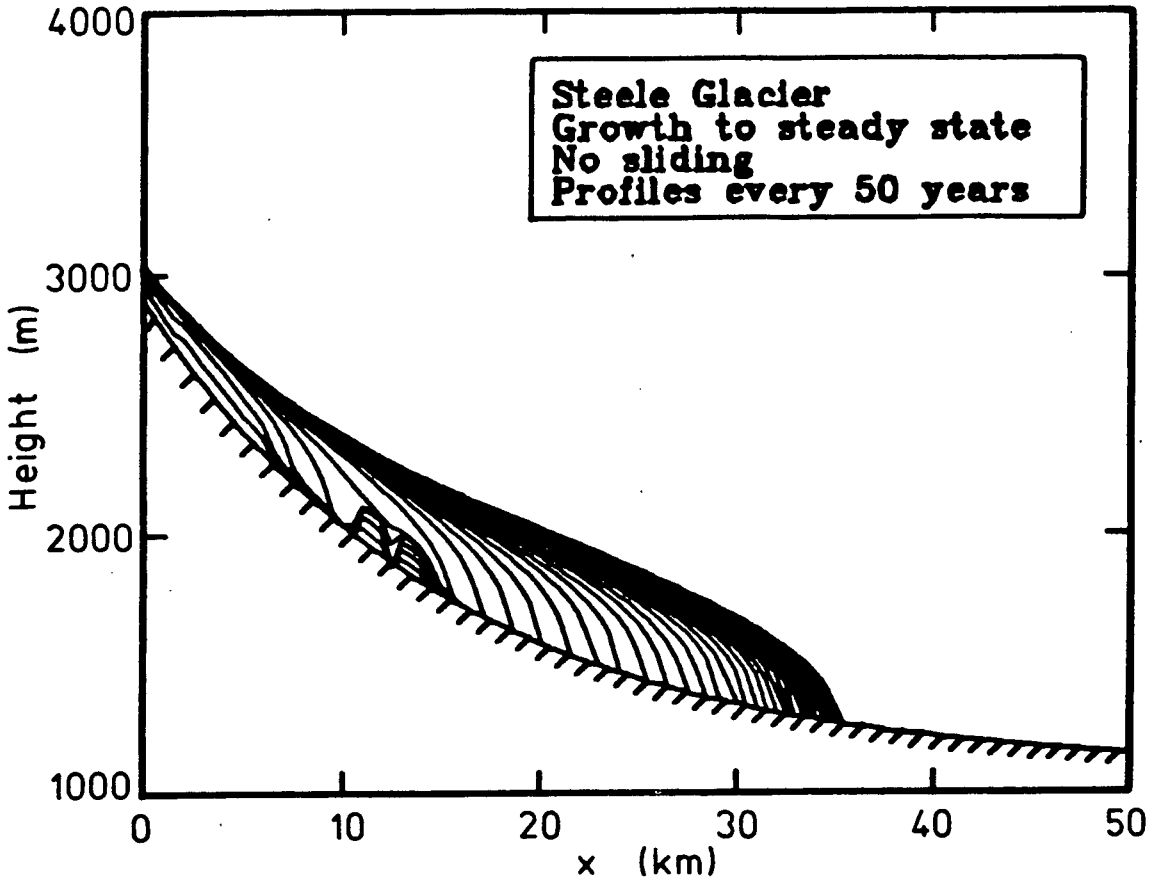

FIGURE 3.5. Steele Model 1 Growth To Steady State. There was no sliding. The model parameters are given in Table 3.1. The ice surface profiles are shown at 50 year intervals starting from ice-free conditions. The ice lobes at 11 km and 13 km are caused by ice from tributaries (1) and (2).

maximum depth is 444 m at x=25 km.

The surface profiles from Model 1 appear to be reasonable,

and the model coped with the rapidly-varying mass balance and width functions in Figure 3.3. However, I calculated some of the steady state streamlines for Model 1; these are shown in Figure 3.6 (note that the abscissa is ice thickness rather than elevation). The vertical mesh increment for the velocity

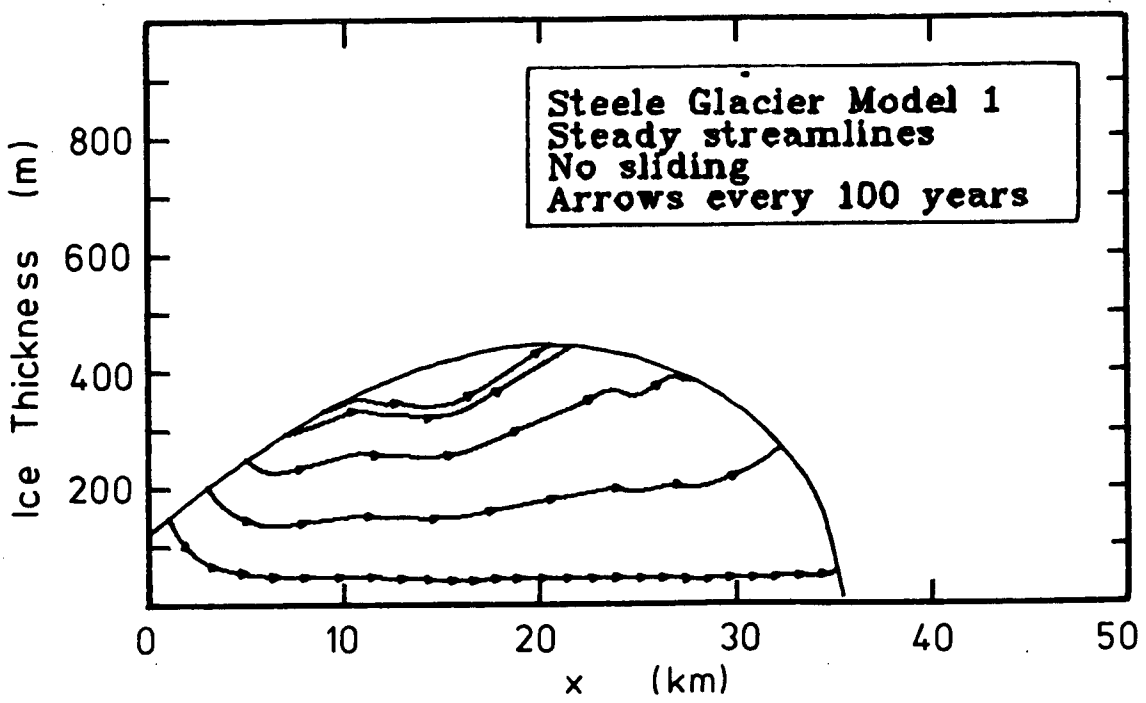

FIGURE 3.6. Steady State Streamlines For Model 1.
This cross-section shows ice depth. Arrows on the streamlines indicate each 100 years of flow. There was no sliding. The perturbations to the smooth streamlines are due to the addition of ice flux from tributaries through mass balance terms.

calculations (see Figure 2.8) was

$$DZ = 15 \text{ m}$$

The perturbations in the streamlines are caused by the additions of tributary ice flux through the mass balance function. I am looking for irregularities in streamline shape and in isotope distribution resulting from surging; to have features of this

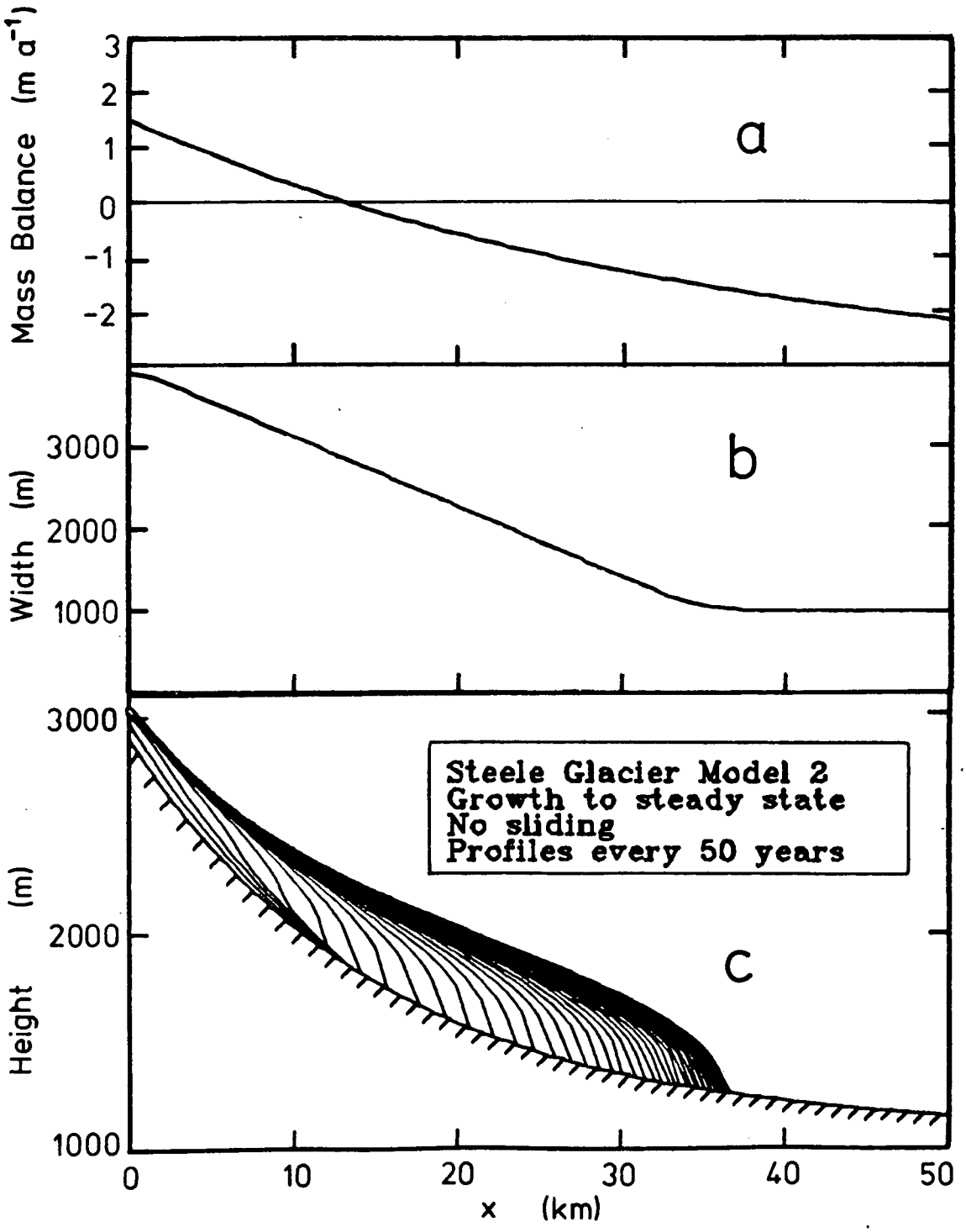

FIGURE 3.7. Model 2 For Steele Glacier.
(a) Mass balance.
(b) Glacier width.
(c) Bed topography and ice surface profiles at 50 year intervals during growth to steady state with no sliding.

form introduced through the mass balance function is

undesirable. Adding the tributary flux at the glacier surface rather than at the channel margins is an adequate approximation if only the ice surface shape is desired. If particle trajectories are also desired, this approximation is unacceptable.

An additional problem arises with Model 1 when sliding is added. The width function (Figure 3.3 (b)) is a detailed representation of the valley of Steele Creek. The spatial distribution of the surging velocity of the Steele Glacier is not known with the same resolution; Wood (1972) and Stanley (1969) obtained only spatially and temporally averaged velocities. Forcing the ice to slide at nearly constant velocity through a channel of highly variable width can result in some unrealistic surface configurations. For instance, in regions where the channel width gradient is large and negative, the ice can thicken rapidly and obtain a reversed surface slope. More detailed data on how the glacier actually changes speed to prevent this situation are not available for the 1966-67 surge. It is necessary to use a width function which has the same degree of spatial detail as the sliding data.

When a network computer model for tributaries is developed, and when more detailed sliding observations are available, the amount of detail in Model 1 can be justified.

3.4.2 SIMPLIFICATIONS

Figure 3.7 (a) and (b) show a simplified model for the Steele Glacier. This model resembles Model 1 in its gross features, yet avoids the difficulties I described in the previous section.

Figure 3.7(c) shows the growth of Model 2 to steady state with no sliding, using the parameters in Table 3.1, and starting from ice-free conditions. The steady state length is 36.5 km, the maximum ice thickness is 452 m at x=21 km, and the maximum velocity (averaged over depth) is 30.4 m a^{-1} at x=11 km. These values are close to the values for Model 1 (see Section 3.4.1).

3.5 STABLE ISOTOPES IN GLACIOLOGY

3.5.1 DEFINITION OF THE DEL SCALE

The standard method of describing the isotopic composition of oxygen and hydrogen in water is the DEL scale (δ). The ratio R of the concentrations of the heavy and light isotopes O^{18}/O^{16} and D/H can be measured with a mass spectrometer; a practical concentration scale should be based on R. The δ value (3.5.1) of an ice sample is the relative difference between R_s of the sample and R_{SMOW} of a reference sample known as Standard Mean Ocean Water (SMOW) (Craig, 1961).

$$\delta = \left[\frac{R_S - R_{SMOW}}{R_{SMOW}} \right] 10^3 \qquad (3.5.1)$$

A drawback of true SMOW is the fact that no samples are available. Samples of other O^{18}/O^{16} isotopic standards from the U.S. National Bureau of Standards have been distributed in the past by the International Atomic Energy Agency, Vienna. In September 1976, at Vienna, the Consultants' Meeting on Stable Isotope Standards and Intercalibration in Hydrology and Geochemistry set up a standard sample called Vienna SMOW. The difference between true SMOW (Craig, 1961) and Vienna SMOW is $-0.05^{o}/_{oo}$. This difference is not significant for my glaciological applications. The reports of isotopic data for the Icefield Ranges (West and Krouse, 1972; West, unpublished; Ahern, unpublished [b]) predate this change. Dansgaard (1969) reported a reproducibility of $\pm 0.12^{o}/_{oo}$ (per mil) for routine mass spectrometer measurements of δ. Ahern (unpublished [b], p. 158) reported $\pm 0.03^{o}/_{oo}$ for samples from the Steele Glacier. Dansgaard's laboratory in Copenhagen also now achieves this level. This is adequate for work on glaciers, since δ may vary by several parts$^{o}/_{oo}$ to tens of parts$^{o}/_{oo}$ for samples from any one glacier.

3.5.2 FACTORS AFFECTING DEL

The nonzero value of DEL (δ) for an ice sample from a glacier is the result of a long series of processes in the hydrological cycle since the water left the well-mixed ocean (where δ is close to zero). At 0°C, the vapour pressures of the three major isotopic forms of water have the approximate ratios (e.g. Dansgaard, 1964)

$$H_2O^{16} : H_2O^{18} : HDO = 1.000 : 0.989 : 0.904 \qquad (3.5.2)$$

and the differences increase with decreasing temperature. The resulting differences in volatility lead to temperature dependent isotopic fractionation in evaporation and condensation processes. Under fast evaporation or condensation conditions (i.e. equilibrium conditions do not exist between the vapour and the liquid phases) the fractionation factor (the ratio of the concentrations of a particular isotopic species in the two phases) is complicated. The process which tends to control the δ values in glacier precipitation is the condensation of droplets from cloud vapour; fortunately, this can, in most cases, be adequately modelled by a Rayleigh condensation process, i.e. a slow condensation (quasi-equilibrium of the vapour and liquid phases) with immediate removal of the condensate (Dansgaard, 1964). For slow condensation or evaporation, the fractionation factor is just a ratio of the vapour pressures of the different isotopic species of water at the ambient temperature. These ratios are well known above 0°C from laboratory measurements, and have been extrapolated to -20°C (Dansgaard, 1964, Table 1) using a formula of Zhavoronkov and others, (1955). When the

Rayleigh condensation model is applicable, the δ value of the precipitation is primarily an indication of the condensation temperature. In general terms, δ values tend to decrease with altitude and with latitude, and, at any one site, to be more negative in winter than in summer. A continental effect is also sometimes observed (Dansgaard, 1964); the δ values of precipitation at constant condensation temperature may decrease with distance from the ocean due to depletion of heavy isotopes from the storm systems through precipitation, and due to dilution with isotopically light vapour from freshwater sources.

Factors other than temperature can influence the δ value of precipitation. Dansgaard (1964) discussed the effects of evaporation from falling droplets, isotopic exchange between drops and air through which they fall, non-equilibrium phase changes, and variations in the frequency and isotopic composition of the source storms. While these processes can cause variations in δ from storm to storm, their effect on the average summer or winter δ value tends to be constant from year to year. $\delta(O^{18}/O^{16})$ and δ(D/H) are linearly related under Rayleigh conditions (Dansgaard, 1964); simultaneous measurement of $\delta(O^{18}/O^{16})$ and δ(D/H) can be used to reveal the presence of non-equilibrium condensation.

Several processes in snow and firn tend to homogenize the isotopic distribution, obliterating differences between individual storms, and sometimes the summer to winter difference. In regions with summer melting, recrystallization in the presence of percolating meltwater can bring the whole vertical column of snowpack to the average δ-value (Dansgaard

and others, 1973). However, the effects of meltwater are not always simple; Ahern (unpublished [a], p. 109) found that percolating meltwater could enhance rather than smooth the isotopic variations in a cold snowpack with variable density. In regions with no summer melting, some smoothing of the isotopic profile occurs due to sublimation and recrystallization in the firn. Vertical vapour motion is most pronounced in regions of high vertical gradients of temperature in the firn (e.g. due to large seasonal temperature variations), or in stormy regions with frequent barometric pressure changes (Dansgaard, and others, 1973).

Below the depth at which firn reaches a density of 550 kg m^{-3}, the vapour spaces in the firn are isolated. The isotopic profile is smoothed only by solid diffusion. This process is too slow to have an appreciable effect on ice in the Steele Glacier.

3.5.3 PREVIOUS ISOTOPIC STUDIES

Assuming (1) that the precipitating air masses follow similar tracks with similar frequency the year around and from year to year, (2) that Rayleigh condensation occurs, (3) that surface and condensation temperatures can be simply related, (4) that the δ-temperature relationship is constant with time, and (5) that the flow pattern of the ice mass can be calculated, then δ values in ice cores can be related to climate at the time of precipitation. This was first pointed out by Dansgaard (1954). A thorough discussion of ice core studies can be found

in Chapter 15 of Paterson (1981).

The Greenland ice sheet provides the most suitable ice flow and meteorological conditions for a simple climatic interpretation of a deep ice core (Dansgaard and others, 1973). The first major drilling program was undertaken in 1956 by S.I.P.R.E. (U.S. Army Snow, Ice, and Permafrost Research Establishment, now called CRREL, Cold Regions Research and Engineering Laboratory); a 411 m core was recovered at Site 2, in northwest Greenland. This was followed by deep cores at Camp Century, Greenland in 1966 (1387 m), and at Byrd Station, Antarctica, in 1968 (2164 m). The Camp Century core has been used to derive climate variations over the past 100,000 years (Dansgaard and Johnsen, 1969[a], 1969[b]; Dansgaard and others, 1969, 1971). The Byrd Station core also shows long term climate variations (Epstein and others, 1970; Johnsen and others, 1972), but is more difficult to date absolutely, because the annual variations of δ were not preserved during the ice formation process. The length of the flowline, and the time scale for this hole are in dispute (Robin, 1977).

Coring programs and climatic interpretations have also been undertaken at other sites in Greenland (Dansgaard and others, 1973), in Antarctica, including Vostok (Barkov and others, 1974, 1975, 1977), Dome C (Lorius and others, 1979), Little America V (Dansgaard and others, 1977), and Terre Adelie (Lorius and Merlivat, 1977), and at sites in the Canadian Arctic, including Meighen Ice Cap (Koerner and others, 1973; Koerner and Paterson, 1974), Devon Ice Cap (Paterson and others, 1977; Paterson and Clarke, 1978; Fisher, 1979), and Agassiz Ice Cap, Ellesmere

Island (D. Fisher, personal communication). Ice cores for isotopic analysis have been obtained from the plateau at 5400 m on Mount Logan, Yukon Territory by G. Holdsworth.

During periods of extensive glaciation, deep sea sediments are enriched in O^{18}; the isotopic composition of sea water is altered because of the large volume of O^{18}-depleted ice on land. Measurements of the isotopic composition of deep sea sediments (e.g. Hayes and others, 1976) have complemented the climatic studies of deep ice cores.

The validity of the climate interpretation of ice cores has also been supported by other studies. Robin (1976) and Johnsen (1977) found that the temperature history derived from the isotopic records was compatible with the present vertical distribution of temperature in boreholes. Paterson and Clarke (1978) used the isotopically-derived temperature history as a boundary condition for a time-dependent heat flow model for the Devon Island boreholes.

Picciotto and others, (1960) demonstrated the existence of a linear relationship between cloud temperature and δ on the coast of East Antarctica, and Lorius and Delmas (1975) found a linear relationship between δ(D/H) and ten metre firn temperatures. Picciotto and others, (1968), and Lorius and others, (1970) used the annual variation of δ in near-surface samples to measure the recent accumulation rate at Antarctic sites. Lorius and others, (1969) measured regional variations of δ(D/H) in Antarctic precipitation.

West and Krouse (1972) measured isotopic ratios at several sites in the St. Elias Mountains, Yukon Territory, including

Mount logan, Divide Station, and Rusty Glacier, obtaining mass balance estimates and relating isotopic composition to weather patterns. A longitudinal surface sampling of Rusty Glacier (a small surge-type glacier in the Steele Creek basin) showed a systematic increase of δ with height in the ablation zone, demonstrating that the general isotopic pattern of the glacier was not destroyed by surging.

Ahern (unpublished [b], p. 162) obtained an isotopic profile to a depth of 36 m in a borehole at x=15 km (Figure 3.2) on the Steele Glacier. This profile appeared to show periodic oscillations of wavelength 7 metres and amplitude $\pm 1.5^{o}/_{oo}$ in $\delta(O^{18}/O^{16})$.

Isotopic studies on glaciers and ice sheets are closely related to studies of ice flow. The age of the ice must be determined, and annual layers cannot always be detected isotopically. Time scales for ice cores have been derived by Dansgaard and Johnsen (1969[a]), by Philberth and Federer (1971), and by Hammer and others (1978), using assumptions of steady state, proximity to an ice divide, and specific forms of vertical strain rate or temperature gradient. Paterson and others (1977) measured the vertical deformation in the Devon boreholes; this allowed them to eliminate the strain rate assumptions when deriving a time scale from the flow. For boreholes at large distances from ice divides, the horizontal velocity influences the time scale calculation, and two-dimensional flow simulations, such as given by Budd and others (1971, p. 148) for the Byrd station flowline, must be used to date the ice.

A conceptual inconsistency can arise with the use of steady state flow models; the existence of the climatic variations, which the isotopic profiles attempt to determine, could preclude the existence of steady state conditions. In addition, the ice surface elevation may vary in the absence of climatic variations. For this reason, time-dependent flow models are essential to the interpretation of some isotopic data. Jenssen (1978) investigated the effect of ice sheet elevation changes on the isotopic profile in the Vostok core. He calculated ice trajectories and simulated isotopic profiles on the Antarctic ice sheet flowline from Vostok to Mirny, assuming periodic surges; the time-dependent ice surface profiles were computed by Budd and McInnes (1978, 1979). This is the only previous work of which I am aware in which trajectories and isotopic distribution are calculated in a time-varying ice mass. Jenssen (1978) was interested in the effect of surging on the climatic interpretation; in this chapter, I investigate the feasibility of using isotopic information to reveal the surge history. Jenssen (1978) used a linear isotopic-elevation relation similar to equation (3.5.3) below. The details of the flowline calculations were not described.

3.5.4 DEL RELATIONS FOR THE MODEL

In the computer model, I assume that:

(1) all precipitation has the annual average value for the given elevation or location, (i.e. rapid isotopic homogenization in the firn), and

(2) isotopic diffusion is negligible in the solid ice.

I use two δ-precipitation models, representing opposite extremes of topographic control of precipitation. The first, which I call Model δ1, is based on the assumption that the isotopic composition of snowfall is completely controlled by the surface elevation of the glacier h(x,t), and can be approximated by a linear relationship over the range of elevations considered, i.e.

$$\delta(x,t) = \delta_0 + c\, h(x,t) \qquad (3.5.3)$$

Values of the constants δ_0 and c consistent with the few measurements in the Steele Creek basin (West and Krouse, 1972) and on the Steele Glacier (Ahern, unpublished [b]) are

$$\delta_0 = -15.0\ {}^{o}/_{oo}$$
$$c = -0.004\ m^{-1}\ {}^{o}/_{oo} \qquad (3.5.4)$$

The gradient c is close to the value of $-0.005\ m^{-1}\ {}^{o}/_{oo}$ found by Sharp and others, (1960) for c at Blue Glacier, Washington, U.S.A. It is within a factor of two of the value of $-0.002\ m^{-1}\ {}^{o}/_{oo}$ reported by Dansgaard (1961). Jenssen (1978) used $c=-0.006\ m^{-1}\ {}^{o}/_{oo}$ in a modelling study of an Antarctic flowline. Isotopic values on ice sheets and ice caps can be described by Model δ1, because the ice sheet surface height strongly influences the vertical motion of incoming air masses.

The second model, called Model δ2, assumes that the isotopic composition of the snowfall is completely controlled by the regional mountain topography and by distance from the storm source in the Gulf of Alaska; δ is assumed to be a function only of position x. Approximating the 1951 Steele Glacier surface (Topographical Survey, 1969) by a straight line in the

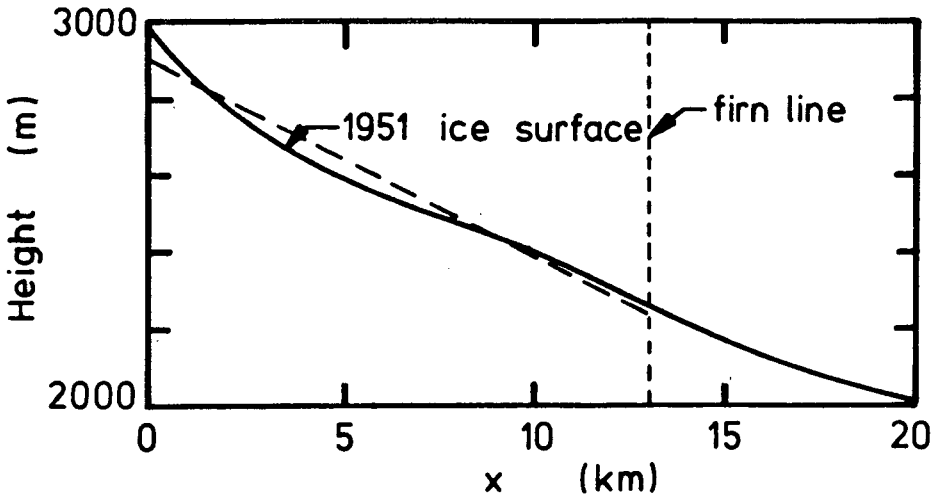

FIGURE 3.8. Reference Surface For δ-x Function.
The accumulation area of the Steele Glacier is assumed to extend (see Figure 3.7 (a)) to x=13 km (vertical broken line). The curved line is the observed ice surface elevation in 1951. Applying the δ-elevation relation (3.5.3) to the linear approximation (dashed line) to this surface, and using the constants (3.5.4) gives a linear δ-x relationship with the constants in (3.5.6).

accumulation area, as shown in Figure 3.8, and applying the δ-h relationship to this line, with the constants (3.5.4), gives the x-δ relationship

$$\delta(x,t) = \delta_0 + k\,x \qquad (3.5.5)$$

with the constants

$$\delta_0 = -26.6\ {}^{o}/_{oo}$$
$$k = 0.00022\ m^{-1}\ {}^{o}/_{oo} \qquad (3.5.6)$$

Model δ2 is more appropriate than Model δ1 for small valley glaciers. The Steele Glacier, being a large valley glacier, probably falls between the two extremes.

Because Model δ1 allows the isotopic composition of snowfall to vary with both position and time, while Model δ2 allows only variation with position, Model δ1 can produce larger variations or discontinuities in $\delta(O^{18}/O^{16})$. Models δ1 and δ2

can be considered to give the maximum and minimum structure respectively to the isotopic distribution within the Steele Glacier.

3.6 MODEL RESULTS: SURGE PERIOD AND TRAJECTORIES

3.6.1 INTRODUCTION

The surge periodicity of the Steele Glacier is unknown. In Section 3.6.2, I show three computer simulations of the Steele Glacier using surge periods spanning the range of 50 to 150 years suggested by field observations. I used the same velocity pattern during the surge in all three cases. The period (97 years) which gave the most reasonable ice thickness profiles at all times was selected for trajectory and isotopic calculations. In Section 3.6.3, I present typical trajectories for ice particles in this model. These trajectories show periodic abrupt changes of direction and speed.

3.6.2 PERIODICALLY REPEATING STATE

To obtain a periodically repeating surge cycle, I used the constants in Table 3.2 to generate the sliding velocity. This sliding pattern is shown at intervals of 0.25 years in Figure 3.9. The surge duration was two years. I used three surge periods; 47, 97, and 147 years span the range of possible periods described in Section 3.2.4. Starting from the nonsliding steady state in Figure 3.6, I ran the Steele Glacier Model 2 through fifteen surge cycles of length t_4. By that time, the

t_0 (a)	0.0	$x_{-2}(t_0)$ (km)	8.0
t_1 (a)	0.75	$x_{-1}(t_0)$ (km)	18.0
t_2 (a)	1.5	$x_1(t_0)$ (km)	19.0
t_3 (a)	2.0	$x_2(t_0)$ (km)	26.0
t_4 (a)	1) 47.0		
	2) 97.0	$c_{-2}(t_0)$ (m a^{-1})	-1000.0
	3) 147.0	$c_{-1}(t_0)$ (m a^{-1})	7500.0
f	0.0	$c_1(t_0)$ (m a^{-1})	15000.0
U_0 (m a^{-1})	5000.	$c_2(t_0)$ (m a^{-1})	15000.0

TABLE 3.2. Velocity pattern for Steele surge.
The three values of surge period t_4 were used for Figures 3.10, 3.11, and 3.12 respectively.

model no longer "remembered" the initial steady state condition; it repeated the same surface profile sequence to one part in 10^4 with each new cycle for 97 and 147 year periods, and to a few parts in 10^3 with a 47 year period. The time steps in the computer model must be very small when the glacier is surging in order to maintain accuracy (see Section A1.5). Table 3.3 summarizes the numerical time step sequence used. The other numerical and physical constants had the values shown in Table 3.1. Figures 3.10 through 3.12 show the pre-surge glacier surface (solid line) at t_0, and the post-surge surface (broken line) at t_3 for the three surge periods of 47, 97, and 147 years respectively. The model with a 47 year surge period (figure 3.10) has a pre-surge profile (solid line) which is less than 100 m thick beyond x=20 km. The post-surge profile is less than 100 m thick beyond x=25 km. It seems unlikely that a surge of ice always less than 100 m thick could advance 12 km in two years. The profiles shown in this diagram are unrealistic. This conclusion indicates that the Steele Glacier accumulation area cannot provide sufficient mass in just 47 years to generate

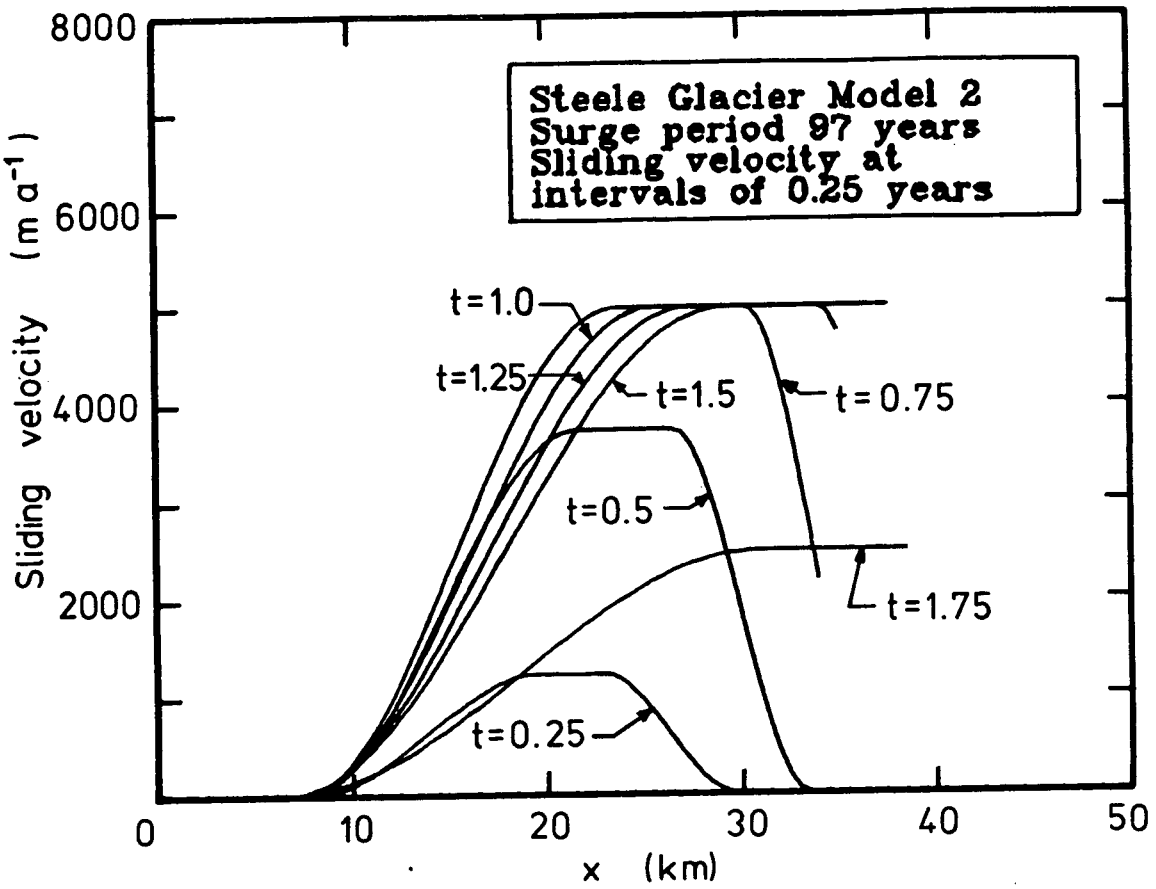

FIGURE 3.9. Sliding Velocity: Steele Glacier Model.
The sliding velocity profile is shown at intervals of 0.25 years during the surge of two years duration. The end of each curve indicates the position of the advancing terminus (for the model with 97 year surge period.)

surges which move as quickly or as far as the 1966-67 example. Either some surges must be less vigorous, or the surge period must be substantially longer than 47 years. The model with a period of 147 years (Figure 3.12) is reasonably thick at all times. It could be criticized on the basis of the exceptionally thick ice lobe below x=25 km following the surge. Radio echo sounding (e.g. Narod and Clarke, 1980) of the Steele Glacier would resolve the validity of this criticism. This model could be acceptable for the trajectory analysis, but I did not use it because the observations of Stanley (1969), Wood (1972) and

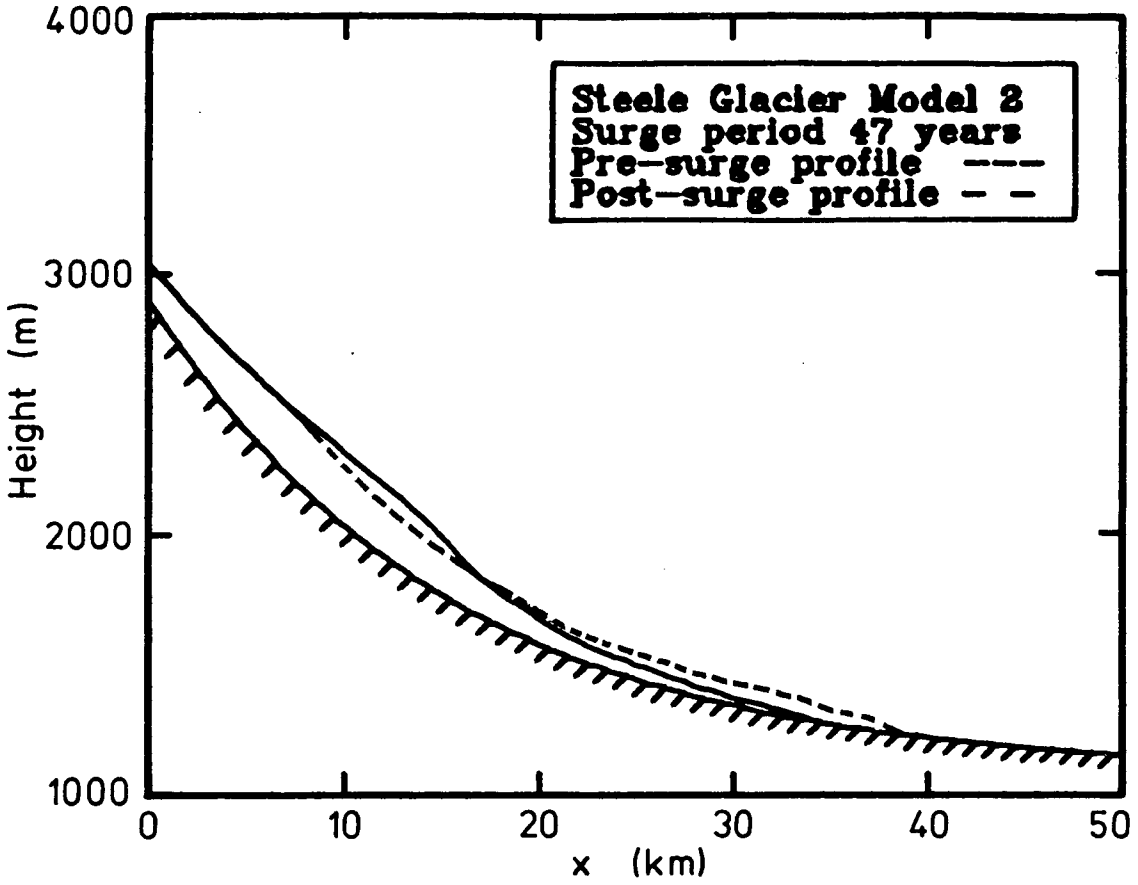

FIGURE 3.10. Pre- And Post-surge Profiles: 47 Year Period. The solid curve shows the glacier as the surge begins. The broken curve shows the surface elevation as the surge ends two years later. The sliding function is given in Table 3.2 and Figure 3.9. The ice depths of the lower glacier are unreasonably thin; the Steele has insufficient accumulation to surge as vigorously as the 1966-67 event as frequently as every 47 years.

Sharp (1947), described in Section 3.2.4, indicate that 150 years is an upper limit for the time between surges.

The surge period of 97 years is the most acceptable of the three. There is little change in the ice surface elevation above x=8 km. Between 8 km and 20 km, the surface drops by up to 110 m, while below 20 km, the surface rises during the surge by up to 120 m. This pattern agrees well with the zones described by Stanley (1969). I used this model for the trajectory and

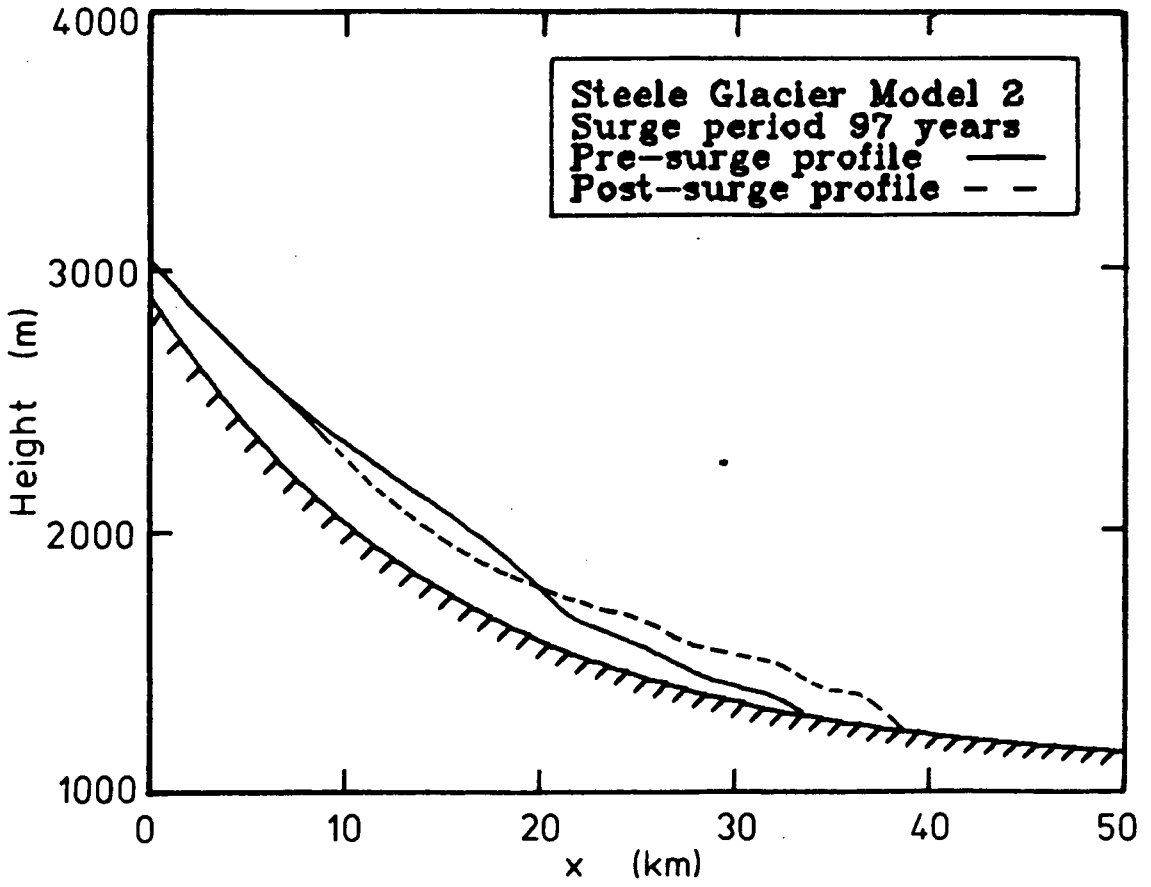

FIGURE 3.11. Pre- And Post-surge Profiles: 97 Year Period. The solid curve shows the glacier as the surge begins. The broken curve shows the surface elevation as the surge ends two years later. The sliding function is given in Table 3.2 and Figure 3.9. This model is used in Section 3.7.

isotopic calculations.

Figure 3.13 shows an orthographic view of the ice thickness h(x,t) during one complete surge cycle for the case with a 97 year period. The rapid decrease in surface elevation between x=8 km and x=20 km and between time zero and two years is hidden by the pre-surge profile, but the rapid surface rise of the lower glacier can be seen. The subsequent slow ablation of the terminus region, and the buildup and advance of the ice in the source region are evident. Three steps or waves can be seen in the ablation zone. One wave forms during each surge. The ice

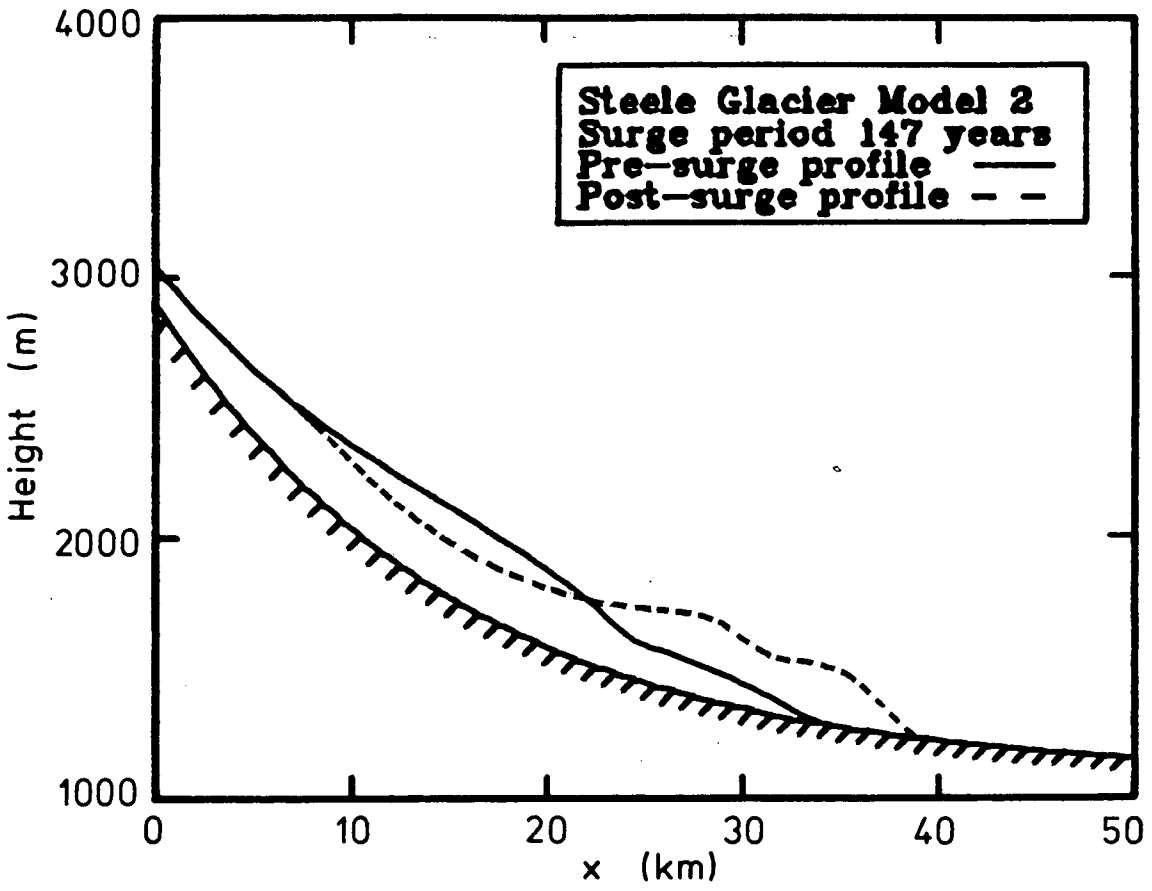

FIGURE 3.12. Pre- And Post-surge Profiles: 147 Year Period. The solid curve shows the glacier as the surge begins. The broken curve shows the surface elevation as the surge ends two years later. The sliding function is given in Table 3.2 and Figure 3.9. This model is physically reasonable, but 147 years is an upper limit on the surge period based on the observations of Stanley (1969), Wood (1972), and Sharp (1947).

Interval	Time (a)	Δt (a)
t_0-t_1	0.0 - 0.75	0.01
t_1-t_2	0.75 - 1.5	0.01
t_2-t_3	1.5 - 2.0	0.01
t_3-t_4	2.0 - 7.0	0.1
	7.0 - 97.0	1.0

TABLE 3.3. Numerical time steps for Steele surge.

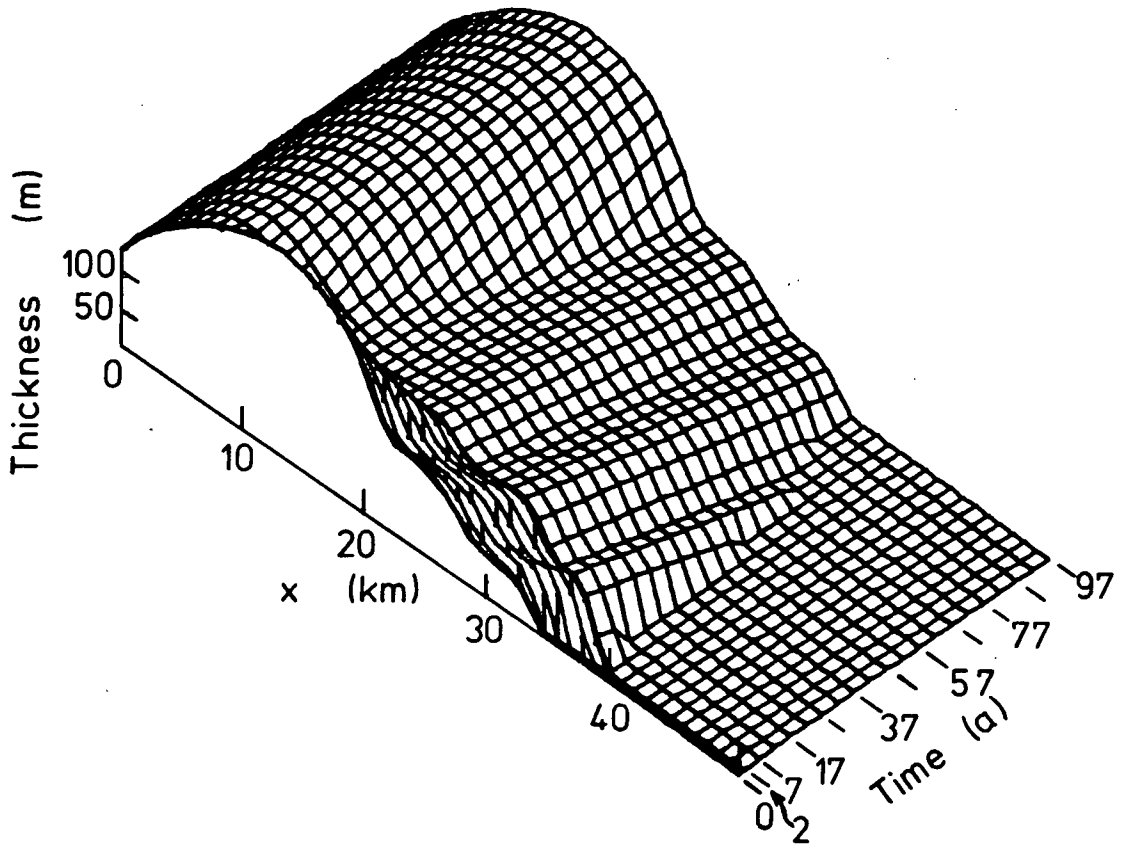

FIGURE 3.13. Steele Glacier Thickness: One Surge Cycle.
Ice thickness h(x,t) in orthographic view from a point 45° above the x axis, and 45° around the thickness axis from the time axis. The model used the constants in Tables 3.1, 3.2, and 3.3. The surge started at time=0.0 and ended at 2 years. The surge period was 97 years. The transverse lines indicate 1 km intervals, and the longitudinal lines are spaced at intervals of 5 years.

thickens as a result of being forced into the converging channel (see Figure 3.7 (b)). The observed profile of the Steele Glacier in 1951 (Figure 3.3 (c)) has long surface undulations, but these could result from bed topography. Repeated surface mapping and a radio-echo depth survey would resolve this question. The undulations in Figure 3.13 may be an artifice of the model due to the poorly-known spatial variation of the surge velocity, and the inclusion of the Hodgson Glacier through the width function

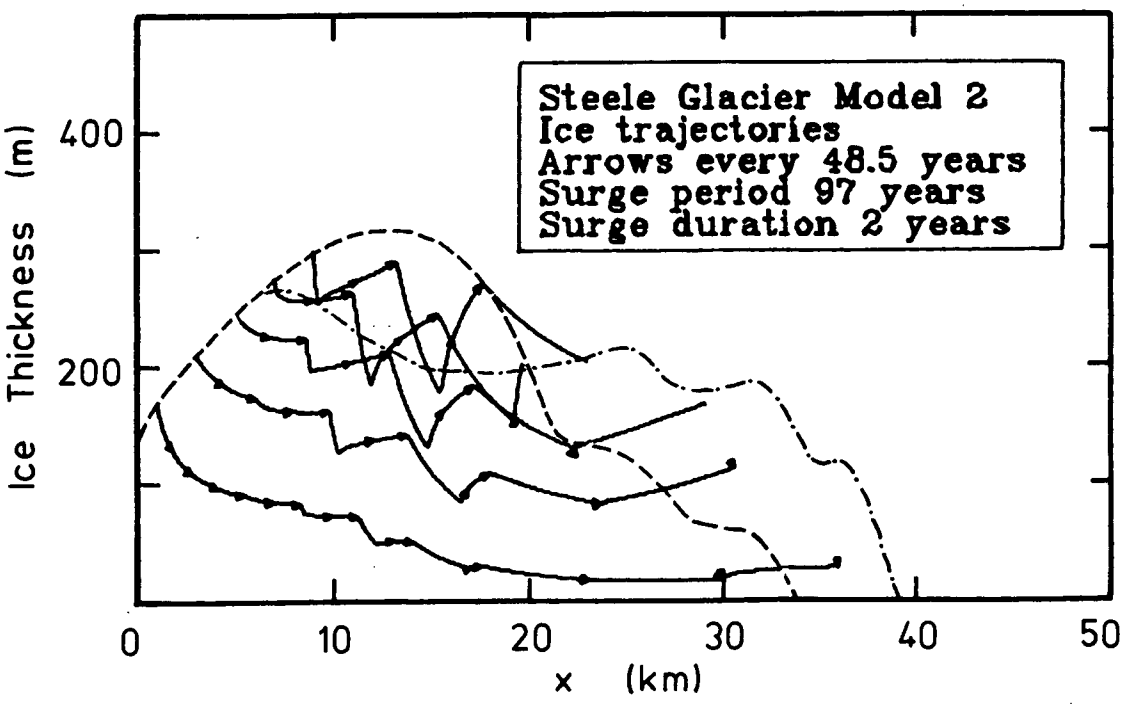

FIGURE 3.14. Ice Trajectories For 97 Year Surge Period. Trajectories for 5 particles starting on the ice surface as a surge begins. The dashed profile is the ice thickness at t_0. The dashed-dotted profile is the post-surge ice thickness at t_3=2 years. The arrows on the trajectories indicate time intervals of 48.5 years, i.e. the midpoint and end of each 97 year surge cycle. Beyond x=22 km, the ice is virtually stagnant between surges, and the arrows for mid-period and for the end of the period are superimposed.

shown in Figure 3.3 (b).

3.6.3 ICE TRAJECTORIES

Figure 3.14 shows the trajectories of particles starting on the ice surface at t_0 as a surge begins. The arrows on the trajectories show the particle locations each 48.5 years, i.e. at the midpoint and at the termination of each 97 year surge cycle. The pre-surge (dotted curve) and the post-surge

(dotted-dashed curve) ice thickness are also shown. The ice beyond x=22 km is virtually stagnant between surges, and the arrows indicating the end of each surge cycle are superimposed on the mid-cycle arrow. Between x=8 km and x=20 km, the trajectories descend abruptly during the surge; the high longitudinal strain rate resulting from the gradient of the sliding velocity in Figure 3.9 causes a general thinning in this zone. The trajectories rise during the surge in the region below x=20 km because the velocity gradient is small and the ice thickens as it flows into a channel of decreasing width. The endpoint of each trajectory indicates the position of ice surface at the time the ice particle came to the surface.

3.7 MODEL RESULTS: DISTRIBUTION OF ISOTOPES

3.7.1 INTRODUCTION

In this section, I show the isotopic distributions found by calculating ice trajectories for the surge model with 97 year period (Figures 3.11 and 3.13) and the precipitation-δ models 61 and 62. I have chosen to look at the isotope distribution at four times during the cycle: (1) when the surge begins at t=0.0, (2) at mid-surge, t=1.0 years, (3) at t=10.0 years, when it is again possible to walk over most of the glacier surface, and (4) at t=50.0 years, near the midpoint of the quiescent period.

Since the velocity field is smoothly-varying even during a surge (Stanley, 1969), discontinuities cannot be introduced into the isotope distribution within the ice by the rapid flow alone;

this would require shear fracturing and dislocation on a large scale. Discontinuities or sharp changes in the gradient of δ can be introduced only by abrupt changes in the δ-value of precipitation falling onto a given element of ice at the glacier surface. When δ is considered to be a function of position and surface elevation (Section 3.5.2), the δ-value of new precipitation falling on an element of ice at the surface can change abruptly only if (1) the surface elevation changes abruptly, or (2) the surface element is rapidly moved to a new position at which snowfall has a different δ-value. Thus, isotopic discontinuities can be formed only in ice which (1) is at the ice-air interface at the moment a surge begins, (2) is in the accumulation region, and (3) participates in the surge through forward motion or a decrease in ice thickness. The region above x=8 km on the Steele Glacier did not take part in the 1966-67 surge (Stanley, 1969); this feature is incorporated into the computer model. Since all the ice downstream from x=25, and the deep ice throughout the glacier comes from the region upstream from x=8 km, there cannot be any discontinuities or abrupt variations in δ in this ice. (The surges do, of course, alter the positions and distort the gradients of the isodel lines, but all quantities remain slowly-varying; this would be a difficult and subtle matter to interpret in a flow regime as complicated as that of a surging valley glacier).

In Section 3.7.2, I show longitudinal vertical sections of the Steele Glacier between x=5 km and x=25 km at the four times metioned above using the height-dependent precipitation model 61. I present detailed surface profiles of δ at the same

four times in Section 3.7.3. In Section 3.7.4, I show sections and profiles at the same times using the the precipitation model δ2.

3.7.2 MODEL δ1: LONGITUDINAL δ SECTIONS

Would a well-placed borehole, or series of boreholes in the Steele Glacier recover convincing isotopic evidence of past surges? In Figure 3.15, I show the expected isotopic distributions in a longitudinal section at the four times 0, 1, 10, and 50 years measured from the initiation of a surge. The region from x=5 km to x=25 km contains all the ice which is capable of containing discontinuities in δ and its gradient (see Section 3.7.1). A δ-value was assigned to each point on a mesh (indicated by dots) with a horizontal spacing of 500 m, and a vertical spacing of 5 m. The δ-value was calculated by applying the isotopic model δ1 to the starting coordinates of the ice

---

Overleaf:
FIGURE 3.15. Longitudinal δ sections: Model δ1.
The δ-values within the Steele Glacier are contoured at intervals of $0.1^{o}/_{oo}$. The dots show the 5x500 m mesh at which δ was evaluated using Model δ1. (Section 3.5.4). The surge model (Figures 3.11 and 3.13) had a period of 97 years. Each line of steep δ gradient which intersects the ice surface and is attenuated with distance upstream and into the ice outlines the relict ice-air interface at the start of a previous surge.
a) t=0 year; pre-surge profile.
b) t=1 year; mid-surge.
c) t=10 years; post-surge profile. Foot travel would again be possible.
d) t=50 years; this is approximately the midpoint of the quiescent period.
In Model δ1, precipitation is a linear function of ice surface elevation; this tends to over-estimate the magnitude of isotopic discontinuities due to surging.

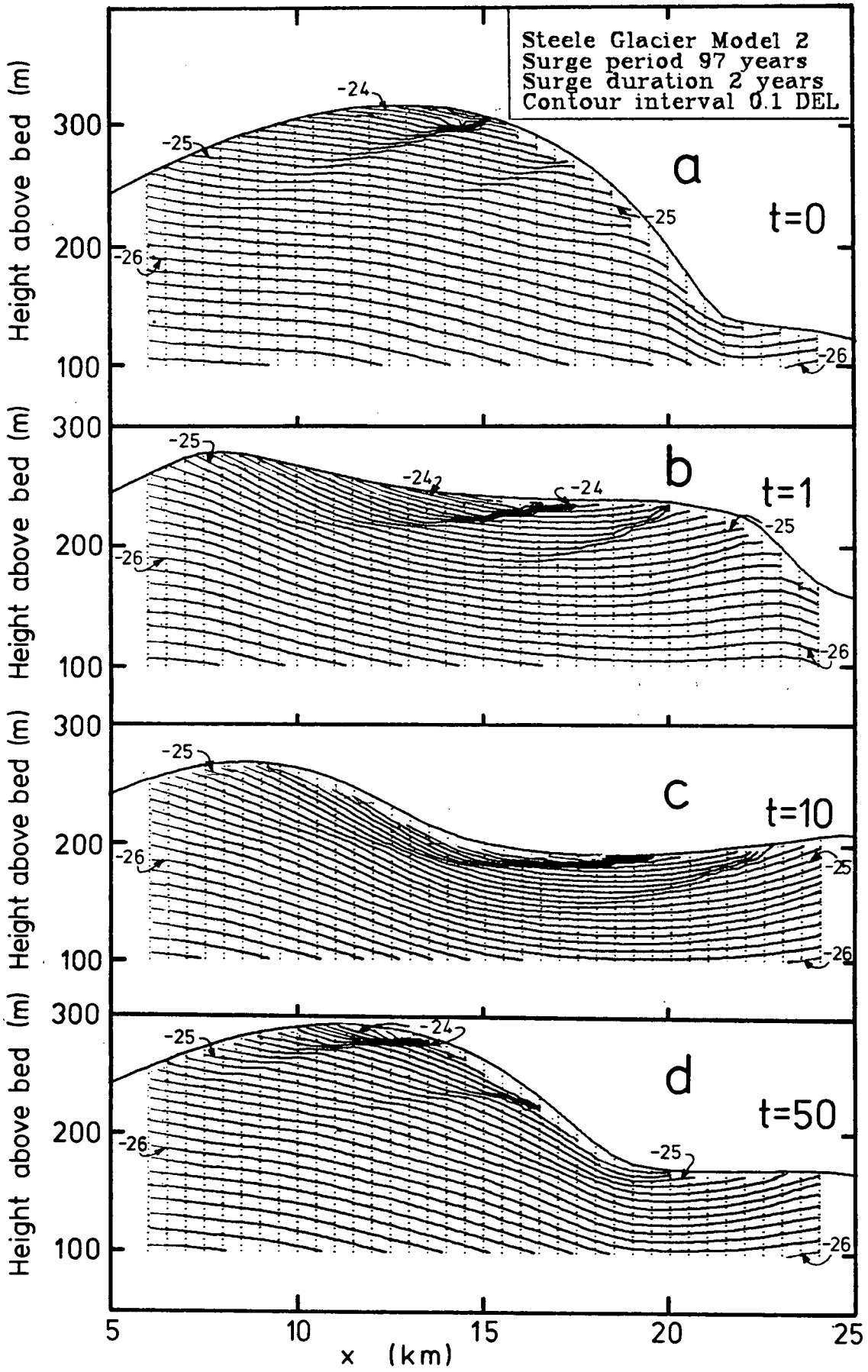
Steele Glacier Model 2
Surge period 97 years
Surge duration 2 years
Contour interval 0.1 DEL
a
t=0
b
t=1
c
t=10
d
t=50
-24
-25
-26
Height above bed (m)
300
200
100
5
10
15
20
25
x (km)

trajectories which passed through the meshpoints at the time of the cross-section. The Model 61 (Section 3.5.4) assumes that the isotopic ratio of precipitation is a linear function of the ice surface elevation. I calculated the trajectories using the velocity evaluated on a mesh (Figure 2.8) with

$$DZ = 15 \text{ m} \qquad \Delta x = 500 \text{ m} \qquad (3.7.1)$$

(The velocity mesh can be coarser than the isotopic mesh because there are no discontinuities in the velocity field). The δ-values for the isotopic mesh were contoured automatically with an interval of $0.1^{o}/_{oo}$.

The only features in the otherwise smooth isotopic distributions are curved lines which intersect the glacier surface and dip upstream into the ice. Crossing one of these lines from above to below, δ decreases by an amount which varies from $0.8^{o}/_{oo}$ or more at the surface near the firn line (x=13 km) to near zero at depth. Each of these lines reveals the present location of ice which was at the surface in the accumulation region at the time a previous surge began. The line generated by the surge cycle shown in Figure 3.15 is not visible until (d) at 50 years. From zero to ten years, the discontinuity is too close to the ice surface and to the edge of the 5 m mesh to be displayed in the contour plots. I discuss the ice surface further in the next section.

To understand the creation and evolution of one of these relict pre-surge surface lines, consider the ice at x=12 km where the $-24^{o}/_{oo}$ contour intersects the ice surface in Figure 3.15 (a). During the surge, this element of ice moves rapidly downstream and to a lower elevation. In (b), it is at

x=8 km. The combined effect of bed slope and ice thinning has lowered this ice element by approximately 100 m, so, using the value of c from (3.5.4), the snow falling on this element of ice has a δ-value of $-23.6^{o}/_{oo}$. At the end of the surge, this ice element is further downstream and still lower; the δ-value of new snow on this element is near $-23^{o}/_{oo}$. A δ discontinuity of the order of $1^{o}/_{oo}$ has been created. As snow accumulates during the quiescent phase, the discontinuity is buried; it is at a depth of 20 m in (d). The magnitude of the δ transition across the relict surface decreases with distance up the glacier, because the sliding velocity during the surge and the amount of surface-lowering also decrease in this direction (see Figures 3.9 and 3.11). After one complete surge, this line is clearly visible in Figure 3.15 (a); it intersects the ice surface at x=15 km. During the subsequent surge (b) and (c), this line is seen to move down the glacier. Since it then intersects the glacier surface in the ablation zone (at x=20 km in (c)), the downstream part, with the largest δ contrast, is rapidly destroyed by melting (d), until, at the start of the third surge cycle (a), all that remains is a slight perturbation of the isodel lines near x=17.5 km.

An isotopic profile in a single borehole would show, at best, a single abrupt decrease of about $0.8^{o}/_{oo}$ to $0.5^{o}/_{oo}$ at the most recent or second most recent relict pre-surge surface. Because this ice is displaced by three to five km during each surge, it is not possible to see more than one discontinuity in a single borehole. A large number of boreholes (5-30) would be required to interpret the δ pattern with reliability and

precision. This would be an expensive field project.

3.7.3 MODEL 61: SURFACE δ PROFILES

A cheap alternative to borehole drilling is detailed surface sampling in the ablation zone. In Figure 3.16, I show the isotopic δ-values along the glacier surface for the same models and the same times as for the cross-sections in Section 3.7.2. The δ-values were poorly determined by the computer model where the profiles are broken. When an ice particle is very near the surface, and its velocity is nearly parallel to the surface, small truncation errors in the normal velocity component (see Section 2.5.3) can cause the trajectory to intersect the ice surface at a large distance from the correct position; this gives an incorrect value for δ. I estimate the error in δ to be $\pm 0.1^{o}/_{oo}$ in this region. Elsewhere, the trajectories intersect the ice surface at larger angles, giving reliable intersection positions and δ-values.

At any given time, isotopic discontinuities due to three previous surges can be seen, diminishing in amplitude from $0.8^{o}/_{oo}$ to $0.2^{o}/_{oo}$ with age. As in the previous section, it is possible to follow the motion of any relict pre-surge surface, this time seeing only where it intersects the present ice surface. The four isotopic peaks and discontinuities labelled t=0, t=1, t=10, and t=50 in Figure 3.16 show the position and the amplitude change across a relict surface during the cycle in which it forms. The discontinuities labelled simply 1, 10, and 50 show how the pattern moves downstream with the ice in the

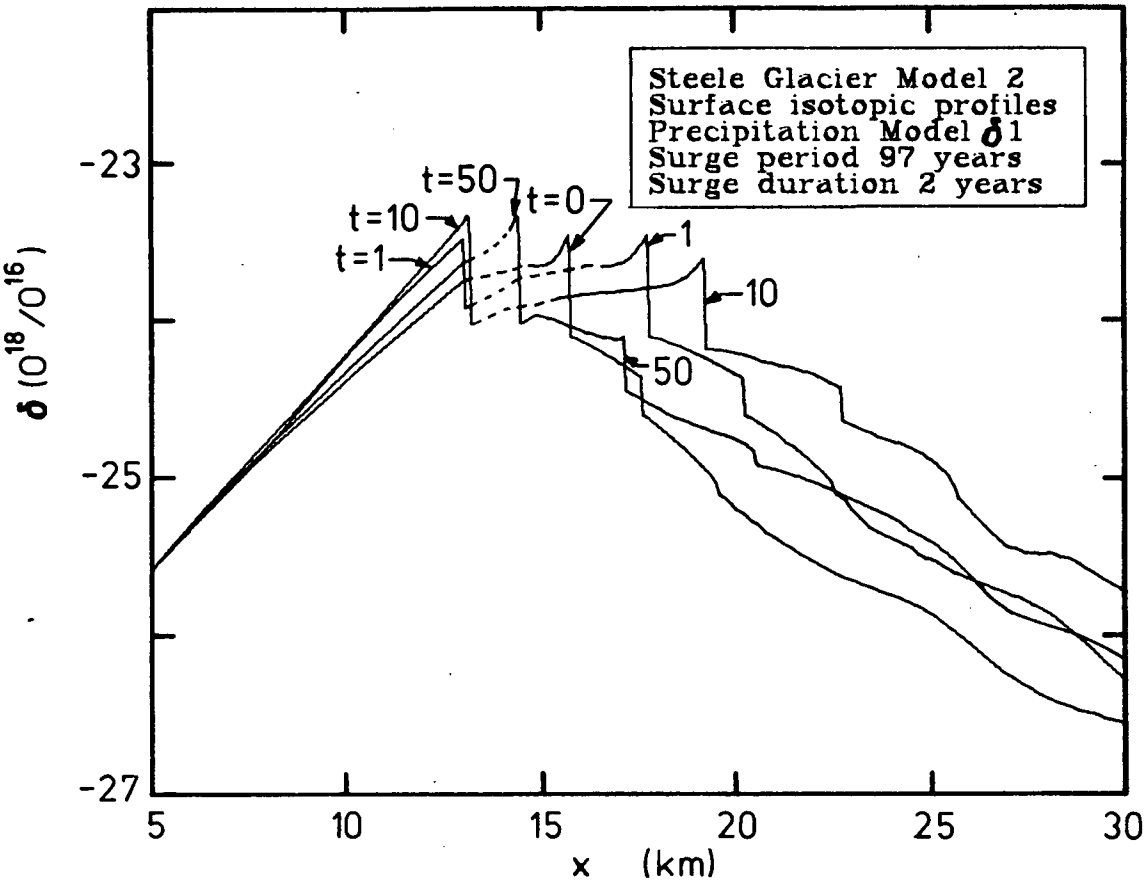

FIGURE 3.16. Model 61: Surface δ Profiles.
δ was calculated at 50 m intervals along the surface of the Steele Glacier model with 97 year surge period (Figures 3.11 and 3.13). The profiles correspond to the longitudinal sections in Figure 3.15. The discontinuities in δ occur where the relict pre-surge surfaces in Figure 3.15 intersect the ice surface. The δ-values may be in error by $\pm 0.1^{o}/_{oo}$ where the lines are broken, due to small vertical velocity errors in trajectories nearly parallel to the surface. The firn line is at x=13 km.

second surge (1 and 10), then how the intersection point retreats back upstream (50) as the shallow downstream portion of the relict surface is melted off.

Information on either surge periodicity, or on ice displacement during previous surges could be derived from a surface isotopic sampling program if Model 61 is appropriate for

the Steele Glacier, and if the background noise in $\delta(O^{18}/O^{16})$ is small. Some shallow coring could help to control the uncertainties in surface intersection points of the relict surfaces; these points may be difficult to locate precisely due to the small angles between ice surfaces and relict pre-surge surfaces.

3.7.4 MODEL 62: SECTIONS AND SURFACE PROFILES

Model 61 assumes that the δ-value of snowfall is determined by the surface height of the ice. In fact, cloud height (and thus δ) is probably strongly influenced by the height of the mountains in the vicinity of the Steele Glacier, and is thus also a function of location x. Figure 3.17 shows isotopic cross-sections at times t=0 and t=10 years using the δ-precipitation Model 62 (Section 3.5.4). The surge period, surface height, velocity field, and trajectories are identical to those used for Figure 3.15; only the relationship between δ and the point of origin of the snow has been changed. Compared to Figure 3.15 (a) and (c), the amplitude of the δ change across each relict pre-surge surface is reduced by a factor of approximately one half, and only the most recent pre-surge surface can be seen plainly.

Figure 3.18 shows the surface δ profiles at the same for times as the profiles in Figure 3.16, using the same flow models, but isotope model 62. The same discontinuities are visible in both figures, but the amplitudes are smaller by a factor of two to three using Model 62. During a surge, ice

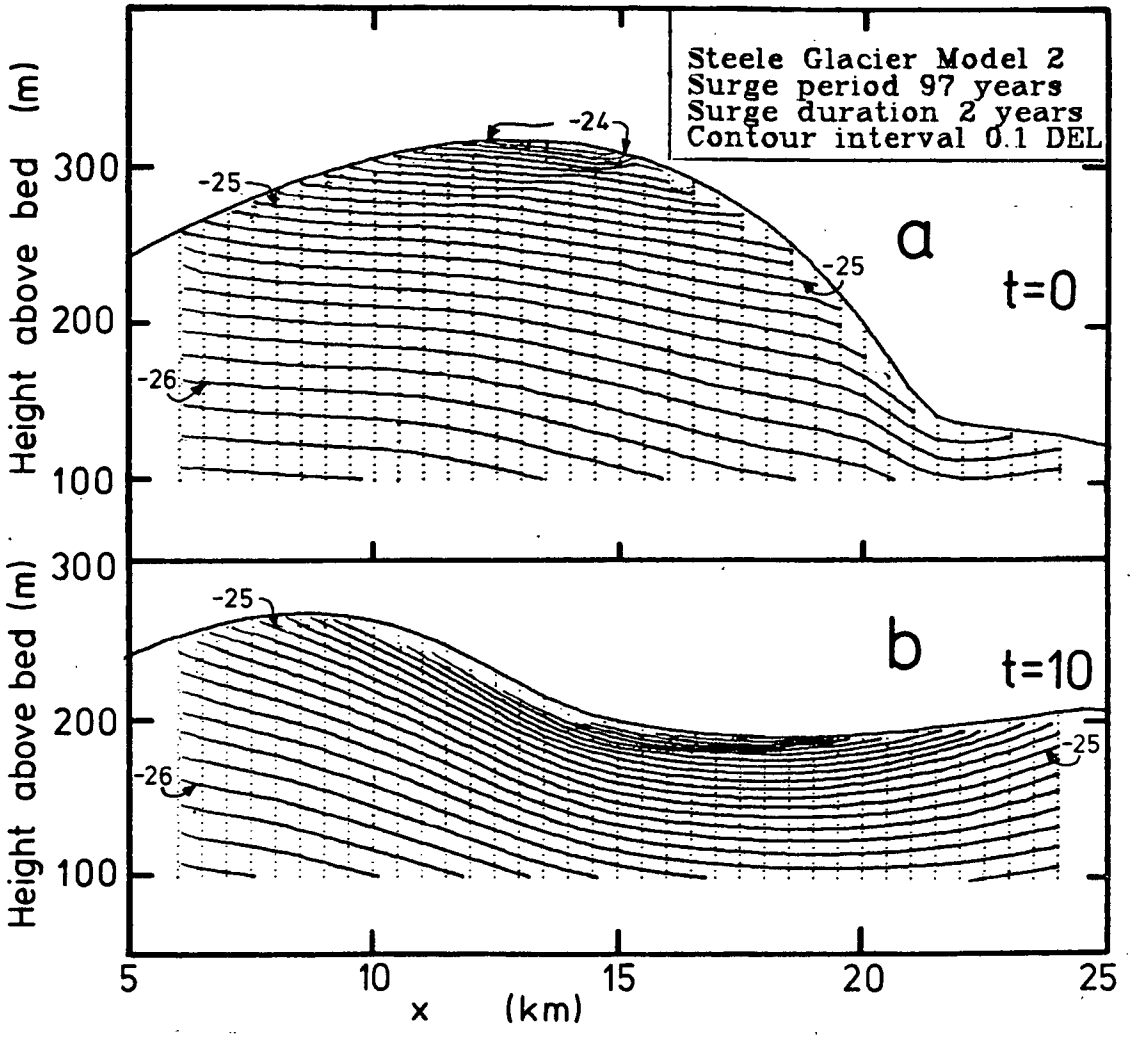

FIGURE 3.17. Model 62: Longitudinal δ Sections.
The isotopic content of precipitation is assumed to depend only on location x. The surge period, surface height, and trajectories are identical to those used for Figure 3.15 (a) and (c). The amplitude of the δ discontinuities is reduced by a factor of 1/3 to 1/2 by the change in precipitation-δ model.
(a) t=0; pre-surge cross-section
(b) t=10 years; 8 years after the end of a surge.

particles on the surface a few kilometres above the firn line both (1) move downstream approximately 3 km, losing roughly 150-200 m of elevation due to the slope of the glacier bed, and (2) are lowered a further 100-120 m by the thinning of the glacier. Both these factors are used to calculate δ with

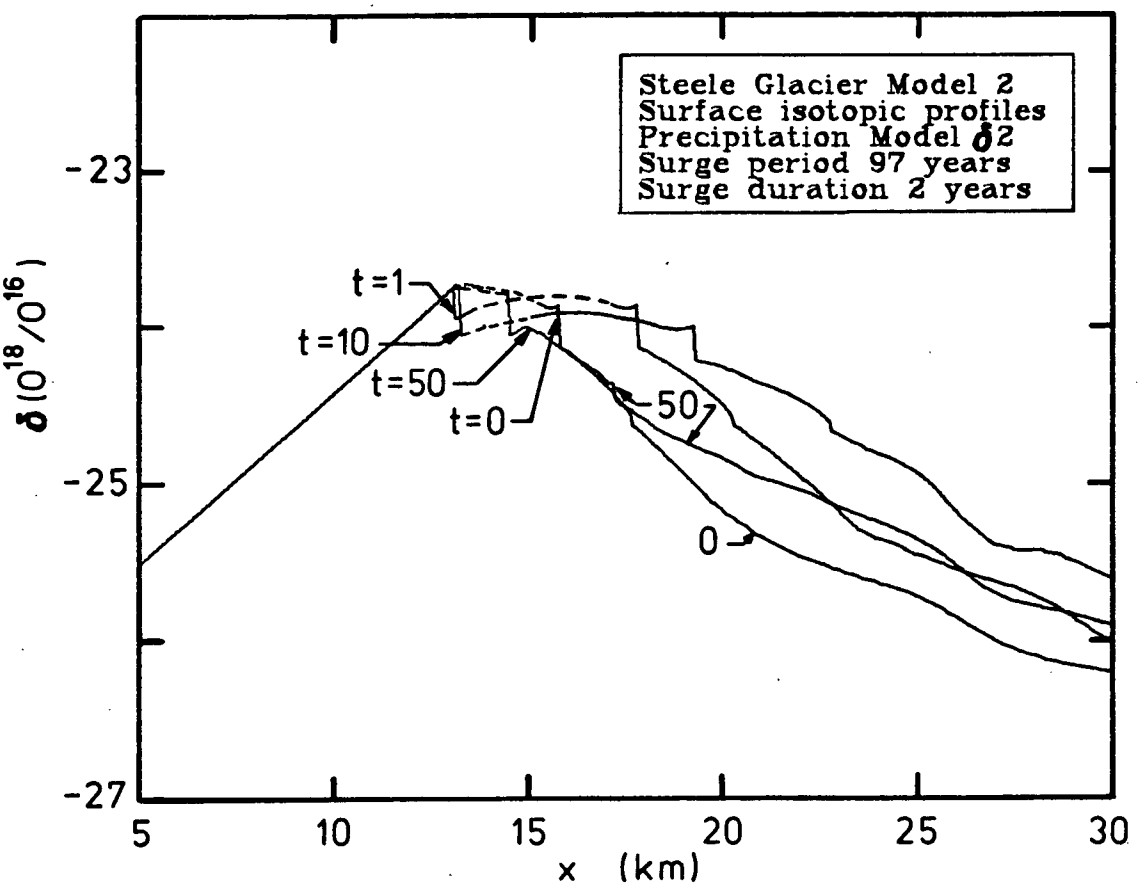

FIGURE 3.18. Model 62: Surface δ Profiles.
Isotopic variations expected on the surface along the central flowline of the Steele Glacier if the δ-value of snow depends only on x. The flow model is identical to that used for Figure 3.16. The amplitude of the δ discontinuities is reduced by approximately 1/2 from the amplitudes in Figure 3.16.

Model 61. With Model 62, the variation of δ with x is based on the elevation drop of an average slope (see Figure 3.8), but δ is considered to be independent of the second factor; hence the δ contrast at the buried pre-surge surfaces is smaller by a factor given, approximately, by the ratio of the height changes considered relevant in the two cases. Since the Steele is a large glacier, its surface height may influence the flow of local air masses. The amplitude of δ discontinuities on the

Steele should fall between the limits set by models δ1 and δ2.

3.7.5 ARE THE PREDICTED EFFECTS OBSERVABLE?

The computational results in Figures 3.15 through 3.18 predict that isotopic features with amplitudes in the range $0.2°/_{oo}$ to $0.8°/_{oo}$ should outline several relict pre-surge surfaces now buried in the ice. This amplitude is an order of magnitude larger than the measurement repeatability error of mass spectrometers (Ahern, unpublished [b], p. 158). The principle obstacle to a successful match of observed δ profiles and numerical predictions is the unknown level of natural background noise in the isotopic distribution. How large are the isotopic effects of (1) meltwater percolation, (2) wind scour and wind-blown deposition of snow, (3) accumulation from avalanches, (4) annual and year-to-year variations of precipitation and temperature, (5) crevassing and shear displacement of seracs during surges, and (6) surging tributaries? The effect of these processes can be evaluated only after systematic data collection on and around the Steele Glacier.

A crude estimate of the background noise level can be obtained from the isotopic profile to a depth of 35 m at x=15 km on the Steele Glacier by Ahern (unpublished [b], p. 162) in 1975, nine years after the start of the 1966-67 surge. Ahern measured δ-values for water samples obtained at intervals of approximately two metres by periodically bailing a hole made by a hot point drill. The data points varied from $-29.8°/_{oo}$ to

$-26.5^{o}/_{oo}$. From the surface to 10 metres depth, the points fall close to a line with slope $-0.1^{o}/_{oo}$ m^{-1}. Below 10 metres, Ahern fit the data with a sawtooth wave with amplitude $\pm 1.5^{o}/_{oo}$ and wavelength 7 metres, and a small amount of scatter. Ahern (unpublished [b], p. 165) suggested that the wave pattern resulted from periodic surging; the computed longitudinal section (Figure 3.15 (c)) at the time and location of this borehole does not support this interpretation. I also calculated the isotopic distribution (not shown) using a tighter mesh (2x100 m) to look for fine structure not found in Figure 3.15 (c); none was found. This same simulation found that the approximate thickness of annual layers in the vicinity of the borehole was 0.5 m. The wavelength seen by Ahern is an order of magnitude too large to be an annual effect, and an order of magnitude too small to be a surge period effect. With the present limited understanding of the isotopes on the Steele Glacier, I can only say that the variations seen by Ahern are a source of noise which could easily obscure the presence of buried pre-surge surfaces. If Ahern's observations can be explained by a simple physical mechanism which allows a prediction of their spatial distribution, amplitude, and phase, then it might be possible to recover the signals due to surges by data filtering methods.

3.7.6 CONCLUSIONS

I have carried out a computer simulation of the flow of the Steele Glacier using a simplified model based on observations of the 1966-67 surge, and on limited surveys and mass balance estimates extending back to the late 1930's. The numerical model is accurate, but due to uncertainties in the data (mass balance, bed topography, flow law constants, shape factor, ice temperature, surge period and surge velocity), I do not expect the model profiles to give more than qualitative information; one figure accuracy in ice depth is the most that can be claimed (no more should be claimed of any simulations of complicated glacier flow).

By comparing surface profiles for a suite of models with differing surge periods, I chose a surge period of 97 years. My calculations of ice trajectories and isotope distributions in this model indicate that it is possible to locate the buried pre-surge surface ice from the accumulation area for the previous one to three surges, by drilling a series of boreholes to a depth of 50 to 100 m in the region from x=10 to x=20 km. Detailed surface sampling along the centreline can also reveal surge-created isotopic discontinuities. If the background isotopic noise is large everywhere on the glacier, then the signal due to surges may be overwhelmed; Ahern's (unpublished [b], p. 162) data show a high noise level. I conclude that the isotopic signal due to surges of the Steele Glacier would be difficult to measure without a much better understanding of the precipitation-δ relationship and the causes

of noise in the isotopic record. The technique may be more feasible on glaciers for which the surge reservoir region (Stanley, 1969) and the accumulation region have a larger overlap.

CHAPTER 4: WAVE OGIVES

4.1. INTRODUCTION

4.1.1 DESCRIPTION OF OGIVE SYSTEMS

Ogives are transverse surface features which form at the rate of one per year at icefalls on some alpine glaciers. Ogives travel downglacier at the surface velocity of the ice, so that the wavelength of an ogive pattern is the distance ice flows in one year. There are two related types of ogives; topographic waves, called "wave ogives", and pairs of alternating light and coloured bands, called "Forbes bands". There are some types of bands on glaciers which do not repeat annually, and are not associated with icefalls. These bands are not considered to be true ogives (e.g. Lliboutry, 1965, p. 386). Ogives occur in many parts of the world e.g. the Alps (Forbes, 1845), Norway (King and Lewis, 1961), Iceland (Ives and King, 1954), Greenland (Atherton, 1963), the Canadian Rockies (Sherzer, 1907, p. 50), the Andes (Lliboutry, 1957; 1958[a]), the Karakoram (Yafeng and Wenying, 1980), the Himalayas (Haefeli, 1957) and Alaska (Leighton, 1951).

Typical wave ogives may have a crest-to-trough amplitude of 10 metres right below the icefall. The amplitude usually decays with distance travelled down the glacier, so that often only 10 to 20 waves are seen. Some wave ogive trains persist, however, for many more years, e.g. Trimble Glacier North Branch, Alaska

Range (frontispiece, p. 2).

Forbes bands were first described by Forbes (1845, p. 162) on the Mer de Glace, although Agassiz (1840, p. 121) may have seen them earlier, in 1833. In French nomenclature, Forbes bands are also called "chevrons", because, due to differential flow, they become convex downglacier. The name "bandes brunes" (e.g. Lliboutry, 1965, p. 338) has also been used. It probably refers to the colour of morainic material often found on the dark bands. The bands often become more visible with distance down the glacier from the icefall.

King and Lewis (1961) who worked on Odinsbreen icefall at Austerdalsbreen, an outlet glacier of Jostedalsbre in western Norway, gave a complete description of the origins of the coloured bands. In their view, crevasses near the top of the Odinsbreen icefall collect dust in summer, and snow in winter. Years later, when these closed and compressed crevasses are below the icefall, they are seen as narrow structural bands (1 - 100 cm thick) of dirty and bubbly ice respectively, extending to a large depth in the glacier. The Forbes bands are the result of variations in the numbers of these narrow structural bands per unit distance down the glacier. Leighton (1951), Lliboutry (1957), and Fisher (1951; 1962) also discussed the likelihood that the structure of ogives extended deep into the ice. On the Mer de Glace, Vallon (unpublished), Reynaud (1979), and Lliboutry and Reynaud (1981) indicate that the colour and structural differences extend to a depth of several hundred metres in the ice immediately downstream of the icefall Séracs du Géant. However, Lliboutry (1958[a]; 1965) reported

that in some circumstances the colouration appeared to be purely surficial rather than continuing into the body of the glacier.

It has long been known that there is some connection between wave ogives and Forbes bands. Tyndall (1874, p. 131) and King and Lewis (1961) associated the dark bands with the troughs of the wave ogives, and the light bands with the crests. Atherton (1963) and Elliston (1957), who worked in a variety of different climatic regimes, associated the dark bands with the leading slopes of the waves.

Since the earliest observations, there has been a tradition of controversy in the literature concerning the origin of the layered structure in ogives. Agassiz (1840, p. 40) thought that all layering and foliation in glaciers was sedimentary in origin, whereas Forbes (1845) realized that this was not true for the bubbly ice and dirt layers of ogives. The controversy persisted into this century. Vareschi (1942), (and reported by Godwin, 1949), using a careful pollen analysis on Grosser Aletschgletscher, attempted to correlate ogives with annual layering in the accumulation zone, but King and Lewis (1961) were able to trace the ogives back to a steep avalanching icefall.

Fisher (1947) suggested that ogives in northern climates were sedimentary in origin, and proposed a category called "Alaskan bands". This interpretation is probably incorrect, and Alaskan ogives are similar to ogives elsewhere.

I propose in this chapter to consider only wave ogives, and these can be modelled on the large scale using mass conservation. Therefore, the controversy about the small scale

processes of crevassing and dirt accumulation does not affect my conclusions.

4.1.2 THEORIES OF WAVE OGIVE FORMATION

Early theories of ogive wave formation (Forbes, 1845; Streiff-Becker, 1952; Haefeli, 1951[a]; 1951[b]; 1957) favoured a seasonally varying longitudinal stress at the foot of the icefall; these variations were assumed to be caused by seasonal changes in the sliding velocity. In fact, in early terminology, wave ogives were called "pressure waves", an unfortunate choice of words that may have biased future thinking on ogive origins.

The pressure mechanism is still a topic of research. Williams (1979) [abstract only] reported a theoretical derivation of wave trains on glaciers as a second order creep effect. Pressure does appear to be the cause of some wave trains on cold glaciers, in particular on Meserve Glacier in Wright Valley, Antarctica (Holdsworth, 1969; Hughes, 1971, 1975). The waves on Meserve Glacier are associated with the glacier terminus rather than with an icefall, so they are not ogives in the classical sense (Lliboutry, 1965, p. 386).

From observations on Austerdalsbreen, however, Nye (1959[a]; 1959[b]) calculated the distribution of stress and found that the ogives there could not be explained by pressure. Nye (1958[b]) proposed another mechanism for creating wave ogives. He showed that annual waves should be expected below an icefall due to the annually periodic nature of the seasonal mass balance, and the large plastic deformations taking place in the

icefall, even when the velocity was independent of time. Vallon (unpublished, p. 51) applied Nye's theory to the generation of ogives by les Séracs du Géant on the Mer de Glace. Martin (1977) showed that this mechanism could also generate kinematic waves at icefalls in response to fluctuations of climate. The Nye theory is the basis of the developments reported in this chapter.

Some authors (Atherton, 1961; Elliston, 1957; Ives and King, 1954; King and Ives, 1956) reported multiple systems of ogives with more than one wave or pair of bands per year. Sharp (1960) reported that the ogive bands on the Blue Glacier, Washington State, USA, were not annual. He attributed the periodicity to the regular passage of serac blocks over the icefall, rather than to annual balance variations. Waves due to serac blocks are seen on the Mer de Glace below Séracs du Géant (Tyndall, 1874, p. 180), and Vallon (unpublished, p.80) found four new waves in a six month period. Washburn (1935) and Fisher (1947) also suggested this mechanism for forming waves. There may be a range of periodic sources or a combination of sources which generate waves, but I will consider only the annual ablation-stretching mechanism.

4.1.3 DISAPPEARANCE OF THE WAVES

The wave crests are free of snow earlier in the melt season (e.g. North Trimble Glacier, frontispiece, p. 2; Gilkey Glacier, Post and LaChapelle, 1971, Plate 66, p. 56) and tend to receive less shadowing than the troughs. Nye (1958[b]) reported 30%

higher ablation on the crests than in the troughs at Austerdalsbreen. Kamb (1964) favoured this mechanism of wave decay. It appears likely, however, that, for some glaciers, there is enough dirt or meltwater in the troughs to cause the ablation there to be just as high as on the crests, due to lowered albedo and increased absorption of solar radiation.

A compressive longitudinal strain rate as the ice slows and thickens below the icefall can lead to amplification of the waves (Nye, 1958[b]). Glen (1958) pointed out that the associated longitudinal stress could effectively soften the ice in the region downstream from an icefall, allowing the waves to decay by flow under their own weight. The presence of the waves themselves also causes a perturbation of the stress field near the ice surface, and Vallon (unpublished, p. 54) suggested that, on the Mer de Glace, the waves may decay in amplitude due to viscous relaxation of the stress perturbation. However, due to the nonlinear rheology of ice, the effective viscosity increases as the waves (and the stress perturbation) decrease. Lick (1970) indicated that this effect increased the relaxation time by an order of magnitude in the case of the Vaughn Lewis Glacier. He concluded that the wave decay was due almost entirely to differential ablation.

The relative importance of these processes on a particular glacier will determine how long the wave train remains visible. I do not model any of these processes in this thesis.

4.2 NYE'S THEORY OF WAVE OGIVES

4.2.1 OUTLINE OF THE NYE THEORY

To give a concise and lucid description of Nye's wave producing mechanism, I quote from the abstract to Nye (1958[b]):

> "The widely held theory that the waves are the result of pressure requires that the forward velocity of the ice U, depends both on distance x down the glacier and on the time t. The simpler case where U depends only on x is treated analytically, and it is found that, owing to the essentially periodic nature of the ablation, even this case gives waves. All elements are stretched out as they pass through the icefall, owing to the high local velocity, and they therefore present greater surface area. Those passing through the icefall in the summer therefore lose more ice by ablation than those which spend the summer in regions of lower velocity. Waves are thus produced by a combination of plastic deformation and ablation."

Washburn (1935) also suggested that the annual mass balance cycle could cause wave ogives, but he did not attempt to formulate the principle mathematically. He attributed the troughs to increased summer melt made possible by an increased exposed surface area due to shattering in the icefall, whereas Nye (1958[b]) attributed the greater surface area to thinning in regions of rapid flow.

4.2.2 NYE'S ANNUALLY REPEATING STATE SOLUTION

Since the wavelength of wave ogives where they become visible below an icefall rapidly becomes less than the ice thickness (due to compressive flow), the waveforms are too short to propagate as kinematic waves (Nye (1958[b]) discussed this possibility), and essentially the waves do not perturb the flow. This is consistent with the assumption that U(x) is independent

of time, i.e.

$$\frac{\partial U}{\partial t} = 0 \qquad (4.2.1)$$

The waves are simply carried forward at the velocity of the ice surface, which is treated strictly as a "conveyor belt" in this theory. Nye defined an Annually Repeating State (A.R.S.) by

$$h(x,t) = h(x,t+1) \qquad (4.2.2)$$

for time measured in years, and used the continuity equation (1.3.5) repeated here as (4.2.3)

$$\frac{\partial h}{\partial t}(x,t) + \frac{1}{W(x)} \frac{\partial Q}{\partial x}(x,t) = A(x,t) \qquad (4.2.3)$$

where h is ice thickness, W(x) is the transverse width, A(x,t) is the mass balance rate, and Q is the ice flux given by

$$Q(x,t) = h(x,t)\ U(x)\ W(x) \qquad (4.2.4)$$

U(x) is the forward velocity of the ice. Because the theory concerns regions of thin and rapidly sliding ice, the difference between V(x) of (1.4.38), the average velocity through a column, and u(x,h), the surface velocity from (1.4.34), is very small. U(x) may be identified with the ice surface velocity.

For unit width following a section of ice moving at U(x), introducing the total derivative DQ/Dx (e.g. Malvern, 1969, p. 211) and using the assumption (4.2.1), Nye found

$$\frac{DQ}{Dx}(x,t) = A(x,t) \qquad (4.2.5)$$

Nye assumed that, at Austerdalsbreen, where Odinsbreen icefall is in the ablation zone, the amount of winter snowfall was unimportant to the wave generation process, being merely a protective covering for the true glacier surface. To simplify the analysis, he also assumed that the net annual ablation of

ice occurred instantaneously each year at time t_o, i.e.

$$A(x,t) = b(x) \sum_{n=-\infty}^{\infty} \delta(t-t_o+n) \qquad (4.2.6)$$

where $\delta(t)$ is the Dirac delta function (e.g. Morse and Feshbach, 1953, p. 122), n is an integer, and b(x) is the net annual balance given by

$$b(x) = \int_0^1 A(x,t)\, dt \qquad (4.2.7)$$

He then derived a recursion relation for the glacier thickness profile h(x) in an A.R.S. immediately after the ablation at t_o

$$h(x) = \frac{U(x-\lambda)}{U(x)}\, h(x-\lambda) - b(x) \qquad (4.2.8)$$

for ice that was at position $(x-\lambda)$ one year previously. Assuming an input ice thickness at the origin x=0 (13.8 m and constant with time for Odinsbreen icefall), Nye used (4.2.8) to predict the wave pattern at Austerdalsbreen. The spatial balance b(x) and the surface velocity U(x) shown in Figure 4.1 (redrawn from Nye, 1958[b]), were a fit to the observations of the Cambridge Austerdalsbreen Expedition.

The agreement between the observed and the predicted waves was good, except for the decay of the waves (which the theory does not attempt to predict), and the sharpness of the troughs, which resulted from the assumption (4.2.6). The ablation season at Austerdalsbreen actually lasts about three months (Nye, 1958[b]).

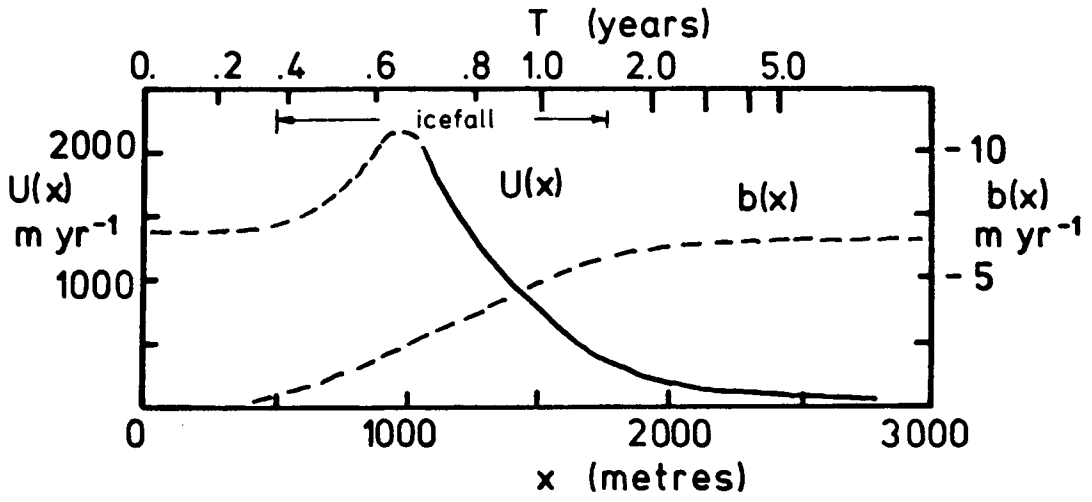

FIGURE 4.1. Austerdalsbreen Velocity And Mass Balance. Odinsbreen icefall: curves redrawn from Nye (1958[b]). T(x) is the time in years for ice to flow from the origin to position x.

4.2.3 OGIVES ABOVE THE FIRN LINE

Fisher (1962) thought that the head of an icefall that generated ogives had to be at or below the firn line. This is now known to be incorrect. Post and LaChapelle (1971, plate 68, p. 57) showed distinct wave ogives in firn on the Grand Pacific Glacier, Fairweather Range, British Columbia, and Atherton (1963) reported wave ogives in the accumulation zone of Eldridge Glacier, Alaska. Atherton thought that Nye's (1958[b]) theory was inadequate above the firn line, perhaps because he thought that the instantaneous mass balance form (4.2.6) was essential to the theory. In fact, it is not, and Nye (1959[a]) pointed out that a related process would produce waves above the firn line. (Atherton also thought that, by Nye's theory, the wavelength of ogives should increase going down an icefall above the firn

line. He must have misunderstood some aspect of the theory, because the wavelength is related to the velocity U(x) and not to the mass balance.)

Above the firn line, the ratio of winter accumulation to summer melt is important to the wave generation process, and the mass balance in the vicinity of the icefall might be better expressed, to a first approximation, as the sum of the net annual mass balance $\overline{x}(x)$ and an annual variation T(t) independent of x, so that

$$A(x,t) = \overline{x}(x) + T(t) \qquad (4.2.9)$$

This simple function will generate wave ogives above the firn line by Nye's mechanism.

4.2.4 AN UNANSWERED QUESTION

The ablation-plastic deformation mechanism is capable of producing very large waves. The question which is often asked (e.g. Post and LaChapelle, 1971, p. 57) is why large ogives are not present below many active icefalls? In particular (Nye,1958[b], p. 153), why are waves from the ablation-plastic stretching mechanism absent?

In Section 4.3, I solve the continuity equation (4.2.3) in a manner that answers this question.

4.3 A NEW SOLUTION FOR OGIVES

4.3.1 USING METHOD OF CHARACTERISTICS

In this section, I solve the continuity equation (4.2.3) with velocity U(x) independent of time (4.2.1), in a more general form. The solution includes the wave ogives caused by the mechanism Nye described.

Multiplying the continuity equation (4.2.3) by U(x) and by W(x) gives

$$\frac{\partial Q}{\partial t}(x,t) + U(x)\,\frac{\partial Q}{\partial x}(x,t) = A(x,t)\,U(x)\,W(x) \qquad (4.3.1)$$

I used (4.2.1) and (4.2.4) to take all the factors inside the time derivative.

Now I change the distance variable x to a new variable T(x), the time required for ice to flow from the origin (x=0) to position x, travelling at the ice velocity U(x).

$$T(x) = \int_0^x \frac{ds}{U(s)} \qquad (4.3.2)$$

Nye also used this transformation when evaluating (4.2.8). (When the variable T is used, λ becomes unity.)

Using the chain rule gives

$$U(x)\,\frac{\partial Q}{\partial x}(x,t) = \frac{dx}{dT}\,\frac{\partial Q}{\partial x}(x,t) = \frac{\partial Q}{\partial T}(T,t) \qquad (4.3.3)$$

so that (4.3.1) becomes

$$\frac{\partial Q}{\partial t}(T,t) + \frac{\partial Q}{\partial T}(T,t) = A(T,t)\,U(T)\,W(T) \qquad (4.3.4)$$

This equation is readily solved by the method of characteristics (e.g. Whitham, 1974, p. 19) to give

$$\frac{dQ}{dT} = A(T,t)\ U(T)\ W(T) \tag{4.3.5}$$

along the characteristic curves

$$\frac{dT}{dt} = 1 \tag{4.3.6}$$

or

$$T = t - \phi \tag{4.3.7}$$

These characteristics are straight lines at 45° to both axes in the T-t plane, Figure 4.2. They are the space-time trajectories

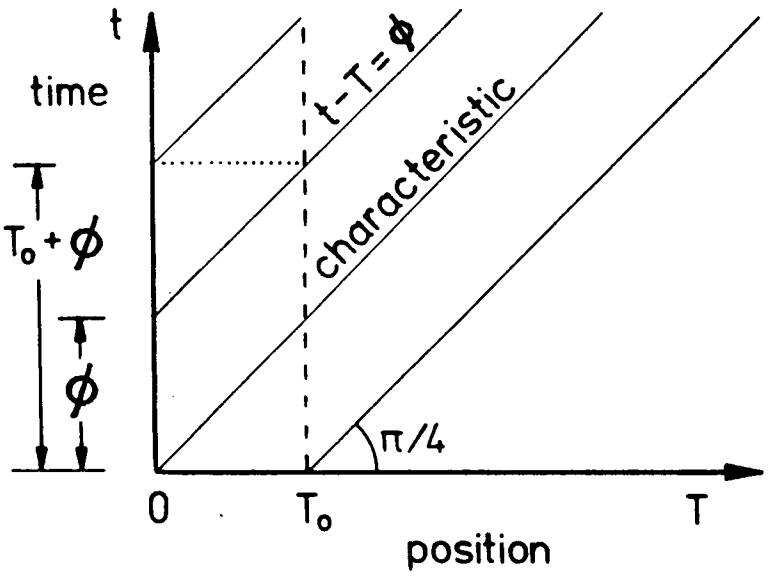

FIGURE 4.2. The Characteristics In T-t Space.
T(x) is the time taken by ice to flow from the origin to x, so it measures position on the glacier, and t is time. Each characteristic, representing the trajectory of an ice column, is parameterized by ϕ, the time the ice passed the origin T=0.

of the vertical ice columns. Each characteristic is labelled by a value of ϕ, the time when that ice passed the origin x=0.

The equation (4.3.5) is a single total derivative in one variable T. It is quite similar to equation (4.2.5) used by Nye (1958[b]). It is easily integrated to give

$$Q(T,T+\emptyset) - Q(T_o,T_o+\emptyset) = \int_{T_o}^{T} A(s,s+\emptyset)\ U(s)\ W(s)\ ds \qquad (4.3.8)$$

where T_o is a reference position where the boundary condition is applied.

Now I want to show that the solution (4.3.8) contains terms of the form Q(t-T), which are waveforms travelling down the glacier at the speed of the ice, i.e. at one year's flow distance per year. I also need to show that this propagating solution has a spatial periodicity of one year's flow distance below the icefall.

4.3.2 SEPARABLE MASS BALANCE

To proceed further, I will assume that the mass balance A(T,t) is separable into the summation

$$A(T,t) = \sum_{i=1}^{N} x_i(T)\ T_i(t) \qquad (4.3.9)$$

This form includes, as a special case,

$$A(T,t) = \bar{x}(T)\ T(t) \qquad (4.3.10)$$

where the annual cycle T(t) is weighted by the annual net balance $\bar{x}(T)$ at each position T. The mass balance (4.2.6) that Nye used for Austerdalsbreen had this form.

It also includes the special case (4.2.9) which I discussed

in connection with waves above the firn line. In this case, an annual cycle T(t) is added to the annual net balance.

It is possible to introduce travelling waveforms into the solution through propagating mass balance waves having the form

$$A(T,t) = b(T-t) \qquad (4.3.11)$$

when N is larger than unity in (4.3.9). In fact, the disappearance of the wave ogives (see Section 4.1.3) can be represented by such a term; zones of excessive ablation rate may propagate down the glacier so as to remain on wave crests. However, I have not included this effect in the examples I show. Any propagating waves formed between T_0 and T in the examples arise from the ablation-stretching mechanism.

Because (4.3.8) is linear in the mass balance, the summation in (4.3.9) will carry through all the linear operations which follow. To keep the expressions as simple as possible, I can consider the case N=1, and drop the subscripts, without loss of generality.

It will be useful, subsequently, to define a function B(t) which is an integral of the temporal variation T(t) of the mass balance.

$$B(t) = \int_0^t T(s)\, ds \qquad (4.3.12)$$

4.3.3 THE GENERALIZED VELOCITY

To simplify the appearance of the equations, I will define a 'generalized velocity function' v(T)

$$v(T) = U(T)\ W(T)\ x(T) \qquad (4.3.13)$$

which comprises the total spatial dependence of the integrand in (4.3.8). I have called it a velocity because, of the three factors, U(T) is likely to have the largest relative changes in an icefall.

4.3.4 THE UPSTREAM BOUNDARY CONDITION

In this section, I derive an expression for the input flux at the upstream boundary $T=T_o$.

By substituting the mass balance (4.3.9) into the flux continuity equation (4.3.4) evaluated at the boundary T_o, I get

$$\frac{\partial Q}{\partial t}(T_o,t) = v(T_o)\ T(t) - \frac{\partial Q}{\partial T}(T_o,t) \qquad (4.3.14)$$

Integrating this from time zero to time

$$t = T_o + \emptyset \qquad (4.3.15)$$

i.e. up the vertical boundary line at T_o in the T-t plane (Figure 4.2), gives

$$Q(T_o,T_o+\emptyset) = Q(T_o,0) + v(T_o)B(T_o+\emptyset) - \int_0^{T_o+\emptyset} \frac{\partial Q}{\partial T}(T_o,s)ds \qquad (4.3.16)$$

This is the input flux at the boundary T_o for the characteristic $\emptyset$. It is composed of three terms. The first is a constant which may be thought of as a datum flux, the flux which was crossing

the boundary T_0 at time t=0.

The second term is the change in flux at the boundary due to the synchronous rise and fall B(t) of the whole surface in response to the seasonal changes.

The final term is a function of $\emptyset=[t-T]$, so it represents a waveform travelling at the speed U(x) of the ice. It gives the flux changes at the boundary due to advection of spatial variations across the boundary.

4.3.5 THE TERMS OF THE FLUX SOLUTION

When I substitute the mass balance (4.3.9) into the flux solution (4.3.8) using the generalized velocity (4.3.13), I get

$$Q(T,T+\emptyset) - Q(T_o,T_o+\emptyset) = \int_{T_o}^{T} T(s+\emptyset)\, v(s)\, ds \qquad (4.3.17)$$

Using integration by parts on the right side,

$$Q(T,T+\emptyset) - Q(T_o,T_o+\emptyset)$$

$$= \left[v(s) \int_{T_o}^{S} T(s+\emptyset)ds \right]_{S=T_o}^{T} - \int_{T_o}^{T} \frac{dv(s)}{dT} \left[\int_{T_o}^{S} T(r+\emptyset)dr \right] ds \qquad (4.3.18)$$

Evaluating the first expression on the right at its limits, and recalling the definition (4.3.12) of B(t),

$$Q(T,T+\emptyset) - Q(T_o,T_o+\emptyset)$$

$$= v(T)[B(T+\emptyset) - B(T_o+\emptyset)] - \int_{T_o}^{T} \frac{dv}{dT}(s)[B(s+\emptyset) - B(T_o+\emptyset)]ds \qquad (4.3.19)$$

Taking the second term in the integrand outside the integral, substituting the boundary condition (4.3.16), and setting $T+\emptyset=t$ from (4.3.7), two terms cancel, and

$$Q(T,t) = Q(T_o,0) - \int_{0}^{T_o+(t-T)} \frac{\partial Q}{\partial T}(T_o,s)\, ds$$

$$+ v(T)\, B(t) - \int_{T_o}^{T} \frac{dv}{dT}(s)\, B(s+[t-T])\, ds \qquad (4.3.20)$$

If the summation is carried through from (4.3.9),

$$Q(T,t) = Q(T_o,0) - \int_{0}^{T_o+(t-T)} \frac{\partial Q}{\partial T}(T_o,s)\, ds$$

$$+ \sum_{i=1}^{N} v_i(T)\, B_i(t) - \sum_{i=1}^{N} \int_{T_o}^{T} \frac{dv_i}{dT}(s)\, B_i(s+[t-T])\, ds \qquad (4.3.21)$$

To find the waves in the ice thickness profile h(T,t), divide through by U(T). To see the waves as a function of distance x rather than the travel time T, stretch the T axis by the inverse transformation to (4.3.2), i.e.

$$x(T) = \int_0^T U(s)\, ds \qquad (4.3.22)$$

4.3.6 PHYSICAL INTERPRETATION

The equation (4.3.21) is the complete solution for the flux at all times t and positions $T>T_0$ with the assumptions

1) velocity is independent of time (4.2.1), and

2) mass balance is separable (4.3.9).

The first two terms were discussed in Section 4.3.4. The first term is the datum flux that existed at the origin at time t=0. It has no effect on the generation of waves.

The second term is the advection of spatial flux variations $\partial Q/\partial T$ across the boundary at T_0. If waves exist above T_0, this term will represent their propagation through the region of interest. Nye's assumption of constant velocity and ice thickness above the Austerdalsbreen icefall eliminated this effect from his analysis. I will also avoid introducing waves through the boundary condition in the examples I show.

The third term represents the synchronous rise and fall of the whole glacier surface due to the changing seasons. There can be no propagating wave of the form Q(t-T) from this term.

The final term contains the ogive waves. It is a function of the limits T_0 and T, and of [t-T], the phase shift of the balance integral B(t).

$$P(T_o,T,[t-T]) = \int_{T_o}^{T} \frac{dv}{dT}(s)\ B(s+[t-T])\ ds \qquad (4.3.23)$$

The dependence on [t-T] indicates that this term contains a disturbance propagating in the positive direction at the same speed as the ice.

If the annual balance variation T(t) is cyclic with a period of one year, then so is its integral B(t) (4.3.12), to within a linear trend which is made zero by a suitable choice of the terms in (4.3.9), i.e.

$$B(t) = B(t+1) \qquad (4.3.24)$$

This suggests that the propagating disturbance (4.3.23) also has a strong periodic component at one year. For example, if I consider a region below the icefall where the generalized velocity is constant, then the upper integration limit of (4.3.23) can be put to ∞, and substituting (4.3.24) into (4.3.23) shows that

$$P(T_o,T+1,[t-T+1]) = P(T_o,T,[t-T]) \qquad (4.3.25)$$

i.e. that the propagating disturbance is a wave that repeats with a period of one year's flow distance.

The wave term (4.3.23) has the physical interpretation that any incremental step change δv in the generalized velocity at position T_1, or, equivalently, an impulse of strength δv in the velocity gradient, generates a set of waves downstream given by

$$G([t-T];T_1) = \delta v\ B(T_1+[t-T]) \qquad (4.3.26)$$

Nye (1958[b]) illustrated the wave generating mechanism by

an example of an A.R.S. shown in Figure 4.3 (redrawn from Nye (1958[b]). The ice velocity (curve(a)) is doubled from U_0 to

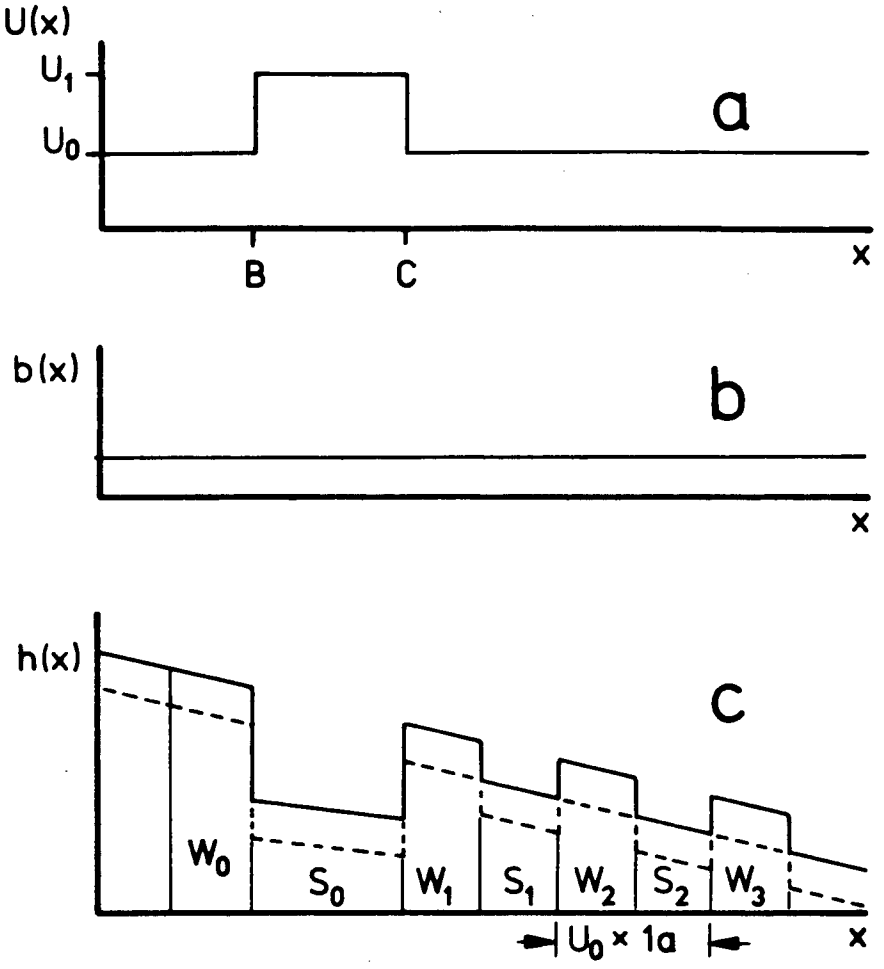

FIGURE 4.3. Double Step Icefall Model.
The ice travels the distance BC in 6 months. The mass balance is applied instantaneously each year.
(a) the ice velocity.
(b) the average annual mass balance.
(c) solid curve: ice thickness just before ablation.
broken curve: immediately after ablation.

$U_1=2U_0$ between B and C. The ice travels this distance in six months. The mass balance function (curve (b)) is spatially

constant, and is applied instantaneously each year at the same time. The resulting ice thickness (Figure 4.3 (c)) immediately before the ablation occurs is shown by the solid line. The ice thickness immediately after ablation is shown by the broken line. The volume elements S_0 and W_0 are nearly equal before ablation. S_0 is on the fast section BC during the summer ablation, and W_0 is not. The square waves result from the fact that the ablation removes approximately twice as much mass from the element S_0 as from the elements W_0 and W_1 on either side, because S_0 has approximately twice as much surface area exposed to ablation. Downstream, the volumes S_j which were in the icefall in summer are shorter than the elements W_j, and so form troughs.

However, the result (4.3.26) indicates that there is an even simpler wave generating model. If the velocity merely increases or decreases, but not both, waves are still generated. This model is shown in Figure 4.4 for a decreasing velocity step from U_0 to $U_1=U_0/2$, with an instantaneous mass balance. As before, the solid curve in (c) is the ice thickness just before ablation, and the broken curve is immediately after.

In this case, the ablation removes twice the volume from the column A_0, immediately upstream from the velocity decrease, as from the column B_0 of equal volume immediately below. Later, when both A_0 and B_0 have moved downstream, and are travelling at the same velocity, B_0 will be higher than A_0. A new discontinuity is generated in this way every year, giving the sawtooth pattern.

From the definition (4.3.13) of the generalized velocity

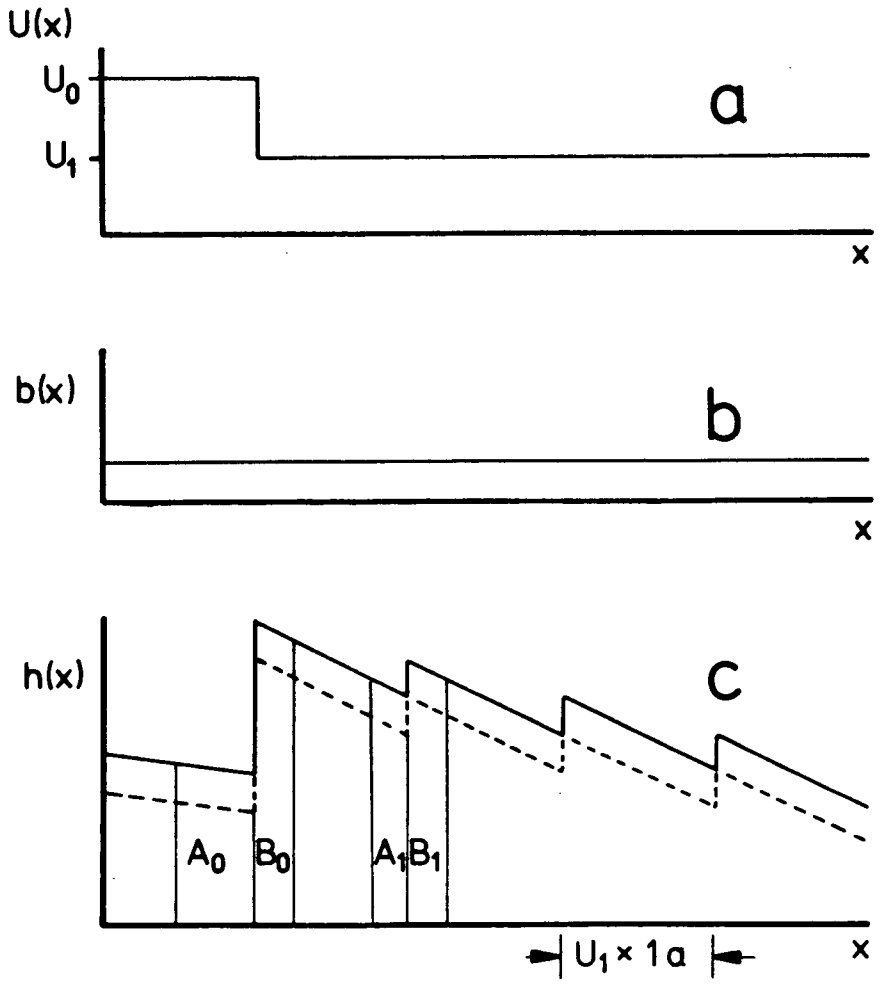

FIGURE 4.4. Single Velocity Step Model.
(a) the ice velocity.
(b) the average annual mass balance.
(c) solid curve: ice thickness just before ablation.
broken curve: immediately after ablation.
The mass balance is applied instantaneously each year.

gradient, it is apparent that spatial changes in the mass balance and in the channel width contribute annual waves in the same manner as do velocity changes. However, the relative changes in these factors on actual glaciers are usually less than the relative velocity changes in an icefall. Nye (1958[b]) mentioned waves due to changes in mass balance with x. A theory was presented at a meeting of the British Glaciological Society,

November 1, 1957.

These three factors would be expected to influence the wave amplitude on simple physical grounds. If I consider the ice in terms of vertical prisms, then the waves arise because the mass balance removes or adds a different amount to prisms immediately above and below the position $x(T_1)$ (To relate x to T, see the transformation (4.3.22)).

As illustrated in Figure 4.5 (a), a change of velocity achieves this by stretching the ice prism in the downstream direction to expose a different surface area.

A change in glacier width achieves this by stretching the ice prism laterally (Figure 4.5 (b)) to expose a different surface area.

A change in mass balance achieves this by removing ice to a different depth in prisms presenting equal surface area (Figure 4.5 (c)).

Of course, a longer ablation season would generate smoother waves.

Overleaf:
FIGURE 4.5. Three factors generating waves.

(a) a change of velocity U(x). W(x) and x(x) are constant.
(b) a change of width W(x). U(x) and x(x) are constant.
(c) a change of mass balance x(x). U(x) and W(x) are constant.
The mass balance is assumed to be applied instantaneously for the purpose of illustration. The A.R.S. profiles are shown immediately before the ablation is applied. The shaded volumes indicate the mass about to be ablated from previously equal volumes of ice above and below the transition point $x(T_1)$.

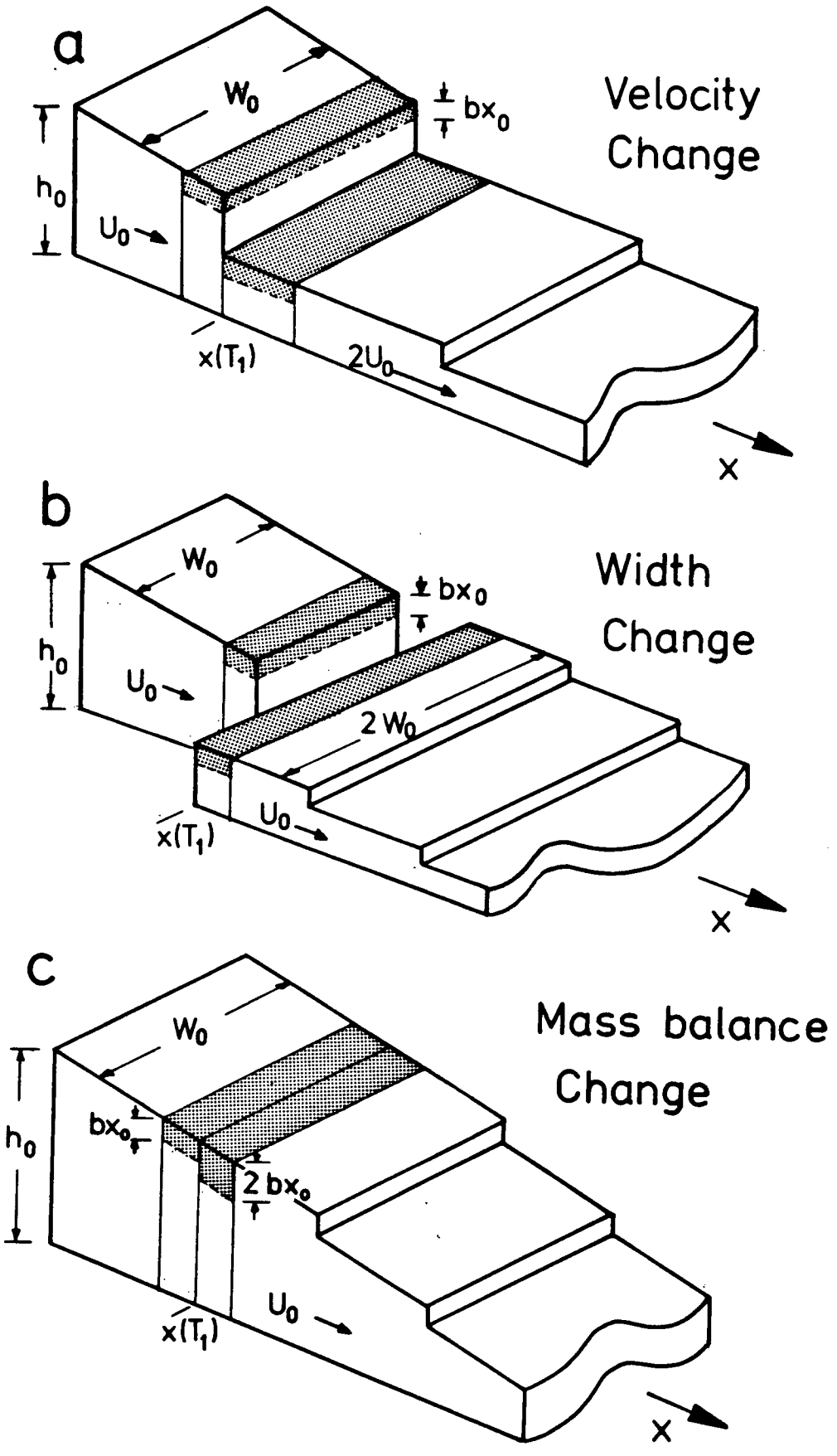
a
W0
± bx0
h0
U0
x(T1)
2U0
x
Velocity
Change
b
W0
± bx0
h0
U0
2 W0
x(T1)
U0
x
Width
Change
c
W0
h0
bx0
2 bx0
U0
x(T1)
x
Mass balance
Change

4.3.7 THE GREEN'S FUNCTION FOR OGIVES

The function (4.3.26) is the Green's function (e.g. Morse and Feshbach, 1953, p. 791) or impulse solution for wave ogives. The total resultant wave pattern (4.3.23) is the integral of the Green's function over the whole upstream region where the generalized velocity varies.

The reason that annual waves are not seen on all glaciers is that all the small waves due to spatial changes in velocity, mass balance, or channel width tend to have differing phase, which makes them interfere destructively. Only on glaciers where the spatial changes are large and localized, such as in an icefall, can these waves add together constructively to give visible ogives.

4.3.8 A CONVOLUTION FORMULATION FOR OGIVES

If I define a reversed cumulative balance function $B_r(t)$ by

$$B_r(t) = B(-t) \tag{4.3.27}$$

and if the generalized velocity $v(T)$ is constant above the boundary T_0 and below the observation point T, the ogive term (4.3.23) takes the standard form of a simple linear convolution (with variable $[t-T]$), of the time-dependent term B_r with the spatial velocity gradient term dv/dT.

$$P(t-T) = \int_{-\infty}^{\infty} \frac{dv}{dT}(s)\, B_r([t-T]-s)\, ds \tag{4.3.28}$$

The theory of convolutions, and algorithms to do convolutions, are widely known. For example, the velocity gradient dv/dT may

be treated as a smoothing filter applied to the wave term B_r.

If the velocity gradient is nonzero downstream from T, the truncated convolution with finite limits must be used for the exact solution. If the gradient below T is small, or is uniform for a large distance, however, the convolution (4.3.28) is a good approximation, because a small, uniform gradient has little effect on wave generation. I shall illustrate this in the next section. The only effect of a small negative velocity gradient is to cause longitudinal compression. This amplifies existing waves expressed in terms of ice thickness and has no effect on waves expressed in terms of ice flux.

4.4 SOME SIMPLE EXAMPLES

4.4.1 INTRODUCTION

I shall consider two very simple types of generalized velocity changes, and use the convolution equation (4.3.28) to illustrate how destructive interference can occur, even on active icefalls, to prevent the formation of observable waves. Combinations of these simple velocity patterns can be applied to any icefall to get a rough but easy estimate of the expected ogive wave amplitude.

4.4.2 EXAMPLE: LINEAR VELOCITY GRADIENT

Equation (4.3.26) showed that the simplest feature generating wave ogives is an impulsive velocity change from v_0 to v_1. A generalization of this step change is a constant velocity gradient from v_0 at T_0 to v_1 at T_1, a distance I will call τ, as shown in Figure 4.6 (b).

The velocity gradient dv/dT in Figure 4.6 (b) is a "boxcar" function of length τ.

$$\frac{dv}{dT} = \begin{cases} \dfrac{v_1 - v_0}{\tau} & T_0 < T < T_1 \\ 0 & T < T_0 \text{ or } T > T_1 \end{cases} \qquad (4.4.1)$$

Some general results for this velocity gradient are immediately apparent. First, the wave amplitude will, in general, tend to decrease as the gradient decreases, i.e. as τ lengthens, or as v_0 approaches v_1. Second, because convolution using (4.4.1) is (except for a constant factor) just a running average over a distance τ, (4.3.28) must be identically zero whenever τ is an integer and the mass balance integral B(t) is

---

Overleaf:
FIGURE 4.6. Ogives from a velocity gradient.
T is a measure of distance downglacier, and t is time.
(a) Generalized velocity.
(b) Generalized velocity gradient.
(c) Mass balance.
(d) Normalized crest-to-trough wave amplitude as function of τ, the spatial extent of the gradient. The solid triangles are the amplitude of waves in numerical solutions (Figure 4.7).

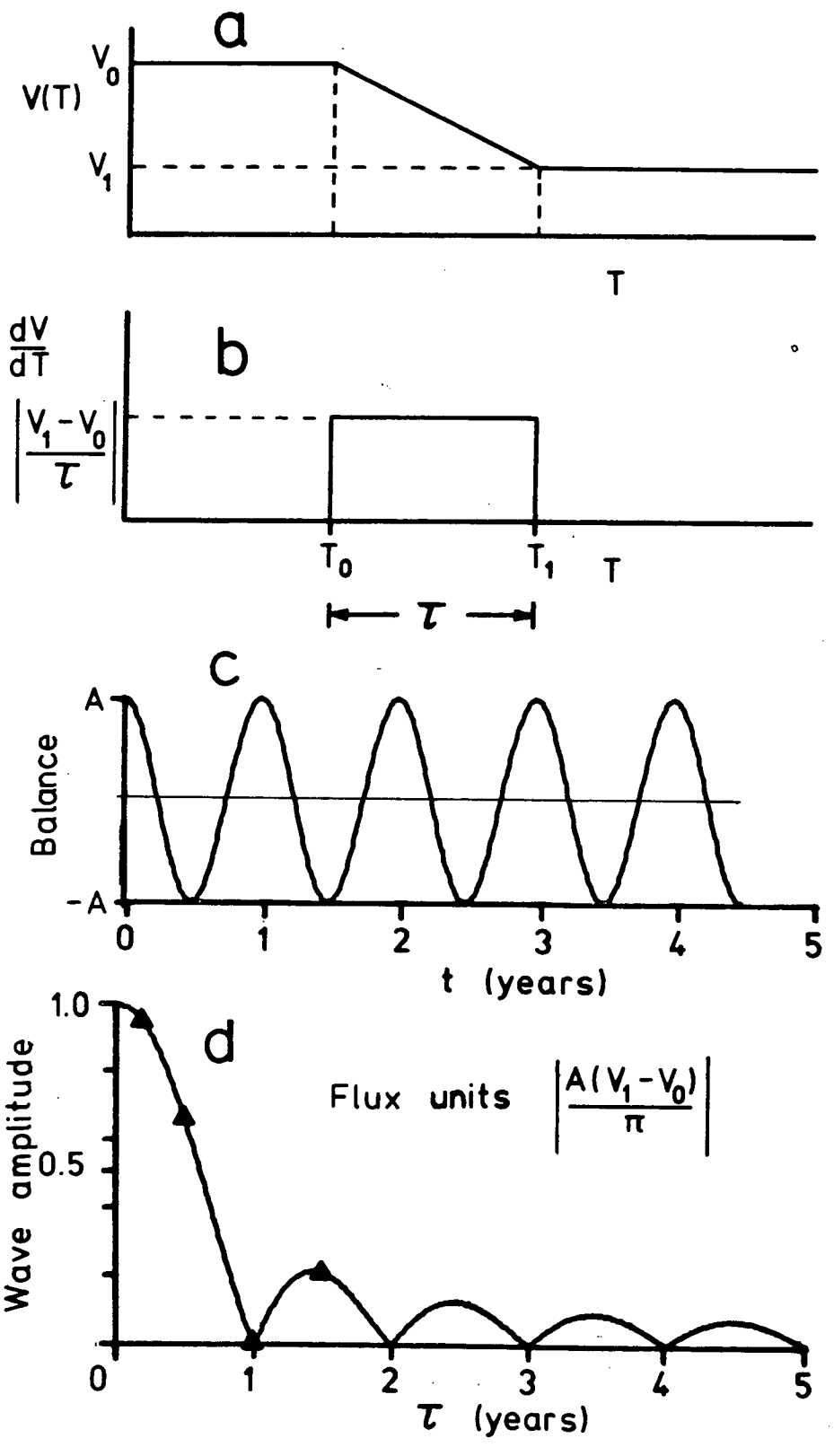
a
V(T)
V_0
V_1
T
b
$\frac{dV}{dT}$
$\left|\frac{V_1 - V_0}{\tau}\right|$
T_0
T_1
T
τ
c
Balance
A
-A
0
1
2
3
4
5
t (years)
d
Wave amplitude
1.0
0.5
Flux units $\left|\frac{A(V_1 - V_0)}{\pi}\right|$
0
1
2
3
4
5
τ (years)

an annually repeating function with zero mean.

If, for example, the mass balance (4.3.9) is a simple harmonic function

$$T(t) = A \cos(2\pi t) \tag{4.4.2}$$

as shown in Figure 4.6 (c), then

$$B_r(t) = -\frac{A}{2\pi} \sin(2\pi t) \tag{4.4.3}$$

Performing the convolution (4.3.28) using (4.4.1) and (4.4.3), and using the standard addition formula for cosines (e.g. Abramowitz and Stegun, 1965, formula (4.3.17), p. 72) gives

$$P(t-T) = -\frac{A}{2\pi}(v_1 - v_0)\left[\frac{\sin(\pi\tau)}{\pi\tau}\right] \sin(2\pi[t-T] + \pi[T_1 + T_0]) \tag{4.4.4}$$

The final factor is the propagating annual wave train. The crest-to-trough amplitude of this wave train is modulated by

$$M(\tau) = \left|\frac{A(v_1 - v_0)}{\pi} \frac{\sin(\pi\tau)}{\pi\tau}\right| \tag{4.4.5}$$

which is shown in Figure 4.6 (d). A velocity gradient over an integer number of years generates no waves at all, and the amplitude of the ogive waves falls rapidly with increasing length of the gradient region between zero and one year. It is always small for lower gradients, i.e. larger τ. Because of the processes which can destroy wave ogives (Section 4.1.3), waves formed by gradients longer than 6 months may, in most cases, be too small to be observable.

Figure 4.7 shows the numerical solution to the continuity equation (4.3.4) for a suite of models with velocity gradient sections of varying lengths τ as shown in Figure 4.6 (a), using $v_1 = v_0/4$ and the mass balance (4.4.2). The constant A is $0.1h_0$

per year, where h_0 is the average input ice thickness at the boundary. I used the numerical model described in Chapter 2. The numerical solutions are presented as orthographic projections of the ice flux Q(T,t), seen from a position rotated 45° up about the t axis, and 30° forward about the Q axis.

In these numerical solutions, the terms in the analytical solution (4.3.20) can be identified. The first term $Q(T_0,0)=Q_0$ is the amplitude at the point T=0, as the ice surface passes through its average level in the middle of the accumulation season. The second term is zero, because there are no input waveforms at the boundary T=0.

The annual variations on lines parallel to the time axis are the third term, the whole glacier surface going up and down with the changing seasons. This is clearest on Figure 4.7 (c).

Finally, the fourth term, the wave ogives, describes the annual disturbances which propagate at a velocity of unity (one year per year). The triangular data points on Figure 4.6 (d) are the wave amplitudes from these numerical solutions. Figure 4.7 is a graphic illustration of the differences in wave amplitude due to slightly different geometrical situations.

Overleaf:

FIGURE 4.7. Flow past a velocity gradient: numerical solution. Orthographic projections of ice flux Q(T,t) for various gradient lengths τ. T is a measure of distance downglacier, and t is time. Surface profiles are at intervals of 1.5 months. The velocity and the mass balance have the form shown in Figure 4.6.
(a) τ = 0.2
(b) τ = 0.5
(c) τ = 1.0
(d) τ = 1.5

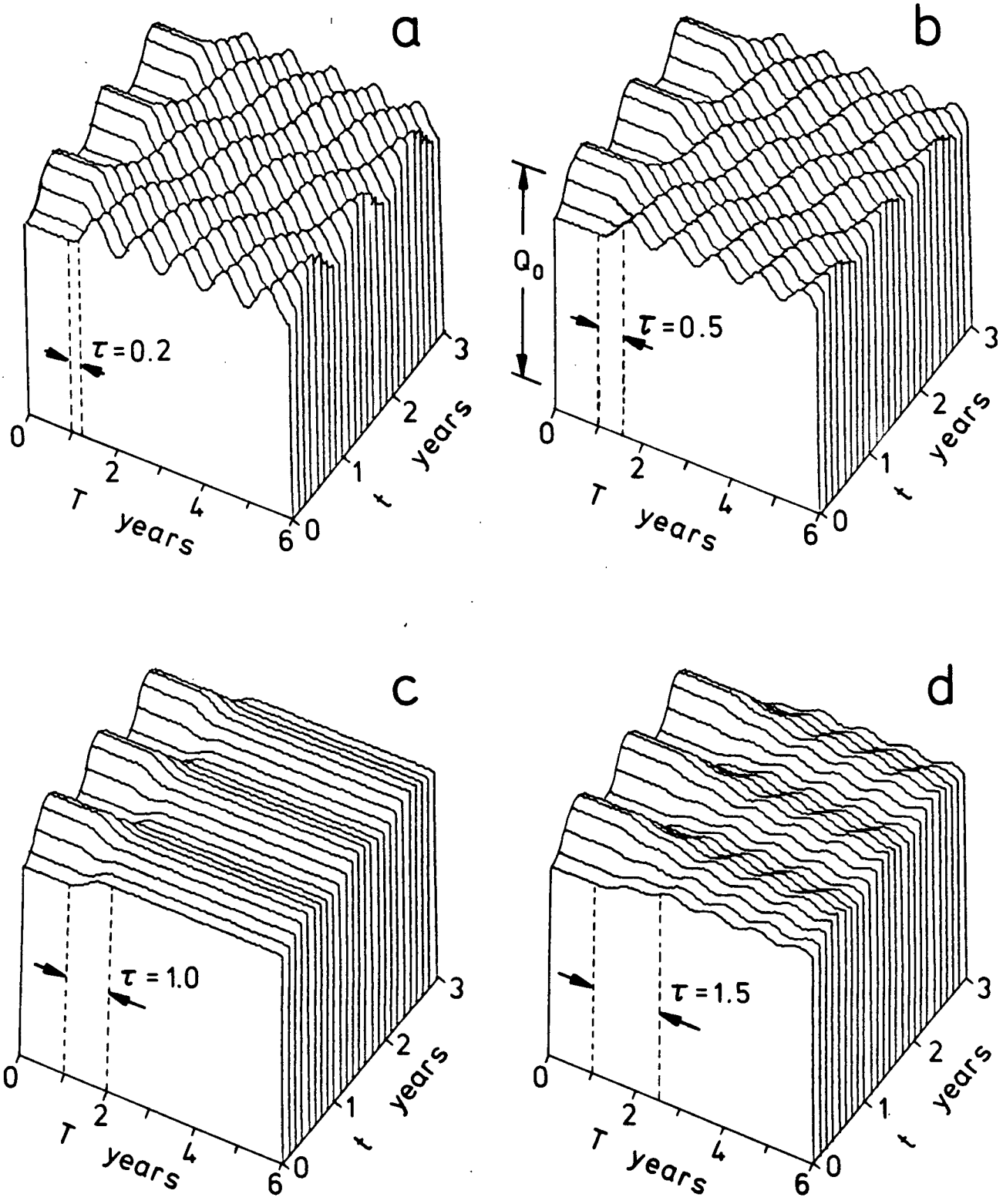
a
τ = 0.2
0
2
4
T years
6
0
1
2
3
t years
b
Q_0
τ = 0.5
0
2
4
T years
6
0
1
2
3
t years
c
τ = 1.0
0
2
4
T years
6
0
1
2
3
t years
d
τ = 1.5
0
2
4
T years
6
0
1
2
3
t years

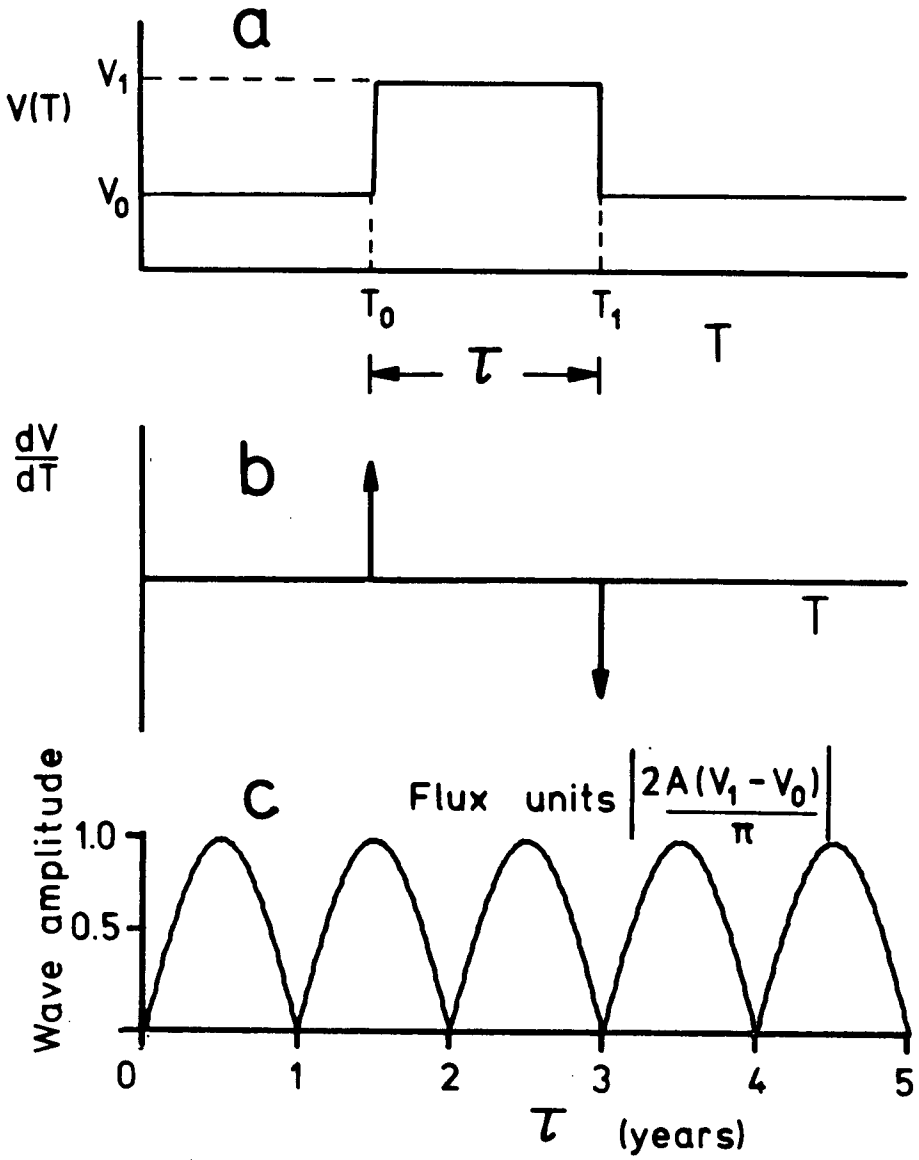

FIGURE 4.8. Double Step Icefall Model.
T is a measure of distance downglacier, and t is time. The mass balance is given in Figure 4.7 (c).
(a) Generalized velocity.
(b) Generalized velocity gradient.
(c) Normalized crest-to-trough amplitude of waves in flux as a function of icefall length τ.

4.4.3 EXAMPLE: DOUBLE STEP ICEFALL MODEL

The second simple example (Figure 4.8) of a velocity distribution and the resulting ogives is a generalization of

Nye's (1958[b]) simple illustrative model previously shown in Figure 4.3 (a). This time, I will look at the amplitude of the waves as a function of τ, the length of the 'icefall', as shown in Figure 4.8 (a)

In this case, the velocity gradient dv/dT is two Dirac delta functions (e.g. Morse and Feshbach, 1953, p. 122) of opposite polarity, shown in Figure 4.8 (b). If B_r is annually repeating, and if τ is an integer, these two delta functions will contribute equal and opposite amounts to the convolution (4.3.28), i.e. no waves are formed.

For example, using the harmonic mass balance (4.4.2), the convolution (4.3.28) becomes

$$P(t-T) = -\frac{A}{\pi}(v_1 - v_0) \sin(\pi\tau) \sin(2\pi[t-T] + \pi[T_1 + T_0]) \qquad (4.4.6)$$

The peak-to-trough amplitude is given by

$$M(\tau) = \left| \frac{2A}{\pi}(v_1 - v_0) \sin(\pi\tau) \right| \qquad (4.4.7)$$

which is shown in Figure 4.8 (c). Even when the velocity changes are abrupt, the wave interference from the speed-up phase and from the slowdown phase modulates the ogive amplitude, depending on the length of the icefall.

4.5 AUSTERDALSBREEN

4.5.1 INTRODUCTION

King and Lewis (1961) attributed the Forbes bands on Austerdalsbreen to seasonal differences in dust accumulation, melting, and snow accumulation in the crevasses formed in the upper part of the Odinsbreen icefall, where the ice undergoes a longitudinal extension. This region is between x=500 metres and x=1000 metres in Figure 4.1. Since wave ogives are often associated with Forbes bands, it is interesting to see which sections of the Odinsbreen icefall are most important for forming the waves.

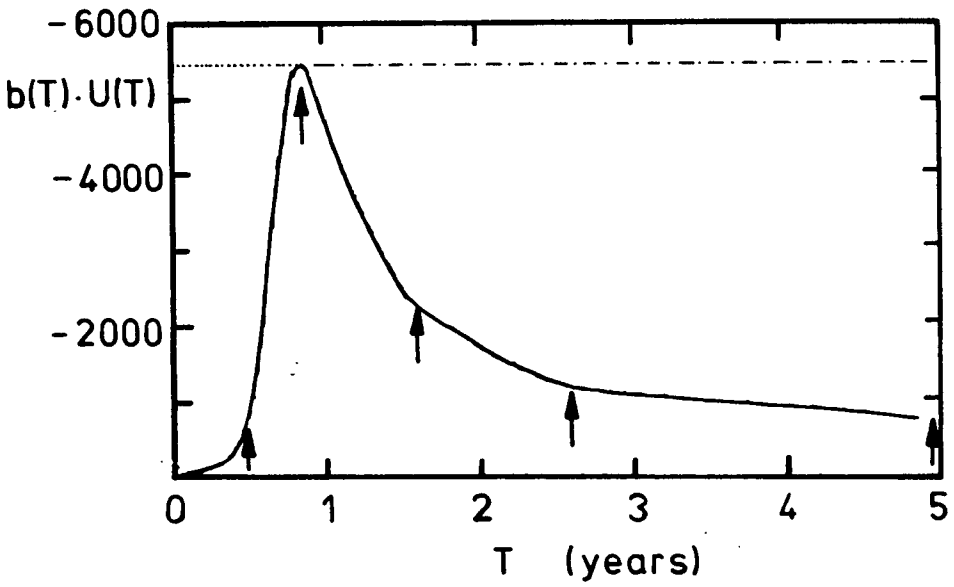

FIGURE 4.9. Odinsbreen: Generalized Velocity Per Unit Width. The arrows indicate the ends of the approximately linear sections in Table 4.1.

4.5.2 ESTIMATED WAVE GENERATION

If I assume that the width variations are unimportant (Nye (1958[b]) also assumed this), then, by multiplying the curves U(x) and b(x) in Figure 4.1, and using the transformation (4.3.2), I get the generalized velocity v(T) for unit width on Odinsbre. This is shown in Figure 4.9. In rough terms, this curve can be approximated by four sections of constant gradient, as described in Table 4.1. The wave amplitude function $M(\tau)$ in

T_0 years	T_1 years	τ years	$(v_1 - v_0)$ $m^3 a^{-2}$	$M(\tau)$ normalized
0.5	0.9	0.4	-5500.	0.76
0.9	1.6	0.7	2200.	0.15
1.6	2.6	1.0	1100.	0.0
2.6	5.0	2.4	400.	0.01

TABLE 4.1. Approximation to Odinsbreen by linear velocity sections. The endpoints are shown by arrows on Figure 4.9. Values of generalized velocity v are given per metre width. The wave amplitude factor M has been normalized using $\tau=0$ and $v_1-v_0=5500.\ m^3a^{-2}$. (Note that the units of generalized velocity are not $m\ a^{-1}$).

Table 4.1 is the value of $M(\tau)$ from equation (4.4.5) normalized to $\tau=0$ and $v_1-v_0=5500.\ m^3\ a^{-2}$. Although (4.4.5) is exact only for the mass balance (4.4.2), other annually varying mass balance functions would show similar rapid falloff of the wave amplitude with τ. The $M(\tau)$ column in Table 4.1 suggests that the largest contribution to the generation of the waves comes from the initial section of the generalized velocity as the ice accelerates to maximum speed. This is the same section that King

and Lewis (1961) identified as the region controlling the formation of the Forbes bands.

4.5.3 OGIVE SOLUTION FOR AUSTERDALSBREEN

To test this idea, I have used the Odinsbreen icefall profile (Figure 4.9) to solve the continuity equation (4.3.4) with the numerical model described in Chapter 2.

The upstream boundary condition was satisfied by a constant input flux. Using the values of ice thickness ($h = 13.8$ m) and ice velocity ($U = 1375.$ m a^{-1}) at the upstream boundary from Nye (1958[b]), the input flux per metre width was

$$Q_o = h_o U_o = 18975. \text{ m}^3 \text{ a}^{-1} \qquad (4.5.1)$$

(For Nye's model of Austerdalsbreen, the input flux was constant in time because the mass balance at the top of the icefall was zero.)

Because the finite difference model cannot accurately represent an instantaneous mass balance of the form (4.2.6), I used a constant ablation rate for three months each year, i.e.

$$T(t) = 4[H(t-t_o) - H(t-t_o-1/4)] \qquad (4.5.2)$$

where H(t) is the unit Heaviside step function (e.g. Morse and Feshbach, 1953, p. 123). Nye (1958[b]) indicated this was

---

Overleaf:
FIGURE 4.10. Austerdalsbreen wave ogives.
The numerical solution using the generalized velocity in Figure 4.9, with constant input flux at T=0, and a 3 month constant ablation season. Profiles at 1.5 month intervals. T is a measure of distance downglacier, and t is time.
(a) ice flux Q(T,t).
(b) ice thickness h(x,t).

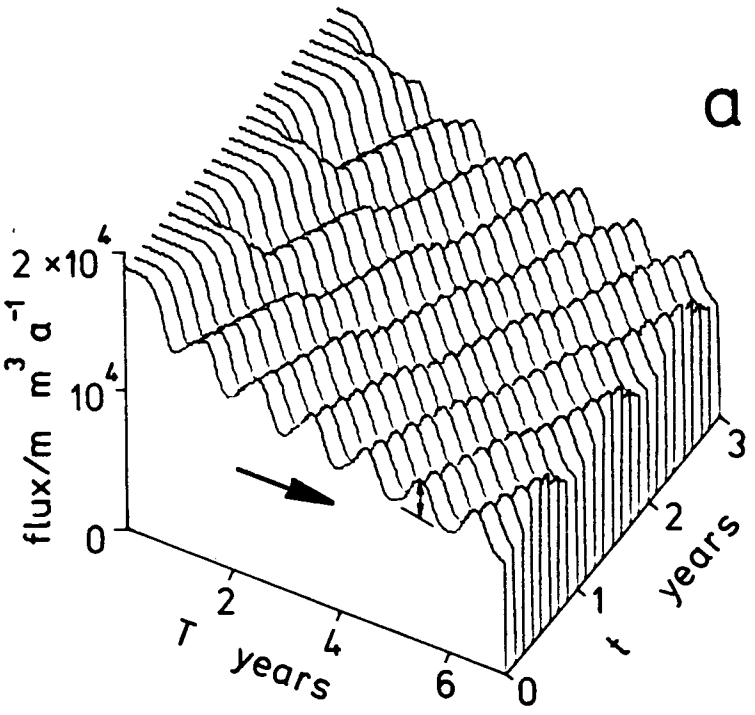
a
2 ×10^4
10^4
0
flux/m m^3 a^-1
2
4
6
T years
0
1
2
3
t years

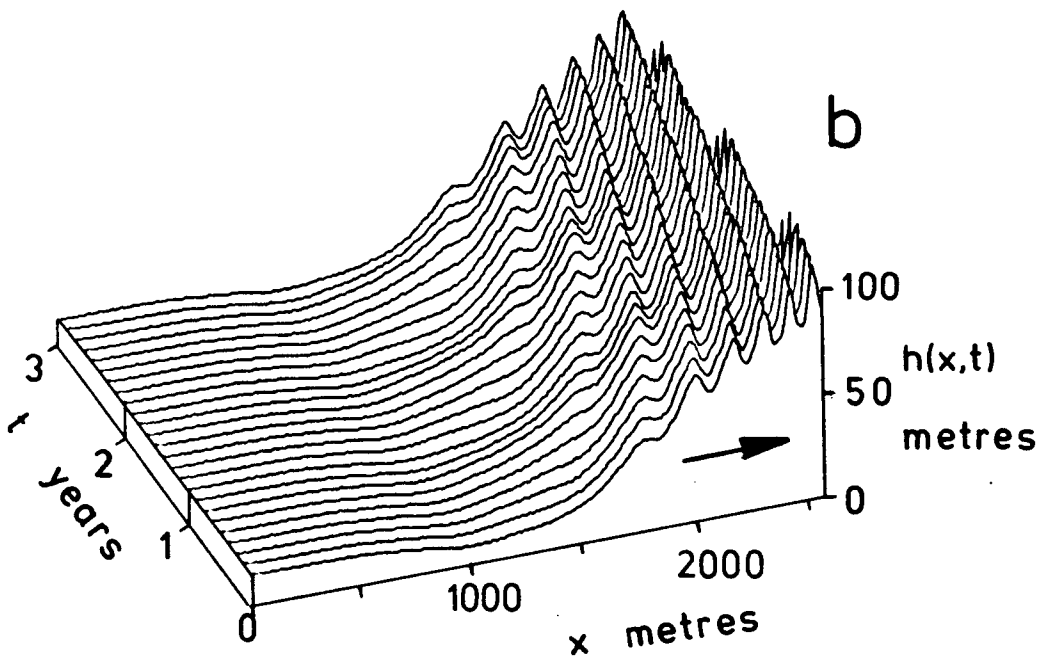
b
3
2
1
0
t years
1000
2000
x metres
100
50
0
h(x,t)
metres

actually a more realistic representation of the Austerdalsbreen mass balance.

Figure 4.10 (a) shows the computed ice flux Q(T,t) in an orthographic view from an angle 30° forward about the Q axis, and 45° up about the t axis. Figure 4.10 (b) shows the transformation to ice thickness h(x,t). The view is from 20° back about the h axis, and 30° up about the t axis. The wave ogives are evident in both plots. The amplification of the waves due to compressive flow can be seen in Figure 4.10 (b).

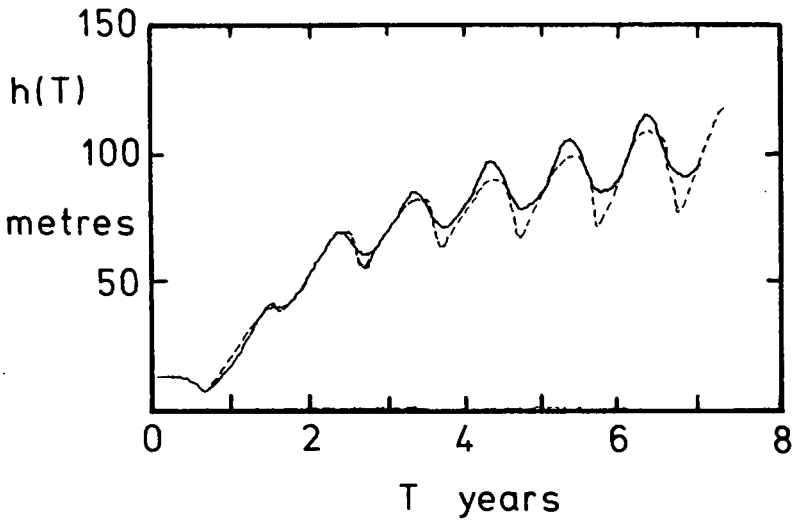

FIGURE 4.11. Austerdalsbreen Ice Thickness.
Ice thickness h(T) at the midpoint of the ablation season. T(x) is a measure of distance downglacier (the time to flow from the origin to position x).
solid curve: numerical solution with 3 month ablation season.
broken curve: Nye (1958[b]) with instantaneous ablation.

The solid curve in Figure 4.11 shows the ice thickness profile h(T) in the middle of the ablation season. For comparison, the broken line is the wave pattern found by Nye

using an instantaneous ablation season. The longer ablation season smooths out the sharp troughs on the waves.

4.5.4 FINDING THE WAVE GENERATING REGION

To test whether the steep gradient of v(T) in the upper icefall essentially causes the wave ogives, I then used the numerical model with two modified velocity profiles.

To generate the annual repeating state in Figure 4.12 (a), I brought the ice into the icefall already travelling at the high generalized velocity of -5500. m^3a^{-2}, i.e. using the dotted horizontal curve in Figure 4.9, then let the ice slow down on the standard Odinsbreen curve (solid line). The upstream boundary condition for this A.R.S. model is time-dependent, because b(x) cannot be zero at the boundary. The boundary flux is

$$Q_o(0,t) = h_o U_o + \int_0^t T(s)\, ds \qquad (4.5.3)$$

the waves generated in this model have only 15%-20% of the amplitude of those in Figure 4.10 (a). The prediction in Table 4.1 was 15%.

Next, I ran the numerical model using the standard Odinsbreen curve (solid line in Figure 4.9) up to the peak of the generalized velocity curve, but letting the ice leave the icefall and travel down Austerdalsbreen without slowing down, i.e. using the broken horizontal curve. The boundary condition was (4.5.1). The average slope of the flux surface is much

larger in this case, because the ice remains thin, and ablation takes a larger proportion of the mass each year, but the amplitude of the waves in this case, Figure 4.12 (b), is approximately 80% of the amplitude in Figure 4.10 (a). The prediction in Table 4.1, based on the approximating linear velocity gradient segments, was 76%. This agreement suggests that the simple estimates are quite adequate. These results also substantiate the idea that the rapid velocity increase in the upper region of Odinsbreen causes the waves at Austerdalsbreen, and the subsequent slowdown of the ice only amplifies the waves in ice thickness by compressive flow. It appears that the rapid extension, which is responsible for the crevassing controlling Forbes bands, is also responsible for the formation of wave ogives.

The velocity and ablation data for Séracs du Géant in Vallon (unpublished, p. 52) suggest that the slowdown phase at Mer de Glace also contributes very little to the wave ogives on that glacier.

Overleaf:
FIGURE 4.12. Variations on Odinsbreen icefall.
T is a measure of distance downglacier, and t is time. the vertical arrows at T=5 show the wave amplitude.
(a) The ice enters the icefall already travelling at the maximum generalized velocity (dotted curve in Figure 4.9). It slows down following the solid curve. The wave amplitude is small.
(b) The ice reaches peak generalized velocity and maintains it as it descends the icefall (broken curve in Figure 4.9). The wave amplitude is comparable to the amplitude in Figure 4.10 (a).

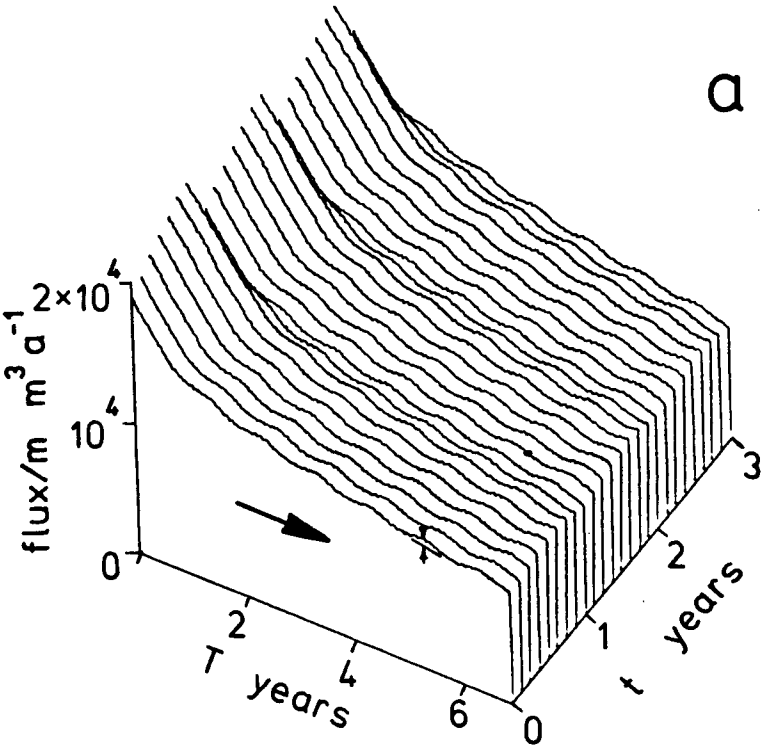
a
flux/m m³ a⁻¹
2×10⁴
10⁴
0
T years
2
4
6
t years
0
1
2
3

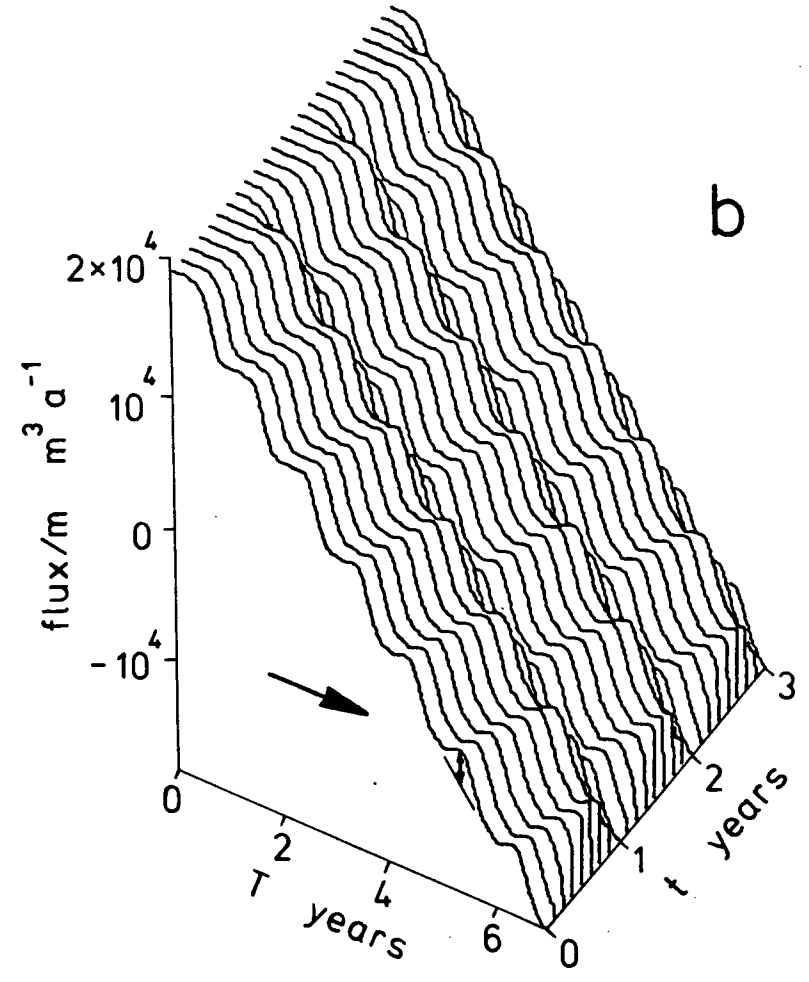
b
flux/m m³ a⁻¹
2×10⁴
10⁴
0
-10⁴
T years
0
2
4
6
t years
0
1
2
3

4.6 CONCLUSIONS

The ablation-plastic stretching mechanism of Nye (1958[b]) has been re-examined through a solution of the continuity equation for ice flux by the method of characteristics. The total wave ogive pattern on a glacier can be written as a convolution of a spatial term, the velocity-width-mass balance gradient, with a temporal term, the time-integrated mass balance. Nye's plastic stretching is in the spatial term, and the annual mass balance is in the time term. The convolution describes their interaction.

The integrated mass balance has an annual periodicity. The velocity gradient can be viewed as a filter applied to this periodic function. Wave ogives appear in the filter output (the glacier flux profile), only if the filter does not heavily attenuate the annual component. The theory predicts that factors such as the icefall length, and the magnitude and spatial extent of velocity changes in the icefall modulate the amplitude of the resulting wave ogives. The modulation factor may go to zero.

Since small annual waves may go unnoticed, or be rapidly obliterated by differential ablation, this modulation effect may be why some icefalls with rapid ice velocities and large annual balance variations do not generate observable wave ogives by the ablation-stretching mechanism.

Several points of physical interest can also be made:

1. Longitudinal variation of ice velocity, channel width, and mass balance all can generate annual waves in the same way. The waves due to velocity changes are usually the largest.

2. Every incremental change with x of any of these three factors generates a wave train downglacier. This annually periodic wave train is the Green's function for the total wave pattern.
3. Waves are not observed on all glaciers, because the velocity gradients are small, and waves generated over a large spatial range tend to be out of phase and to interfere destructively.
4. Only large and localized gradients traversed by the ice in six months or less can generate waves sufficiently coherent to form large wave ogives.
5. Wave ogives and Forbes bands often are found together, because, while the physical processes causing them are different, they both depend on the occurrence of a short zone of rapid ice acceleration, such as the upper stretch of some icefalls.

LIST OF SYMBOLS

SYMBOL	SECTION[1]	MEANING
A	1.4.3	temperature dependent coefficient in Glen's flow law
A	1.4.3	coefficient in general stress-strain rate relationship
A	2.5.2	coefficient in Weertman sliding law
A	4.4.2	half amplitude of seasonal mass balance
A	A2.3.2	coefficient in quadratic equation for δx
$A(m)$	A13.4	real term common to numerator and denominator of $T(m)$
$A'(x,t)$	A5.4	mass balance normal to glacier surface
$\bar{A}$	A1.3.4	mass balance averaged over wedge terminus
A_j	A1.1.2	sub-diagonal element of $\underline{M}$ row j
A_0	1.4.3	constant in Arrhenius temperature relation for A in Glen's flow law
A_0	4.3.6	a vertical prism of ice at lower edge of icefall during ablation
A_1	4.3.6	a vertical prism of ice which occupied position A_0 one year previously
$\underline{A}$	2.2.2	tridiagonal matrix in iterations for $\underline{\delta h}$
$A(x,t)$	1.3.3	mass balance normal to bed
A_j^n	2.2.2	mass balance normal to bed at mesh point j, time step n

[1]The SECTION column indicates the section in the text where this particular definition of the symbol is first used.

$A_o(x)$	A6	mass balance for a datum (steady) state
$a(x,t)$	A6	perturbation to mass balance $A_o(x)$
$\underline{a}$	A5.2	a vector in a set whose endpoints define mass balance as a function of position everywhere on the glacier surface
a_{jk}	A1.2	element in row j column k of matrix $\underline{\underline{A}}$
a_j	A1.2	sub-diagonal element in row j matrix $\underline{\underline{A}}$ equal to $a_{j+1,j}$
B	1.4.3	coefficient in general stress-strain rate relationship
B	A2.3.2	coefficient in quadratic equation for δx
B_o	4.3.6	a vertical prism of ice which left icefall just prior to ablation
B_1	4.3.6	a vertical prism of ice which occupied position B_o one year previously
$\underline{B}$	1.4.2	total body force on a deforming continuum
B_i	1.4.2	ith component of body force $\underline{B}$
B_j	A1.1.2	row j main diagonal element of matrix $\underline{\underline{M}}$
B(t)	4.3.2	temporal integral of bt(t)
$B_r(t)$	4.3.8	time reversal of B(t) i.e. B(-t)
B(m)	A13.4	real factor common to imaginary parts of numerator and denominator of T(m)
B(x)	A15.3.1	mass balance for Nagata ice sheet model
b	2.5.2	constant term in mass balance of Nagata ice sheet model
b	A15.2	constant mass balance for Nye ice sheet model
$\underline{b}$	A5.2	vector in a set whose endpoints define basal melting rate over bottom surface

b_j	A11	glacier bed elevation at gridpoint j
b_j	A1.2	diagonal element a_{jj} of matrix $\underline{\underline{A}}$
b(x)	4.2.2	total depth of accumulation in one year
C	1.4.3	coefficient in general stress-strain rate relationship
C	A2.3.2	coefficient in quadratic equation for δx
C_j	A1.1.2	super-diagonal element in row j matrix $\underline{\underline{M}}$
c	2.3.2	scale constant in analytical solution for terminus motion test
c	3.5.4	rate of change of $\delta(O^{18}/O^{16})$ with height
c	A15.3.3	streamline parameter for Nagata model
c_j	A1.2	super-diagonal element in row j matrix $\underline{\underline{A}}$
c(H)	2.3.3	rate of change of flux Q_1 with H (variable for Burgers' equation)
c(x,t)	2.3.3	same as c(H)
$c_{-2}(t)$	3.3.5	velocity of transition region edge $x_{-2}(t)$
$c_{-1}(t)$	3.3.5	velocity of transition region edge $x_{-1}(t)$
$c_1(t)$	3.3.5	velocity of transition region edge $x_1(t)$
$c_2(t)$	3.3.5	velocity of transition region edge $x_2(t)$
$c_0(x)$	A6	rate of change of flux Q with depth H in datum state
c_{0j}	A13.4	value of $c_0(x)$ at gridpoint j
D	4.2.2	material derivative or total derivative of a function of both space and time
$\underline{D}$	2.2.2	right side column vector containing known terms in equation for $\underline{H}$
D_j	A1.1.2	element j of vector $\underline{D}$

$D_0(x)$	A6	rate of change of ice flux Q with surface slope in datum state
D_{o_j}	A13.4	value of $D_0(x)$ at gridpoint j
DX_T	A1.3.4	length of wedge terminus region
DX_{ij}	2.4.2	grid interval in x direction at position i and height j
DZ	2.4.2	grid interval in z direction
DX_0	A2.3.1	DX_{ij} between meshpoints $\underline{P}_0$ and $\underline{P}_2$
DX_1	A2.3.1	DX_{ij} between meshpoints $\underline{P}_1$ and $\underline{P}_3$
$d\underline{P}$	A2.3.1	displacement vector $(\delta x, \delta z)$ of an ice particle relative to a meshpoint $\underline{P}_0$
E_h	A1.5.4	fractional interpolation error in ice thickness h at midpoint of mesh interval
e	A1.5.4	error in $\partial Q/\partial x$ resulting from E_h
e(x)	1.4.4	fractional error in ice velocity due to assumption of simple shear deformation
e_h	A11	an error in h_j at some meshpoint j
F(m)	A3.1	Fourier transform of a function f(x)
F(Z)	A3.1	Z transform of a sampled function f_j
$\underline{F}$	A5.2	a length vector tangent to glacier surface
F_g	A7.3	gravitational term in expression (A7.2.20)
F_l	A7.3	longitudinal stress term in (A7.2.20)
F_s	A7.3	shear stress-dependent term in (A7.2.20)
f	3.3.5	ratio of sliding velocity between surges to peak sliding velocity during surges

f	A1.5.4	fractional error in flux Q due to error E_h
f_j	A3.1	jth point of a sampled arbitrary function f
$\underline{f}(\underline{r})$	1.4.2	specific body forces at position $\underline{r}$
$f_i(\underline{r})$	1.4.2	ith component of $\underline{f}(\underline{r})$
$f(\underline{P})$	A2.3.1	value of an arbitrary scalar function f at a point $\underline{P}$ in a vertical longitudinal section
$f_0,\ldots f_3$	A2.3.1	values of arbitrary function $f(\underline{P})$ at meshpoints $\underline{P}_0,\ldots\underline{P}_3$
$\underline{G}$	A5.2	arbitrary vector tangent to ice surface (units of mass balance)
g	1.4.2	acceleration due to gravity 9.8 m s^{-2}
H	2.3.3	gas density
H	2.5.2	thickness of Nagata ice sheet at x=0
$\underline{H}$	2.2.2	column vector with jth element h_j^{n+1}
$H_0(x)$	1.3.3	initial condition for ice thickness
$H(t)$	4.5.3	Heaviside step function =0 t<0 =1 t>0
$H^n(z)$	A1.4.2	polynomial Z transform of $\{h_j \mid j=1,J\}$
$H_0(x)$	A6	ice thickness in datum (steady) state
$H(x,t)$	A6	total ice thickness $H_0(x)+h(x,t)$
$h(x,t)$	A6	perturbation to ice thickness $H_0(x)$
$h(x,t)$	1.3.2	ice thickness normal to glacier bed
h_j^n	2.2.2	ice thickness at meshpoint j, time step n

$\underline{h}$	A5.2	a position vector from a set whose endpoints define the ice surface
$h'(x,t)$	A5.4	ice thickness measured normal to glacier surface
$\tilde{h}(m,t)$	A1.5.1	Fourier transform of $h(x,t)$
h_o	2.3.2	ice thickness at x=0 for analytical solution testing terminus motion
i	A1.4.2	$i^2 = -1$
J	2.2.2	number of finite difference meshpoints between bergschrund and terminus
$K(m)$	A1.5.2	a real term in the transfer function $T(m)$
$K(Z)$	A1.4.2	a real term in the transfer function $T(Z)$
k	3.5.4	rate of change of $\delta(O^{18}/O^{16})$ with x
k	A1.3.1	nonzero element in last row of matrix $\underline{\underline{M}}$
k	A16.2	flow law constant used by Budd and McInnes (related to Glen's flow law through $k=2A/[n+1]$)
$L(t)$	1.3.3	length of glacier
$\underline{\underline{M}}$	2.2.2	coefficient matrix in equation for $\underline{H}$
$M(\tau)$	4.4.2	amplitude of wave ogives generated by velocity changes over a distance τ
$M(t)$	A5.1	mass inside a volume V of a continuum
M_i	A19	width of ith tributary of Steele Glacier
m	2.2.4	wavenumber
m	2.5.2	exponent in Weertman sliding relation
m_N	2.2.4	Nyquist wavenumber; highest wavenumber which can be detected on a discrete grid
$\underline{m}$	A7.2	ice surface downslope unit tangent vector
N	2.2.2	total number of time steps Δt

n	1.4.3	exponent in Glen's flow law for ice
$\underline{n}$	1.4.2	unit vector normal to a surface
n_j	1.4.2	jth component of $\underline{n}$
$O[x]$	1.4.4	f=O[x] means f is of the order of x It is used in the approximate sense: $\|10^{-1}x\|<\|f\|<\|10x\|$ Technically it means $\lim_{x\to 0}(f)$ is bounded
$\underline{P}_0$	2.4.2	initial position of an ice particle
$\underline{P}_0,\ldots\underline{P}_3$	A2.3.1	four meshpoints at the vertices of a quadrilateral mesh cell in vertical longitudinal section (used for 4-point interpolation scheme)
$\underline{P}(t)$	2.4.2	trajectory of an ice particle
$P(T_0,T,[t-T])$	4.3.6	term containing wave ogives in solution of continuity equation
p	1.4.3	pressure
p_j	2.2.2	constant $\Delta t/(2\Delta x W_j)$ at gridpoint j
Q	1.4.3	activation energy for creep
$Q(x,t)$	1.3.3	ice flux through a vertical transverse cross-section
$Q^n_{j+1/2}$	2.2.2	ice flux at time step n, midway between gridpoints j and j+1
$Q'_{j+1/2}$	A11	estimate of $Q^n_{j+1/2}$ when h^n_j has error e_h
$Q_0(t)$	2.2.1	ice flux at x=0 (boundary condition)
$Q_0(x)$	A6	ice flux in datum (steady) state
$Q_1(H)$	2.3.3	flux term depending on H (derivation of Burgers' equation)
Q_1	A5.2	ice flux through surface S_1

Q_2	A5.2	ice flux through surface S_2
$Q_{bal}(x)$	A16.4	balance flux for steady glacier
Q_i	A19	discharge of ith tributary of Steele Glacier
$q(x,t)$	A6	perturbation to datum flux $Q_0(x)$
R	1.4.3	gas constant 8.314 J $^{o}K^{-1}$ mol^{-1}
R	2.3.3	Reynold's number for Burgers' equation
R_S	3.5.1	isotopic concentration ratio of a sample
R_{SMOW}	3.5.1	isotopic concentration ratio of Standard Mean Ocean Water
r_j^{n+1}	2.2.2	residual in iterative solution for h_j^{n+1} at gridpoint j, time step n+1
$\underline{r}$	2.2.2	residual vector with jth element r_j^{n+1}
$\underline{r}$	1.4.2	position vector of a point in a continuum
S	1.4.2	surface enclosing a deforming continuum V
S_1	A5.2	upstream surface of a thin transverse vertical prism
S_2	A5.2	downstream surface of a thin transverse vertical prism
S_0	4.3.6	prism of ice in icefall during ablation (Summer ice)
S_1	4.3.6	prism of ice which occupied position S_0 one year previously
$S(x',t)$	A5.3	transverse cross-sectional area of glacier channel
s	1.4.4	shape factor (may be x dependent)
$s(t)$	2.3.2	slope of analytical solution to continuity equation (used to test terminus motion)

s_0	2.3.2	initial value of s(t)
$\dot{s}$	2.3.2	rate of change of s(t)
T	1.4.3	temperature (^oK)
$\underline{T}$	1.4.2	surface traction vector for a deforming volume V of a continuum
T_k	1.4.2	kth component of $\underline{T}$
T_1, T_2, T_3	1.4.3	scalar invariants of stress tensor σ_{jk}
T_1', T_2', T_3'	1.4.3	invariants of stress deviator tensor σ'_{jk}
T(m)	2.2.4	transfer function for numerical scheme when using Fourier transform
T(Z)	A1.4.2	transfer function for numerical scheme when using Z transform
T(t)	3.3.5	amplitude function used to model surge velocity of Steele Glacier
T(x)	4.3.1	time for ice to flow from origin to x (For ogive problem, this is a nonlinear measure of distance)
T_o	4.3.1	reference position at which boundary condition $Q_o(t)$ is applied
T_o	4.4.2	upstream end of a linear gradient in generalized velocity v
T_1	4.4.2	downstream end of a linear gradient in generalized velocity v
t	1.3.3	time
t_o	2.3.3	initial time
t_1	A2.3.2	time subsequent to t_o: $t_1=t_o+\Delta t$
t_o	3.3.5	time at which a surge starts
t_1	3.3.5	time at which a surge reaches peak sliding velocity

t_2	3.3.5	time at which a surge begins to slow
t_3	3.3.5	time at which a surge ends
t_4	3.3.5	surge period
U_0	3.3.5	maximum sliding velocity in Steele Glacier surge simulations
$U(x)$	4.2.2	surface velocity of ice for ogive models
U_0	4.3.6	velocity of ice at upstream edge of transition zone for simple ogive models
U_1	4.3.6	velocity of ice at downstream edge of transition zone for simple ogive models
$u(\underline{x})$	1.3.1	velocity component parallel to bed when $\underline{x}$ is the triplet (x,y,z)
u_i	1.4.3	velocity component in direction x when $\underline{x}$ is (x_1,x_2,x_3) i
u_{max}	A2.2.3	maximum value of $u(\underline{x})$ on $[0,L(t)]$
$u_s(x,t)$	1.4.4	basal sliding velocity
u_{sj}	2.4.1	$u_s(x)$ at gridpoint j
$u_0,\ldots u_3$	A2.3.2	velocity component u at mesh points $\underline{P}_0$, $\underline{P}_1$, $\underline{P}_2$, $\underline{P}_3$
u_x	A2.3.2	first difference of u in x direction between $\underline{P}_0$ and $\underline{P}_2$
u_z	A2.3.2	first difference of u in z direction between $\underline{P}_0$ and $\underline{P}_1$
u_{xz}	A2.3.2	first difference of u_x in z direction
V	1.4.2	volume of a deforming continuum
V(x,t)	1.3.3	downslope velocity component $u(\underline{x})$ averaged over width and depth
$V^n_{j+1/2}$	2.2.2	V(x,t) at time step n, midway between gridpoints j and j+1

$V_0(x)$	A15.3.1	vertical velocity component at ice surface for Nagata ice sheet model
V_{phase}	A1.5.2	phase velocity of wavenumber component m
VOL_T	A1.3.4	volume of wedge terminus
$VW_{j-1/2}$	A10	ice velocity $V_{j-1/2}$ times width $W_{j-1/2}$
$\underline{v}(\underline{x})$	1.3.1	velocity vector (u,w,v)
$v(\underline{x})$	1.3.1	z component of $\underline{v}(\underline{x})$
$v(T)$	4.3.3	generalized velocity function for ogives
$v_0,...v_3$	A2.3.2	velocity component v at mesh points $\underline{P}_0$, $\underline{P}_1$, $\underline{P}_2$, $\underline{P}_3$
v_x	A2.3.2	first difference of v in x direction between $\underline{P}_0$ and $\underline{P}_2$
v_z	A2.3.2	first difference of v in z direction between $\underline{P}_0$ and $\underline{P}_1$
v_{xz}	A2.3.2	first difference of v_x in z direction
$W(x)$	1.3.1	channel width
W_j	2.2.2	width W(x) at gridpoint j
W_0	2.3.2	channel width at x=0 for analytical solution used to test terminus
W'	2.3.2	x gradient of channel width for analytical solution used to test terminus
W_0	4.3.6	a prism of ice above icefall during ablation (in icefall in Winter)
W_1	4.3.6	ice which occupied volume W_0 one year previously
$\bar{W}$	A1.3.4	average width of wedge terminus
W_i	A19	width of Steele Glacier at confluence with ith tributary

$w(\underline{x})$	1.3.1	velocity component in y direction
X	A1.3.4	nondimensional length of wedge terminus
X(x,t)	3.3.5	spatial pattern of sliding velocity for Steele Glacier surge simulations
$\underline{x}$	1.3.1	position vector (x,y,z)
x	1.1.2	axis along glacier bed on a flowline (positive downstream)
x_1	1.4.2	equivalent to x axis
x_2	1.4.2	equivalent to y axis
x_3	1.4.2	equivalent to z axis
x'	A5.2	axis along glacier surface (positive downstream)
x_T	A1.3.4	position of glacier terminus (equivalent to L(t))
x_e	A15.3.2	equilibrium line for Nagata steady ice sheet model
$x_{.2}(t)$ $x_{.1}(t)$ $x_1(t)$ $x_2(t)$	3.3.5	points defining zone in which sliding takes place in simulations of surges of the Steele Glacier
y	1.1.2	transverse horizontal axis
Z	A1.4.1	Z transform variable $Z=e^{im\Delta x}$
z	1.1.2	axis in vertical plane and normal to x (positive upward)
z'	A5.2	axis in vertical plane and normal to x'
$\mathcal{A}$	A6	inclination of ice surface slope in datum (steady) state
α	1.4.4	inclination of ice surface slope
α	A6	perturbation to $\mathcal{A}$
α	2.3.3	coefficient in quadratic relation between gas flux Q_1 and gas density H (Burgers'equation)

β	1.4.2	inclination angle of glacier bed
β	2.3.3	coefficient in quadratic relation between gas flux Q_1 and gas density H
γ	2.3.3	coefficient in quadratic relation between gas flux Q_1 and gas density H
Δt	2.2.2	time increment for finite difference solution of continuity equation
Δx	2.2.2	horizontal grid interval for finite difference scheme
Δx_j	2.2.2	grid interval along bed at grid point j for finite difference scheme
$\delta(O^{18}/O^{16})$	3.5.1	isotopic composition of oxygen
δt	1.3.4	a small time interval
δx	1.3.4	a small increment in x direction
$(\delta x, \delta z)$	2.4.3	position of an ice particle relative to a meshpoint $\underline{P}_o$
δ_{ij}	1.4.3	Kroenecker delta function: =1 if i=j, =0 if i≠j
$\delta(x)$	2.3.3	Dirac delta distribution
δ_o	3.5.4	isotopic composition at a reference location
δV_{bal}	A1.3.4	volume change of wedge terminus in time Δt due to surface melting
δV_{flux}	A1.3.4	volume change of wedge terminus in time Δt due to ice flow through upstream boundary
δb_i	3.3.4	perturbation to Steele Glacier mass balance to simulate ice discharge from ith tributary
δh_j	2.2.2	iterative correction to h_j^{n+1}
$\underline{\delta h}$	2.2.2	correction vector: ith element is δh_j

δv	4.3.6	magnitude of a step change in generalized velocity v
$\delta\tau$	1.4.4	difference between effective shear stress τ and shear stress σ_{xz}
ϵ	A1.4.5	numerical viscosity (Lax-Wendroff scheme)
ϵ_j^n	2.2.5	truncation error at gridpoint j at time step n
$\dot{\epsilon}_{ij}$	1.4.3	strain rate tensor
$\dot{\epsilon}$	1.4.3	effective strain rate (square root of second invariant of $\dot{\epsilon}_{ij}$)
η	A8.3.1	Newtonian viscosity for longitudinal strain (Budd, 1975)
Θ	2.2.2	weighting parameter between 0 and 1, used to mix past and future time steps in finite difference scheme
λ	4.2.2	displacement of surface ice in one year
ν	2.3.3	diffusion coefficient
ρ	1.3.4	density of glacier ice
σ_{jk}	1.4.2	stress tensor
σ'_{jk}	1.4.3	deviatoric stress tensor
τ	1.4.3	effective shear stress (square root of T'_2)
τ	4.4.2	time for ice to travel the length of a channel section with a velocity gradient
τ_c	A8.3.1	simple gravitational shear stress given by $s\rho gh \sin\alpha$
τ_c^*	A8.3.1	local lubrication-lowered stress (Budd, 1975)

τ_b	A8.3.1	'actual' basal shear stress (Budd, 1975)
$T(t)$	4.2.3	temporal term in mass balance for ogives
$\emptyset$	4.3.1	time when ice passes origin (this is also the label for characteristic curves)
$\emptyset$	A8.3.1	basal lubrication factor (Budd, 1975)
$\emptyset$	A13.3	baseline halflength for finite difference estimate of $\partial Q/\partial x$
$\emptyset_{pde}(m)$	A1.5.2	phase angle of transfer function T(m) for partial differential equation at wavenumber m
$\emptyset_{fd}(m)$	A1.5.2	phase angle of transfer function T(m) for finite difference scheme at wavenumber m
$\emptyset_0, \ldots \emptyset_9$	A1.5.3	real numbers between 0 and 1/2 giving x locations of remainder terms in truncated Taylor expansions of h(x) and Q(x)
$x(x)$	4.2.3	spatial term in mass balance for ogives
Ψ	A13.3	baseline halflength for finite difference estimate of slope α
Ψ_1, Ψ_2	A1.5.4	real numbers between 0 and 1 giving x locations of remainder terms for Taylor expansions for interpolation error analysis
$\underline{\ }$		underscore indicating a vector. double underscore indicates a matrix
*	A1.4.2	convolution operator
$\cdot$		superior dot indicating time derivative
$\bar{\ }$		superior bar indicating spatial average

LITERATURE CITED

Abramowitz, M., and Stegun, I. A. 1965. Handbook of mathematical functions. Dover, New York. 1046 p.

Agassiz, L. 1840. Etudes sur les glaciers. [privately printed] Neuchâtel. 18 plates. 331 p.
--- 1966. Dawsons of Pall Mall. 2 Volumes. 347 p. 18 plates. [reprint of 1840.]

Agassiz, L. 1967. Studies on glaciers. Hafner Publishing Co. New York. lxxii. 18 plates. 213 p. [translation of Agassiz (1840) by A. V. Carozzi.]

Agassiz, L. 1847. Nouvelles études et expériences sur les glaciers actuels: leur structure, leur progression, et leur action physique sur le sol. Victor Masson. Paris. 598 p.

Ahern, T. K. Unpublished [a]. An O^{18}/O^{16} study of water flow in natural snow. [M.Sc. thesis. University of British Columbia. 1975. 164 p.]

Ahern, T. K. Unpublished [b]. The development of a completely automated oxygen isotope mass spectrometer. [Ph.D. thesis. University of British Columbia. 1980. 181 p.]

Ahlmann, H. W:son 1935[a]. Scientific results of the Norwegian-Swedish Spitzbergen Expedition in 1934. Introduction. General outline of the expedition. Geografiska Annaler, Vol. 17, p. 22-28. (with one map plate).

Ahlmann, H. W:son 1935[b]. The stratification of the snow and firn on Isachsen's Plateau. Geografiska Annaler, Vol. 17, p. 29-42. [Scientific Results of the Norwegian-Swedish Spitzbergen Expedition in 1934. Part I.]

Ahlmann, H. W:son 1935[c]. Ablation measurements at the headquarters on Isachsen's Plateau. Geografiska Annaler, Vol. 17, p. 43-52. [Scientific Results of the Norwegian-Swedish Spitzbergen Expedition in 1934. Part II.]

Ahlmann, H. W:son 1935[d]. The Fourteenth of July Glacier. Geografiska Annaler, Vol. 17, p. 167-218. (and one fold-out map). [Scientific Results of the Norwegian-Swedish Spitzbergen Expedition in 1934. Part V.]

Ahlmann, H. W:son 1936. The firn structure on Isachsen's Plateau. Geografiska Annaler, Vol. 18, p. 48-73. [Scientific Results of the Norwegian-Swedish Spitzbergen Expedition in 1934. Part VII.]

Aleschow, A. 1930. Ein rezenter Gletscher im nordlichen Ural. Zeitschrift für Gletscherkunde, Vol. 18, p. 58-62. [cited by Matthes (1942), p. 176.]

Andrews, J. T. 1974. Glacial isostasy. Dowden, Hutchinson and Ross. Stroudsburg, Pennsylvania. 491 p. [Benchmark Papers in Geology series.]

Andrews, J. T., and Mahaffy, M. A. W. 1976. Growth rate of the Laurentide ice sheet and sea level lowering. Quaternary Research, Vol. 6, No. 2, p. 167-83.

Atherton, D. 1963. Comparisons of ogive systems under various regimes. Journal of Glaciology, Vol. 4, No. 35, p. 547-57.

Bader, H. 1939. Der Schnee und seine Metamorphose. Beiträge zur Geologie der Schweiz, Series Hydrologie, part 3. [cited by Matthes, (1942) p. 165.]

Ball, J. 1870. On the cause of the descent of glaciers. Philosophical Magazine, Ser. 4, Vol. 40, p. 1-10. [cited by Croll (1875, p. 501) and Russell (1897, p. 176).]

Barkov, N. I., and others. 1974. First results of the study of an ice core from the borehole at Vostok Station (Antarctica) by the oxygen isotope method, by N. I. Barkov, F. G. Gordienko, E. S. Korotkevich, and V. M. Kotlyakov. Doklady Akademii Nauk SSSR, Vol. 214, p. 1383-86. [cited by Paterson and others, (1977).]

Barkov, N. I., and others. 1975. Isotope oxygen (sic) studies of 500 m ice core taken from drillhole at Vostok station, by N. I. Barkov, F. G. Gordienko, E. S. Korotkevitch, and V. M. Kotlyakov. Bulletin of the Soviet Antarctic Expedition, No. 90, p. 39-49. [cited by Jenssen (1978).]

Barkov, N. I., and others. 1977. The isotope analysis of ice cores from Vostok station (Antarctica) to the depth of 950 m, by N. I. Barkov, Ye. S. Korotkevitch, F. G. Gordienko, and V. M. Kotlyakov. In Isotopes and impurities in snow and ice symposium: symposium isotopes et impurités dans les neiges et glaces. Proceedings of the Grenoble Symposium, Aug.-Sept. 1975. p. 382-87. [IAHS Publication No. 118].

Barnes, P., and others. 1971. The friction and creep of polycrystalline ice, by P. Barnes, D. Tabor, and J. C. F. Walker. Proceedings of the Royal Society, Ser. A, Vol. 324, No. 1557, p. 127-55.

Battle, W. R. 1951. Early discoverers V. Louis Agassiz on "extrusion flow". Journal of Glaciology, Vol. 1, No. 9, p. 510.

Bayrock, L. A. 1967. Catastrophic advance of the Steele Glacier, Yukon, Canada. Boreal Institute for Northern Studies, University of Alberta. Edmonton. 35 p. [Publication No. 3.]

de Beer, G. R. 1950. Johann Heinrich Hottinger's description of the ice mountains of Switzerland (1703). Annals of Science, Vol. 6, No. 4, p. 327-60.

Benoist, J.-P. 1979. The spectral power density and shadowing function of a glacial microrelief at the decimetre scale. Journal of Glaciology, Vol. 23, No. 89, p. 57-66.

Benoist, J.-P., and Lliboutry, L. 1978. Fonction d'éclairment d'un profil aléatoire gaussien. Annales de Géophysique, Vol. 34, No. 2, p. 163-75.

Bindschadler, R. A. Unpublished. A time dependent model of temperate glacier flow and its application to predict changes in the surge type Variegated Glacier during its quiescent phase. [Ph.D. thesis, University of Washington, 1978. 245 p.]

Bindschadler, and others. 1977. Geometry and dynamics of a surge-type glacier, by R. A. Bindschadler, W. D. Harrison, C. F. Raymond, and R. Crosson. Journal of Glaciology, Vol. 18, No. 79, p. 181-94.

Blumcke, A., and Hess, H. 1899. Untersuchungen am Hintereisfirner. Zeitschrift d. Deutsch und Osterrech Alpen-Verein, Wissenschaftliche Erganzungshefte, Vol. 1, No. 2, [cited by Deeley and Parr (1913); Shumskiy (1978) p. 128.]

Bodvarsson, G. 1955. On the flow of ice-sheets and glaciers. Jökull, Vol. 2, p. 1-8.

Bordier, 1773. Picturesque journey to the glaciers of Savoy. Geneva. [cited by Tyndall (1874, p. 157).]

Bostock, H. S. 1948. Physiography of the Canadian Cordillera, with special reference to the area north of the fifty-fifth parallel. Geological Survey of Canada Memoir 247. 106 p.

Boulton, G. S. 1979. Processes of glacial erosion on different substrata. Journal of Glaciology, Vol. 23, No. 89, p. 15-38.

Bowden, F. P., and Tabor, D. 1964. Friction and librication of solids, Part 2. Clarendon Press, Oxford. 544 p.

Brockamp, B., and Mothes, H. 1930. Seismische Untersuchungen auf dem Pasterzegletscher. Zeitschrift für Geophysik, Vol. 6, No. 1, p. 482-500.

Bryson, R. A., and Goodman, B. M. 1980. Volcanic activity and climate changes. Science, Vol. 207, No. 4435, p. 1041-44.

Buchanan, J. Y. 1887[a]. On ice and brines. I. Nature, Vol. 35, p. 608-11.

Buchanan, J. Y. 1887[b]. On ice and brines. II. Nature, Vol. 36, p. 9-12.

Buchanan, J. Y. 1887[c]. On ice and brines. Proceedings of the Royal Society of Edinburgh, Vol. 14, p. 129-47. [largely verbatim from 1887[a] and 1887[b].]

Buchanan, J. Y. 1912. In and around the Morteratsch Glacier. Scottish Geographical Magazine, Vol. 28, p. 169-189.

Budd, W. F. 1968. The longitudinal velocity profile of large ice masses. UGGI-AIHS assemblee generale de Berne, 25 sept.-7 oct. 1967. p. 58-77. [AIHS Publication No. 79.]

Budd, W. F. 1969. The dynamics of ice masses. Antarctic Division, Dept. of Supply, Melbourne. 216 p. [ANARE Scientific Reports, Series A(IV). Publication No. 108.]

Budd, W. F. 1970[a]. The longitudinal stress and strain-rate gradients in ice masses. Journal of Glaciology, Vol. 9, No. 55, p. 19-27.

Budd, W. F. 1970[b]. Ice flow over bedrock perturbations. Journal of Glaciology, Vol. 9, No. 55, p. 29-54.

Budd, W. F. 1971. Stress variations with ice flow over undulations. Journal of Glaciology, Vol. 10, No. 59, p. 177-95.

Budd, W. F. 1975. A first simple model for periodically self-surging glaciers. Journal of Glaciology, Vol. 14, No. 70, p. 3-21.

Budd, W. F., and Jenssen, D. 1975. Numerical modelling of glacier systems. UGGI-AIHS Proceedings of the Moscow symposium, August 1971. Snow and ice - symposium - neiges et glaces. p. 257-91. [IASH-AIHS Publication No. 104.]

Budd, W. F., and McInnes, B. J. 1974. Modelling periodically surging glaciers. Science, Vol. 186, p. 925-27.

Budd, W. F., and McInnes, B. J. 1978. Modelling surging glaciers and periodic surging of the Antarctic ice sheet. (In Pittock, A. B., and others. Climatic change and variability - a southern perspective, edited by A. B. Pittock, L. A. Frakes, D. Jenssen, J. A. Petersen, and J. W. Zillman. Cambridge University Press. 455 p.) p.228-34.

Budd, W. F., and McInnes, B. J. 1979. Periodic surging of the Antarctic ice sheet: an assessment by modelling. Hydrological Sciences Bulletin, Vol. 24, No. 1, p. 95-104.

Budd, W. F., and Radok, U. 1971. Glaciers and other large ice masses. Reports on Progress in Physics, Vol. 34, No. 1, p. 1-70.

Budd, W. F., and others. 1971. The derived physical characteristics of the Antarctic ice sheet, by W. F. Budd, D. Jenssen, and U. Radok. Antarctic Division, Dept. of Supply, Melbourne. 178 p. [ANARE Interim Reports, Series A(IV). Publication No. 120.]

Burgers, J. M. 1948. A mathematical model illustrating the theory of turbulence. Advances in Applied Mathematics, Vol. 1, p. 171-99.

Campbell, W. J, and Rasmussen, L. A. 1969. Three-dimensional surges and recoveries in a numerical glacier model. Canadian Journal of Earth Sciences, Vol. 6, No. 4, p. 979-86.

Campbell, W. J., and Rasmussen, L. A. 1970. A heuristic model for three-dimensional time-dependent glacier flow. In UGGI-AIHS International symposium on Antarctic glaciological exploration (ISAGE) Hanover, N.H., U.S.A. 3-7 Sept., 1968. p. 177-90. [AIHS-IASH Publication No. 86.]

Canada. Unpublished. The influence of glaciers on the hydrology of streams affecting the proposed Alcan pipeline route. [Report dated 1977 on file at Glaciology Division, Inland Waters Directorate, Dept. of Fisheries and Environment, Ottawa.]

Carnahan, B., and others. 1969. Applied numerical methods, by B. Carnahan, H. A. Luther, and J. O. Wilkes. Wiley, New York. 604 p.

Carozzi, A. V. 1967. Editor's introduction. (In Agassiz, L. Studies on glaciers. Hafner, New York. lxxii. 213 p. 18 plates. [translated and edited by A. V. Carozzi.]

Chamberlin, R. T. 1928. Instrumental work on the nature of glacier motion. Journal of Geology, Vol. 36, No. 1, p. 1-30.

Chamberlin, R. T. 1934. Comments on paper 'The motion of glaciers', by O. D. von Engeln. Science, Vol. 80, No. 2084, p. 526-27.

Chamberlin, R. T. 1936. Glacier motion as typical rock deformation. Journal of Geology, Vol. 44, No. 1, p. 93-104.

Chamberlin, T. C. 1895. Recent glacial studies in Greenland. Bulletin of the Geological Society of America, Vol. 6, p. 199-220.

de Charpentier, J. 1841. Essai sur les glaciers et sur le terrain erratique du bassin du Rhône. M. Ducloux. Lausanne. x. 363 p. 7 plates.

Claerbout, J. 1976. Fundamentals of geophysical data processing with application to petroleum prospecting. McGraw-Hill, New York. 274 p.

Clarke, G. K. C. 1973. Velocity, stress and temperature solutions for rectilinear glacier flows with sliding at the bed. Geophysical Journal of the Royal Astronomical Society, Vol. 35, p. 71-81.

Clarke, G. K. C. 1976. Thermal regulation of glacier surging. Journal of Glaciology, Vol. 16, No. 74, p. 231-50.

Clarke, G. K. C. In press. Glacier outburst floods from "Hazard Lake", Yukon Territory, and the problem of flood magnitude prediction. Journal of Glaciology, in press.

Clarke, G. K. C., and Jarvis, G. T. 1976. Post-surge temperatures in Steele Glacier, Yukon Territory, Canada. Journal of Glaciology, Vol. 16, No. 74, p. 261-68.

Clarke, G. K. C., and Mathews, W. H. 1981. Estimates of the magnitude of glacier outburst floods from Lake Donjek, Yukon Territory, Canada. Canadian Journal of Earth Sciences, Vol. 18, No. 9, p. 1452-63.

Clarke, G. K. C., and others. 1977. Strain heating and creep instability in glaciers and ice sheets, by G. K. C. Clarke, U. Nitsen, and W. S. B. Paterson. Reviews of Geophysics and Space Physics, Vol. 15, No. 2, p. 235-47.

Colbeck, S. C., and Evans, R. J. 1973. A flow law for temperate glacier ice. Journal of Glaciology, Vol. 12, No. 64, p. 71-86.

Cole, J. D. 1951. On a quasilinear parabolic equation occurring in aerodynamics. Quarterly of Applied Mathematics, Vol. 9, p. 225-36.

Collins, I. F. 1968. On the use of the equilibrium equations and flow law in relating the surface and bed topography of glaciers and ice sheets. Journal of Glaciology, Vol. 7, No. 50, p. 199-204.

Collins, S. G. Unpublished. Steele Glacier surveys 1974 and 1975: data and analysis. 7 p. VII Tables. [report to principal investigator, G. K. C. Clarke].

Cooley, J. W., and Tukey, J. W. 1965. An algorithm for the machine computation of complex Fourier series. Mathematics of Computation, Vol. 19, No. 90, p. 297-301.

Craig, H. 1961. Standard for reporting concentrations of deuterium and oxygen-18 in natural waters. Science, Vol. 133, No. 3467, p. 1833-34.

Crank, J., and Nicolson, P. 1947. A practical method for numerical integration of solutions of partial differential equations of heat-conduction type. Proceedings of the Cambridge Philosophical Society, Vol. 43, p. 50.

Croll, James 1869. On the physical cause of the motion of glaciers. Philosophical Magazine, Vol. 38, p. 201-06. [cited by Croll (1875, p. 504) and Russell (1897, p. 181).]

Croll, James 1875. Climate and time in their geological relations: a theory of secular changes of the earth's climate. D. Appleton and Co. New York. 577 p. [Chapters XXX and XXXI review glacier flow.]

Cunningham, A. 1970. Ladak, physical, statistical and historical, with notices of the surrounding countries. Sagar Publications, New Delhi. 485 p. [first published 1854.]

Dansgaard, W. 1954. The oxygen-18 abundance of fresh water. Geochimica et Cosmochima Acta, Vol. 6, p. 241-60.

Dansgaard, W. 1961. The isotopic composition of natural waters. Meddelelser om Grønland, Vol. 165, No. 2, 120 p.

Dansgaard, W. 1964. Stable isotopes in precipitation. Tellus, Vol. 16, No. 4, p. 436-68.

Dansgaard, W. 1969. Oxygen-18 analysis of water. Meddelelser om Grønland, Vol. 177, No. 2, p. 33-36.

Dansgaard, W., and Johnsen, S. J. 1969[a]. A flow model and a time scale for the ice core from Camp Century, Greenland. Journal of Glaciology, Vol. 8, No. 53, p. 215-23.

Dansgaard, W., and Johnsen, S. J. 1969[b]. Comment on paper by J. Weertman 'Comparison between measured and theoretical temperatures of the Camp Century, Greenland, borehole'. Journal of Geophysical Research, Vol. 74, No. 4, p. 1109-10.

Dansgaard, W., and others. 1969. One thousand centuries of climatic record from Camp Century on the Greenland ice sheet, by W. Dansgaard, S. J. Johnsen, J. Moller, and C. C. Langway Jr. Science, Vol. 166, No. 3903, p. 377-81.

Dansgaard, W., and others. 1971. Climatic record revealed by the Camp Century ice core, by W. Dansgaard, S. J. Johnsen, H. B. Clausen, and C. C. Langway Jr. (In Turekian, K. K., editor. The late Cenozoic glacial ages. Yale University Press, New Haven. 606 p.) p. 37-56.

Dansgaard, W., and others. 1973. Stable isotope glaciology, by W. Dansgaard, S. J. Johnsen, H. B. Clausen, and N. Gundestrup. Meddelelser om Grønland, Vol. 197, No. 2, p. 1-53.

Dansgaard, W., and others. 1977. Stable isotope profile through the Ross Ice Shelf at Little America V, Antarctica, by W. Dansgaard, S. J. Johnsen, H. B. Clausen, C. U. Hammer, and C. C. Langway Jr. In Isotopes and impurities in snow and ice symposium: symposium isotopes et impurités dans les neiges et glaces. Proceedings of the Grenoble Symposium, Aug.-Sept. 1975. p. 322-25. [IAHS Publication No. 118].

Deeley, R. M. 1888. A theory of glacial motion. Philosophical Magazine, Vol. 25, p. 136-64. [cited by Russell (1897, p. 185).]

Deeley, R. M. 1895. The viscous flow of glacier ice. Geological Magazine, Decade IV, Vol. 2, No. 9, p. 408-15.

Deeley, R. M. 1908. The viscosity of ice. Proceedings of the Royal Society, Ser. A, Vol. 81, No. 547, p. 250-59.

Deeley, R. M. 1910. Glacier granule-markings. Geological Magazine, Decade V, Vol. 7, No. 3, p. 112-14.

Deeley, R. M., and Parr, P. H. 1913. The viscosity of glacier ice. Philosophical Magazine, S.6, Vol. 26, No. 151, p. 85-111.

Deeley, R. M., and Parr, P. H. 1914. The Hintereis Glacier. Philosophical Magazine, S.6, Vol. 27, No. 157, p. 153-76.

Demorest, M. 1937. Glaciation of the upper Nugssuak Peninsula, West Greenland. Zeitschrift für Gletscherkunde, Vol. 25, No. 1, p. 36-56.

Demorest, M. 1938. Ice flowage as revealed by glacier striae. Journal of Geology, Vol. 46, No. 5, p. 700-725.

Demorest, M. 1941. Glacier flow and its bearing on the classification of glaciers. Bulletin of the Geological Society of America, Vol. 52, No. 12, part 2, p. 2024-25. [abstract]

Demorest, M. H. 1942. Glacier regimes and ice movement within glaciers. American Journal of Science, Vol. 240, No. 1, p. 29-66. [Part I of 'Glacier thinning during deglaciation', by R. F. Flint, and M. Demorest.]

Demorest, M. 1943. Ice sheets. Bulletin of the Geological Society of America, Vol. 54, No. 3, p. 363-96.

Dolgoushin, L. D., and Osipova, G. B. 1975. Glacier surges and the problem of their forecasting. UGGI-AIHS Proceedings of the Moscow symposium, August 1971. Snow and ice - symposium - neiges et glaces. p. 292-304. [IASH-AIHS Publication No. 104.]

Drake, L. D., and Shreve, R. L. 1973. Pressure melting and regelation of ice by round wires. Proceedings of the Royal Society, Ser. A, Vol. 332, No. 1588, p. 51-83.

von Drygalski, E. 1938. Die Bewegung von Gletschern und Inlandeis. Mitteil. der Geogr. Gesellschaft in Wien, Vol. 81, No. 9-10, p. 273-83. [cited by Matthes (1942), p. 187.]

Elliston, G. R. 1957. A study of the ogives on some of the outlet glaciers of Oraefajokull. Jokull, No. 7, p. 26-32.

von Engeln, O. D. 1915. Experimental studies and observations on ice structure. American Journal of Science, Vol. 190, No. 239, p. 449-73.

von Engeln, O. D. 1934. The motion of glaciers. Science, Vol. 80, No. 2079, p. 401-03.

von Engeln, O. D. 1935. Reply to R. T. Chamberlin's comments on 'The motion of glaciers'. Science, Vol. 81, No. 2106, p. 459-61.

Englehardt, H. F., and others. 1978. Basal sliding and conditions at the glacier bed as revealed by borehole photography, by H. F. Englehardt, W. D. Harrison, and Barclay Kamb. Journal of Glaciology, Vol. 20, No. 84, p. 469-508.

Epstein, S., and others. 1970. Antarctic ice sheet: stable isotope analyses of Byrd Station cores and interhemispheric climatic implications, by S. Epstein, R. P. Sharp, and A. J. Gow. Science, Vol. 168, No. 3939, p. 1570-72.

Evans, S. 1963. Radio techniques for the measurement of ice thickness. Polar Record, Vol. 11, No. 73, p. 406-10.

Finsterwalder, R. 1950. Some comments on glacier flow. Journal of Glaciology, Vol. 1, No. 7, p. 383-88.

Finsterwalder, S., 1897. Der Vernagtferner, seine Geschichte und seine Vermessung in den Jahren 1888-1889. Zeitschrift d. Deutsch und Osterrech Alpen-Verein, Wissenschaftliche Erganzungshefte, Vol. 1, No. 1, [cited by Shumskiy (1978)]

Finsterwalder, S. 1907. Die Theorie der Gletscherschwankungen. Zeitschrift für Gletscherkunde, Vol. 2, p. 81-103. [cited by Nye (1958[a]).]

Fisher, D. A. 1979. Comparison of 10^5 years of oxygen isotope and insoluble impurity profiles from the Devon Island and Camp Century ice cores. Quaternary Research, Vol. 11, No. 3, p. 299-305.

Fisher, D. A., and Jones, S. J. 1971. The possible future behaviour of Berendon Glacier, Canada - a further study. Journal of Glaciology, Vol. 10, No. 58, p. 85-92.

Fisher, J. E. 1947. Forbes' and Alaskan dirt bands on glaciers and their origins. American Journal of Science, Vol. 245, No. 3, p. 137-45.

Fisher, J. E. 1951. The formation of Forbes bands. Journal of Glaciology, Vol. 1, No. 10, p. 580-81. [correspondence about Haefeli (1951[a]).]

Fisher, J. E. 1952. Extrusion flow. Comments on Dr. J. F. Nye's paper. Journal of Glaciology, Vol. 2, No. 11, p. 51-52. [discussion of Nye (1951).]

Fisher, J. E. 1962. Ogives of the Forbes type on alpine glaciers and a study of their origin. Journal of Glaciology, Vol. 4, No. 31, p. 53-61.

Forbes, J. D. 1845. Travels through the Alps of Savoy. A. and C. Black, Edinburgh, 460 p. [second edition.] [first edition (1843) Simpkin. Edinburgh.]

Forbes, J. D. 1855. Remarks on the Rev. H. Moseley's theory of the descent of glaciers. Philosophical Magazine, S.4, Vol. 10, No. 66, p. 300-304.

Forbes, J. D. 1859. Occasional papers on the theory of glaciers. Adam and Charles Black. Edinburgh. 278 p.

Fowler, A. C. 1979. The use of a rational model in the mathematical analysis of a polythermal glacier. Journal of Glaciology, Vol. 24, No. 90, p. 443-56.

Gary, J. 1975. The numerical solution of partial differential equations, Parts I and II. Dept. of Computer Sciences, University of Colorado, Boulder. [lecture notes. Available at nominal cost from the publisher.]

Geikie, James 1894. The great ice age and its relation to the antiquity of man. Edward Stanford. London. 850 p. [third edition.]

Georgi, J. 1933. Greenland as a switch for cyclones. Geographical Journal, Vol. 81, p. 344-45.

Gerrard, J. A. F., and others. 1952. Measurement of the velocity distribution along a vertical line through a glacier, by J. A. F. Gerrard, M. F. Perutz, and A. Roch. Proceedings of the Royal Society, Ser. A, Vol. 213, No. 1115, p. 546-58.

Gibson, G. R., and Dyson, J. L. 1939. Grinnell Glacier, Glacier National Park, Montana. Bulletin of the Geological Society of America, Vol. 50, No. 5, p. 681-96.

Glen, J. W. 1952. Experiments on the deformation of ice. Journal of Glaciology, Vol. 2, No. 2, p. 111-14.

Glen, J. W. 1955. The creep of polycrystalline ice. Proceedings of the Royal Society, Ser. A, Vol. 228, No. 1175, p. 519-38.

Glen, J. W. 1958. The flow law of ice. IUGG Symposium de Chamonix, 16-24 sept. 1958, Physique du mouvement de la glace. p. 171-83. [AIHS Publication no. 47.]

Godwin, H. 1949. Pollen analysis of glaciers in special relation to the formation of various types of banding. Journal of Glaciology, Vol. 1, No. 6, p. 325-33. [report on work of Vareschi.]

Gribbin, J. 1979. Eighteenth century climate may indicate future patterns. New Scientist, Vol. 83, No. 1173, p. 891-93.

Gruner, G. S. 1760. Die Eisgebirge des Schweizerlandes. 3 Volumes in 8°. A. Wagner. Bern. [cited by Agassiz (1840).]

Haefeli, R. 1951[a]. Some observations on glacier flow. Journal of Glaciology, Vol. 1, No. 9, p. 496-500.

Haefeli, R. 1951[b]. The formation of Forbes bands. Journal of Glaciology, Vol. 1, No. 10, p. 581-82. [discussion with J. E. Fisher about Haefeli (1951[a]).]

Haefeli, R. 1957. Notes on the formation of ogives as pressure waves. Journal of Glaciology, Vol. 3, No. 21, p. 27-29.

Haefeli, R. 1961. Contribution to the movement and the form of ice sheets in the Arctic and Antarctic. Journal of Glaciology, Vol. 3, No. 30, p. 1133-51.

Haefeli, R. 1963[a]. Observations in ice tunnels and the flow law of ice. (In Kingery, W. D., editor. Ice and snow. Properties, processes, and applications. Proceedings of a conference at M.I.T., Feb. 12-16, 1962. M.I.T. Press, Cambridge, Mass. 684 p.) p. 162-86.

Haefeli, R. 1963[b]. A numerical and experimental method for determining ice motion in the central parts of ice sheets. UGGI-AIHS General Assembly of Berkeley, 19-31 Aug., 1963. Commission of snow and ice. p. 253-60. [AIHS Publication No. 61.]

Hallet, B. 1976. The effect of subglacial chemical processes on glacier sliding. Journal of Glaciology, Vol. 17, No. 76, p. 209-22.

Hallet, B. 1979. A theoretical model of glacial abrasion. Journal of Glaciology, Vol. 23, No. 89, p. 39-50.

Haltiner, G. J. 1971. Numerical weather prediction. John Wiley and Sons. New York. 317 p.

Haltiner, G. J., and Williams, R. T. 1980. Numerical prediction and dynamic meteorology. John Wiley and Sons. New York. 477 p.

Hammer, C. U., and others. 1978. Dating of Greenland ice cores by flow models, isotopes, volcanic debris, and continental dust, by C. U. Hammer, H. B. Clausen, W. Dansgaard, N. Gundestrup, S. J. Johnsen, and N. Reeh. Journal of Glaciology, Vol. 20, No. 82, p. 3-26.

Hansen, B. L., and Langway, C. C. Jr. 1966. Deep core drilling in ice and core analyses at Camp Century, Greenland, 1961-66. Antarctic Journal of the United States, Vol. 1, p. 207-08.

Hansen, J., and others. 1981. Climate impact of increasing atmospheric carbon dioxide, by J. Hansen, D. Johnson, A. Lacis, S. Lebedeff, P. Lee, D. Rind, and G. Russell. Science, Vol. 213, No. 4511, p. 957-66.

Harrison, W. D. 1972. Temperature of a temperate glacier. Journal of Glaciology, Vol. 11, No. 61, p. 15-29.

Hattersley-Smith, G. 1964. Rapid advance of glacier in northern Ellesmere Island. Nature, Vol. 201, p. 176.

Hawkes, L. 1930. Some notes on the structure and flow of ice. Geological Magazine, Vol. 67, No. 3, p. 111-123.

Hays, J. D., and others. 1976. Variations in the earth's orbit: pacemaker of the ice ages, by J. D. Hays, John Imbrie, and N. J. Shackleton. Science, Vol. 194, No. 4270, p. 1121-32.

von Helmholtz, H. L. F. 1865. Populäre Vorträge. Braunschweig. [cited by Buchanan (1912).]

von Helmholtz, H. L. F. 1873. Popular lectures on scientific subjects. Longmans, Green, and Co. London. 397 p. [translation of Helmholtz (1865) by E. Atkinson.] [Lecture IV. Ice and glaciers. p. 107-152.]

Hess, H. 1904. Die Gletscher. Braunschweig. Friedrich Vieweg und Sohn. 426 p. [cited by Matthes (1942).]

Hess, H. 1933. Das Eis des Erde: Handbuch der Geophysik. Vol. 8, Berlin. p. 1-121. [cited by Matthes (1942).]

Hewitt, K. 1969. Glacier surges in the Karakoram Himalaya (Central Asia). Canadian Journal of Earth Sciences, Vol. 6, No. 4, p. 1009-18.

Hill, R. 1950. Mathematical theory of plasticity. Clarendon Press. Oxford. 356 p.

Hobbs, P. V. 1974. Ice physics. Clarendon Press, Oxford, 837 p.

Hobbs, W. H. 1911. Characteristics of existing glaciers. Macmillan. New York. 301 p.

Hobbs, W. H. 1921. The fixed glacial anticyclone compared to the migrating anticyclone. Proceedings of the American Philosophical Society, Vol. 60, No. 1, p. 34-42.

Hobbs, W. H. 1926. The glacial anticyclone, the poles of the atmospheric circulation. Michigan University Studies, Science Series Vol. 4. MacMillan, New York. [cited by Matthes (1942)]

Hobbs, W. H. 1934. The glaciers of mountain and continent. Science, Vol. 79, No. 2054, p. 419-22.

Hobbs, W. H. 1941. Greenland expeditions 1926-1933. University of Michigan Press. Ann Arbor.

Hodge, S. M. 1974. Variations in the sliding of a temperate glacier. Journal of Glaciology, Vol. 13, No. 69, p. 349-69.

Holdsworth, G. 1969. Structural glaciology of Meserve Glacier. Antarctic Journal of the United States, Vol. 4, No. 4, p. 126-28.

Hollin, J. T. 1969. Ice sheet surges and the geological record. Canadian Journal of Earth Sciences, Vol. 6, No. 4, p. 903-10.

Hopf, E. 1950. The partial differential equation $du/dt+u\ du/dx=\mu\ d^2u/dx^2$. Communications on Pure and Applied Mathematics, Vol. 3, p. 201-30.

Hughes, T. J. 1971. Nonhomogeneous strain studies on Antarctic glaciers. Antarctic Journal of the United States, Vol. 6, No. 4, p. 89-90.

Hughes, T. J. 1975. A differential ablation-longitudinal compression mechanism for generating wave trains on cold alpine glaciers. UGGI-AIHS Proceedings of the Moscow symposium, August 1971. Snow and ice - symposium - neiges et glaces. p. 307-15. [IASH-AIHS Publication No. 104.]

Hughes, T. P., and Seligman, G. 1939. The temperature, meltwater movement, and density increase in the neve of an Alpine glacier. Monthly Notices of the Royal Astronomical Society, Geophysical Supplement, Vol. 4, No. 8, p. 616-47. [Publication No. 2 of the Jungfraujoch Research Party.]

Hughes, T. P., and Seligman, G. In press. The bearing of snow permeability and retentivity on the density increase of firn and ice-band formation in glaciers. Bulletin of the International Association of Scientific Hydrology, [Publication No. 3 of the Jungfraujoch Research Party.] [cited as in press by Seligman (1941), but Bull. Int. Assoc. Sci. Hydrol. did not begin publication until 1956.]

Hugi, F. J. 1830. Naturhistoriche Alpenreise in 8°. Solothurn, Amiet-Lutiger. [cited by Agassiz (1840).]

Hutter, K. 1980. Time-dependent surface elevation of an ice slope. Journal of Glaciology, Vol. 25, No. 92, p. 247-66.

Hutter, K. 1981. The effect of longitudinal strain on the shear stress of an ice sheet. In defence of using stretched coordinates. Journal of Glaciology, Vol. 27, No. 95, p. 39-56.

Hutter, K. In press. Theoretical glaciology. Vol. 1. Reidel Book Co.

Hutter, K., and Legerer, F. J. 1979. First-order stresses and deformations in glaciers and ice sheets. Journal of Glaciology, Vol. 24, No. 90, p. 481. [abstract only.]

Hutter, K., and others. 1981. First order stresses and deformations in glaciers and ice sheets, by K. Hutter, F. Legerer, and U. Spring. Journal of Glaciology, Vol. 27, No. 96, p. 227-70.

Ives, J. D., and King, C. A. M. 1954. Glaciological observations on Morsarjökull S. W. Vatnajökull. Part I: The ogive banding. Journal of Glaciology, Vol. 2, No. 18, p. 423-28.

Jarvis, G. T., and Clarke, G. K. C. 1974. Thermal effects of crevassing on Steele Glacier, Yukon Territory, Canada. Journal of Glaciology, Vol. 13, No. 68, p. 243-54.

Jenssen, D. 1977. A three-dimensional polar ice sheet model. Journal of Glaciology, Vol. 18, No. 80, p. 373-89.

Jenssen, D. 1978. Climatic and topographic changes from glaciological data. (In Pittock, A. B., and others. Climatic change and variability - a southern perspective, edited by A. B. Pittock, L. A. Frakes, D. Jenssen, J. A. Petersen, and J. W. Zillman. Cambridge University Press. 455 p.) p. 77-81.

Jenssen, D., and Radok, U. 1963. Heat conduction in thinning ice sheets. Journal of Glaciology, Vol. 4, No. 34, p. 387-97.

Johnsen, S. J. 1977. Stable isotope profiles compared with temperature profiles in firn with historical temperature records. In Isotopes and impurities in snow and ice symposium: symposium isotopes et impurités dans les neiges et glaces. Proceedings of the Grenoble Symposium, Aug.-Sept. 1975. p. 388-92. [IAHS Publication No. 118].

Johnsen, S. J., and others. 1972. Oxygen isotope profiles through the Antarctic and Greenland ice sheets, by S. J. Johnsen, W. Dansgaard, H. B. Clausen, and C. C. Langway Jr. Nature, Vol. 235, No. 5339, p. 429-34.

Johnson, J. N. 1968. Steady profile of a finite-amplitude kinematic wave on a glacier. Journal of Glaciology, Vol. 7, No. 49, p. 117-19.

Johnston, J., and Adams, L. H. 1913. On the effect of high pressures on the physical and chemical behaviour of solids. American Journal of Science, Vol. 35, Series 4, No. 207, p. 205-53.

Jones, S. J., and Brunet, J.-G. 1978. Deformation of ice single crystals close to the melting point. Journal of Glaciology, Vol. 21, No. 85, p. 445-55.

Kamb, W. B. 1964. Glacier geophysics. Science, Vol. 146, No. 3642, p. 353-65.

Kamb, W. B. 1970. Sliding motion of glaciers: theory and observation. Reviews of Geophysics and Space Physics, Vol. 8, No. 4, p. 673-728.

Kamb, W. B., and LaChapelle, E. R. 1964. Direct observation of the mechanism of glacier sliding over bedrock. Journal of Glaciology, Vol. 5, No. 38, p. 159-72.

Kanasewich, E. R. 1975. Time sequence analysis in geophysics. University of Alberta Press, Edmonton. 364 p. [second edition.]

Kaplan, W. 1952. Advanced calculus. Addison-Wesley, Reading, Mass. 679 p.

Keeler, C. M. 1969. Snow accumulation on Mount Logan, Yukon Territory, Canada. Water Resources Research, Vol. 5, p. 719-23.

King, C. A. M., and Ives, J. D. 1956. Glaciological observations on some of the outlet glaciers of south-west Vatnajökull, Iceland, 1954. Part II: Ogives. Journal of Glaciology, Vol. 2, No. 19, p. 646-51.

King, C. A. M., and Lewis, W. V. 1961. A tentative theory of ogive formation. Journal of Glaciology, Vol. 3, No. 29, p. 912-39.

Koerner, R. M., and Paterson, W. S. B. 1974. Analysis of a core through the Meighen Ice Cap, arctic Canada, and its paleoclimatic implications. Quaternary Research, Vol. 4, No. 3, p. 253-63.

Koerner, R. M., and others. 1973. $\delta^{18}O$ profile in ice formed between the equilibrium and firn lines, by R. M. Koerner, W. S. B. Paterson, and H. R. Krouse. Nature, Physical Science, Vol. 245, No. 148, p. 137-40.

Kreiss, H. 1964. On difference approximations of the dissipative type for hyperbolic differential equations. Communications on Pure and Applied Mathematics, Vol. 17, No. 3, p. 335-53.

Lagally, M. 1930. Die Zahigkeit des Gletschereises und die Tief der Gletscher. Zeitschrift für Gletscherkunde, Vol. 18, p. 1-8. [cited by Perutz (1947).]

Lagally, M. 1934. Mechanik und Thermodynamik des stationarem Gletschers. Leipzig. 94 p. [no publisher indicated in the copy available (University of Washington library). Shumskiy (1978) gives:
...1933. Ergebnisse der Kosmischen Physik hrg. V. Konard und 1. Weickmann, Bd. 2. Lepzig.]

Lax, P., and Wendroff, B. 1960. Systems of conservation laws. Communications on Pure and Applied Mathematics, Vol. 13, No. 2, p. 217-37.

Leighton, F. B. 1951. Ogives on the East Twin Glacier, Alaska, their nature and origin. Journal of Geology, Vol. 59, No. 6, p. 578-89.

Lick, W. 1970. The propagation of disturbances on glaciers. Journal of Geophysical Research, Vol. 75, No. 12, p. 2189-97.

Lighthill, M. J., and Whitham, G. B. 1955. On kinematic waves: I. Flood movement in long rivers; II. Theory of traffic flow on long crowded roads. Proceedings of the Royal Society, Ser. A, Vol. 229, No. 1178, p. 281-345.

Lliboutry, L. 1957. Banding and volcanic ash on Patagonian glaciers. Journal of Glaciology, Vol. 3, No. 21, p. 20-25.

Lliboutry, L. 1958[a]. Studies of the shrinkage after a sudden advance, blue bands and wave ogives on Glaciar Universidad (central Chilean Andes). Journal of Glaciology, Vol. 3, No. 24, p. 261-71.

Lliboutry, L. 1958[b]. La dynamique de la Mer de Glace et la vague de 1891-1895 d'après les mesures de Joseph Vallot. UGGI-AIHS Symposium de Chamonix, 16-24 sept., 1958. p. 125-38. [IASH-AIHS Publication No. 47.]

Lliboutry, L. A. 1964. Instability of temperature (sic) ice-sheets owing to a feedback mechanism. Nature, Vol. 203, No. 4945, p. 627-29.

Lliboutry, L. 1965. Les Chevrons. (In Lliboutry, L., Traité de glaciologie, Masson et Cie, Paris, 1040 p. Tome I, p. 386-90.)

Lliboutry, L. 1968[a]. General theory of subglacial cavitation and sliding of temperate glaciers. Journal of Glaciology, Vol. 7, No. 49, p. 21-58.

Lliboutry, L. 1968[b]. Théorie complète du glissement des glaciers, compte tenu du fluage transitoire. UGGI-AIHS assemblée générale de Berne, 25 sept.-7 oct. 1967. p. 33-48. [AIHS Publication No. 79.]

Lliboutry, L. 1969[a]. The dynamics of temperate glaciers from the detailed viewpoint. Journal of Glaciology, Vol. 8, No. 53, p. 185-205.

Lliboutry, L. 1969[b]. Contribution à la théorie des ondes glaciaires. Canadian Journal of Earth Sciences, Vol. 6, No. 4, p. 943-53.

Lliboutry, L. A. 1971[a]. Permeability, brine content and temperature of temperate ice. Journal of Glaciology, Vol. 10, No. 58, p. 15-29.

Lliboutry, L. A. 1971[b]. The glacier theory. (In Ven te Chow, editor. Advances in hydroscience, Vol. 7. Academic Press, New York. p. 81-167.)

Lliboutry, L. 1975. Loi de glissement d'un glacier sans cavitation. Annales de Géophysique, Vol. 32, No. 2, p. 207-25.

Lliboutry, L. 1978. Glissement d'un glacier sur un plan parsemé d'obstacles hemisphériques. Annales de Géophysique, Vol. 34, No. 2, p. 147-62.

Lliboutry, L. 1979. Local friction laws for glaciers: a critical review and new openings. Journal of Glaciology, Vol. 23, No. 89, p. 67-95.

Lliboutry, L., and Reynaud, L. 1981. "Global dynamics" of a temperate glacier, Mer de Glace, and past velocities deduced from Forbes Bands. Journal of Glaciology, Vol. 27, No. 96, p. 207-26.

Lliboutry, L., and others. 1977. Glaciological problems set by the control of dangerous lakes in Cordillera Blanca, Peru. 1. Historical failures of morainic dams, their causes and prevention, by L. Lliboutry, B. M. Arnas, A. Pautre and B. Schneider. Journal of Glaciology, Vol. 18, No. 79, p. 239-54.

Løken, O. H. 1969. Evidence of surges on the Barnes Ice Cap, Baffin Island. Canadian Journal of Earth Sciences, Vol. 6, No. 4, p. 899-901.

Lorius, C., and Delmas, R. 1975. Géochimie des calottes polaires: aspects atmosphériques et climatiques. Journal de Physique, Vol. 36, No. C8, p. 37-43.

Lorius, C., and Merlivat, L. 1977. Distribution of mean surface stable isotope values in East Antarctica: observed changes with depth in the coastal area. In Isotopes and impurities in snow and ice symposium: symposium isotopes et impurités dans les neiges et glaces. Proceedings of the Grenoble Symposium, Aug.-Sept. 1975. p. 127-37. [IAHS Publication No. 118].

Lorius, C., and others. 1969. Variation in the mean deuterium content of precipitations [sic] in Antarctica, by C. Lorius, L. Merlivat, and R. Hagemann. Journal of Geophysical Research, Vol. 74, No. 28, p. 7027-31.

Lorius, C., and others. 1970. Dating of firn layers in Antarctica: application to the determination of the rate of snow accumulation, by C. Lorius, G. Lambert, R. Hagemann, L. Merlivat, and J. Ravoir. In UGGI-AIHS International symposium on Antarctic glaciological exploration (ISAGE) Hanover, N.H., U.S.A. 3-7 Sept., 1968. p. 3-14. [AIHS-IASH Publication No. 86.]

Lorius, C., and others. 1979. A 30,000-year isotopic climatic record from Antarctic ice, by C. Lorius, L. Merlivat, J. Jouzel, and M. Pourchet. Nature, Vol. 280, p. 644-48.

Mahaffy, M. A. W. Unpublished. A three-dimensional numerical method for computing the load distribution of ice sheets as a function of time. [M.Sc. thesis, University of Colorado, 1974.]

Mahaffy, M. A. W. 1976. A three dimensional numerical model of ice sheets: tests on the Barnes Icecap, Northwest Territories. Journal of Geophysical Research, Vol. 81, No. 6, p. 1059-66.

Mahaffy, M. A. W., and Andrews, J. T. 1976. The speed of glacierization of Canada during the Wisconsin Ice Age. Journal of Glaciology, Vol. 16, No. 74, p. 300-302. [abstract and discussion.]

Main, J. F. 1887. Note on some experiments on the viscosity of ice. Proceedings of the Royal Society, Vol. 42, p. 329-30.

Malvern, L. E. 1969. Introduction to the mechanics of a continuous medium. Prentice-Hall. Englewood Cliffs, New Jersey. 713 p.

Marcus, M. G., and Ragle, R. H. 1970. Snow accumulation in the Icefield Ranges, St. Elias Mountains. Arctic and Alpine Research, Vol. 2, p. 277-92.

Martin, S. 1977. Analyse et reconstitution de la série des bilans annuelles du Glacier de Savennes, sa relation avec les fluctuations du niveau de trois glaciers du Massif du Mont-Blanc (Bossons, Argentière, Mer de Glace). Zeitschrift für Gletscherkunde und Glazial-geologie, Bd. 13, Ht. I-II, p. 127-53.

Mathews, W. H. 1959. Vertical distribution of velocity in Salmon Glacier, British Columbia. Journal of Glaciology, Vol. 3, No. 26, p. 448-54.

Matthes, F. E. 1942. Glaciers. (In O. E. Meinzer, editor, Hydrology - Physics of the earth series, Vol. 9, McGraw-Hill, New York. 712 p.) p. 149-219.

McConnel, J. C. 1890. On the plasticity of an ice crystal (preliminary note). Proceedings of the Royal Society, Vol. 48, No. 244, p. 259-60.

McConnel, J. C. 1891. On the plasticity of an ice crystal. Proceedings of the Royal Society, Vol. 49, No. 299, p. 323-43.

McConnel, J. C., and Kidd, D. A. 1888. On the plasticity of glacier and other ice. Proceedings of the Royal Society, Vol. 44, No. 270, p. 331-67.

McInnes, B. J. Unpublished. Numerical modelling of self-surging glaciers. [M.S. thesis, University of Melbourne, 1976. 165 p.]

McSaveney, M. J. 1972. Ogive systems on polar alpine glaciers. Antarctic Journal of the United States, Vol. 7, No. 4, p. 101-102.

Meier, M. F. 1958. Vertical profiles of velocity and the flow law of glacier ice. UGGI-AIHS Symposium de Chamonix, 16-24 sept. 1958, Physique du mouvement de la glace. p. 169-70. [AIHS Publication no. 47.]

Meier, M. 1960. Mode of flow of Saskatchewan Glacier, Alberta, Canada. U.S. Geological Survey. 70 p. [Professional Paper No. 351.]

Meier, M. F., and Post, A. 1969. What are glacier surges? Canadian Journal of Earth Sciences, Vol. 6, No. 4, p. 807-17.

Meier, M. F., and Tangborn, W. V. 1961. Net budget and flow of South Cascade Glacier, Washington. Journal of Glaciology, Vol. 5, p. 547-66.

Meier, M. F., and others. 1974. Flow of Blue Glacier, Olympic Mountains, Washington, U.S.A., by M. F. Meier, W. B. Kamb, C. R. Allen, and R. P. Sharp. Journal of Glaciology, Vol. 13, No. 68, p. 187-212.

Mesinger, F., and Arakawa, A. 1976. Numerical methods used in atmospheric models. World Meteorological Organization, Geneva, 64 p. [GARP publication series No. 17.]

Morland, L. W. 1976[a]. Glacier sliding down an inclined wavy bed. Journal of Glaciology, Vol. 17, No. 77, p. 447-62.

Morland, L. W. 1976[b]. Glacier sliding down an inclined wavy bed with friction Journal of Glaciology, Vol. 17, No. 77, p. 463-77.

Morland, L. W., and Johnson, I. R. 1980. Steady motion of ice sheets. Journal of Glaciology, Vol. 25, No. 92, p. 229-46.

Morris, E. M. 1976. An experimental study of the motion of ice past obstacles by regelation. Journal of Glaciology, Vol. 17, No. 75, p. 79-98.

Morse, P. M., and Feshbach, H. 1953. Methods of theoretical physics. McGraw-Hill, New York. 1978 p. [two volumes.]

Moseley, H. 1862. On the motion of a plate of metal on an inclined plane, when dilated and contracted; and on the descent of glaciers. Philosophical Magazine, Ser. 4, Vol. 23, p. 72-79. [cited by Croll (1875, p. 498) and Russell (1897, p. 176).]

Muraltuf, 1669. Concerning the icy and crystallin mountains of Helvetia, call'd the Gletscher. Philosophical Transactions of the Royal Society of London, Vol. 4, p. 932-3. [described in Journal of Glaciology, 1948. Vol. 1, No. 3, p. 144.]

Nagata, T. 1977. A theoretical steady state profile of ice sheet (sic). Antarctic Record, Vol. 60, p. 13-27.

Nagata, T. 1978. A possible mechanism of concentration of meteorites within the Meteorite Ice Field in Antarctica. (In Nagata, T., editor. Proceedings of the Second Symposium on Yamato Meteorites. National Institute of Polar Research, Tokyo, 267 p.) p. 70-92. [Memoirs of NIPR special issue No. 8.]

Narod, B. B. Unpublished. U.H.F. radio echo sounding of Yukon Glaciers. [Ph.D. thesis, University of British Columbia, 1979. 183 p.]

Narod, B. B., and Clarke, G. K. C. 1980. Airborne UHF radio echo-sounding of three Yukon glaciers. Journal of Glaciology, Vol. 25, No. 91, p. 23-31.

NASA. Unpublished. ICEX Ice and climate experiment. Report of Science and Applications Working Group. National Aeronautical and Space Administration. Goddard Space Flight Center, Greenbelt Maryland. December 1979.

Nayfeh, A. H. 1973. Perturbation methods. Wiley-Interscience, New York. 425 p.

Nielsen, L. E., and Stockton, F. D. 1956. Flow patterns in glacier ice. Journal of Applied Physics, Vol. 27, No. 5, p. 448-53.

NOAA. Unpublished. Ice sheet modeling studies. A program plan for investigating the past and future of polar ice sheets. National Oceanic and Atmospheric Administration. United States Dept. of Commerce. June 1980. 21 p.

Nye, J. F. 1951. The flow of glaciers and ice sheets as a problem in plasticity. Proceedings of the Royal Society, Ser. A, Vol. 207, No. 1091, p. 554-72.

Nye, J. F. 1952[a]. The mechanics of glacier flow. Journal of Glaciology, Vol. 2, No. 12, p. 82-93.

Nye, J. F. 1952[b]. A comparison between the theoretical and the measured long profile of Unteraar Glacier. Journal of Glaciology, Vol. 2, No. 12, p. 103-107.

Nye, J. F. 1952[c]. A method for calculating the thicknesses of the ice sheets. Nature, Vol. 169, No. 4300, p. 529-30.

Nye, J. F. 1952[d]. Reply to Mr. Joel E. Fisher's comments. Journal of Glaciology, Vol. 2, No. 11, p. 52-53.

Nye, J. F. 1953. The flow law of ice from measurements in glacier tunnels, laboratory experiments, and the Jungfraufirn borehole experiment. Proceedings of the Royal Society, Ser. A, Vol. 219, p. 477-89.

Nye, J. F. 1957. The distribution of stress and velocity in glaciers and ice sheets. Proceedings of the Royal Society, Ser. A, Vol. 239, No. 1216, p. 113-33.

Nye, J. F. 1958[a]. Surges in glaciers. Nature, Vol. 181, No. 3621, p. 1450-51.

Nye, J. F. 1958[b]. A theory of wave formation in glaciers. UGGI - IUGG Symposium de Chamonix, 16-24 sept. 1958, Physique du mouvement de la glace, p. 139-54. [IASH-AIHS Publication No. 47.]

Nye, J. F. 1959[a]. The deformation of a glacier below an icefall. Journal of Glaciology, Vol. 3, No. 25, p. 387-408.

Nye, J. F. 1959[b]. A method of determining the strain-rate tensor at the surface of a glacier. Journal of Glaciology, Vol. 3, No. 25, p. 409-19.

Nye, J. F. 1959[c]. The motion of ice sheets and glaciers. Journal of Glaciology, Vol. 3, No. 26, p. 493-507.

Nye, J. F. 1960. The response of glaciers and ice-sheets to seasonal and climatic changes. Proceedings of the Royal Society, Ser. A, Vol. 256, No. 1287, p. 559-84.

Nye, J. F. 1961. The influence of climatic variations on glaciers. UGGI-AIHS assemblée générale de Helsinki, 25 July-6 August, 1960. p. 397-404. [AIHS-IASH Publication No. 55.]

Nye, J. F. 1963[a]. On the theory of the advance and retreat of glaciers. Geophysical Journal of the Royal Astronomical Society, Vol. 7, No. 4, p. 431-56.

Nye, J. F. 1963[b]. The response of a glacier to changes in the rate of nourishment and wastage. Proceedings of the Royal Society, Ser. A, Vol. 275, No. 1360, p. 87-112.

Nye, J. F. 1963[c]. Theory of glacier variations. (In Kingery, W. D., editor. Ice and snow. Properties, processes, and applications. Proceedings of a conference at M.I.T., Feb. 12-16, 1962. M.I.T. Press, Cambridge, Mass. 684 p.) p. 151-61.

Nye, J. F. 1965[a]. The frequency response of glaciers. Journal of Glaciology, Vol. 5, No. 41, p. 567-87.

Nye, J. F. 1965[b]. A numerical method of inferring the budget history of a glacier from its advance and retreat. Journal of Glaciology, Vol. 5, No. 41, p. 589-607.

Nye, J. F. 1965[c]. The flow of a glacier in a channel of rectangular, elliptic or parabolic cross-section. Journal of Glaciology, Vol. 5, No. 41, p. 661-90.

Nye, J. F. 1967. Plasticity solution for a glacier snout. Journal of Glaciology, Vol. 6, No. 47, p. 695-715.

Nye, J. F. 1969[a]. The effect of longitudinal stress on the shear stress at the base of an ice sheet. Journal of Glaciology, Vol. 8, No. 53, p. 207-13.

Nye, J. F. 1969[b]. A calculation on the sliding of ice over a wavy surface using a Newtonian viscous approximation. Proceedings of the Royal Society, Ser. A, Vol. 311, No. 1506, p. 445-67.

Nye, J. F. 1970. Glacier sliding without cavitation in a linear viscous approximation. Proceedings of the Royal Society, Ser. A, Vol. 315, No. 1522, p. 381-403.

Nye, J. F. 1973[a]. Water at the bed of a glacier. UGGI - IUGG Symposium of Cambridge, Sept. 7-13, 1969. Hydrology of glaciers. p. 189-94. [IASH-AIHS Publication No. 95.]

Nye, J. F. 1973[b]. The motion of ice past obstacles. (In Whalley, E., and others, editors. Physics and chemistry of ice. Edited by E. Whalley, S. J. Jones, and L. W. Gold. Royal Society of Canada. Ottawa. 403 p.) p. 387-99.

Nye, J. F. 1976. Water flow in glaciers: jokulhlaups, tunnels, and veins. Journal of Glaciology, Vol. 17, No. 76, p. 181-208.

Olsson, H. 1936. Radiation measurements on Isachsen's Plateau. Geografiska Annaler, Vol. 18, p. 225-44. [Scientific Results of the Norwegian-Swedish Spitzbergen Expedition in 1934. Part VIII.]

Orowan, E. 1949. The flow of ice and other solids. Journal of Glaciology, Vol. 1, No. 5, p. 231-40.

Paterson, W. S. B. 1969. The physics of glaciers. Pergamon Press, Oxford. 250 p.

Paterson, W. S. B. 1972. Laurentide ice sheet: estimated volumes during late Wisconsin. Reviews of Geophysics and Space Physics, Vol. 10, No. 4, p. 885-917.

Paterson, W. S. B. 1977. Secondary and tertiary creep of glacier ice as measured by borehole closure rates. Reviews of Geophysics and Space Physics, Vol. 15, No. 1, p. 47-55.

Paterson, W. S. B. 1980. Ice sheets and ice shelves. (In Colbeck, S., C., editor. Dynamics of snow and ice masses. Academic Press, New York. 512 p.) p. 1-78.

Paterson, W. S. B. 1981. The physics of glaciers. Pergamon Press. Oxford. 380 p. [second edition.]

Paterson, W. S. B., and Clarke, G. K. C. 1978. Comparison of theoretical and observed temperature profiles in Devon Island ice cap, Canada. Geophysical Journal of the Royal Astronomical Society, Vol. 55, p. 615-32.

Paterson, W. S. B., and Savage, J. C. 1963[a]. Geometry and movement of the Athabasca Glacier. Journal of Geophysical Research, Vol. 68, No. 15, p. 4513-20.

Paterson, W. S. B., and Savage, J. C. 1963[b]. Measurements on Athabasca Glacier relating to the flow law of ice. Journal of Geophysical Research, Vol. 68, No. 15, p. 4537-43.

Paterson, W. S. B., and others. 1977. An oxygen-isotope climatic record from the Devon Island Ice Cap, Arctic Canada, by W. S. B. Paterson, R. M. Koerner, D. Fisher, S. J. Johnsen, H. B. Clausen, W, Dansgaard, P. Bucher, and H. Oeschger. Nature, Vol. 266, p. 508-11.

Perutz, M. F. 1947. Report on problems relating to the flow of glaciers. Journal of Glaciology, Vol. 1, No. 2, p. 47-51.

Perutz, M. F. 1950. Direct measurement of the velocity distribution in a vertical profile through a glacier. Journal of Glaciology, Vol. 1, No. 7, p. 382-83.

Perutz, M. F., and Seligman, G. 1939. A crystallographic investigation of glacier structure and the mechanism of glacier flow. Proceedings of the Royal Society, Ser. A, Vol. 172, No. 950, p. 335-60. [Publication No. 1 of the Jungfraujoch Research Party.]

Philberth, K., and Federer, B. 1971. On the temperature profile and the age profile in the central part of cold ice sheets. Journal of Glaciology, Vol. 10, No. 58, p. 3-14.

Philipp, H. 1920. Geologische Untersuchungen uber den Mechanismus der Gletscherbewegung und die Entstehung der Gletscherstrukter. Neues Jahrbuch für Mineralogie, Geologie und Paleontologie, Vol. 43, p. 439-56. [cited by Matthes (1942), p. 171.]

Phillips, N. A. 1957. A coordinate system having some special advantages for numerical forecasting. Journal of Meteorology, Vol. 14, No. 2, p. 184-85.

Phillips, N. A. 1959. An example of nonlinear computational instability. (In Bolin, B., editor. The atmosphere and the sea in motion. Rockefeller Institute Press. New York. 509 p.) p. 501-04.

Picciotto, E. E., and others. 1960. Isotopic composition and temperature of formation of Antarctic snows, by E. E. Picciotto, X. De Maere, and I. Friedman. Nature, Vol. 187, p. 857-59.

Picciotto, E., and others. 1968. Determination of the rate of snow accumulation at the Pole of Relative Inaccessibility, Eastern Antarctica: a comparison of glaciological and isotopic methods, by E. Picciotto, R. Cameron, G. Crozaz, S. Deutsch, and S. Wilgain. Journal of Glaciology, Vol. 7, No. 50, p. 273-87.

Post, A. 1969. Distribution of surging glaciers in western North America. Journal of Glaciology, Vol. 8, No. 53, p. 229-40.

Post, A., and LaChapelle, E. R. 1971. Glacier ice. University of Toronto Press, Toronto, 110 p.

Prager, W. 1973. Introduction to mechanics of continua. Dover, New York. 230 p. [first edition 1961, Ginn and Co.]

Quincke, G. 1905[a]. The formation of ice and the grained structure of glaciers. Nature, Vol. 72, No. 1874, p. 543-45.

Quincke, G. 1905[b]. The formation of ice and the grained structure of glaciers. Proceedings of the Royal Society, Ser. A, Vol. 66, No. 512, p. 431-39. [same paper as 1905[a].]

Rankine, W. J. M. 1870. On the thermodynamic theory of waves of finite longitudinal disturbance. Philosophical Transactions of the Royal Society, Vol. 160, p. 277-88.

Rasmussen, L. A., and Campbell, W. J. 1973. Comparison of three contemporary flow laws in a three-dimensional time-dependent glacier model. Journal of Glaciology, Vol. 12, No. 66, p. 361-73.

Raymond, C. F. 1971. Flow in a transverse section of Athabasca Glacier. Journal of Glaciology, Vol. 10, No. 58, p. 55-84.

Raymond, C. F. 1976. Some thermal effects of bubbles in temperate glacier ice. Journal of Glaciology, Vol. 16, No. 74, p. 159-72.

Raymond, C. F. 1980. Temperate valley glaciers. (In Colbeck, S. C., editor. Dynamics of snow and ice masses. Academic Press, New York. 512 p.) p. 79-139.

Raymond, C. F., and others. Unpublished. Variegated Glacier studies - 1979, by C. F. Raymond, W. Harrison, and E. Senear. February, 1981.

Reeh, N., and others. 1978. Secular trends of accumulation rates at three Greenland stations, by N. Reeh, H. B. Clausen, W. Dansgaard, N. Gundestrup, C. U. Hammer, and S. J. Johnsen. Journal of Glaciology, Vol. 20, No. 82, p. 27-30.

Reid, H. F. 1896. The mechanics of glaciers. Journal of Geology, Vol. 4, No. 8, p. 912-28.

Rendu, Canon. 1841. Théorie des glaciers de Savoie. Memoirs of the Royal Academy of Sciences of Savoy, Vol. 10. [cited by Tyndall (1874, p. 158); Agassiz (1847, p. xxii); Forbes (1859, p. 253).]

Rendu, Canon. 1874. Theory of the glaciers of Savoy. Macmillan. [translation of Rendu (1841). Cited by Russell (1897).]

Reynaud, L. 1977. Glacier fluctuations in the Mont Blanc area. Zeitschrift für Gletscherkunde und Glazial-geologie, Vol. 13, No. 1-2, p. 155-66.

Reynaud, L. 1979. Reconstruction of past velocities of Mer de Glace using Forbes Bands. Zeitschrift für Gletscherkunde und Glazial-geologie, Vol. 15, No. 2, p. 149-63.

Richtmyer, R. D., and Morton, K. W. 1967. Difference methods for initial value problems. Wiley, Interscience, New York, 406 p.

Rigsby, G. P. 1958. Effect of hydrostatic pressure on velocity of deformation of single ice crystals. Journal of Glaciology, Vol. 3, No. 24, p. 273-78.

Rink, H. 1889. Bemaerkningen om Inlandsisen og Isfjeldenes Oprindelse. Meddelelser om Grønland, Vol. 8, p. 271-79.

Roberts, B. 1933. The Cambridge expedition to Vatnajökull, 1932. Geographical Journal, Vol. 81, No. 4, p. 289-313.

Robin, G. de Q. 1955. Ice movement and temperature distribution in glaciers and ice sheets. Journal of Glaciology, Vol. 2, No. 18, p. 523-32.

Robin, G. de Q. 1967. Surface topography of ice sheets. Nature, Vol. 215, No. 5105, p. 1029-32.

Robin, G. de Q. 1969. Initiation of glacier surges. Canadian Journal of Earth Sciences, Vol. 6, No. 4, p. 919-28.

Robin, G. de Q. 1976. Reconciliation of temperature-depth profiles in polar ice sheets with past surface temperatures deduced from oxygen-isotope profiles. Journal of Glaciology, Vol. 16, No. 74, p. 9-22.

Robin, G. de Q. 1977. Ice cores and climatic change. Philosophical Transactions of the Royal Society of London, Ser. B, Vol. 280, p. 143-48.

Robin, G de Q., and Weertman, H. 1973. Cyclic surging of glaciers. Journal of Glaciology, Vol. 12, No. 64, p. 3-18.

Roots, E. F. 1967. Yukon Centennial projects- a variety of survey problems. Canadian Surveyor, Vol. 21, p. 250-59.

Rothlisberger, H. 1968. Erosive processes which are likely to accentuate or reduce the bottom relief of valley glaciers. UGGI-IUGG Assemblée générale de Berne. 25 sept. - 7 oct. 1967. p. 87-97. [IASH-AIHS Publication No. 79.]

Rothlisberger, H. 1972. Water pressure in intra- and subglacial channels. Journal of Glaciology, Vol. 11, No. 62, p. 177-203.

Russell, I. C. 1897. Glaciers of North America. Ginn and Co. Boston. 210 p.

Ryder, C. H. 1889. Undersögelse af Grönlands Vesthyst fra 72° til 74°35' N. Br. Meddelelser om Grønland, Vol. 8, p. 203-70.

de Saussure, H. B. 1779-96. Voyages dans les Alpes, précédés d'un essai sur l'histoire naturelle des environs de Genève.
Vol. 1: S. Fauche. Neuchâtel. 1779.
Vol. 2: Barde, Manget & Co. Genève. 1786.
Vol. 3: L. Fauche-Borel. Neuchâtel, 1796.
Vol. 4: L. Fauche-Borel. Neuchâtel, 1796.

Scheuchzer, J. J. 1723. Ouresifoigez Helveticus sive itinera per Helvetiae Alpinas Regiones facta, annis 1702-1711. 4 Volumes. Lugdini Batavorum, P. Vander Aa. [cited by Agassiz (1840).]

Schneider, S. H., and Mesirow, L. E. 1976. The genesis strategy. Plenum Press. Dell Publishing Co., New York. 419 p. [a well-annotated popular publication]

Seligman, G. 1936. Snow structure and ski fields. Macmillan, London, 555 p. [reprinted, Jos Adam, Brussels, 1962.]

Seligman, G. 1941. The structure of a temperate glacier. Geographical Journal, Vol. 97, No. 5, p. 295-317.

Seligman, G. 1947. Extrusion flow in glaciers. Journal of Glaciology, Vol. 1, No. 1, p. 12-21. [report of work by Streiff-Becker, with discussion.]

Sharp, R. P. 1943. Geology of the Wolf Creek area, St. Elias Range. Bulletin of the Geological Society of America, Vol. 54, p. 625-50.

Sharp, R. P. 1947. The Wolf Creek glaciers, St. Elias Range, Yukon Territory. The Geographical Review, Vol. 37, No. 1, p. 26-52. [now known as Steele Glacier.]

Sharp, R. P. 1951. Glacial history of Wolf Creek, St. Elias Range, Canada. Journal of Geology, Vol. 59, p. 97-117.

Sharp, R. P. 1953. Deformation of a vertical borehole in a piedmont glacier. Journal of Glaciology, Vol. 2, No. 13, p. 182-84.

Sharp, R. P. 1960. Glaciers. Oregon State System of Higher Education. Eugene. 78 p. [Condon Lecture Series.]

Sharp, R. P., and others. 1960. Oxygen isotope ratios in the Blue Glacier, Olympic Mountains, Washington, by R. P. Sharp, S. Epstein, and I. Vidziunas. Journal of Geophysical Research, Vol. 65, No. 12, p. 4043.

Sherzer, W. H. 1907. Glaciers of the Canadian Rockies and Selkirks. Smithsonian Contributions to Knowledge, Vol. 34, Article 4, 135 p.

Shreve, R. L., and Sharp, R. P. 1970. Internal deformation and thermal anomalies in lower Blue Glacier, Mount Olympus, Washington, USA. Journal of Glaciology, Vol. 9, No. 55, p. 65-86.

Shumskiy, P. A. 1961. On the theory of glacier motion. UGGI-AIHS assemblée générale de Helsinki, 25 July-6 August, 1960. p. 142-49. [AIHS-IASH Publication No. 55.]

Shumskiy, P. A. 1963. On the theory of glacier variations. Bulletin de l'Association Internationale d'Hydrologie Scientifique, 8e An., No. 1, p. 45-56.

Shumskiy, P. A. 1967. The distribution of stress, velocity, and temperature in glaciers. (In Oura, H., editor. Physics of snow and ice: international conference on low temperature science. Vol. 1. Proceedings of conference on physics of snow and ice. August 14-19 1966, Sapporo, Japan. Sapporo, Institute of Low Temperature Science, Hokkaido University, 1967. xxix 711 p.) p. 371-84.

Shumskiy, P. A. 1978. Dynamic glaciology. Amerind Publishing Co. Pvt. Ltd. New Delhi. 161 p. [translated from the Russian by U. Radok and V. J. Vinocuroff.]

Simler, Josias 1574. Vallesiae descriptio: libri duo, de Alpibus commentarius. Tiguri, excudebat C. Froschoverus. [cited by Agassiz (1840).]

SMIC. 1971. Inadvertent climate modification. Report of the study of man's impact on climate. M.I.T. Boston. 201 p.

Somigliana, C. 1921. Sulla profondità dei ghiacciai. Atti della Reale Academia Nationale dei Lincei, Rendiconti Classe di Scienze fisiche, matematiche e naturali, Vol. 30, Serie 5, 1° semestre p. 291-96, 323-27, 360-64. 2° semestre p. 3-7.

Somigliana, C. 1927. The viscosity of glacier ice and the determination of the depth of glaciers. Zeitschrift für Gletscherkunde, Vol. 15. [report by S. Finsterwalder.]

Sorge, E. 1933. The scientific results of the Wegener expedition to Greenland. Geographical Journal, Vol. 81, No. 4, p. 333-44.

Stanley, A. D. 1969. Observations on the surge of Steele Glacier, Yukon Territory, Canada. Canadian Journal of Earth Sciences, Vol. 6, No. 4, p. 819-30.

Steinemann, S. 1958. Resultats experimentaux sur la dynamique de la glace et leur correlation avec le mouvement et la petrographie des glaciers. IUGG Symposium de Chamonix, 16-24 sept. 1958, Physique du mouvement de la glace. p. 184-98. [AIHS Publication no. 47.]

Stokes, G. G. 1848. On a difficulty in the theory of sound. Philosophical Magazine, Vol. 23, No. 3, p. 349-56. [cited by Whitham (1974).]

Streiff-Becker, R. 1938. Zur Dynamik des Firneises. Zeitschrift für Gletscherkunde, Vol. 26, No. 1-2, p. 1-21.

Streiff-Becker, R. 1952. Probleme der Firnschichtung. Zeitschrift für Gletscherkunde und Glazial-geologie, Vol. 2, No. 1, p. 1-9.

Streiff-Becker, R. 1953. Extrusion flow in glaciers. Journal of Glaciology, Vol. 2, No. 13, p. 181-82.

Sverdrup, H. U. 1935[a]. The temperature of the firn on Isachsen's Plateau, and general conclusions regarding the temperature of the glaciers of West Spitzbergen. Geografiska Annaler, Vol. 17, p. 53-88. [Scientific Results of the Norwegian-Swedish Spitzbergen Expedition in 1934. Part III.]

Sverdrup, H. U. 1935[b]. The ablation on Isachsen's Plateau and on the Fourth of July Glacier in relation to radiation and meteorological conditions. Geografiska Annaler, Vol. 17, p. 145-66. [Scientific Results of the Norwegian-Swedish Spitzbergen Expedition in 1934. Part IV.]

Sverdrup, H. U. 1936. Results of the meteorological observations on Isachsen's Plateau. Geografiska Annaler, Vol. 18, p. 34-47. [Scientific Results of the Norwegian-Swedish Spitzbergen Expedition in 1934. Part VI.]

Tammann, G., and Dreyer, K. L. 1929. Die Rekristallisation leicht schmelzender Stoffe und die des Eises. Zeitschrift für Anorganische Chemie, Vol. 182, No. 3, p. 289-313.

Tarr, R. S. and von Engeln, O. D. 1915. Experimental studies of ice with reference to glacier structure and motion. Zeitschrift für Gletscherkunde, Vol. 9, p. 81-139. [cited by Hawkes (1930).]

Tarr, R. S., and Martin, L. 1914. Alaskan glacier studies. The National Geographic Society, Washington, D.C. 498 p.

Tarr, R. S., and Rich, J. L. 1912. The properties of ice - experimental studies. Zeitschrift für Gletscherkunde, Vol. 6, No. 4, p. 225-49. [cited by Hawkes (1930).]

Taylor, G. I. 1910. The conditions necessary for discontinuous motion in gases. Proceedings of the Royal Society, Ser. A, Vol. 84, No. 571, p. 371-77.

Thomas, R. H. 1973. The creep of ice shelves: interpretation of observed behaviour. Journal of Glaciology, Vol. 12, No. 64, p. 55-70.

Thomas, R. H., and others. 1979. Effect of climate warming on the West Antarctic ice sheet, by R. H. Thomas, T. J. O. Sanderson, and K. E. Rose. Nature, Vol. 277, p. 355-58.

Thomson, S. 1972. Movement observations on the terminus area of the Steele Glacier. (in V. C. Bushnell and R. H. Ragle, editors. Icefield Ranges research project. Scientific results. Vol. 3. Arctic Institute of North America. Montreal. 259 p.) p. 29-37.

Thomson, W. (Lord Kelvin). 1888. Polar ice caps and their influence on changing sea levels, (in Thomson, W., Popular lectures and addresses, Vol. 2, Geology and general physics, MacMillan. London. 1894. 599 p.) p. 319-59.

Thorarinsson, S. 1969. Glacier surges in Iceland, with special reference to the surges of Bruarjökull. Canadian Journal of Earth Sciences, Vol. 6, No. 4, p. 875-82.

Topographical Survey. 1969. Steele Glacier Map. Dept. of Energy, Mines and Resources, Ottawa. November, 1969. [Topographic map at scale 1:25,000, contour interval 20 metres. Compiled from aerial photography - flight lines A13232/3, July 1951. Two sheets.]

Truesdell, C., and Toupin, R. A. 1960. The classical field theories. (in Flugge, S., editor, Handbuch der physik, Vol. 3, No. 1, Principles of classical mechanics and field theory. Springer-Verlag. Berlin. 902 p.) p. 226-793.

Tyndall, J. 1874. The forms of water. Henry S. King and Co. London. 192 p. [fourth edition.]

Tyndall, J. 1896. Glaciers of the Alps, being a narrative of excursions and ascents, an account of the origin and phenomenon of glaciers, and an exposition of the physical principles to which they are related. Longmans, Green and Co. London. 445 p. [first edition 1860]

Tyndall, J. 1906. Glaciers of the Alps, part 1, and Mountaineering in 1861. J. M. Dent and Co. London. 274 p.

Untersteiner, N., and Nye, J. F. 1968. Computations of the possible future behaviour of Berendon Glacier, Canada. Journal of Glaciology, Vol. 7, No. 50, p. 205-13.

Vallon, M. Unpublished. Contribution a l'étude de la Mer de Glace. [Thèse d'Etat. Publication No. 102 du Laboratoire de Glaciologie du CNRS, Grenoble, 1975.]

Vallot, J. 1900. Expériences sur la marche et la variation de la Mer de Glace. Annales de l'Observatoire metéorologique, physique et glaciaire du Mont-Blanc. G. Steinheil, Paris. Vol. 4, p. 35-157. Vol. 5, 61 plates. [cited by Lliboutry (1958[b]).]

Vareschi, V. 1942. Die pollenanalytische Untersuchung der Gletscherbewegung. Veroffentlichungen des Geobotanischen Instituts Rubel in Zurich, Ht. 19, 142 p. [cited by King and Lewis (1961).]

Venetz, I. 1830. Actes Soc. Helv Sc. Nat. 15ème session, Hospice du Grand St. Bernard, 21-23 juillet, 1829. P. 31. [cited by Carozzi (1967)]

Venetz, I. 1833. Memoir sur les variations de la température dans les Alpes de la Suisse. Denkschriften der allg. schweiz. Gesellschaft gesaaten Naturwissenschaften, Vol. 1, No. 2, p. 1-38. [cited by Agassiz (1840)].

Vialov, S. S. 1958. Regularities of glacial shields (sic) movement and the theory of plastic viscours (sic) flow. UGGI-AIHS Symposium de Chamonix, 16-24 sept. 1958, Physique du mouvement de la glace. p. 266-75. [AIHS Publication no. 47.]

Vivian, R. 1980. The nature of the ice-rock interface: the results of investigation of 20000 m² of the rock bed of temperate glaciers. Journal of Glaciology, Vol. 25, No. 92, p. 267-77.

Vivian, R., and Bocquet, G. 1973. Subglacial cavitation phenomena under the Glacier d'Argentière, Mont Blanc, France. Journal of Glaciology, Vol. 12, No. 66, p. 439-51.

Waddington, E. D. 1979. Testing numerical models of glacier flow. Journal of Glaciology, Vol. 24, No. 90, p. 508-09. [abstract and discussion.]

Washburn, H. B. 1935. Morainic banding of Malaspina Glacier and other Alaskan glaciers. Bulletin of the Geological Society of America, Vol. 46, No. 12, p. 1879-90.

Weertman, J. 1957. On the sliding of glaciers. Journal of Glaciology, Vol. 3, No. 21, p. 33-38.

Weertman, J. 1958. Travelling waves on glaciers. UGGI-AIHS Symposium de Chamonix, 16-24 sept. 1958, Physique du mouvement de la glace. p. 162-68. [AIHS Publication no. 47.]

Weertman, J. 1961[a]. Stability of ice age ice sheets. Journal of Geophysical Research, Vol. 66, No. 11, p. 3783-92.

Weertman, J. 1961[b]. Equilibrium profile of ice caps. Journal of Glaciology, Vol. 3, No. 30, p. 953-64.

Weertman, J. 1962. Catastrophic glacier advances. UGGI-AIHS Colloque d'Obergurgl, sept. 10-18, 1962. Variations of glaciers. Commission des neiges et glaces. p. 31-39. [IASH-AIHS Publication No. 58.] [discussion in AISH Bulletin Vol. 8, No. 2, p. 61-68.]

Weertman, J. 1963. Profile and heat balance at the bottom surface of an ice sheet fringed by mountain ranges. UGGI-AIHS General Assembly of Berkeley, 19-31 Aug., 1963. Commission of snow and ice. p. 245-52. [AIHS Publication No. 61.]

Weertman, J. 1964[a]. Rate of growth or shrinkage of nonequilibrium ice sheets. Journal of Glaciology, Vol. 5, No. 38, p. 145-58.

Weertman, J. 1964[b]. The theory of glacier sliding. Journal of Glaciology, Vol. 5, No. 39, p. 287-303.

Weertman, J. 1966. Effect of basal water on the dimensions of ice sheets. Journal of Glaciology, Vol. 6, No. 44, p. 191-207.

Weertman, J. 1968. Comparison between measured and theoretical temperatures of the Camp Century, Greenland, borehole. Journal of Geophysical Research, Vol. 73, No. 8, p. 2691-2700.

Weertman, J. 1969. Water lubrication mechanism of glacier surges. Canadian Journal of Earth Sciences, Vol. 6, No. 4, p. 929-42.

Weertman, J. 1972. General theory of water flow at the base of a glacier or ice sheet. Reviews of Geophysics and Space Physics, Vol. 10, No. 1, p. 287-333.

Weinberg, V. B. 1907. Ueber den Koefficienten der inneren Reibung des Gletschereises und seine Bedeutung für die Theorie der Gletscherbewegung. Zeitschrift für Gletscherkunde, Vol. 1, No. 5, [cited by Deeley and Parr (1913) and Somagliana (1921).]

West, K. E. Unpublished. $H2O^{18}/H2O^{16}$ variations in ice and snow of mountainous regions of Canada. [Ph.D. thesis. University of Alberta. 1972. 123 p.]

West, K. E., and Krouse, H. R. 1972. Abundances of isotopic species of water in the St. Elias Mountains. (in V. C. Bushnell and R. H. Ragle, editors. Icefield Ranges research project. Scientific results. Vol. 3. Arctic Institute of North America. Montreal. 259 p.) p. 117-30.

Whitham, G. B. 1974. Linear and nonlinear waves, Wiley-Interscience. New York. 636 p.

Williams, F. M. 1979. Wave ogives as second order effects in the creep of large ice masses. Journal of Glaciology, Vol. 24, No. 90, p. 509-10. [abstract and discussion.]

Wilson, A. T. 1969. The climatic effects of large scale surges of ice sheets. Canadian Journal of Earth Sciences, Vol. 6, No. 4, p. 911-18.

Wood, W. A. 1972. Steele Glacier 1935-1968. (in V. C. Bushnell and R. H. Ragle, editors. Icefield Ranges research project. Scientific results. Vol. 3. Arctic Institute of North America. Montreal. 259 p.) p. 1-8.

Yafang, S., and Wenying, W. 1980. Research on snow cover in China and the avalanche phenomena of Batura Glacier in Pakistan. Journal of Glaciology, Vol. 26, No. 94, p. 25-30.

Zhavoronkov and others. 1955. Primenenie Mechenykh, by Zhavoronkov, Uvarof, and Sevryugova. Atomov Anal. Khim. Akad Nauk. USSR., p. 223-33. [cited by Dansgaard, (1964).]

APPENDIX 1: CONTINUITY MODEL

"A mighty maze! But not without a plan;
A wild, where weeds and flowers promiscuous shoot,
Or garden, tempting with forbidden fruit."[1]

A1.1 THE NUMERICAL SCHEME

A1.1.1 THE CONTINUITY EQUATION

The solution of the partial differential equation (A1.1.1)

$$\frac{\partial h}{\partial t}(x,t) + \frac{1}{W(x)} \frac{\partial Q}{\partial x}(x,t) = A(x,t)$$

$$0 \le x \le L \qquad 0 \le t \le T \qquad \text{(A1.1.1)}$$

is approximated by the solution of a corresponding set of algebraic equations (A1.1.4) for $\{h_j^n \mid j=1,J; n=1,N\}$, the values of h(x,t) at a set of mesh points in x-t space.

$$\{(\sum_{i=1}^{j-1} \Delta x_i \;,\; n\Delta t) \mid j=1,J;\; n=1,N\}$$

$$L = \sum_{j=1}^{J-1} \Delta x_j \qquad n = \Delta t/T \qquad \text{(A1.1.2)}$$

The x axis runs along the glacier bed, and the thickness h and the source term A are measured normal to it. Q is the ice flux through the cross section normal to the bed. W is the width of the glacier channel. The mesh points are chosen with a uniform spacing Δx in the horizontal direction. The intervals along the x axis on the glacier bed are then

[1] An essay on man. Alexander Pope.

$$\Delta x_j = \Delta x/\cos(\beta_j) \qquad \text{(A1.1.3)}$$

The slope of the glacier bed is β. This is illustrated in Figure A1.1.

$$\frac{h_j^{n+1} - h_j^n}{\Delta t} + \frac{\theta}{W_j}\frac{(Q_{j+1/2}^{n+1} - Q_{j-1/2}^{n+1})}{\Delta x_j} + \frac{(1-\theta)}{W_j}\frac{(Q_{j+1/2}^{n} - Q_{j-1/2}^{n})}{\Delta x_j}$$

$$= \theta A_j^{n+1} + (1-\theta)A_j^n \qquad \text{(A1.1.4)}$$

$$1 \le j \le J \quad 1 \le n \le N$$

The weight factor θ is a constant between 0 and 1 used to

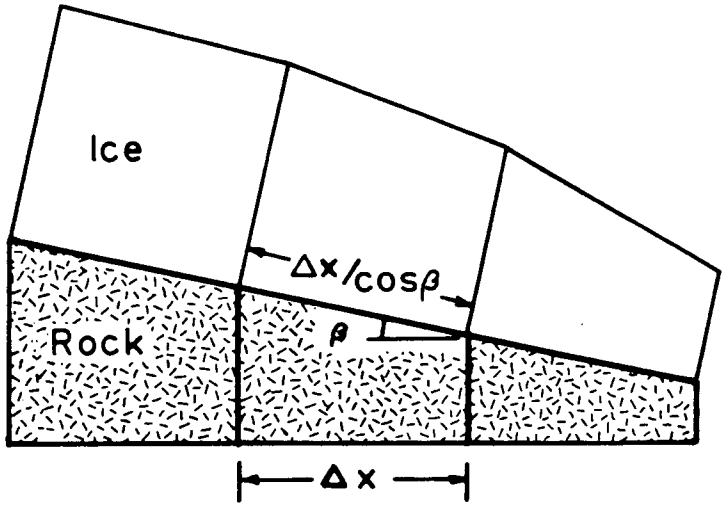

FIGURE A1.1. Mesh Increment On Bed.

stabilize the numerical scheme by mixing estimates of the spatial partial derivative at successive time steps. This is discussed further in Section A1.4 below.

The ice flux $Q_{j+1/2}$ can be written in terms of the ice thickness h_j at the mesh points by

$$Q_{j\pm1/2} = V_{j\pm1/2}\, W_{j\pm1/2}\, \frac{(h_{j\pm1} + h_j)}{2} \qquad \text{(A1.1.5)}$$

where $V_{j+1/2}$ is the ice velocity midway between the mesh points and averaged over the depth $h_{j+1/2}$ normal to the glacier bed. $W_{j+1/2}$ is the channel width.

After substituting (A1.1.5) into (A1.1.4), separating past and future values of thickness h and setting

$$p_j = \Delta t/(2\Delta x\, W_j) \qquad \text{(A1.1.6)}$$

(A1.1.4) gives

$$[1 + p_j\,\theta(V^{n+1}_{j+1/2} W_{j+1/2} - V^{n+1}_{j-1/2} W_{j-1/2})]\, h^{n+1}_j$$

$$+ [-\theta p_j W_{j-1/2} V^{n+1}_{j-1/2}]\, h^{n+1}_{j-1} + [\theta p_j W_{j+1/2} V^{n+1}_{j+1/2}]\, h^{n+1}_{j+1}$$

$$= [1 - p_j (1-\theta)(V^{n}_{j+1/2} W_{j+1/2} - V^{n}_{j-1/2} W_{j-1/2})]\, h^{n}_j$$

$$+ [(1-\theta)p_j W_{j-1/2} V^{n}_{j-1/2}]\, h^{n}_{j-1} - [(1-\theta)p_j W_{j+1/2} V^{n}_{j+1/2}]\, h^{n}_{j+1}$$

$$+ [\theta A^{n+1}_j + (1-\theta) A^{n}_j]\, \Delta t$$

$$1 \le j \le J \qquad 1 \le n \le N \qquad \text{(A1.1.7)}$$

Starting from an initial condition $\{h^0_j \mid j=1,J\}$, this system of equations is solved for $\{h^1_j \mid j=1,J\}$. This time stepping method of solution is continued until n=N. Since the left side of (A1.1.7) contains more than one of the unknowns i.e. h^{n+1}_{j-1}, h^{n+1}_j, and h^{n+1}_{j+1}, this is an implicit numerical scheme for $\{h^{n+1}_j \mid j=1,J\}$.

A1.1.2 A MATRIX FORMULATION

The system of equations (A1.1.7) can be written as a matrix equation

$$\begin{bmatrix} B_1 & C_1 & 0 & \cdots & 0 & \cdots \\ A_2 & B_2 & C_2 & 0 & \cdots & 0 \\ 0 & A_3 & B_3 & C_3 & \cdots & 0 \\ \vdots & & \ddots & & & \\ & & 0 & A_j & B_j & C_j \\ & & & \ddots & & \\ & & & A_{J-1} & B_{J-1} & C_{J-1} \\ & & & 0 & A_J & B_J \end{bmatrix} \begin{bmatrix} h_1^{n+1} \\ \vdots \\ h_j^{n+1} \\ \vdots \\ h_J^{n+1} \end{bmatrix} = \begin{bmatrix} D_1 \\ \vdots \\ D_j \\ \vdots \\ D_J \end{bmatrix}$$

$$\text{or } \underline{\underline{M}}\,\underline{H} = \underline{D} \qquad \text{(A1.1.8)}$$

where D_j is the expression on the right side of (A1.1.7) containing only known quantities. B_1, C_1, A_J, B_J, D_1, and D_J are determined by the choice of boundary conditions discussed below in Section A1.3. The matrix $\underline{\underline{M}}$ is tridiagonal and is diagonally dominant because the diagonal terms B_j, the coefficients of h_j^{n+1} in (A1.1.7), are of order unity, while the off-diagonal terms are of the order of pQ, which is usually less than unity for reasonable glacier models, and choices of mesh. This means that the matrix equation is easily solved by Gaussian elimination without using any special pivoting strategy (Carnahan and others, 1969, p. 272).

A1.2 NONLINEARITY

If the velocities $\{V_j^{n+1} | j=3/2, 5/2,...J+1/2\}$ were perfectly known, the complete solution would be obtained by simply solving the matrix equation (A1.1.8). Since the $\{V_j^{n+1} | j=3/2, 5/2,...J+1/2\}$ depend in general on $\{h_j^{n+1} | j=1,J\}$ through some flow and sliding law, (A1.1.8) only appears to be linear in $\{h_j^{n+1} | j=1,J\}$. The standard technique to solve nonlinear equations of the form of (A1.1.8) is to use an iterative method to improve the coefficient values (here, the $\{V_j^{n+1} | j=3/2, 5/2,...J+1/2\}$) based on the values of the unknowns $\{h_j^{n+1} | j=1,J\}$ at the previous iteration. Specifically, letting the sublevel prescripts indicate the iteration number, $\{{}_0V_j^{n+1} | j=3/2, 5/2,...J+1/2\}$ at the new time step are approximated by $\{V_j^n | j=3/2, 5/2,...J+1/2\}$, the velocity at the previous time step. Using these values for the coefficients, (A1.1.8) is solved for $\{{}_0h_j^{n+1} | j=1,J\}$. This thickness profile estimate is then put into the flow and sliding law to find a better velocity profile $\{{}_1V_j^{n+1} | j=3/2, 5/2,...J+1/2\}$. The residuals $\{ r_j^{n+1} | j=1,J\}$ are then calculated.

$$r_j^{n+1} = 2p\,\Theta[Q_{j+1/2}^{n+1} - Q_{j-1/2}^{n+1}] + 2p_j(1-\Theta)[Q_{j+1/2}^{n} - Q_{j-1/2}^{n}]$$

$$+ h_j^{n+1} - h_j^{n} - [\Theta A_j^{n+1} - (1-\Theta)A_j^{n}]\Delta t$$

$$1 \le j \le J \qquad 1 \le n \le N \qquad \text{(A1.2.1)}$$

and

$$p_j = \Delta t/(2\Delta x\, W_j\, j) \qquad (A1.1.6)$$

The residuals are a measure of the degree to which the continuity equation is satisfied by the current values of $\{h_j^{n+1} | j=1,J\}$ and $\{V_j^{n+1} | j=3/2,\ 5/2,\ldots J+1/2\}$. The quantity r_j is the volume of ice created or destroyed in one time step per unit length and width at mesh point j, through error either in the surface elevation, or in the amount of ice flowing in and out from the adjacent mesh points.

It is then necessary to calculate the corrections $\{\delta h_j | j=1,J\}$ to the thicknesses such that the residuals will be reduced to zero using

$$h^{n+1}_{k+1\ j} = h^{n+1}_{k\ j} - \delta h_j \qquad (A1.2.2)$$

This can be done using a multidimensional Newton-Raphson technique. A variation of this method was used by Bindschadler (unpublished, p. 84), who did not solve the matrix equation (A1.1.8) for the first estimate $\{{}_0h_j^{n+1} | j=1,J\}$, but instead set

$$\{{}_0h_j^{n+1} | j=1,J\} = \{h_j^n | j=1,J\}$$

i.e. used a steady state starting estimate. The procedure described in this study gives a better starting estimate of $\{{}_0h_j^{n+1} | j=1,J\}$ when the profile is changing with time, but requires the extra computing effort of solving (A1.1.8).

The residuals $\{ r_j^{n+1} | j=1,J\}$ are a function of the thickness values $\{h_j^{n+1} | j=1,J\}$ either directly, or through the ice surface slope or higher derivatives. Dropping iteration prescripts for the moment, the first order Taylor expansion of r_j^{n+1} about zero is

$$r_j^{n+1} = \sum_{k=1}^{J} \frac{\partial r_j^{n+1}}{\partial h_k^{n+1}} \delta h_k$$

or, in matrix form,

$$\underline{\underline{A}}\ \underline{\delta h} = \underline{r} \ . \qquad \text{(A1.2.3)}$$

This is a set of algebraic equations which can be solved for $\{\delta h_j \mid j=1,J\}$. The elements of matrix $\underline{\underline{A}}$ can be found by differentiating the residuals in (A1.2.3)

$$a_{jk} = \frac{\partial r_j^{+1}}{\partial h_k^{+1}} \qquad \text{(A1.2.4)}$$

This is another implicit system of equations that can be solved by Gaussian elimination (e.g. Carnahan and others, 1969, p. 272) for the corrections to the ice thickness.

A common modelling case is that in which the flux at x is a function of the thickness at x and the slope at x. In this case, the matrix $\underline{\underline{A}}$ is also tridiagonal. For models with a flow law such that the flux depends on thickness and slope over a range of x, the diagonal band of $\underline{\underline{A}}$ becomes wider than three. These models are no more difficult in theory, but merely require more computational time.

For the case that flux Q(x) depends only on thickness and slope at x,

$$a_j = \frac{\partial r}{\partial h}_j \Bigg|_{\substack{h_j \\ h_{j-1}\ h_{j+1}}} = -2p_j \theta \frac{\partial Q}{\partial h}_{j-1/2} \Bigg|_{\substack{h_j \\ h_{j-1}\ h_{j+1}}}$$

$$b_j = \frac{\partial r}{\partial h}_j \Bigg|_{\substack{h_{j-1} \\ h_j\ h_{j+1}}} = 1+2p_j \theta \left[\frac{\partial Q}{\partial h}_{j+1/2} - \frac{\partial Q}{\partial h}_{j-1/2} \right] \Bigg|_{\substack{h_{j-1} \\ h_j\ h_{j+1}}}$$

$$c_j = \frac{\partial r}{\partial h}_j \Bigg|_{\substack{h_{j-1} \\ h_j\ h_{j+1}}} = 2p_j \theta \frac{\partial Q}{\partial h}_{j+1/2} \Bigg|_{\substack{h_{j-1} \\ h_j\ h_{j+1}}} \qquad \text{(A1.2.5)}$$

where each partial derivative is evaluated with all the other h_i held constant. The b_j's are the main diagonal elements a_{jj} and the a_j's, and c_j's are the sub- and super-diagonal elements $a_{j+1,j}$ and $a_{j,j+1}$.

For computations it is more convenient to express the coefficients in the matrix $\underline{\underline{A}}$ as partials with respect to thickness between mesh points $h_{j+1/2}$ and the slope between mesh points $\alpha_{j+1/2}$, since these are the quantities from which the flux is directly calculated. This form of the coefficients is derived in Appendix 10.

As with the matrix equation (A1.1.8) for the full thickness for the first iteration at a new time step, the coefficients in rows 1 and J are determined by the boundary conditions. The details are described below in Section A1.3.

If the residuals were truly a linear function of the $\{h_j^{n+1} | j=1,J\}$, the solution would be obtained exactly after solving the residual equation (A1.2.3) once. Since the matrix equation (A1.2.3) was obtained by linearization through a Taylor series, the iterations must be continued until the the largest

residual in absolute value is smaller than some preset test criterion. The choice of such a criterion is discussed in Appendix 11.

A1.3 BOUNDARY CONDITIONS

A1.3.1 THE UPPER BOUNDARY

The first order partial differential equation (A1.1.1) requires one boundary condition. The condition for the finite difference system (A1.1.4) is applied at the upstream end j=1 in complete analogy to the condition on equation (A1.1.1). The various possible types of condition are described below.

1) Zero flux input: wedge type

The thickness h_1 is zero. This models alpine glaciers starting on a steep slope. In the equations (A1.1.8) for the first iteration,

$$B_1 = 1.0 \quad C_1 = 0.0 \quad D_1 = 1.0 \qquad \text{(A1.3.1)}$$

For subsequent iterations to find $\{\delta h_j \mid j=1,J\}$, the same values are used.

2) Zero flux input: zero slope

The surface slope is zero at x=0. This is the model for a stable ice divide on an ice sheet. The boundary condition is implemented by reflection at j=1 by using an image point in the equations (A1.1.7) with subscript 0 such that

$$h_0 = h_2$$

$$W_{1/2} = W_{3/2}$$

$$V_{1/2} = -V_{3/2} \qquad \text{(A1.3.2)}$$

In the matrix equation (A1.1.8)

$$B_1 = 1 + 2p_1 \Theta V_{3/2}^{n+1} W_{3/2}$$

$$C_1 = 2p_1 \Theta V_{3/2}^{n+1} W_{3/2}$$

$$D_1 = h_1 - 2(1-\Theta)p_1 V_{3/2}^{n} [h_2^{n} + h_1^{n}] W_{3/2} \qquad \text{(A1.3.3)}$$

$$+ \Theta A_1^{n+1} \Delta t + (1-\Theta) A_1^{n} \Delta t$$

3) Flux input $Q_0(t)$

The flux $Q_0(t)$ at $x=-\Delta x/2$, or $j=1/2$, is substituted into (A1.1.7). This models a section of an ice mass starting some distance below the bergschrund or ice divide. For example this model is used to investigate the generation of wave ogives at an icefall when the input flux from the upper glacier is $Q_0(t)$. Note that in the limit of $Q_0(t)$ going to zero, this is not equivalent to boundary conditions 1) or 2) above, since in this case neither the slope nor the thickness is specifically set to zero at the boundary, and the boundary is located at $x=-\Delta x/2$ rather than at $x=0$. In the matrix (A1.1.8)

$$B_1 = 1 + p_1 \theta V^{n+1}_{3/2} W_{3/2}$$

$$C_1 = p_1 \theta V^{n+1}_{3/2} W_{3/2}$$

$$D_1 = -2p_1 [\theta Q^{n+1}_0 + (1-\theta) Q^{n}_0] - p_1 (1-\theta) V^{n}_{3/2} [h^{n}_2 + h^{n}_1] W_{3/2}$$

$$+ (1-\theta) A^{n}_1 \Delta t + \theta A^{n+1}_1 \Delta t + h^{n}_1 \qquad \text{(A1.3.4)}$$

A1.3.2 THE DOWNSTREAM BOUNDARY

Since the partial differential equation (A1.1.1) is first order, it requires only one boundary condition. However, to implement the numerical scheme (A1.1.7) it is necessary to impose some condition at the lower boundary j=J so that the the matrix $\underline{\underline{M}}$ can be terminated i.e. to eliminate $h^{n}_{J+\frac{1}{2}}$.

A1.3.3 NONZERO FLUX LEAVES DOWNSTREAM BOUNDARY

This treatment is useful when modelling a short section of an ice mass which does not include the terminus region. No mesh points are added to or removed from the grid as time advances, and a nonzero ice flux exists at $\Delta x/2$ beyond the last mesh point j=J. This ice flux is given by

$$Q^{n+1}_{J+1} = V^{n+1}_{J+1/2} \; h^{n+1}_{J+1/2} \; W_{J+1/2}$$

where $h^{n}_{J+\frac{1}{2}}$ is estimated by the second order Newton's divided

difference polynomial (e.g., Carnahan and others, 1969, p. 12)

$$h_{J+1/2} =$$

$$h_J + \frac{\Delta x}{2}\left[\frac{h_J - h_{J-1}}{\Delta x}\right] + \left[\frac{\Delta x}{2}\right]\left[\frac{3\Delta x}{2}\right]\left[\frac{\dfrac{h_J - h_{J-1}}{\Delta x} - \dfrac{h_{J-1} - h_{J-2}}{\Delta x}}{2\Delta x}\right] \qquad \text{(A1.3.5)}$$

This quadratic extrapolation ignores the third order term $(\partial^3 h/\partial x^3)\Delta x^3$, so that the extrapolated flux has an error that is $O(V\,[\partial^3 h/\partial x^3]\Delta x^3)$, and the flux gradient has an error term that is $O(V\,[\partial^3 h/\partial x^3]\Delta x^2)$, which is the same order as the truncation error described in Section A1.5. To use any extrapolation with a larger error than the truncation error would reduce the accuracy of the total solution. This was done by Budd and Jenssen (1975) who used a linear extrapolation. The 'shocks' at the boundaries described by these authors are possibly a result of this treatment.

However, this extrapolation introduces a nonzero coefficient k for $h_J^{n+\frac{1}{2}}$ in the last row J of the matrix (A1.1.8), so that the matrix is no longer tridiagonal, but has the form

$$\begin{bmatrix} 0 & . & A_{J-2} & B_{J-2} & C_{J-2} & 0 \\ . & 0 & . & 0 & A_{J-1} & B_{J-1} & C_{J-1} \\ & & . & & k & A_J & B_J \end{bmatrix} \begin{bmatrix} h^{n+1}_{J-2} \\ h^{n+1}_{J-1} \\ h^{n+1}_{J} \end{bmatrix} = \begin{bmatrix} D_{J-2} \\ D_{J-1} \\ D_J \end{bmatrix} \qquad \text{(A1.3.6)}$$

in the last three rows. When k is nonzero, the matrix can be restored to tridiagonal form by subtracting (k/A_J) times the

(J-1)st row from the Jth row to give

$$\begin{bmatrix} \cdot & A_{J-2} & B_{J-2} & C_{J-2} & & 0 \\ \cdot & 0 & A_{J-1} & B_{J-1} & C_{J-1} & \\ & & 0 & A_J - kB_{J-1} & B_J - kC_{J-1} & \end{bmatrix} \begin{bmatrix} h^{n+1}_{J-2} \\ h^{n+1}_{J-1} \\ h^{n+1}_{J} \end{bmatrix} = \begin{bmatrix} D_{J-2} \\ D_{J-1} \\ D_J - kD_{J-1} \end{bmatrix} \qquad (A1.3.7)$$

A1.3.4 MOVING WEDGE TERMINUS

For some applications it is essential to include the terminus in the glacier model, and allow it to move so as to satisfy mass conservation and the flow law for ice. For example, the terminus of a surging glacier may advance and retreat by 10% or more of the glacier length during one cycle. This requires a procedure to add meshpoints to the grid, or to remove them, based on a calculation of the terminus position at each time step.

To calculate the terminus position when it lies between mesh points, it is necessary to make some assumptions. The velocity (1.4.34) based on an integration of Glen's flow law (Glen, 1955) for simple shear cannot be used near the terminus (Nye, 1967). The scheme described below is based on the one used by Bindschadler (unpublished, p. 105), with some modifications to the x increments. Referring to Figure A1.2, the terminus is assumed to be wedge-shaped i.e. the ice thickness h(x) is linear with distance from the last mesh point x_J to the terminus

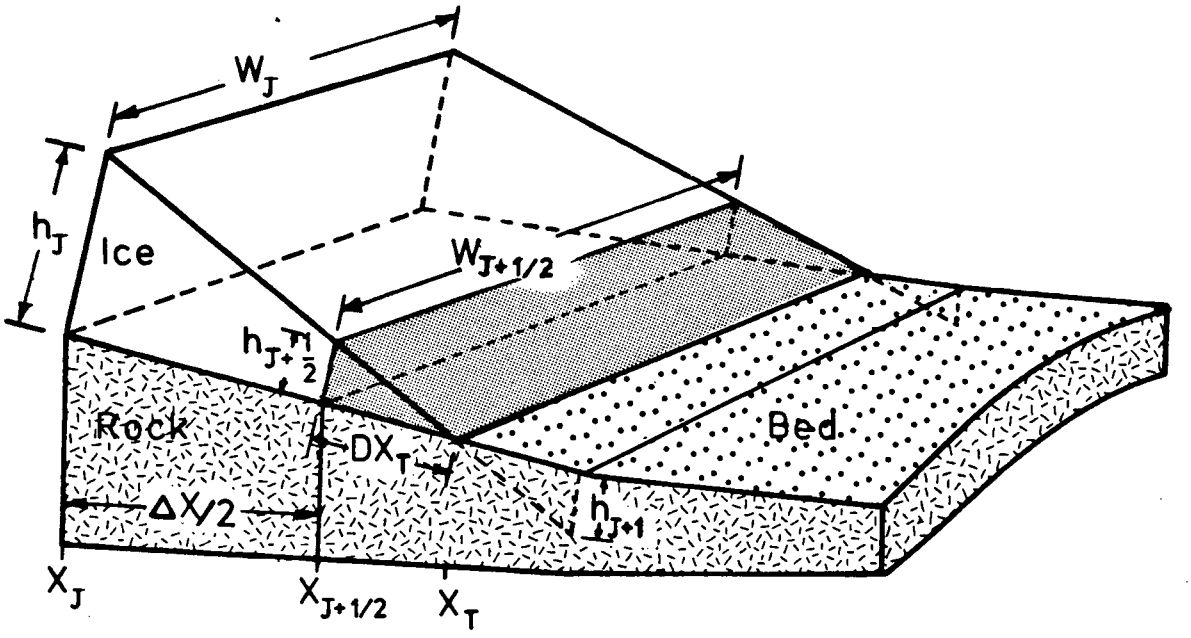

FIGURE A1.2. Model Terminus.

position x_T, at which the thickness is zero. Mass is conserved in the shaded wedge beyond $x_{J+1/2}$ in Figure A1.2. The volume of this terminus section is

$$VOL_T = \int_0^{DX_T} h(x)\, W(x)\, dx \qquad \text{(A1.3.8)}$$

where x is measured parallel to the bed, and $h(x)$ is normal to the bed. Neglecting the possibility that dW/dx may change slightly below x_{J+1},

$$h(x) = h_J + h'x \qquad h' = -h_{J+1/2} \Big/ DX_T$$

$$W(x) = W_J + W'x \qquad W' = (W_{J+1} - W_J) \Big/ DX_T \qquad \text{(A1.3.9)}$$

Substituting (A1.3.9) into (A1.3.8) gives

$$VOL_T = \frac{h_{J+1/2}\, W_{J+1/2}\, DX_T}{2} + \frac{W'\, h_{J+1/2}\, DX_T^2}{6} \qquad (A1.3.10)$$

and, using the similar triangles of height h_J and $h_{J+1/2}$ shown in Figure A1.2,

$$DX_T = \left[\frac{h_J + h_{J+1}}{h_J - h_{J+1}}\right] \frac{\Delta x_J}{2} \qquad (A1.3.11)$$

Changes in the volume VOL_T occur due to the mass balance acting on the surface, and ice flowing into VOL_T through the cross-section at $x_{J+1/2}$. The average mass balance (normal to the bed) on the surface of the wedge, to the same accuracy as used elsewhere on the grid, is

$$\bar{A} = \frac{A(x_{J+1/2}) + A(x_T)}{2} \qquad (A1.3.12)$$

The surface area exposed normal to this ablation is

$$\bar{W}\, DX_T = \left[\frac{W(x_{J+1/2}) + W(x_T)}{2}\right] DX_T \qquad (A1.3.13)$$

Bars over variables indicate average values. $W(x_T)$ and $A(x_T)$ can be interpolated linearly between their values at x_J and x_{J+1}. Setting

$$X = \frac{2\, DX_T}{\Delta x_J} \qquad (A1.3.14)$$

then the change in volume of the wedge terminus due to melting on the top surface in a time interval Δt is

$$\delta V_{bal} = \bar{A}\,\bar{W}\,DX_T =$$

$$= \frac{\Delta t}{16} DX_T \left[(2-X)W_J + (2+X)W_{J+1}\right]\left[(2-X)A_J + (2+X)A_{J+1}\right] \qquad \text{(A1.3.15)}$$

The change in volume of the wedge due to influx of ice through the cross-section at $x_{J+1/2}$ during the same time interval Δt is

$$\delta V_{flux} = W_{J+1/2}\; h_{J+1/2}\; V_{J+1/2}\; \Delta t \qquad \text{(A1.3.16)}$$

Conservation of mass in the terminus from time step n to time step (n+1) requires

$$VOL_T^{n+1} - VOL_T^{n} = \left[\frac{\delta V_{bal}^{n+1} + \delta V_{bal}^{n}}{2} + \frac{\delta V_{flux}^{n+1} + \delta V_{flux}^{n}}{2}\right] \qquad \text{(A1.3.17)}$$

On substituting (A1.3.10) through (A1.3.16), the unknowns in this equation are h_J^{n+1} and $h_{J+\frac{1}{2}}^{n+\frac{1}{2}}$. Since it is not linear in these unknowns, it cannot be included directly in the matrix equation (A1.1.8) at the first iteration for $\{h_j^{n+1} | j=1,J+1\}$. Instead, an initial guess at $h_{J+\frac{1}{2}}^{n+\frac{1}{2}}$ must be used. For instance, I can assume that the terminus has the same slope as at the previous step, i.e.

$$h_{J+1}^{n+1} - h_J^{n+1} = h_{J+1}^{n} - h_J^{n} \qquad \text{(A1.3.18)}$$

and use this in (A1.1.8) by setting

$$A_{J+1} = -1.0 \qquad B_{J+1} = 1.0 \qquad D_{J+1} = h_{J+1} - h_J \qquad \text{(A1.3.19)}$$

After dividing through (A1.3.17) by a surface area $W_{J+1/2}\Delta x_J$ to give the same units as the other residuals in (A1.2.1), the

residual at x_{J+1} is

$$r^{n+1}_{J+1} = \left[\frac{VOL_T^{n+1} - VOL_T^{n} - \frac{1}{2}\left[\delta V_{bal}^{n+1} + \delta V_{bal}^{n} \right] - \frac{1}{2}\left[\delta V_{flux}^{n+1} + \delta V_{flux}^{n} \right]}{W_{J+1/2} \, \Delta x_J} \right] \tag{A1.3.20}$$

Using the Taylor expansion (A1.2.3) on (A1.3.20) gives a (J+1)th equation for the corrections $\{\delta h_j \mid j=1,J+1\}$. The coefficients in (A1.2.3) are

$$a_{J+1,J} = \frac{\partial r}{\partial h}_J$$

$$= \frac{DX_T}{4\Delta x_J} + \frac{W' \, DX^2_T}{12 W_{J+1/2} \, \Delta x_J} - \frac{\Delta t \, V_J}{4\Delta x_J} - \frac{\Delta t \, h_{J+1/2}}{2 \, \Delta x_J} \frac{\partial V_J}{\partial h_J} +$$

$$\frac{\partial DX_T}{\partial h_J} \left[\frac{h_{J+1/2}}{2\Delta x_J} + \frac{h_{J+1/2} \, W' DX_T}{3 W_{J+1/2} \, \Delta x_J} - \delta V_{bal} \frac{1}{\Delta x_J \, DX_T \, W_{J+1/2}} \right.$$

$$\left. - \frac{\Delta t \, DX_T}{16 \Delta x^2_J \, W_{J+1/2}} \left[[W_{J+1} - W_J] [(2-X)A_J + (2+X)A_{J+1}] \right.\right.$$

$$\left.\left. + [A_{J+1} - A_J] [(2-X)W_J + (2+X)W_{J+1}] \right] \right] \tag{A1.3.21}$$

The coefficient at J+1 has the same form, with the changes

$$\left(\frac{\partial DX_T}{\partial h_J}\right) \longrightarrow \left(\frac{\partial DX_T}{\partial h_{J+1}}\right)$$

$$\left(\frac{\partial V_J}{\partial h_J}\right) \longrightarrow \left(\frac{\partial V_J}{\partial h_{J+1}}\right) \qquad \text{(A1.3.22)}$$

The derivatives of V_J can be found in equation (A10.5). The derivatives of DX_T are

$$\left(\frac{\partial (DX_T)}{\partial h_J}\right) = - \frac{2DX_T \, h_J}{h^2_{J+1} - h^2_J} \qquad \text{(A1.3.23)}$$

$$\left(\frac{\partial (DX_T)}{\partial h_{J+1}}\right) = \frac{2DX_T \, h_{J+1}}{h^2_{J+1} - h^2_J} \qquad \text{(A1.3.24)}$$

At each iteration for the thickness, DX_T is calculated from (A1.3.11). When the residuals have been reduced sufficiently at the (n+1)th time step, the value of DX_T determines whether the number J+1 of mesh points must be changed.

The terminus region is a critical region for any numerical model. If the model terminus advances too slowly due to incorrect use of the flow law at the terminus, it tends to dam up the ice behind. This creates a model solution which is too thick and flows too slowly. If the model terminus advances too quickly, it can stretch the whole model profile beyond the correct length, even though continuity is satisfied everywhere.

There are two points to consider:

The equation (A1.3.16) uses the flow law only in the flux term δV_{flux} through the velocity factor $V_{J+1/2}$. If the terminus is allowed to advance too far beyond $x_{J+1/2}$, the terminus will

satisfy continuity, but will bear little similarity to the expected terminus shape of a real ice mass governed by the flow law. This can lead to grossly inaccurate behaviour of the whole model.

On the other hand, integrated forms of Glen's flow law (Glen, 1955), as discussed in Appendix 7, assume small slopes and thick ice with the major deformation being shearing parallel to the glacier bed. This is not the case near the terminus. The sliding velocity near the terminus is also difficult to model. This means that x_T must not be allowed to get too close to $x_{J+1/2}$ either, because then the value of $V_{J+1/2}$ would be in question. A reasonable compromise is to keep the length DX_T of the wedge terminus of the order of the average ice thickness. If maximum and minimum acceptable lengths are DXmax and DXmin respectively, then a new meshpoint is added when x_T exceeds $x_{J+1/2}$ +DXmax. Similarily, if x_T is less than $x_{J+1/2}$ +DXmin, then the meshpoint J+1 is discarded at the subsequent time step.

A1.4 NUMERICAL STABILITY

A1.4.1 INTRODUCTION

Physically realizable solutions of the partial differential equation (A1.1.1) are bounded for all time t. Solutions of the set of finite difference equations (A1.1.4) must be bounded also. For what values of Δt, Δx, and Θ is this true? Assuming that the source term A_j will not affect stability, it can be set to zero without loss of generality. A large positive mass balance will result in faster flow of a bounded solution, while a large negative mass balance will terminate the computations in a bounded time by eliminating the ice mass.

Rigourous stability analysis of nonlinear equations is in general not possible. However, the stability conditions for the linearized system of equations used in the iterative procedure are a helpful guide.

The approach I take in the next few sections, to find stability conditions involving Θ, is a variation on the von Neumann, or Fourier series method. (e.g., Richtmyer and Morton, 1967, p. 70). I use Z transform notation (Claerbout, 1976, p. 2) because it is equivalent to Fourier series, but more direct and notationally simpler. (see Appendix 3). The method in brief is to find the transfer function $T(Z)$ in the wavenumber domain which takes the transform $H^n(Z)$ of the ice profile $\{h_j^n | j=1,J\}$ at time n to the transform $H^{n+1}(Z)$ at time $(n+1)$. If $|T(Z)| \leq 1$ for all Z or wavenumbers that can be sensed by the grid, then the profile $\{h_j^{n+1} | j=1,J\}$ is also bounded for all n,

i.e. the scheme is stable. Accuracy of the scheme can be estimated by comparing the amplitude and phase of the transfer functions for the partial differential equation and the finite difference equations.

There are two questions to ask about numerical stability. First, how should the mesh increments Δx and Δt be chosen for stability of the linearized equations? Second, what effects are introduced by the nonlinearity, and how should they be handled? The scheme used for the flux gradient is a critical factor for both questions.

A1.4.2 THE LINEAR COMPUTATIONAL INSTABILITY

If Θ is set to zero giving the explicit numerical scheme, no effect can propogate through the mesh faster than the characteristic speed $\Delta x/\Delta t$. This is unrealistic for a system with diffusive characteristics (see Appendix 6). In this model diffusion arises from the dependence of the ice flux on the surface slope. Explicit schemes for diffusion equations are usually numerically unstable unless the time steps are very small, giving a high characteristic speed $\Delta x/\Delta t$ (e.g. Richtmyer and Morton, 1967, p. 18). Using an implicit scheme, i.e. $\Theta>0$ lets the domain of dependence (e.g., Mesinger and Arakawa, 1976, p. 5) for each mesh point be the entire mesh at the subsequent time step. For diffusion equations, this tends to alleviate stability problems (e.g. Richtmyer and Morton, 1967, p. 18).

The velocities $\{V_j^{n+1} | j=3/2, 5/2, \ldots J+1/2\}$ are treated as constants at each iteration in Section A1.2. Here, they are all

set equal to one constant value V to get an approximate stability criterion involving Θ. The channel width W(x) is also held constant. Similarily, the differences in the $\{\Delta x_j \mid j=1,J\}$ due to the bed slope are not expected to be important. All Δx_j are set equal to Δx. The actual variation with x will presumably alter the criterion in a minor way. The signal h is assumed to be periodic with period 2JΔx in the x direction, so that Fourier series can be used. (This is also a form of boundary condition.) With zero mass balance, the finite difference system of equations can be written as convolutions (e.g. Claerbout, 1976, p. 5)

$$\{h_1^{n+1}, h_2^{n+1}, \ldots h_J^{n+1}\} * \{pVW\Theta, 1, -pVW\Theta\}$$

$$= \{h_1^{n}, h_2^{n}, \ldots h_J^{n}\} * \{-pVW(1-\Theta), 1, pVW(1-\Theta)\} \qquad \text{(A1.4.1)}$$

After taking the Z transform the convolutions become multiplications in the Z domain, and the series become sums.

$$H^{n+1}(Z)\frac{[pVW\Theta+1-pVW\Theta Z]}{Z} = H^{n}(Z)\frac{[-pVW(1-\Theta)+1+pVW(1-\Theta)Z]}{Z} \qquad \text{(A1.4.2)}$$

Since Z is a complex number of the form $e^{im\Delta x}$, the Z transform is equivalent to a discrete Fourier transform with wavenumber m. The factor (Z-1/Z) is purely imaginary and is equal to i[2 sin(mΔx)] where "i" is the square root of minus one. Setting

$$i\,K(Z) = WpV(Z-1/Z)$$

$$= i\,\frac{\Delta t V \sin(m\Delta x)}{\Delta x} \qquad \text{(A1.4.3)}$$

where K(Z) is real, the transfer function is

$$T(Z) = \frac{1 + (1-\Theta)iK(Z)}{1 - \Theta iK(Z)} \qquad \text{(A1.4.4)}$$

Setting $|T(Z)| \leq 1$ gives

$$K^2 (K^2\Theta^2+1) (1-2\Theta) \leq 0 \qquad \text{(A1.4.5)}$$

Since the first two factors are nonnegative for all Z, the stability criterion is

$$\Theta \geq 1/2 \qquad \text{for all } \Delta t \text{ and } \Delta x. \qquad \text{(A1.4.6)}$$

The case $\Theta=1/2$ gives $|T(Z)|=1$ for all Z and thus is marginally stable at all wavenumbers. The presence of nonlinearity could alter the stability criterion (A1.4.6). A velocity dependent on ice slope tends to stabilize the scheme (Section A1.4.6 and stability analysis of Budd and Jenssen, 1975). However, a velocity dependent on ice thickness tends to form shocks, and is a destabilizing factor. To guarantee stability, I could be tempted to use a larger value of Θ. However, the accuracy of the scheme also depends on Θ. This is discussed in Section A1.5.1 and Section A1.5.3.

A1.4.3 THE NONLINEAR INSTABILITY

In this Section, I will discuss the nonlinear instability (NLI) (e.g. Haltiner, 1971, p. 199; Mesinger and Arakawa, 1976, p. 35; Gary, 1975, p. 8.41; Haltiner and Williams, 1980, p. 170), a problem which arises in any numerical solution of a differential equation using a discrete mesh, and having terms which are nonlinear in some combination of the dependent and the independent variables. In (A1.1.1), $\partial Q/\partial x$ is such a term.

Basically, the nonlinearity pumps energy (squared amplitude of the wavenumber spectrum) into the high wavenumber part of the wavenumber spectrum of the dependent variable, and the aliasing (Appendix 3) due to discrete sampling folds this energy back to the lower wavenumbers, where it distorts the solution.

Assuming that the initial profile $\{h_j^o | j=1,J\}$ and the velocity $\{V_j^o | j=3/2, 5/2, \ldots J+1/2\}$ derived from it are periodic with period $2J\Delta x$, they can be expressed as Fourier series with wavenumbers $(l\pi)/(J\Delta x)$ from $-m_N$ to the Nyquist wavenumber m_N (see Appendix 3, Section A3.2).

$$m_N = \pi/\Delta x \tag{A1.4.7}$$

$$h_j^o = \sum_{l=-\frac{J}{2}}^{J/2} H_l \, e^{\frac{i2\pi l}{J\Delta x}} \tag{A1.4.8}$$

$$V_j^o = \sum_{k=-\frac{J}{2}}^{J/2} V_k \, e^{\frac{i2\pi k}{J\Delta x}} \tag{A1.4.9}$$

The flux $Q(x,t)$ in a channel of unit width, however, is the product of these two series.

$$Q_j^o = \sum_{l=-\frac{J}{2}}^{J/2} \sum_{k=-\frac{J}{2}}^{J/2} H_l \, V_k \, e^{\frac{i2\pi(l+k)}{J\Delta x}} \tag{A1.4.10}$$

This flux has harmonic components up to $2\pi/\Delta x$, or twice the Nyquist wavenumber. The energy in these high wavenumbers should not appear in the solution because the solution is bandlimited; however, due to the discrete mesh this energy is aliased (see

Appendix 3, Section A3.2) back into the wavenumber interval $[0,\pi/\Delta x]$ and thus distorts the solution. Most important, however, is the fact that more energy is aliased into the solution at each time step. This numerical effect can increase without bound and will dominate the true solution of the partial differential equation (A1.1.1) in a finite time. The situation can be avoided if the numerical scheme allows damping of the higher wavenumbers, so that aliased energy is attenuated; this also leaves little energy available at the wavenumbers from which it can be pumped up past the Nyquist wavenumber by the nonlinearity.

In principle, the nonlinear instability can be completely eliminated if, at every time step, the wavenumber spectra of the velocity profile and of the ice thickness profile contain no energy above 2/3 of the Nyquist wavenumber m_N. Then, in the following time step, the highest wavenumber component activated by the nonlinearity (see (A1.4.10)) is $4/3\ m_N$. The spectral band from m_N to $4/3\ m_N$ is folded back onto the band from $2/3\ m_N$ to m_N, making the spectrum of Q in this latter band incorrect. This is illustrated schematically in Figure A1.3. The important point to note, however, is that the band from 0 to $2/3\ m_N$, to which I originally band limited h and V, is unaffected by the aliasing. If the energy above $2/3\ m_N$ can be eliminated at every time step, the signal in 0 to $2/3\ m_N$ will always be correct. Choosing Δx small enough can always push the cutoff $(2\pi)/(3\Delta x)$ out beyond the wavenumber of any feature of interest in the glacier spectrum, no matter how short its wavelength.

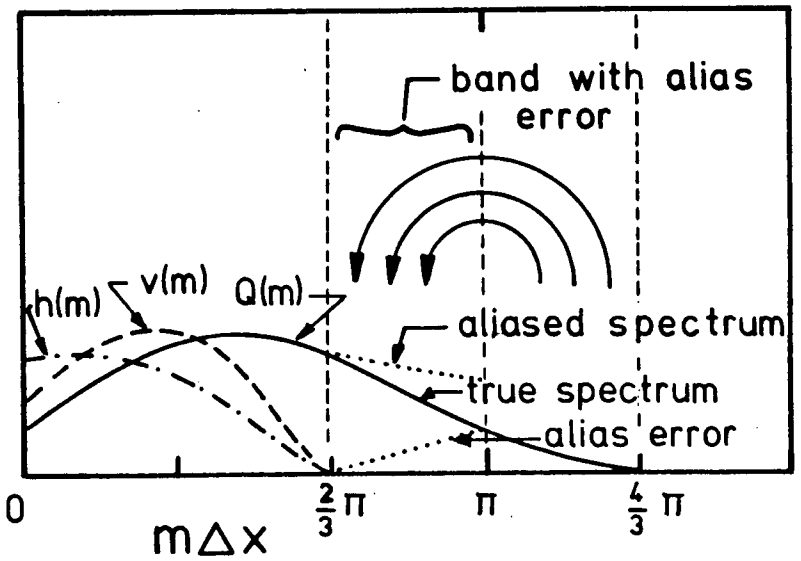

FIGURE A1.3. Aliasing And The Nonlinear Instability. The spectrum of $Q(m)=v(m)h(m)$ beyond the Nyquist wavenumber at $m\Delta x=\pi$ is folded back (lower dotted curve) as an aliasing error between $2\pi/3$ and π. The upper dotted line is the spectrum of the sampled $Q(m)$ with aliasing.

There are several ways to damp the instability in the aliased part of the spectrum. Some are more satisfactory than others. I will discuss four methods. The first two have conceptual drawbacks. I have used the third and fourth methods in this study.

A1.4.4 VELOCITY SMOOTHING

Budd and Jenssen (1975), who attributed the instability to machine roundoff, replaced the velocity profile $V(x)$ by a version smoothed by a second derivative operator

$$V(x) \longleftarrow V(x) + \frac{1}{4}\frac{\partial^2 V}{\partial x^2}\Delta x^2 \qquad \text{(A1.4.11)}$$

whenever they saw high wavenumber components in the velocity profile. To see what (A1.4.11) does to the spectrum of $V(x)$,

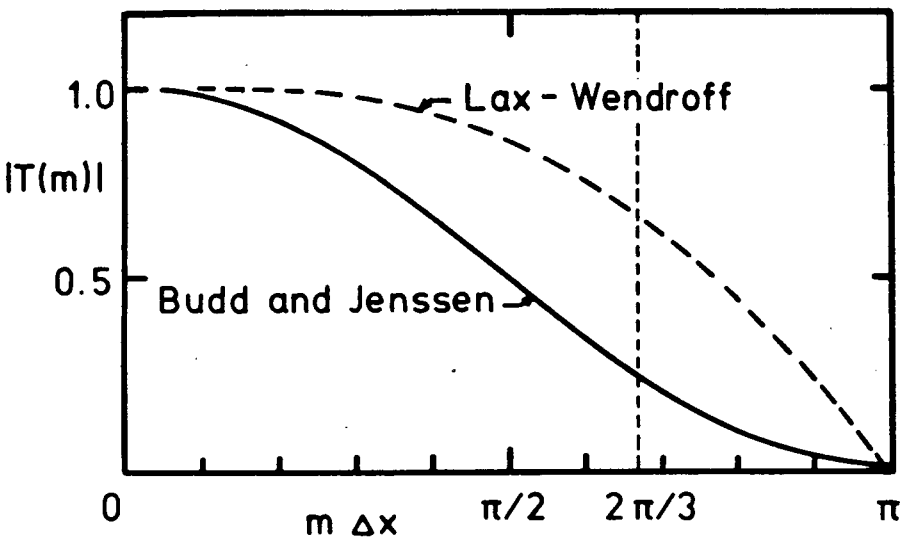

FIGURE A1.4. Transfer Functions Of Smoothing Schemes.
Solid curve: Budd and Jenssen smoothing applied occasionally to velocity profile.
Broken curve: Lax-Wendroff numerical scheme with maximum dissipation. This would be applied to h(x) at each time step.

take the Z transform (Appendix 3) of the right side using the standard finite second difference estimate

$$\frac{\partial^2 V}{\partial x^2} = \frac{V_{j+1} - 2V_j + V_{j-1}}{\Delta x^2} \qquad \text{(A1.4.12)}$$

to get

$$V(Z) \longleftarrow V(Z) + \frac{1}{4} V(Z) \left(Z - 2 + \frac{1}{Z}\right) \qquad \text{(A1.4.13)}$$

or, in terms of wavenumber m,

$$V(m) \longleftarrow V(m) \left[\frac{1 + \cos(m\Delta x)}{2}\right] \qquad \text{(A1.4.14)}$$

since $Z = e^{i m \Delta x}$ (Section A1.4.2). The smoothing filter (the second factor on the right side of (A1.4.14)) is shown in Figure A1.4. Although it substantially reduces the signal beyond 2/3 m_N, it does not totally eliminate it. Since Budd and Jenssen (1975)

applied it only to the velocity, and not to the ice thickness profile, and only at infrequent times when the solution was already seriously in error, it could not completely or correctly remove the nonlinear instability. It could only keep it from totally dominating the physical solution.

In addition, the filter attenuates the amplitude at all wavenumbers except zero.

Both these effects distort the shape and total energy content (integral of the squared amplitude) of the velocity profile. This can cause errors in mass conservation through the flux gradient term. The effect in many cases may be small. However, better methods are available.

A1.4.5 NUMERICAL DISSIPATION

A second method to stabilize the equations (A1.1.4) is to add a dissipative diffusion term of the form

$$\epsilon \frac{\partial^2 h}{\partial x^2}$$

where ϵ is small, directly into the differential equation (A1.1.1). Kreiss (1964) showed that a wide class of difference schemes for linear hyperbolic equations could be stabilized this way, rather than by using implicit schemes such as (A1.1.4). Dissipative terms control instabilities by preferentially damping the high wavenumbers at which instabilities typically arise. They can also be used to control the nonlinear instability.

For example, consider the transfer function which results from adding the dissipative term to the linear form of the

continuity equation, a simple special case of (A1.1.1) with constant width and velocity.

$$\frac{\partial h}{\partial t} + V\frac{\partial h}{\partial x} - \epsilon\frac{\partial^2 h}{\partial x^2} = 0 \qquad \text{(A1.4.15)}$$

The simple finite difference scheme for (A1.4.15)

$$\frac{h_j^{n+1} - h_j^n}{\Delta t} + \frac{V(h_{j+1}^n - h_{j-1}^n)}{2\Delta x} - \epsilon\frac{(h_{j+1}^n - 2h_j^n + h_{j-1}^n)}{\Delta x^2} = 0 \qquad \text{(A1.4.16)}$$

has the transfer function

$$T(m) = 1 + \frac{2\epsilon\Delta t}{\Delta x^2}[1 - \cos(m\Delta x)] + iV\frac{\Delta t}{\Delta x}\sin(m\Delta x) \qquad \text{(A1.4.17)}$$

The derivation parallels Section A1.4.2. When

$$\epsilon = V^2\frac{\Delta t}{2} \qquad \text{(A1.4.18)}$$

Gary (1975, p. 3.69) showed that (A1.4.16) is the standard Lax-Wendroff dissipative formulation (Lax and Wendroff, 1960) which is stable for

$$\frac{V\Delta t}{\Delta x} < 1 \qquad \text{(A1.4.19)}$$

and approaches the solution of

$$\frac{\partial h}{\partial t} + V\frac{\partial h}{\partial x} = 0 \qquad \text{(A1.4.20)}$$

in the limit $\Delta t \to 0$. Using (A1.4.18), the modulus of the transfer function is

$$|T(m)| = \left[1 - 4c(1-c)\sin^4(m\Delta x/2)\right]^{1/2} \qquad \text{(A1.4.21)}$$

where c is given by

$$c = \left[\frac{2\epsilon\Delta t}{\Delta x^2}\right]^2 = \frac{V^2\Delta t^2}{\Delta x^2} \qquad \text{(A1.4.22)}$$

The magnitude of the damping term is largest when c=1/2, i.e.

when material advances $(1/2)^{1/2}$ mesh intervals per time step. $|T(m)|$ is shown for that case in Figure A1.4. For other values of Δt, there is less damping of the high wavenumber components. This scheme would be preferable to the method of Budd and Jenssen (1975). Because it is applied at every time step, it is more likely to keep the nonlinear instability in check at all times.

It nevertheless suffers from some of the same drawbacks. It attenuates the low wavenumbers. The damping term also changes the equation from first order to second order. This means a second boundary condition is needed. Because the new term has no physical meaning, there is no immediately obvious physical boundary condition to apply, and the amplitude of the solution to partial differential equations can often be very sensitive to the boundary conditions.

The reason that these two methods appear to work in practice is that the nonlinear instability tends to grow at least exponentially. It either totally dominates the solution, or it is insignificantly small. It seldom exists undetected with a magnitude comparable to that of the physical solution, although this is always a possibility with these second derivative schemes.

A1.4.6 DISSIPATION FROM THE VELOCITY EQUATION

A more aesthetically pleasing way to avoid the nonlinear instability is to utilize the damping inherent in the flow properties of ice, rather than to introduce an artificial diffusive term, as in the previous section. For any realistic flow model of glacier ice, the flow velocity of ice increases with increasing ice surface slope.

By using the linearized perturbation form (Appendix 6) of the continuity equation with a velocity dependent on ice thickness and surface slope, I illustrate, in Appendix 13, the main features of this method of suppressing the nonlinear instability. The modulus $|T(m)|$ of the transfer function (A13.2.5) of the differential equation, with parameters in (A13.2.6), is shown by a dotted curve in Figure A1.5 . The slope dependence leads to substantial damping at high wavenumbers. In Appendix 13, I show that, in order to achieve acceptable damping with the numerical scheme, it is necessary to calculate the ice surface slope over at most one mesh interval Δx, and to evaluate the ice flux between the mesh points, so that the flux gradient is also evaluated over a distance of at most Δx. The solid curve in Figure A1.5 shows the transfer function modulus for the difference scheme when these restrictions are met.

Like the previous two methods, this transfer function does not completely eliminate the components above $2/3\ m_N$. However, in practice, the attenuation is adequate to prevent growth of the nonlinear instability. There are advantages to this method. Although it attenuates wave numbers below $2/3\ m_N$, this

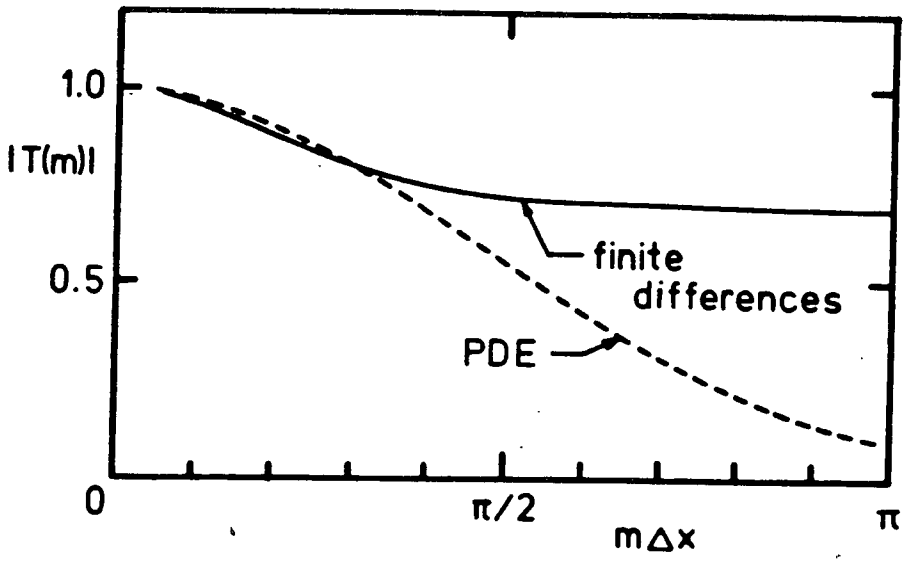

FIGURE A1.5. Transfer Functions: Slope-dependent Damping.
Solid curve: transfer function modulus for the finite difference scheme with space increment Δx.
Broken curve: transfer function modulus for the linear partial differential equation.
The Nyquist wavenumber is at $m\Delta x=\pi$.

attenuation has a physical basis, i.e. the diffusive nature of ice flow. The two curves in Figure A1.5 are similar at low wavenumber, indicating that the numerical scheme models this diffusive property quite well.

Since no artificial damping term is introduced, the order of the equation is unchanged, and no extra boundary conditions are required.

This method was used by Mahaffy (unpublished), Mahaffy (1976), Mahaffy and Andrews (1976) and Bindschadler (unpublished) to control the nonlinear instability. It is also used in this study for the Steele Glacier model.

A1.4.7 WAVENUMBER SPECTRAL TRUNCATION

The most straightforward way to eliminate energy above 2/3 m_N without altering the spectrum up to that wavenumber is to apply a lowpass filter with cutoff at 2/3 m_N to the Fourier transforms of the ice thickness and velocity in the wavenumber domain. Phillips (1959) did this in the original paper identifying the nonlinear instability. At that time, to calculate the discrete Fourier series of a long profile was an

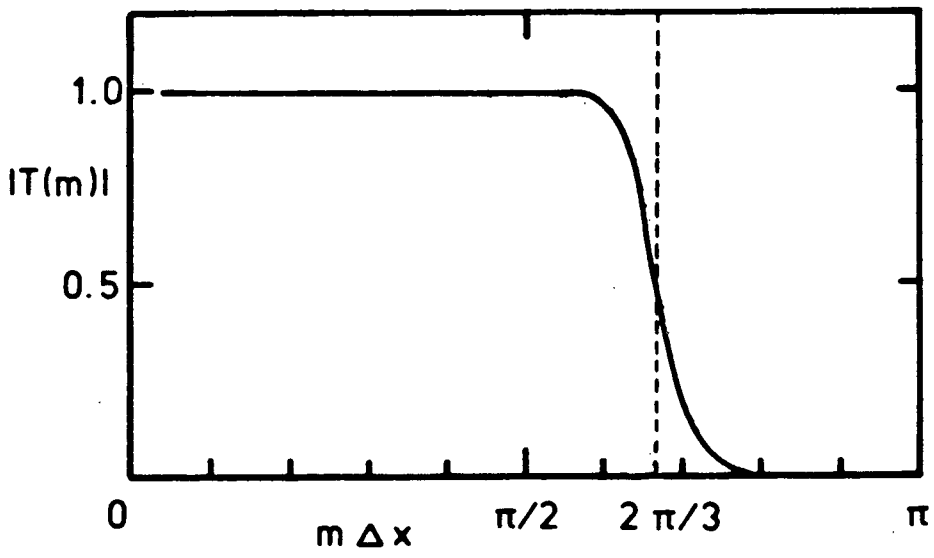

FIGURE A1.6. Filter To Suppress Nonlinear Instability. The length of the taper at $2\pi/3$ is exaggerated for the purpose of illustration. The Nyquist wavenumber is at $m\Delta x=\pi$.

expensive procedure, so the method was rarely used. Since the introduction of the Fast Fourier Transform (FFT) by Cooley and Tukey (1965), however, it is quite feasible to use the lowpass filter in Figure A1.6 at each time step with only a modest increase in cost. The filter is smoothed at the corner at 2/3 m_N

with a raised cosine to prevent spurious ripple or sidelobe formation in the spatial domain (e.g. Kanasewich, 1975, p. 96). The length of the cosine taper is exaggerated in Figure A1.6.

Briefly, the procedure is to remove the mean value and trend from the glacier profile, take its FFT to get the wavenumber spectrum, multiply it by the filter in Figure A1.6 to remove the high wavenumbers, then take the inverse FFT to get back to the spatial domain, then finally add back the trends and mean value originally removed.

This method is the most appropriate one when the velocity of the ice does not depend on the local surface slope.

Some observations (Meier and others, 1974; Bindschadler and others, 1977; Budd, 1968) and theory (Budd, 1968; 1970[a]; 1970[b]) indicate that glacier flow responds to an effective slope averaged over several times the ice thickness, rather than to the local slope, due to the influence of longitudinal stress gradients. Bindschadler (unpublished) used a weighted average of a long-scale slope, to match observations, and the local slope to get numerical stability. Using the lowpass filter eliminates the need to include an amount of local slope in the effective slope definition. The effective slope can be based strictly on the physics of glacier flow, and not on the numerical difficulties.

A1.5 ACCURACY

A1.5.1 θ PARAMETER: ACCURACY

In Section A1.4.2, I concluded that for numerical stability, $\theta \geq 1/2$, and that using a value strictly greater than 1/2 would help ensure stability when nonlinearity is included. However, the accuracy with which the finite difference scheme represents the partial differential equation also depends on θ, leading to a tradeoff situation. I will now compare the transfer function (A1.4.4) with the transfer function for the corresponding partial differential equation, to find conditions on θ for an accurate solution.

When the velocity V is a constant, and mass balance is zero, (A1.1.1) for unit width reduces to

$$\frac{\partial h}{\partial t} + V\frac{\partial h}{\partial x} = 0 \qquad \text{(A1.5.1)}$$

Taking the Fourier transform represented by tildes, with respect to x (e.g. Morse and Feshbach, 1953, p. 453), and using the derivative property

$$\frac{dh}{dx} = i\, m\tilde{h}(m) \qquad \text{(A1.5.2)}$$

where m is the wavenumber, and $i^2=-1$, gives

$$\frac{\partial \tilde{h}}{\partial t}(m,t) + iVm\tilde{h}(m,t) = 0 \qquad \text{(A1.5.3)}$$

The solution of (A1.5.3) is

$$\tilde{h}(m,t) = \tilde{h}_o e^{imVt} \qquad \text{(A1.5.4)}$$

In a time interval Δt, the transfer function is then

$$T(m) = e^{imV\Delta t} \qquad (A1.5.5)$$

The transfer function T(m) for the partial differential equation has unit modulus at all wavenumbers. Figure A1.7 shows the modulus of the numerical transfer function for several stable values of θ, using

$$\frac{V\Delta t}{\Delta x} = 1 \qquad (A1.5.6)$$

which means that waveforms travel one mesh interval in one time step. It is evident that I must keep θ near 1/2 to minimize discrepancies between the two transfer functions. Systematic differences in modulus can spuriously create or destroy mass in the glacier. Figure A1.7 indicates that this would be most evident as a nonphysical decay of features at one half the Nyquist wavenumber, or at a wavelength of four meshpoints.

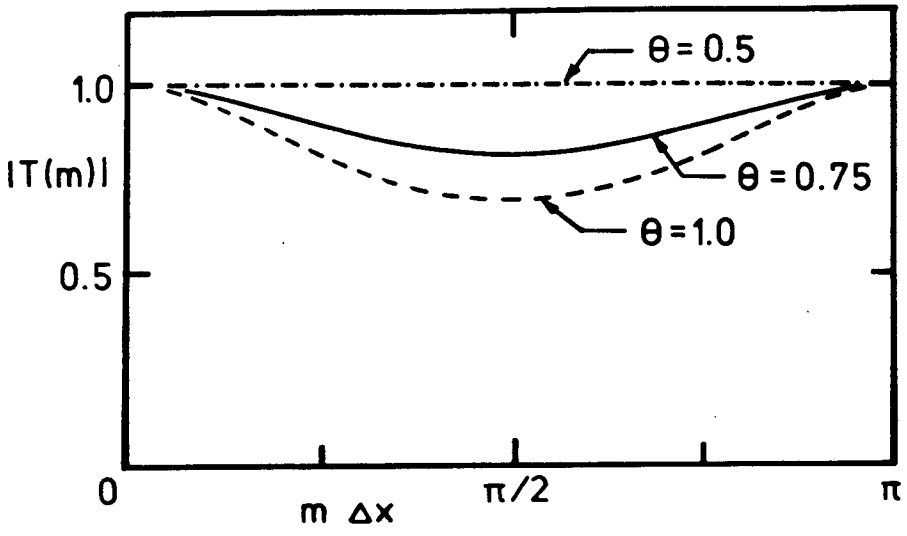

FIGURE A1.7. Transfer Function Modulus For Various θ.

The analysis of the truncation error by a spatial domain method with different assumptions in Section A1.5.3 also

indicates that $\Theta=1/2$ is the best choice for an accurate scheme.

To compromise between the accuracy problem and the marginal stability at $\Theta=1/2$, I usually used values of Θ in the range 0.50 to 0.55 .

A1.5.2 PHASE ERRORS

Any differences in phase between the transfer functions (A1.5.5) of the partial differential equation and (A1.4.4) of the numerical scheme will distort the glacier thickness, by causing errors in phase velocity, leading to incorrect dispersion. The phase speed at which the component at wavenumber m propagates is

$$V_{phase}(m) = \frac{\phi}{m\Delta t} \qquad (A1.5.7)$$

where ϕ is the phase of the transfer function. The phase of the transfer function (A1.5.5) of the partial differential equation is

$$\phi_{pde}(m) = mV\Delta t \qquad (A1.5.8)$$

Its phase velocity is V, a constant for all wavenumbers. The phase increases linearly with m. The straight line in Figure A1.8 is the phase (A1.5.8) when $V\Delta t=\Delta x/4$.

The phase of the finite difference transfer function (A1.4.4) using $\Theta=1/2$, is

$$\phi_{fd}(m) = \tan^{-1}\left[\frac{K(m)}{1 - K^2(m)/2}\right] \qquad (A1.5.9)$$

By using the multiple angle formula for arctangent (Abramowitz

and Stegun, 1965, (4.3.26), p. 73)

$$\phi_{fd}(m) = 2\tan^{-1}[K(m)/2] \qquad \text{(A1.5.10)}$$

K(m) is given by (A1.4.3). The phase (A1.5.10) is also shown in

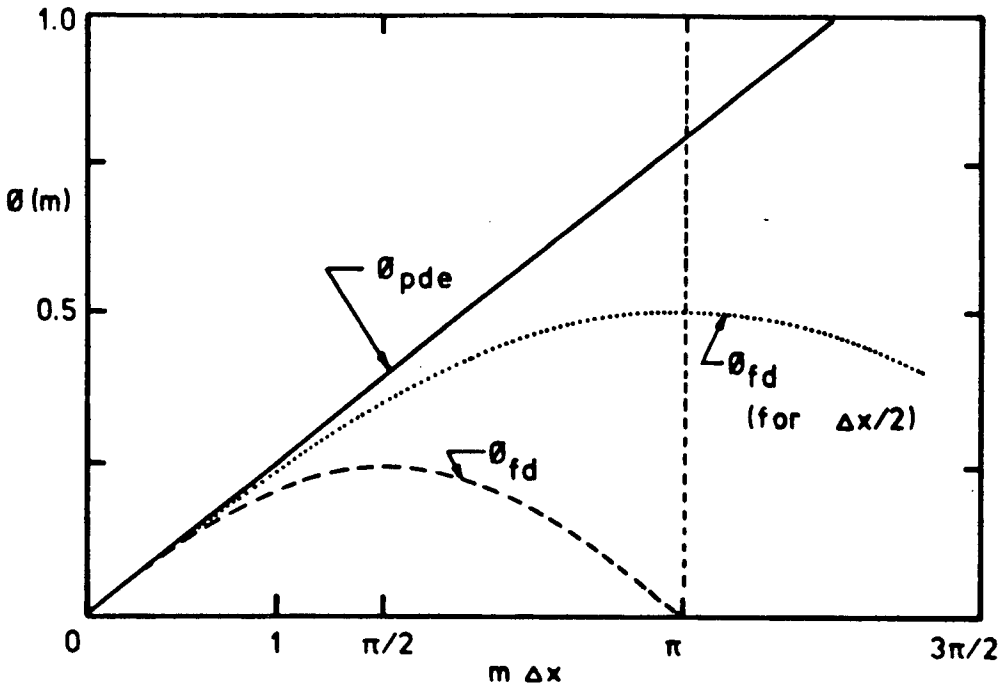

FIGURE A1.8. Transfer Function Phase Comparison.
Solid curve: phase for solution to partial differential equation.
Broken curve: phase for the finite difference scheme with mesh interval Δx.
Dotted curve: phase for the finite difference scheme with mesh interval $\Delta x/2$.

Figure A1.8 (broken line) for the same time step Δt as in (A1.5.8). The finite difference phase obviously diverges badly from the correct value at wavenumbers above one half the Nyquist wavenumber $\pi/\Delta x$, giving large errors in phase speed. In fact, at the Nyquist wavenumber, the phase velocity goes to zero. Any waves sampled at two points per wavelength do not propagate at

all! Gary (1975, p. 2.21) discussed this behaviour for a mixed differential-difference hyperbolic system. The numerical scheme causes gross dispersion of the high wavenumber components. The difficulty is due almost entirely to inadequate spatial sampling. When the single time step Δt is replaced by 100 time steps of $10^{-2}\Delta t$, there is almost no change in the cumulative phase. The differences cannot be distinguished on the scale of Figure A1.8.

If, on the other hand, the spatial mesh increment Δx is halved, keeping the same large time step, the phase is given by the dotted curve in Figure A1.8. The agreement with the correct phase is greatly improved out to higher wavenumbers (note that the Nyquist wavenumber has also been increased. It is now at

$$m\Delta x = 2\pi$$

when the mesh increment is $\Delta x/2$).

It is evident that, to maintain phase accuracy, I must choose Δx sufficiently small so that the spectrum of the glacier profile $h(x)$ is essentially bandlimited to the region

$$m\Delta x << 1 \qquad \text{(A1.5.11)}$$

which means that there are many mesh points per wavelength for all wavelengths having significant amplitude in the spectrum.

In the region (A1.5.11), I can evaluate the error in the phase (A1.5.10) relative to (A1.5.8) by expanding $\sin(m\Delta x)$ as a Taylor series to third order (Abramowitz and Stegun, 1965, (4.3.65), p. 74) in the small parameter $m\Delta x$. When

$$K(m)/2 \leq 1 \qquad \text{(A1.5.12)}$$

or

$$\frac{\Delta x}{\Delta t} \geq \frac{V}{2} \qquad \text{(A1.5.13)}$$

i.e. material moves less than two mesh increments per time step, the power series expansion (4.4.12) of Abramowitz and Stegun (1965, p. 81) can be used for the arctangent. With the restrictions (A1.5.11) and (A1.5.13), the phase is

$$\phi_{fd}(m) = mV\Delta t\left[1 - (m\Delta x)^2\left[\frac{1}{6} + \frac{V^2\Delta t^2}{12\Delta x^2}\right] + O(m\Delta x)^4\right] \qquad \text{(A1.5.14)}$$

No matter how small I choose the time step Δt, the fractional error in the phase is still at least

$$(m\Delta x)^2/6 \qquad \text{(A1.5.15)}$$

This error can be reduced by smaller mesh intervals Δx subject to (A1.5.13).

The results in this section are based on the analysis of the linear equation (A1.5.1), but similar phenomena occur in numerical solutions of the nonlinear analogue, and the restrictions derived here give excellent guidance for the nonlinear case.

A1.5.3 TRUNCATION ERROR

In the previous sections, I examined the accuracy of the finite difference scheme (A1.1.4) as a function of wavenumber, assuming constant velocity. In this section, I will examine the accuracy of the scheme starting from different assumptions. The truncation error is the difference between an exact solution h(x,t), indicated by tildes, of the partial differential equation (A1.1.1) and an exact solution $\{h_j^n \mid j=1,J\}$ of the

corresponding system of algebraic equations (A1.1.4). The name arises because the finite differences can be represented by truncated Taylor expansions of the solutions $h(x,t)$ and $Q(x,t)$ of the partial differential equation. The assumption in this analysis is that $h(x,t)$ and $Q(x,t)$ are infinitely differentiable in x and t. This is reasonable since glacier profiles are so smooth. The accuracy is expressed in terms of neglected derivatives at each spatial position, rather than in terms of wavenumber.

To derive an expression for the truncation error, first expand all the quantities in the finite difference equations (A1.1.4) as Taylor series with remainder about the point $((j-1)\Delta x,(n+1/2)\Delta t))$ in terms of the exact solution $h(x,t)$ and its derivatives there.

$$h_j^{n+1} = h_j^{n+1/2} + \frac{\Delta t}{2}\frac{\partial h}{\partial t}\bigg|_j^{n+1/2} + \frac{\Delta t^2}{8}\frac{\partial^2 h}{\partial t^2}\bigg|_j^{n+1/2} + \frac{\Delta t^3}{48}\frac{\partial^3 h}{\partial t^3}\bigg|_j^{n+1/2+\emptyset_0}$$

$$h_j^{n} = h_j^{n+1/2} - \frac{\Delta t}{2}\frac{\partial h}{\partial t}\bigg|_j^{n+1/2} + \frac{\Delta t^2}{8}\frac{\partial^2 h}{\partial t^2}\bigg|_j^{n+1/2} - \frac{\Delta t^3}{48}\frac{\partial^3 h}{\partial t^3}\bigg|_j^{n+1/2-\emptyset_1}$$

$$Q_{j+1/2}^{n+1} = Q_j^{n+1} \pm \frac{\Delta x}{2}\frac{\partial Q}{\partial x}\bigg|_j^{n+1} + \frac{\Delta x^2}{8}\frac{\partial^2 Q}{\partial x^2}\bigg|_j^{n+1} \pm \frac{\Delta x^3}{48}\frac{\partial^3 Q}{\partial x^3}\bigg|_{j-\emptyset_3}^{n+1} \quad j-1/2 \qquad j+\emptyset_2$$

(cont'd)

$$Q^{n}_{\substack{j+1/2\\ j-1/2}} = Q^{n}_{j} \pm \frac{\Delta x}{2}\frac{\partial Q}{\partial x}\bigg|^{n}_{j} + \frac{\Delta x^2}{8}\frac{\partial^2 Q}{\partial x^2}\bigg|^{n}_{j} \pm \frac{\Delta x^3}{48}\frac{\partial^3 Q}{\partial x^3}\bigg|^{n}_{\substack{j+\emptyset_4\\ j-\emptyset_5}}$$

(A1.5.16)

The derivatives in the expressions for the flux Q are expanded in the same way.

$$\frac{\partial Q}{\partial x}\bigg|^{n+1}_{n}_{j} = \frac{\partial Q}{\partial x}\bigg|^{n+1/2}_{j} \pm \frac{\Delta t^2}{2}\frac{\partial^2 Q}{\partial x^2}\bigg|^{n+1/2}_{j} + \frac{\Delta t^3}{8}\frac{\partial^3 Q}{\partial x^3}\bigg|^{n+1/2+\emptyset_6}_{n+1/2-\emptyset_7}_{j}$$

$$\frac{\partial^2 Q}{\partial x^2}\bigg|^{n+1}_{n}_{j} = \frac{\partial^2 Q}{\partial x^2}\bigg|^{n+1/2}_{j} \pm \frac{\Delta t}{2}\frac{\partial^3 Q}{\partial x^3}\bigg|^{n+1/2+\emptyset_8}_{n+1/2-\emptyset_9}_{j}$$

(A1.5.17)

The bars followed by subscripts and superscripts indicate the mesh indices at which the derivatives are evaluated. The $\emptyset_i$ in the remainder terms are real numbers between zero and 1/2. The existence of remainder terms of this form is guaranteed by the Taylor Formula with Remainder Theorem, (e.g. Kaplan, 1952, Theorem 41, p. 357).

After substituting these expressions into the finite difference equations (A1.1.4), assuming unit width, and cancelling the terms which identically satisfy the partial differential equation (A1.1.1), the truncation error which remains is

$$\epsilon_j = \Delta t \left[\frac{(2\theta-1)}{2} \left. \frac{\partial^2 Q}{\partial x \partial t} \right|_j^{n+1/2} \right]$$

$$+ \frac{\Delta t^2}{48} \left[6\theta \left. \frac{\partial^3 Q}{\partial x \partial t^2} \right|_j^{n+1/2+\phi_6} + 6(1-\theta) \left. \frac{\partial^3 Q}{\partial x \partial t^2} \right|_j^{n+1/2-\phi_7} \right.$$

$$\left. + \left. \frac{\partial^3 h}{\partial t^3} \right|_j^{n+1/2+\phi_0} + \left. \frac{\partial^3 h}{\partial t^3} \right|_j^{n-1/2-\phi_1} \right]$$

$$+ \frac{\Delta x^2}{48} \left[\theta \left. \frac{\partial^3 Q}{\partial x^3} \right|_{j+\phi_2}^{n+1/2} + \theta \left. \frac{\partial^3 Q}{\partial x^3} \right|_{j-\phi_3}^{n+1/2} \right.$$

$$\left. + (1-\theta) \left. \frac{\partial^3 Q}{\partial x^3} \right|_{j+\phi_4}^{n+1/2} + (1-\theta) \left. \frac{\partial^3 Q}{\partial x^3} \right|_{j-\phi_5}^{n+1/2} \right] \qquad \text{(A1.5.18)}$$

In terms of dependence on the mesh increments,

$$\epsilon_j = (2\theta-1)\, O(\Delta t) + O(\Delta t^2) + O(\Delta x^2) \qquad \text{(A1.5.19)}$$

It appears that using the scheme with $\theta=1/2$ results in a minimum truncation error; as the term $O(\Delta t)$ goes to zero. This advantage must be traded off against the marginal numerical stability at this value.

The coefficients of Δx^2, Δt, and Δt^2 cannot be evaluated exactly because the derivatives of the exact solution $h(x,t)$ are not known exactly, and the shifts ϕ_i at which they are to be evaluated are also unknown. However, useful estimates of the

coefficients can be obtained for order of magnitude effects.

First, assume that the derivatives change slowly with time and space, so that the $\emptyset_i$ can be ignored without large error. Then note that for time-independent mass balance,

$$\frac{\partial}{\partial t}\left[\frac{\partial Q}{\partial x}\right] = -\frac{\partial^2 h}{\partial t^2} \qquad \text{(A1.5.20)}$$

by using the continuity equation (A1.1.1). The truncation error is then approximately

$$\epsilon_j = \Delta t\left[\frac{(1-2\Theta)}{2}\frac{\partial^2 h}{\partial t^2}\Big|_j^n\right] + \Delta t^2\left[\frac{1}{6}\frac{\partial^3 h}{\partial t^3}\Big|_j^n\right] + \Delta x^2\left[\frac{1}{24}\frac{\partial^3 Q}{\partial x^3}\Big|_j^n\right] \qquad \text{(A1.5.21)}$$

and the coefficients can be estimated by the finite difference analogues of these simple partial derivatives, using the numerical solution.

A1.5.4 INTERPOLATION ERROR

There is an error introduced by representing the thickness $h_{j+1/2}$ at the midpoints of the mesh intervals by a linear interpolation from the primary grid, i.e. by using

$$h_{j+1/2} = (h_{j+1} + h_j)/2 \qquad \text{(A1.5.22)}$$

To estimate this error, write the thickness values at the mesh points as Taylor series with remainder about the true value at a point $j+\emptyset$ between j and j+1.

$$h_{j+1} = h_{j+\phi} + (1-\phi)\,\Delta x \left.\frac{\partial h}{\partial x}\right|_{j+\phi} + (1-\phi)^2 \frac{\Delta x^2}{2} \left.\frac{\partial^2 h}{\partial x^2}\right|_{j+\psi_1} \qquad \phi<\psi_1<1$$

$$h_{j} = h_{j+\phi} + \phi\,\Delta x \left.\frac{\partial h}{\partial x}\right|_{j+\phi} + \phi^2 \frac{\Delta x^2}{2} \left.\frac{\partial^2 h}{\partial x^2}\right|_{j+\psi_2} \qquad 0<\psi_2<\phi$$

(A1.5.23)

The interpolation error E_ϕ at $j+\phi$ is then

$$E_\phi = h_{j+\phi} - (\phi h_{j+1} + (1-\phi)h_j)$$

$$= \phi(1-\phi)\frac{\Delta x^2}{2}\left[(1-\phi)\left.\frac{\partial^2 h}{\partial x^2}\right|_{j+\psi_1} + \phi \left.\frac{\partial^2 h}{\partial x^2}\right|_{j+\psi_2}\right]$$

(A1.5.24)

The interpolation error at $\phi=1/2$ is approximately

$$E_{1/2} = \frac{\Delta x^2}{8}\left.\frac{\partial^2 h}{\partial x^2}\right|_{j+1/2} \qquad \text{(A1.5.25)}$$

when $\partial^2 h/\partial x^2$ is slowly varying with x.

The fractional interpolation error is

$$\frac{E_h}{h} = \frac{E_{1/2}}{h} = \frac{\partial^2 h}{\partial x^2}\frac{\Delta x^2}{8h} \qquad \text{(A1.5.26)}$$

For example, on a glacier of unit length, with a mesh chosen so that Δx and h are $O(10^{-2})$ and thickness and slope change by of the order of 10% between adjacent mesh points, the fractional interpolation error is

$$E_h = 10^{-5} \qquad \text{(A1.5.27)}$$

which is quite acceptable. The error is largest where the curvature is largest. The interpolation error also propagates into the $\partial Q/\partial x$ term. For instance, if flux Q is proportional to

h^m, as in the simple case of slab flow with Glen's flow law, (Glen, 1955), the fractional error in Q is

$$f = E_Q = m E_h \qquad \text{(A1.5.28)}$$

How does this error in Q affect the flux gradient estimates? Let $\{Q_j \mid j=1,J\}$ be the true values of the ice flux, and $\{Q'_j \mid j=1,J\}$ with primes be the estimates including the interpolation error. Then

$$Q'_{j+1/2} = Q_{j+1/2}(1 + f) \qquad \text{(A1.5.29)}$$

and the error in the representation of $\partial Q/\partial x$ is

$$e = \frac{Q'_{j+1/2} - Q'_{j-1/2}}{\Delta x} - \frac{Q_{j+1/2} - Q_{j-1/2}}{\Delta x}$$

$$= \left[Q_{j+1/2} f_{j+1/2} - Q_{j-1/2} f_{j-1/2} \right] \Big/ \Delta x$$

$$= \left[\frac{Q_{j+1/2} - Q_{j-1/2}}{\Delta x} \right] \left[\frac{f_{j+1/2} + f_{j-1/2}}{2} \right]$$

$$+ \left[\frac{Q_{j+1/2} + Q_{j-1/2}}{2} \right] \left[\frac{f_{j+1/2} - f_{j-1/2}}{\Delta x} \right]$$

$$\doteq \frac{\partial Q}{\partial x} f + Q \frac{\partial f}{\partial x} \qquad \text{(A1.5.30)}$$

Substituting (A1.5.28) for f,

$$e = \frac{m\Delta x^2}{8}\left[\frac{\partial Q}{\partial x} + \frac{\partial^2 h}{\partial x^2}\frac{1}{h} + \frac{Q}{h} + \frac{\partial^3 h}{\partial x^3} - \frac{Q}{h^2}\frac{\partial^3 h}{\partial x^3}\frac{\partial h}{\partial x}\right]$$

$$= \frac{m\Delta x^2}{8}\left[\frac{1}{h}\frac{\partial^2 h}{\partial x^2}\left[\frac{\partial Q}{\partial x} - \frac{Q}{h}\frac{\partial h}{\partial x}\right] + \frac{Q}{h}\frac{\partial^3 h}{\partial x^3}\right]$$

$$= \frac{m\Delta x^2}{8}\left[\frac{\partial^2 h}{\partial x^2}\frac{\partial V}{\partial x} + V\frac{\partial^3 h}{\partial x^3}\right] \qquad \text{(A1.5.31)}$$

using Q=hV. Thus

$$e = \frac{m\Delta x^2}{8}\left[\frac{\partial}{\partial x}\left[V\frac{\partial^2 h}{\partial x^2}\right]\right] \qquad \text{(A1.5.32)}$$

which can be kept small by suitably small choice of Δx. This is the same requirement as found previously for the truncation error and transfer function error. The coefficient of Δx^2 can be estimated from the solution profile. It is generally small, because velocity and ice thickness usually vary slowly with x.

APPENDIX 2: ICE TRAJECTORY MODEL

A2.1 INTRODUCTION

This Appendix describes the procedures I have used in the computer model which calculates the trajectories of individual particles of ice, as they travel through the time-varying glacier.

At each time step, the glacier profile obtained with the continuity equation model (Appendix 1) is used to determine the velocity field within the glacier on a two dimensional vertical surface through the glacier centreline, as shown in Figure A2.1. The x axis is along the glacier bed, z is up and normal to x, and y is transverse and horizontal making a right handed system. The gridpoints lie at equal intervals of DZ along lines normal to the bed. These lines are rooted on the bed at the midpoints of the intervals Δx used in the continuity model (Appendix 1, Section A1.1.1, i.e. at equal horizontal increments of Δx, starting at $\Delta x/2$ from the origin). The meshpoint (i,j) is the jth point above the bed over X_i. The meshpoints divide the glacier section into quadrilateral cells (see Figure A2.1). The top and bottom of each cell are parallel, but the sides may diverge slightly due to the curvature of the glacier bed. This makes necessary some minor geometric corrections, but has definite advantages over a rectangular Cartesian grid when I calculate the velocity components.

Jenssen (1977) used a grid with a vertical mesh increment

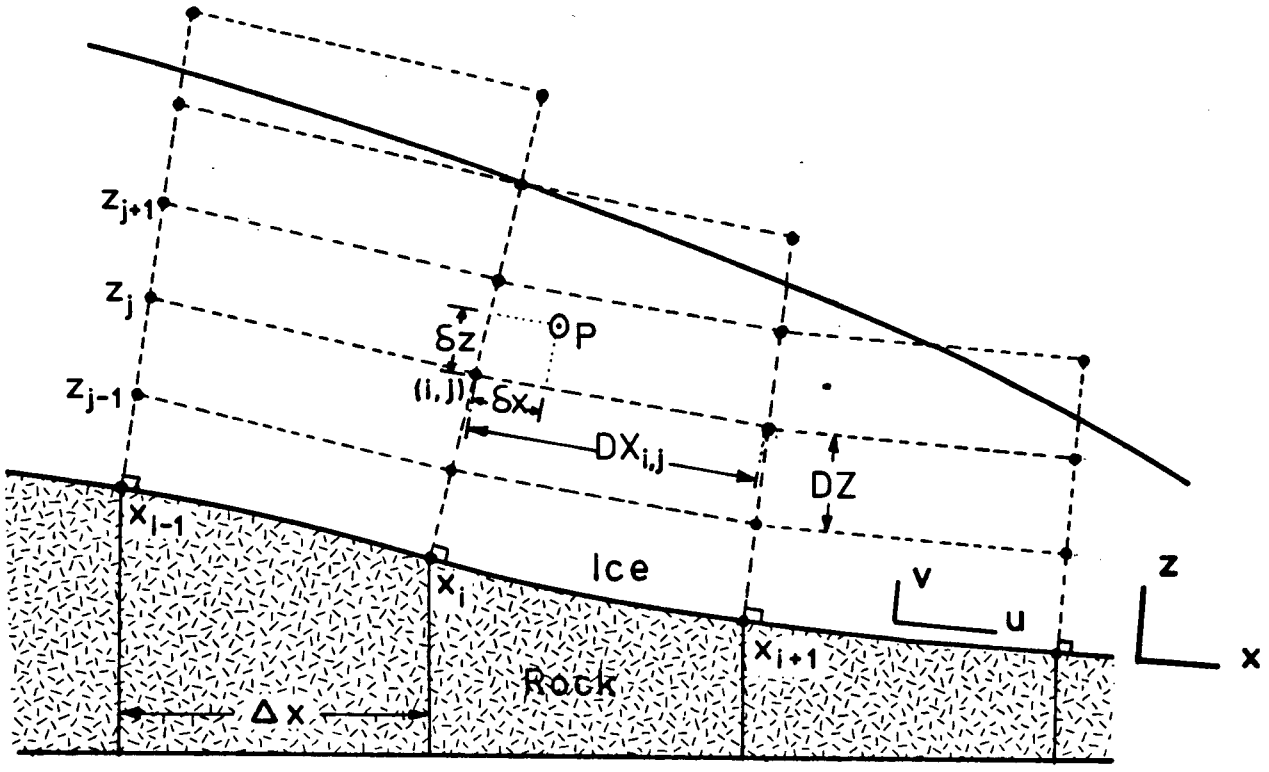

FIGURE A2.1. Mesh For Ice Displacement Calculations.

which varied with the ice thickness, based on a atmospheric modelling scheme of Phillips (1957). This scheme simplifies the boundary treatment, at the expense of more complicated derivatives.

A2.2 THE VELOCITY FIELD

A2.2.1 THE RECTANGULAR FLOW MODEL

The velocity vector $\underline{v}(\underline{x})$ at a point $\underline{x}$ within the glacier has components

$$\underline{v}(\underline{x}) = (u,w,v) \qquad (A2.2.1)$$

on the x,y,z axes. The glacier channel (Figure A2.2) is rectangular in cross-section, with width W(x). The ice thickness

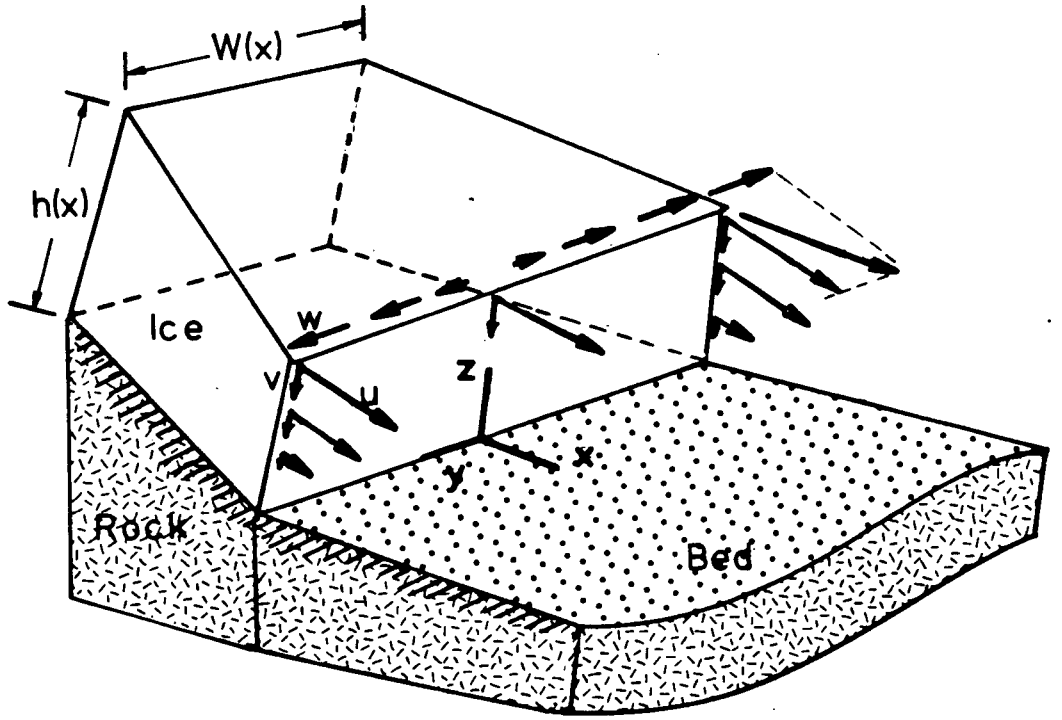

FIGURE A2.2. The Rectangular Flow Model.
The triad x-y-z is the coordinate system, and the bold arrows u, v, and w show the vector components of the velocity field $\underline{v}$.

h(x,t) and the velocity components u(x,z,t) and v(x,z,t) are assumed to be independent of y, the lateral position in the channel. Only the lateral velocity w(x,y,z,t) varies with y. At

the sidewalls of the flow tube (Figure A2.2), the total velocity vector $\underline{v}(\underline{x},t)$ must be in the local plane of the sidewalls, i.e.

$$w(x,\pm\frac{W}{2},z,t) = \pm\frac{u(x,z,t)}{2}\frac{dW}{dx} \qquad (A2.2.2)$$

and assuming constant lateral strain rate across the channel,

$$\frac{dw}{dy}(x,z,t) = \frac{u(x,z,t)}{W(x)}\frac{dW}{dx} \qquad (A2.2.3)$$

A2.2.2 THE DOWNSLOPE VELOCITY

The component of velocity $u(x,z,t)$ parallel to the glacier bed at height z where the ice thickness normal to the bed is $h(x,t)$ and the ice surface slope angle is α, is given in Appendix 7 (A7.5.8) as

$$u(x,z,t)-u_s(x,t) = \frac{2A}{n+1}\left[h^{n+1} - (h-z)^{n+1}\right][s(x)\rho g\sin\alpha]^n \qquad (A2.2.4)$$

plus some correction terms for stresses and strain rates other than shear parallel to the bed. A and n are the constants in Glen's flow law (Glen, 1955) (see 1.4.22)), ρ is the density of glacier ice, g is the acceleration due to gravity at the surface of the earth, and $u_s(x,t)$ is the basal sliding velocity which I discussed in Section 1.4.

A2.2.3 THE LONGITUDINAL STRAIN RATE

After u(i,j) is obtained at each mesh point (i,j) as in Figure A2.1, the gradient $\partial u/\partial x$ is estimated by the first term of the finite difference

$$\frac{\partial u}{\partial x}(i,j) = \frac{u(i+1,j) - u(i-1,j)}{DX_{i-1,j} + DX_{i,j}} + O\left(\frac{\partial^3 u}{\partial x^3}\,\Delta x^2\right) \quad (A2.2.5)$$

If any of the points (i±1,j) on the right side of (A2.2.5) are above the glacier surface, the velocities there are estimated by extrapolation from within the ice mass (purely for the numerical procedure). The error term in (A2.2.5) due to the use of the finite difference is made small by a suitably small choice of Δx. The factor $\partial^3 u/\partial x^3$ is also small, since glacier flow tends to be smooth.

Using (A2.2.4) for the velocity gradient (A2.2.5) neglects all the stress and strain rate components in the error terms in (A7.5.9), repeated below as (A2.2.8), yet purports to give the longitudinal strain rate, which is related to the longitudinal stress deviator by Glen's flow law (Glen, 1955). Is this inconsistent? I will show in the following pages that the estimate of the velocity gradient is in fact accurate to within an error term which is usually small. The error term contains stress and strain rate terms other than those parallel to the bed.

If u(x,z) is the velocity due to internal deformation by simple shearing from (A7.5.8), without the correction terms (A7.5.9)

$$u(x,z) = \frac{2A}{n+1}\left[h^{n+1} - (h-z)^{n+1}\right][s(x)\rho g \sin\alpha]^{n} \qquad (A2.2.6)$$

then the total velocity component parallel to the bed is

$$u(x,z) = u_{s}(x) + u(x,z)[1+ e(x)] \qquad (A2.2.7)$$

where $e(x)$ is the error term containing other stress and strain rate components subject to the assumptions in Appendix 7.

$$e(x) = O\left[\left[\left[n\left[\frac{2h\frac{\partial\overline{\sigma'_{xx}}}{\partial x} + h\frac{\partial\overline{\sigma'_{yy}}}{\partial x}}{\rho g h \alpha}\right] + (n-1)\frac{\delta\tau_{xz}}{\sigma} - \frac{\partial v}{\partial x}\Big/\frac{\partial u}{\partial z}\right]_{max}\right]\right] \qquad (A2.2.8)$$

Taking the x derivative of (A2.2.7) gives

$$\frac{\partial u}{\partial x}(x,z) = \frac{\partial u_{s}}{\partial x}(x) + \frac{\partial u}{\partial x}(x,z) + \frac{\partial}{\partial x}[u(x,z)\, e(x)] \qquad (A2.2.9)$$

The procedure I described in (A2.2.5) to estimate the longitudinal velocity used the first two terms of (A2.2.9), but neglected the third. In the most favourable case, i.e. $e(x)$ does not vary with x, (A2.2.9) reduces to

$$\frac{\partial u}{\partial x}(x,z) = \frac{\partial u_{s}}{\partial x}(x) + \frac{\partial u}{\partial x}(x,z)[1 + e(x)] \qquad (A2.2.10)$$

and the error in my method is always a small fraction of the longitudinal velocity gradient.

In the more general case, both $e(x)$ and $u(x,z)$ can vary with x, and the relative error in $\partial u/\partial x$ in (A2.2.9) is

$$\frac{\partial}{\partial x}[u(x,z)\, e(x)] \Big/ \frac{\partial u}{\partial x}(x,z) \qquad (A2.2.11)$$

which can be large when $u(x,z)$ changes slowly with x. This may be the case if the glacier near position x behaves like a parallel-sided slab in simple shear. This implies that where the

longitudinal gradient $\partial u/\partial x$ is very small, i.e.

$$\left|\frac{\partial u}{\partial x}(x,z)\right| << \left|u_{max}/L\right| \qquad \text{(A2.2.12)}$$

where L is the glacier length, and u_{max} is the greatest downslope velocity in the glacier, or

$$\left|\frac{\partial u}{\partial x}(x,z)\right| << \left|\frac{v(x,h(x))}{h(x)}\right| \qquad \text{(A2.2.13)}$$

then estimates of $\partial u/\partial x$ in the computer model are unreliable.

However, in absolute terms, the error is likely always small, because e(x) is small and presumably slowly varying with x. Unless the glacier has pronounced icefalls, or other steep bed gradient changes, the error is likely to satisfy

$$\left|\frac{\partial}{\partial x}[u\ e]\right| << u_{max}/L \qquad \text{(A2.2.14)}$$

and the gross flow pattern of the glacier model will be essentially correct.

A2.2.4 VELOCITY NORMAL TO THE BED

Because ice is incompressible, the divergence of the velocity field $\underline{v}(\underline{x},t)$ is zero, i.e.

$$\frac{\partial u}{\partial x} + \frac{\partial v}{\partial z} + \frac{\partial w}{\partial y} = 0 \qquad \text{(A2.2.15)}$$

The first term is calculated in (A2.2.5), and the third term is given by (A2.2.3) with (A2.2.4). Neglecting basal melt, which is usually less than a few centimetres per year (except during surging, when it may be comparable to surface melting for short periods), gives a boundary condition

$$v(x,0,t) = 0 \qquad \text{(A2.2.16)}$$

so that integrating (A2.2.7) from the bed to level z gives

$$v(x,z,t) = -\int_0^z \left[\frac{\partial u(x,z,t)}{\partial x} + \frac{u(x,z,t)}{W(x)} \frac{dW}{dx}\right] dz \qquad \text{(A2.2.17)}$$

This integral is evaluated at each meshpoint using Simpson's Rule (e.g. Carnahan and others, 1969, p. 73). This completes the solution for the velocity field $\underline{v}(\underline{x},t)$ at each time t.

At the glacier surface with normal vector $\underline{n}$, the condition

$$\underline{v}\cdot\underline{n} - \frac{\partial \underline{h}}{\partial t}\cdot\underline{n} - \underline{a}\cdot\underline{n} = 0 \qquad \text{(A2.2.18)}$$

must be satisfied. The terms $\underline{a}\cdot\underline{n}$ and $(\partial\underline{h}/\partial t)\cdot\underline{n}$ are the mass balance and the rate of change of ice thickness measured normal to the ice surface. Input values of $\underline{h}$ and $\underline{a}$, and $\underline{v}$ derived by the numerical procedure described above, when substituted into (A2.2.11) will leave a residual, the size of which indicates the accuracy achieved in determining $\underline{v}$. This is used as an independent test of this model in Chapter 2.

A2.3 ICE DISPLACEMENT FIELD

A2.3.1 FOUR POINT INTERPOLATION

Since ice particles may be located anywhere in the cross-section at the beginning of any time step, I must be able to relate any arbitrary quantity $f(\underline{P})$ at an arbitrary point $\underline{P}$ inside a mesh cell to the values of f at the four vertices labelled $\underline{P}_0$ through $\underline{P}_3$ as shown in Figure A2.3. Let $\underline{P}$ be displaced by an amount $d\underline{P}$ from $\underline{P}_0$.

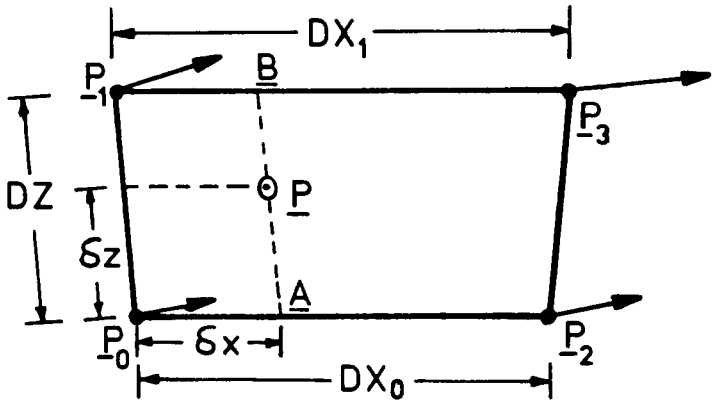

FIGURE A2.3. Four Point Interpolation Scheme.

$$d\underline{P} = (\delta x, \delta z) \qquad \text{(A2.3.1)}$$

To find $f(\underline{P})$, first find $f(\underline{A})$ and $f(\underline{B})$ on the boundaries of the mesh cell on the line through $\underline{P}$ parallel to $\underline{P}_0\underline{P}_1$ using a linear interpolation. Letting subscripts j on f_j indicate the meshpoint (see Figure A2.4),

$$f(\underline{A}) = f_0 + \left[\frac{f_2 - f_0}{DX_0}\right] \delta x \qquad (A2.3.2)$$

$$f(\underline{B}) = f_1 + \left[\frac{f_3 - f_1}{DX_1}\right] \delta x \qquad (A2.3.3)$$

Then, interpolating between $f(\underline{A})$ and $f(\underline{B})$,

$$f(\underline{P}) = f(\underline{A}) + \left[\frac{f(\underline{B}) - f(\underline{A})}{DZ}\right] \delta z$$

$$= f_0 + \left[\frac{f_2 - f_0}{DX_0}\right] \delta x + \left[\frac{f_1 - f_0}{DZ}\right] \delta z + \left[\frac{\frac{f_3 - f_1}{DX_1} - \frac{f_2 - f_0}{DX_0}}{DZ}\right] \delta x \delta z \qquad (A2.3.4)$$

The interpolated values $f(\underline{P})$ then lie on the surface sketched in Figure A2.4. This surface is linear along any line parallel to the x or z axes.

A2.3.2 DISPLACEMENTS AT MESHPOINTS

The next step is to find the displacement from time t_0 to time $t_1 = t_0 + \Delta t$ of the ice which was at meshpoint $\underline{P}$ at time t_0. This is given by

$$d\underline{P} = \int_{t_0}^{t_1} \underline{v}(t)\, dt \qquad (A2.3.5)$$

This can be approximated by using the arithmetic mean of the velocities at its position at the beginning and at the end of the time step, so that

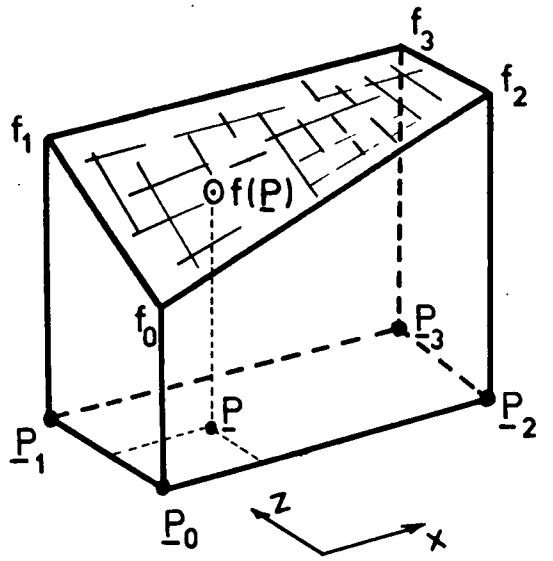

FIGURE A2.4. Interpolation Surface f(P).

$$d\underline{P} = \left[\frac{\underline{v}(\underline{P}(t_0),t_0)+\underline{v}(\underline{P}(t_1),t_1)}{2}\right] \Delta t \qquad \text{(A2.3.6)}$$

After using the interpolation scheme (A2.3.4) to express the velocity vector $\underline{v}(\underline{P}(t_1),t_1)$ in terms of the components δx and δz of $d\underline{P}$, letting integer subscripts on the velocity component u indicate the vertex number, and introducing the notation (A2.3.7) for the partial differences of the component u,

$$u_x = \frac{u_2(t_1) - u_0(t_1)}{DX_0}$$

$$u_z = \frac{u_1(t_1) - u_0(t_1)}{DZ}$$

$$u_{xz} = \frac{\dfrac{u_3(t_1) - u_1(t_1)}{DX_1} - \dfrac{u_2(t_1) - u_0(t_1)}{DX_0}}{DZ} \qquad \text{(A2.3.7)}$$

together with the obvious equivalent definitions for v, the two

components of the vector equation (A2.3.6) yield two coupled nonlinear equations (A2.3.8) and (A2.3.9) for δx and δz.

$$\delta x = \frac{\Delta t}{2}\left[u_o(t_o) + u_o(t_1) + u_x \delta x + u_z \delta z + u_{xz}\, \delta x \delta z\right] \tag{A2.3.8}$$

$$\delta z = \frac{\Delta t}{2}\left[v_o(t_o) + v_o(t_1) + v_x \delta x + v_z \delta z + v_{xz}\, \delta x \delta z\right] \tag{A2.3.9}$$

Solving (A2.3.9) for δz and substituting it into (A2.3.8) gives

$$A\,\delta x^2 + B\,\delta x + C = 0 \tag{A2.3.10}$$

where

$$\begin{aligned} A &= u_x v_{xz} - u_{xz} v_x - \frac{2}{\Delta t} \\ B &= v_{xz}\left[u_o(t_o) + u_o(t_1)\right] - u_{xz}\left[v_o(t_o) + v_o(t_1)\right] \\ &\quad + u_x v_z - u_z v_x - \frac{2}{\Delta t}\left[u_x + v_z\right] + \frac{4}{\Delta t^2} \\ C &= v_z\left[u_o(t_o) + u_o(t_2)\right] - u_z\left[v_o(t_o) + v_o(t_1)\right] \\ &\quad + \frac{2}{\Delta t}\left[u_o(t_o) + u_o(t_1)\right] \end{aligned} \tag{A2.3.11}$$

The solution of (A2.3.10) is given by the standard quadratic formula taking the positive square root. The other displacement component δz is found by substituting δx into (A2.3.8).

If the point $\underline{P}$ is in a region where v is positive (upward flow), the procedure described above is used. This is the usual situation in the ablation region of a glacier. However, if $v<0$,

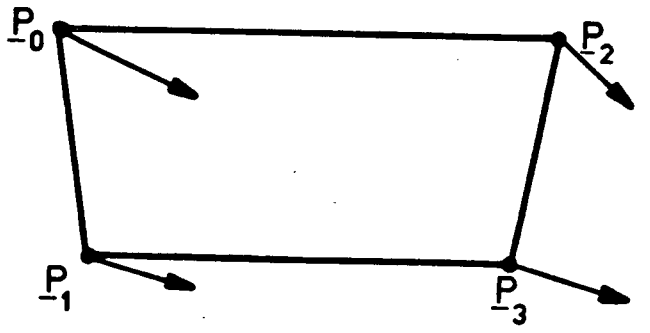

FIGURE A2.5. Cell Vertex Notation For Downward Velocity.

the ice at $\underline{P}_0$ would flow into the cell below the cell illustrated in Figure A2.3. In this case $\underline{P}_0$ is chosen to be the upper left vertex of the cell, DZ is negative, and similar equations are derived for δx and δz. The vertex notation for this case is illustrated in Figure A2.5. This is the usual situation in the accumulation zone.

This procedure is repeated for each mesh point (i,j) to find the displacement field throughout the longitudinal section of the glacier. Figure A2.6 shows the displacement field calculated by this method for a glacier in steady state.

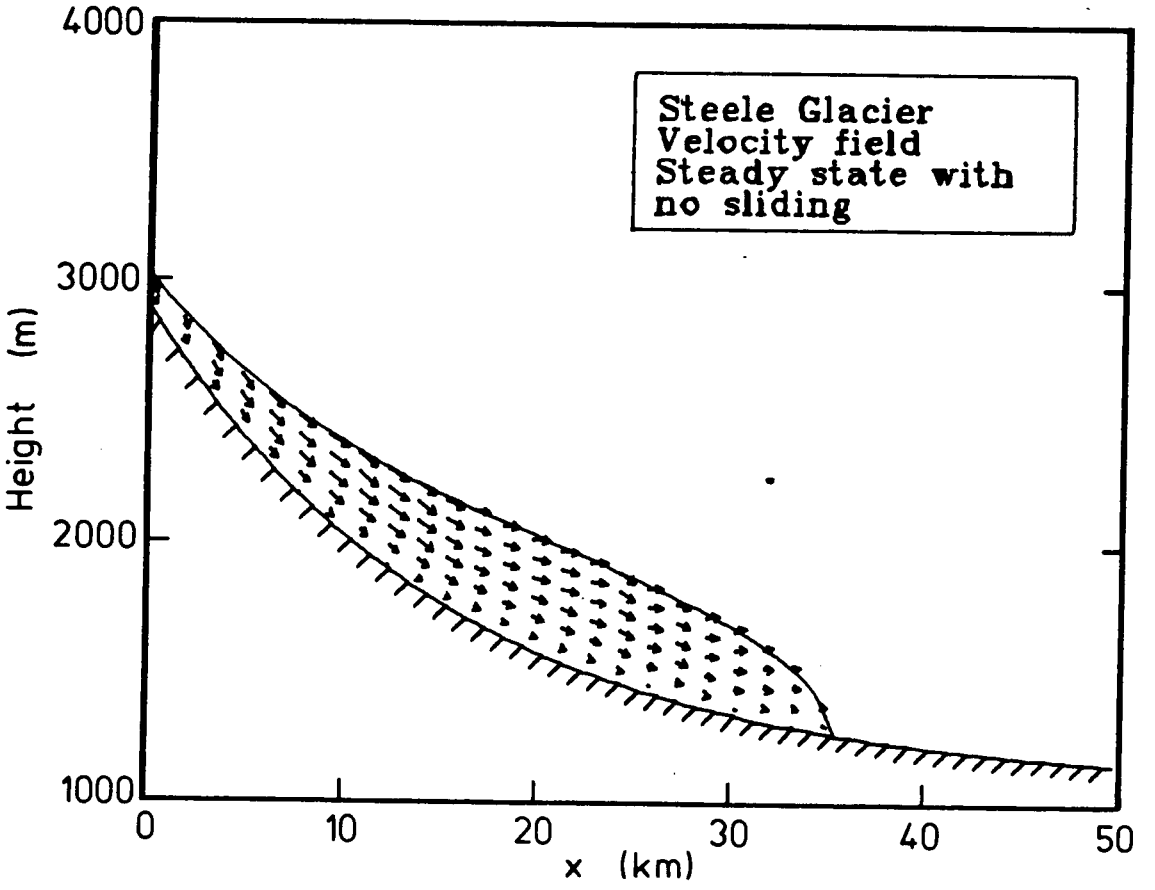

FIGURE A2.6. Displacement Field In A Steady State.
The mass balance and the width for this Steele Glacier model are shown in Figure 3.3. The displacement vectors indicate the flow for 25 years in a steady state with no sliding.

A2.4 ICE PARTICLE TRAJECTORIES

A2.4.1 TRACKING PROCEDURE

At time t_o, the cell occupied by each particle $\underline{P}$ currently being tracked is identified, and the coordinates $(\delta x, \delta z)$ of the particle relative to the vertex $\underline{P}_o$ are determined. Then, using the interpolation scheme (A2.3.4) where $f(\underline{P})$ is a Cartesian displacement component, the displacement components $f(\underline{P})$ at $\underline{P}$ are found using the known displacements at the surrounding

vertices. The new Cartesian coordinates of the particle at time t_1 are then saved. The program then checks to see whether the particle has moved into a new cell, and calculates the new $(\delta x, \delta z)$ for the next time step. This procedure is repeated at each time step for each particle being tracked.

A2.4.2 PARTICLES WHICH REACH ICE SURFACE

If the calculated position of a particle at the end of a time step is above the glacier surface, it has obviously gone too far! The position and time at which it actually reached the glacier surface are interpolated from the surface position and particle position at the two times involved, and this information is saved.

A2.4.3 TRACKING BACKWARDS IN TIME

For some applications, I do not want to know where the ice is going, but from where it came. For instance, given a sample of ice from a position $\underline{P}'$ in a borehole at time t', I may wish to know where and when it was precipitated at the glacier surface as snow. To do this I run the model described above backwards through time from t', using $\Delta t<0$. Then $(\delta x, \delta z)$ in (A2.3.8) and (A2.3.9) are the displacements of ice particles which arrived at mesh point $\underline{P}_0$ at time t_0, rather than displacements of ice which left $\underline{P}_0$ at time t_0. When $\Delta t<0$, $\underline{P}_0$ is chosen to be on the downstream boundary of the mesh cell, as in Figure A2.7.

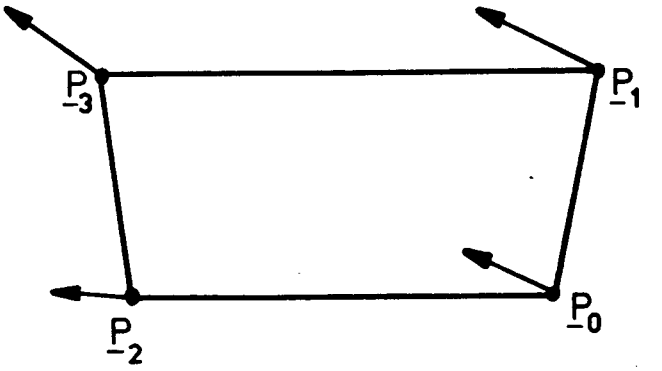

FIGURE A2.7. Cell Vertex Notation For Negative Time.

A2.4.4 BOUNDARY CONDITION AT UPSTREAM END

If the boundary condition at x=0 is zero input flux with zero surface slope (ice divide model), then image points at $-\Delta x/2$ are assigned the velocities

$$u(-\frac{\Delta x}{2},z,t) = -u(\frac{\Delta x}{2},z,t)$$

$$v(-\frac{\Delta x}{2},z,t) = v(\frac{\Delta x}{2},z,t) \qquad \text{(A2.4.1)}$$

This prevents the ice particles from flowing across the transverse section at x=0 .

If there is a nonzero input flux $Q_0(t)$ into the model at x=0, then the fictitious points at $-\Delta x/2$ are assigned velocities derived by extrapolation from the mesh points at x>0, and ice particles tracked back across the section at x=0 disappear from the model.

APPENDIX 3: ASPECTS OF DISCRETE DATA SERIES

A3.1 THE Z TRANSFORM

A digitized function on a grid with spacing Δx can be represented as a series

$$f(x) = [f_0, f_1, f_2, \ldots f_J] \qquad (A3.1.1)$$

It can also be represented by a polynomial F(Z), where the coefficients are the $\{f_j | j=1,J\}$, and Z is the unit space shift operator.

$$F(Z) = \sum_{j=0}^{J} f_j Z^j \qquad (A3.1.2)$$

(A3.1.2) is the Z transform of (A3.1.1). If the substitution

$$Z = e^{im\Delta x} \qquad (A3.1.3)$$

is made into (A3.1.2), the Fourier transform of the digitized function is obtained.

$$F(m) = \sum_{j=0}^{J} f_j e^{imj\Delta x} \qquad (A3.1.4)$$

As the wavenumber m goes from zero to $2\pi/\Delta x$, Z moves counterclockwise around the unit circle in the complex plane, as shown in Figure A3.1.

Convolution of time series is equivalent to multiplying the Z polynomials. The forward Fourier transform is equivalent to summing the terms in the Z polynomial, and the inverse Fourier transform is equivalent to identifying the coefficients of each

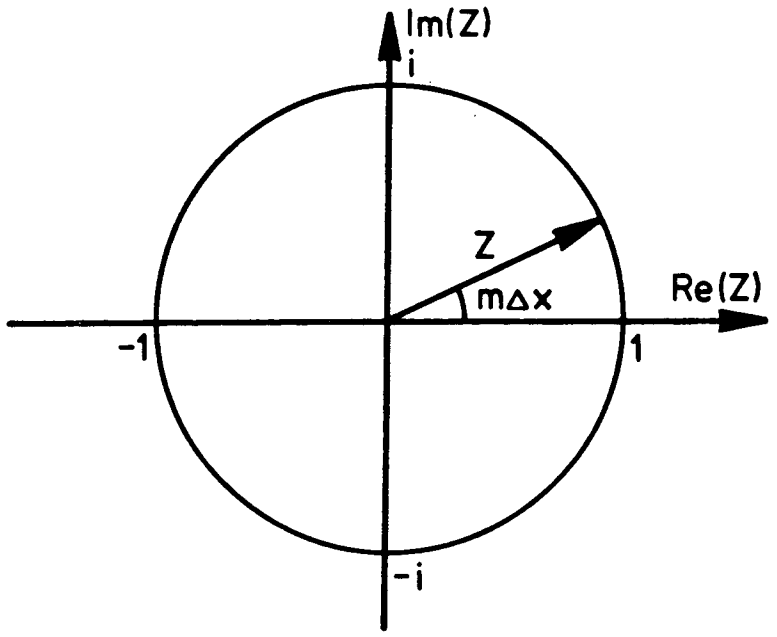

FIGURE A3.1. The Z Plane.

power of Z in the polynomial.

A3.2 ALIASING

A mesh with spacing Δx cannot resolve a sinusoidal variation with a wavelength less than $2\Delta x$, i.e. with less than two mesh points per wavelength. A signal with a wavelength less than $2\Delta x$ will be misinterpreted by the mesh as a signal at a longer wavelength. Figure A3.2 shows how a signal with the wavelength $1.5\Delta x$, or wavenumber $4\pi/(3\Delta x)$, is indistinguishable from a signal with a wavelength $3\Delta x$, or wavenumber $2\pi/(3\Delta x)$.

The limiting wavenumber which is detectable, i.e. $\pi/\Delta x$ is called the Nyquist wavenumber m_N. It is also called the folding wavenumber. In general, energy in a signal at the wavenumber $(2m_N - m)$ with $0<m<m_N$, will be 'folded' back to the wavenumber m within the 'principal alias' $[0,m_N]$. This phenomenon is called

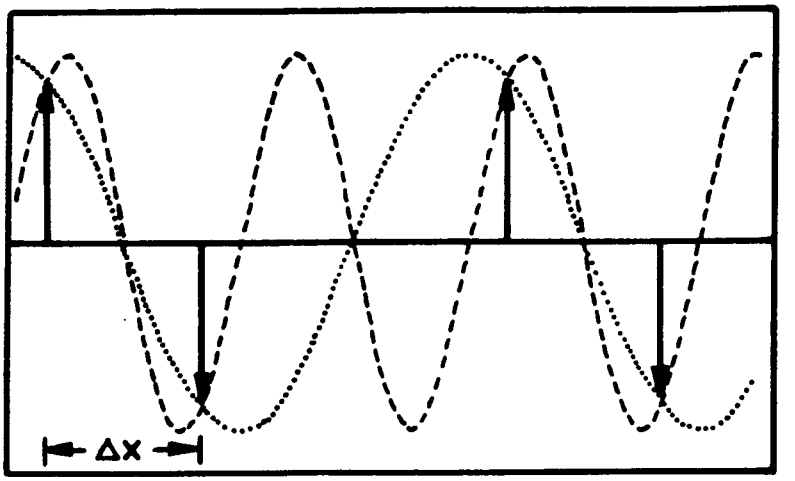

FIGURE A3.2. Signals With Wavelengths 1.5Δx And 3.0Δx. The sampled signal (spikes) is identical for both the continuous signals.

aliasing because the energy at high wavenumbers is disguised as energy at lower wavenumbers due to the discrete mesh.

To demonstrate this, consider the signal

$$f_j = \sin[(\frac{2\pi}{\Delta x} - m)j\Delta x] \quad j=1,J \qquad \text{(A3.1.1)}$$

which has a wavenumber beyond m_N. Basic trigonometric manipulation gives

$$\sin[(\frac{2\pi}{\Delta x} - m)j\Delta x] = -\sin[mj\Delta x] \qquad \text{(A3.1.2)}$$

This shows that the high wavenumber $(2m_N - m)$ signal takes on the same values at the mesh points as a signal at the lower wavenumber m. Similarily, signals at wavenumbers higher than $2m_N$ are folded back into the principal alias. All the energy at wavenumbers $(2nm_N \pm m)$ for integer n in the Fourier spectrum of a signal appears in the mesh at the wavenumber m. This aliasing causes signal distortion.

The aliasing problem arises in this study because of the

nonlinearity of the flux gradient term in the continuity equation. The nonlinearity pumps energy into wavenumbers above m_N at each time step. This energy is then aliased back into the principal alias by the discrete nature of the mesh. This misplaced energy can grow with time and dominate the true solution. This nonlinear instability is discussed in Appendix 1 Section (A1.4.3).

APPENDIX 4: DENSITY OF GLACIER ICE

A4.1 FIRN AS EQUIVALENT ICE THICKNESS

While the firn is generally restricted to the upper 10% or less of an ice mass, the deformation by shearing is concentrated near the bed. In a region of laminar flow parallel to the bed, the ice velocity depends only on σ_{xz}, the shear stress parallel to the x axis. Balancing forces on an ice element above a bed with slope α as in Figure A4.1,

$$\sigma_{xz}(z+\delta z) - \sigma_{xz}(z) = \rho(z)\, g \sin(\alpha)\, \delta z \qquad \text{(A4.1.1)}$$

where $\rho(z)$ is ice density, g is the acceleration due to gravity, and α is ice surface slope. In the limit as δz goes to zero,

$$\frac{\partial \sigma_{xz}}{\partial z} = \rho(z)\, g \sin(\alpha) \qquad \text{(A4.1.2)}$$

Integrating (A4.1.2) gives

$$\sigma_{xz}(z) = g \sin(\alpha) \int_0^z \rho(y)\, dy \qquad \text{(A4.1.3)}$$

where z is positive downward and the free surface is at z=0. (A4.1.3) shows that the shear stress parallel to the bed depends only on the integral of the density above level z, i.e. the total mass above, and not on its distribution. For z below the firn, the shear stress is not affected by representing the firn by an ice layer of equal mass. Within the firn itself, the stresses are generally too small to cause significant deformation other than compaction. When comparing model results

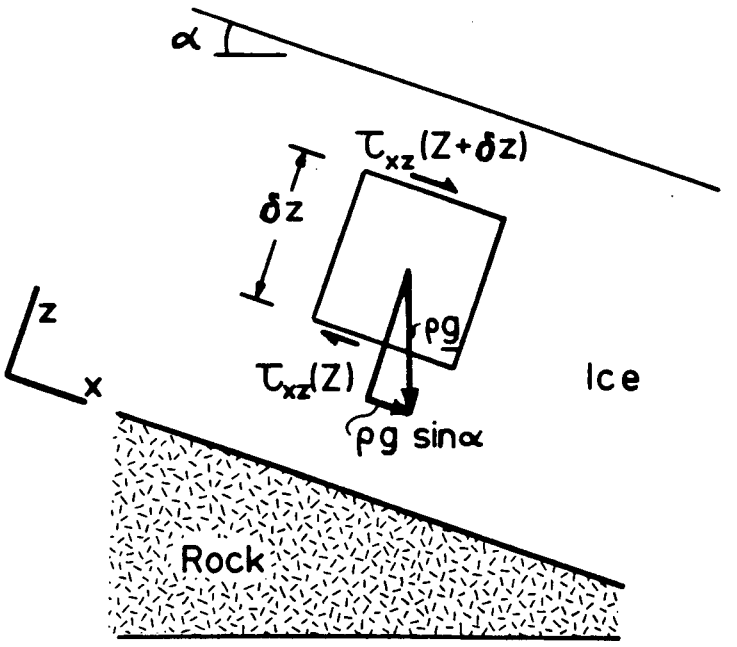

FIGURE A4.1. Force Balance On An Ice Element.

with field observations, it must be remembered, however, to use the elevation of the equivalent ice layer, not the observed glacier surface.

A4.2 CONSTANT DENSITY ASSUMPTION

New snow may have a density as low as 50 kg m^{-3} (Seligman, 1936) on falling. The density increases with depth of burial due to compression and metamorphism of snow and firn crystals, until at a density of about 850 kg m^{-3}, the interconnecting air passages between grains are sealed off. The depth at which this occurs can vary widely. Paterson (1969, p. 16) gives two examples. On the upper Seward Glacier (a wet snow regime) the transition to ice occurs at a depth of 13 metres, while at Site 2, Greenland, (a dry snow regime) the transition is at 80

metres. In climates with significant summer ablation, ice can also form by the freezing of meltwater percolating down into soaked firn. This is called superimposed ice (e.g. Paterson, 1969, p. 9).

The density of glacier ice itself varies with temperature, pressure, bubble content and debris content.

The coefficient of cubical expansion of ice in the range -10°C to -50°C is of the order of 1.5×10^{-4} deg^{-1} (Hobbs, 1974, p. 350). Thus the total variation in density of ice that could be expected due to a temperature difference of 50°C is of the order of 10^{-2}, or 1%. This is negligible given the other uncertainties in glacier parameters.

Values of the bulk modulus of polycrystalline ice at -5°C (Hobbs, 1974, p. 258) are of the order of 10^{10}Pa (10^5 bar). Since maximum basal pressures (overburden load) in ice sheets are of the order of 10^7Pa, the maximum variation in density to be expected due to pressure contraction is 10^{-3}, or 0.1%. The assumption that ice is incompressible is included explicitly in Glen's formulation of the flow law for ice (Glen, 1955).

The presence of gas bubbles within glacier ice can have a larger effect on density. Seligman (1936, p. 119) gives a variation of 38 kg m^{-3} or about 3% between measurements on white bubbly ice and blue bubble-free ice. The bubbly ice could be compressed by pressure on flowing to depth by up to this 3% by merely compressing the gas in the bubbles. Even a 3% variation is negligible, however, given other assumptions of modelling.

The inclusion of debris in the basal layers of a glacier may increase the local density considerably. For example, 50%

debris by volume (a large amount) with a density of 2100 kg m^{-3} would raise the density of the ice-debris mixture to 1500 kg m^{-3}, or by over 50%. It would presumably also alter the flow law parameters in the basal region where a large part of the deformation of a glacier takes place. There is very little that one can do about this source of error in the numerical model. The only salvation is the observation that extensive debris is usually restricted to within a few metres of the glacier bed.

For most computations carried out in this study, the density of glacier ice was taken as 900 kg m^{-3}.

APPENDIX 5: CONTINUITY EQUATION FOR AN ICE MASS

A5.1 MASS CONSERVATION IN A MOVING CONTINUUM

Let M(t) be the volume integral of a continuously differentiable function $\rho(\underline{x},t)$ defined in a volume $V(\underline{x},t)$ enclosed by a surface $S(\underline{x},t)$ moving with the velocity $\underline{v}(\underline{x},t)$ of the continuum. The position vector is $\underline{x}$ and t is time. Underscores indicate vector quantities. Then

$$M(t) = \iiint_V \rho(\underline{x},t)\, d^3r \qquad \text{(A5.1)}$$

When $\rho(\underline{x},t)$ is the material density, M(t) is the mass contained within V. The material derivative DM/Dt is the rate of change of M(t) with respect to time 't' (e.g. Malvern, 1969, p. 211).

$$\frac{DM}{Dt} = \iiint_V \frac{\partial \rho(\underline{x},t)}{\partial t}\, d^3r + \iint_S \rho(\underline{x},t)\, \underline{v}(\underline{x},t)\cdot\underline{n}\, ds \qquad \text{(A5.2)}$$

where $\underline{n}$ is the outward unit normal to S. By the law of conservation of mass,

$$\frac{DM}{Dt} = 0 \qquad \text{(A5.3)}$$

For ice masses in this study, the firn and the mass balance are expressed as equivalent ice thickness, and the density of ice is taken constant. These assumptions are examined in Appendix 4.

Under these assumptions, (A5.2) reduces to

$$\iint_S \underline{v}(\underline{x},t)\cdot\underline{n}\, ds = 0 \qquad \text{(A5.4)}$$

A5.2 IN A STATIONARY GLACIER CROSS-SECTION

Although (A5.4) was derived assuming the surface S moved with the continuum, (A5.4) is also true for a stationary surface that corresponds to S at the instant considered. Since $\rho \underline{v} \cdot \underline{n}$ is the mass flux density, (A5.4) states that the net ice flux across the surface S is zero. To put this into a usable form, let S comprise two transverse sections S_1 and S_2 through the ice

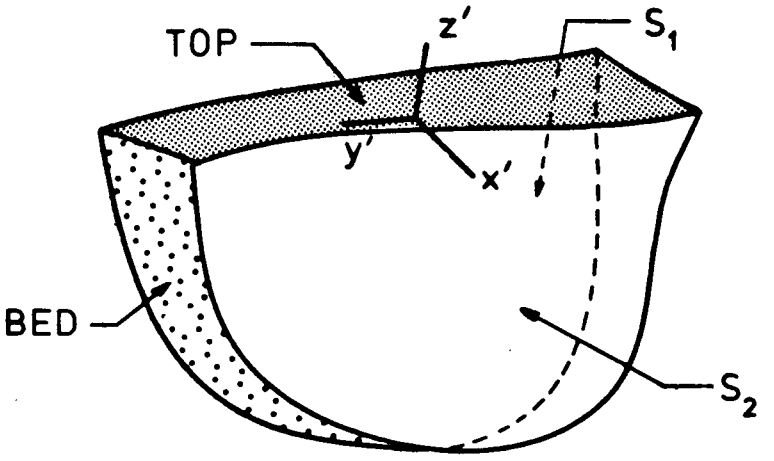

FIGURE A5.1. Surfaces for Derivation of Continuity Equation.

mass in Figure A5.1, plus the annular surface joining them, i.e. the sections TOP and BED. Then (A5.4) is

$$\iint_{S_1} \underline{v} \cdot \underline{n} \, ds + \iint_{S_2} \underline{v} \cdot \underline{n} \, ds + \iint_{TOP} \underline{v} \cdot \underline{n} \, ds + \iint_{BED} \underline{v} \cdot \underline{n} \, ds = 0 \qquad \text{(A5.5)}$$

Now consider the motion of the free surface TOP defined as the endpoints of position vectors $\underline{h}$. As the surface TOP moves, $\partial \underline{h}/\partial t \cdot \underline{n}$ is the normal velocity of the free surface. The vector

$\partial \underline{h}/\partial t$ is determined only to within an arbitrary constant vector $\underline{F}$ normal to $\underline{n}$, or tangent to the surface TOP, i.e.

$$\frac{\partial \underline{h}}{\partial t} = \left[\frac{\partial \underline{h}}{\partial t}\cdot\underline{n}\right]\underline{n} + \underline{F} \qquad \underline{F}\cdot\underline{n} = 0 \tag{A5.6}$$

Similarily, the mass balance $\underline{a}(\underline{x},t)$ at the surface is arbitrary to within a constant vector $\underline{G}$ tangent to the surface TOP, but the component $\underline{a}\cdot\underline{n}$ is the normal velocity of the melting surface or accumulation surface with respect to the material.

$$\underline{a}(\underline{x},t) = (\underline{a}\cdot\underline{n})\,\underline{n} + \underline{G} \qquad \underline{G}\cdot\underline{n} = 0 \tag{A5.7}$$

It is apparent that the net normal velocity of the surface must be the sum of the normal velocity $\underline{v}(\underline{x},t)\cdot\underline{n}$ of the material at the surface plus the normal velocity into the material of the melting surface, i.e.,

$$\frac{\partial \underline{h}}{\partial t}\cdot\underline{n} = \underline{v}\cdot\underline{n} + \underline{a}\cdot\underline{n} \tag{A5.8}$$

where $\underline{v}(\underline{x},t)$ is the material velocity.

Similarily, on the constrained surface BED

$$\underline{v}\cdot\underline{n} + \underline{b}\cdot\underline{n} = 0 \tag{A5.9}$$

where $\underline{b}(x,t)$ is the rate of melting or freezing at the bed. Letting Q_1 and Q_2 be the total fluxes through S_1 and S_2 using the downslope unit normal, (A5.5) becomes

$$Q_2 - Q_1 + \iint_{TOP} \frac{\partial \underline{h}}{\partial t}\cdot\underline{n}\, ds - \iint_{TOP} \underline{a}\cdot\underline{n}\, ds - \iint_{BED} \underline{b}\cdot\underline{n}\, ds = 0 \tag{A5.10}$$

To proceed further, it is necessary to choose some axes. Let the x' axis run along the glacier surface down the "centre" of the channel (how this is defined is not crucial). The z' axis is

orthogonal to x' and positive upward in the vertical surface containing the centreline. The horizontal y' axis completes a right-handed orthogonal coordinate system. These axes are shown in Figure A5.1.

Next, let the surface S become thin such that S_1 and S_2 intersect the glacier surface at x'_1 and x'_2 separated by a small amount $\delta x'$ (see Figure A5.2). Then, when W(x',Z') is the channel

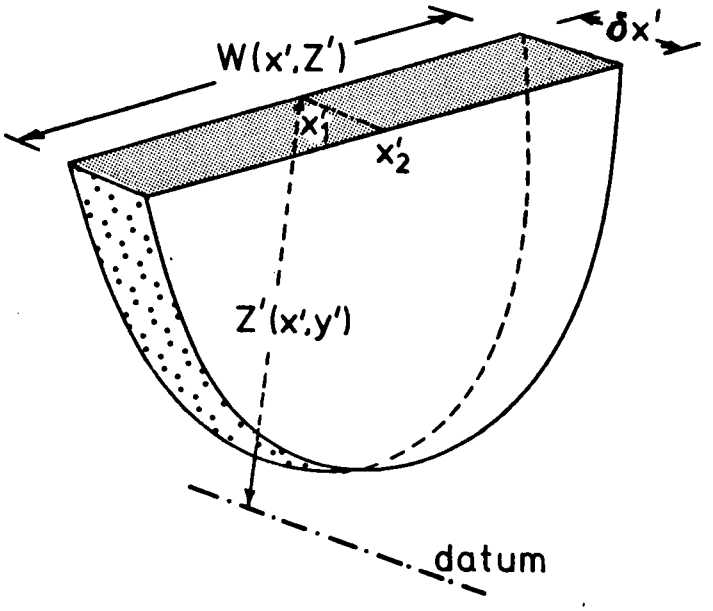

FIGURE A5.2. The Thin Cross-section Limit.

width at the level Z'(x',y') of the ice surface above some datum level, (A5.10) becomes

$$0 = Q_2(x'_2) - Q_1(x'_1) + \delta x' \left[\int_0^{W(x',Z')} \frac{\partial \underline{h}}{\partial t} \cdot \underline{n} \, dy - \int_0^{W(x',Z')} \underline{a} \cdot \underline{n} \, dy - \int_0^{W(x',Z')} \underline{b} \cdot \underline{n} \, dy \right] \quad \text{(A5.11)}$$

A5.3 IN AN ARBITRARY CHANNEL

At this point there are two possible lines of development, dependent on the form of channel cross-section to be modelled. Letting (A5.12) define a scalar B(x',t) which is mass balance plus basal melting per unit channel width normal to the ice surface at height z'=0 and averaged across the glacier channel width W(x',0) ,

$$B(x',t)\, W(x',0) = \int_0^{W(x',0)} (\underline{a} \cdot \underline{n} + \underline{b} \cdot \underline{n}) \, dy' \quad \text{(A5.12)}$$

and recognizing

$$\frac{\partial \underline{h}}{\partial t} \cdot \underline{n} \, dy = \frac{\partial S(x',t)}{\partial t} \quad \text{(A5.13)}$$

where S(x',t) is the transverse cross sectional area of the glacier in the y'-z' plane, (A5.11) becomes

$$\frac{Q_2(x'_2) - Q_1(x'_1)}{\delta x'} + \frac{\partial S(x',t)}{\partial t} = B(x',t)\, W(x',0) \quad \text{(A5.14)}$$

In the limit as $\delta x' \rightarrow 0$,

$$\frac{\partial S(x',t)}{\partial t} + \frac{\partial Q(x',t)}{\partial x'} = A(x',t)\, W(x',0) \qquad (A5.15)$$

This formulation (A5.15) is useful when the channel width varies with depth z' (e.g. Bindschadler, unpublished; Raymond, 1980).

A5.4 IN A RECTANGULAR CHANNEL

In this study, however, I use models with rectangular cross section, so that the cross sectional area S need not be introduced. In such a channel (Figure A5.3), the thickness and the x' and z' velocity components are assumed to be independent of y'. The transverse velocity component is such that at every point on the channel wall, the total velocity vector is in the plane of the wall, i.e. there are no voids along the margins. The transverse strain rate is then assumed to be constant across the channel. I have described this model in Section A2.2.1. This approach was suggested by Nye (1959[c]). It is quite a good model for nonparallel flowlines on ice sheets, where the "walls" of the "channel" are fictitious. Even for valley glaciers, the same approach may be used. W(x) may be thought of as the width of a narrow band of flow lines near the glacier centreline, e.g. a few percent of the valley width at the level of the ice surface. The bed is likely to be nearly flat over a narrow band at the centre of the channel, and u and v are usually almost independent of y near the centreline. Then, v is essentially the centreline velocity, not the average across the whole channel. Shape factors (Nye, 1965[c]) can be used to account qualitatively for the drag from the valley walls. This approach does allow me to get an approximate solution to a

three-dimensional problem using a two-dimensional model.

With these assumptions, the first integral in (A5.11) reduces to

$$\int_0^{W(x')} \frac{\partial \underline{h}}{\partial t} \cdot \underline{n} \, dy' = W(x') \frac{\partial \underline{h}(x',t)}{\partial t} \cdot \underline{n} \qquad \text{(A5.16)}$$

where $\underline{h}(x',t)$ is now independent of the transverse coordinate y', and $W(x')$ is independent of surface elevation Z'. Defining a total source term $\underline{A}(x',t)$ independent of y' through (A5.17)

$$\int_0^{W(x')} (\underline{a}\cdot\underline{n} + \underline{b}\cdot\underline{n}) \, dy' = W(x') \, \underline{A}(x',t)\cdot\underline{n} \qquad \text{(A5.17)}$$

and letting $\delta x' \rightarrow 0$ puts the continuity equation (A5.11) into the form

$$\frac{\partial \underline{h}(x',t)}{\partial t} \cdot \underline{n} + \frac{1}{W(x')} \frac{\partial Q}{\partial x'} = \underline{A}(x',t)\cdot\underline{n} \qquad \text{(A5.18)}$$

If the vectors $\underline{h}(x',t)$ and $\underline{A}(x',t)$ are $\underline{h}'(x',t)$ and $\underline{A}'(x',t)$ oriented normal to the ice surface (see Figure A5.3), i.e. parallel to $\underline{n}$, (A5.18) reduces immediately to

$$\frac{\partial h'(x',t)}{\partial t} + \frac{1}{W(x)} \frac{\partial Q(x',t)}{\partial x} = A'(x,t) \qquad \text{(A5.19)}$$

where the scalars $h'(x',t)$ and $A'(x',t)$ are just the magnitudes of the vector quantities. However, a coordinate system that moves with the time-varying ice surface is computationally inconvenient. I will now show that other more convenient choices of coordinates lead to a equation of the same form as (A5.19).

A5.5 IN BED-NORMAL COORDINATES

Let an x axis lie anywhere in the x'-z' plane. The z axis is in the same plane, and positive up. The y axis is the same as the y' axis. These coordinates are shown in Figure A5.3. Let

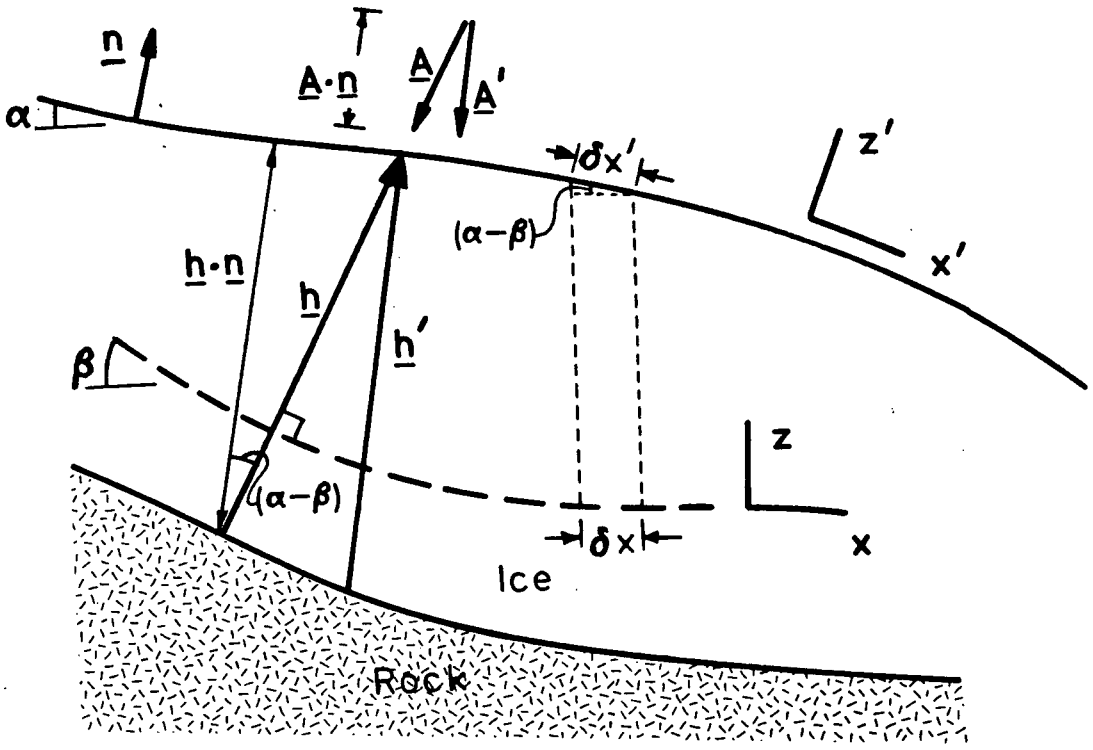

FIGURE A5.3. Coordinates And Variables In Rectangular Channel.

$\alpha(x')$ and $\beta(x)$ be the inclinations of the ice surface (x' axis) and the x axis respectively, and let the vector $\underline{h}$ be measured normal to the x axis. Then

$$\frac{\partial \underline{h}}{\partial t} \cdot \underline{n} = \frac{\partial h}{\partial t} \cos(\alpha - \beta) \qquad \text{(A5.20)}$$

and

$$\underline{A}\cdot\underline{n} = A\cos(\alpha-\beta) \tag{A5.21}$$

The difference between $\underline{h}$ normal to the x axis and $\underline{h}'$ normal to the ice surface is just the vector $\underline{F}$ in (A5.6); a similar result holds for the balance and $\underline{G}$ in (A5.7).

It is also seen from Figure A5.3 that the x axis is related to the x' axis by

$$\frac{dx'(x)}{dx} = \frac{1}{\cos(\alpha-\beta)} \tag{A5.22}$$

so that using the chain rule

$$\frac{\partial Q}{\partial x'} = \frac{\partial Q}{\partial x}\frac{dx}{dx'} = \frac{\partial Q}{\partial x}\cos(\alpha-\beta) \tag{A5.23}$$

and (A5.18) reduces to

$$\frac{\partial h(x,t)}{\partial t}\cos(\alpha-\beta) + \frac{1}{W(x)}\frac{\partial Q(x,t)}{\partial x}\cos(\alpha-\beta)$$

$$= A(x,t)\cos(\alpha-\beta) \tag{A5.24}$$

The cosine factors divide out, leaving an equation of exactly the same form as (A5.19) when h(x,t) and A(x,t) are measured normal to, and the flux gradient is taken along, <u>any</u> x axis in the x'-z' plane that can be related to the x' axis by a one-to-one transformation through integrating (A5.22). This restriction means that the curvature of the x axis must be small enough that vectors normal to it do not intersect within the ice mass.

Some obvious choices for the x axis are (1) the glacier surface: this is impractical because it moves in time; (2) horizontal Cartesian axis; and (3) the glacier bed: this is used in this study because it is stationary, and the integrated form of Glen's flow law (see Appendix 7) uses thickness normal to the glacier bed.

When $u(x,z,t)$ is the x-component of velocity, the flux $Q(x,t)$ is

$$Q(x,t) = W(x) \int_0^{h(x,t)} u(x,z,t)\, dz \qquad \text{(A5.25)}$$

After defining $V(x,t)$, the velocity averaged over depth, by

$$V(x,t) = \frac{Q(x,t)}{W(x)\, h(x,t)} = \frac{1}{h(x,t)} \int_0^{h(x,t)} u(x,z,t)\, dz \qquad \text{(A5.26)}$$

$Q(x,t)$ can be written as

$$Q(x,t) = V(x,t)\, h(x,t)\, W(x) \qquad \text{(A5.27)}$$

When the ice deforms mainly by shear near the bed, $V(x,t)$ is close to the velocity at the ice surface. In fact, using Glen's flow for ice, the surface velocity $u(x,h,t)$ is equal to $(n+2)/(n+1)$ times the average velocity $V(x,t)$ in (A5.26).

The form of the continuity equation that is solved in this study is

$$\frac{\partial h}{\partial t}(x,t) + \frac{1}{W(x)} \frac{\partial}{\partial x}[h(x,t)V(x,t)W(x)] = A(x,t) \qquad \text{(A5.28)}$$

where $h(x,t)$ and $A(x,t)$ are measured normal to the glacier bed, and the flux gradient is measured along the bed.

APPENDIX 6: EQUATIONS FOR PERTURBATIONS

This appendix follows the work of Weertman (1958) and of Nye (1960; 1963[a]; 1963[b]). The continuity equation (1.3.5) has the form

$$\frac{\partial H}{\partial t}(x,t) + \frac{\partial Q}{\partial x}(x,t) = A(x,t) \tag{A6.1}$$

when the width W(x) of the channel is unity. H(x,t) is the ice thickness normal to the ice surface, Q(x,t) is the ice flux through H(x,t), and A(x,t) is the mass balance. Letting subscripts 0 indicate a steady state configuration, (A6.1) becomes

$$\frac{\partial Q}{\partial x}_{o}(x) = A_{o}(x) \tag{A6.2}$$

If the steady state quantities are perturbed by small amounts indicated by lower case variables, (A6.1) becomes

$$\frac{\partial}{\partial t}[H_{o}(x)+h(x,t)] + \frac{\partial}{\partial x}[Q_{o}(x)+q(x,t)] = [A_{o}(x)+a(x,t)] \tag{A6.3}$$

Using (A6.2), (A6.3) becomes

$$\frac{\partial h}{\partial t}(x,t) + \frac{\partial q}{\partial x}(x,t) = a(x,t) \tag{A6.4}$$

when the width W(x) of the channel is unity. When the flux Q(x,t) depends on the thickness H(x,t) and the ice surface slope $\alpha(x,t)$, the flux perturbation can be linearized by a first order expansion about the steady state in terms of the thickness perturbation h(x,t) and the slope perturbation $\alpha(x,t)$.

$$Q(x,t) = c_o(x)h(x,t) + D_o(x)\alpha(x,t) \tag{A6.5}$$

where

$$c_o(x) = \left.\frac{\partial Q}{\partial H}\right|_0$$

$$D_o(x) = \left.\frac{\partial Q}{\partial \text{斗}}\right|_0 \tag{A6.6}$$

Since

$$\frac{\partial H}{\partial x}(x,t) = \beta(x) - \text{斗}(x,t) \tag{A6.7}$$

where β is the slope of the glacier bed, it follows that

$$\frac{\partial h}{\partial x}(x,t) = -\alpha(x,t) \tag{A6.8}$$

Substituting (A6.5) and (A6.8) into (A6.4) gives

$$\frac{\partial h}{\partial t} = -c_o'(x)\,h - [c_o(x) - D_o'(x)]\frac{\partial h}{\partial x} + D_o(x)\frac{\partial^2 h}{\partial x^2} + a(x,t) \tag{A6.9}$$

where primes indicate x derivatives.

The nonlinear equation (A6.1) has been transformed into a linear equation with variable coefficients to obtain solutions for the perturbations to the steady state.

The fact that (A6.9) is a diffusion equation demonstrates the diffusive nature and thus high wavenumber damping of the ice surface profile as discussed in Section (A1.4.6).

APPENDIX 7: VELOCITY EQUATION FOR AN ICE MASS

A7.1 INTRODUCTION

In this Appendix, I will derive an equation for the ice flux $Q(x)$, and the downstream velocity component $u(x,z)$, using the stress equilibrium equations (1.4.8) through (1.4.10), and Glen's flow law (1.4.22), maintaining the small error terms so that the error in the formulae (1.4.34) and (1.4.36) can be estimated. Orowan (1949), Shumskiy (1961), Lliboutry (1958[b]), and Robin (1967) pointed out the importance of longitudinal stress gradients. My derivation of the shear stress contains concepts drawn from Nye (1952[b]), who showed that the shear stress depends on surface slope rather than bed slope, from Collins (1968) who derived a correction term depending on the longitudinal stress deviator gradient, and from the summary of both by Paterson (1969, p. 92-105). Nye (1969[a]) put the analytical shear stress equation in a particularly simple form by an appropriate choice of axes.

Budd has written several papers on the effects of longitudinal stress gradients on the flow field (1968; 1970[a]; 1970[b]; 1971), deriving correction terms to the basal shear stress in (1.4.23), together with estimates of the scale lengths over which they may be important.

Hutter and Legerer (1979), Hutter (1980), Hutter (1981), and Hutter and others (1981) derived equations for the shear stress including longitudinal strain and nonparallel surfaces,

using stretched coordinates.

A7.2 THE SHEAR STRESS EQUATION

The stress equilibrium equations (1.4.8) and (1.4.9) are

$$\frac{\partial \sigma_{xx}}{\partial x} + \frac{\partial \sigma_{xy}}{\partial y} + \frac{\partial \sigma_{xz}}{\partial z} + \rho g \sin(\beta) = 0 \qquad \text{(A7.2.1)}$$

$$\frac{\partial \sigma_{xz}}{\partial x} + \frac{\partial \sigma_{yz}}{\partial y} + \frac{\partial \sigma_{zz}}{\partial z} - \rho g \cos(\beta) = 0 \qquad \text{(A7.2.2)}$$

These can be integrated from the surface h(x) to depth z above the bed

$$\sigma_{xz}(x,z) = \sigma_{xz}(x,h) + \rho g(h-z)\sin(\beta(x)) + \int_z^{h(x)} \frac{\partial \sigma_{xx}}{\partial x}\, dz' \qquad \text{(A7.2.3)}$$

and

$$\sigma_{zz}(x,z) = \sigma_{zz}(x,h) - \rho g(h-z)\cos(\beta(x)) + \int_z^{h(x)} \frac{\partial \sigma_{xz}}{\partial x}\, dz' \qquad \text{(A7.2.4)}$$

The first and last terms on the right side of (A7.2.4) can be combined through the surface boundary condition. Let $\underline{n}$ be the unit outward surface normal vector

$$\underline{n} = [\sin(\alpha-\beta), \cos(\alpha-\beta), 0] \qquad \text{(A7.2.5)}$$

and let $\underline{m}$ be the downslope unit tangent vector

$$\underline{m} = [\cos(\alpha-\beta), -\sin(\alpha-\beta), 0] \qquad \text{(A7.2.6)}$$

The surface traction vector $\underline{T}$ is then (using the summation convention for repeated indices)

$$T_k = n_j \sigma_{jk} \qquad \text{(A7.2.7)}$$

The normal stress on the boundary is the atmospheric pressure p, and the shear stress on the surface is zero, i.e.

$$\underline{T}\cdot\underline{n} = -p \qquad \text{(A7.2.8)}$$

$$\underline{T}\cdot\underline{m} = 0 \qquad \text{(A7.2.9)}$$

which give the two equations

$$\sin^2(\alpha-\beta)\sigma_{xx} + 2\sin(\alpha-\beta)\cos(\alpha-\beta)\sigma_{xz} + \cos^2(\alpha-\beta)\sigma_{xz} = -p \qquad \text{(A7.2.10)}$$

$$\sin(\alpha-\beta)\cos(\alpha-\beta)[\sigma_{xx} - \sigma_{zz}] + [\cos^2(\alpha-\beta)\alpha-\beta\sin^2(\alpha-\beta)]\sigma_{xz} = 0 \qquad \text{(A7.2.11)}$$

which can be reduced to

$$[\sigma_{xx}(h) + p]\frac{dh}{dx} = \sigma_{xz}(h) \qquad \text{(A7.2.12)}$$

$$\sigma_{zz}(h) + p = \sigma_{xz}(h)\frac{dh}{dx} \qquad \text{(A7.2.13)}$$

since

$$\tan(\alpha-\beta) = -\frac{dh}{dx} \qquad \text{(A7.2.14)}$$

The Leibnitz formula for differentiation of integrals (e.g. Kaplan, 1952, p. 220) gives the identity

$$\int_z^{h(x)} \frac{\partial \sigma_{xz}}{\partial x}\, dz' = \frac{\partial}{\partial x}\int_z^{h(x)} \sigma_{xz}\, dz' - \sigma_{xz}(x,h(x))\,\frac{dh}{dx} \qquad \text{(A7.2.15)}$$

Using (A7.2.13) and (A7.2.15) in (A7.2.4) gives

$$\sigma_{zz}(x,z) = -p - \rho g(h-z)\cos(\beta(x)) + \frac{\partial}{\partial x}\int_z^{h(x)} \sigma_{xz}(x,z')dz' \qquad \text{(A7.2.16)}$$

I will now evaluate the influence of the final term in (A7.2.3) on the shear stress, using (A7.2.16) and the definitions (1.4.18) of stress deviators to get σ_{xx}.

Nonparallel bed and ice surface will generate a correction term to the gravitational stress, and longitudinal variation of the stress deviators will generate a dynamic stress correction term.

Solving (1.4.18) for σ_{xx} and σ_{yy} gives

$$\sigma_{xx} = \sigma_{zz} + 2\sigma'_{xx} + \sigma'_{yy} \qquad \text{(A7.2.17)}$$

$$\sigma_{yy} = \sigma_{zz} + 2\sigma'_{yy} + \sigma'_{xx} \qquad \text{(A7.2.18)}$$

Substituting (A7.2.16) into (A7.2.17) and differentiating with respect to x yields

$$\frac{\partial \sigma_{xx}(x,z)}{\partial x} = -\rho g[\cos(\beta(x))\frac{dh}{dx} - (h-z)\sin(\beta(x))\frac{d\beta}{dx}]$$

$$+ \frac{\partial^2}{\partial x^2}\int_z^{h(x)} \sigma_{xz}(x,z')dz' + \frac{\partial}{\partial x}[2\sigma'_{xx} + \sigma'_{yy}] \qquad \text{(A7.2.19)}$$

This derivative can then be used in the integral term in (A7.2.3) to give an equation (A7.2.20) for the shear stress in an ice mass. It is exact, except for the neglect of the acceleration terms in the stress balance equations (1.4.18). Unfortunately, (A7.2.20) is still an implicit solution for σ_{xz}.

$$\sigma_{xz}(x,z) = \sigma_{xz}(x,h(x)) + \rho g(h-z)\left[\sin(\beta(x)) - \cos(\beta(x))\frac{dh}{dx} - (h-z)\sin(\beta(x))\frac{d\beta}{dx}\right] + \int_z^{h(x)} \frac{\partial^2}{\partial x^2} \int_{z''}^{h(x)} \sigma_{xz}(x,z')dz'\,dz'' + \int_z^{h(x)} \frac{\partial}{\partial x}\left[2\sigma'_{xx} + \sigma'_{yy}\right]dz' \qquad \text{(A7.2.20)}$$

A7.3 APPROXIMATIONS

Throughout this section, I will assume that the width of the ice mass is much greater than its thickness. The effect of the valley walls is considered in Section A7.4 below.

First, note that for the case of a parallel-sided slab ($\alpha=\beta$), all x derivatives are zero, the boundary term in (A7.2.20) is zero by (A7.2.12), and the exact solution for the shear stress reduces to

$$\sigma_{xz}(z) = \rho g(h-z)\sin(\alpha) \qquad \text{(A7.3.1)}$$

Since a parallel-sided slab is often a good first approximation to a glacier or an ice sheet (except near the bergschrund or the terminus), I will introduce some approximations and show when the other terms in (A7.2.12) can be neglected or treated as correction terms to (A7.3.1).

I will assume that the slope $\alpha(x)$ of the ice surface $s(x)$ and the slope $\beta(x)$ of the bed $b(x)$ are small

$$|\alpha(x)| << 1 \tag{A7.3.2}$$

$$|\beta(x)| << 1 \tag{A7.3.3}$$

An implication of this is

$$|\alpha(x) - \beta(x)| << 1 \tag{A7.3.4}$$

A further result of (A7.3.3) is

$$h \left|\frac{d\beta}{dx}\right| << 1 \tag{A7.3.5}$$

because the bed slope cannot change by an amount near unity (e.g. 0° to 45°) in a distance equal to the ice thickness if the bed slope β is always small. Results analogous to (A7.3.5) apply to $\alpha(x)$ and to $[\alpha(x)-\beta(x)]$.

I will now consider the gravitational term which I will call F_g, on the right side of (A7.2.20). Using (A7.2.14), and expanding the trigonometric functions as Taylor series to two terms,

$$F_g = \rho g(h-z)\{\beta - \frac{\beta^3}{6} + [1-\frac{\beta^2}{2}][\alpha-\beta-(\frac{\alpha-\beta}{3})^3] - (h-z)[\beta-\frac{\beta^3}{6}]\frac{d\beta}{dx}\} \tag{A7.3.6}$$

Retaining only terms to third order in the small quantities,

$$F_g = \rho g(h-z)\alpha \left[1-\frac{\alpha^2}{3}+\alpha\beta -3\frac{\beta^2}{2}\right] + \rho g(h-z)\beta \left[\frac{\beta^2}{3}-(h-z)\frac{d\beta}{dx}\right] \tag{A7.3.7}$$

Unless $\alpha<<\beta$ (which is possible at ice divides, for instance), the first term is dominant because the leading term in the square bracket is unity. The other terms in the square brackets are small by (A7.3.2) through (A7.3.5), and

$$F_g = \rho g(h-z)\alpha \left[1-\frac{\alpha^2}{3}+\alpha\beta -3\frac{\beta^2}{2}+\frac{\beta^3}{\alpha}-\frac{\beta}{\alpha}(h-z)\frac{d\beta}{dx}\right] \tag{A7.3.8}$$

An important point to note in (A7.3.8) is that, to a good approximation, the shear stress depends only on the ice surface slope $\alpha(x)$, and not on the bed slope angle $\beta(x)$.

If $\alpha<<\beta$, the form (A7.3.7) must be retained.

Now I will consider the term involving the gradient of the x and y normal stress deviators. Defining the average value of the gradient of the normal stress deviator above depth z by

$$\overline{\frac{\partial \sigma'_{xx}}{\partial x}} = \left(\frac{1}{h-z}\right)\int_z^{h(x)} \frac{\partial \sigma'_{xx}}{\partial x}\, dz' \qquad z<h \tag{A7.3.9}$$

$$= 0 \qquad z=h$$

$$\overline{\frac{\partial \sigma'_{yy}}{\partial x}} = \left(\frac{1}{h-z}\right)\int_z^{h(x)} \frac{\partial \sigma'_{yy}}{\partial x}\, dz' \qquad z<h \tag{A7.3.10}$$

$$= 0 \qquad z=h$$

lets me write this term in (A7.2.20) as

$$F_1 = [\rho g(h-z)\alpha]\left[\frac{2h\frac{\partial \overline{\sigma'_{xx}}}{\partial x} + h\frac{\partial \overline{\sigma'_{yy}}}{\partial x}}{\rho g h \alpha}\right] \qquad \text{(A7.3.11)}$$

The leading factor in (A7.3.11) is just the dominant term (A7.3.1). For an ice column from surface to bed, the nondimensional term in the square bracket is, roughly speaking, (apart from the factor of two), the ratio of the net longitudinal force (plus transverse force) to the basal shear force acting on the column. This ratio is usually quite small for most glaciological situations. This term will be retained in the analysis in this Appendix, as an estimate of the error due to neglect of nonzero longitudinal and transverse stress gradients.

All the stress components near the free surface are small, and $\sigma_{xz}(h)$ is also proportional to $(\alpha-\beta)$ from (A7.2.12) and (A7.2.14). It will only make a significant fractional change in σ_{xz} near z=h, where there is very little shear deformation in any case. Neglecting $\sigma_{xz}(h)$ will not cause a significant absolute error in the shear stress at any depth.

Now I will show that the shear term involving the double integral of $\sigma_{xz}(x,z)$ in (A7.2.20) is negligible under most conditions. I call it F_s. This is the term that makes the equation implicit; eliminating it will lead to an explicit solution for the shear stress.

Because of the assumptions (A7.3.2) and (A7.3.3) of small angles, I know that the solution for σ_{xz} is approximately (A7.3.1). I will substitute this approximate solution into the term in question, and show that the result is very much smaller

than the approximate solution (A7.3.1). The substitution gives

$$F_s = \rho g(h-z)\{(h-z)\frac{d\alpha}{dx}\frac{dh}{dx} - \frac{(h-z)^2}{6}\frac{d^2\alpha}{dx^2} + \frac{(h-z)}{2}\alpha\frac{d^2h}{dx^2} + \alpha(\frac{dh}{dx})^2\} \quad \text{(A7.3.12)}$$

Noting that, by the chain rule,

$$(h-z)^2\frac{d^2\alpha}{dx^2} = (h-z)\frac{d}{dx}[(h-z)\frac{d\alpha}{dx}] - (h-z)\frac{dh}{dx}\frac{d\alpha}{dx} \quad \text{(A7.3.13)}$$

and by differentiating (A7.2.14) to get

$$\frac{d^2h}{dx^2} = \frac{-d(\alpha-\beta)}{dx} \quad \text{(A7.3.14)}$$

by using (A7.2.14) with a first order expansion of the tangent, (A7.3.12) becomes

$$F_s = \rho g(h-z)\alpha\left[-\frac{5}{3}(h-z)\frac{d\alpha}{dx} + \frac{(h-z)}{2}\frac{d\beta}{dx} + (\alpha-\beta)^2\right]$$

$$- \rho g(h-z)\beta\left[\frac{7}{6}(h-z)\frac{d\alpha}{dx}\right] - \rho g(h-z)\left[\frac{(h-z)}{6}\frac{d}{dx}[(h-z)\frac{d\alpha}{dx}]\right] \quad \text{(A7.3.15)}$$

All the terms in the first two brackets are much less than unity, by (A7.3.2) through (A7.3.5). The third term is more of a problem. Since

$$(h-z)\frac{d\alpha}{dx} \quad \text{(A7.3.16)}$$

is the change in slope over a distance equal to (h-z), it must satisfy

$$\left|(h-z)\frac{d\alpha}{dx}\right| < \alpha_{max} \quad \text{(A7.3.17)}$$

where α_{max} is the maximum surface slope on the glacier. By assuming that the surface slope α is nonzero and slowly varying,

i.e.

$$\left|(h-z)\,\frac{d\alpha}{dx}\right| \ll \alpha \qquad \text{(A7.3.18)}$$

the whole quantity inside the curled bracket in (A7.3.12) is the change in a distance (h-z) of a quantity which is always much less than α; therefore it too is much less than α. This implies that the third term in (A(7.3.15) satisfies

$$\left|\rho g(h-z)\{(h-z)\frac{d}{dx}[(h-z)\frac{d\alpha}{dx}]\}\right| \ll \rho g(h-z)\alpha \qquad \text{(A7.3.19)}$$

(A7.3.18) is usually true in all regions of a glacier, except where the surface slope goes to zero, such as at an ice divide. In that circumstance, the shear stress is very small in absolute value, and the normal stresses may give the dominant deformation. The correction term F_l from (A7.3.11) is a major contribution to the shear stress in (A7.2.20). Then, reasonable assumptions about slow variation of F_l with x can be used to give

$$F_s \ll F_l \qquad \text{(A7.3.20)}$$

by using F_l as an estimate of σ_{xz} to evaluate F_s. Budd (1968; 1970[a]) also derived the result that a term similar to F_s was negligible when only undulations of long wavelength (greater than 4h) were considered. In either case, the term F_s can be neglected without drastically affecting the estimate of the error in σ_{xz}, so that, approximately,

$$\sigma_{xz}(x,z) = \rho g(h-z)\sin\alpha \left[1 + \left[\frac{2h\,\overline{\partial\sigma'_{xx}}/\partial x + h\,\overline{\partial\sigma'_{yy}}/\partial x}{\rho g h \alpha}\right]\right] \qquad \text{(A7.3.21)}$$

with the assumptions (A7.3.2), (A7.3.3), and (A7.3.18), and α is not small compared to β (see(A7.3.7)).

The surface slope α was replaced in (A7.3.21) by $\sin\alpha$ to make it consistent with the standard result (A7.3.1) for a parallel-sided slab. The difference between α and $\sin\alpha$ is $O(\alpha^3)$; this is the same order as other neglected terms.

A7.4 SHAPE FACTORS

The derivation of the shear stress (A7.3.21) was based on the assumption of a very wide channel, such that the total downslope component of the weight of the ice is supported by σ_{xz} shear forces. However, in valley glaciers, σ_{xy} shear forces also support some of the glacier weight.

Nye (1965[c]) considered rectilinear flow in channels with rectangular, elliptical, and parabolic cross-section. He found that the shear stress σ_{xz} was linear with depth on the central axis of a semicircular channel, and was exactly half the value (A7.3.1) at the same depth in an infinitely wide channel. For the other channels considered, the stress σ_{xz} was nearly linear with depth on the central axis, so Nye suggested the approximation

$$\sigma_{xz}(z) = s\rho g(h-z)\sin\alpha \qquad \text{(A7.4.1)}$$

where s is a "shape factor" varying from zero for an infinitely

deep channel, to unity for an infinitely wide channel. The shape factor is chosen so that the integration of the shear strain rate given by (A7.4.1) and Glen's flow law gives the correct downslope velocity component u at the ice surface. Nye's method was numerical and can be adapted to any arbitrary cross-section. He tabulated values of s for a series of rectangular, elliptical, and parabolic channels.. When the channel cross-section varies with distance x, the flow is no longer rectilinear, and longitudinal forces may be present, but it is common practice (e.g. Bindschadler, unpublished; Budd and Jenssen, 1975) to introduce a shape factor s(x) depending on position x, to try to account for the drag of the valley walls in an approximate way. I include a shape factor of this type in the model used in Chapter 3 for the Steele Glacier.

The shape factor can be a large source of uncertainty for the quantitative interpretation of computed velocities, because the shear stress is raised to the nth power when using Glen's flow law (see next section).

A7.5 SHEAR STRAIN RATE

The shear strain rate $\dot{\epsilon}_{xz}$ is defined by

$$\dot{\epsilon}_{xz} = \frac{1}{2}\left[\frac{\partial u}{\partial z} + \frac{\partial v}{\partial x}\right] \qquad (A7.5.1)$$

If I assume that the shear parallel the bed is the dominant deformation, i.e.

$$\left|\frac{\partial v}{\partial x}\Big/\frac{\partial u}{\partial z}\right| << 1 \qquad (A7.5.2)$$

then (A7.5.1) can be written as

$$\dot{\epsilon}_{xz} = \frac{1}{2}\frac{\partial u}{\partial z}\left[1 + \frac{\partial v}{\partial x}\Big/\frac{\partial u}{\partial z}\right] \qquad (A7.5.3)$$

where the second term in the bracket is a small correction term.

The velocity u(x,z) can be obtained by integrating (A7.5.3) from the bed to level z.

$$u(x,z) = u_s(x) + 2\int_0^z \frac{\dot{\epsilon}_{xz}}{\left[1 + \frac{\partial v}{\partial x}\Big/\frac{\partial u}{\partial z}\right]}\, dz' \qquad (A7.5.4)$$

where $u_s(x)$ is the basal sliding velocity. When I substitute Glen's flow law (A1.4.22) for $\dot{\epsilon}_{xz}$, use the identity (A7.5.5), for τ, the effective shear stress (1.4.20), assuming the second term is small,

$$\tau = \sigma_{xz}\left[1 + \frac{(\tau - \sigma_{xz})}{\sigma_{xz}}\right] = \sigma_{xz}\left[1 + \frac{\delta\tau}{\sigma_{xz}}\right] \qquad (A7.5.5)$$

together with Taylor expansions of (A7.5.5) to the (n-1) power

and of the velocity gradient term in the denominator to the power -1

$$u(x,z) = u_s(x) + 2A \int_0^z \sigma_{xz}^n(x,z') \left[1+(n-1)\frac{\delta\tau}{\sigma}_{xz} - \frac{\partial v}{\partial x}\Big/\frac{\partial u}{\partial z}\right] dz' \qquad \text{(A7.5.6)}$$

In taking A, the coefficient of Glen's flow law, outside the integral, I am assuming an isothermal ice mass. If the temperature varies spatially in a known manner, the integral may be evaluated numerically. Substituting (A7.3.21) for the shear stress in (A7.5.6), with a Taylor expansion of the correction terms in (A7.3.21) raised to the nth power, I get

$$u(x,z) - u_s(x) =$$

$$2A \int_0^z [s(x)\rho g(h-z)\sin(\alpha(x))]^n \left[1 + n\left[2h \frac{\overline{\partial\sigma'}_{xx}}{\partial x} + h \frac{\overline{\partial\sigma'}_{yy}}{\partial x}\right] + (n-1)\frac{\delta\tau}{\sigma}_{xz} - \frac{\partial v}{\partial x}\Big/\frac{\partial u}{\partial z} \right] dz' \qquad \text{(A7.5.7)}$$

The leading term is easily integrated, but the error terms all depend on z' in unknown ways depending on the geometry of the ice mass. However, an estimate of the magnitude of the error in u(x,z) can be found by replacing the z' dependent errors in (A7.5.7) by the maximum amplitude of their sum over the depth range of zero to z. This estimation allows me to bring the factor in the large square bracket outside the depth integral. Then

$$u(x,z) - u_s(x) =$$

$$2A[s(x)\rho g \sin(\alpha(x))]^n \frac{[h^{n+1} - (h-z)^{n+1}]}{(n+1)} [1 + e(x)] \qquad (A7.5.8)$$

where the error e(x) is estimated to be of the order of

$$e(x) = O\left[\left[n\left[\frac{2h\overline{\frac{\partial \sigma'}{\partial x}}_{xx} + h\overline{\frac{\partial \sigma'}{\partial x}}_{yy}}{\rho g h \alpha}\right] + (n-1)\frac{\delta\tau}{\sigma_{xz}} - \frac{\partial v}{\partial x}\Big/\frac{\partial u}{\partial z}\right]_{max}\right] \qquad (A7.5.9)$$

$\delta\tau$ is defined by (A7.5.5) as the difference between the stress invariant and the shear stress parallel to the glacier bed. The longitudinal stress gradients are given by (A7.3.11). The subscript 'max' indicates the maximum value taken anywhere by the term in the inner large square bracket. This gives a conservative estimate of the accuracy obtained.

A7.6 ICE FLUX AND AVERAGE VELOCITY

The downslope ice flux for use in the continuity equation (1.3.5) is

$$Q(x,t) = \int_0^{h(x,t)} u(x,z,t)\, dz$$

$$= u_s(x,t)\, h(x,t) + 2A\frac{[s\rho g \sin\alpha]^n}{(n+2)} [h(x,t)]^{n+2} [1 + e(x)] \qquad (A7.6.1)$$

The error term involving e(x) is small with the assumptions discussed in the previous section, and is neglected in the

computer model.

The average velocity V(x,t) used in Section 1.3 and Appendix 1 is defined as the

$$V(x,t) = Q(x,t)/h(x,t) \qquad \text{(A7.6.2)}$$

which is

$$V(x,t) = u_s(x,t) + 2A\left[s\frac{\rho g \sin\alpha}{(n+1)}\right]^n [h(x,t)]^{n+1} [1+ e(x)] \qquad \text{(A7.6.3)}$$

The term on the right due to the internal deformation is just (n+1)/(n+2) times the downslope velocity component at the ice surface u(x,h(x),t).

The surface slope α should be considered to be an average over at least 4h, because of the neglect of the term F_s in (A7.3.12).

APPENDIX 8: GLACIER SLIDING

A8.1 MEASUREMENTS

Measurements at the glacier bed are obviously difficult. Direct access is possible only in a few places, such as at cavities at the glacier margin, or in tunnels into the ice itself, or in galleries in bedrock directly below the glacier (e.g. Glacier d'Argentiere (Vivian and Bocquet, 1973) and other sites in Europe (Vivian, 1980)). These are obviously not representative of the glacier bed as a whole.

Boreholes may reach the glacier bed. Hotpoint probes are often stopped by debris-laden ice at some distance above the bed, but cable tool drilling (Englehardt and others, 1978) or rotary drilling (Newmont Mining, at South le Duc Glacier, and at Burroughs Glacier (W. H. Mathews, personal communication, 1981)) usually gets to the ice-rock interface. The method is time consuming. Observations by borehole television cameras provide sliding data, but can be limited by turbidity in the basal water, and by unknown motion of a thin layer of subsole drift (possibly a few cm thick).

Indirect measurements of sliding may be obtained by subtracting a calculated internal deformation velocity (using (1.4.34)) from the surface measurement of the total velocity. This method is limited by the assumptions in deriving (1.4.32), and by uncertainty in the appropriate local values of the constants in Glen's flow law (1.4.22) in the basal ice.

Surface measurements of ice velocity show variations on time scales of hours or days, often with correlations with rainfall or intense surface melting. Deformation velocities in the ice are unlikely to vary that rapidly; this suggests that pressure in the basal water influences sliding.

A8.2 PHYSICAL PROCESSES IN SLIDING

Weertman (1957; 1964[b]) identified two main processes controlling sliding, on the assumption that bed irregularities or roughness prevent the glacier from sliding downslope as a rigid body. Weertman suggested that the basal ice moved past small obstacles by regelation, a sliding process originally discussed by Deeley and Parr (1914). Because the upstream side of an obstacle supports some of the downslope component of the glacier weight, the pressure in the ice there is elevated above average. This lowers the pressure melting temperature. Ice approaching an obstacle cools and gives up some of its internal energy to melting. Meltwater from the upstream side of an obstacle flows around to the lee side, where the pressure is lower than average, and the pressure melting temperature is correspondingly higher, so that the water refreezes. The heat of fusion so released diffuses along the temperature gradient to the upstream side of the obstacle, where it contributes to further melting. This process is limited by reduced temperature gradients as the obstacle size increases.

The presence of excess pressure upstream from large obstacles increases the second scalar invariant T_2' of the stress

deviator tensor, leading to enhanced deformation rates, i.e. softer ice and more rapid flow (see (1.4.19)). For small obstacles, this process is limited by less significant stress perturbations.

The combination of these two processes is postulated to allow basal ice to move past obstacles on any roughness scale.

Kamb and LaChapelle (1964) interpreted structures in the basal ice of Blue Glacier, Washington, U.S.A. as evidence of both regelation and enhanced plastic flow.

Weertman (1957) developed a mathematical model of sliding using these concepts, with a bed modelled by an array of cubic obstacles on a plane (the "tombstone model"). Nye (1969[b]; 1970) and Kamb (1970) presented theories using the same sliding concepts with a Fourier spectral representation of the glacier bed. These theories assumed small sliding velocities, and further, that clean ice was in contact with the bedrock. Morland (1976[a]; 1976[b]) included the effects of glacier thickness and bed friction.

Raymond (1980) summarized a number of other physical complications of this simple sliding concept which limit its quantitative applicability in a computer model.

Drake and Shreve (1973) and Morris (1976) indicated that solutes in the basal water can alter the pressure melting point, inhibiting regelation by lowering the temperature gradient through obstacles. Hallet (1976) gave field evidence that this process is significant for at least some glaciers.

Nye (1973[b]) pointed out that temperature gradients in the basal water film may affect regelation, and Harrison (1972) and

Raymond (1976) showed that water and bubbles in the basal ice could also affect the diffusion of heat, and the amount of regelation.

Lliboutry (1968[a]) pointed out that transient creep may be significant in the time scales involved in flow around obstacles. Glen's flow law (1.4.22) is applicable only to secondary creep.

Vivian and Bocquet (1973) suggested that ice texture, impurities, and water content in basal ice may affect its mechanical properties, and Weertman (1969) pointed out that local stress near obstacles may be large enough to exceed the range of validity of Glen's flow law.

Permeability of the bed could, of course, significantly affect regelation, and rock load in the glacier sole, and a layer of subsole drift can alter the mechanical properties of the interface itself (e.g. Englehardt and others, 1978).

Lliboutry (1968[a]; 1968[b]; 1978) made an important contribution to the theory of sliding by including the possibility of a separation of basal ice and bedrock to form cavities in the lee of obstacles. This can alter the apparent roughness of the bed, and there may be a reduced contact area to support the ice load. This can be expressed by a shadowing function (Benoist and Lliboutry, 1978; Benoist, 1979; Lliboutry, 1979).

Cavities beneath a glacier may be connected, leading to a complicated basal water system. Weertman (1972) gave a review of water flow beneath glaciers, and its relation to sliding. Flow may occur in subglacial drift, in channels incised in the

bedrock (Nye, 1973[a]), or in time-varying channels incised in the basal ice (Rothlisberger, 1968; 1972; Nye, 1976).

A8.3 COMPUTER MODELS OF SLIDING

A8.3.1 USING WEERTMAN SLIDING

The Weertman model is incorporated into my computer model by

$$u_s(x) = C \tau_b^{(n+1)/2} \qquad \text{(A8.3.1)}$$

where n is the exponent in Glen's flow law (1.4.22), C is a constant related to bed roughness (Weertman, 1957; 1964[b]), and τ_b is the basal shear stress. However, I have not used it in this study (except for the Nagata ice sheet model, Appendix 15), because it is valid only for small sliding velocities; in addition, all the possible complications outlined in Section A8.2 would make any results numerically suspect.

A8.3.2 BUDD-MCINNES MODEL

Budd and McInnes (1974) and Budd (1975) used a quite different approach to model basal sliding. Rather than attempting to quantitatively model the processes described in Section A8.2, they started from the premise that meltwater produced by sliding or internal friction can lower or redistribute the effective basal shear stress, or shear resistance, which would otherwise prevent the glacier from sliding. If the downslope component of the weight was everywhere

balanced locally by a shear stress at the base, this shear stress would be approximately

$$\tau_c = s\rho g h \sin\alpha \qquad \text{(A8.3.2)}$$

This is the simple result (A7.3.1) for a parallel-sided slab. Budd (1975) chose a simple feedback function (A8.3.3) having the desired qualitative behaviour; at low sliding velocities, the basal shear stress and sliding velocity increase together, but at higher sliding velocities, increased sliding reduces the basal shear stress, due to meltwater lubrication of the bed. The constant $\emptyset$ was called the 'basal lubrication factor', and the stress (A8.3.3) was called the "local lubrication-lowered stress"

$$\tau_c^* = \frac{\tau_c}{1 + \emptyset \tau_c V} \qquad \text{(A8.3.3)}$$

Since V is the average downslope velocity, the factor $\tau_c V$ is approximately the power dissipated per unit area of bed by sliding friction and internal deformation. This is directly related to meltwater production. To maintain the global force equilibrium of the glacier, i.e. to prevent it from accelerating off the bedrock slope, Budd added a constant stress to (A8.3.3). Letting bars represent averages over the total glacier length, Budd took the basal shear stress to be

$$\tau_b = \tau_c^* + (\bar{\tau}_c - \bar{\tau}_c^*) \qquad \text{(A8.3.4)}$$

Obviously, (A8.3.4) is only one of many possible ways to maintain gross equilibrium. For instance, (A8.3.4) does not exclude uphill sliding; this would be a logical constraint. The

procedure (A8.3.4) redistributes the basal shear stress so that sections with the highest meltwater production are partially unsupported by their local basal shear stress, and throw their weight on sections upstream and downstream. This leads to longitudinal strain rates. By assuming that the longitudinal extension, when averaged over the ice thickness, is viscous, with viscosity η, i.e.

$$2\eta \dot{\epsilon}_{xx} = \overline{\sigma'}_{xx} \qquad \text{(A8.3.5)}$$

and that the extension is due entirely to gradients in the basal sliding, i.e.

$$\dot{\epsilon}_{xx} = \frac{\partial u_s(x)}{\partial x} \qquad \text{(A8.3.6)}$$

Budd was able to perform two x integrals of a stress equation similar to (1.4.25) (neglecting the lateral term in y) to get a sliding velocity. (Shumskiy (1961) also thought that sliding could be best expressed as the integrated longitudinal strain rate.)

The Budd model is not restricted to small sliding velocities, and it incorporates longitudinal gradients; sliding at any point depends on conditions at other points in the glacier. This was an important and realistic advance. Some of the overly simple assumptions such as (A8.3.5) and (A8.3.6) can be eliminated easily (Budd, 1975). Budd (1975) suggested that periodic surging could exist with no special requirements other than some feedback mechanism like (A8.3.3) to give a multi-valued sliding velocity as a function of basal shear stress.

The Budd model reduces the sliding problem to one physical process (meltwater production), two qualitative functions (A8.3.3) and (A8.3.4) to express its effect on basal stress, and two free fitting parameters $\emptyset$ and n. This simplicity makes the Budd model appealing to computer modellers.

On the other hand, its connection to physical processes is indirect. There are, presumably, a large or infinite number of relationships involving the meltwater production $\tau_c V$ that could perform the same qualitative roles as (A8.3.3) and (A8.3.4) in redistributing the basal shear stress, and, as far as I am aware, there is little physical basis for selecting any particular ones over the others. This makes it difficult to justify interpreting the output in anything more than a qualitative sense.

The fitted parameters $\emptyset$ and n implicitly contain information about the local glacier geometry, ice composition and structure, bed composition, interface structure, drainage structure, etc., as well as about the fundamental properties of sliding, so that new values of $\emptyset$ and n are required for each glacier. The model can perhaps be used to predict the future behaviour of a given glacier; it cannot be used to predict the sliding behaviour if the physical conditions at the bed are altered, and it cannot be used to predict the behaviour of new glaciers without first measuring their sliding velocity.

A8.3.3 SLIDING IN THIS STUDY

Nye (1965[c]) used a no-slip condition when deriving the flow in channels of various cross-section, because of a lack of knowledge of the form of a sliding law, and of the numerical values of the parameters of such a law. Bindschadler (unpublished, p. 5), who used a numerical model similar to the one I described in Appendix 1, chose not to attempt to model sliding, due to the lack of agreement between proposed sliding theories and his data from the Variegated Glacier, Alaska, and the lack of any simple relationship between glacier geometry and sliding.

I agree with Bindschadler's assessment of sliding models. In the computations for this thesis (excluding Appendix 16), I have not tried to calculate sliding velocities based on physical processes or the glacier geometry. In Chapter 3, I have used a predetermined sliding velocity $u_s(x,t)$ to drive the computer model through periodic surge cycles. My sole purpose was then to observe the resulting internal deformation in the model as a consequence of the given surge behaviour.

APPENDIX 9: BURGERS' EQUATION

The material in this appendix is based on Whitham (1974, p. 96). Burgers' equation from (2.3.9)

$$\frac{\partial c}{\partial t}(x,t) + c(x,t)\,\frac{\partial c}{\partial x}(x,t) = \nu\,\frac{\partial^2 c}{\partial x^2}(x,t) \qquad \text{(A9.1)}$$

is an exact equation for waves described by

$$\frac{\partial H}{\partial t}(x,t) + \frac{\partial Q}{\partial x}(x,t) = 0$$

$$Q = \alpha H^2 + \beta H + \gamma - \nu\,\frac{\partial H}{\partial x} \qquad \text{(A9.2)}$$

Cole (1951) and Hopf (1950) showed that using the nonlinear transformation

$$c(x,t) = -2\nu\,\frac{\frac{\partial \phi}{\partial x}(x,t)}{\phi(x,t)} \qquad \text{(A9.3)}$$

reduces (A9.1) to a linear diffusion equation. Doing the substitution in two steps,

$$c = \frac{\partial \Psi}{\partial x} \qquad \text{(A9.4)}$$

and integrating (A9.1) over x,

$$\frac{\partial \Psi}{\partial t} + \frac{1}{2}\left[\frac{\partial \Psi}{\partial x}\right]^2 = \nu\,\frac{\partial^2 \Psi}{\partial x^2} \qquad \text{(A9.5)}$$

Introducing

$$\Psi = -2\nu \log(\phi) \qquad \text{(A9.6)}$$

(A9.5) becomes

$$\frac{\partial \phi}{\partial t} = \nu\,\frac{\partial^2 \phi}{\partial x^2} \qquad \text{(A9.7)}$$

The solution of this linear differential equation is

$$\phi(x,t) = \frac{1}{(4\pi\nu t)^{1/2}} \int_{-\infty}^{\infty} \phi(y,0) \exp[-(x-y)^2/(4\nu t)]dy \qquad (A9.8)$$

The initial condition $\phi(x,0)$ is derived from the initial condition $c(x,0) = F(x)$ for any arbitrary function $F(x)$ through (A9.4)

$$\phi(x,0) = \exp[-\frac{1}{2\nu} \int_{0}^{x} F(y)\, dy\ ] \qquad (A9.9)$$

and the solution $c(x,t)$ derived from (A9.4) and (A9.8) is

$$c(x,t) = \frac{\int_{-\infty}^{\infty} \frac{(x-y)}{t} e^{-G/2\nu} dy}{\int_{-\infty}^{\infty} e^{-G/2\nu} dy} \qquad (A9.10)$$

where

$$G(y:x,t) = \int_{0}^{y} F(z)\, dz + \frac{(x-y)^2}{2t} \qquad (A9.11)$$

When the initial condition is

$$c(x,0) = A\, \delta(x) \qquad (A9.12)$$

(A9.11) reduces to

$$\begin{aligned} G(y:x,t) &= \frac{(x-y)^2}{2t} + A \qquad y>0 \\ &= \frac{(x-y)^2}{2t} \qquad y<0 \end{aligned} \qquad (A9.13)$$

Substituting (A9.13) into (A9.10), setting $A/2\nu = R$, and using the variable change

$$z = \frac{(x-y)}{(4\nu t)^{1/2}} \qquad (A9.14)$$

puts (A9.10) into the form

$$c(x,t) = \frac{2\nu \int_{x/\sqrt{4\nu t}}^{\infty} (2z)\, e^{-z^2}\, dz + e^{R}\, 2\nu \int_{-\infty}^{x/\sqrt{4\nu t}} (2z)\, e^{-z^2}\, dz}{-(4\nu t)^{1/2} \int_{x/\sqrt{4\nu t}}^{\infty} e^{-z^2}\, dz + e^{R}\, (4\nu t)^{1/2} \int_{-\infty}^{x/\sqrt{4\nu t}} e^{-z^2}\, dz} \qquad \text{(A9.15)}$$

Evaluating the integrals in the numerator, and using the property

$$\int_{-\infty}^{\infty} e^{-z^2}\, dz = \pi^{1/2} \qquad \text{(A9.16)}$$

in the denominator,

$$c(x,t) = \sqrt{\frac{\nu}{t}}\, \frac{e^{-x^2/(4\nu t)}\, (e^{R} - 1)}{\pi^{1/2} + (e^{R} - 1) \int_{x/\sqrt{4\nu t}}^{\infty} e^{-z^2}\, dz} \qquad \text{(A9.17)}$$

This analytical solution of (A9.1) is used in Chapter 2 to verify that the numerical model solves nonlinear and kinematic wave problems correctly.

APPENDIX 10: MATRIX COEFFICIENTS

The tridiagonal matrix $\underline{\underline{A}}$ of coefficients in equation (A1.2.3) has sub-, main, and super-diagonal elements $\{a_j, b_j, c_j \mid j=1,J\}$. These are given by

$$a_j = \left.\frac{\partial r}{\partial h}_j\right|_{\substack{h_{j-1} \\ h_{j+1}}} = -2p_j \Theta \left.\frac{\partial Q}{\partial h}_{j-1/2}\right|_{\substack{h_j \\ h_{j+1}}}$$

$$b_j = \left.\frac{\partial r}{\partial h}_j\right|_{\substack{h_{j-1} \\ h_{j+1}}} = 1+2p_j \Theta \left[\left.\frac{\partial Q}{\partial h}_{j+1/2}\right|_{h_j} - \left.\frac{\partial Q}{\partial h}_{j-1/2}\right|_{h_j}\right]_{\substack{h_{j-1} \\ h_{j+1}}}$$

$$c_j = \left.\frac{\partial r}{\partial h}_j\right|_{\substack{h_{j+1} \\ h_{j-1}}} = 2p_j \Theta \left.\frac{\partial Q}{\partial h}_{j+1/2}\right|_{\substack{h_j \\ h_{j-1}}} \qquad \text{(A10.1)}$$

by differentiating in equation (A1.2.1). The quantities following the vertical bar are held constant while performing the partial differentiation. The purpose of this appendix is to derive expressions for the coefficients in terms of the thickness and slope midway between mesh points, rather than in terms of the thickness at mesh points. First, I will evaluate a_j. I know the ice flux $Q_{j-1/2}(h_{j-1/2}, \alpha_{j-1/2})$, where the thickness $h_{j-1/2}$ is

$$h_{j-1/2} = \frac{(h_{j-1} + h_j)}{2} \qquad \text{(A10.2)}$$

and the ice surface slope is

$$\tan(\alpha_{j-1/2}) = \frac{\{[b_j + h_j/\cos(\beta_j)] - [b_{j-1} + h_{j-1}/\cos(\beta_{j-1})]\}}{\Delta x} \tag{A10.3}$$

The glacier bed elevation is $\{b_j | j=1,J\}$, the bed slope is $\{\beta_j | j=1,J\}$, and the thickness $\{h_j | j=1,J\}$ normal to the bed is divided by $\cos(\beta_j)$ to give the vertical ice thickness to within a fractional error of $([\alpha-\beta]\beta)$ with the assumptions $\alpha<<1$ and $\beta<<1$. This is derived in Appendix 14. Figure A10.1 illustrates the geometry of the slope calculation. The ice flux is

$$Q_{j-1/2} = h_{j-1/2} \, VW_{j-1/2} \tag{A10.4}$$

where $VW_{j-1/2}$ is the velocity V parallel to the bed averaged over the ice depth $h_{j-1/2}$, and multiplied by the channel width $W_{j-1/2}$. Then

$$a_j = 2p_j \Theta \left[\frac{\partial Q}{\partial h}_{j-1/2} \bigg|_{\alpha_{j-1/2}} \frac{\partial h}{\partial h}_{j-1/2} \bigg|_{h_j} + \frac{\partial Q}{\partial \alpha}_{j-1/2} \bigg|_{h_{j-1/2}} \frac{\partial \alpha}{\partial h}_{j-1/2} \bigg|_{h_j} \right] \tag{A10.5}$$

$$= p_j \Theta \left[VW_{j-\frac{1}{2}} + h_{j-\frac{1}{2}} \left[\left| \frac{\partial VW}{\partial h} \right|_{j-\frac{1}{2}} - \frac{2\cos^2(\alpha_{j-1/2})}{\Delta x \cos(\beta_{j-1})} \left| \frac{\partial VW}{\partial \alpha} \right|_{j-\frac{1}{2}} \right] \right]$$

Similarily for b_j and c_j,

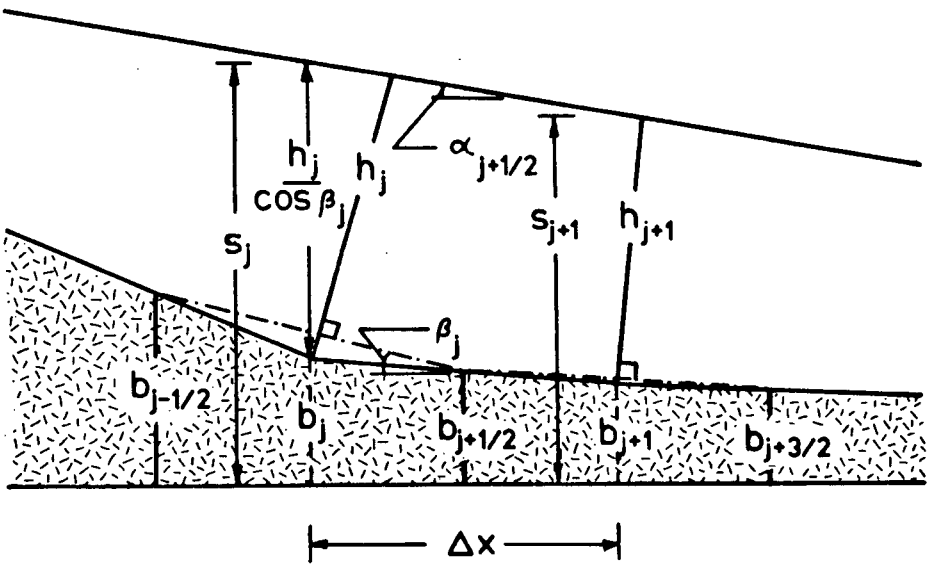

FIGURE A10.1. Quantities In Slope Calculation.

$$b_j = p_j \Theta \left[\begin{array}{l} h_{j+\frac{1}{2}} \left[\left| \frac{\partial VW}{\partial h} \right|_{j+\frac{1}{2}} - \frac{2\cos^2(\alpha_{j+1/2})}{\Delta x \cos(\beta_j)} \left| \frac{\partial VW}{\partial \alpha} \right|_{j+\frac{1}{2}} \right] \\ - h_{j-\frac{1}{2}} \left[\left| \frac{\partial VW}{\partial h} \right|_{j-\frac{1}{2}} - \frac{2\cos^2(\alpha_{j-1/2})}{\Delta x \cos(\beta_j)} \left| \frac{\partial VW}{\partial \alpha} \right|_{j-\frac{1}{2}} \right] \\ + VW_{j+1/2} - VW_{j-1/2} \end{array} \right] \tag{A10.6}$$

$$c_j = p_j \Theta \left[VW_{j+\frac{1}{2}} + h_{j+\frac{1}{2}} \left[\left| \frac{\partial VW}{\partial h} \right|_{j+\frac{1}{2}} - \frac{2\cos^2(\alpha_{j+1/2})}{\Delta x \cos(\beta_{j+1})} \left| \frac{\partial VW}{\partial \alpha} \right|_{j+\frac{1}{2}} \right] \right] \tag{A10.7}$$

The vertical brackets with subscripts indicate where the partials are evaluated. The bars indicating the other

independent variables held constant have been dropped, since there is no confusion when the flux is a function of only two variables $h_{j+1/2}$ and $\alpha_{j+1/2}$.

APPENDIX 11: CONVERGENCE CRITERIA

The numerical scheme uses an iterative procedure to solve the nonlinear continuity and flow law equations. The iterations are terminated when the largest residual in absolute value is smaller than some criterion. The residuals are the the error left when the solution is substituted back into the continuity equation. The residuals $\{ r_j^{n+1} | j=1,J\}$ are

$$r_j^{n+1} = 2p_j\,\Theta[Q_{j+1/2}^{n+1} - Q_{j-1/2}^{n+1}] + 2p_j\,(1-\Theta)[Q_{j+1/2}^{n} - Q_{j-1/2}^{n}]$$

$$+ h_j^{n+1} - h_j^{n} - [\Theta A_j^{n+1} + (1-\Theta)A_j^{n}]\Delta t$$

$$1 \le j \le J \qquad 1 \le n \le N \qquad \text{(A11.1)}$$

$$p_j = \Delta t/(2\Delta x_j W_j) \qquad \text{(A1.1.6)}$$

For practical purposes, however, it is convenient to stop when the changes in ice thickness are below some value. This is easier to relate to measurable quantities on real ice masses. How are the residuals $\{ r_j^{n+1} | j=1,J\}$ related to errors in $\{h_j^{n+1} | j=1,J\}$?

Using the Glen flow law (Glen, 1955) for laminar slab flow in a channel of unit width with a small surface slope α gives for the flux $Q_{j+1/2}$

$$Q_{j+1/2} = A(h_{j+1/2})^{m+2}(\alpha_{j+1/2})^{m} \qquad \text{(A11.2)}$$

where the exponent m is about 3. A is a constant (see Section 1.4). $\{b_j | j=1,J\}$ is the bedrock topography. First note that the

ice surface slope α is given by

$$\alpha_{j+1/2} = h_{j+1} + b_{j+1} - h_j - b_j \qquad \text{(A11.3)}$$

Now suppose that there is an error e_h in h_j due to imperfect convergence in the iterations; all the other $\{h_i \mid i=1,J,\ i\neq j\}$ are correct. Letting the calculated values of $Q_{j+1/2}$ and $h_{j+1/2}$ have primes, and quantities without primes be the values that would be obtained when the residuals are zero,

$$Q'_{j+1/2} = A\left[\frac{h_{j+1} + h'_j}{2}\right]^{m+2}\left[\frac{h_{j+1} + b_{j+1} - h'_j - b_j}{\Delta x}\right]^{m}$$

$$= Q_{j+1/2}\left[1 + \frac{e_h}{h_{j+1} + h_j}\right]^{m+2}\left[1 - \frac{e_h}{h_{j+1} + b_{j+1} - h_j - b_j}\right]^{m}$$

$$\doteq Q_{j+1/2}\left[1 + \frac{(m+2)e_h}{2h_j} - \frac{m\,e_h}{\Delta x \alpha_{j+1/2}}\right] \doteq Q_{j+1/2}\left[1 - \frac{m\,e_h}{\Delta x \alpha_{j+1/2}}\right] \qquad \text{(A11.4)}$$

since $\alpha << h/\Delta x$ for reasonable slopes and mesh selection.

Similarily

$$Q'_{j-1/2} \doteq Q_{j-1/2}\left[1 + \frac{m\,e_h}{\Delta x \alpha_{j-1/2}}\right] \qquad \text{(A11.5)}$$

The flux gradient estimate is then

$$\frac{Q'_{j+1/2} - Q'_{j-1/2}}{\Delta x} \doteq \left[\frac{Q_{j+1/2} - Q_{j-1/2}}{\Delta x}\right]\left[1 - \frac{2m\,e_h}{\Delta x \alpha_j}\right] \qquad \text{(A11.6)}$$

using the assumption that the slope and flux vary slowly with x, i.e.

$$\left| \frac{\alpha_{j+1/2} - \alpha_{j-1/2}}{\alpha_j} \right| << 1$$

$$\left| \frac{Q_{j+1/2} - Q_{j-1/2}}{Q_j} \right| << 1 \qquad \text{(A11.7)}$$

If the glacier is in steady state, then

$$\frac{Q_{j+1/2} - Q_{j-1/2}}{\Delta x} = A_j \qquad \text{(A11.8)}$$

where A_j is the mass balance. Then the error in the flux gradient is approximately

$$\epsilon = -2A_j \frac{m\, e_h}{\Delta x \alpha_j} \qquad \text{(A11.9)}$$

For unit width and $\Theta=0$, the residual (A11.1) is then approximately

$$r_j = e_h \left[1 - \frac{2A_j\, m\Delta t}{\Delta x \alpha_j} \right] \qquad \text{(A11.10)}$$

This order of magnitude estimate is valid only at some distance from the bergschrund or ice divide, and from the terminus, due to the restriction (A11.7). To get an estimate of a residual criterion for the program that will reduce changes in thickness h_j to less than e_h, replace A_j by $a=\max|A_j|$ and the surface slope α_j by the average slope β of the bed. Then

$$r_j = e_h \left[1 - \frac{2am}{\beta} \frac{\Delta t}{\Delta x} \right] \qquad \text{(A11.11)}$$

For example, if $m=3$, $\Delta t=1$, $\Delta x=10^{-2}$, $\beta=10^{-2}$ and $a=10^{-2}$ for a

glacier of unit length, then the residual error is

$$|r_j| = 10^{-3} |e_h| \tag{A11.13}$$

For example, if the ice thickness is approximately 10^{-1}, and we want to find the thickness to six figure accuracy, then

$$|e_h| < 10^{-7} \tag{A11.14}$$

and the residual convergence criterion must be set to

$$|r_j| < 10^{-4} \tag{A11.15}$$

APPENDIX 12: MACHINE ROUNDOFF ERRORS

The truncation error is reduced by taking smaller mesh intervals Δx and Δt. The reduction of the mesh increments is limited, however, by the machine roundoff error. Single precision real floating point arithmetic on the Amdahl 470 V/8 computer at the University of British Columbia is limited to six significant figures. Extended precision results in 14 significant figures. The Amdahl 470 V/8 is similar in architecture to an IBM 370 computer.

Any finite difference estimate of a derivative has the form

$$(f_{j+1} - f_j)/\Delta p \qquad \text{(A12.1)}$$

where Δp is Δx or Δt, and the index j can be either space or time. As Δp becomes small, f_{j+1} approaches f_j since f is assumed to be continuous. When f_{j+1} gets sufficiently close to f_j that they are the same in their first M digits, then M significant figures are lost in the subtraction for the finite difference estimate.

At each time step, there are three operations in which accuracy can be lost. First, the ice surface slope is calculated by a finite difference of the ice surface elevation. This slope is used in the flow law equation to find the ice velocity and flux. A further finite differencing is used to get the ice flux gradient. Finally, in the calculation of the residuals, there is a comparison of the flux gradient and the mass balance.

For example, if in each of these operations, the quantities being differenced differ by less than 1% over Δx, there are zero significant figures left using single precision arithmetic on

the Amdahl 470 V/8. For most models and mesh selections extended precision should be used.

APPENDIX 13: DIFFERENCING SCHEME FOR THE FLUX GRADIENT

A13.1 INTRODUCTION

This Appendix describes how the finite difference form of $\partial Q/\partial x$ must be handled in the spatial dimension to get a stable solution when the flux is a not a linear function of the ice thickness, and I wish to use the diffusive nature of the flow equation for ice to control the nonlinear instability.

To show that the solution of the nonlinear equations (A1.1.4) is bounded for all positions x and all time t is a very difficult problem. Bindschadler (unpublished, p. 87) derived constraints on the form of the the flux gradient scheme for one example of a nonlinear advection equation. He obtained a linear equation by treating $h^2(x,t)$ as the dependent variable. The applicability of the result to other nonlinear equations could be questioned; it is easy to show that the scheme for the special case analysed by Bindschadler reduces to the standard Crank-Nicolson scheme for the linear diffusion equation. The approach I follow here is instead, to find the local numerical stability criterion for perturbations to a steady state solution of the partial differential equation (A1.1.1). This at least gives necessary conditions for global stability, and allows me to eliminate some schemes from further consideration. It is also applicable to any nonlinear form of flux.

A13.2 PERTURBATION EQUATIONS

For small perturbations h(x,t) to a steady state ice mass of unit width with thickness profile H(x) and ice flux Q(x), the continuity equation (A1.1.1) can be written as (see Appendix 6)

$$\frac{\partial h}{\partial t}(x,t) = - \frac{\partial}{\partial x}[c_o(x)\, h(x,t)] + \frac{\partial}{\partial x}[D_o(x)\, \frac{\partial h}{\partial x}(x,t)] \tag{A13.2.1}$$

when the source term a(x,t) is zero. 'Small' means

$$\left|\frac{h(x,t)}{H_o(x)}\right| << 1 \tag{A13.2.2}$$

when the region near the terminus is not included. Letting $\alpha(x)$ be the slope of the steady state ice surface,

$$D_o(x) = \left[\frac{\partial Q(x)}{\partial \alpha}\right]_0 \tag{A13.2.3}$$

$$c_o(x) = \left[\frac{\partial Q(x)}{\partial H}\right]_0$$

Treating $c_o(x)$ and $D_o(x)$ and their derivatives as locally constant (this assumption is the one most likely to be questionable in this section, although Gary (1975, p. 8.42) and Richtmyer and Morton (1967, p. 91) indicate that this is a standard assumption in this type of stability analysis), I can get the wavenumber domain solution of (A13.2.1) by first taking the Fourier transform (Morse and Feshbach, 1953, p. 453) indicated by tildes, with respect to x. Primes indicate spatial derivatives, and m is the wavenumber. Then

$$\tilde{h}(m,t) = \tilde{h}_o \, e^{im(D_o'-c_o)t} \, e^{-c_o' t} \, e^{-D_o m^2 t} \qquad \text{(A13.2.4)}$$

and the transfer function for a time interval Δt is

$$T(m) = e^{im(D_o'-c_o)\Delta t} \, e^{-c_o'\Delta t} \, e^{-D_o m^2 \Delta t} \qquad \text{(A13.2.5)}$$

The complex exponential factor gives the phase shifts for advection analogous to (A1.5.6), the real exponential factor with c_o' gives the decay or growth due to extending or compressing flow, and the factor with D_o is the damping due to the diffusive nature of ice flow. It is evident that the higher wavenumbers are preferentially attenuated in this analytical solution. The modulus of the transfer function (A13.2.5) is shown as a dotted line in Figure A13.1 for the case

$$D_o' = c_o' = 0 \qquad \frac{D_o \Delta t}{\Delta x^2} = \frac{1}{4} \qquad \text{(A13.2.6)}$$

A13.3 SPACE DIFFERENCING SCHEME

Because the mesh is discrete, the highest wavenumber which can be sampled is

$$m_N = \pi/\Delta x \qquad \text{(A13.3.1)}$$

i.e. two samples per wavelength. This is the Nyquist wavenumber. I will derive conditions on the form of the finite difference scheme for the flux gradient so that the slope dependence in the flow equation can suitably damp all high wavenumbers up to the Nyquist wavenumber m_N.

Primes indicate x spatial derivatives. To set up a finite

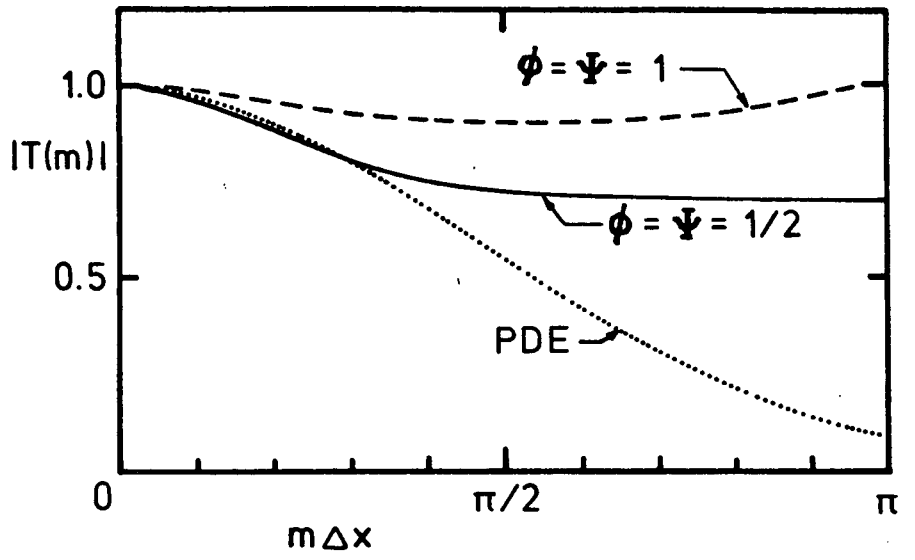

FIGURE A13.1. Damping Using The Ice Surface Slope.
Dotted curve: partial differential equation.
Broken curve: finite difference scheme with slope measured over $2\Delta x$. This scheme cannot suppress the nonlinear instability at the Nyquist wavenumber.
Solid curve: finite difference scheme with slope measured over Δx.

difference analogue of (A13.2.1), let the differences outside the square brackets, i.e. those representing $\partial q/\partial x$, have the form

$$q'_j = \frac{q_{j+\phi} - q_{j-\phi}}{2\phi\Delta x} \qquad \text{(A13.3.2)}$$

where $\phi>0$ and

$$q_{j+\phi} = q([j-1+\phi]\Delta x,\ n\Delta t) \qquad \text{(A13.3.3)}$$

and let the differences representing the surface slope inside the last bracket in (A13.2.1) have the form

$$h'_j = \frac{h_{j+\Psi} - h_{j-\Psi}}{2\,\Psi\Delta x} \qquad \text{(A13.3.4)}$$

A13.4 TRANSFER FUNCTION

The procedure is now to find the transfer function T(Z), just as in Section (A1.4.2) and find restrictions on $\emptyset$ and Ψ such that T(Z) is similar to the transfer function (A13.2.5) for the partial differential equation (A13.2.1) and has a form that can suppress the nonlinear instability. The finite difference equation is

$$\frac{h_j^{n+1} - h_j^{n}}{\Delta t} = -c'_{oj}\left[\theta h_j^{n+1} + (1-\theta)h_j^{n}\right]$$

$$- \frac{c_{oj}}{2\emptyset\Delta x}\left[\theta(h_{j+\emptyset}^{n+1} - h_{j-\emptyset}^{n+1}) - (1-\theta)(h_{j+\emptyset}^{n} - h_{j-\emptyset}^{n})\right]$$

$$+ \frac{D'_{oj}}{2\Psi\Delta x}\left[\theta(h_{j+\Psi}^{n+1} - h_{j-\Psi}^{n+1}) - (1-\theta)(h_{j+\Psi}^{n} - h_{j-\Psi}^{n})\right]$$

$$+ \frac{D_{oj}}{4\Psi\emptyset\Delta x^2}\left[\theta(h_{j+\emptyset+\Psi}^{n+1} - h_{j+\emptyset-\Psi}^{n+1} - h_{j-\emptyset+\Psi}^{n+1} + h_{j-\emptyset-\Psi}^{n+1}) + (1-\theta)(h_{j+\emptyset+\Psi}^{n} - h_{j+\emptyset-\Psi}^{n} - h_{j-\emptyset+\Psi}^{n} + h_{j-\emptyset-\Psi}^{n})\right] \qquad \text{(A13.4.1)}$$

Treating $c_o(x)$ and $D_o(x)$ and their derivatives as locally constant and forming a transfer function as in Section (A1.4.2) gives

$$T(m) = \frac{\left[1-(1-\theta)\Delta t\left[c_o' + \frac{D_o}{\phi\psi\Delta x^2}\sin(m\psi\Delta x)\sin(m\phi\Delta x)\right] - i\left[\begin{matrix} D_o'(1-\theta)\,\Delta t\,\sin(m\psi\Delta x)/(2\psi\Delta x) \\ -c_o(1-\theta)\,\Delta t\,\sin(m\phi\Delta x)/(2\phi\Delta x)\end{matrix}\right]\right]}{\left[1+\theta\,\Delta t\left[c_o' + \frac{D_o}{\phi\psi\Delta x^2}\sin(m\psi\Delta x)\sin(m\phi\Delta x)\right] + i\left[\begin{matrix} D_o'\theta\,\Delta t\,\sin(m\psi\Delta x)/(2\psi\Delta x) \\ -c_o\theta\,\Delta t\,\sin(m\phi\Delta x)/(2\phi\Delta x)\end{matrix}\right]\right]} \qquad \text{(A13.4.2)}$$

A13.5 CONDITIONS ON THE MESH INTERVAL

When $\theta=0.5$, which was the minimum value for stability from Section (A1.4.2), the imaginary parts of the numerator and denominator are equal, and $|T(Z)|\leq 1$ requires

$$\sin(m\phi\Delta x)\sin(m\psi\Delta x) \geq \frac{-c_o'\psi\phi\Delta x^2}{D_o}$$

$$0 \leq m \leq \pi/\Delta x \qquad \text{(A13.4.3)}$$

First, note that $D_o(x)>0$, because any realistic flow law gives increasing ice flow with increasing surface slope. Consider the simple case $c_o'(x)=0$. If $\phi=\psi$, then (A13.4.3) is satisfied for all ϕ and wavenumbers m. However, to achieve the strict inequality i.e. damping at the high wavenumbers, both ψ and ϕ must be strictly less than unity. When $\phi\neq\psi$, the left side of (A13.4.3)

is positive when

$$0 < m < \min\left[\frac{\pi}{\Theta\Delta x} , \frac{\pi}{\Psi\Delta x}\right] \qquad \text{(A13.4.4)}$$

This also requires both Ψ and $\emptyset$ less than unity to satisfy (A13.4.3). When $c_0'<0$ (compressive flow), both $\emptyset$ and Ψ must be smaller still. Since the nonlinear instability tends to grow exponentially, merely keeping $|T(m)|\leq 1$ may not be sufficient damping to curb its growth. For example, the broken curve in Figure A13.1 for $\Psi=\emptyset=1$ shows that there may be no damping at all at the Nyquist wavenumber. Since the damping term in (A13.2.5) decreases monotonically with increasing wavenumber, it is reasonable to demand the same of the numerical scheme.

Noting that, when $\Theta=1/2$, (A13.4.2) has the form

$$T(m) = \frac{1 - A(m) + iB(m)}{1 + A(m) - iB(m)} \qquad \text{(A13.4.5)}$$

and that (A13.4.3) implies

$$A(m) \geq 0 \qquad \text{(A13.4.6)}$$

it is evident that $|T(m)|$ decreases monotonically with wavenumber m as long as A(m) increases with m. Setting the first derivative of A(m) to zero gives an equation (A13.4.7) for the maximum wavenumber m for which A(m) increases with m.

$$\Psi\sin(m\emptyset\Delta x)\cos(m\Psi\Delta x) + \emptyset\cos(m\emptyset\Delta x)\sin(m\Psi\Delta x) = 0 \qquad \text{(A13.4.7)}$$

For the case $\Psi=\emptyset$, (A13.4.7) reduces to

$$\sin(2m\emptyset\Delta x) = 0 \qquad \text{(A13.4.8)}$$

or

$$m = \frac{1}{2\phi} \frac{\pi}{\Delta x} \qquad \text{(A13.4.9)}$$

To keep this turning point m above the Nyquist wavenumber $\pi/\Delta x$,

$$\psi = \phi \leq 1/2 \qquad \text{(A13.4.10)}$$

The modulus of T(m) is plotted as the solid curve in Figure A13.1 for

$$\psi = \phi = \frac{1}{2} \qquad c'_o = D'_o = 0$$

$$\frac{c_o \Delta t}{\Delta x} = 4 \qquad \frac{D_o \Delta t}{\Delta x^2} = \frac{1}{4} \qquad \text{(A13.4.11)}$$

It evidently provides better damping at high wavenumbers than did the choice $\psi=\phi=1$. The choice of 1/2 is quite convenient for computations. The flux is evaluated at the midpoints of the mesh intervals, and can be used twice, i.e. for the gradient estimates at the points both ahead and behind.

If, for some reason, a value other than 1/2 is used for either ψ or ϕ, (A13.4.7) can be solved with $m=m_N$ to find the maximum usable value of the other.

APPENDIX 14: ICE SURFACE ELEVATIONS

To find the slope α of the glacier surface for the flow equation (1.4.38), I must know the elevation s of the ice surface. From the geometry shown in Figure A14.1, it is evident that the surface elevation at x_j is

$$s = b + h[\cos(\beta) + \sin(\beta)\tan(\alpha)] \qquad (A14.1)$$

where b is the bed elevation, β is the bed slope angle, h is the ice thickness normal to the bed, and α is the ice surface slope

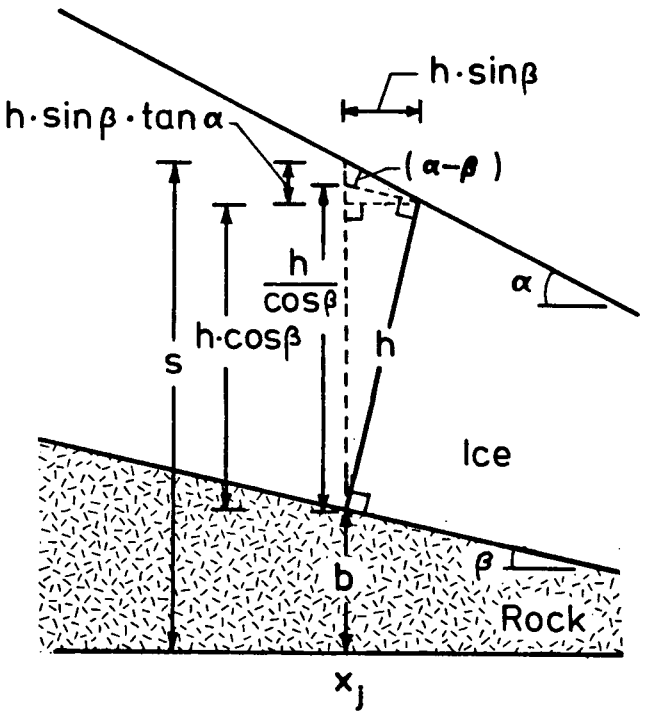

FIGURE A14.1. Ice Surface Elevation.

angle. By writing $\tan(\alpha)$ as $\tan([\alpha-\beta]+\beta)$, and expanding it by the addition formula (4.3.18) of Abramowitz and Stegun (1965, p. 72),

$$s = b + h\left[\cos(\beta) + \sin(\beta)\left[\frac{\tan(\alpha-\beta) + \tan(\beta)}{1-\tan(\alpha-\beta)\tan(\beta)}\right]\right] \qquad (A14.2)$$

Assuming

$$|\alpha| << 1 \qquad (A14.3)$$

$$|\beta| << 1 \qquad (A14.4)$$

and neglecting third power terms in tangent of α, β, or $(\alpha-\beta)$,

$$s = b + h[\tan(\alpha-\beta)\sin(\beta) + \tan(\beta)\sin(\beta) + \cos(\beta)] \qquad (A14.5)$$

Using one term expansions for the trigonometric functions in the first term in the square brackets, and combining the last two terms,

$$s = b + h[(\alpha-\beta)\beta + \frac{1}{\cos(\beta)}] \qquad (A14.6)$$

Because of (A14.4), this can be rewritten as

$$s = b + \frac{h}{\cos(\beta)}[1 + O(\beta[\alpha-\beta])] \qquad (A14.7)$$

Because α depends on s, (A14.7) is an implicit equation for s. However, the term $O(\beta[\alpha-\beta])$ is small when (A14.3) and (A14.4) hold, so in the computer model I have used

$$s = b + \frac{h}{\cos(\beta)} \qquad (A14.8)$$

This estimate is exact when $\alpha=\beta$.

APPENDIX 15: ANALYTIC MODELS OF ICE SHEETS

A15.1 INTRODUCTION

In order to test the accuracy of the ice trajectory model (Section 2.4) I compared the numerical trajectory results to analytical trajectories using ice sheet models which included the two-dimensional velocity field (u,v). In Section A15.2 I discuss the Nye (1959[c]) ice sheet model which was the basis for several later models. In Section A15.3, I present the Nagata ice sheet model, used as a test including basal sliding velocities. In Section A15.4, I point out other models which can be used as tests.

A15.2 NYE ICE SHEET MODEL

Nye (1959[c]) derived the surface profile h(x) of a steady state two-dimensional ice sheet on a plane horizontal bed with a positive constant mass balance b, assuming that the horizontal ice velocity u at any position x was strictly basal sliding, or shear concentrated very near the bed. This model was never intended to be used near the edge of an ice sheet, because the ice velocity in the model goes to infinity as the ice thickness goes to zero. This model approximates the central region of ice sheets in which ice flux is discharged from the terminus by iceberg calving.

A15.3 NAGATA ICE SHEET MODEL

A15.3.1 BASIC EQUATIONS

A misunderstanding of Nye's meaning of mass balance led Nagata (1977) to develop a related ice sheet model which has an equilibrium line and an ablation area, and no velocity singularity at the terminus. The Nagata model can be described by the following equations.

Global continuity for a steady state requires that the ice flux Q(x) be given by

$$Q(x) = h(x)u(x) = \int_0^x B(s)ds \qquad \text{(A15.3.1)}$$

where B(x) is the mass balance. Nagata chose the mass balance to be

$$B(x) = b + u\frac{dh}{dx} \qquad \text{(A15.3.2)}$$

where b is the constant balance from the Nye model. Nagata's reason for using (A15.3.2) is, I think, questionable on physical grounds, but the resulting model is still mathematically consistent. By comparing (A15.3.2) with (A2.2.18), the condition for mass conservation at the ice surface, it is apparent that (A15.3.2) can be true only if

$$V_0(x) = -b \qquad \text{(A15.3.3)}$$

i.e., the downward velocity component $V_0(x)$ at the ice surface must be everywhere constant.

As in Nye's model, the horizontal velocity u(x) is independent of depth z, and the basal sliding is given by

$$u(x) = A\left[-\rho g\, h(x)\, \frac{dh}{dx}\right]^{m} \qquad \text{(A15.3.4)}$$

where m is approximately 2 or 3, and A is a constant. This is the form of the sliding law proposed by Weertman (1957). The term in parentheses is just the simple basal shear stress (1.4.25). Because of the assumption that all of the horizontal velocity is basal slip, the horizontal velocity u(x) is constant in any vertical column. This means that the longitudinal strain rate du/dx is also constant in any vertical column. Local application of incompressibility then implies that the vertical strain rate dv/dz must also be constant in each vertical column. Integrating a constant strain rate from the bed to depth z, using the basal boundary condition

$$v(x,0) = 0 \qquad \text{(A15.3.5)}$$

gives the vertical velocity

$$v(x,z) = -\left[\frac{du}{dx}(x)\right] z \qquad \text{(A15.3.6)}$$

A15.3.2 ICE DEPTH, MASS BALANCE, AND VELOCITY

Nagata's model is found by solving (A15.3.1) through (A15.3.6) for the five functions h(x), u(x), $V_0(x)$, v(x,z) and B(x). The ice thickness solution h(x) using the boundary conditions

$$h(0) = H \qquad h(L) = 0 \qquad \text{(A15.3.7)}$$

is given implicitly by

$$\left[1+\left[\frac{m}{m+1}\right]\frac{h(x)}{H}\right]\left[1-\frac{h(x)}{H}\right]^{\frac{m}{m+1}} = \frac{x}{L} \qquad \text{(A15.3.8)}$$

where the ice thickness H at the centre of the ice sheet is related to the length L of the ice sheet by

$$\frac{(m+1)^2}{m(2m+1)} H^{\frac{2m+1}{m+1}} = \left[\frac{m+1}{m} b\right]^{\frac{1}{m+1}} \left[\rho g\right]^{\frac{-m}{m+1}} A^{\frac{-1}{m+1}} L \qquad \text{(A15.3.9)}$$

This equation for h(x) can be solved at each x by Newton's method (e.g. Carnahan and others, 1969, p. 319) supplemented by interval halving whenever estimates of h(x) exceed H.

By setting B(x)=0 in (A15.3.2), it is easy to show that the equilibrium line occurs at

$$x_e = \left[\frac{3m+1}{2m+1}\right]\left[\frac{m}{2m+1}\right]^{\frac{m}{m+1}} \qquad \text{(A15.3.10)}$$

and the ice thickness at this point is

$$\frac{h_e}{H} = \frac{m+1}{2m+1} \qquad \text{(A15.3.11)}$$

The velocity solution is

$$u(x) = \left[\frac{2m+1}{m+1}\right] \frac{bx}{H\left[1+\left[\frac{m}{m+1}\right]\frac{h(x)}{H}\right]} \qquad \text{(A15.3.12)}$$

$$v(x,z) = \frac{-bz}{h(x)} \qquad \text{(A15.3.13)}$$

The mass balance solution for the Nagata ice sheet is found

by differentiating (A15.3.8) and substituting dh/dx into (A15.3.2) to get

$$B(x) = b\left[1 - \frac{x}{L}\frac{H}{h}\left[\frac{m+1}{m}\right]\frac{\left[1-\frac{h}{H}\right]^{\frac{m}{m+1}}}{\left[1+\left[\frac{m}{m+1}\right]\frac{h}{H}\right]}\right] \qquad \text{(A15.3.14)}$$

From (A15.3.14), it is apparent that, although the Nagata model eliminates the singularity in the horizontal velocity at x=L, it introduces a mass balance singularity and an indeterminate vertical velocity at x=L, because h(L)=0.

A15.3.3 STREAMLINES

The streamlines in the Nagata model are found by integrating

$$\frac{dz}{dx} = \frac{v}{u} \qquad \text{(A15.3.15)}$$

to get the family of curves

$$\left[\frac{m}{2m+1}\right] \ln\left[\frac{\left[1-\frac{h}{H}\right]}{\left[1+\left[\frac{m}{m+1}\right]\frac{h}{H}\right]}\right] + \left[\frac{m}{2m+1}\right]\ln(x) + \ln(z) = c' \qquad \text{(A15.3.16)}$$

where c' is a constant identifying each streamline. Exponentiating (A15.3.16) and using (A15.3.8) gives the streamline curves

$$\frac{z}{H}\frac{x}{L}\left[1+\left[\frac{m}{m+1}\right]\frac{h}{H}\right]^{-1} = c \qquad \text{(A15.3.17)}$$

where c is a new constant identifying each streamline. (There appears to be an error in the exponent of the outer bracketed term in Nagata's original derivation (his equation (28))).

It is evident that c=0 corresponds to a vertical flowline at the ice divide x=0, and using the equations (A15.3.10) and (A15.3.11), it can be shown that the streamline with

$$c = \left(\frac{m+1}{2m+1}\right)\left[\frac{m}{2m+1}\right]^{\frac{m}{m+1}} \qquad \text{(A15.3.18)}$$

just touches the ice surface at the equilibrium line. All streamlines in the ice sheet are represented by constants falling between these extremes.

For each acceptable value of c, the two endpoints x_0 and x_1 at which the streamline enters and leaves the icemass are found by setting z=h in (A15.3.17), solving (A15.3.17) for h(x), and substituting this expression into (A15.3.8); this gives an implicit solution (A15.3.19) for x_0 and x_1.

$$\left[\frac{x}{L}-\left[\frac{2m+1}{m+1}\right]c\right]^{m}-\left[\frac{x}{L}-\left[\frac{mc}{m+1}\right]\right]^{2m+1} = 0 \qquad \text{(A15.3.19)}$$

For values of c between zero and (A15.3.18), this equation can be solved by Newton's method for x_0 and x_1.

The shape of the streamlines in the nondimensional form, i.e. using the variables

$$Z = \frac{z}{H} \qquad X = \frac{x}{L} \qquad D = \frac{h}{H} \tag{A15.3.20}$$

does not depend on the flow law constant A, or on the accumulation constant b. These two constants only affect the rate at which ice moves along these streamlines.

Because the horizontal velocity u(x) is independent of depth, the time taken by any ice particle to flow from x_o to x is given by

$$t - t_o = \int_{x_o}^{x} \frac{ds}{u(s)} \tag{A15.3.21}$$

Substituting (A15.3.12) for u(x) leads to

$$t - t_o = \frac{(m+1)}{(2m+1)} \frac{H}{b} \ln\left[\frac{x}{x_o}\right] + \frac{m}{(2m+1)b} \int_{x_o}^{x} \frac{h(s)}{s}\, ds \tag{A15.3.22}$$

The integral in (A15.3.22) can be evaluated by Simpson's Rule (e.g. Carnahan and others, 1969, p. 73).

Figure A15.1 shows the Nagata ice sheet in nondimensional form for m=2 with five streamlines at equal intervals of c between zero and the limit in (A15.3.18). For the steady state case, the streamlines and particle paths coincide. The velocity field is also shown in Figure A15.1 using the parameters in Table A15.1.

The plot has been nondimensionalized using (A15.3.20). The arrows show velocity multiplied by 250 years, i.e. displacement. These particular numbers are not meant to represent any existing ice sheet; they were simply chosen as round numbers to give a model test.

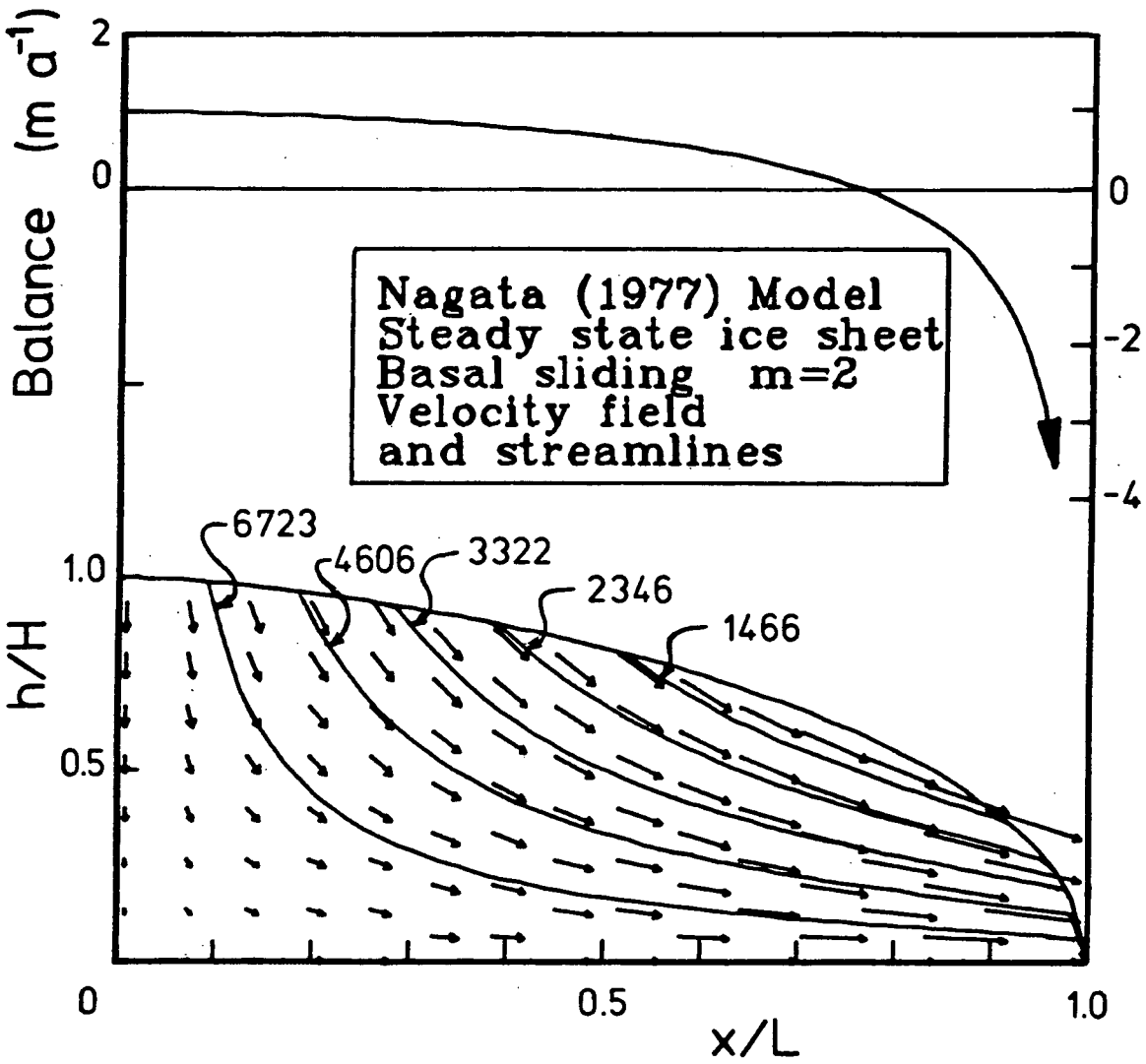

FIGURE A15.1. Nagata Steady Ice Sheet.
Distance and height are shown in nondimensional form. The mass balance goes to $-\infty$ at X=1.0 . The numbers give the time in years for ice to travel the length of the indicated trajectory. The streamlines are shown for equal intervals of the constant c (see equation A15.3.17). The velocity vectors correspond to the case m=2 A=100 bar^{-2} m a^{-1}, with b=1 m a^{-1} and H=3000 m. Using (A15.3.9), L is found to be 454.6 km. The velocities have been multiplied by 250 years so that the vectors effectively show 250 year displacements.

Nagata (1977, p. 19) attempted to find an equilibrium line in Nye's (1959[c]) ice sheet model. The result obtained is

m	A $bar^{-2}a^{-1}$	b ma^{-1}	H m	L km	ρ $kg\ m^{-3}$	g $m\ s^{-2}$
2	100.	1.0	3000	454.6	910	9.8

TABLE A15.1. Parameters for Nagata ice sheet.

incorrect because (A15.3.2) does not hold in the Nye ice sheet. The Nye model does not have an equilibrium line.

A15.4 HAEFELI-PATERSON ICE SHEET MODEL

The Nagata ice sheet model can be used to test the computer model of Appendix 2 for the case of basal sliding. For the case of internal deformation in simple shear using Glen's flow law (1.4.22), Haefeli (1961) derived the steady surface profile for the accumulation area of an ice sheet with a spatially constant mass balance b. Haefeli used the leading term of (1.4.38) for the ice velocity with $u_s(x)=0$. Paterson (1972) derived the same profile for the accumulation region, added an ablation region of constant ablation rate c, and matched the two solutions to get a continuous profile. He also included the effect of isostatic depression of the originally horizontal bed. The velocity field (u,v) can be derived in analytic form for this model, and used as another check of the numerical model. This model has not been included in this study.

APPENDIX 16: TESTS OF THE BUDD-MCINNES MODEL

"You've got to show me - I'm from Missouri."[1]

A16.1 INTRODUCTION

A basal sliding treatment proposed by Budd (1975) was incorporated into a numerical model of glacier flow by McInnes (unpublished), Budd and McInnes (1974) and Budd (1975), and used to simulate surges of several valley glaciers (Budd and McInnes, 1974; Budd, 1975; McInnes, unpublished) and of the East Antarctic ice sheet (Budd and McInnes, 1978; 1979). This model suffered from a numerical instability (McInnes, unpublished, p. 57) which in my opinion appears to be the nonlinear instability (see Section 2.2.4). This instability was treated by the unorthodox method of smoothing the solution profiles whenever high wavenumber oscillations appeared (McInnes, unpublished, p. 64). Since Budd (1975) has become a widely read paper on glacier surges, I wished to verify the accuracy of the final results.

---

[1] American traditional.

A16.2 ICE FLOW IN THE BUDD-MCINNES MODEL

Budd (1975) reported that the ice velocity due to internal deformation in the Budd-McInnes model was calculated from

$$V(x) = k \tau^{n} h(x) \qquad \text{(A16.2.1)}$$

where k is a constant given by

$$k = \frac{2A}{(n+1)} \qquad \text{(A16.2.2)}$$

when A and n are the constant and exponent of Glen's flow law for ice. Both Budd (1975, p. 5) and McInnes (unpublished, p. 88) gave the values of these parameters as

$$n=2 \qquad k=0.15 \text{ bar}^{-2} \text{ a}^{-1} \qquad \text{(A16.2.3)}$$

The basal shear stress τ is given by

$$\tau = s\rho g h \alpha \qquad \text{(A16.2.4)}$$

which I have discussed in Section 1.4.4. The ice thickness is h(x), the surface slope is α, s is a shape factor, and ρg is the weight of ice per unit volume.

The basal sliding was controlled in the Budd-McInnes model by a basal lubrication factor $\emptyset$ and a viscosity η for longitudinal extension. Details have been given by Budd (1975); a summary can be found in Appendix 8, Section 8.3.2. An important point for this discussion is that the basal sliding velocity goes to zero as $\emptyset$ goes to zero.

A16.3 VATNAJÖKULL MODEL: NONLINEAR INSTABILITY

My attention was first caught by Figure 4.3 of McInnes (unpublished, p. 58). Since this figure is not widely available, I show a redrawn version in Figure A16.1. Figure 4.3 of McInnes illustrated the growth of a high wavenumber numerical instability of the sort which required smoothing in the Budd-McInnes model. The figure caption in McInnes (unpublished) indicated that the profiles show the ice surface at 50 year intervals, starting on an ice-free bed, and using the bed and mass balance of "the Vatnajökull model". This model is different from the Vatnajökull (Bruarjökull ice stream) model used later by McInnes (unpublished, p. 107) and shown in Figure 5 of Budd (1975).

McInnes (unpublished, p. 58) used a simple two-point finite difference scheme to compute the dashed profiles in Figure A16.1. For subsequent work he used (unpublished, p. 68) a higher order scheme. The higher order schemes increase accuracy by reducing the truncation error (Section A1.5.3), but do not remove the aliasing problem (Section A3.2) which causes the nonlinear instability.

Since McInnes was discussing stability in the absence of basal sliding, I assumed that, for this example, the basal lubrication parameter $\emptyset$ was equal to zero.

To compare these profiles, for which the nonlinear instability was a problem, to the profiles from a numerical model in which the nonlinear instability was adequately treated, I ran my computer model using the bed and mass balance functions

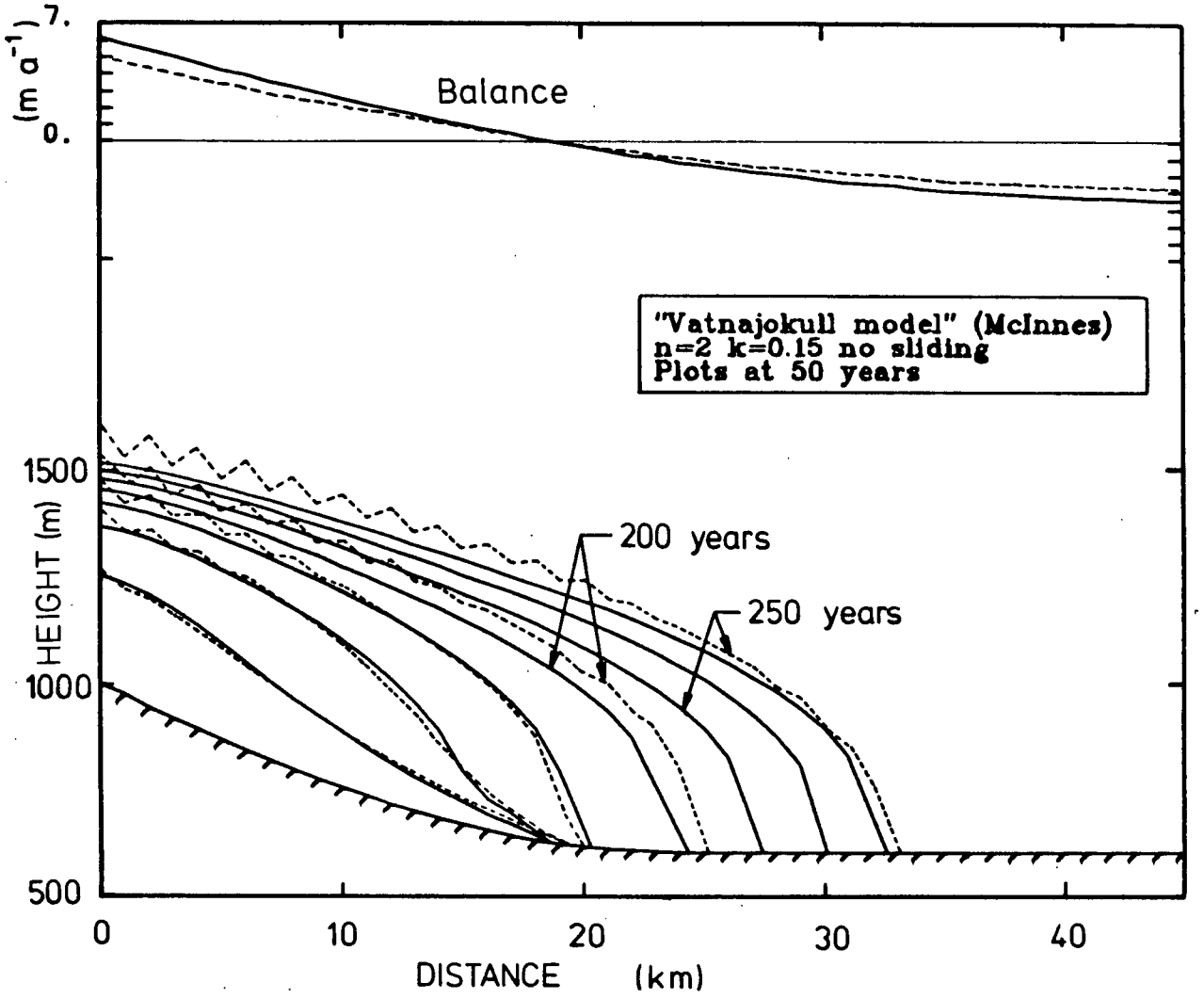

FIGURE A16.1. Vatnajökull: Instability And Growth Rate.
Growth of the Bruarjökull ice stream on Vatnajökull (Iceland) from ice-free conditions at 50 year intervals using Model 1. The dashed ice surface profiles are redrawn from McInnes (unpublished, Figure 4.3). The original caption on that figure was:

> "Profiles from the Vatnajökull model at fifty year intervals, showing the increase in the amplitude of the oscillations with time, due to the two point finite difference approximation. In this case there was no smoothing."

The solid curves are from the numerical model described in this thesis. I used the mass balance given by the solid curve, rather than the broken curve (from McInnes (unpublished) and Budd (1975)) in order to match (approximately) the first 50 year profile. The bed topography is also different from that used later by McInnes (unpublished, p. 107) and Budd (1975). The Budd-McInnes model suffers from the nonlinear instability precipitated by inadequate treatment of the boundary x=0. It also appears to create mass.

scaled from Budd (1975) Figure 5. McInnes (unpublished, p. 53 and p. 106) gave the parameters in the first six columns of Table A16.1 for the Vatnajökull model. The time step of one year

n	k $bar^{-n} a^{-1}$	s	g ms^{-2}	ρ $kg\ m^{-3}$	Δx m	Δt a
2	0.15	1.0	9.8	910.	1000.	1.0

TABLE A16.1. Parameters for Vatnajökull (Bruarjökull) model.

gave stable and accurate results with my model, i.e. the profiles were smooth, and were unchanged by a smaller time step. (The Budd-McInnes model was unstable for a time step of one year (McInnes, p. 56), but this was the linear computational instability (see Appendix 1, Section A1.4.2) due to the explicit scheme used by McInnes and Budd.)

From reading all the published accounts of the Budd-McInnes model, I was unable to discover exactly how the boundary condition was implemented. McInnes (unpublished, p. 53) indicated that for most models, the ice surface slope was equal to zero at x=0 (ice divide condition). However, none of the published profiles in Budd (1975) or the dashed curves in Figure A16.1 appears to be flattening out near x=0. Budd (1975) did not mention the boundary condition. For all the profiles I generated in this Appendix, I used the ice divide boundary condition of zero slope at x=0. (see Section A1.3.1). I also ran some tests using the boundary condition number 3 of Section A1.3.1, i.e.

$$Q_o\left(-\frac{\Delta x}{2},t\right) = 0 \qquad \text{(A16.4.1)}$$

where Δx is the spatial mesh interval, and the mass balance and bed functions were shifted appropriately so that $x=-\Delta x/2$ corresponded to $x=0$ in Figure A16.1. The resulting profiles were visibly different from the solid curves in Figure A16.1 only in the three km stretch nearest the ice divide. Any differences further downglacier could not be resolved on the plotted display.

To match the bed in Figure A16.1, it is necessary to multiply the topographic gradient in Budd (1975, Figure 5) by a factor of roughly 1.18 to get the elevation drop of 400 m. The base level must also be adjusted.

Using the mass balance from Budd (1975), my glacier profiles (not shown) for Vatnajökull also grew much less rapidly than the dashed curves in Figure A16.1, even in the first 50 year period when there is likely very little ice flow; the glacier changes shape mainly by mass accretion due to snowfall. After multiplying the mass balance function shown by Budd (1975) and by McInnes (unpublished, p. 107) by a factor of 1.25, I ran the model again to get the solid curves in Figure A16.1. My first 50 year profile agrees reasonably closely in shape and total ice volume with the first 50 year profile from McInnes. Both the mass balance from Budd, and the mass balance I actually had to use are shown in Figure A16.1. I will use the notation "Vatnajökull model" or "Model 1" for the model in Figure A16.1, and "Bruarjökull model" or "Model 2" for the version in Budd (1975) and in McInnes (p. 107).

It is evident that the profiles from my computer model are free of the nonlinear instability. Due to the choice of finite difference scheme, no smoothing is necessary with this computer model.

A16.4 VATNAJÖKULL (MODEL 1): MASS CONSERVATION

In addition to the high wavenumber instability, the dashed profiles in Figure A16.1 appear to have another serious problem. The computer model appears to create mass. During the first 150 years (three profiles), my glacier simulation (solid curves) grows at about the same rate as Budd-McInnes model (dashed curves). The agreement is as close as I could expect, given the manner in which I had to deduce the mass balance function. At 200 years (fourth profile), however, the terminus has begun to move, and the Budd-McInnes model contains a substantially larger volume of ice than my model. By 250 years, the Budd-McInnes model has a larger volume of ice than my model could amass by 350 years. No amount of high wavenumber smoothing can alter this apparent discrepancy in the total glacier mass. Since my computer model satisfied the tests for continuity described in Chapter 2, I am confident that the results from my model are correct.

The apparent peculiar behaviour of the Budd-McInnes model can be illustrated graphically in two simple ways. First, note that the glacier mass can grow most rapidly when the terminus is at the equilibrium line X defined by

$$b(X) = 0 \qquad \text{(A16.4.1)}$$

where $b(x)$ is the mass balance. At this position, the accumulation area is maximized, and the ablation area is minimized. At all times the growth rate of the glacier mass M must then satisfy

$$\frac{dM}{dt} \leq \dot{M}_{max} = \int_0^X \rho W(s) b(s) ds \qquad \text{(A16.4.2)}$$

where $W(x)$ is the channel width (assumed independent of height. See Appendix 2, Section A2.2.1), and ρ is the density of glacier ice (assumed constant). On a plot of glacier mass as a function of time (Figure A16.2), a glacier is forbidden by (A16.4.2) to exist above the straight line through the origin with slope $\dot{M}_{max}$, regardless of the flow law or sliding law used. The mass of ice in my model is obtained at each time step by a trapezoidal rule integration of

$$M(t) = \int_0^L \rho h(s) W(s) ds \qquad \text{(A16.4.3)}$$

L is the current glacier terminus position, and $h(x)$ is ice thickness. The mass in the Budd-McInnes model was obtained by using a razor blade to cut out a copy of each profile on paper of uniform weight; I then weighed the cutouts on a microbalance. In Figure A16.2, the simulation using the model described in Chapter 2 follows the solid curve. The Budd-McInnes model, however, plots above the straight line, in the forbidden region when there is significant ice flow.

Another simple test of continuity is a plot of dM/dt against glacier length L. Irrespective of the glacier thickness,

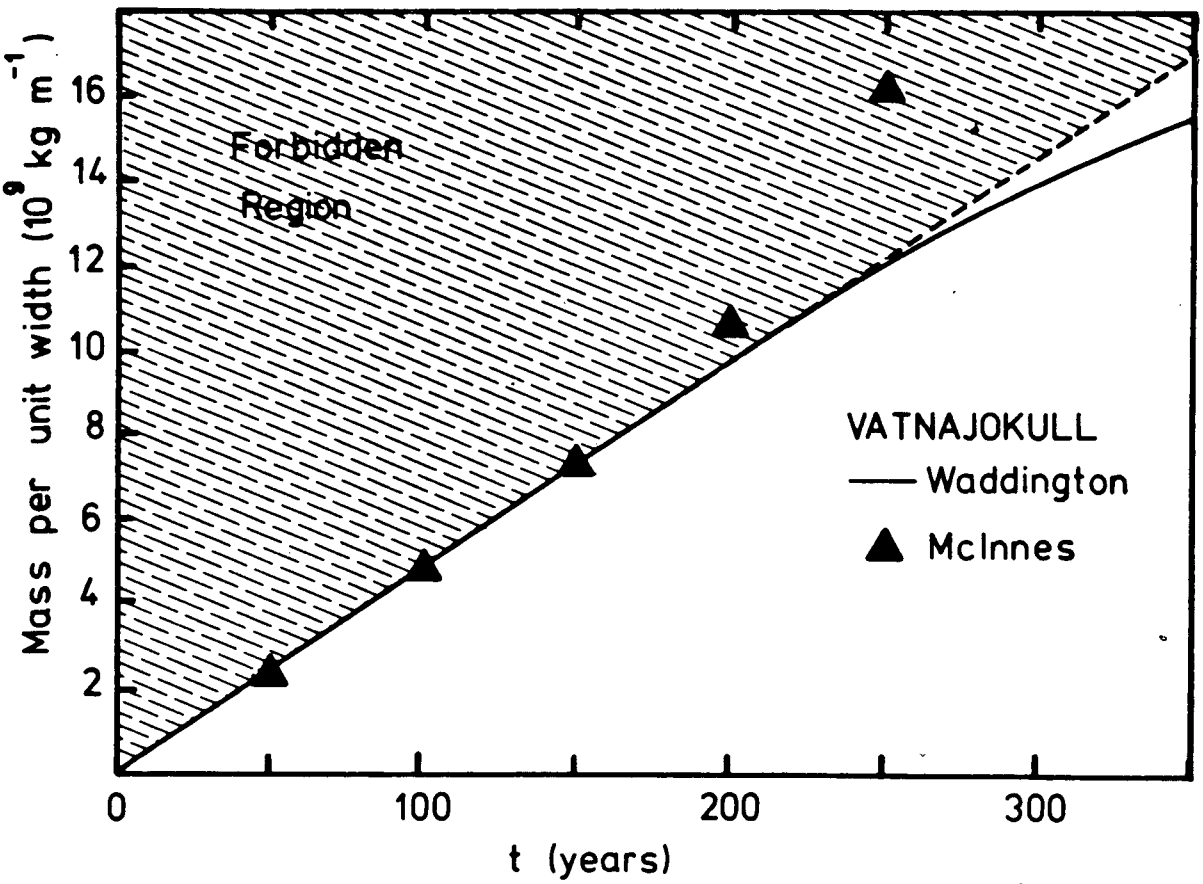

FIGURE A16.2. Glacier Mass As A Function Of Time.
Vatnajökull model continuity test. The broken straight line gives the maximum possible growth rate. The solid line is the mass of the Waddington simulation. It stays in the permitted region. The triangles are the values for the McInnes simulation (McInnes, unpublished, Figure 4.3). These points fall in the forbidden region after 150 years.

or the rate of terminus advance, or the sliding and flow law used, dM/dt at L should equal the balance flux at L. The balance flux Q_{bal}, the flux that would exist in a steady state, is completely specified by the mass balance b(x) and the glacier width W(x). For all models in this Appendix, W(x) is equal to unity, and I use flux per unit width.

$$Q_{bal}(x) = \left[\int_0^x \rho W(s)b(s)ds\right] \Big/ W(x) \qquad \text{(A16.4.4)}$$

The balance flux (A16.4.4) is shown by the broken line in Figure A16.3. The numerical values of dM/dt found by integrating the thickness profiles from my model (using (A16.4.3)) are shown

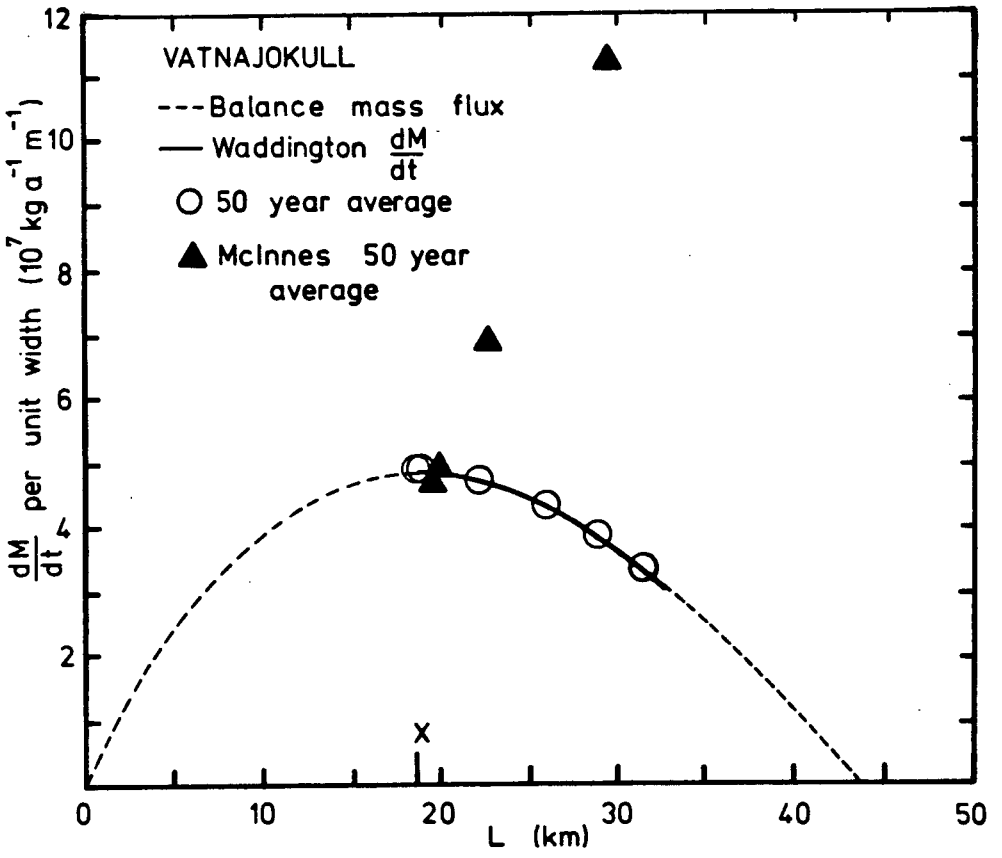

FIGURE A16.3. Rate Of Growth As A Function Of Length L.
The broken curve is the balance flux per metre width (A16.4.4) for Vatnajökull using the dashed mass balance curve in Figure A16.1. X is the equilibrium line. The solid curve is the numerical estimate of mass change rate from integrating the ice thickness changes of the Waddington simulation. The triangles are 50 year averages (all that is available) for the McInnes simulation. These numbers fall well off the correct curve. The 50 year averages for the Waddington runs are shown by circles.

by a solid line. The agreement is very good. For the Budd-McInnes model, the best I can get from Figure A16.1 (dashed curves) is 50 year averages of dM/dt. When the terminus advances, these plot well above the correct curve. For comparison, the 50 year averages for my model are also shown.

Both these simple continuity tests appear to indicate that the Budd-McInnes model has a serious mass creation error. There may be several other possible explanations for the apparent mass discrepancy, but they seem improbable:

(1) The mass balance used for this particular model run may have been altitude-dependent. As the glacier thickened, the accumulation rate could increase, leading to a more rapid growth. However, I was unable to find any mention of an altitude-dependent mass balance in any of the descriptions of this model (Budd and McInnes, 1974, 1978, 1979; Budd, 1975; McInnes, unpublished).

(2) The glacier channel could constrict at or below the equilibrium line, leading to a narrower and deeper glacier cross-section. However, the map of Bruarjökull from Thorarinsson (1969) which McInnes used as a data source does not show a constriction. In any case, McInnes (unpublished, p. 54) and Budd (1975, p. 17) indicate that width variations are absorbed into the mass balance function.

(3) The figure caption on Figure 4.3 in McInnes (unpublished) may be incorrect. However, the first three profiles (150 years) agree well with my results, so they, at least, appear to be at uniform intervals as stated in the caption. The fourth profile could be at 225 years (75 year interval) and the fifth could

conceivably be at 350 or 375 years (125 or 150 year interval), but this is a peculiar sequence, especially in light of the fact that the instability is just becoming interesting, and the terminus is just beginning to advance. Such a sequence would surely be mentioned in the caption.

A16.5 BRUARJÖKULL (MODEL 2): STEADY STATE FLUX

Since the Budd-McInnes model appeared to have some mass creation difficulties in the initial glacier buildup phase, I also wished to compare their final steady state solutions with the results from my model. I chose the nonsurging case because the surging models could be especially sensitive to the details of the numerical schemes, and hard to duplicate under the best of circumstances.

Using the bed shape and the mass balance from Budd (1975, Figure 5) for the Bruarjökull model (Model 2), the parameters in Table A16.1, and no sliding, I ran my computer model for 1500 years to obtain the 50 year profiles in Figure A16.4.

When describing surges of the Fedchenko Glacier (which I discuss below), McInnes distinguished the model with no sliding, called the "steady state case" (unpublished, Section 6.2.1) from models with nonzero basal sliding parameter $\emptyset$, called "surging case" (unpublished, Section 6.2.2) (although in fact for small nonzero values of $\emptyset$, the model may not surge). Since McInnes did not mention any value of $\emptyset$ for what he called "the steady state" in his Figure 6.15, I first assumed that he used $\emptyset=0$. That figure (Figure 6.15, p. 110) showed steady state profiles for

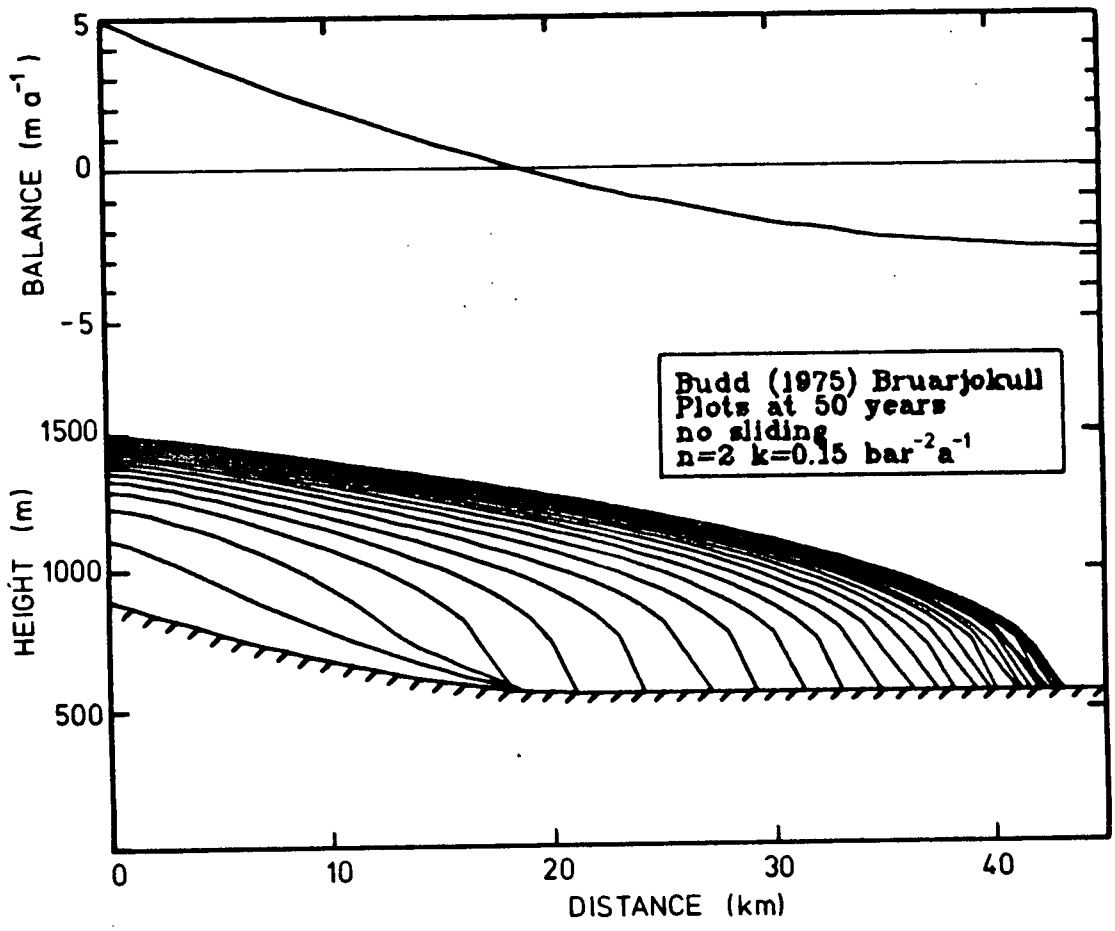

FIGURE A16.4. Bruarjökull Ice Profiles (Model 2).
The mass balance and bed are from Budd (1975). The Waddington model (Chapter 2) was run using the parameters in Table A16.1 and no sliding. The ice surface elevation is shown at 50 year intervals, starting from ice-free conditions.

ice elevation and ice velocity for the Bruarjökull model. The ice elevation and the ice velocity, given by its logarithm by McInnes, are redrawn in Figure A16.5 (a) and (c) as broken curves. I have converted the ice velocity to a linear scale, plotted as the broken curve in (b). I estimated the error in measuring log(V) from that curve as ±0.03, which is ±7% in V.

These limits are shown by the shaded area. The solid lines in Figure A16.5 are the profiles from the steady state reached by my simulation in Figure A16.4. The difference in terminus location is not significant. If a small constant amount of the order of 10 to 20 cm a^{-1} were to be added to the mass balance, my terminus would advance the required amount without noticeably altering the profile upglacier (see Nye, 1963[a]). A change of 10 cm a^{-1} could barely be resolved on Figure 5 of Budd (1975). Elsewhere, the agreement is not good. The velocity in the McInnes profile exceeds my velocities by up to 40%. The ice thickness in my model is greater by up to 65 m. Discrepancies in this direction would be expected if the Budd-McInnes profiles were in fact from a model with some sliding ($\emptyset \neq 0$).

However, the mass flux per unit width (A16.5.1)

Overleaf:

FIGURE A16.5. Bruarjökull flux test.
The final steady state velocity, ice elevation, and mass flux for Model 2, the Bruarjökull model of Budd (1975). McInnes plotted the logarithm of ice velocity, reproduced here as curve (a). I have converted this to velocity on a linear scale (broken curve in (b)). The shaded area shows the maximum error limits (±7%) in measuring the velocity from (a). From 10 to 35 km, it substantially exceeds the velocity from my model (solid curve). The broken ice surface curve in (c) is redrawn from McInnes (unpublished, p. 110). There appears to be a draughting error at x=12 km (arrow), making a direct comparison with my ice profile (solid curve) of dubious value. In (d), the solid curve is the balance flux (A16.4.4) using the mass balance in Figure A16.4. The shaded area indicates the limits of the balance flux due to an estimated maximum error of ±10 cm a^{-1} in measuring the mass balance from Budd (1975, Figure 5). At steady state, the mass flux (A16.5.1) should equal the balance flux. The mass flux in my model lies on the solid curve. The flux in the Budd-McInnes model is given by the broken curve. The shaded area indicates ±10% error limits due to scaling the velocity and thickness from curves (a) and (c). The Waddington model used the parameters in Table A16.1 and no sliding.

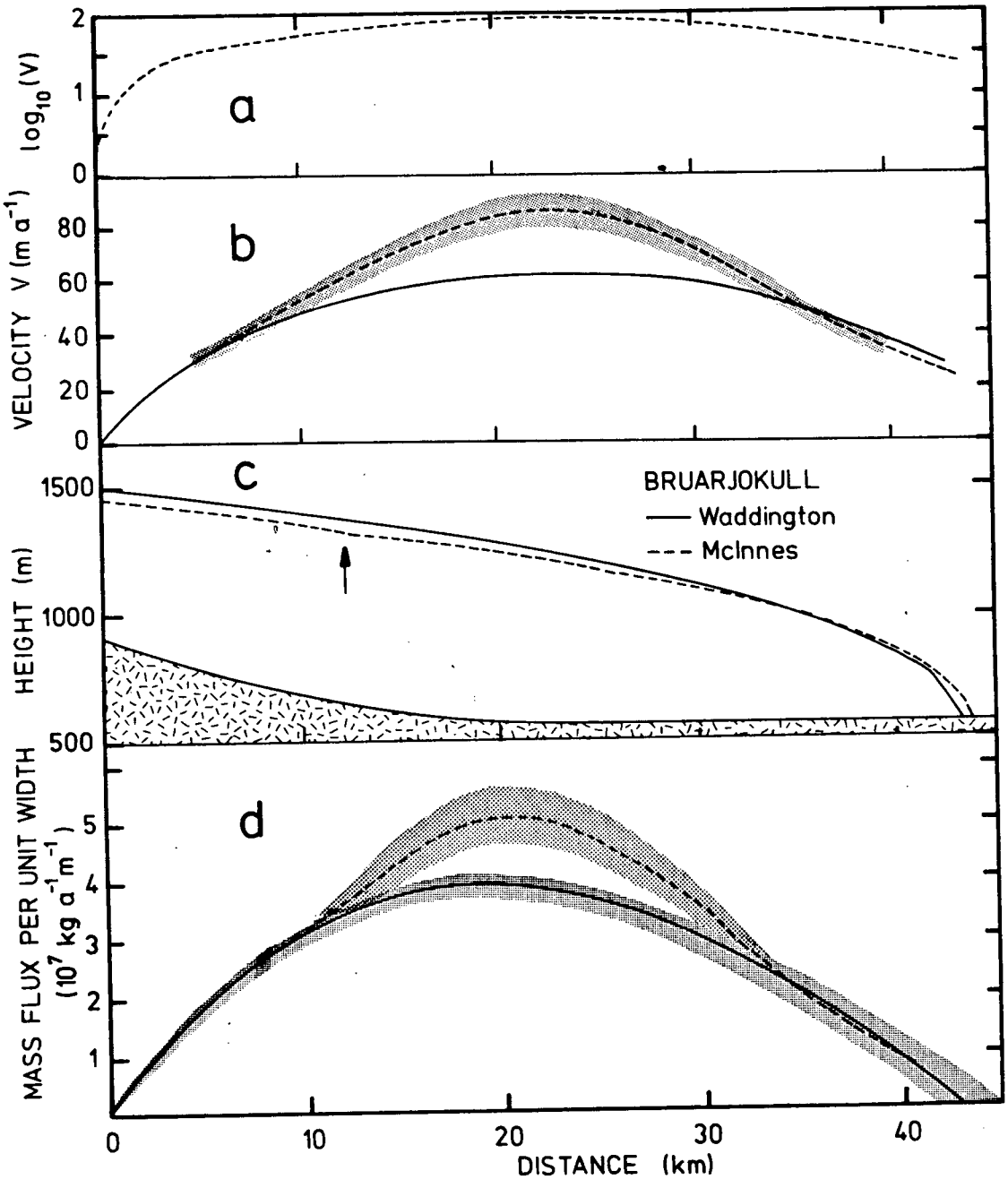
a
b
c
d
log10(V)
VELOCITY V (m a-1)
HEIGHT (m)
MASS FLUX PER UNIT WIDTH (10^7 kg a-1 m-1)
DISTANCE (km)
BRUARJOKULL
Waddington
McInnes
0
1
2
20
40
60
80
500
1000
1500
3
4
5
10
30

$$Q(x) = \rho\, h(x)\, V(x) \qquad \text{(A16.5.1)}$$

should, at steady state, equal the balance flux (A16.4.4), regardless of the flow law or state of sliding. In Figure A16.5 (d), the solid curve is the balance flux (A16.4.4) using the mass balance in Figure A16.4. The limits of the shaded band represent the addition of ±10 cm a^{-1} along the whole glacier length when measuring b(x) from Budd (1975, Figure 5). This is roughly the width of an ink line on the figures. The mass flux (A16.5.1) for my model falls right on the solid curve. The broken curve is the Budd-McInnes model mass flux using the profiles in (b) and (c). The shaded area represents my estimate of ±10% for the maximum total error in measuring V(x) and h(x) from the figures. The Budd-McInnes mass flux is grossly different from the expected curve between 15 and 25 km. This result suggests that the Budd-McInnes model does not conserve mass locally, even in a steady state. This test is independent of the sliding state or flow law used for the glacier simulation.

There are some other possible explanations for the discrepancy:

First, if McInnes actually used a larger mass balance (such as the solid curve in Figure A16.1) rather than the curve which he (p. 107) and Budd (1975, Figure 5) state was used, the balance flux in Figure A16.5 (d) could be increased enough to overlap the mass flux curve.

Second, if the ice velocity or ice thickness profiles in McInnes (Figure 6.15), were incorrectly drawn too large, the

correct mass flux curve (their product) could be reduced enough to overlap the balance flux curve. The cusp at 12 km (arrow) on the ice thickness curve (Figure A16.5 (c)) in fact suggests that there may be a draughting error in the McInnes figure. There are also some apparent contradictions in the text concerning these profiles. The figure caption and the text (p. 109) in McInnes state that the maximum ice thickness was 650 m, but I measured a thickness of 690 m at x=17 km on the dashed curve. The McInnes text also states (p. 109) that the ice thickness in the steady state is less than the thickness observed by Thorarinsson (1969), but Figure 6.13 (McInnes, p. 107) to which McInnes refers, showing the observed elevation from Thorarinsson's (1969) map, has a maximum ice depth of only 570 m. Both in the text (p. 109) and in the caption to Figure 6.15, McInnes stated that the maximum ice deformational velocity was 400 m a^{-1}, but the velocity profile shown does not exceed 90 m a^{-1}.

Because of these apparent unresolved contradictions, I can only conclude that either the Budd-McInnes model works incorrectly for Bruarjökull, or the curves in McInnes (unpublished) or Budd (1975) are inaccurately drawn or incorrectly labelled.

The only other profiles shown by Budd (1975) or McInnes (unpublished) for the Bruarjökull model are in one diagram showing a few profiles during the advance and retreat phases of a surge (McInnes, unpublished, p. 120; Budd, 1975; Budd and McInnes, 1978). These profiles, for $n=1$ bar a and $\emptyset=1.7\ 10^{-4}$ $bar^{-1}m^{-1}a$ would be very difficult to verify because the surge cycle in Budd (1975, Figure 6) does not repeat itself

exactly, and there may be significant model-dependent truncation errors associated with the rapid changes when a surge begins.

A16.6 FEDCHENKO GLACIER: STEADY STATE FLUX

Budd (1975) and McInnes (unpublished) also presented numerical model results for the Fedchenko Glacier. I measured the bed topography and the mass balance profiles from Figure 6.2 of McInnes; this same diagram appears as Figure 3 of Budd (1975). I show these functions in Figure A16.8.

McInnes (Figure 6.10, p. 100) showed the velocity and ice surface profiles for a steady state he obtained for the model, without stating the values he used for the sliding parameters. I have redrawn these profiles as the dashed curves in Figure A16.6 (a) and (c). The ice thickness was exaggerated by a factor of two (McInnes, caption to Figure 6.10). The actual steady state thickness was the curve shown by the dot and dash pattern. The

---

Overleaf:

FIGURE A16.6. Fedchenko Glacier flux test.
The final steady state velocity, ice elevation, and mass flux for the Fedchenko Glacier model of Budd (1975). McInnes plotted the logarithm of ice velocity, reproduced here as curve (a). I have converted this to velocity on a linear scale (broken curve in (b)). The shaded area shows the maximum error limits (±7%) in scaling the velocity from (a). The broken ice surface curve in (c) is redrawn from McInnes (unpublished, p. 100). Because McInnes used a x2 vertical exaggeration, the actual ice surface was the dot-dash line. In (d), the solid curve is the balance flux (A16.4.4) using the mass balance in Figure A16.8. The shaded area indicates the limits of the balance flux due to an estimated maximum error of ±10 cm a^{-1} in measuring the mass balance from Budd (1975, Figure 3). At steady state, the mass flux (A16.5.1) should equal the balance flux. The flux in the Budd-McInnes model is given by the broken curve. The shaded area indicates ±10% error limits due to scaling the velocity and thickness from curves (a) and (c).

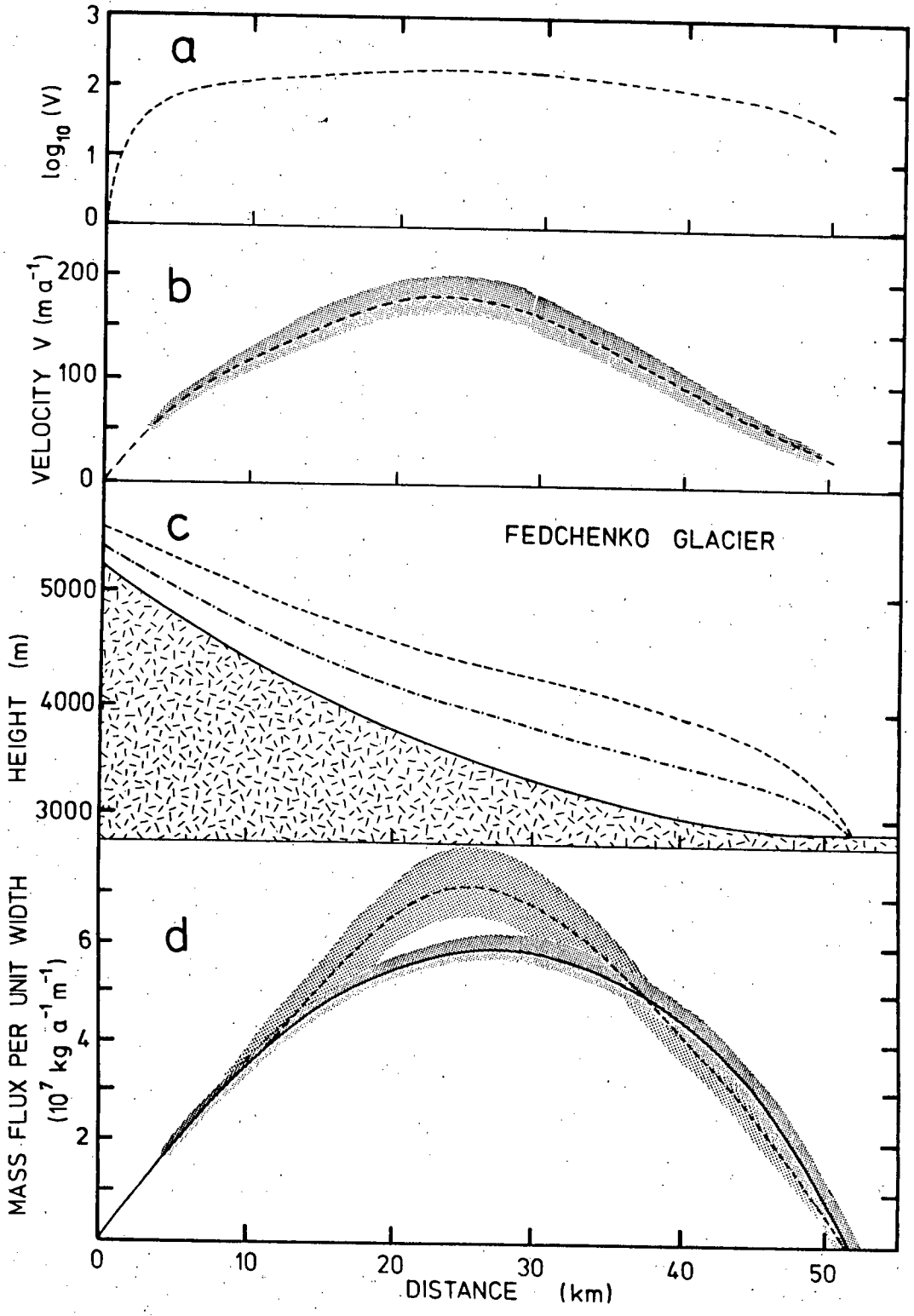
a
b
c
d
FEDCHENKO GLACIER
log10 (V)
VELOCITY V (m a-1)
HEIGHT (m)
MASS FLUX PER UNIT WIDTH (10^7 kg a^-1 m^-1)
DISTANCE (km)
0
1
2
3
100
200
3000
4000
5000
4
6
10
20
30
40
50

shaded band in (b) approximates the error limits (±7%) which I estimated in reading the velocity from (a).

In Figure A16.6 (d), I compare the mass flux (dashed line) using the profiles (b) and (c) to the balance flux (solid curve) obtained by integrating the mass balance from Budd (1975, Figure 3). The shaded bands indicate the maximum error limits associated with measuring V(x), h(x), and b(x) from the Budd and the McInnes figures.

In the central portion of the glacier, the Budd-McInnes mass flux exceeds the balance flux by significantly more than the error limits. Figure A16.6 (d) is remarkably similar to the result (Figure A16.5 (d)) for Bruarjökull, suggesting that the problem lies in the Budd-McInnes computer model itself, rather than in draughting problems or incorrect figure captions. The model does not appear to conserve mass locally, even in a steady state configuration. This test result holds regardless of the flow law parameters, shape factor, or sliding parameters used by Budd and McInnes.

A16.7 FEDCHENKO GLACIER: NONSLIDING MODEL

I then tried to verify the nonsliding steady state of the Fedchenko Glacier model. On Figure 3b of Budd (1975), and Figure 6.2b of McInnes (unpublished), is a profile which I show as a dashed line in Figure A16.7. McInnes (unpublished, p. 88) stated that he used the parameters in Table A16.2 (except for dt), and (p. 91) indicated that the profile redrawn here in Figure A16.7 was the resulting steady state. Budd (1975), however, may have thought that this profile resulted from a nonzero value of $\emptyset$, because his only reference to this profile (p. 13) was

> "...for small values of $\emptyset$ and reasonable n, the ice masses grow up to a steady state as shown, e.g. in Figure 3b."

Assuming McInnes, who ran the models, to be correct, I attempted to duplicate this profile. To get my model runs to reach the steady state length of 52 km as reported by McInnes (unpublished, p. 91), I adjusted the mass balance within the limits of resolution on the published figure (± 10 cm a^{-1}). This procedure has no discernible effect on the thickness profile upstream from the terminus region (see Nye, 1963[a]). I then ran a nonsliding simulation of the Fedchenko Glacier using the parameters in Table A16.2. The resulting set of 50 year profiles is shown in Figure A16.8. In Figure A16.7, the final steady state profile from Figure A16.8 is given by the solid line. It is thicker than the Budd-McInnes profile (dashed curve) by approximately 8% along most of its length. This difference is significantly larger than either the resolution limit on the

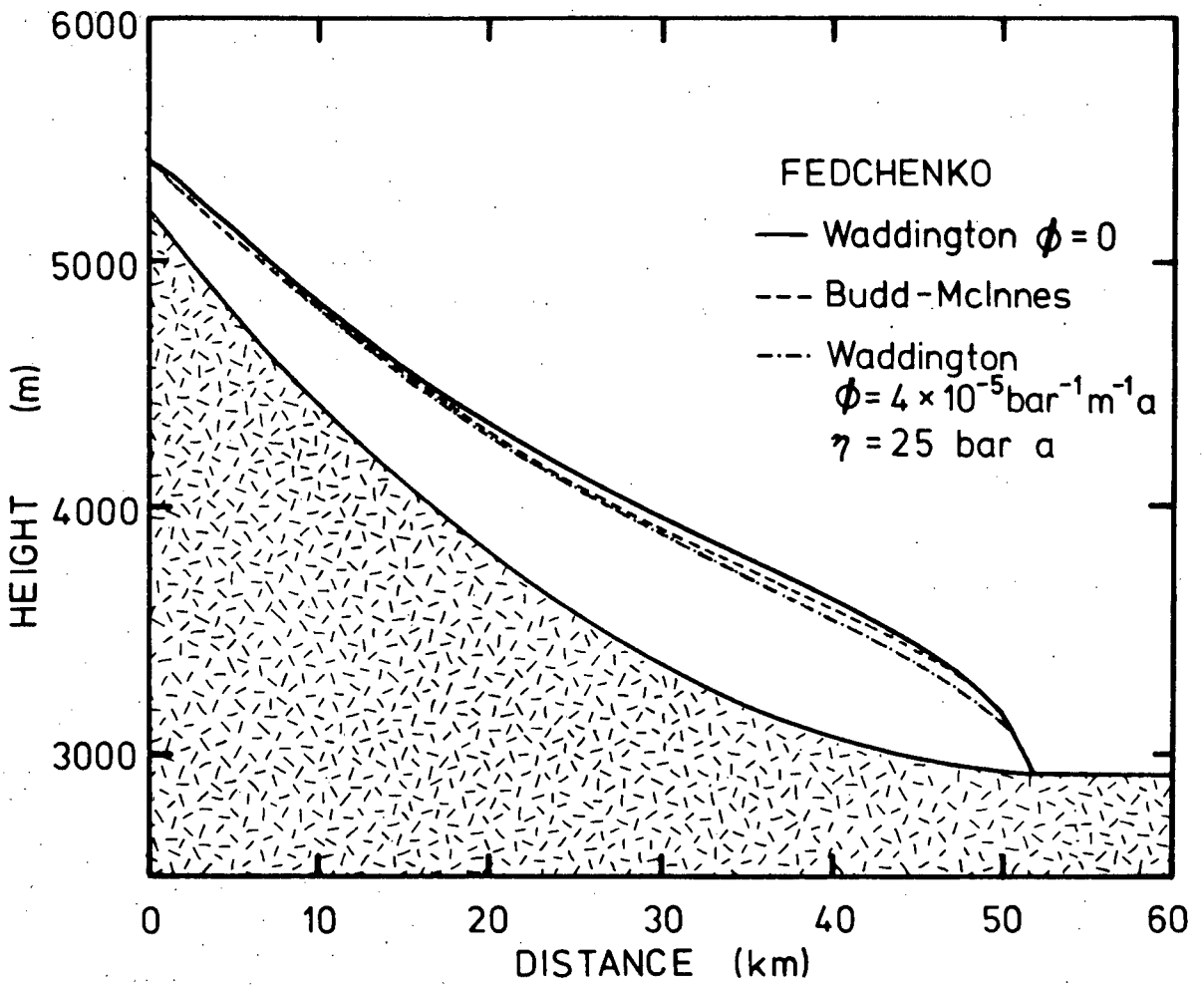

FIGURE A16.7. Fedchenko Steady State Ice Profiles.
The solid line is the final steady state reached by the Waddington model in Figure A16.8. The dashed profile is redrawn from Budd (1975, Figure 3). The dash-dot curve is the steady state reached by the Waddington model with a small amount of sliding (ϕ=4. 10^{-5} $bar^{-1}m^{-1}a$ and η=25 bar a). The flow law parameters n, k, and s are given in Table A16.2.

published diagrams, or the expected truncation error.

Either the Budd-McInnes model does not reach the correct steady state ice thickness, or at least one of the parameters in Table A16.2 is incorrect, due to incomplete or inaccurate documentation in McInnes (unpublished) and Budd (1975). In fact, changing the flow law parameters to

$$n=3 \qquad k=0.15 \text{ bar}^{-3} \text{ a}^{-1} \qquad \text{(A16.7.1)}$$

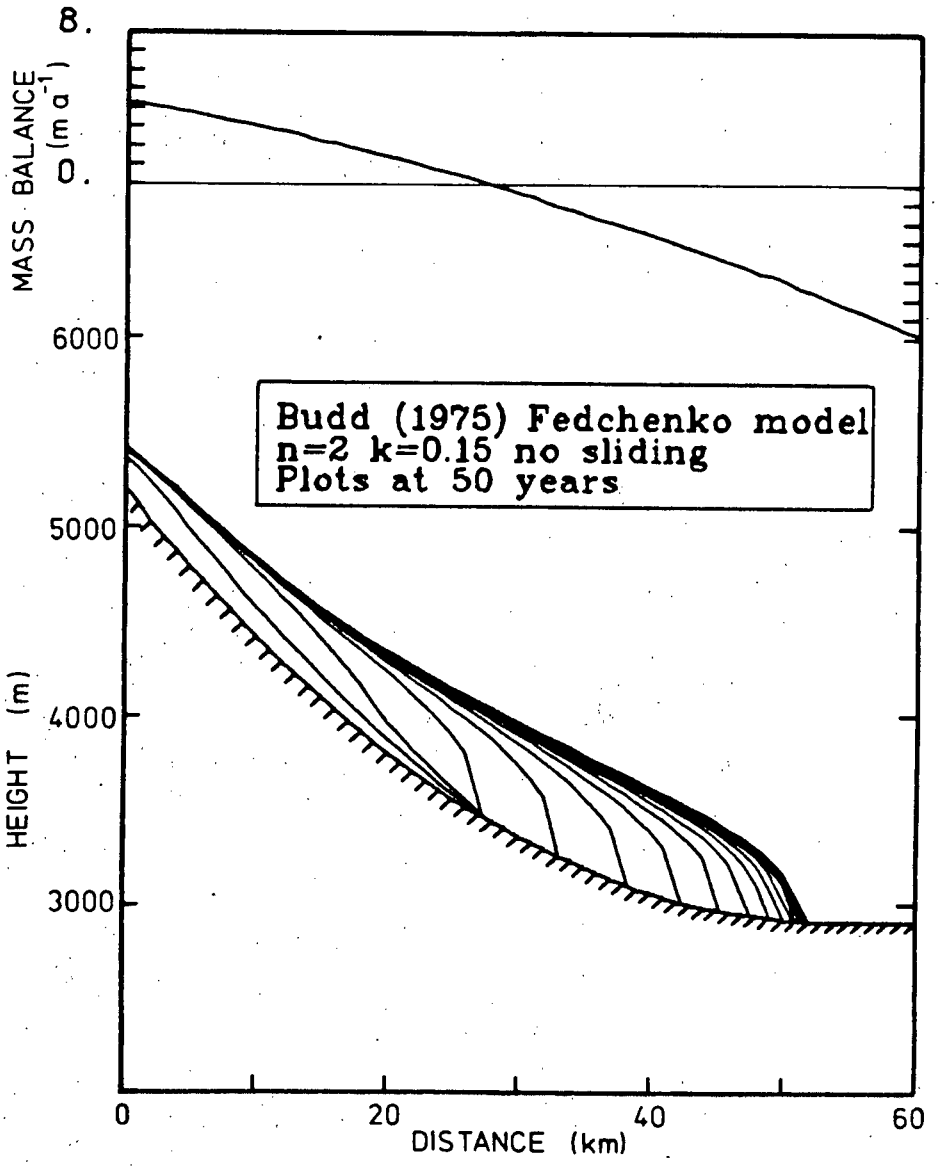

FIGURE A16.8. Fedchenko Nonsliding Model.
Ice surface profiles at 50 year intervals using the Waddington computer model with the parameters in Table A16.2, and the bed and mass balance from Budd (1975) Figure 3.

gave me a model (Figure A16.9) which grew to a steady state matching the Budd-McInnes curve exactly. A model with some sliding ($\emptyset$=4 10^{-5} $bar^{-1}m^{-1}a$ and n=25 bar a) shown by the dot-dash pattern in Figure A16.7 is slightly thinner than the Budd-McInnes profile; presumably a smaller $\emptyset$ or a larger n could

n	k $bar^{-n} a^{-1}$	s	g $m\ s^{-2}$	ρ $kg\ m^{-3}$	Δx m	Δt a
2	0.15	0.7	9.8	910.	1000.	1.0

ϕ $bar^{-1} m^{-1} a$	η bar a
0.	25.0

TABLE A16.2. Parameters for Fedchenko Glacier model.

give a better fit. The only conclusion I can draw from this is the observation that, if Table A16.2 contains the correct parameters, my model disagrees with the Budd-McInnes model; if the values in Table A16.2 are incorrect, then some combinations exist which could give the profile in question.

A16.8 FEDCHENKO GLACIER: DYNAMIC BEHAVIOUR

Because McInnes (unpublished) and Budd (1975) do not show a set of profiles such as Figure A16.8 during the growth to steady state, it is difficult to test the dynamic behaviour of their model. However, they do show (Budd, 1975, Figure 4; McInnes, Figure 5.7, p. 86) a diagram illustrating the change in glacier length, the maximum ice velocity, and the position of the velocity maximum as functions of time. The curves which reach steady state are redrawn as dashed lines in Figure A16.10. I have converted the velocity from a logarithmic to a linear scale; the shaded band approximates the maximum error in reading from the logarithmic scale.

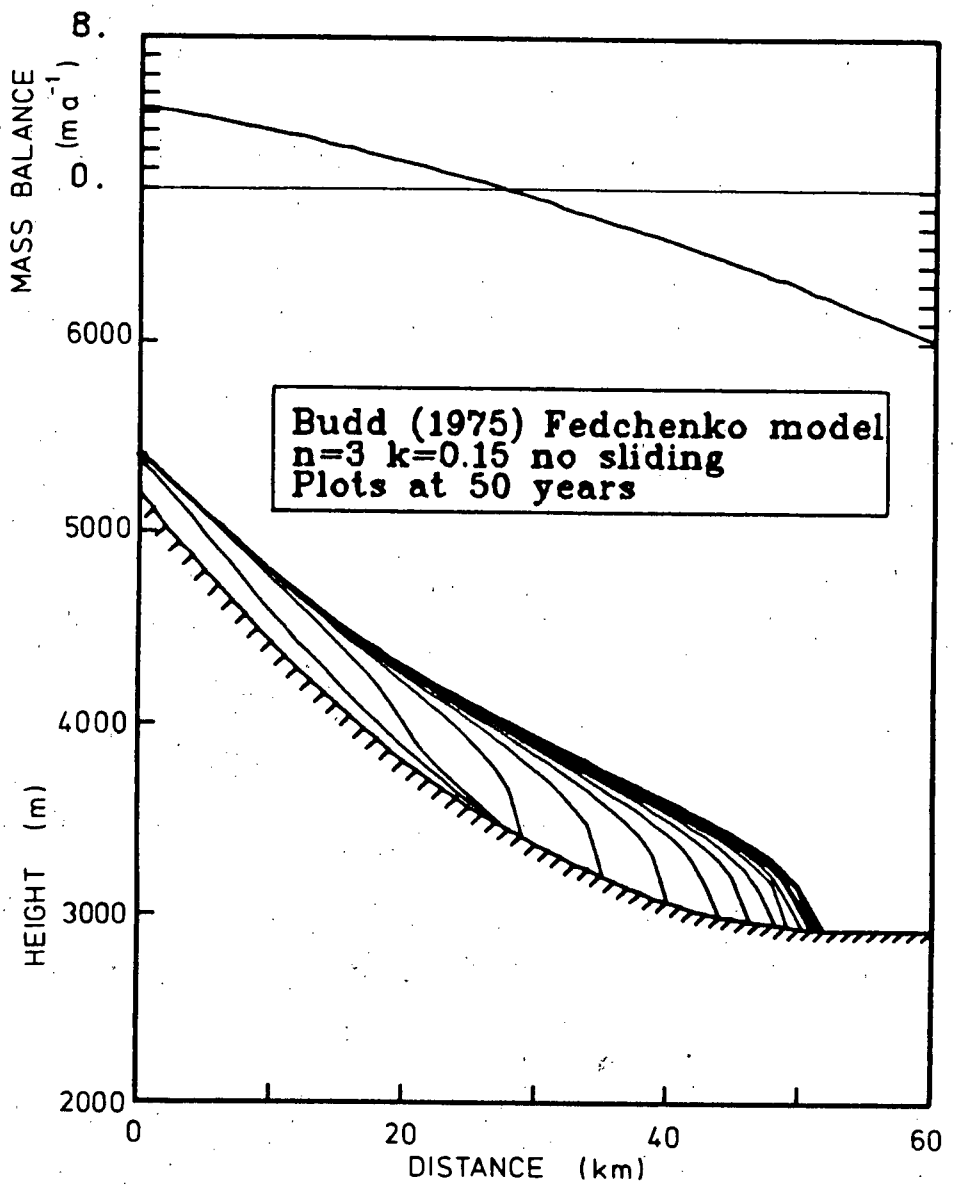

FIGURE A16.9. Fedchenko nonsliding model with n=3. Ice surface profiles at 50 year intervals with n=3 and k=0.15 bar^{-3} a^{-1} and other parameters as listed in Table A16.2.

Neither Budd (1975) nor McInnes (unpublished) state the values of the sliding parameters $\emptyset$ and n used to obtain these functions. Because the maximum velocity reaches a steady state value of 115±10 m a^{-1} which is very close to the value of 112 m a^{-1} in my nonsliding model (Figure A16.8), I began by

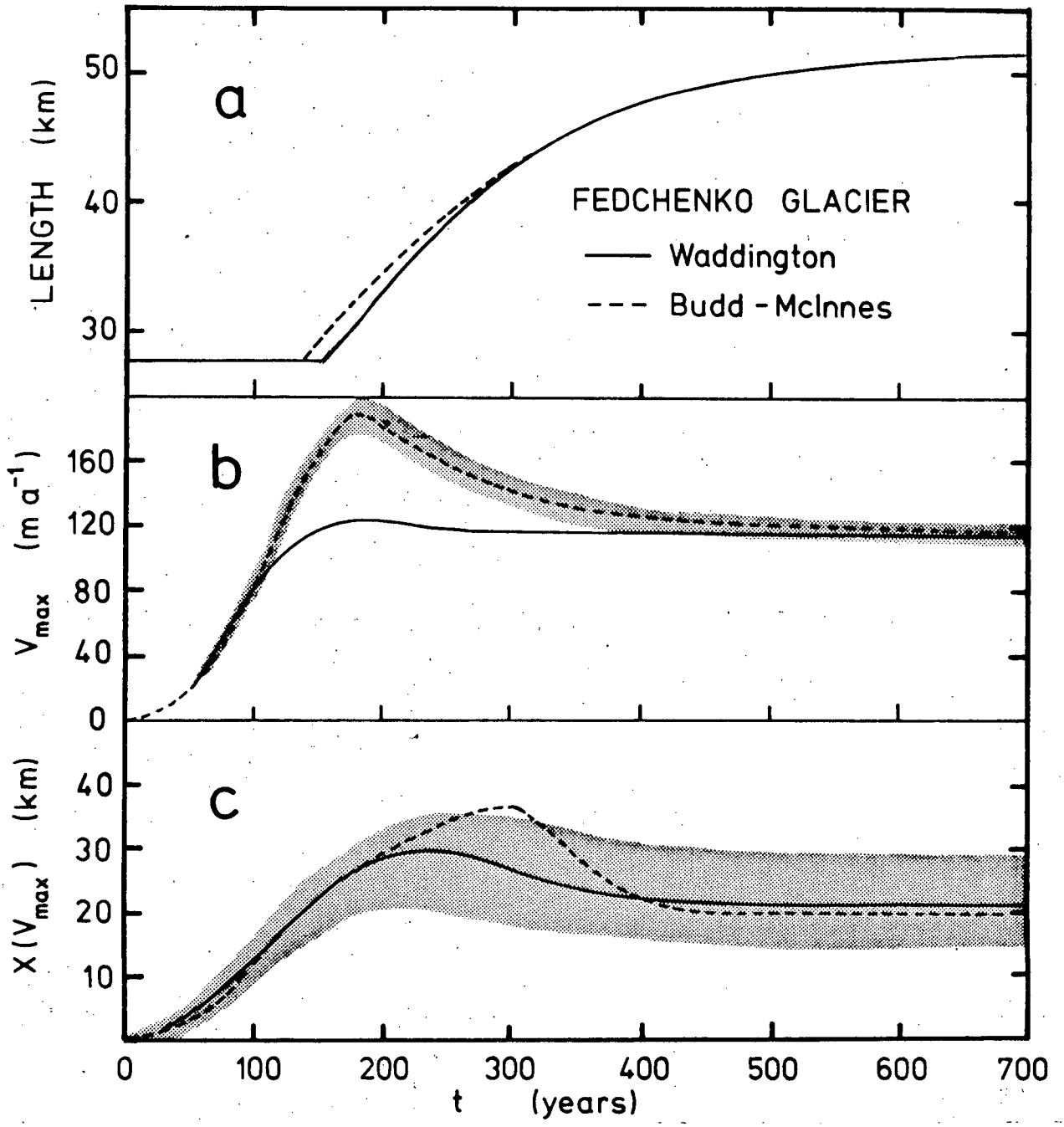

FIGURE A16.10. Growth Of Fedchenko Glacier.
Terminus location, maximum velocity, and position of velocity maximum. The dashed curves are from Budd (1975, Figure 4). The solid curves are from the Waddington model using the parameters in Table A16.2. The shaded band in (b) is the uncertainty in measuring log(V) from Budd. The velocity in the Waddington model was within 5% of the peak value within the shaded band in (c); thus the position of the peak velocity is not a sensitive test. The agreement in velocity at 700 years suggests that the Budd-McInnes curves are also a nonsliding model, but the large velocity during buildup is not present in the Waddington model.

comparing the dashed curves in Figure A16.10 to the corresponding curves (solid) for my nonsliding case using the parameters in Table A16.2. The Budd-McInnes terminus begins to move earlier, and is up to 2.5 km ahead of the terminus of my model. Both models reach the same steady state length. The lack of agreement is disturbing, but it should be noted that different ways of modelling the terminus numerically may give differences in terminus locations which can be of the order of Δx which, in this case, is 1 km.

The maximum velocity curves in (b) differ by up to 50% between 100 and 400 years, although they reach the same steady state value. Because the power of the flow law for ice is low (n=2), substantial differences in ice thickness and slope are required to produce this discrepancy. Either the Budd-McInnes model advances too rapidly (as was also the case for the Vatnajökull model in Figure A16.1) with too high a velocity, or the two models used different parameters for ice deformation and sliding due to incomplete documentation of the curves in Budd (1975, Figure 4) and McInnes (Figure 5.7).

The dashed curve in Figure A16.10 (c) shows the Budd-McInnes position of maximum velocity travelling nearly 10 km farther downglacier and persisting 100 years later than the peak position in my results. However, the velocity peak in my model was nearly constant over a wide distance; the velocity varied by less than 5% from the peak value throughout the shaded band. This test is therefore not discriminating.

The unanswered question about Figure A16.10 is whether Budd and McInnes used parameters different from those in Table A16.2,

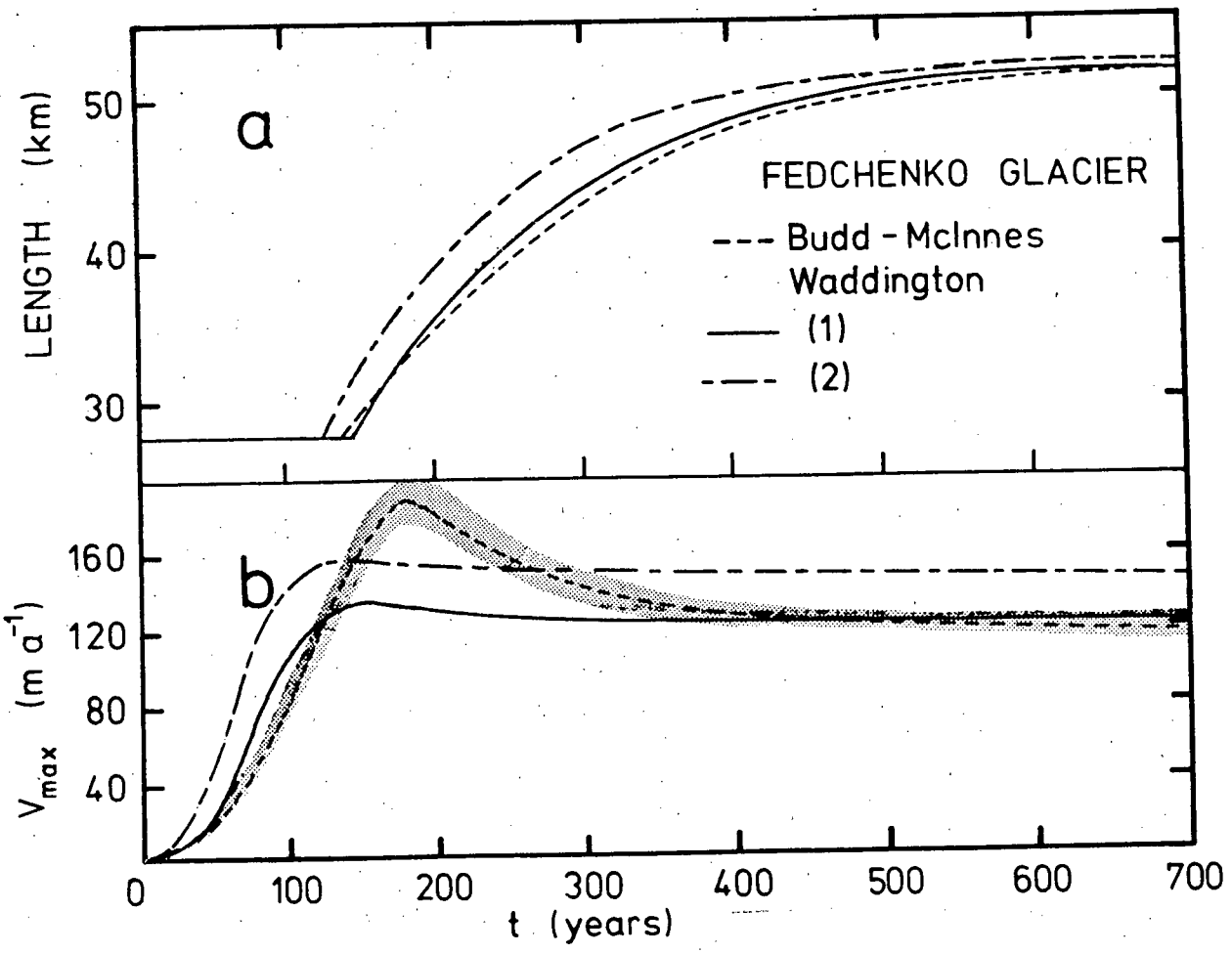

FIGURE A16.11. Fedchenko Growth: Other Nonsliding Models. The terminus position and maximum velocity. The dashed curves are from Budd (1975, Figure 4). The other curves are attempts to match the Budd curves by varying the flow and sliding parameters from the values in Table A16.2. The solid curves (1) are from the n=3 model in Figure A16.9. The double-dashed curves (2) are from a model with $k=0.408$ bar^{-2}a^{-1}.

and whether any possible combination of parameters is likely to give curves resembling the dashed lines in Figure A16.10. It was not feasible to run a complete set of models spanning all possible variations of n, k, s, Ø and ɳ. I did try a few variations, altering at most two of the parameters in Table A16.2 at any one time, and I was able to reach some

conclusions. For the nonsliding case, I was unable to both keep the maximum velocity at steady state down near 115 m a^{-1} and at the same time obtain peak velocities near 190 m a^{-1} during the growth phase. For example, in Figure A16.11, the solid curves (1) are for the model shown in Figure A16.9 with n=3. This model reproduced the Budd-McInnes steady state in Figure A16.7 (dashed curve). However, in Figure A16.11, it does not match the growth functions any better than did the n=2 model (Figure A16.10).

I also tried using a larger value of k. The long-short dashed pattern (2) in Figure A16.11 shows the behaviour of the model with k=0.408 bar^{-2} a^{-1}. The terminus position advances much earlier than the Budd-McInnes terminus, and the steady state maximum velocity (at 700 years) is much larger than the Budd-McInnes value, while the peak between 100 and 200 years is still significantly lower.

It is evident from (A16.2.1) and (A16.2.4) that changing the shape factor s is equivalent to changing k.

Although my tests were not exhaustive, I conclude that it is unlikely that a nonsliding model exists which can match the velocity curve (Figure A16.11 (b)).

To test whether any sliding models can match the dashed curves in Figure A16.11, I have written a computer subroutine to implement the Budd (1975) sliding algorithm. Because the sliding velocity in Budd's formulation depends on the whole glacier profile, it was most convenient to include the contribution due to sliding by explicit terms; i.e. at a given time step, the sliding depends only on the glacier configuration at the old time step. This makes the $O(\Delta t)$ term nonzero in the truncation

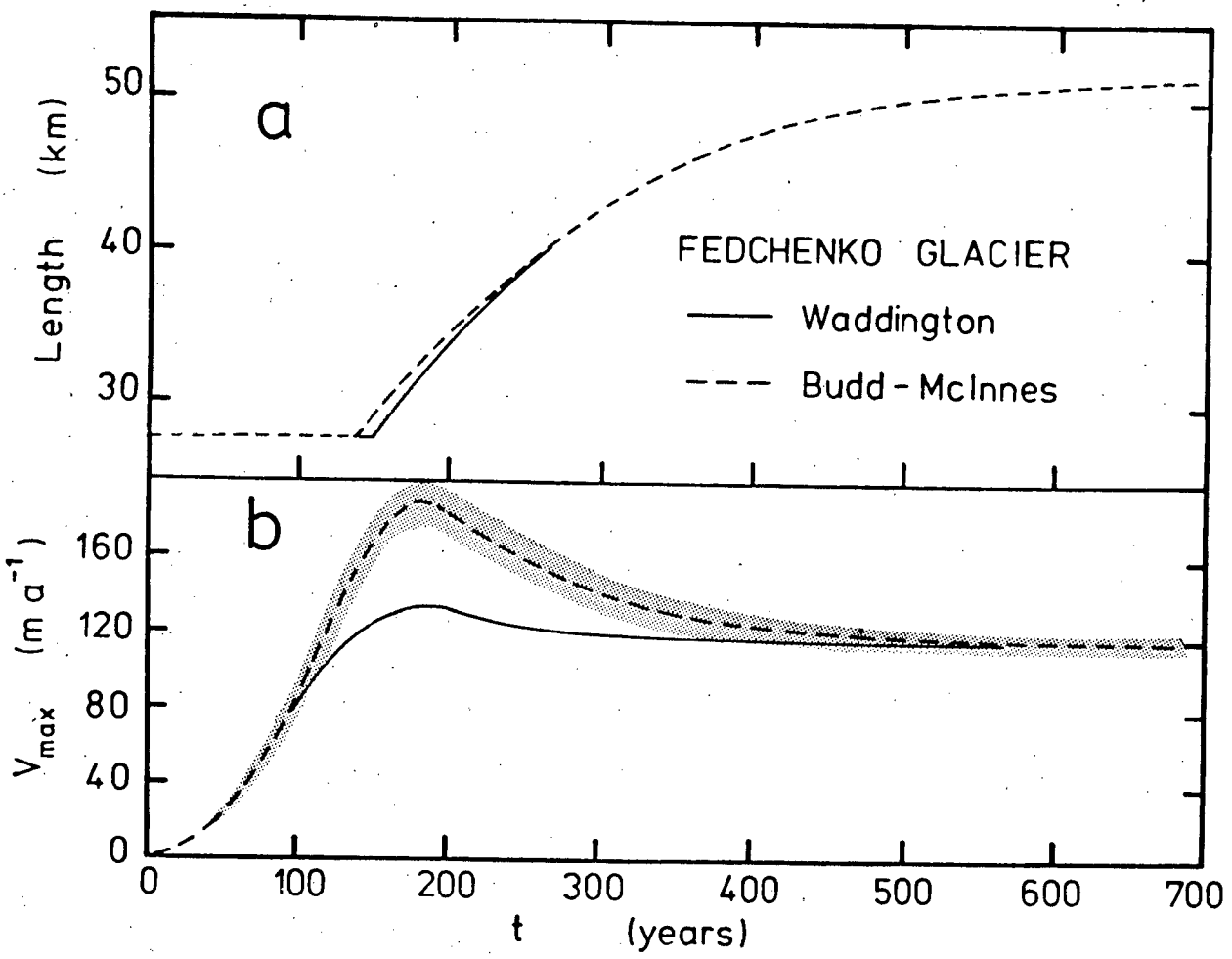

FIGURE A16.12. Fedchenko Growth: Moderate Sliding.
Terminus position and maximum velocity for the growth of the Fedchenko Glacier to steady state for model (1) in Table A16.3. The dashed lines are the Budd-McInnes model. The maximum velocity falls short of the value for the Budd-McInnes model.

error (A1.5.21), forcing the use of much smaller time steps to maintain accuracy. The solid curves in Figure A16.12 give the result with a small amount of sliding ($\emptyset$=4.0 10^{-5} $bar^{-1}m^{-1}a$ and n=25.0 bar a). This model does at least show a peak in maximum velocity at 150 years, although it is not large enough to match the Budd-McInnes curve (broken line).

The broken curve in Figure A16.13 of the $\emptyset$-n plane shows the dividing line which separated surging from steady state

MODEL	ϕ $bar^{-1}m^{-1}a$	η bar a	Δt a
1	$4.0\ 10^{-5}$	25.0	0.1
2	$1.5\ 10^{-4}$	25.0	0.1
3	$5.0\ 10^{-6}$	1.0	0.1
4	$5.0\ 10^{-7}$	0.1	0.1

TABLE A16.3. Parameters for sliding models.
The entries under Δt are the smallest time steps used during the run. Larger values were used during the initial growth (before 100 years) and near steady state (after 300 years).

models in McInnes (unpublished, Figure 6.4, p. 94). A similar figure for the Bruarjökull model can be seen in Budd (1975, Figure 7).

In my attempt to get a high maximum velocity during the glacier advance, I used the values of η and ϕ (2), (3), and (4) in Table A16.3. These points are shown in Figure A16.13. They lie close to the surge-nonsurge transition line; in fact, (4) is in the surge region. The terminus advance and the maximum velocities for these three models are shown in Figures A16.14, A16.15, and A16.16. All three models reached a steady state.

In all three cases, the terminus advanced more rapidly than the Budd-McInnes terminus (broken lines in (a)). The maximum sliding velocity was not a smooth function of time in my simulations; it varied erratically within the the shaded bands in (b) of each figure. Smaller time steps Δt did not reduce the width of the shaded bands. The upper limit of each shaded envelope is compatible with the Budd-McInnes curve (To keep the diagram simple I did not include the shaded band indicating my uncertainty in measuring their curve. It can be seen in

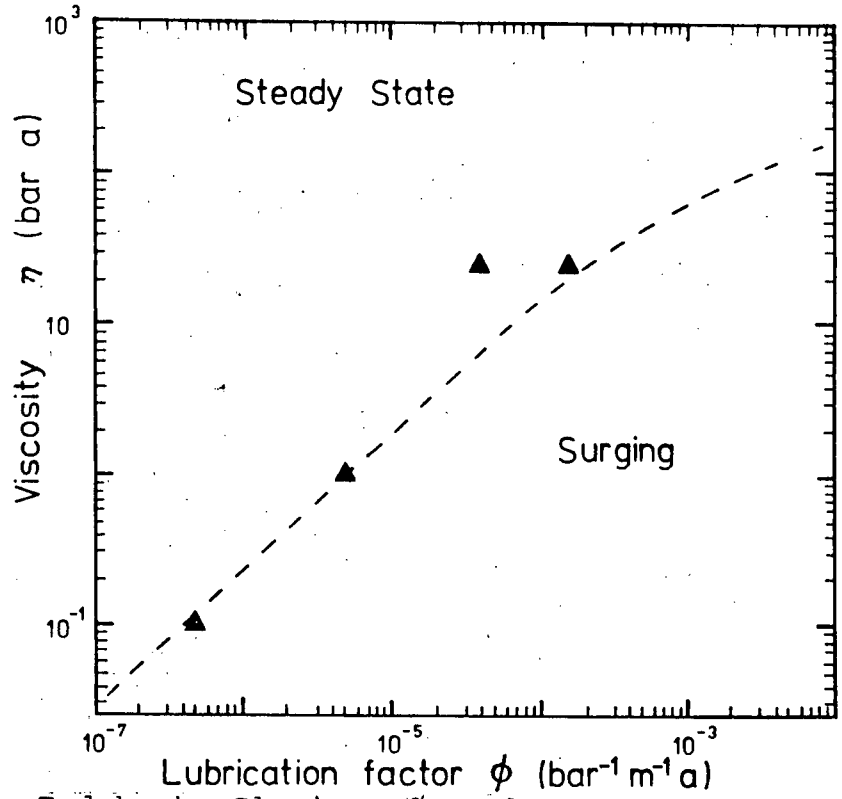

FIGURE A16.13. Fedchenko Glacier: ϕ-η Plane.
The broken line is the boundary between surging and steady state glaciers from McInnes (unpublished, Figure 6.4). The triangles are models reported in this appendix; all reached steady state.

Figure A16.10 (b)). However, the erratic variations in maximum velocity appear to be a purely numerical effect resulting from insufficient spatial sampling. I used a grid spacing of Δx=1 km, because McInnes (unpublished, p. 88) used this value. At each time step, the position and angle of the glacier model terminus are chosen so as to conserve mass; they are not chosen to maintain a constant or well-behaved basal shear stress τ_c (A8.3.2). As the terminus advances and adds meshpoints or alters the angle beyond the last meshpoint (Section A1.3.4), the basal shear stress τ_c near the terminus also varies, in a manner that bears little relationship to the forces acting on the glacier upstream. Unfortunately, the shear stress τ_c near the terminus

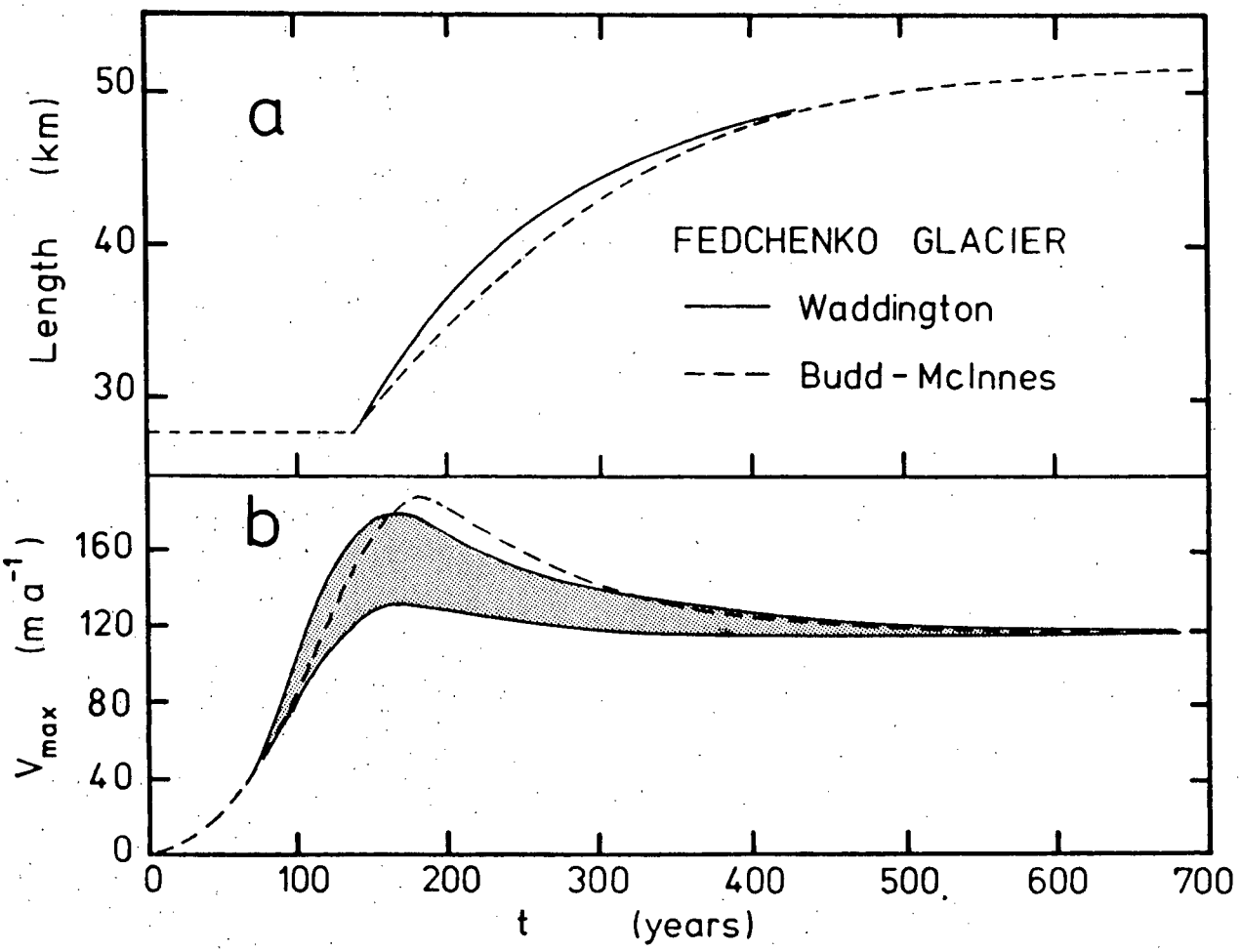

FIGURE A16.14. Fedchenko Growth: Sliding Model (2). Terminus motion (a) and maximum velocity (b) for model (2) in Table A16.3. The curves from Budd (1975) are shown by broken lines. The maximum velocity varied erratically throughout the shaded region because the mesh interval of 1 km (used by both Waddington and Budd (1975)) was too large for accurate stress estimates near the terminus. The correct curve is probably near the lower limit of the shaded zone. My estimated uncertainty in drawing the Budd curve is shown in Figure A16.10 (b).

then affects Budd's local basal shear stress τ_b (A8.3.4) through the average value $\overline{\tau_c}$ in equation (A8.3.4). Each time that the basal stress τ_b is altered by a terminus change of this type, unbalanced longitudinal forces are created in the computer model, and the glacier adjusts to the new stress conditions by

rapid sliding. The effect should be reduced by repeating the calculations with a smaller grid interval (e.g. 500 m or 250 m) to minimize the contribution of the point nearest to the terminus.

If this interpretation of the variance in the maximum velocity is correct, I expect that the maximum velocity should stay near the lower boundary of the shaded bands in Figures A16.14 through A16.16. In Figure A16.15 (c), I show the maximum velocity curve for model (3) of Table A16.3 when Δx was reduced by a factor of four, i.e. to 250 m. The velocity maximum for this case falls within a much narrower band, indicated by the shaded region, and this band lies along the lower boundary of the region in Figure A16.15 (b). This substantiates the hypothesis that the large velocities were caused by a spatial numerical truncation error. It is possible that a similar truncation error causes or contributes to the large velocity during the advance of the Budd-McInnes model (e.g. broken curve in Figure A16.10 (b)). If the rapid sliding is in fact being driven by numerical truncation errors at the terminus as a

---

Overleaf:

FIGURE A16.15. Fedchenko growth: sliding model (3).
Terminus motion (a) and maximum velocity (b) for model (3) in Table A16.3. The curves from Budd (1975) are shown by broken lines. The maximum velocity varied erratically throughout the shaded region because the mesh interval of 1 km (used by both Waddington and Budd (1975)) was too large for accurate stress estimates near the terminus. When Δx was reduced to 250 m (a factor of 1/4), the erratic variations of the maximum velocity were restricted to the shaded region in (c). The correct curve is probably near the lower limit of the shaded zone. My estimated uncertainty in drawing the Budd curve is shown in Figure A16.10 (b).

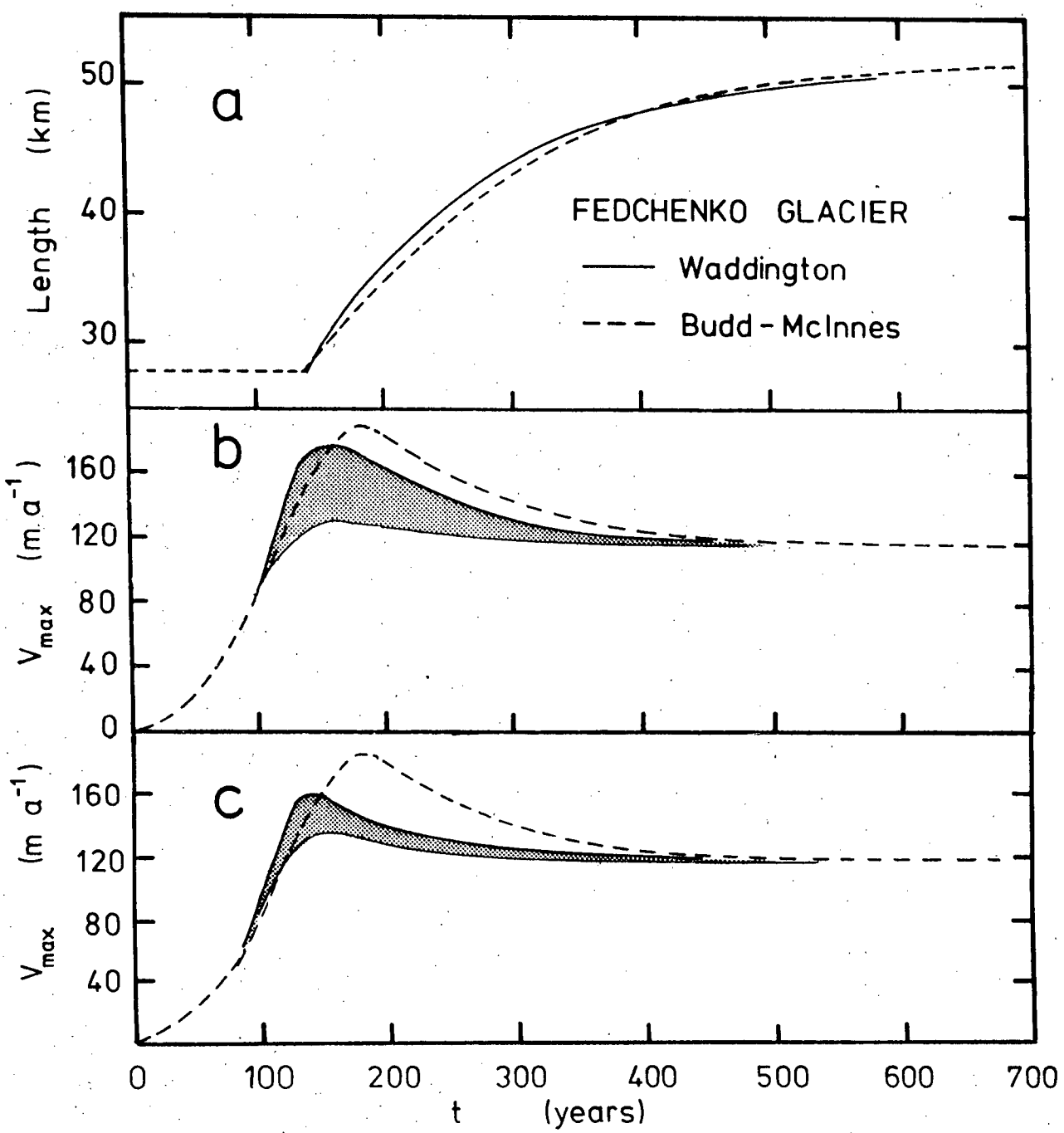
a
b
c
FEDCHENKO GLACIER
Waddington
Budd - McInnes
Length (km)
50
40
30
V_{max} (m a^{-1})
160
120
80
40
0
0
100
200
300
400
500
600
700
t (years)

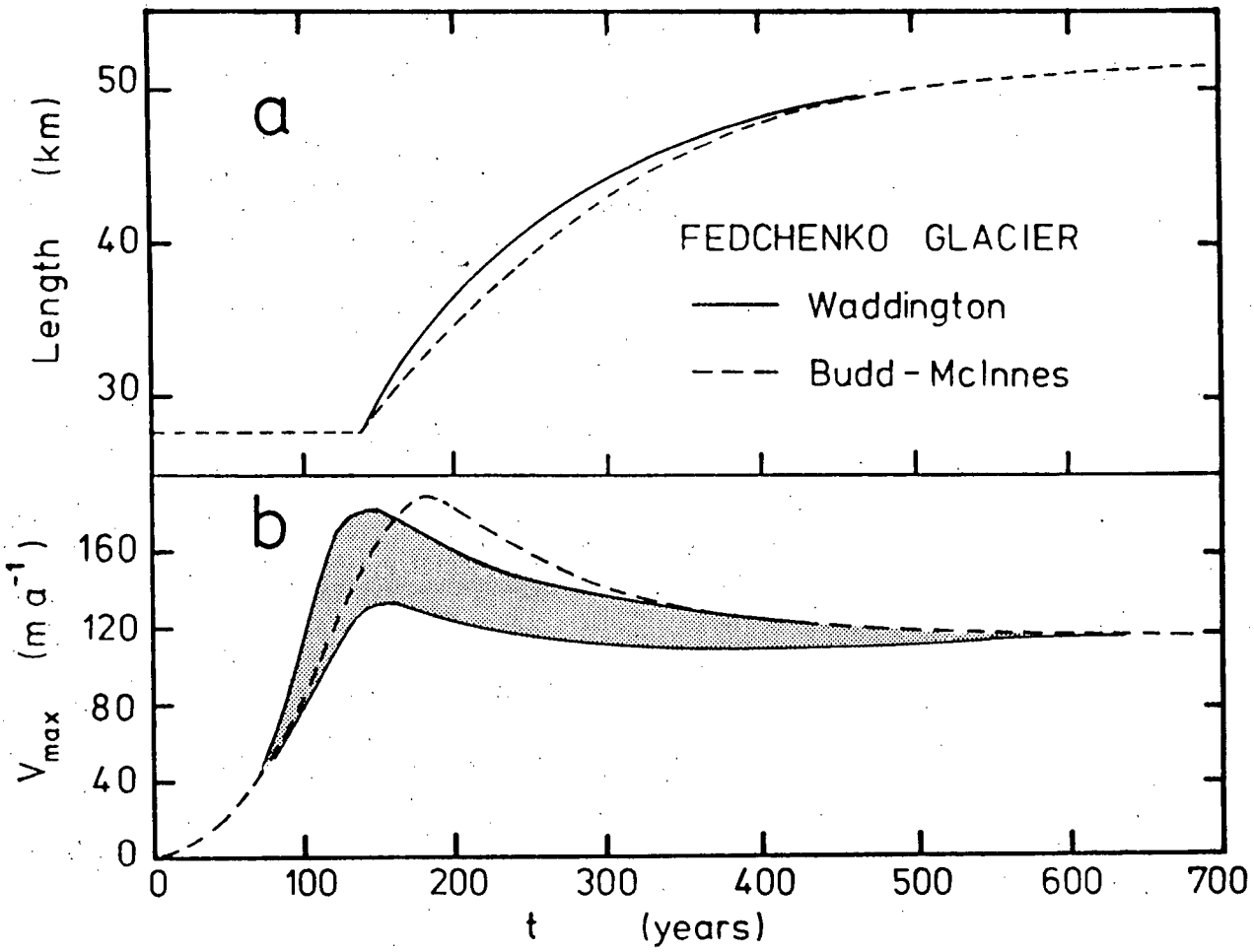

FIGURE A16.16. Fedchenko Growth: Sliding Model (4). Terminus motion (a) and maximum velocity (b) for model (4) in Table A16.3. The curves from Budd (1975) are shown by broken lines. The maximum velocity varied erratically throughout the shaded region because the mesh interval of 1 km (used by both Waddington and Budd (1975)) was too large for accurate stress estimates near the terminus. The correct curve is probably near the lower limit of the shaded zone. My estimated uncertainty in drawing the Budd curve is shown in Figure A16.10 (b).

result of using a large grid interval Δx, then the surge-nonsurge transition line from McInnes (unpublished, Figure 6.4) shown in Figure A16.13 is incorrectly placed; it should be further to the right.

The possibility also exists that the surging instability in

the Budd theory (1975) is so sensitive to details of the numerical schemes at the glacier terminus, that only qualitative comparisons are possible, i.e. none of our numerical models is adequate to quantify the Budd surge mechanism.

Although I may have overlooked some possible combination of parameters, it appears unlikely that I could find a model to duplicate the Budd-McInnes Fedchenko Glacier growth to steady state. The terminus advance rate is best matched by nonsliding models, while the peak velocity during the advance stage appears to require significant sliding, if it can be duplicated at all.

A16.9 CONCLUSIONS

There are several indications that the Budd (1975) and McInnes (unpublished) computer model has serious flaws. I was unable to find any tests which indicated that it works correctly:

The instability problem was pointed out by McInnes (p. 58), but, following Budd and Jenssen (1975), was incorrectly attributed.

The mass flux-balance flux tests (Figures A16.5 and A16.6 suggest that the model creates mass on the local scale at a rate of about 25% of the mass balance.

The profiles shown for the Vatnajökull model (Figure A16.1) suggest that the model creates mass globally during times of active flow.

Figure A16.1 and Figure A16.10 suggest the possibility that the Budd-McInnes model may on occasion advance much too quickly

due to purely numerical effects. This would be an unfortunate characteristic for a computer model designed to verify a physical mechanism of triggering glacier surges.

For one of the few profiles with an apparently complete set of parameters given (McInnes, p. 88), my well-tested computer model found a steady state thickness 8% greater than the one shown by Budd (1975, Figure 3) and by McInnes (p. 90).

Curves in Budd (1975, Figure 4) and in McInnes (unpublished, p. 86) showed terminus position and maximum velocity for the Fedchenko Glacier during growth to a steady state. The documentation of all the physical parameters was incomplete. Using my computer model, I was unable to find any combinations which could match the Budd-McInnes curves. Although my search was not exhaustive, due to other time and computational commitments, I covered the most probable areas of the $\emptyset$-$_n$ plane.

It is possible that rapid sliding in the computer model is triggered or driven by a numerical truncation error resulting from the the coarse mesh interval (1000 m). This possibility is being tested further.

Verification of the accuracy of the Budd-McInnes model is made difficult by incomplete documentation of the numerical values of the physical parameters used for the published model results. However, the tests I have been able to devise indicate that, if the existing documentation is accurate, the model has serious deficiencies. These problems may cause it to give incorrect results which at first glance appear to be "physically reasonable", but which may be no more accurate than intuition.

The surge model proposed by Budd is a useful addition to our concepts of glacier sliding. However its numerical confirmation remains to be conclusively demonstrated.

APPENDIX 17: FOUR CENTURIES OF GLACIER FLOW THEORY

> "Yes, that's all very well, but which really advanced further in four hundred years, the glacier ice or the theory?"[1]

A17.1 INTRODUCTION

Our contemporary understanding of glacier flow has been formed mainly in the past three decades, as a result of several important developments. Nye (1951, 1952[a], 1957) established continuum mechanics and mathematical methods as indispensible research tools. Glen (1952, 1955, 1958) determined a realistic flow law for ice, following the general realization (Orowan, 1949) that metallurgical research could shed light on the constitutive relations of ice. Deep ice coring techniques (Hansen and Langway, 1966) and radio-echo sounders (Evans, 1963) gave another dimension to data acquisition. Nonetheless, this should not obscure the fact that inquiries into the causes of glacier flow date back four hundred years. In this appendix, I outline some of the major questions, controversies, and results in the period prior to the rapid developments in the years 1950-1981. In Section A17.2, I outline some of the better-known writings prior to 1840. Studies on glaciers by Louis Agassiz in that year marked a transition point. In Section A17.3, I summarize the observations and theories in the period 1840-1915, when physical scientists dominated research on glaciers. In Section A17.4, I describe the period 1915-1953, in which

---

[1] an anonymous (and disrespectfully impudent) colleague.

glaciological research (with some important exceptions) was often descriptive and sometimes speculative; the physics of ice flow was occasionally ignored when many research programs were geologically or meteorologically oriented.

This history may show a bias toward English language sources; some German language sources were difficult to obtain.

A17.2 THE YEARS 1570 TO 1840

A17.2.1 EARLIEST PIONEERS

One classical view (based on limited observation and no knowledge of thermodynamics, e.g. Muraltuf, 1669) held that glaciers were not ordinary ice, but a form of rock crystal like quartz. One of the early scientific writers on glaciers was Simler (1574), who realized that glaciers resulted from snow accumulation. He made a clear distinction between neves and glaciers; glaciers had the ability to carry material downslope. Hottinger (see de Beer, 1950) in 1703 observed the stratification of glaciers, and advances and retreats of glacier termini. Scheuchzer, a physicist from Zurich, was one of the early glaciologists to make an impression on Louis Agassiz. Scheuchzer (1723) also discussed glacier stratification and the forward motion of glacier termini. He related the opening of crevasses to gas bubbles and temperature changes. Scheuchzer first proposed the dilatation theory of glacier flow. Agassiz adopted this theory in 1840, but later realized it was incorrect. According to the dilatation theory, melt water flowed

into the interstices and cracks in the ice each day, then froze at night. The volume expansion upon freezing then pushed the lower tongue of the glacier forward.

Gruner (1760) may have been the first to realize that melting takes place almost entirely on the lower reaches of alpine glaciers. He was also the first to suggest that glaciers move forward by sliding on their base. His ideas on glacier growth were incorrect. He thought accumulation of ice was primarily caused by water which filled crevasses, then spilled out over the surface and froze there.

A17.2.2 H. B. DE SAUSSURE

One of the earliest comprehensive studies of the glaciers of the Alps can be found in Voyages dans les Alpes by H. B. de Saussure (1779-96). This work, in four volumes, is a marvellous natural history covering geology, glaciology, meteorology, and geography of the Alps. De Saussure (Vol. 1, Section 523) obtained a lower limit on the thickness of the Mer de Glace at Chamonix by observing crevasse depths. He favoured the sliding theory of Gruner, but Forbes (1859, p. 97-101) was convinced that de Saussure and Gruner thought of glaciers as rigid blocks, rather than as viscous fluid or plastic solids. De Saussure assigned too large a role to the geothermal heat flux when he considered ablation, but correctly identified solar radiation, warm wind and rain as other important melting agents (Vol. 1, Section 531-34).

De Saussure also investigated glacial moraines (Vol 1, Section 536) and had the idea of using them to determine the history of advance and retreat of valley glaciers. However, he thought that the huge erratic boulders on the Swiss plain were deposited by water currents rather than by glacial ice (Vol. 1, Section 210-13).

De Saussure was one of the first to visit the upper reaches of glaciers and to write about his observations there. He was the first to use the term 'seracs' (a name for a local cheese) for the large blocks of ice and firn seen in icefalls (Vol. 4, Section 1975), and, by observing the annual layering exposed in them, was able to correctly describe the transition from snow through firn to glacier ice. He also described glacier tunnels and correctly assigned their formation to meltwater and warm valley winds.

De Saussure was apparently the first to describe 'red snow', which we now know to be caused by blue-green algae. From chemical tests of samples, he reached the correct conclusion (Vol. 2, Section 646) that the colour was due to organic matter, although he tentatively identified it as pollen (Vandalism is not a new problem; one of his early sample collecting trips on Mont Brevent ended when someone stole the cloth filter in which he was melting some red snow).

The earliest writer to suggest that ice flowed as a viscous or ductile substance, in spite of the apparent rigidity of small specimens, was Bordier (1773). In his book entitled Picturesque journey to the glaciers of Savoy, he observed that ice behaved like "softened wax, flexible and ductile to a certain point",

which flowed downward "after the manner of fluids" (quoted by Tyndall (1874, p. 157)).

Hugi (1830) made one of the earliest measurements of glacier motion. In 1826, he built a stone shelter on the medial moraine of the Finsteraar and Lauteraar Glaciers, right at their confluence. In 1830, he found that the hut had moved 30 m downstream. In 1836 (Agassiz, 1840, p. 150) Hugi found that it had moved a further 650 m, and in 1839, Agassiz (1840) found it 1350 m from its starting point.

A17.2.3 RENDU

Rendu, a Catholic priest who subsequently became Bishop of Annecy, presented a paper entitled 'Theorie des glaciers de Savoie' to the Royal Academy of Savoy in 1841 (Rendu, 1841, 1874). He pointed out the similarities of glacier and river flow, and predicted that a glacier should move most rapidly (1) at the surface and (2) near the centre of the channel. His measurements of the displacement of surface features substantiated the second prediction (Tyndall, 1874, p. 159). Rendu attributed to ice

> "a kind of ductility which enables it to mould itself to its locality, to thin out, to swell, and to contract as if it were a soft paste"

(quoted by Tyndall, (1874, p. 159)), and postulated that ice could fracture and flow when the pressure exceeded a certain amount. He realized that further experiments to measure the solidity of ice were necessary (Tyndall, 1896, p. 302). We now

know that the plasticity of ice depends on the stress deviator, rather than on pressure. Rendu's appreciation of the importance of stress was a major advance, but the misconception about the role of hydrostatic pressure persisted into the twentieth century.

A17.3 1840 TO 1915

A17.3.1 LOUIS AGASSIZ

The decade 1840-1850 saw the beginnings of experimental glaciology. As Tyndall expressed it (1874, p. 160):

> "In science thought, as far as possible, ought to be wedded to fact. This was attempted by Rendu, and in great part accomplished by Agassiz and Forbes."

In 1840, Louis Agassiz published Etudes sur les glaciers. This book was a landmark for glacier research. For several years, Venetz (1830, 1833) and de Charpentier had been formulating 'the Glacial Theory', i.e. the idea that the glaciers of the Alps had previously been much more extensive, and were responsible for the striae, erratic boulders and morainic ridges of the Jura and the Swiss plain. Agassiz published these ideas together with his own observations on glacial geomorphology and glacier flow. In the concluding chapter of the book, Agassiz became highly speculative; he thought that the ice age preceded the uplift of the Alps, and that this subsequent uplift, combined with the heat from new species of warm-blooded animals, caused the disintegration of

the ice sheet (Agassiz was not well versed in thermodynamics). This idea was justifiably attacked by the leading geologists of the day, Leopold von Buch, and Elie de Beaumont. The controversy tended to put the whole work into question. This was unfortunate, because when Agassiz controlled his exuberance and wrote about his own observations, his work was logical and organized. Prior to 1840, Agassiz had devoted most of his effort to geomorphology; he had spent very little time observing glacier flow. Agassiz originally accepted Scheuchzer's dilatation theory, and this assumption led him into several pitfalls. Since there was more meltwater near glacier margins than in the centre of the channel, and, often, more crevasses as well, Agassiz (1840, p. 86) assumed that glaciers flowed most rapidly near their edges. He also thought that glaciers did not flow in winter when there was little or no meltwater (1840, p. 212). When basal meltwater was present, Agassiz thought that the basal ice could flow down the slope more rapidly than the surface ice. This improbable pattern of deformation, called 'extrusion flow', was to reappear a century later. To Agassiz' credit, he himself corrected some of these errors. His stake network on the Aar Glacier in 1841-42 moved during the winter, and transverse lines became convex downstream (Carozzi, 1967, p. xxx; Tyndall, 1896, p. 273). Between 1840 and 1847, when he published his second book Nouvelles études et expériences sur les glaciers actuels, he conducted one of the first extensive and scientific observation programs on glacier movement. By 1847, he was aware that his extrusion flow idea was mere conjecture (see Battle, 1951). Joint observations by Agassiz and

Forbes (Forbes, 1845, p. 441; 1859, p. 69) revealed that the velocity at the glacier surface tended to be largest near the firn line; it did not increase monotonically from bergschrund to terminus as the dilatation theory predicted. Agassiz also came to realize (Tyndall, 1874, p. 156) that temperate glaciers could not extract heat from water in deep cracks to cause it to freeze as the dilatation theory required, because the ice was already at the melting point.

A17.3.2 J. D. FORBES

In 1841, Agassiz invited J. D. Forbes, professor of natural history at Edinburgh, to join him at the Aar Glacier. Forbes became interested in glacier flow, and introduced accurate surveying techniques to glacier observations. Forbes (1845) compiled the first accurate topographic map of a glacier and its surroundings; his map of the Mer de Glace at Chamonix has been used as baseline information for modern studies. Forbes made detailed observations of ablation rate and of glacier motion, detecting movement over times as short as one hour (1845, p. 133), and showing that the ice generally moved steadily (1845, p. 444), rather than with a stick-slip motion. In 1842, at the Mer de Glace, he confirmed Agassiz' observation (at the Aar) that the ice at midchannel flowed more rapidly than marginal ice; their results were published nearly simultaneously.

Forbes was the first structural glaciologist. He noticed

and investigated the foliation of glacier ice (1845, p. 162). He found narrow bands of hard, clear ice a few centimetres thick, alternating with bands of bubbly ice; he called this "the ribboned structure" or "the veined structure" of glaciers. From investigations on the Mer de Glace, Forbes saw that the ribboned structure formed spoon-shaped surfaces, concave upward, and dipping upglacier. He realized (1845, p. 402) that the ribboned structure was not stratigraphic, but was caused by, and could be used to map the glacier flow. Describing these structures, he wrote (1845, p. 406):

> "their figure at once gives the idea of fluid motion, freest in the middle, obstructed by friction towards the sides and bottom;"

He suggested (1845, p. 406) that the hard clear bands represented crevasses which had filled with meltwater, frozen, and been stretched by differential flow (this is partially correct; foliation can also arise from recrystallization and redistribution of bubbles (Sharp, 1960, p. 57), and foliation often extends to greater depths than crevasses). He pointed out (1845, p. 27 and p. 438) the similarity between foliation and slaty cleavage in metamorphic rocks.

Forbes is associated with "the viscous theory" of glacier flow, although a concise statement of this theory is elusive even now. Forbes frequently emphasized the viscous or plastic nature of glacier flow (he did not differentiate the two; continuum mechanics was an unknown field in 1845). His observations of differential motion, even in areas free of crevasses (1845, p. 438) led him to conclude of glaciers, that (1845, p. 445):

> "the extreme inequality of motion of the central and lateral parts of glaciers is the best direct proof of the very considerable plasticity of their mass;"

Forbes reproduced some features of large scale flow patterns by using plaster of Paris scale models of glaciers; these models developed differential flow, crevasses, and foliation (1859, p. 77). He also commented on similarities between glacier flow and the flow of lava at Mt. Etna and Mt. Vesuvius (1859, p. 82). In this sense, the viscous theory was, as Tyndall pointed out (1896, p. 311), not a theory at all, but a statement of uncontested facts. On several occasions Forbes appears to have changed his views concerning the the details of the way in which ice flowed in a viscous manner. In his discussion of the viscous theory in Travels through the Alps of Savoy (1845) he considered the flow pattern of a glacier as a whole; he did not state that ice, on the scale of hand specimens, or individual crystals, was necessarily viscous or isotropic. Yet, in 1855, Forbes stated:

> "the viscosity, though it cannot be traced in the parts if very minute, nevertheless exists there, as unequivocally proved by experiments on the large scale".

(This conclusion may appear to strain the use of the scientific method!) Yet, on other occasions, Forbes invoked physical processes other than microscopic viscous flow. In Travels ... (1845, p. 428), he described glacier ice as a mixture of ice, water, and cracks, undergoing melting, freezing, and relative motion, and in Occasional papers on the theory of glaciers, (1859, p. 47), Forbes, discussing the apparent lack of ductility of small specimens of ice, wrote:

> "it is this fragility precisely which, yielding to the hydrostatic pressure of the unfrozen water contained in the countless capillaries of the glacier, produces the crushing

> action which shoves the ice over its neighbouring particles".

How Forbes reconciled crushed ice with continuous viscous deformation is not clear. (like Rendu, Forbes in this passage incorrectly attributed deformation to pressure, rather than to deviatoric stress.)

Forbes is probably best known for his discovery of annual band ogives (now also known as Forbes bands) on the Mer de Glace (see Chapter 4). He correctly related the light and dark bands to differences in surficial dirt on areas with differing foliation.

A17.3.3 JOHN TYNDALL

John Tyndall, professor of natural philosophy at the Royal Institution, published two books about glacier physics. Glaciers of the Alps (1860) was divided into two sections; the first was a travelogue and mountaineering guide, and the second, observations and discussion of glacier flow (Unfortunately, this clean division tempted some later publishers (e.g. J. M. Dent and Co., 1906) to delete the second part on the grounds that it was of no possible interest to anybody). Tyndall's second book, entitled The forms of water, (fourth edition, 1874), resulted from a Christmas lecture series for young people in 1871 at the Royal Institution. Clouds, rain, and ice of rivers, lakes, and sea were given cursory treatment compared to Tyndall's main interest, glaciers.

Tyndall conducted further surveys on the Mer de Glace,

obtaining, among his observations, firm evidence that the flow was most rapid at the glacier surface, and decreased with depth (1874, p. 80), and the observation that the point of maximum surface velocity on any transverse line was often displaced toward the outside of valley bends.

Tyndall looked to the microscopic level for an explanation of glacier flow. He was the original advocate of the 'regelation flow theory'. In 1850, Faraday had found that two clean surfaces of melting ice, when brought into contact, would freeze together, and Bottomley (cited by Tyndall, 1874, p. 170) had performed the classic regelation experiment, wherein a weighted wire was passed through a block of thawing ice in one half hour, leaving the block of ice in one piece; the pressure of the wire reduced the melting point of the ice, allowing the ice to melt, and the water subsequently refroze above the wire. Tyndall (1874, p. 165) compressed blocks of ice in moulds, showing that, when the ice was near 0°C, the ice fractured, then was reunited by regelation into a new block of a different shape, and, if the pressure was applied carefully, the shape could be changed without total fracture (1874, p. 166). Since glacier ice is under pressure due to the weight of overlying ice, he concluded (1874, p. 166) that:

> "by the slow and constant application of pressure the ice gradually moulds itself to the valley, which it fills."

Tyndall envisioned ice as a brittle material crushed by pressure and shear stresses, and reunited by regelation after minor rearrangement of the fragments. The process of regelation is important in basal sliding, and, as Tyndall realized, in

crevasse closure (1874, p. 166) and in the transformation of firn to ice (1874, p. 165), but it is not a complete explanation of the internal deformation of glaciers. It does not take account of the crystalline properties of ice, and it is inapplicable to cold ice masses.

Tyndall frequently criticized Forbes' viscous theory (e.g. Tyndall, 1896, p. 327). Forbes' theory had obvious weaknesses, but then, so did Tyndall's regelation theory. Because of this controversy, some glaciologists thought of the glacier flow problem as simply a choice between the viscous or the regelation model. This impeded the development of a complete description. Russell (1897, p. 186) appreciated the difficulty, and proposed the adoption of an 'eclectic model'.

Tyndall is often remembered for his discovery and explanation of 'Tyndall flowers'. These are small melt figures inside ice crystals. If a clear crystal of ice is left for a few minutes in direct sunlight, internal melting parallel to the basal plane produces discs of liquid and vapour about 5 mm to 10 mm in diameter. These discs continue to grow with continued exposure to sunlight, eventually forming delicate crenulated shapes with 6-fold symmetry. Tyndall (1874, p. 36) used crystals of lake ice; the figures can also be produced in large crystals of glacier ice, such as are often found in old ice near a glacier terminus.

A17.3.4 MANY WONDROUS THEORIES

During the last decades of the nineteenth century, a number of theories of glacier flow were proposed. Like Tyndall, most writers looked for small-scale processes to explain large scale glacier motion. The apparent brittleness of small lumps of ice coupled with the observed laminar flow of glaciers was a puzzling paradox. Most of the new theories were controversial, ingenious, and almost invariably inadequate. Like the viscous theory and the regelation theory, they often contained some elements of truth. For example, Canon Moseley (1862) showed that a plate of lead could creep down an inclined plane if it was repeatedly warmed and cooled. This process accounts for some of the motion of talus slopes (e.g. Russell. 1897, p. 176); Moseley suggested that it also caused the motion of glaciers, due to diurnal expansion and contraction. Forbes (1855) and Ball (1870) strongly refuted this suggestion, on the grounds that:

(1) the vertical diurnal displacement necessary to cause the creep phenomenon was not observed;

(2) heat diffusion into glaciers was too slow and too small to achieve any diurnal effect; and

(3) alpine glaciers were invariably observed to be at the pressure melting point.

Moseley objected to most flow theories other than his own on the grounds that they required ice to shear. Moseley measured the force required to cleanly and abruptly shear off one square inch bars of ice; he then leapt to the unjustified conclusion that a glacier would need to be at least 34 times thicker than the Mer

de Glace (i.e. at least several km) to deform by shear. As Ball pointed out, Moseley totally neglected the rate at which deformation occurred. Continuum mechanics was not one of Moseley's strong points. This discussion, and others like it, occupied a large portion of the glaciological literature of the period (e.g. see Croll (1875) Chapters XXX and XXXI).

Croll (1869, 1875, Chapter XXXI) proposed the 'hypothesis of molecular change'. Solar radiation at the glacier surface could produce melting; this water would flow downhill, then refreeze; the latent heat released would melt the adjacent ice, which could then flow downhill before refreezing. This chain reaction would extend throughout the glacier mass. Deeley (1888) proposed a similar theory. Russell (1897, p. 182) pointed out that, in the St. Elias Mountains, surface ice and snow above 13,000 feet (4000 m) was always at a temperature well below the melting point. In addition, where surface melting occurs, most of the water is quickly lost to runoff in glacial streams.

Various authors, including T. C. Chamberlin (1895), proposed a related theory called 'the hypothesis of granular change'. According to this theory, each ice crystal was assumed to undergo pressure melting where it touched neighbouring crystals. With these obstructing points removed, the crystal was free to settle downslope under the influence of gravity; the meltwater would refreeze, leaving a new crystal shape and orientation, with a downslope displacement. This idea resembled Tyndall's regelation theory applied to individual crystals. The process does exist in glaciers (e.g. the development of foliation), but it is insufficient to account for observed

glacier motions.

In 1894, Chamberlin observed shear planes and thrust features in stratified ice in the termini of some Greenland glaciers. Using less than rigorous arguments (e.g. entrained boulders did not visibly sink through glacier ice), he then (1895) challenged the concept of flow by continuous viscous yielding. He suggested, instead, that individual sedimentary layers moved as cohesive units, possibly bending and sliding relative to one another, but maintaining their identity throughout their flow history (i.e. deforming like a deck of playing cards). I suspect that the layering which Chamberlin (1895) observed was a secondary foliation (e.g. Sharp, 1960) rather than the initial bedding, and the thrusts which he observed were probably of local extent. In fact, both shearing and plastic yielding play some part in glacier flow under various conditions (e.g. Nye, 1951).

A17.3.5 ICE DEFORMATION EXPERIMENTS

By the end of the century, field glaciologists had begun to examine ice at the crystalline level. J. C. McConnel performed some of the earliest experiments. Part of Tyndall's rationale for the regelation theory was the assumption that (1874, p. 167) ice could not deform in tension without fracturing. Main (1887) and McConnel and Kidd (1888) showed that a bar of polycrystalline ice deformed under both compression and tension. They also found that, for a given stress, the deformation rate

decreased rapidly with decreasing temperature below 0°C, but they were unable to quantify this result; they worked in winter at the edge of glaciers, and had poor temperature control and large structural variations in the ice bars. They found that monocrystalline bars were highly anisotropic; they were unable to produce a measurable deformation by applying tension or compression at right angles to the optic axis. Further experiments by McConnel (1890, 1891) showed that the ice crystal

> "behaved as if it consisted of an infinite number of indefinitely thin sheets of paper, normal to its optic axis, attached to each other by some viscous substance which allowed one to slide over the next with great difficulty."

This process of gliding on the basal plane is fundamental to our modern understanding of the flow of glaciers. Further work by others substantiated this important result and led to a refined understanding of the deformation of ice crystals. For example, Tarr and Rich (1912) showed that the laminae normal to the optic axis could bend as well as glide, if the stress was nonuniform.

R. M. Deeley was one of the last in the series of notable glacier physicists of the pre-1914 period. In a paper on granule markings (1910), he showed that striae on the surface of ice crystals were the edges of McConnel's laminae.

A17.3.6 MATHEMATICAL GLACIOLOGY

In an early paper, Deeley (1895) made the first clear distinction in the glaciological literature between viscous and plastic materials, and derived some simple solutions for viscous flow in cylindrical channels and on inclined planes. Deeley (1908) used these results together with estimates of glacier thicknesses and observed flow rates at ten locations on four glaciers in the Alps to estimate the bulk viscosity of polycrystalline ice. There was a large scatter; we now know that the viscosity of ice is stress-dependent. (Deeley (1895) was also aware that the viscosity might not be constant). Deeley found that the viscosity of a single ice crystal shearing normal to the optic axis was several orders of magnitude less than the viscosity of polycrystalline ice.

Previously, Thomson (Lord Kelvin) (1888) had approached the reverse problem; he had estimated the thickness of the floating arctic ice pack and of the East Antarctic ice sheet using a viscosity calculated from the data by Main (1887).

Some of the earliest mathematical modelling of glacier flow appeared at the end of the nineteenth century. Reid (1895) and Finsterwalder (1897) calculated streamlines through steady glaciers. The results were only approximate, because they took no account of the rheological properties of glacier ice. Finsterwalder (1907) was the first to solve the continuity (mass conservation) equation to find glacier thickness changes; this procedure forms the basis of most modern models of ice masses.

Blumcke and Hess (1899) carried out one of the most

comprehensive glacier surveys of that era. They measured ablation rate, surface altitude, and ice velocity along a series of transverse profiles on the Hintereis Glacier. In addition, they used borehole information coupled with the Finsterwalder (1897) kinematic theory to estimate the ice thickness.

Weinberg (1907) had estimated the viscosity of the Hintereis Glacier by using the equations for viscous flow in an elliptical channel to approximate the observations of Blumcke and Hess (1899). Deeley and Parr (1913, 1914) also used the Hintereis data of Blumcke and Hess (1899) in two outstanding papers. Deeley and Parr (1913) found a solution to the Poisson equation for viscous flow in a uniform channel having a more general cross-section than an ellipse. They showed that this type of channel (called "Parr's curve") gave an improved fit over Weinberg's result (1907) to the observed flow of the Hintereis Glacier.

They also addressed the difficult question of separating basal slip from internal shear deformation. They estimated the basal sliding velocity by assuming it was proportional to the basal shear stress, and inversely proportional to the frictional resistance. They pointed out that, since ice must flow around some obstacles on the bed, the flow and sliding questions were connected.

In this paper (1913), Deeley and Parr also pointed out the fact that flow is controlled primarily by the ice surface slope, rather than by the slope of the glacier bed. They were the first to propose the name "Poise" (after Poiseuille) for the C.G.S. unit of viscosity.

Their second paper (Deeley and Parr, 1914) focused primarily on the basal sliding problem. They presented a conceptual model of sliding which is remarkably similar to the widely known model put forward independently by Weertman in 1957. Deeley and Parr (1914) envisioned flow by regelation around small basal obstacles. Instead of modelling bed roughness by a plane with an array of cubes with a characteristic separation (the Weertman (1957) 'tombstone model'), Deeley and Parr modelled the glacier bed by a plane covered by an array of pyramids with a characteristic slope angle. In both models, the parameter could be adjusted to balance the downslope component of gravity against the resistance offered by the uphill faces of the obstacles. Deeley and Parr pointed out that ice moved past large obstacles, channel curves and other irregularities by viscous flow; they did not envision the enhancement of flow due to stress concentrations as pointed out by Weertman (1957), because they assumed a linear (viscous) constitutive relation for ice.

Deeley and Parr (1914) tested their ideas on slip by measuring the sliding rate of a loaded piece of ice on an inclined, grooved rock slab in their laboratory, noting that the slip rate decreased as the temperature dropped below 0°C. They expected this result from the regelation mechanism.

Several other phenomena of interest to the glaciological community of 1914 were discussed in this landmark paper. Vallot (1900) had observed a wave on the Mer de Glace; Deeley and Parr (1914) mentioned waves which they called Schwellungswellen

travelling down glaciers at three to four times the ice velocity. These waves were thought to result from thickening in the lower accumulation region and from changes in the elevation of the firn line (Weertman (1958) presented a mathematical treatment of these kinematic waves). Deeley and Parr also discussed a second type of wave called Druckwellen, which they said arose from thickening and thrusting in the upper accumulation region. These waves were said to travel at 20 to 150 times the velocity of the ice. Few authors since 1914, with the exception of Hodge (1974) and Fowler (1979), have mentioned Druckwellen-type waves.

Johnston and Adams (1913) pointed out that uniform pressure could cause an elastic compression, but could not permanently deform solid bodies; significant permanent distortion resulted only from nonuniform pressure, or stress deviators. This important fact had been overlooked by Rendu and Forbes, and was sometimes overlooked later in this century (e.g. Demorest, 1938, p. 36).

A17.3.7 THE BRINY DEPTHS OF GLACIERS

One other question about glacier flow arose near the end of this period. What effect do solutes and impurities have on the deformation rate of ice? Johnston and Adams (1913) had argued that permanent deformation of a solid near its melting point took place through real melting of the constituent particles under the greatest stress. Quincke (1905[a], 1905[b]) and

Buchanan (1912) had suggested that brine in glaciers could account for melt features on crystal laminae and grain boundaries. Both authors thought that the salts came from rock and dirt inclusions, while Buchanan (1887[a], 1887[b], 1887[c]) suggested that snow and rain could also supply the impurities. Tarr and Engeln (1915) used these ideas to interpret their compression and extrusion experiments on ice bars. They suggested that salts turned the liquid fraction (proposed by Johnston and Adams, 1913) into a brine which formed an intergranular film at temperatures down to -22°C (its eutectic point). They envisioned individual rigid ice crystals readjusting their relative positions by displacing the fluid phase, to give a net bulk flow. In addition, since the fluid volume was hypothesized to increase with shear stress, the ice would soften with increasing stress. While grain boundary sliding does occur in ice near 0°C, we now know that deformation within ice crystals is the major contribution to the creep of ice below -8°C (Barnes and others, 1971), and that glacier ice is often purer than Tarr and Engeln (1915) thought it to be; however, brines do affect the apparent viscosity of ice, and the subject is still worthy of research (e.g. Bowden and Tabor, 1964, p. 137; Lliboutry, 1971[a]). Because the 1914-1918 World War disrupted research and international communication, Engeln (1915) republished the work on solutes in The American Journal of Science.

A17.4 1915 TO 1953

A17.4.1 INTRODUCTION

Following the 1914-1918 World War, glaciological studies were resumed at many institutions. While most work in Europe and in the U.K. continued to emphasize the mathematics of glacier flow and the physics of ice deformation, some studies, particularily in North America, were interested in glaciers as agents of geomorphological change, or as components of hydrological or meteorological cycles. Several controversies arose in the glaciological literature as a result of misconceptions advanced by writers whose expertise lay elsewhere. I will mention the ongoing debate on the roles of shear plane slip (Chamberlin, 1928) and viscous flow (Engeln, 1934), the glacier anticyclone theory of Hobbs (1921,1926,1934) and the extrusion flow theory of Demorest (1937, 1938, 1941, 1942) and Streiff-Becker (1938).

The leading glaciological journal of the period was Zeitschrift für Gletscherkunde; the Journal of Glaciology began publication in 1947. Two books by Hans Hess, Die Gletscher (1904) and Das Eis der Erde (1933) were frequently cited authorities on glacier physics. Review articles on glacier flow were published in English by Hawkes (1930), Matthes (1942), Perutz (1947), and Orowan (1949).

A17.4.2 SHEAR PLANE SLIP OR VISCOUS FLOW?

In the nineteenth century, Tyndall and Forbes, and their respective followers, hotly debated the merits of "the regelation theory" (a solid deformation theory) and "the viscous theory". Both solid and viscous theories survived well into the twentieth century with new variations and new champions. Since 1894, mounting evidence suggested the existence of significant shear thrusting in glaciers. T. C. Chamberlin (1895) had pointed out the existence of shear planes at glacier termini, and was sceptical of the ability of glacier ice to behave as a isotropic viscous fluid on a scale length of centimetres to metres. Scherzer (1907, p. 34) measured an offset of 5.9" (15 cm) at a shear plane spanned by a line of spikes in the Victoria Glacier in the Canadian Rockies. Philipp (1920) thought that the thin bands of blue ice in glaciers were slippage planes, along which ice had been crushed, melted, and refrozen. R. T. Chamberlin (1928) used a recording strainmeter to measure episodic overthrust displacements along shear surfaces at the margin of Glacier de la Brenva on Mont Blanc. He postulated three other types of solid flow in addition to slip on shear planes. They were:

(1) flow by ideomolecular exchange between crystals, i.e. some crystals could grow at the expense of others due to ambient conditions of stress, surface energy, etc.,

(2) solid shearing of ice aggregates, and,

(3) sliding of the whole glacier over the bedrock.

Having presented this careful and timely work, Chamberlin (1928)

then attacked the concept of viscous flow (a type of motion his experiment was not designed to measure). He first labelled two apparently mutually exclusive schools of thought, "the declared adherents of the viscous theory", and "the distinct advocates of the ideomolecular theory" (leaving everyone else among "those who play fast and loose with both sides and entertain more or less vague notions of the mechanics of moving glaciers"). He then concluded (1928, p. 1) that

> "The results speak definitely for the solidity and elastic rigidity of moving glacier ice, and decisively against liquid or viscous flow as the main type of adjustment under stress"

and further (1928, p. 21), that

> "it shows that the common conception of viscous liquid flow has to be eliminated from the picture completely before any real understanding of glacier motion is possible."

These were fighting words, and they stirred up a controversy. Engeln, who had proposed (1915) a "viscous" flow model based on intergranular brine films, apparently took umbrage at Chamberlin's sweeping conclusions. When Hess (1933, p. 79) (translated by Engeln) described glacier motion to be

> "due solely to gravity and ... the motion is to be considered comparable to the streaming of a very viscous fluid",

Engeln (1934) with some delight quoted Hess in a letter to Science, and claimed Hess' support for the viscous theory. After outlining Chamberlin's four types of solid flow, Engeln concluded that

> "Such shear concept Hess, now, and the present author earlier, hold to be fundamentally and completely erroneous."

These were also fighting words, and a debate (Chamberlin, 1934;

Engeln, 1935) ensued in the pages of Science.

Demorest (1934) provided evidence supporting viscous deformation in basal ice. The glacial striations which he mapped on rock steps, around obstacles, and in transverse trenches in deglaciated terrain formed patterns suggestive of fluid flowlines. Eventually, as more data accumulated, even the protagonists realized that glacier motion involved both episodic shearing and continuous deformation. R. T. Chamberlin wrote (1936, p. 104):

> "To advocate either a 'plastic theory of glacier motion', or...perforce advocate a 'shear theory' is to seize upon only a part instead of the whole and to have but a very imperfect understanding of the actual composite phenomenon. The plastic theory is little more than a name for the familiar fact that glaciers move en masse and change in shape. The so-called 'shear theory' ... would imply belief that shearing is the only process producing glacier motion. ... The discovery that a particular process is in operation does not signify that that is the whole story. Unfortunately, this has been all too commonly overlooked in scientific investigations."

After nearly a century, glaciologists could realize that neither Forbes nor Tyndall had been wrong, that neither had been wholly correct, but that both had contributed to the theory of glacier flow.

A17.4.3 CONTINUUM MECHANICS FOR GLACIERS

Two Europeans made important contributions to the mathematical description of glacier motion. Somagliana (1921, 1927) derived the equations of motion for steady flow of a heavy viscous fluid in a channel of constant slope and cross-section. This treatment was notable for its clarity and its discussion of

all the assumptions made. Somagliana also derived expressions for the glacier channel cross-section when the longitudinal surface velocity profile could be approximated by a second or third order polynomial. Somagliana cited Weinberg's (1907) derivation of the viscosity of the Hintereis Glacier, but did not appear to be aware of the work on viscous flow by Deeley and Parr (1913).

Lagally (1930) extended the Somagliana viscous flow theory, and used it to predict the ice depth of the Pasterze Glacier (Austria); seismic soundings by Brockamp and Mothes (1930) showed the predictions to be correct. In 1934, Lagally published Mechanik und Thermodynamik des stationarem Gletschers. This important monograph formulated the glacier flow problem in the mathematical framework of continuum mechanics. For example, Lagally discussed glacier flow in terms of the Navier-Stokes equation, and the temperature of glaciers in terms of the heat diffusion equation. Various early authors had considered some aspects of the thermodynamics of glaciers (e.g. Helmholtz (1865, p. 133; 1873, p. 151) had shown that as much as 7% of the Mer de Glace was melted by internal viscous heating), but in this work, Lagally established a comprehensive and consistent framework for thermodynamic studies. This was an important step, since the viscosity of ice depends strongly on temperature.

A17.4.4 THE GLACIER ANTICYCLONE

During the nineteenth and twentieth centuries, there have been many expeditions to glaciers and ice sheets in the arctic and in Antarctica. The tone of these expeditions has developed from the early heroic (and romantic) efforts to explore unknown lands, into a desire to carry out rigorous scientific inquiries. I discuss only those few expeditions which I think led to a new understanding of the flow of ice masses.

W. H. Hobbs, a meteorologist at the University of Michigan, was the earliest proponent of the glacial anticyclone theory. Hobbs (1911, p. 149; 1921, 1926, 1934) pointed out that a zone of high atmospheric pressure could be expected over an ice sheet, because the air would be cold and dense. This cold sinking air would tend to flow radially out, down the surface slope of the ice sheet. It would be replaced by air drawn down from aloft. This air would be cooled by the ice sheet, causing fog, some frost and rime, and generally light and variable winds with little precipitation over the centre of the ice sheet. These atmospheric conditions do often occur over the East Antarctic ice sheet; however, Hobbs attributed to the glacial anticyclone a stability which is not justified for these atmospheric conditions, and he attempted to predict the glacial flow regime of the Greenland ice sheet on the basis of a permanent glacial anticyclone. Hobbs (1934) thought that precipitation in central Greenland was very small, and that this small amount of light snow and rime was blown out radially by the downslope winds. He thought that cyclonic depressions from

the Atlantic and from Baffin Bay were unable to penetrate the interior; all the precipitation from these storms would be dropped within 80 km to 150 km of the ice sheet margin. Consequently, he postulated that the ice in the centre of Greenland had to be motionless, and the large outlet ice streams were fed only by the marginal zone. He 'supported' this view with two additional claims of questionable merit:

(1) there were no crevasses in the interior, and thus no evidence for motion, and

(2) "the glaciated rock surface overridden by the continental glaciers bears a record of erosional work beneath the marginal zone only ... It thus supplies no warrant whatever for supposing that such action has gone on beneath the vast central area." (1934, p. 421).

(Hobbs' theory of motionless ice was a refreshing break with the traditional debate over shear slip or viscous flow!)

Little was known about the climate or the glacier conditions in the interior, but the high discharge observed at West Greenland glaciers by Ryder (1889) and by Rink (1889) and by subsequent observers required either a large positive mass balance in the marginal zone, or a large collection area; this posed a problem for Hobbs' theory. Hobbs (1941) led four expeditions between 1926 and 1933 attempting to demonstrate the existence of the anticyclone. His results were inconclusive. Observations in 1929 and 1930-1931 by the Alfred Wegener Greenland Expedition (Sorge, 1933) showed that Hobbs had been led to erroneous conclusions about the flow of the ice sheet. Wegener's expedition over-wintered in 1930-1931 at three

stations, Scoresby Sound on the east coast, a station at the western margin of the ice sheet, and at Eismitte, a station near 3000 metres elevation and close to the ice divide 400 km from the west coast. Their observations (Georgi, 1933; Matthes, 1942) established that:

(1) the mean mass balance over roughly a twelve year period was 31 cm a^{-1} water equivalent at the ice divide. This was too large for the Hobbs theory, and

(2) gravity currents of cold air often flowed down the slope of the ice sheet, as Hobbs predicted; however, they were frequently disrupted by cyclonic disturbances which penetrated the central regions of Greenland.

Matthes (1942, p. 187) summarized the anticyclone theory when he wrote:

> "It is thus manifest that the ice sheet of Greenland is nourished, not by the glacial anticyclone, as Hobbs supposed, but in spite of it".

The Wegener expedition was notable for its geophysical work. Sorge (1933) obtained the first seismic soundings of the Greenland ice sheet, finding the ice thickness at twelve points on a profile from Eismitte to the west coast. Temperature measurements showed the diffusion of the annual cold wave into the firn, and density measurements determined the mass balance and firn compaction rates. In November 1930, the expedition leader Alfred Wegener died of a heart problem while travelling from Eismitte to the western station, and his companion Villumsen was lost trying to reach the west coast alone.

A17.4.5 FIELD STUDIES: 1934 SPITZBERGEN EXPEDITION

W. H:son Ahlmann and H. U. Sverdrup led the Norwegian - Swedish Spitzbergen Expedition (Ahlmann, 1935[a]) in the summer of 1934. They carried out quantitative investigations of the mass and energy balance of the Fourteenth of July Glacier and the icefield on Isachsen's Plateau. The interaction of glaciers and climate is critical to understanding glacier motion and variations; this expedition made the most comprehensive observations to that time.

Olsson (1936) measured the total incoming radiation, the albedo of the snow and ice surfaces under various conditions, and the absorption properties of the snow. Ahlmann (1935[c]) measured ablation rates using lines of surveyed stakes and a recording ablatograph, and mapped the stratification of firn in pits and boreholes (1935[b], 1935[d], 1936) to derive the net annual mass balance. Sverdrup (1935[a]) measured the temperature gradient in the firn, and (1935[b]) used all these observations together with meteorological data (Sverdrup, 1936) to formulate the mass and energy balance equations. He was then able to determine the relative roles of radiation, conduction from the air or from below, vapour condensation, evaporation, and fusion. This work had fundamental importance to our knowledge of how and why glaciers vary in response to climate.

The temperature measurements in the firn on Isachsen's Plateau held some surprises. Because the mean annual temperature was below 0°C, Sverdrup (1935[a]) had expected the firn to be frozen to a great depth, as the Wegener expedition had found at

Eismitte (Sorge, 1933); however, he found that in June the temperature was at the melting point everywhere below ten metres depth. The thermocouples and thermometers in shallow boreholes showed that even this surface layer of firn warmed to the melting point everywhere during the summer. To explain this observation, Sverdrup (1935[a]) showed that the latent heat available each summer in meltwater percolating from the surface was sufficient to warm the total thickness of firn if the water refroze, thus completely eliminating the diffusing cold wave from the previous winter. Sverdrup realized that the transformation from firn to glacier ice occured at shallower depths and in younger firn when meltwater was present. In addition, the discovery of ice at the melting point in cold climates had implications for the distribution of viscosity and thus flow rate in the upper reaches of many glaciers.

Ahlmann (1935[d]) studied the hydrology of the Fourteenth of July Glacier, showing that the largest contribution to subglacial runoff came from surface melting. This was true even in winter, because there was a large time lag for percolation through firn and ice crevices. The temporal and spatial distribution of subglacial water is now widely thought to be important for basal sliding.

The work of this Spitzbergen expedition was an admirable model for later studies of glacier physics.

A17.4.6 FIELD STUDIES: JUNGFRAUJOCH RESEARCH PARTY

Most studies of ice structure prior to 1938 had been confined to the ablation zones, the most accessible regions of glaciers. The Jungfraujoch Research Party, led by Hughes, Perutz, and Seligman from Cambridge, was a field study of processes and ice structure in an accumulation area. Seligman (1936, Chapters 5 and 6) had previously studied the transformation of snow into firn, and the Norwegian - Swedish Spitzbergen Expedition had made some observations of firn temperature and metamorphosis. Did similar processes occur in the Alps? An additional goal was to shed some light on the controversy surrounding the relative importance of shear plane slip and continuous deformation. The results of the expedition were published by Perutz and Seligman (1939), Hughes and Seligman (1939), and Seligman (1941). Seligman (1941) cited a second paper by Hughes and Seligman as "in press" in Bulletin of the International Association of Scientific Hydrology; this paper may have become a war casualty; Volume 1 of the Bulletin was not published until 1956.

The Jungfraujoch is a saddle at 3460 m elevation between the Monch and the Jungfrau in the Swiss Alps. It is accessible by cog railway, and has tourist facilities. The Research Party set up a cold laboratory in an artificial cavern in the ice apron (the Guggifirn) on the north side of the saddle, using an old rock tunnel for access. Members of the research group excavated a 20 metre pit in the Monchfirn, an accumulation area of the Great Aletsch Glacier. They measured temperatures in the

pit walls using thermocouple probes, and collected samples for density measurements and crystallographic studies. Observations of water percolation, firn density, and settling rate were taken in additional shallow pits and boreholes, and in crevasses.

This expedition was one of the first to use the polarizing microscope to examine ice crystals in thin section. This technique is now used routinely to study ice fabric. Perutz and Seligman (1939) charted the increase in grain size and density of the firn with age, until the interconnecting air passages were closed off at a density of 820 to 840 kg m^{-3}. They found no significant discontinuous changes in crystal size, density, or fabric across the transition. They showed that ice fabric developed in several stages. New-fallen snow had randomly oriented crystals. In firn at a depth of about one metre, the C-axes tended to be aligned vertically, due to recrystallization parallel to the temperature gradient. After six to eight years, differential motion had destroyed this fabric; crystals, or clumps of crystals, tended to be rotated by flow. In the glacier ice, flow tended to develop a strong fabric. Crystals could no longer rotate as they had done in the firn. Instead, the crystals with basal planes parallel to the flow were able to grow at the expense of less energetically favoured crystals. Bader (1939) had found that a fabric with basal planes parallel to the direction of shear had developed in blocks of ice deformed in the laboratory. Tammann and Dreyer (1929) had demonstrated the growth of the preferentially oriented crystals during shearing, and had attributed the migration of molecules (to the preferred crystals) to the closer packing of atoms in

the basal plane. The work at the Jungfraufirn showed that the same phenomena occur in Alpine glaciers.

To investigate the relative importance of slip on shear planes and plastic deformation, Perutz and Seligman (1939) inserted lines and arrays of pins and screws in exposed longitudinal vertical faces in the pit, in crevasses, and in ice grottos at the cold lab and in the terminus of the Eigergletscher. The deformation of these lines and arrays showed that:

(1) there was no evidence for shear plane motion in the firn; the ice lenses in firn were purely sedimentary in origin;

(2) both shear plane slip and continuous deformation occurred near the glacier terminus.

Several other interesting questions were addressed during the field season. The temperature measurements throughout the summer (Hughes and Seligman 1939) showed how the winter cold wave was reduced and eliminated from the upper 15 metres of the firn by heat conduction early in the summer, and by latent heat from refreezing meltwater later in the season (as had been shown by Sverdrup, (1935[a]) at Spitzbergen). Simultaneous measurement of meltwater mass transport (using collection pans) and of bulk settling (using the array of pins) allowed Hughes and Seligman (1939) to separate the relative contributions of the two processes in the densification of the firn. Attempts (Perutz and Seligman, 1939) to locate the intergranular brine film hypothesized by Engeln (1934) were unsuccessful down to the resolution of 0.004% NaCl and 0.008% NH_4NO_3. Perutz and Seligman

(1939) attributed three sources to the various blue bands of ice observed at the terminus of the Eigergletscher: (1) the original sedimentary layering, (2) shear planes, and (3) traces of closed crevasses (In view of later work (e.g. Sharp, 1960), I think the case for (1) sedimentary layering was not conclusive).

The Jungfraujoch Research Party had performed one of the most rigorous and comprehensive Alpine glacier studies of the pre-World War II period.

A17.4.7 EXTRUSION FLOW

Extrusion flow is the name given to any velocity field in which the maximum horizontal velocity occurs not at the free upper surface, but at some depth, so that the underlying ice flows out or is 'extruded' from beneath the overlying layer. For the case of two-dimensional flow (plane strain) extrusion flow is clearly impossible. There is no way to apply a retarding force on the surface ice to prevent it being carried along at least as rapidly as the ice below (The analogy of a mortar paste squeezed out from beneath a brick requires a large tensile strength in the brick; the ice of an ice sheet would fail in tension long before extrusion flow could occur). Raymond (1971) pointed out that extrusion flow can exist in the transverse direction of a valley glacier, because the valley walls can provide the retarding force, but in the longitudinal direction, for all but a few implausible valley configurations, plane strain is a good approximation, and any deviations from plane

strain are generally insufficient to retard the upper layers. Nevertheless, extrusion flow has been invoked regularly over the past 130 years by glaciologists who were unfamiliar with Newton's laws of motion. Louis Agassiz (1840, p. 212) postulated extrusion flow, although he realized it was merely a conjecture, and Tyndall and Forbes showed that the idea was untenable at the Mer de Glace. Rink (1889), Drygalski (1938), Hess (1933, p. 113) and Matthes (1942) thought that the west Greenland glaciers were fed from the ice sheet by extrusion flow. Aleschow (1930) reported extrusion flow in a cirque glacier in the Urals, and Gibson and Dyson (1939) invoked extrusion flow to explain the dip of stratification planes in the Grinnell Glacier in Montana. The most dedicated proponent of extrusion flow in the twentieth century was Max Demorest.

Demorest, too, derived his first ideas on extrusion flow from a trip to Greenland (Demorest, 1937). Following his work on striations (1938) to show that viscous flow existed, he developed a four part classification scheme for all glacier flow. Demorest justified the scheme by references to "the principles of fluid mechanics", but he was neither a mathematician nor a physicist, and did not publish any equations to support his proposals. The four flow regimes were "gravity flow", "extrusion flow", "obstructed gravity flow", and "obstructed extrusion flow". The criteria for each category involved surface and bed geometry.

"Gravity flow" was the standard type of deformation which we associate with a viscous material on an inclined plane, i.e. the velocity increased continuously from bed to surface.

The physical reasoning by which Demorest included "extrusion flow" in his system was defective on several points. He thought that hydrostatic pressure increased deformation rates of ice (Johnston and Adams (1913) had pointed out the error in that view), he probably confused strain rate with velocity, and he totally missed the force equilibrium difficulty (i.e. the need for a retarding force on the upper ice surface).

"Obstructed flow" meant that something got in the way and forced the streamlines to rise away from the bed. The difference between "obstructed gravity flow" and "obstructed extrusion flow" was related in some way to the curvature of these streamlines.

Although the system was physically incorrect and logically muddled, Demorest advertized it effectively. Many glaciologists who accepted and quoted his ideas may later have regretted being so uncritical.

Demorest was the theoretician of extrusion flow; Streiff-Becker was the experimentalist. Streiff-Becker (1938) had measured the surface velocity and the net annual mass balance each year since 1916 at a central location on the Claridenfirn, a small cirque glacier. When Streiff-Becker (reported by Seligman, 1947) estimated the cross-section area of the channel below the observation site, and multiplied by the measured velocity to find the ice flux, his result was only one quarter of the balance flux calculated by multiplying the surface area of the glacier upstream by the mass balance rate at the observation site. Yet, the surface of the glacier at the

site had not risen since 1916. Streiff-Becker concluded therefore, (for lack of any better explanations!) that there had to be extrusion flow with a bottom current to carry away the excess mass. This "evidence" for extrusion flow was widely accepted for a decade, despite several obvious difficulties:

(1) The glacier was not enclosed by walls on both sides. It was not clear (Seligman, 1947, p. 18) that all the flow passed through the cross-section at the observation site; some firn or ice could have fallen away transversely over the ledge on the right margin of the glacier.

(2) The bedrock profile and the velocity profile at the site were incompletely known.

(3) Mass balance can be highly variable, especially in a cirque, where turbulent winds and drifts can redistribute snowfall. Measurements at one location are totally inadequate to estimate the basin accumulation.

The definitive test of the extrusion flow theory was obviously the measurement of the deformation of vertical boreholes through glaciers. The borehole casing left in the Hintereis Glacier in 1904 by Blumcke and Hess (Hess, 1933) developed a forward slant, implying that the velocity was greatest at the surface. Other boreholes in the Jungfraufirn (Perutz, 1950; Gerrard and others, 1952), in the Malaspina Glacier (Sharp, 1953), in the Salmon Glacier (Mathews, 1959), and in many other locations all gave the same result; none supported the extrusion flow concept. Faith in an idea persists, nonetheless. Streiff-Becker (1953) suggested that the

Jungfraufirn borehole failed to detect extrusion flow simply because it had been drilled in the wrong section of the glacier.

By the early 1950's, some glaciologists were questioning the extrusion flow concept. The final blow to the theory came in 1952 in correspondence in the Journal of Glaciology. J. E. Fisher (1952) objected to a statement by Nye (1951) that extrusion flow seemed to be impossible. In his reply, Nye (1952[d]) showed that, for an idealized ice sheet with the dimensions of an east-west profile of Greenland (a distance AB), the existence of extrusion flow would require an unbalanced force which would accelerate the ice such that (Nye, 1952[d], p. 53):

> "Starting from rest under this acceleration a particle of ice would move the distance AB in 2 hours. Or, if the acceleration were sustained for 100 years, which is not long compared with the lifetime of a piece of ice in Greenland, the ice would reach nearly one-fifth the velocity of light."

No glaciologists, not even the non-physicists or non-mathematicians among us, have recently postulated the existence of extrusion flow in glaciers.

APPENDIX 18: STABILITY CONDITION FOR A SURGE BULGE

This appendix contains a brief discussion of the equilibrium condition for a monoclinal flood wave. This analysis is well-known in the study of tidal bores (e.g. Whitham, 1974, p. 87). I include it here because of its relevance to the velocity function used to simulate surges of the Steele Glacier in Chapter 3.

Consider the propagation of a velocity change in a continuum with a free top surface lying on a plane bed (Figure A18.1). Behind the velocity transition zone, the material is a parallel sided slab of thickness h_0 sliding forward at velocity U_0. Ahead of the transition zone, the material is a simple slab of thickness h_1 sliding forward at velocity U_1 such that

$$U_0 > U_1 \qquad \text{(A18.1)}$$

The transition zone (shaded in the figure) between $x_0(t)$ and $x_1(t)$ advances along the characteristic line (e.g. Whitham, 1974, p. 19)

$$\frac{dx}{dt} = c_1 \qquad \text{(A18.2)}$$

Note that U_0 and U_1 are material velocities, but c_1 is the propagation velocity of the velocity transition zone. If c_1 is very small, material from behind will overtake the transition region, causing a growing bulge between $x_0(t)$ and $x_1(t)$. If c_1 is only marginally faster than U_0, the transition zone can still plow the slow-moving ice ahead into a growing bulge. On the other hand, if c_1 is very large, there is insufficient material

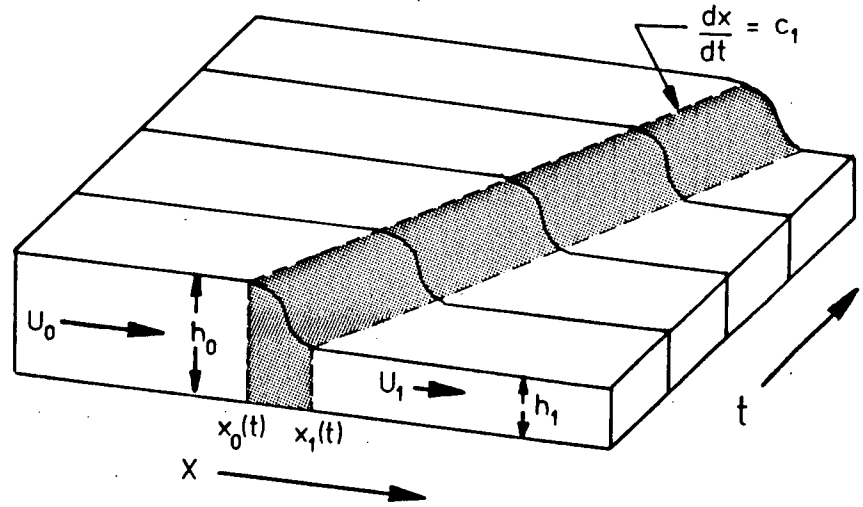

FIGURE A18.1. Advancing Surge Bulge.
The transition zone (shaded) between ice moving at U_0 and ice moving at U_1 moves downstream at c_1. The condition for a stable bulge is given by (A18.4).

available to fill the rapidly lengthening zone behind $x_0(t)$ to the level h_0; the transition profile must flatten out. There is a unique intermediate speed at which the profile can maintain its steady shape (as illustrated in Figure A18.1) with no change of volume in the transition zone. Consider an inertial coordinate system moving at velocity c_1. Assuming no addition or subtraction of mass at the top or bottom surfaces of the continuum, the net flux per unit width δQ across the vertical surfaces at $x_1(t)$ and $x_0(t)$ and into the transition zone in this coordinate system is

$$\delta Q = (U_1 - c_1)\, h_1 - (U_0 - c_1)\, h_0 \qquad \text{(A18.3)}$$

To maintain a constant transition profile, $\delta Q = 0$, and

$$c_1 = \frac{U_0 h_0 - U_1 h_1}{h_0 - h_1} \qquad \text{(A18.4)}$$

If c_1 exceeds this value, δQ is negative (assuming (A18.1) is true) and the transition profile flattens. If c_1 is less than (A18.4), δQ is positive, and a shock, or growing bulge forms in the transition region.

The 1966-67 surge bulge on the Steele Glacier (Stanley, 1969) appeared to maintain a roughly constant height as it moved down the glacier. There are probably physical processes operating in a bulge to increase its speed when the front steepens, and to slow it down when the advancing front flattens out. These trends tend to maintain the equality in (A18.4).

When the ice in front of the transition zone is stagnant ($U_1=0$) (A18.4) reduces to

$$c_1 = U_0 \frac{h_0}{h_0 - h_1} \qquad \text{(A18.5)}$$

It is interesting to note that by observing the speed c_1 of the bulge, the speed U_0 of surface features on the ice, and the height (h_0-h_1) of the bulge, it is possible to obtain an estimate of the ice thickness h_0 from (A18.5).

APPENDIX 19: STEELE GLACIER TRIBUTARIES

The ice flux from the ith tributary glacier is included as a perturbation δb_i to the mass balance function of the Steele Glacier. The flux from each tributary is estimated by two methods:

(1) The surface area of the tributary glacier is multiplied by the average mass balance using the values in Figure 3.3 (a) as a function of elevation. The ice fluxes calculated in this way are listed in Table A19.1.

Number	Area m^2	Average balance $m\ a^{-1}$	Flux $m^3\ a^{-1}$
0	$5.\ 10^6$	2.0	$10.\ 10^6$
1	$10.\ 10^6$	0.7	$7.\ 10^6$
2	$8.\ 10^6$	1.0	$8.\ 10^6$
3	$8.\ 10^6$	0.25	$2.\ 10^6$
4	$5.\ 10^6$	1.0	$5.\ 10^6$
5	$10.\ 10^6$	0.3	$3.\ 10^6$

TABLE A19.1. Ice flux from Steele Glacier tributaries (a). Tributary 0 is the avalanche zone on the north face of Mount Steele (see Figure 3.2). Numbers 1 through 5 are ice streams.

(2) The discharge of each tributary is estimated by simple dynamic considerations. Assuming a basal shear stress of one bar for the tributary glaciers, and using the simple basal stress estimate (1.4.25) without the error term, and with an estimated shape factor of s=0.8, the ice thickness as the tributary enters the trunk ice stream can be estimated from the ice surface slope of the tributary. Narod (unpublished, p. 23) and Narod and

Clarke (1980) suggested that UHF radio echo sounding reflections from within the Hazard Glacier could be the basal moraine of a tributary; if this interpretation is correct, the tributary ice did not change thickness significantly as it was incorporated into the trunk glacier. Wood (1972) reported velocity estimates for the main channel of the Steele Glacier in 1951, and the width of the inset tributary ice streams can be measured on on 1951 air photos. The product of the width w_i of the inset ice stream, the tributary thickness h_i, and the main trunk ice velocity v_i is an estimate of the tributary discharge Q_i.

$$Q_i = w_i v_i h_i \qquad \text{(A19.1)}$$

These estimates are shown in Table A19.2. This estimate assumes that the flow rates given by Wood (1972) are applicable near the margins of the channel, and that and that the tributaries flow at a steady rate. In fact, the only observations of plug flow on the Steele Glacier are during the surge (Stanley, 1969), and, from the moraine pattern on the 1951 air photos, there is some evidence for irregular flow of tributary (4) in the late 1940's.

Both methods give, at best, order of magnitude estimates of tributary discharge. The balance-area method gives consistently larger flux estimates. The values in Table A19.2 may be less reliable. The tributary streams may be deeper and narrower in the main channel than in their own valleys, or they may have been deformed by the episode of rapid sliding (Wood, 1972) in the late 1930's. If the moraine configuration on the 1951 photographs reflects the geometric conditions during a fast flow episode, the rapid (and unknown) velocity during the advance

No	Slope tan(α)	Depth m	Inset width m	Speed m a^{-1}	Flux m^3 a^{-1}
1	0.08	175	750	30.	$3.9\ 10^6$
2	0.13	105	200	30.	$0.6\ 10^6$
3	0.10	140	200	28.	$0.8\ 10^6$
4	0.20	70?	300	25.	$0.5\ 10^6$
5	0.13	105	500	25.	$1.3\ 10^6$

TABLE A19.2. Ice flux from Steele Glacier tributaries (b). The slope of the tributary upstream from the confluence with the main channel is measured from the 1:25,000 map (Topographic Survey; based on 1951 air photos). The ice depth is obtained from the slope assuming a basal shear stress of one bar, and assuming the thickness is not greatly changed as the tributary ice enters the main channel. The velocity estimates (1951) for the main channel are from Wood (1972). The flux estimates are the product of depth, width and speed of the inset tributary ice stream.

would be a more appropriate estimate than the speed for 1951 from Wood (1972). I have used values intermediate between those in Tables A19.1 and A19.2 to calculate additional terms δb_i for the mass balance using the relationship

$$\delta b_i = Q_i / (W_i M_i) \qquad \text{(A19.2)}$$

Q_i is the discharge of tributary i, W_i is the width of the Steele at the confluence, and M_i is the width of the tributary, i.e. the length along the main Steele ice stream within which the flux from the tributary must be absorbed. The solid curve in Figure 3.3 (a) shows the mass balance with the tributary terms δb_i included. Table A19.3 summarizes the contribution of the tributaries to the mass balance. Incorporating tributaries into the mass balance adequately represents their effect on the bulk flow of the glacier, but it introduces an error into the trajectory calculations, because it assumes that the tributary

No	X_i km	Q_i $m^3\ a^{-1}$	W_i m	M_i m	δb_i $m\ a^{-1}$
0	2.	$9.\ 10^6$	3200.	4000.	0.7
1	11.	$4.\ 10^6$	2400.	1000.	1.7
2	13.	$4.\ 10^6$	2500.	1000.	1.6
3	15.	$1.5\ 10^6$	2800.	800.	0.7
4	24.	$3.\ 10^6$	1750.	550.	3.1
5	27.	$2.5\ 10^6$	1750.	800.	1.8

TABLE A19.3. Tributaries: effect on mass balance.
X_i is the distance from the bergschrund of the main ice stream, Q_i is the discharge of the ith tributary, W_i and M_i are the widths of the Steele and the tributary, and δb_i is the term added to the mass balance over a distance M_i to include the flux Q_i. Due to the discrete mesh increment Δx, δb_i may be smaller and be applied over a larger distance M_i in the computer model.

mass is added to the glacier surface; in fact, the tributaries add ice only along the glacier margins.